

The Synthesis of Unimolecular Polymers through Iterative Exponential Growth and their Applications in Block Copolymer Phase Segregation and Biological Systems

By

Yivan Jiang

B.A., Columbia University (2014)

Submitted to the Department of Chemistry
in Partial Fulfillment of the Requirements for the Degree of

Doctor of Philosophy in Chemistry

at the

MASSACHUSETTS INSTITUTE OF TECHNOLOGY

June 2019

© 2019 Massachusetts Institute of Technology. All rights reserved.

Signature redacted

Signature of Author: _____

Signature redacted

Department of Chemistry
May 10, 2019

Certified by: _____

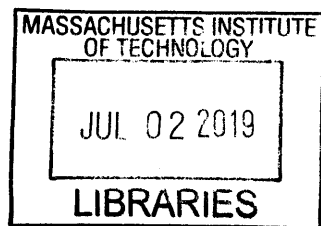
Signature redacted

Jeremiah A. Johnson
Associate Professor of Chemistry
Thesis Supervisor

Signature redacted

Accepted by: _____

Robert W. Field
Haslam and Dewey Professor of Chemistry
Chairman, Departmental Committee on Graduate Students



ARCHIVES

This doctoral thesis has been examined by a committee of the Department of Chemistry as follows:

Signature redacted

Professor Timothy M. Swager: _____ Thesis Committee Chair

Signature redacted

Professor Jeremiah A. Johnson: _____ Thesis Supervisor

Signature redacted

Professor Rick L. Danheiser: _____ Committee Member

The Synthesis of Unimolecular Polymers through Iterative Exponential Growth and their Applications in Block Copolymer Phase Segregation and Biological Systems

By

Yivan Jiang

B.A., Columbia University (2014)

Submitted to the Department of Chemistry on May 10, 2019
in Partial Fulfillment of the Requirements for the Degree of Doctor of Philosophy
in Organic Chemistry at the Massachusetts Institute of Technology

ABSTRACT

Absolute structural control over polymers – in terms of sequence, length, and stereochemistry – is a Holy Grail of polymer science. Inspired by Nature, polymer chemists over the last century have sought new methods and strategies to control these parameters. An inverse relationship exists, however, between the ability to control the primary structure of a macromolecule and the ability to scale the production of the same macromolecule. In this thesis, we describe the application of iterative exponential growth (IEG) toward the scalable synthesis of sequence-defined, unimolecular, chiral polymers. Using this strategy, we have created a wide array of functional molecularly precise polymers of up to 12.1k kDa in molar mass with various side chains for applications in block copolymer phase segregation, lectin binding, and nanoparticle formulations.

Thesis Supervisor: Jeremiah A. Johnson
Title: Associate Professor of Chemistry

To my family and all who supported me

Acknowledgements

I could not have gotten this far without the continuous support of my graduate advisor and most important mentor, Jeremiah Johnson. I cannot overemphasize the appreciation I have for his trust in my ability to push forward my often crazy ideas and turn them into viable projects. Even when I struggled and hit major roadblocks, his creativity, positive attitude, and skilled communication have always been major sources of motivation. He has catalyzed my scientific and personal development far past what I had ever expected.

I am very grateful to my thesis committee chair Tim Swager for his amazingly positive influence on my development as a scientist. He's always been very generous in his advice, wisdom, and perspective. His enthusiasm and thought-provoking suggestions have consistently affected the way I see my research and life directions. I also cannot count the times that I've sought the use of his equipment and laboratory to complete work that I could not have done otherwise. Finally, I am deeply indebted to Tim for mentoring my fiancée Qifan Zhang throughout her PhD and helping her grow into being such an amazing chemist and person.

Many thanks to Rick Danheiser for influencing many aspects of my graduate career. I enjoyed his 5.511 class far more than any other class I took at MIT. His detailed teaching style and class material were critical to my maturation as an organic chemist. Much of my current ability to mentor, instruct, and communicate with others has largely been informed by Rick's teaching style and clarity. He's truly been one of my role model educators. I am also thankful to him for training one of my closest friends at MIT Sam Bartko into becoming a great organic chemist. I've absorbed so many important techniques from simply hanging around the Danheiser lab.

From the Johnson Group, there are so many amazing people I need to thank for being wonderful labmates. Yuwei Gu has always been a wonderful source of inspiration who's always challenged my ideas and changed my perspective. I wouldn't have made it this far without him. Hung Nguyen has never hesitated to disagree with me and this has greatly helped me grow as a person. He's taught and helped me more than I can express here. Thank you Jonathan Barnes for being someone I look up to and pushing me far beyond my limits. You've made me realize I can do so much more than I had originally assumed about myself. I cannot thank Yufeng Wang enough for always calmly evaluating my ideas and providing honest and detailed feedback. Mingjiang Zhong has always been an infinite source of insight into polymer chemistry and I feel a lot of my work would not be possible without him. Thank you Matt Golder for your partnership throughout much of my PhD career and collaboration on many projects that would not have been possible without you. Thanks Manuel Hartweg for always having such an optimistic view on life and all the work that we've done together. Thank you Wenxu Zhang for all of his advice on research projects and many fun conversations. Thank you Mingjun Huang for always believing in my abilities and encouraging me to push outside of my comfort zone. Thank you Junpeng Wang for his thoughtful analysis of my work and companionship. Thank you Yoshiki Shibuya for being such a great person to work with and for entertaining me on my many trips to Japan. Thank you Mashahiro Yoshizawa-Fujita for his kind advice and hospitality when I visited Japan. Thank you Nolan Gallagher for our many discussions both on science and on politics. Thank you Peter Ke Qin for always being so positive and for being a wonderful person to be with. I'd like to also thank Alex Zhukhovitsky, Michelle Macleod, Mao Chen, Farrukh Vohidov, Ken Kawamoto, Qixian Chen, Yongsheng Gao, Jenny Liu, Julian Grundler, Ellane Park, Gabriela Gil Alvaradejo, Shuto Mochizuki, Eileen Burke, Martin Henriksen, Zhihao Huang, Yasmeeen AlFaraj, Gihan Hewage, Katherine Young, Erica Zhou, Teruhiko Saito, Masamichi Shirakura, Peyton Shieh, Bo Qiao, Nate

Oldenhuis, Jessica Lamb, Samantha Kristufek, Julia Zhao, Michael Stolberg, Matthew Pearson, Alexandra Sourakov, Sachin Bhagchandani, Deborah Ehrlich, Keith Husted, David Lundberg, and Alan Enrisco for being amazing labmates through the years. I'd like to thank my mentees Wencong Wang, Kathleen Chen, and Nicole Milos for giving me the wonderful opportunity to give them chemistry training.

From the rest of MIT, there are many other people I must thank. Thank you Steve Buchwald for teaching me so many lessons in my early PhD career, the most important one being that of personal responsibility. I am also very thankful to Jeff Bandar for his personal support and mentorship throughout my time at MIT and Columbia, helping me out whenever I was struggling the most. I am grateful to Adam Willard for always having such advanced theoretical insight into many projects that I simply would not have understood otherwise. Thank you Hyowon Seo for being a great friend who's always there to listen to my worries and concerns with my life. Thank you Sam Bartko for showing me how to do so much chemistry and our many discussions about the meaning of life.

I am deeply thankful for the mentors and teachers from Columbia University that gave me my deep connection to chemistry. I want to thank Luis Campos for being an amazing mentor and PI throughout my undergraduate career. Luis supported me by giving me the freedom to explore my interests to work on whatever project I had an interest in and motivating me to push beyond my limits. Many thanks also to Sujun Wei for being my first mentor in chemistry research, Helen Tran for providing emotional support and professional advice on my many worries, and Jianlong Xia for giving me the confidence and courage to accept my personal demons and adapt to new situations.

I am grateful to Tristan Lambert for introducing me to graduate level chemistry and showing me the importance and nuances of understanding enantioselective reactions and general catalysis. Thank you Scott Snyder for providing some of the most detailed instruction on almost every major aspect of organic chemistry from olefination to the fascinating synthetic problem of quinine. I am so thankful to Sam Danishefsky for his astoundingly interesting classes on the history of the synthesis of steroids and alkaloids, and consequently giving me a great appreciation for the innate beauty of total synthesis and what it has done for human society. I am also indebted to Myles Smith for being the greatest TA I have ever had the pleasure of knowing. Myles was my TA for all 3 of the above classes and gave me essentially one on one tutoring in his many weekly office hours. I was an ignorant undergraduate junior at the time and desperately needed that patience and help.

Thank you Ronald Breslow for having introduced me to organic chemistry and later on teaching me the finer points of bioorganic and medicinal chemistry. Thank you Colin Nuckolls for giving me my introduction to materials chemistry. Thank you Nina Berova and George Ellestad for showing me the history of early analytical chemistry and for the many stories on different natural products. Thank you Koji Nakanishi for being such an encouraging role model and showing me what to aim for in my scientific career. I cannot thank James Valentini and Vesna Gasperov enough for letting me join the first round of the Columbia Science Research Fellows and instigating my scientific career. Without Jim and Vesna, I truly could not have come this far. Also, thank you to my lifelong friends David Xing and Scott Sicong Zhang who have been by my side ever since the Columbia days.

With greatest importance, I must thank my family for their unending and unconditional love and support. I am eternally grateful for the sacrifices that my mother and father have made in order to give me the life I have now. I know both of you have been frequently challenged by my

frequent foolishness and my many mistakes. Thank you both for helping me grow as a human being and I hope to make you both as proud of me as I am of you. My sister has always been my best friend throughout my life. We've had our many ups and downs, fun memories, and many fights. I don't know where I'd be without you and I'm so glad to be your older brother. Finally, I need to thank my fiancée Qifan Zhang who has been my closest friend and most fervent supporter. I am so lucky to have found you and for the opportunity to love you. Because of you, I am able to find happiness when I'm struggling and passion when I'm demotivated. You've changed me into a wiser, more emotionally intelligent, and just overall better human being. I couldn't have asked for a more wonderful partner in life. I can't wait to see what our future has in store for us!

Preface

This thesis is comprised of material adapted from the publications below. Used with permission from the American Chemical Society.

Jiang, Y.; Golder, M. R.; Nguyen, H. V. T.; Wang, Y.; Zhong, M.; Barnes, J. C.; Ehrlich, D. J. C.; Johnson, J. A. Iterative exponential growth synthesis and assembly of uniform diblock copolymers. *J. Am. Chem. Soc.* **2016**, *138*, 9369-9372.

Golder, M. R.†; Jiang, Y.†; Teichen, P. E.; Nguyen, H. V.-T.; Wang, W.; Milos, N.; Freedman, S. A.; Willard, A. P.; Johnson, J. A. Stereochemical sequence dictates unimolecular diblock copolymer assembly. *J. Am. Chem. Soc.* **2018**, *140*, 1596-1599.

In preparation:

Hartweg, M. †; Jiang, Y.†; Yilmaz, G.; Jarvis, C.; Nguyen, H. V.-T.; Primo, G. A.; Monaco, A.; Beyer, V. P.; Mata, A.; Chen, K.; Kiessling, L. L.; Johnson, J. A.; Becer, C. R. Unimolecular chiral glycopolymers for selective lectin binding performance. 2019

Nguyen, H. V.-T. †; Jiang, Y.†; Barnes, J. C.; Oldenhuis, N. J.; Huang, Z.; Wang, W.; Chen, K.; Chen, Q.; Golder, M. R.; Young, K.; Johnson, J. A. Chiral unimolecular-armed bottlebrush polymers as biological probes. 2019

Respective Contributions

This thesis contains work that is the result of collaborative efforts of the author and colleagues in the Johnson group, the Willard group, the Kiessling group, and the Becer group.

Chapter 1. This chapter was a collaborative effort between Jonathan C. Barnes and the author.

Chapter 2. This chapter is composed of material adapted from the following publication:

Jiang, Y.; Golder, M. R.; Nguyen, H. V. T.; Wang, Y.; Zhong, M.; Barnes, J. C.; Ehrlich, D. J. C.; Johnson, J. A. Iterative exponential growth synthesis and assembly of uniform diblock copolymers. *J. Am. Chem. Soc.* **2016**, *138*, 9369-9372.

The work in this chapter was a collaborative effort with Matthew R. Golder, Hung V. T. Nguyen, Yufeng Wang, Mingjiang Zhong, Jonathan C. Barnes, and Deborah J. C. Ehrlich. Matthew R. Golder, Jonathan C. Barnes, and Deborah J. C. Ehrlich assisted with the synthesis design and analysis of the data. Hung V. T. Nguyen performed all Transmission Electron Microscopy (TEM) imaging. Yufeng Wang guided Atomic Force Microscopy (AFM) imaging and sample preparation. Mingjiang Zhong assisted with the analysis of the Small Angle X Ray Scattering (SAXS), TEM, and AFM data. The author performed and led the design of the synthetic routes, characterized all materials, and wrote the chapter.

Chapter 3. This chapter is composed of material adapted from the following publication:

Golder, M. R.†; Jiang, Y.†; Teichen, P. E.; Nguyen, H. V.-T.; Wang, W.; Milos, N.; Freedman, S. A.; Willard, A. P.; Johnson, J. A. Stereochemical sequence dictates unimolecular diblock copolymer assembly. *J. Am. Chem. Soc.* 2018, *140*, 1596-1599.

The work in this chapter was a collaborative effort with Matthew R. Golder, Paul E. Teichen, Hung V. T. Nguyen, Wencong Wang, Nicole Milos, and Seth A. Freedman. Matthew R. Golder performed and analyzed the SAXS experiments. Paul E. Teichen ran simulations on the block copolymers. Hung V. T. Nguyen and Matthew R. Golder performed the TEM imaging. Wencong Wang, Nicole Milos, and Seth A. Freedman assisted in the synthesis of the materials. The author designed the synthetic routes and made all the materials. The writing of the chapter was a collaborative effort between Matthew R. Golder and the author.

Chapter 4. This chapter is composed of material adapted from the following publication:

Hartweg, M. †; Jiang, Y.†; Yilmaz, G.; Jarvis, C.; Nguyen, H. V.-T.; Primo, G. A.; Monaco, A.; Beyer, V. P.; Mata, A.; Chen, K.; Kiessling, L. L.; Johnson, J. A.; Becer, C. R. Unimolecular chiral glycopolymers for selective lectin binding performance. 2019. *In preparation*.

The work in this chapter was a collaborative effort with Manuel Hartweg, Gökhan Yilmaz, Cassie Jarvis, Hung V. T. Nguyen, Gastón A. Primo, Alessandra Monaco, Valentin P. Beyer, Alvaro Mata, and Kathleen Chen. Manuel Hartweg designed and performed the synthesis of the thiomannose sodium salt and its addition onto the allyl-IEG compounds. Manuel Hartweg, Gökhan

Yilmaz, Gastón A. Primo, Alessandra Monaco, Valentin P. Beyer, and Alvaro Mata ran the Surface Plasmon Resonance (SPR) and the cell viability studies. Cassie Jarvis performed the imaging and analysis of the endocytosis of the TAMRA functionalized glycopolymers into Raji B-cells in different conditions. Hung V. T. Nguyen performed all of the TEM and Dynamic Light Scattering (DLS) experiments. Kathleen Chen assisted in the synthesis of the allyl-IEG polymers. The author synthesized all allyl-IEG polymers. The writing of the chapter was a collaborative effort between Manuel Hartweg and the author.

Chapter 5. This chapter is composed of material adapted from the following publication:

Nguyen, H. V.-T. †; Jiang, Y. †; Barnes, J. C.; Oldenhuis, N. J.; Huang, Z.; Wang, W.; Chen, K.; Chen, Q.; Golder, M. R.; Young, K.; Johnson, J. A. Chiral unimolecular-armed bottlebrush polymers as biological probes. 2019. *In preparation*.

The work in this chapter was a collaborative effort of Yivan Jiang, Hung V.-T. Nguyen, Jonathan C. Barnes, Nathan J. Oldenhuis, Zhihao Huang, Wencong Wang, Kathleen Chen, Qixian Chen, Matthew R. Golder, and Katherine Young. Jonathan C. Barnes, Hung V.-T. Nguyen, and the author designed the study. Hung V.-T. Nguyen, Jonathan C. Barnes, Zhihao Huang, and the author synthesized, characterized, and prepared materials and samples for these studies. Hung V.-T. Nguyen, Nathan J. Oldenhuis, and Jonathan C. Barnes performed in vitro studies. H.V.-T.N., J.C.B., and the author performed in vivo studies.

Table of Contents

Title Page	1
Signature Page	2
Abstract	3
Acknowledgements	5
Preface	8
Respective Contributions	9
Table of Contents	11
Chapter 1: Sequence-control in polymer chemistry: Synthetic strategies and potential applications	13
1.1 Introduction	14
1.2 Absolute Control over Structure	17
1.3 Scalable Methods with Partial Control over Structure	25
1.4 Iterative Exponential Growth Strategies	32
1.5 Potential Applications of Sequence-Controlled Polymers	39
1.6 Conclusions and Future Directions	42
1.7 References	43
Chapter 2: Iterative Exponential Growth Synthesis and Assembly of Uniform Diblock Copolymers	51
2.1 Introduction	52
2.2 Results and Discussion	54
2.3 Conclusions	59
2.4 Supplementary Information.....	60
2.5 References	89
Chapter 3: Stereochemical Sequence Dictates Unimolecular Diblock Copolymer Assembly	93
3.1 Introduction	94
3.2 Results and Discussion	95
3.3 Conclusions	103
3.4 Supplementary Information.....	104
3.5 References	179
Chapter 4: Uniform Glycopolymers with Stereo-defined Microstructure for Selective Lectin Binding Performance	182
4.1 Introduction	183
4.2 Results and Discussion	186
4.3 Conclusions	192
4.4 Supplementary Information.....	193
4.5 References	290
Chapter 5: Chiral Unimolecular-armed Bottlebrushes as Biological Probes	294
5.1 Introduction	295

5.2 Results and Discussion	301
5.3 Conclusions	308
5.4 Supplementary Information.....	310
5.5 References	360

Chapter 1.
Sequence-control in polymer chemistry:
Synthetic strategies and potential applications

This chapter was a collaborative effort between Jonathan C. Barnes and the author.

1.1 Introduction

Nature relies on biopolymers with defined microstructures to sustain life. These biopolymers are defined in the sense that they possess precise lengths and stereoconfigurations and are comprised of an exact ordering of monomer units (Figure 1.1); an order which defines the primary sequence and ultimately dictates the secondary and tertiary structure.^{1,2} This absolute control over molecular design at the monomer level sets the stage for encoding sequences with preprogrammed bits of information that designate roles and assign functions for each biomolecule. These designations result in the advent of biological machines and genetic storage materials that proceed to regulate biochemical pathways, often through mechanisms^{3,4} that produce more functional biopolymers. Nature is a masterful polymer chemist.

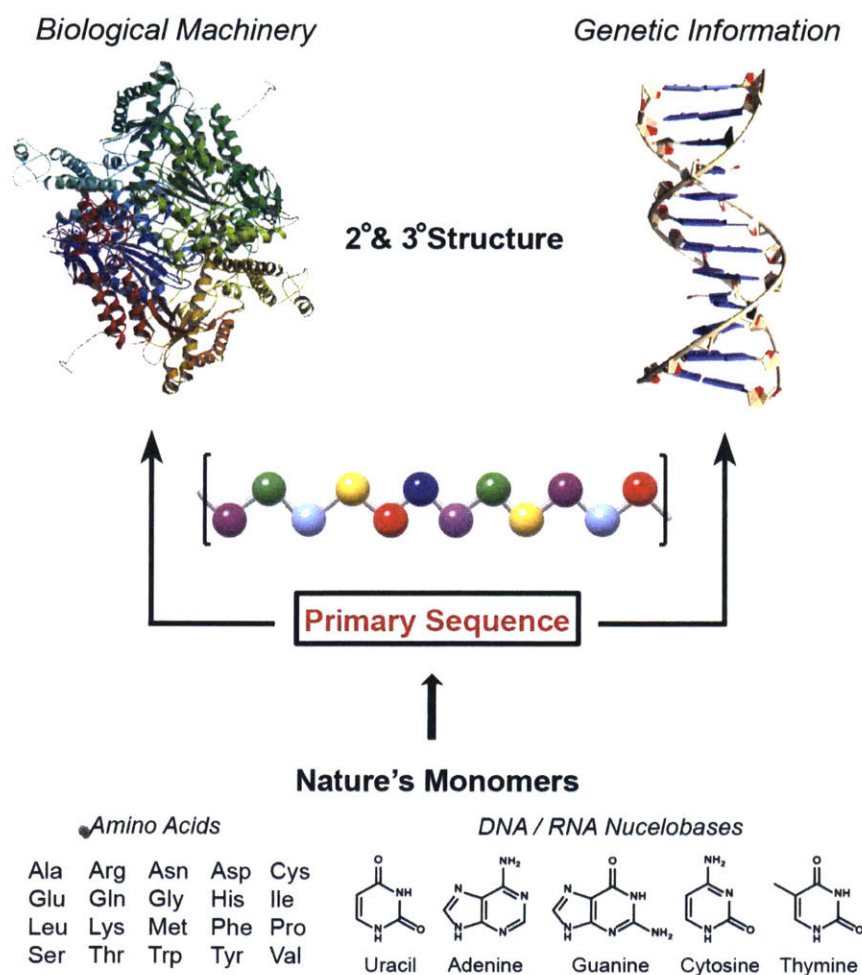


Figure 1.1. Nature's biomolecules serve as the blueprints for absolute control over structure and function. Proteins, DNA, and RNA are sequence-defined precision polymers comprised of a relatively small library of available monomers. The precise arrangement of these monomers

results in well-defined and chiral primary sequences which dictate the formation of secondary and tertiary structures through the advent of multiple noncovalent interactions along the biopolymer chain. These structural modifications lead to the formation of complex biological machinery (such as proteins and enzymes), or genetic storage materials, such as DNA/RNA. The ultimate goal for polymer chemists is to one day be able to develop polymers that are comparable to Nature's biomolecules in terms of sequence, chain length, and stereoconfiguration.

Since 1920, when Staudinger's seminal work⁵ defined the field of polymer science, chemists have strived⁶⁻²¹ (Figure 1.2) to synthesize polymers with Nature's precision, while simultaneously attempting to do so in a scalable manner. One of the first examples of a stereoselective and scalable synthesis of high molecular weight polymers originated from Ziegler and Natta in the mid 1950's, where they demonstrated²²⁻²⁵ the use of a titanium-aluminum catalyst system that could polymerize α -olefins – also referred to as 1-alkenes – and thereby produce polyethylene and either isotactic or syndiotactic polypropylene. Versions of these catalysts are still used²⁶ worldwide in order to generate millions of metric tons of polyolefins for the production of plastics and rubbers. It is important to note that differences in the tacticity alone of a polyolefin can lead to dramatically different properties and provide completely distinct classes of polymer products; control of primary structure is thus key, even for commercial polymers.²⁷ Although very scalable and industrially useful, these catalysts are not able to precisely control the sequence of a growing copolymer chain, a structural feature that can affect^{28,29} the bulk properties of a material. Likewise, other living polymerization methods, such as i) anionic polymerization,³⁰ ii) cationic polymerization,^{16,17} iii) olefin metathesis methods¹³ including ring-opening metathesis polymerization (ROMP),³¹ and iv) free radical polymerizations,³² offer high initiation rates and narrow distributions in chain length, but can only offer statistical control over the sequence of a copolymer. Even controlled radical polymerizations, such as atom transfer radical polymerization (ATRP),³³ reversible addition-fragmentation chain-transfer (RAFT),³⁴ and nitroxide-mediated polymerization (NMP),³⁵ which limit undesirable chain termination reactions and thus provide polymers with excellent control over molecular weight, are still governed by statistical addition of monomers and therefore have limited sequence control.

Timeline | Key advances in macromolecular engineering

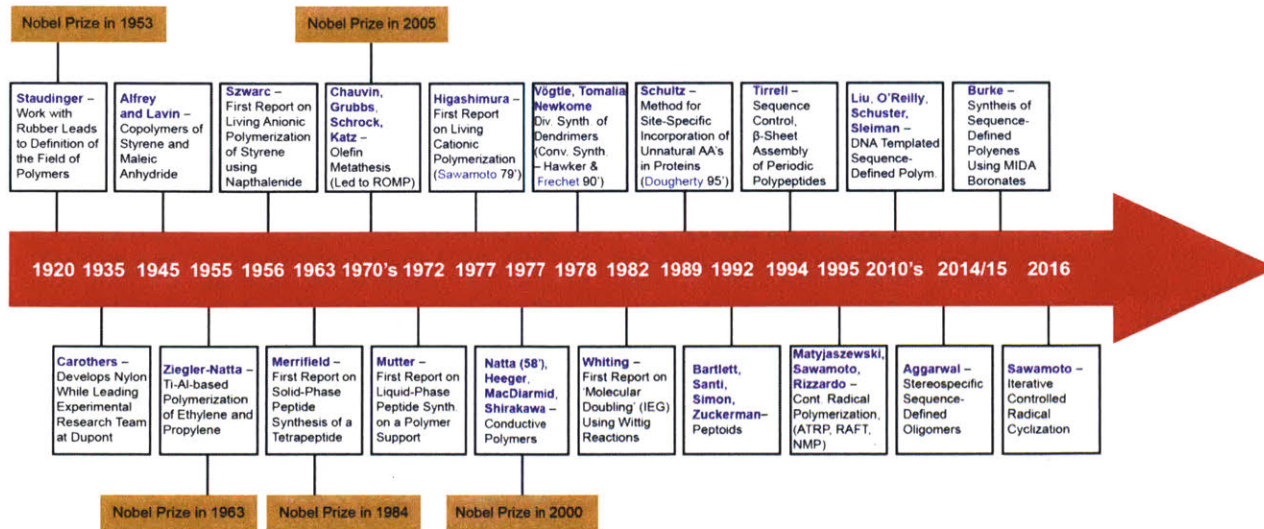


Figure 1.2. Key advances in macromolecular engineering. The timeline depicts the years in which key advances in polymer chemistry – i.e., structural control over sequence, stereconfiguration, polymer chain length, and scalability – were first established. The years that Nobel prizes were awarded for significant discoveries in the polymer field are also provided either directly above or below each corresponding information box listed along the timeline.

On the other end of the spectrum, a solid-phase heterogeneous method¹⁰ based on cross-linked polystyrene resins was developed by Merrifield in the early 1960's (*vide infra*). Solid-phase synthesis is an iterative process capable of constructing, in principle, any arbitrary sequence of monomers. This technique has been used to synthesize a wide-variety of precise polypeptides,³⁶ polynucleotides,³⁷ oligosaccharides,³⁸ and non-natural synthetic polymer³⁹ sequences and can speed up the process of synthesizing a sequence-defined polymer by employing washing steps that remove uncoupled products and excess reagents in between each monomer addition as opposed to more tedious purifications often required in solution-phase synthesis. Solid-phase synthesis is undisputedly the most well-developed approach for sequence-defined polymer synthesis. Despite the mountains of research done in the field, it has become clear that there are inherent limitations to the technique. For example, each step requires the addition of a large excess of the monomer (which can be costly if not recovered) and coupling reagents to ensure quantitative chain growth. Also, the purity of the desired sequence becomes progressively worse as the polymer reaches longer and longer lengths. Once the desired sequence has been obtained, the polymer product must be cleaved from the resin and undergo an additional step of purification, typically by preparative

high performance liquid chromatography (prep-HPLC). These limitations ultimately make it difficult to produce substantial quantities of the sequence-defined polymer; syntheses of polypeptides and polynucleotides with degrees of polymerization greater than 30 are often limited to milligram or smaller scales.

Although these key advances in macromolecular engineering (Figure 1.2) have enhanced our ability to control different features of polymer structure, and each has led to important advances in applications of polymers in academia and industry, there is an apparent tradeoff, or inverse relationship, that exists between microstructural control and scalability. Statistical polymerization methods can produce kilograms of a polymer with limited control, whereas iterative methods yield many orders of magnitude less material with absolute structural control. So far, there is not one particular method or set of practices that can control all of the features associated with precision polymer architectures, while also possessing the quality of being easily scalable. In order to open new arenas of fundamental and applied polymer science, methods that can produce practical quantities of structurally precise polymers are needed, such that perfect synthetic polymers can be explored in a wide range of materials applications. The purpose of this introduction to the synthesis of unimolecular polymers is to examine existing methods that provide either absolute control over polymer structure, or ones that are more scalable but lack complete control. At the end of the introduction, newer strategies based on an iterative exponential growth (IEG) process – a form of iterative step-growth polymerization – are discussed as additions to the ongoing balancing act that exists between sequence-control and scalability.

1.2 Absolute Control over Structure

Nature's Assembly Lines and Solid-Phase Syntheses

Nature's machinery is capable of synthesizing precise biopolymers when provided with a biopolymer template that encodes for a particular sequence. In 1992, Tirrell and co-workers exploited⁴⁰ this process by incorporating DNA fragments that encode for a known nonapeptide sequence into a plasmid, followed by incubating the plasmid with *E. coli* in order to access the biological machinery of the microbe, and expressing a polypeptide with the repeating nonapeptide unit (AlaGly)₃ProGluGly, spaced on either end with methionine residues. This process resulted in the isolation (after precipitation and ion-exchange chromatography) of a polypeptide comprised of a precise sequence of 54 nonapeptide repeat units, which possessed a reversible glass transition

temperature (T_g) of 170 °C, could be cast into an optically clear film, and its thermal properties characterized by differential scanning calorimetry (DSC) and thermogravimetric analysis (TGA). The yield from this process is only on the order of 10 mg/L of fermentation media, but by utilizing the bacteria as microscale reaction vessels, the authors were able to generate new sequences of biopolymers. Tirrell and co-workers later demonstrated⁴¹ the use of this type of protein engineering in *E. coli* to prepare a well-defined and unimolecular polypeptide comprised of AlaGly and GluGly blocks flanked by Glu residues – a particular sequence that is known to form β -sheets and β -sheet crystal stems in the lamellae. With these precise biopolymers, they were able to study fundamental properties and physical dimensions/parameters of the crystalline lamellae. Moreover, there are a number of examples⁴² of residue-specific incorporation of non-canonical amino acids into proteins for materials applications that further demonstrates how precise biopolymers can be obtained using Nature's assembly line machinery.

As introduced above, Merrifield's solid-phase synthesis¹⁰ is another strategy to synthesize polypeptides of any amino acid sequence (Figure 1.3a,b) simply by coupling a protected amino acid to a solid support, followed by removal of the terminal protecting group, which exposes a new functional handle that is coupled to the next residue in the desired sequence. Once the iterative synthetic sequence is complete, the peptide is cleaved from the resin, the side-chain protecting groups are removed, and the product is purified. The importance of solid-phase peptide synthesis cannot be overstated, as it has allowed for the development of completely novel arenas of polymer synthesis with a wide variety of natural and non-natural monomers (vide infra).

Amide-bond formation on solid resins using a submonomer approach⁴³ has been exploited for the preparation of synthetic oligomers known widely as peptoids.⁴⁴ These peptidomimetic structures have side chains that are located on the amide nitrogen atom as opposed to being on the α -carbon atoms like in natural amino acids. Peptoids are achiral and lack the amide hydrogen atom as a result of this functionalization strategy; this change affects a peptoid's ability to control secondary structure, unless of course functional side chains are used⁴⁵ that can help stabilize the formation of secondary structures. Because peptoids are resistant to proteolysis, much like D-peptides, many biomedical applications have been pursued⁴⁶ with various sequence-defined peptoid structures.

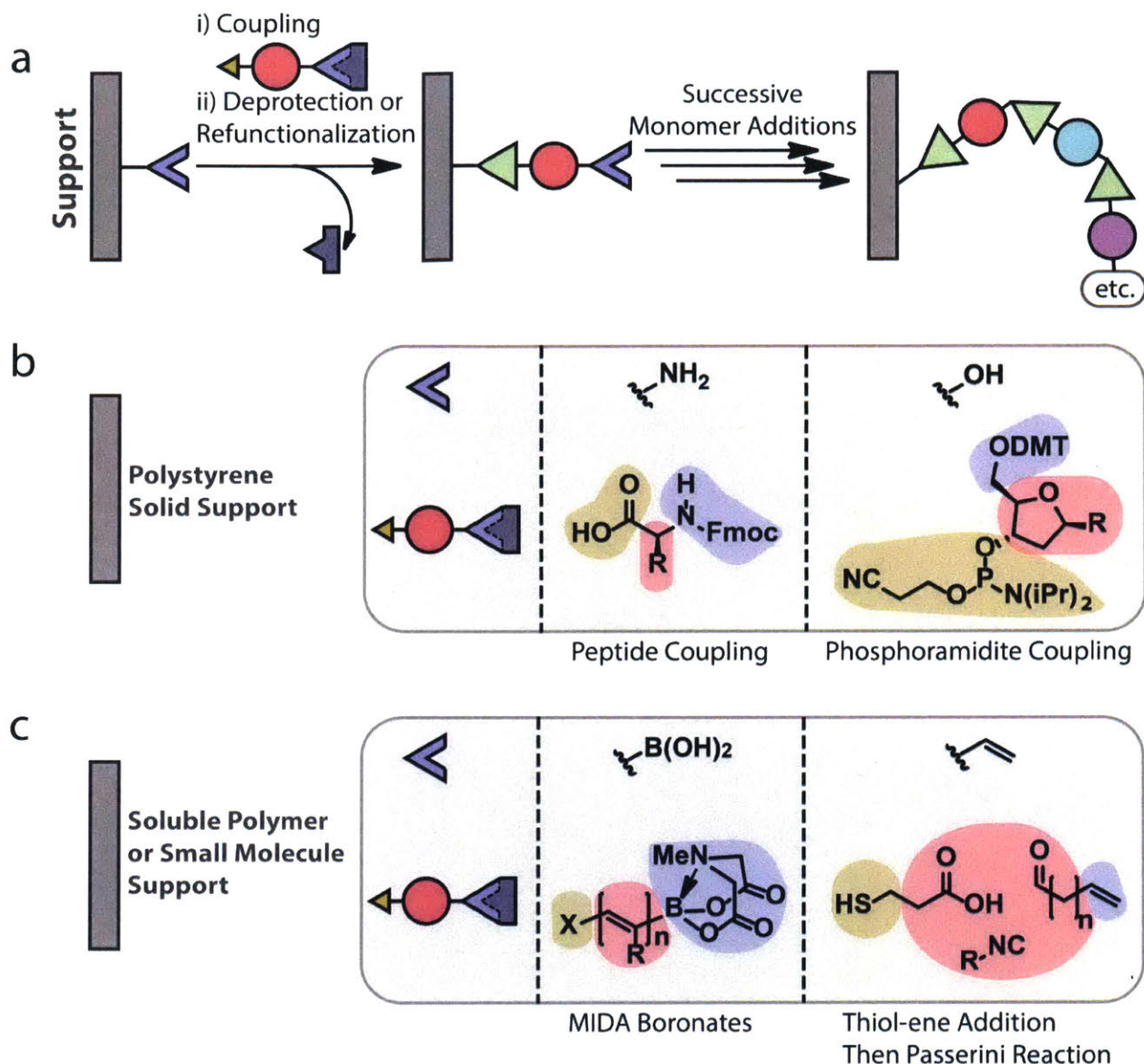


Figure 1.3. Sequential addition of protected monomers to a solid or solution phase support leads to precise macromolecules. **a**, In this general scheme, the support – either solid- or solution-phase – has a reactive functional group which is coupled to a multifunctional monomer. This monomer has an orthogonal functional group that allows for the addition of another monomer upon deprotection or refunctionalization. This process is repeated in cycles to form a macromolecule of precise sequence and length. **b**, Crosslinked polystyrene solid supports are commonly used as they allow for facile purifications. Large excess of reagents are often used to fully react with the terminal functional group of each growing chain. Typical chemistries used on these solid supports include peptide and phosphoramidite coupling. **c**, Linear polymers and short nonfunctional alkyl chains have also been used as soluble supports. These strategies can use protected monomers as in solid-phase syntheses, such as trivalent *N*-methyliminodiacetic acid (MIDA) protected boronic monomers. Another popular strategy is to use monomers with orthogonal functional groups. An example is the use of thiol-ene addition to a small molecule support bonded alkene and a subsequent Passerini three component reaction to regenerate the alkene functionality.

Solid-phase synthesis was expanded to the synthesis of sequence-defined oligonucleotides with the advent of phosphoramidite^{47,48} chemistry (Figure 1.3b) in the 1970's, and oligosaccharides^{49,38} around the same time period with the development of sugar protecting group strategies. In the context of oligonucleotides, the development of the 2-cyanoethyl protecting group resulted in higher selectivity and improved rates of internucleoside linkage. This chemistry is used in most of the nucleoside⁵⁰ and non-nucleoside^{51,52} phosphoramidite building blocks that are employed today for the synthesis of natural and non-natural sequences of DNA and other polymers with phosphate backbones. The power of supported phosphoramidite syntheses comes from the ability to generate any nucleotide sequence (degrees of polymerization up to approx. 200 are possible) for use in a variety of applications, such as functionalization of the 5'-terminus of oligonucleotides with non-natural functional handles,⁵³ siRNA gene knockdown therapies,⁵⁴ DNA origami,^{55,56} as well as spherical nucleic acids,⁵⁷ to name a few. The critical limitations to this technique are those that are inherent to all solid-phase syntheses: i) it requires a large excess of monomer for each addition to ensure complete functionalization of a growing oligomer/polymer chain, ii) the length scales are limited to a few hundred residues on account of the occurrence of potential error strands that arise as more and more residues are added to the sequence, and iii) the need to extensively purify the final product from side products with single monomer deletions, and iv) the amount of materials produced, especially for long sequences (>40–50 units), is typically on the order of a few milligrams, or less. Regardless of these limitations, solid-phase synthesis remains a powerful technique that is used⁵⁸ across many disciplines for a multitude of materials applications.⁵⁹

Solution-Phase Monomer Addition

Solution-phase polymer supports⁶⁰⁻⁶² have also been explored. These supports operate in a similar manner as solid-phase supports, but in this case the product of each coupling step is purified by precipitation of the polymer-bound product in a non-solvent for the polymer. Though in principle solution-phase supports could allow for greater scalability, this approach can lead to additional complications such as the need to identify and synthesize a support that is compatible with the desired chemistry, as well as the need to find the right precipitation conditions for purification. The latter can be especially difficult for longer chains where the solubility of the

product chain can compete with that of the polymer support. Nonetheless, with the advent of native chemical ligation strategies for solution-phase coupling of polypeptides, researchers have achieved the total synthesis of full-length proteins.^{63,64} Though not often widely recognized within the polymer community, these works represent the pinnacle of what is possible in the realm of sequence-controlled polymers synthesis. Nonetheless, the very limited scale of such strategies precludes exploratory syntheses for materials applications.

Moving away from supports of any kind (Figure 1.3c, bottom), there have been numerous examples⁶⁵⁻⁷⁴ of iterative addition processes in solution, where one monomer is added at a time to afford sequence-defined oligomers. Here we highlight only a few of some of the more recent examples, however, there are many others.

Burke and co-workers have demonstrated^{75,76} in recent years the ability to affect sequence control over polyenyl building blocks, which they used for the synthesis of a library of polyene-based natural products. With the development of *N*-methyliminodiacetic acid (MIDA) protected boronates (Figure 1.3c, left), which are Suzuki-Miyaura cross-coupling reagents that are very stable and unreactive under standard coupling conditions while in the ‘off’, or complexed state, the authors can conduct an “iterative cross-coupling” (ICC) strategy, where the MIDA end of the growing sequence is inactive until it is converted into the pinacol ester using mild conditions – namely, pinacol and NaHCO₃ in MeOH at 45 °C. Using the ICC strategy, they demonstrated⁷⁵ the ability to synthesize three natural products starting from MIDA boronate building blocks; specifically, asnipyrone B (36% yield over two steps), physarigin A (4.6% over three steps), and neurosporaxanthin β -D-glucopyranoside (2.8% over four steps). Moving to automation⁷⁷ to speed up the process, Burke and co-workers have capitalized on MIDA boronate’s affinity (and lack thereof) for silica under certain solvent conditions, which allows for the excess reagents or unreacted boronic esters used during the ICC protocol to be washed away, analogous to solid-phase synthetic protocols. One limitation of the MIDA boronate chemistry is that some of the coupling steps have proceeded with low efficiency. This limitation is usually not a problem for natural product syntheses that only require 2–4 coupling steps, but it would be crippling if ICC chemistry were to be used to synthesize longer oligomers in an effort to move towards polymers. The classical isocyanide-based multi-component reaction⁷³ (IMCR) protocols – such as the Passerini 3-component reaction⁷⁸ (P-3CR) (Figure 1.3c, right) and the Ugi 4-component reaction⁷⁹ (U-4CR) – have been applied in polymer synthesis^{80,81} by Meier and co-workers for the synthesis

of oligomeric structures with precise sequences. Discovered in 1921, the P-3CR incorporates an isocyanide, an aldehyde or ketone, and a carboxylic acid to form an α -acyloxy amide. The versatility of this process is based on the interchangeability of the R group on the various substituents; Meier and co-workers used (Figure 1.3c) different isocyanides to define a particular sequence. The same authors showed recently⁸² how it is possible to iteratively synthesize a sequence-defined tetramer by alternating between a Passerini step (to assemble the three components) and a thiol-ene step, which introduces a terminal acid that can be used in a subsequent Passerini reaction. In this way, the need for protecting groups, as is common in iterative synthesis, is replaced by the thiol-ene step. Completing four iterations of this alternating reaction protocol (7 steps in total) resulted in the generation of a tetramer with molar mass of 1.6 kDa in an overall yield of 26%. The yields of this process were better when starting from an acid-functionalized 2 kDa polyethylene glycol (PEG), presumably because the products could be purified by precipitation. In this case, a pentamer was synthesized in 34% overall yield and all of the iterative products synthesized from the 2 kDa PEG were characterized by SEC, which indicated low dispersities around 1.05. The key potential limitation of this synthetic strategy lies in the excess use (10 equiv.) of the thiol reagent, as well as the limited efficiencies associated with each reaction. Furthermore, the reliance on different isocyanides for sequence variation limits this approach to the small selection of commercial isocyanides, or requires the synthesis of new isocyanides, which can be dangerous and difficult. Modified MCR procedures that utilize a single isocyanide and a diverse range of amines or carboxylic acids can be imagined. Nonetheless, the synthesis of a high molar mass polymer using only P-3CR and thiol-ene in an iterative manner may well preclude this method from being a scalable methodology.

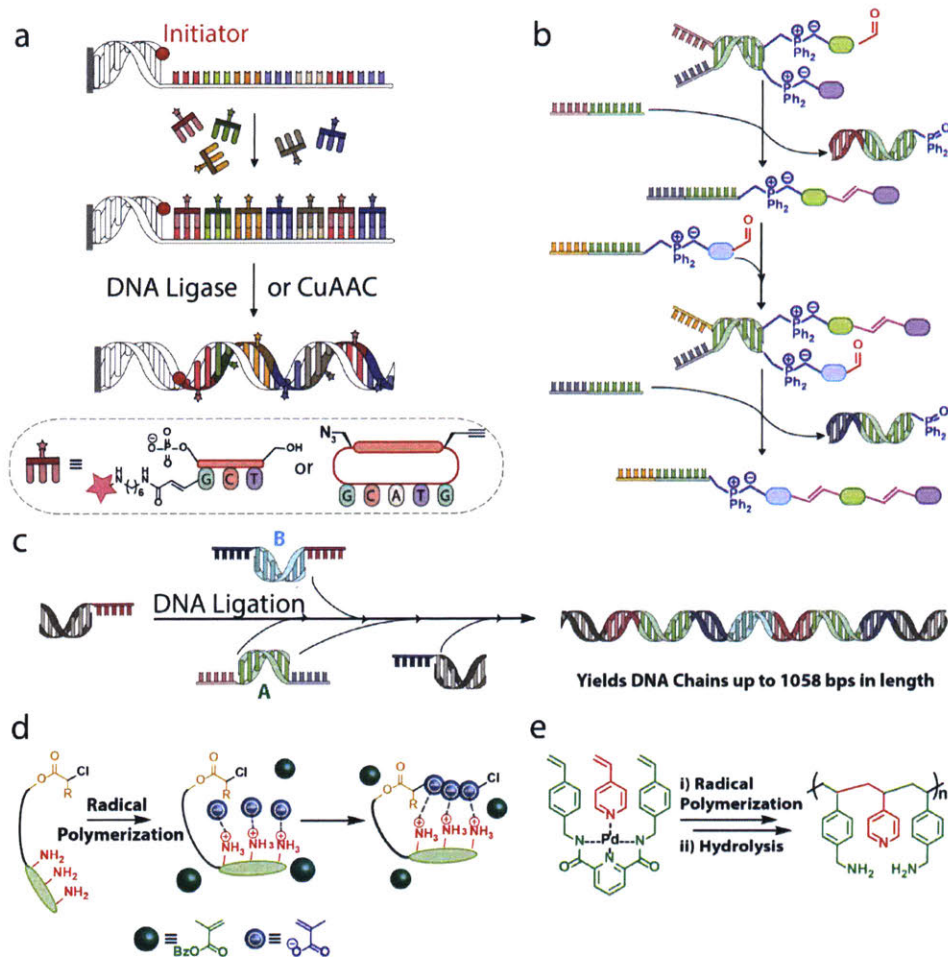


Figure 1.4. DNA-based templation and small molecule templation are strategies to produce sequence and length-controlled polymers. **a**, Differently coded trinucleotide or pentanucleotide monomers can selectively bind and order themselves on a DNA reading frame. Using either DNA ligase or Copper catalyzed Azide Alkyne Cycloaddition (CuAAC), these monomers are covalently bonded to both the DNA template and each other to form a sequence-defined polymer. **b**, Complementary DNA template strands are used to put reactive ylide and aldehyde functional groups in close proximity to one another. Oligomerization propagates in a step wise fashion through successive Wittig reactions with different monomers. Each monomer addition requires the use of an additional DNA strand to dissociate the spent monomer template from the growing chain. **c**, In the presence of a DNA ligase, complementary sticky ends of two propagating A and B polynucleotide monomers are sequentially joined to form a longer DNA polymer. This selective addition of the two monomers leads to the synthesis of sequence and length defined polymers – up to 1058 base pairs in length – which can be amplified subsequently with PCR. **d**, Monomer templation based on small molecules has not reached the precision of DNA based systems, but can be performed on a far greater scale. Directing groups like primary amines can direct the addition of methacrylic acid onto an initiator with radical polymerization conditions. Though a primitive model, this method selectively polymerizes the acid even in the presence of neutral monomers. **e**, Palladium can form a square planar complex with pyridine and amide containing monomers. This association between the monomers leads to the synthesis of an ABA alternating copolymer that, upon hydrolysis, can reveal functional groups, such as primary amines.

DNA Templatation of Sequence-Defined Structures

Templatation is a powerful means to pre-organize individual monomers, such that the functional handles of the monomers are close enough to react with one another and form sequence-controlled polymers. Nature's templates are DNA/RNA, and in combination with a polymerase, they are capable of serving as the blueprints for the production of other nucleotide and polypeptide sequences. This templatation makes polymerase chain reaction (PCR)⁸³ such a powerful tool in biology, medicine, forensic science, and polymer science. It is therefore no surprise that chemists have long sought to utilize analogous DNA templatation strategies to pre-organize synthetic monomers for the synthesis of perfectly sequence-defined synthetic polymers. In some cases synthetic chemical reactions can completely take the place of the ligase enzyme and allow for the production of new classes of sequence-defined polymers. Along these lines, Liu and co-workers demonstrated⁸⁴ that it is possible to use DNA to template the polymerization of peptide nucleic acid aldehyde tetramers through imine and reductive amination reactions. They also showed it was possible to organize eight functionalized trinucleotides onto a reading frame of a particular DNA template (Figure 1.4a) and use T4 DNA Ligase to polymerize the 5'-phosphorylated trinucleotides into sequence-defined polymers of at least 50 trinucleotide blocks, or 150 sequential nucleotides in total. Liu and co-workers later developed⁸⁵ this strategy for use in the absence of ligase enzymes. In this case, the monomers were macrocycles comprised of a non-nucleic acid portion tethered to a peptide nucleic acid portion (5 nucleic acid units long) via disulfide bonds. The non-nucleic acid part of the hybrid monomers contained azide and alkyne functional handles (Figure 1.4a) that could undergo copper-catalyzed azide-alkyne cycloaddition (CuAAC) "click chemistry" to form the synthetic polymer, followed by reduction of the disulfide bonds with dithiothreitol after the polymerization was completed. This work represents the first example of an enzyme-free translation of sequence-defined synthetic polymers with molecular weights of 26 kDa (comprised of 16 monomer) using a DNA template.

In another example of DNA templatation used in a different way, O'Reilly and co-workers demonstrated⁸⁶ (Figure 1.4b) that two monomer-functionalized oligonucleotide strands could be hybridized together to place two reactive functional groups – specifically an aldehyde and ylide – in close proximity with one another. Using Wittig coupling chemistry, these two functional groups were converted to an olefin, followed by the decoupling of the two oligonucleotide strands using a third complementary strand. Once freed, another monomer-functionalized oligonucleotide

strand could be hybridized onto the sequence that is tethered to the growing synthetic oligomer, another Wittig coupling could be conducted, and this cycle could be repeated. With this approach, the authors demonstrated the synthesis of tetramers with yields of 61–95%. Though very elegant, as with most DNA templation strategies, this process is difficult to scale to gram quantities and exhibits poor atom economy, especially since each monomer is required to be a part of an oligonucleotide in order to be brought into close proximity with its coupling partner.

Sleiman and co-workers have also explored precision polymers based on DNA and other polyphosphate sequences in the context of 3D DNA micellar nanostructures,⁸⁷ and with phosphoramidite coupling of non-nucleotide precision polymer sequences tethered to DNA.⁴⁶ A recent powerful example of the synthesis of long nucleotide-based precision polymers⁴⁵ also comes from Sleiman and co-workers, where they showed (Figure 1.4c) how two different oligonucleotide blocks (A and B) – synthesized using solid-phase phosphoramidite chemistry and comprised of 42-nucleotides with 10-nucleotide sticky blocks on both ends – could be alternately ligated to one another for several iterations, followed by capping with primer strands that allowed the sequence to be amplified using PCR. With this method, they were able to produce DNA chains ranging from 480 to 1058 base pairs, and take 4 ng of the starting DNA strand up to 1-2 µg of a product strand. This amount is sufficient to explore other 3D DNA-based structures, such as nanotubes.⁸⁸

The ability of DNA to control polymer structure and template precision polymers is very powerful. Whatever oligonucleotide sequence is desired by the end user, a solid-phase phosphoramidite process can generate it. These precise nucleotide sequences can then be used for a wide range of processes and fundamental applications. The inherent drawback, however, in all of these examples remains the fact that many of these DNA processes cannot be greatly scaled, usually only producing nano- to –micrograms of material. In many of the fundamental applications described here, scaling is not necessary, but if other real world materials applications are to be explored, more material will be a necessity.

1.3 Scalable Methods with Partial Control over Structure

Small Molecule Templation of Sequence-Regulated Polymers

Although DNA is Nature's blueprint for templating precision polymers, there are still issues associated with scaling the processes that produce nucleotide or DNA-translated synthetic

precision polymers. In an effort to address this issue, while admittedly sacrificing some level of control over the precise sequence, synthetic molecules can also function as templates for the synthesis of sequence-regulated polymers. For example, Sawamoto and co-workers demonstrated⁸⁹ how the use of a heterobifunctional designer template initiator comprised of a known initiator for living cationic polymerizations and a known initiator for living radical polymerizations can use electrostatic interactions as a means of templation during the ruthenium-catalyzed radical polymerization of methacrylic acid (MAA). The templation in this system (Figure 1.4d) comes from the cationic polymerization of azido-vinyl ether from one side of the heterobifunctional initiator, followed subsequently by reduction of the azides to amines. Lowering the pH of the template initiator solution resulted in the protonation of the polyamine. This positively charged ammonium strand then functioned as an electrostatic template capable of recruiting methacrylate monomer, which is incorporated during the living radical polymerization, even in the presence of a competitive benzyl methacrylate (BzMA) monomer. As a control, when no template was present, the BzMA monomer polymerized at a faster rate than MAA.

In another elegant example from Sawamoto and co-workers, it was shown⁹⁰ that a styrene-functionalized tridentate 2,6-dicarboxyamido-pyridine monomer and a monodentate 4-vinylpyridine monomer can form a square-planar complex with Pd (Figure 1.4e) – an event which organizes the vinyl groups in an ABA sequence block – and undergo living radical polymerization, generating a sequence-regulated polymer. The secret to maintaining this block structure throughout the polymer synthesis can be attributed to the choice of a bulky fluoroalcohol solvent that hydrogen bonds with the carbonyl of the amide groups, while also running the polymerizations at $-5\text{ }^{\circ}\text{C}$. These additional logistical details help maintain the sequence-regulated structure by minimizing rotation about the carbon-nitrogen bond of the amido group, thus maintaining the close proximity shared by the vinyl groups of the ABA block.

Other synthetic molecular templates exist as well. For example, Leigh and co-workers developed⁹¹ a pseudorotaxane (not shown) that mimics a ribosome and can sequentially pick up amino acids off a molecular strand or ‘track’. The process is a combination of shuttling of the pseudorotaxane ring bearing a cysteine residue along the strand and acyl-shifts after intramolecular attack from the terminal amine. So far, this sequence-specific peptide synthesis has only been achieved up to a trimer length scale, however, it served as a highly novel demonstration capable of generating milligram quantities of the tripeptide. Future work will entail lengthening the track

(which is in itself a sequence-defined polymer synthesis challenge) and increasing the number of amino acid residues that can be coupled in a sequence-specific manner.

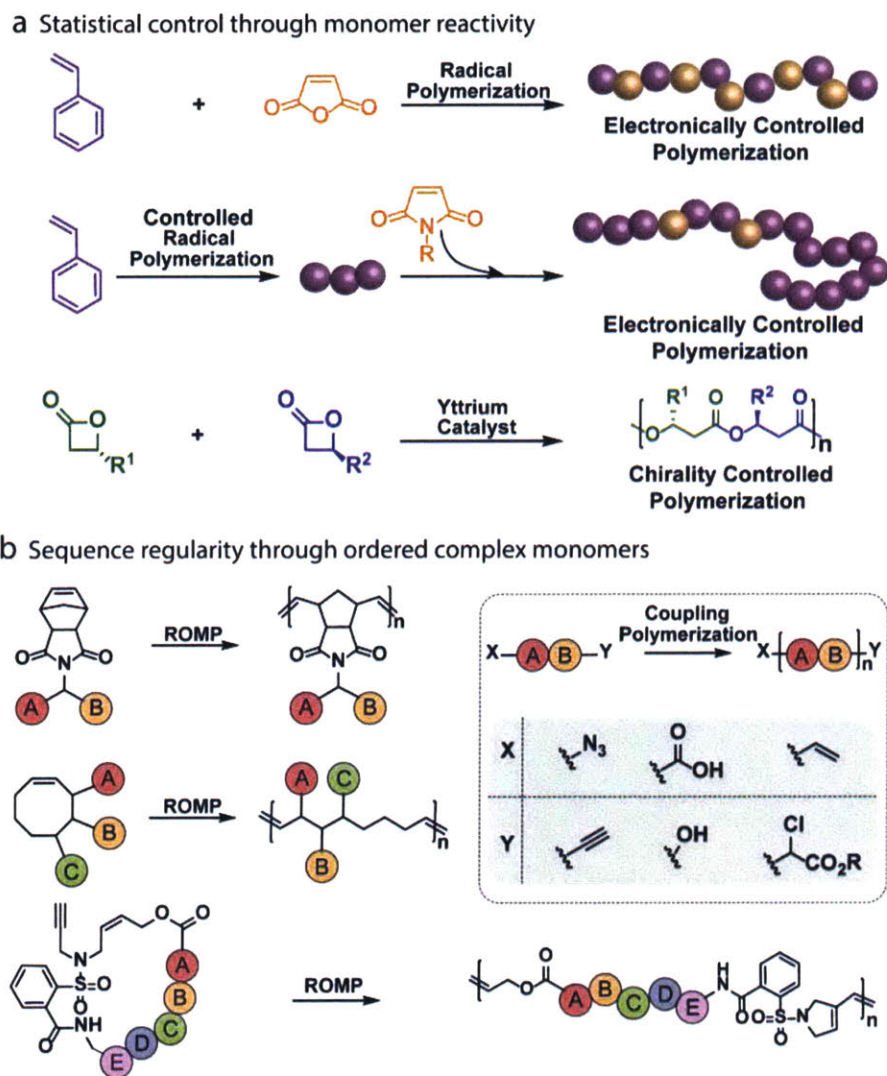


Figure 1.5. Careful monomer design promotes varying degrees of sequence control. **a**, Depending on the type of polymerization, monomers can add on to a growing chain at different speeds. This difference in reactivity and consequently kinetics gives opportunities for sequence control. One old example is the radical polymerization of styrene, an electron-rich monomer, and maleic anhydride, an electron-poor monomer, which due to electronic effects leads to an almost perfectly alternating sequenced polymer. This phenomenon of monomers reacting rapidly with their electronic opposites has been used to position certain monomers in a narrow region on a growing polymer. A popular example involves the precisely timed addition of functional maleimides onto growing styrene polymers. Outside of electronics, a catalyst can bias kinetics to favor the addition of one monomer over another. Syndiospecific Yttrium catalysts are capable of forming alternating copolymers from enantiomerically pure and differently substituted lactone-based monomers. **b**, The sequence of the polymer can also be controlled independent of the

monomer reactivity simply by preordering the sequences on the monomers themselves. Methods of controlled polymerization on these preordered monomers results in the synthesis of sequence regular polymers with approximate length control. Ring Opening Metathesis Polymerization (ROMP) is often used in this strategy with monomers where functionalized side chains are bonded to norbornene and cyclooctene derivatives or the sequence is part of the backbone of enyne functionalized macrocycles. Sequence regular polymers are also synthesized from AB monomers with synergistic functional groups. Couplings like Palladium catalyzed cross-coupling, Wittig reactions, Steglich Esterifications, or radical couplings can result in perfectly alternating AB copolymers.

Monomer Design Directs Sequence Control – Statistical

One of the earliest examples of a sequence-defined copolymer came in 1945 when Alfrey and Lavin demonstrated⁹² the copolymerization (Figure 1.5a, top) of different stoichiometric ratios of styrene and maleic anhydride (MA) in the presence of a radical initiator (benzoyl peroxide) at reflux in benzene. Since the rate of addition of one MA monomer onto another MA monomer of the growing polymer chain is very slow, the authors showed that having either an excess, or 1-to-1 stoichiometry, of MA to styrene affords a copolymer that is roughly 50:50 in composition, which implied a perfectly sequence-defined alternating copolymer. Upon addition of an excess of styrene (i.e. 95% styrene to 5% MA) during the polymerization, however, the composition of the copolymer changed to being approximately two-thirds styrene and only one-third MA. This result implied that the polymer is comprised of styrene blocks after the MA monomers were interspersed in between each styrene monomer in the beginning of the polymerization. This phenomenon is best explained as a kinetically controlled process where the cross-propagation rate vs homopolymerization rate is quite high as a consequence of electronic effects.

Beginning in 2007, Lutz and co-workers examined⁹³ (Figure 1.5a, middle) this kinetically controlled process through sequential additions of four different *N*-substituted maleimide derivatives to an atom transfer radical copolymerization of polystyrene. Again, a high rate of cross-propagation resulted in the incorporation of the four maleimide derivatives at specified times during the polymerization of styrene. Although this method does not provide monomer-level sequence control, the polymer microstructure was well-defined with a molar mass of 6.5 kDa and a $M_w/M_n = 1.16$. This work was expanded in 2008 when Lutz *et al.* investigated⁹⁴ the compatibility of a library of *N*-substituted maleimides as part of a controlled radical copolymerization of styrene. This work established the versatility of the local incorporation (100:1 ratio of styrene to *N*-substituted maleimide) of a variety of functional groups, where one in particular, a propargylic

maleimide, seems to be the most useful since it is eligible for subsequent post-polymerization functionalization either through Sonagashira or CuAAC coupling reactions. Utilizing the ability to incorporate only a few (and in some cases only one) *N*-substituted maleimide(s), Lutz and co-workers set out to investigate⁹⁵ the site-specific incorporation of *N*-propargyl maleimide along a polystyrene chain that had been prepared using ATRP. By installing the propargyl groups at specified locations, followed by azidification of the end groups, CuAAC reactions could be carried out (as well as oxidative Glaser couplings between free alkyne functional groups) to create different topologically interesting structures. The limitations to this synthetic strategy are that it is still a statistically controlled process and there may be chains with more propargyl groups than others, if at all, which could potentially cause a wide variety of shapes and topologies to occur. Nonetheless, by capitalizing on the timing of maleimide additions, and carefully controlling the ratios of donor to acceptor starting monomers throughout the controlled radical copolymerization of styrene and *N*-substituted maleimides, Lutz *et al.* has shown that the ability to hone in on the ultra-precise insertion⁹⁶ of functional monomers can be greatly enhanced.

As mentioned above, tacticity can dramatically affect the thermal and mechanical properties of a polymer. Simultaneous control of sequence and tacticity in statistical polymerization processes is extremely difficult. In an elegant study, Coates and co-workers demonstrated⁹⁷ a syndiospecific, yttrium-catalyzed ring-opening polymerization (Figure 1.5a, bottom) of a 50:50 mixture of two different enantiopure β -lactones, where most polymerization times ran from 5 to 120 minutes at room temperature (depending on the number of equivalents used) and dispersities typically ranged between 1.10 and 1.23. These perfectly alternating syndiotactic polymers possessed lower melting temperatures than the isotactic ones, the latter of which were synthesized as a control using a different catalyst. The difference in melting temperatures of the two isomers is a nice example of how changes in tacticity can affect the physical properties of a material.

Monomer Design Directs Sequence Control – Complex Sequence Monomers

Not wanting to leave anything to chance in terms of the statistical arrangement of monomers in a living/controlled polymerization, chemists have sought ways to design monomers that already possess complex sequences of different functional groups; sequences that will be maintained indefinitely in the polymer. Such an approach inherently requires a polymerization

that can tolerate highly functionalized monomers. One of the more functional-group tolerant living chain-growth polymerization methods is ruthenium-mediated ROMP,³⁰ which is why it is a very popular method for the polymerization of complex monomers. In order to undergo ROMP, the monomer of choice must possess a strained cyclic olefin. Monomer structures that have been explored (Figure 1.5b, ROMP schemes) with this method include bivalent branched AB monomers and macromonomers by Tew and co-workers,⁹⁸ as well as our group,^{99,100} multi-functionalized cyclooctene derivatives,¹⁰¹ and ABCDE enyne macrocycles¹⁰² to name a few examples. In each case, the presence of functional groups from the polymer backbone is locked in during and after the polymerization: the molecular design strategy is taken into consideration pre-polymerization. We showed using electron paramagnetic resonance (EPR) that pseudo-alternating copolymers prepared via ROMP of bivalent-branched AB monomers have inherently homogeneous microstructures, whereas statistical copolymers of analogous AB monomer have heterogeneous microstructures with three distinct regions: A-rich, B-rich, and A-B mixed. Although all of these strategies are very scalable methods that can produce grams of polymer, the drawbacks to this approach are that it leads to polymers that are sequence-regulated, instead of being completely defined (in terms of stereochemistry and mass), and the spacer that constitutes the backbone of the strained ring before polymerization will always exist as part of the polymer chain, and therefore the repeat sequences are permanently separated from one another.

Step-growth polycondensation reactions of A-B-C... monomers inherently provide sequence-regulated polymers. Thus, many researchers have designed sequence-regular monomers with X-AB-Y structures (Figure 1.5b, inset box), where X and Y are complementary functional groups, such as the azide-alkyne,¹⁰³ the carboxylic acid-alcohol,²⁷ and vinyl group-chloride initiator (Figure 1.5b).¹⁰⁴ These AB monomers are then used in step-growth polymerizations, which are very scalable, but generally give molar mass dispersities. Nonetheless, one striking example of the effect of simple sequence control on polymer properties was presented by Meyer and co-workers in 2011. These authors showed²⁷ that perfectly alternating poly(lactide-*co*-glycolide) (PLGA) prepared via polycondensation of an “LG” monomer structure has a drastically different degradation profile than traditional PLGA prepared via random copolymerization of lactide and glycolide monomers. These unique structure/property relationships further motivate the development of new methods for sequence-controlled polymers.

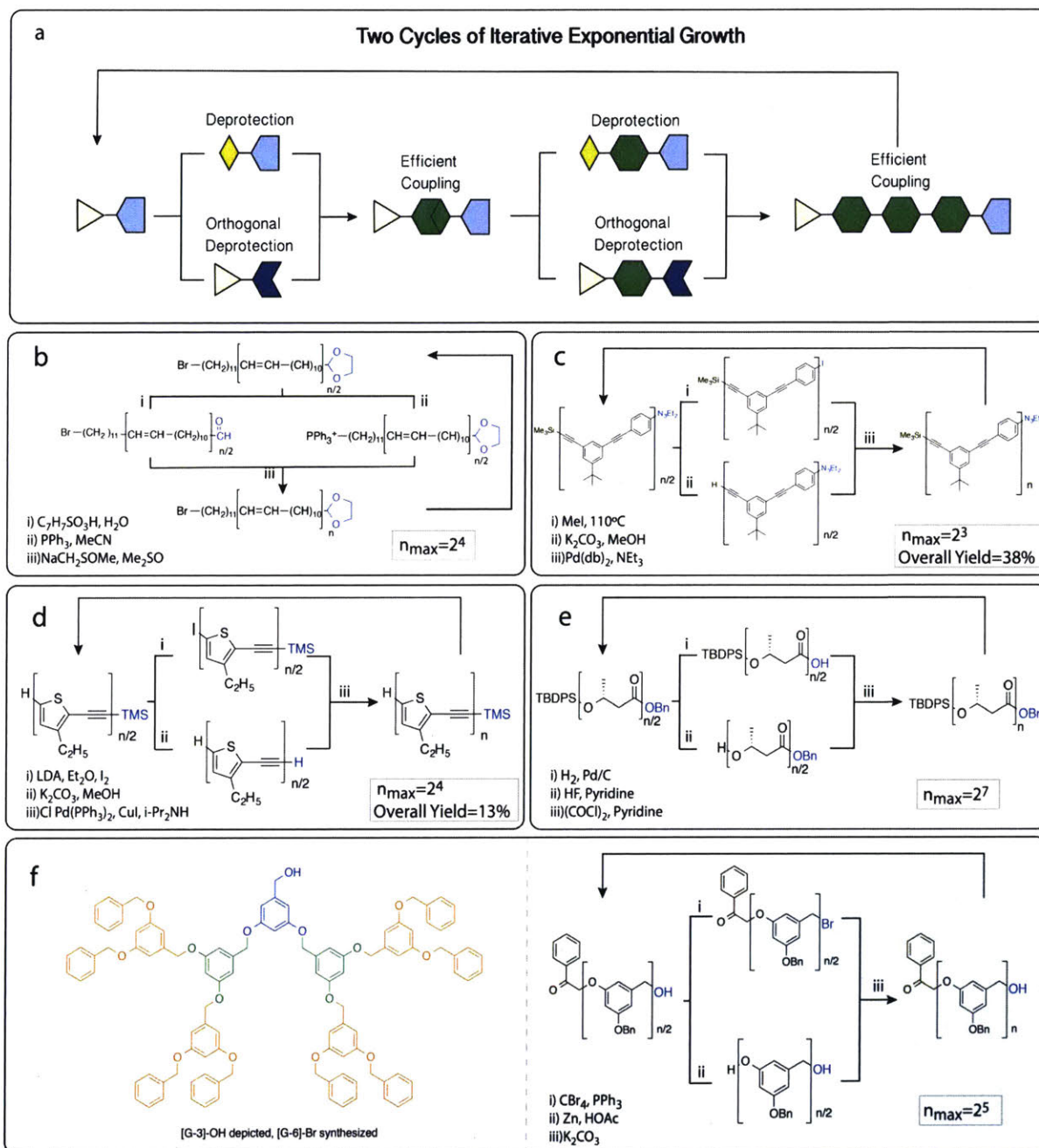


Figure 1.6. Key historical examples of iterative exponential growth. **a**, Pictorial schematic of two cycles of iterative exponential growth. **b**, First example of divergent, convergent growth from Whiting and coworkers, where the convergent step (step iii) is based on Wittig coupling chemistry. **c**, Moore and co-workers employed Sonogashira coupling reactions as part of an IEG cycle to synthesize monomodal conjugated materials. **d**, IEG has been used by Tour and co-workers to synthesize unimolecular thiophene-based materials for single molecule conductance applications. **e**, Although seven IEG cycles were used to create oligomers with 128 repeat units – where each unit possessed a methyl side chain of identical chirality – the efficiency of each cycle suffered. **f**,

Branched and linear dendrimer syntheses also employ the IEG process to generate unimolecular dendritic polyethers.

1.4 Iterative Exponential Growth Strategies

Historical Perspective of Traditional IEG Chemistry

In an effort to develop an iterative synthetic protocol that allows for absolute control over polymer structure, while also doubling the length of the oligomer/polymer each cycle, a solution-phase iterative exponential growth (IEG) strategy was developed¹⁰⁵ in 1982 by Whiting and co-workers. As part of the general IEG strategy (Figure 1.6a), a key monomer is split into two batches and orthogonally deprotected at opposite ends of the molecule. Then, the α - and ω -end functionalized intermediates are coupled together using efficient, often catalytic, reactions. This process results in the formation of a dimer that is twice the degree of polymerization of the starting monomer. Repeating this process leads to tetramer, while a third cycle gives an octamer, and so on. In only a few short cycles, long oligomers and polymers can be obtained. Whiting explored this strategy (Figure 1.6b) in the context of Wittig coupling chemistry, where the orthogonal end-chain protecting groups of choice were a bromide and an aldehyde masked as an acetal group. After converting the bromide to a phosphonium salt and deprotecting the acetal to expose the free aldehyde, strong base was added in order to generate the ylide *in situ*, which then became the coupling partner of the aldehyde. This process was repeated several times in this seminal report, which allowed the authors to synthesize a 104-carbon linear olefin-based structure that was converted to a linear aliphatic chain after hydrogenation of the unsaturated carbon-carbon bonds. Whiting produced several more IEG-related publications¹⁰⁶⁻¹¹¹ that employed the Wittig coupling approach, however, in each case, there were issues with byproduct formation, lack of efficiency in the later stage couplings, and problems with purity of the final hydrogenated products. These issues led Whiting to investigate other uses of IEG chemistry, specifically in the area of Nylon 6¹¹² and Nylon 4,6/6,6.¹¹³ These studies were plagued by solubility problems of the Nylon oligomers, but nonetheless provided important proofs-of-principle for the IEG approach.

A decade after Whiting established the IEG methodology, Moore and co-workers began investigations¹¹⁴⁻¹¹⁶ into the use of meta-substituted phenylacetylene conjugated molecules (Figure 1.6c) as a substrate for IEG chemistry. Specifically, palladium-mediated Sonagashira cross-coupling was carried out after orthogonal deprotections of the terminal protecting groups. With this approach, the authors synthesized a meta-phenylacetylene hexadecamer in 70% yield for the

final coupling step to provide 320 mg total product. Although the yields were more efficient than in Whiting's system, presumably as a consequence of forming less byproducts during each cycle, the Moore process was limited by solubility issues at the hexadecamer stage. For example, when they attempted to synthesize a 32-unit conjugated polymer from their hexadecamer as the precursor, the solubility issues made it difficult to purify and subsequently scale the reaction. Nonetheless, it was shown that the conjugated hexadecamers can behave as a foldamer¹¹⁷ when driven by solvophobic effects and how the secondary helical structure of the foldamer can be controlled in the presence of Ag⁺ ions¹¹⁸ or a chiral guest,¹¹⁹ such as α -pinene.

Shortly after Moore's report of IEG of a meta-phenylacetylene oligomer, Tour and co-workers published investigations¹²⁰⁻¹²² describing an IEG synthetic protocol for a thiophene-ethynylene system (Figure 1.6d) which is based on the iodination of half of the key monomer in the 5 position of the thiophene (63-93% yield), while the other half is desilylated (99-100% yield) using K₂CO₃ in MeOH at room temperature. The final step for each round involves Sonagashira coupling reactions that become increasingly less efficient as the length of the oligomer increases (i.e., 72% for octamer and 50% for hexadecamer), presumably as a consequence of solubility. Tour discusses this solubility issue in later publications, which address some of the problems by installing longer, branched aliphatic side chains onto the thiophene ring. The overall goal of this work, however, was to be able to prepare sufficient amounts of unimolecular material, and in many cases¹²³⁻¹²⁵ with thiol groups at the ends of the oligomer, such that the unimolecular compounds could be sandwiched between two gold electrodes and serve¹²⁶ as a sort of 'molecular wire' for single molecule conductivity measurements. Along these lines, they were able to routinely synthesize ~600 mg or more of the thiophene-based hexadecamers, which allowed them to investigate each derivative in a molecular electronic device setting.

The IEG methodology has also been applied to chiral monomers, as demonstrated¹²⁷⁻¹²⁹ (Figure 1.6e) by Seebach and co-workers beginning in 1996 for poly(*R*-3-hydroxybutanoate) – a 128-mer with a molar mass >11 kDa. In this example, the orthogonal protecting groups are *tert*-butyldiphenylsilane (TBDPS) and a benzyl (Bn) group, which can be deprotected selectively using an HF-pyridine solution and Pd/C hydrogenation, respectively. The final coupling step entails the *in situ* generation of an acyl chloride in place of the free carboxylic acid group at one end by adding oxalyl chloride ((COCl)₂) and pyridine, forming an ester linkage between the deprotected intermediates and essentially doubling the molecular weight. This example represents a

benchmark in IEG chemistry in terms of the number of monomer units that were incorporated using the controlled step-growth polymerization methodology. One drawback from this example is that they were only able to produce small amounts of the 128-mer (i.e., 12 mg) and the yields at the later coupling stages ranged from 2 to 30%, which makes producing an appreciable amount of polymer a difficult task with this particular chemistry. Although scaling the later stage polymers of poly(*R*-3-hydroxybutanoate) is an issue, Seebach and co-workers demonstrated¹³⁰ how shorter oligo(hydroxybutanoate) (OHB) chains – specifically, 32-mers – could form lamellae in phospholipid bilayers and function as membrane ion channels in the presence of calcium polyphosphate. The membrane ion channel application represents a potential example as to why monomodal compounds can be important. The 32-mer OHB chain is the perfect size in the lamellae to form ion channels that span 5.0 nm across the membrane. Other size OHB compounds do not afford an appropriate lamellae cross-section width comparable to the width of the phospholipid bilayer.

Although not technically an IEG-based synthetic strategy – nor necessarily a method used for sequence-controlled materials – unimolecular branched^{21,131} and linear¹³² dendritic architectures (Figure 1.6f, left and right, respectively) have been synthesized using a convergent iterative approach and share a commonality with IEG chemistry in terms of being able to produce materials with little to no dispersity. Early examples of a convergent dendrimer synthetic strategy come from Miller and Neenan¹³³ and later Fréchet, Hawker, and Wooley (Figure 1.6f) in the early 1990's, where the latter researchers capitalized on the difference in acidity of a phenol versus that of a benzyl alcohol (*pKa* of ~10 versus ~15, respectively). Using a mild base such as K₂CO₃, the phenol hydroxyl group is deprotonated and reacts subsequently with a brominated trifunctionalized intermediate to afford the next generation structure where each layer of the dendrimer is chemically similar to the next. The advantage of the branched dendrimer architectures is that large molecular weight 5th and 6th generation dendrimers can be achieved in only a few cycles, and are essentially monomodal species.

Here, we have highlighted representative examples of IEG systems from the literature. There are other examples¹³⁴⁻¹³⁶ of IEG-based chemistries from the last 30 years that were not covered here. For a more comprehensive review of the IEG field alone, please see Hawker and Drockenmuller's 2011 review¹³⁷ on the subject and all references therein.

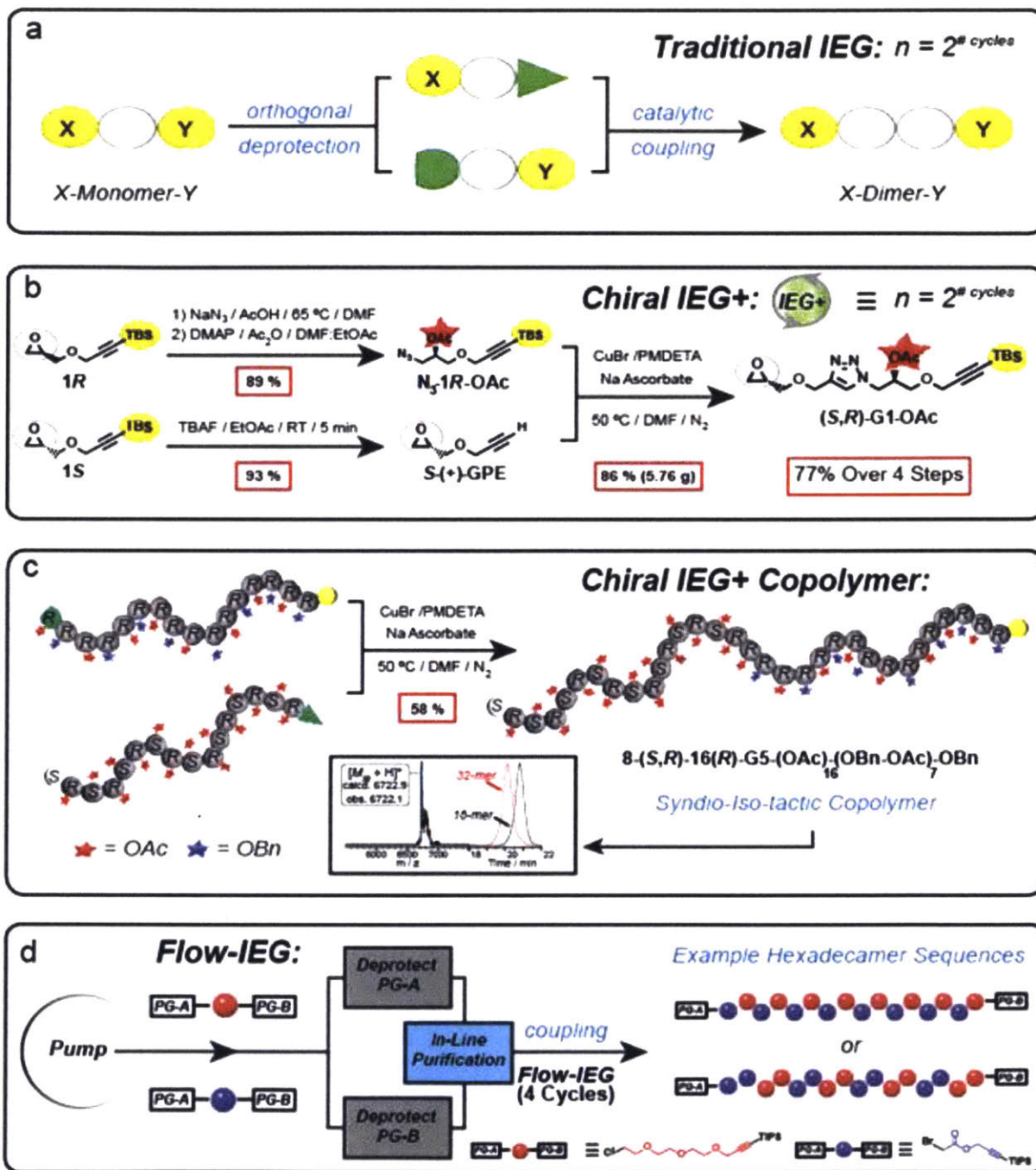


Figure 1.7. Iterative Exponential Growth Plus (IEG+) Side-Chain Functionalization and Flow-IEG. a, Graphical representation of a typical IEG+ cycle that begins with a pair of enantiopure monomers that are either functionalized or deprotected, followed by a catalytic coupling step that affords a 1st generation (G1) stereo-defined dimer. Each IEG+ cycle effectively doubles the molecular weight of the starting precursor, while also introducing the possibility to

control the stereochemistry and side-chain functionality every cycle. **b**, A specific example of IEG+ that starts from key monomers comprised of an enantiopure epoxide (either *R* or *S*) on one end and a silyl-protected alkyne on the other. In one stream, an *R*-configured monomer is subjected to ring-opening of the epoxide under mildly acidic conditions using AcOH and NaN₃. The newly unveiled secondary alcohol is then protected with an acetyl group (OAc; red star) before being coupled to the desilylated alkyne precursor to afford the G1 dimer in 77% yield over 4 steps. **c**, Moving to longer length scales, a 32-unit syndiotactic homopolymer (top) was synthesized after completing 4 more cycles of IEG+ in only about 4 days. The total yield for this process is 19% over 16 steps. After developing a library of hexadecamers (only two shown; lower left), a complex sequenced 32-unit copolymer was synthesized (see inset for MALDI and GPC data of the final polymer) by converging two hexadecamers of disparate tacticity and functionality. **d**, Recently, IEG has been carried out with basic building blocks in a continuous flow reactor in an effort to streamline multiple steps in conjunction with an in-line purification filter prior to CuAAC coupling. Shorter residence times (on the order of minutes instead of hours) and high throughput rates (e.g., 2.75 g/hr for a dimer) allow for the production of a library of hexadecamers (only two shown in graphical form) with precisely controlled sequences. Optimization of the flow system should, in principle, allow for a ‘plug and play’ scenario where any monomer can be incorporated and any sequence of monomers obtained.

Iterative Exponential Growth plus Side-Chain Functionalization (IEG+)

Despite the potential of IEG, it has primarily been used as a method to examine fundamental structure-property relationships of uniform homopolymers. In an effort to improve the scalability of IEG, and to introduce the use of IEG specifically for defining monomer sequences and polymer stereochemistry, the Johnson group developed¹³⁸ a solution-phase IEG strategy (Figure 1.7) that incorporates enantiopure epoxides (obtained from 99.9% pure *R* or *S* epichlorohydrin) and silyl-protected alkynes as the α - and ω -end groups, respectively. Key to our approach is the stereospecific epoxide-opening step (Figure 1.7a, step 1) with azide anion, which generates a new functional handle (secondary alcohol) every cycle. These newly formed secondary alcohols can be functionalized (Figure 1.7a, step 2) with a variety of protecting and functional groups after the ring-opening step, an event which prompted us to name this new modified process ‘Iterative Exponential Growth plus Side-Chain Functionalization’ – or IEG+ for short. In the next step, efficient coupling of the azide intermediate to any combination of stereodefined alkyne monomers affords a 1st generation dimer that is comprised of any of the possible stereoisomer combinations: (*R,R*), (*R,S*), (*S,R*), or (*S,S*). Each reaction step (Figure 1.7b) is very efficient, where the azide-mediated epoxide-opening step, followed by acetyl (Ac) protection using acetic anhydride (Ac₂O), affords an average yield of 89% over two steps, and the

desilylation of the alkyne with tetra-*n*-butylammonium fluoride (TBAF) occurs in less than 5 minutes and routinely gives $\geq 93\%$ yield on multi-gram scales. The final step (Figure 1.7b) involves copper-catalyzed azide-alkyne cycloaddition (CuAAC) of the two intermediates in the presence of 5 mol% CuBr, 10 mol% *N,N,N',N'',N''*-pentamethyldiethylenetriamine (PMDETA), and 10 mol % sodium ascorbate in DMF at 50 °C for 2 h. The yield for the CuAAC coupling step to make the dimer ranges from 86–95% and has been carried out on multi-gram scales, with an overall yield of 77% to make the *S,R*-configured dimer. Elaboration of this dimer through the divergent/convergent IEG+ protocol four times (Figure 1.7c), resulted in a unimolecular syndiotactic polymer (~150 mg, 19% overall yield over 16 steps) of molar mass > 6 kDa, where each side chain alcohol is protected with an Ac group. It is important to point out that although nearly a gram of syndiotactic hexadecamer was prepared using the IEG+ protocol, only a few 100 mgs of it were used as a proof-of-concept to synthesize the 32-unit syndiotactic polymer. It is entirely feasible to make more of this material depending on the length scale desired by the end user. Starting instead with a benzyl protected *R,R*-dimer, this process was repeated to produce an isotactic and perfectly alternating sequence-defined hexadecamer (Figure 7c, red and blue starred graphic). Epoxide-opening of this alternating hexadecamer with azide anion, followed by Ac protection and coupling with a desilylated syndiotactic hexadecamer, resulted in the formation of another unimolecular polymer with complex syndio-iso-tactic and homo-alternating sequence blocks. This level of stereochemical and sequence control in a uniform polymer (Figure 1.7c, inset MALDI and GPC data) would be nearly impossible to reproduce using traditional polymerization techniques and demonstrates the power of the IEG+ methodology. In terms of purification, the products from the first two steps of an IEG+ cycle can be isolated either by running silica plugs or more commonly by way of simple chemical extractions in CH₂Cl₂ or EtOAc against H₂O. The final iterative product obtained after the CuAAC coupling step can be isolated easily using silica flash chromatography. In a matter of only ~3–4 days, a 32-unit polymer can be synthesized with absolute control over mass, monomer sequence, and stereochemistry.

Just like in any system, there are inherent limitations to IEG+. It will not replace solid-phase synthetic methods in general simply because IEG+ is designed for the fast synthesis of polymers that contain alternating sequences, block sequences, or palindromic sequences, with the additional ability to do single point mutations of any orthogonal functional group as a consequence of the epoxide-opening step at the start of each IEG+ cycle. Solid-phase syntheses can provide an

end user with the ability to create any arbitrary sequence they need, and although this can be achieved in a similar number of steps with IEG+, the well-established and automated process of solid-phase syntheses is more suited for fast and random sequence elaboration (e.g., ABCDEFGHI...etc. type sequences) of a particular monomer family. For longer, synthetic polymers with repeat sequences, however, IEG+ could be a superior alternative to solid-phase methods.

To demonstrate true scalability of the IEG+ process, we turn our sights towards continuous flow chemistry as a means to produce these designer polymers on a larger scale than has been demonstrated in batch thus far. As an initial proof-of-concept, non-chiral building blocks were explored¹³⁹ in flow (Figure 1.7d, bottom right), where the deprotections of protecting group A (*PG-A*) and B (*PG-B*) are carried out simultaneously in two separate reaction streams in only a matter of minutes before being passed through an in-line purification membrane that can separate out water and salts from the degassed organic media. Once through the membrane, the azide and alkyne intermediates are brought back together and subjected to CuAAC coupling chemistry for a 3 minute residence period before the product is collected into a flask and purified by silica flash chromatography. The overall yields for this process are nearly similar to those reported for IEG+ chemistry once steady state is achieved, and the automated nature of this process makes it possible to calculate theoretical production rates of 2.75 g/hr, or even 66 g/day, if the system were stocked with enough starting materials and were run non-stop. These rates represent real potential in terms of being able to ‘plug and play’ with different monomers. Looking forward, the ideal scenario of using the IEG+ monomers and chemistry in flow could ultimately lead to large-scale production of designer polymers that may have real-world materials applications.

1.5 Potential Applications of Sequence-Controlled Polymers

Why does sequence definition matter? Bridging nature and technology.

The greatest advantage of perfect polymers lies in the application of their well-defined controllable topology. In past decades, polymer chemistry has gradually shifted focus from making disperse plastics for their bulk properties to understanding the finer effects of chirality, length, and sequence.²⁷ Ziegler and Natta were among the first to start this shift when they found that isotactic or syndiotactic polypropylene had radically different physical properties. More recently, other studies have emerged like that of Ray and coworkers¹⁴⁰ where they found the popularly used thermoresponsive polymer poly(N-isopropylacrylamide) (PNIPAM) exhibits differences in solubility, viscosity, and thermal decomposition with increasing isotacticity. Meyer and coworkers¹⁴¹ have also found that perfectly alternating sequences in poly(lactic-co-glycolic acid) lead to homogenous and sustained degradation of the polymer in comparison to the random sequence alternative. Despite their importance, these advancements do not necessarily require absolute sequence definition. We believe that the greatest potential of perfect polymers lies in bridging the gap between proteins and plastics by rigorously engineering secondary, tertiary, and quaternary structures through primary structure manipulation.

One of the most important early papers that showed the importance of sequence definition was reported by Harada and Kataoka¹⁴² who showed defined length is essential towards core-shell—type supramolecular assemblies. They prepared two types of block copolymers, either cationic poly(ethylene glycol)-*b*-poly(L-lysine) or anionic poly(ethylene glycol)-*b*-poly(α,β -aspartic acid). The sizes of the ionic Lys or Asp blocks were precisely made to be 18 or 78 units long by solid phase peptide synthesis. When an equimolar mixture of the 18 and 78 unit anionic Asp block copolymers was combined with an 18 unit cationic Lys block copolymer, polyion complexes would form exclusively between the 18 unit ionic polymers with no participation from the 78 unit Asp block polymer. Additional mixtures of the ionic block copolymers reach the same conclusion: ionic polymers of opposite charge will only form polyion complexes with one another if each has the same number of charges. This finding has far reaching consequences as the formation of stable polyplexes of cationic polymers with the phosphate backbones of genetic material is necessary to properly transport the desired gene into target cells. Without defined length, it is difficult to obtain the best self-assemblies of ionic polymers.

Early efforts in designing systems that readily assemble into reproducible secondary structures include work done by Moore and coworkers¹¹⁶⁻¹¹⁸ with their oligo(meta-phenylacetylene) foldamers. Though they were unable to make oligomers past the hexadecamer stage due to solubility limitations, they found that even these smaller molecules due to their rigidity and meta-substitutions could assemble into helical structures and hold guest compounds like Ag⁺ ions or the chiral α -pinene. Huc and coworkers¹⁴³ have followed up on the spirit of these studies by synthesizing long, rigid aromatic amide polymers of up to 96 units in length that assemble into helical foldamers. The synthesis of these foldamers requires high concentrations, long reaction times, and lengthy recrystallizations, but it allows for potential of variable side chains that may give these helices some eventual application. A drawback of aromatic based backbones is that there are no examples that have a diversity of topologies the rigidity of the system does allow for much participation of the side chains in the structure.

When dealing with flexible backbones that avoid the rigid structures of aromatic polymers, it is often much more difficult to force the polymers to predominantly adopt a certain conformation. Macrocycles have gained much attention as they so far seem to be an efficient way to impart more order to these structures. Lutz and coworkers⁹⁴ used their effective site-specific incorporation of maleimide along a polystyrene chain prepared by ATRP to install free alkynes along the backbone. Using oxidative Glaser couplings between the free alkyne functional groups or CuAAC couplings between terminal azides and internal free alkynes, they are able to constrain their polystyrenes with macrocycles into “P,” “Q,” “8,” or “ α ” shapes. More recently, Alabi and coworkers¹⁴⁴ have used macrocycles on a more functional backbone. Using their previously developed platform of iterative thiol-ene radical and thiol conjugate addition reactions on a fluorosoluble support, they make sequence-defined oligomers of up to 1 kD. These oligomers are functionalized with alkyl, alcohol, benzaldehyde, azide, and guanidinium groups. In properly functionalized oligomers, removal of the fluorosoluble support with TFA reveals a hydroxylamine functionality and a pendant benzaldehyde along the oligomer. Oxime ligation leads to macrocycles with sizes that can be controlled by the chosen position of the benzaldehyde. When adapted with enhanced functionality such as guanidinium cations, these macrocycles show anti-microbial activity. Though only modest effects were observed, certain macrocyclic oligomers showed significant and superior efficacy when compared to their linear counterparts, depending upon the size of the macrocycle and overall sequence. Thus, constraining topology improved bioactivity.

Despite advancements in functional sequence defined polymers, there is still nothing that can compare to DNA in its recognition properties. The versatility of DNA simply cannot be understated due to its character of precise organization into highly stable double helices after hybridization. Not only has it more than proven its use in nature, but also it is a versatile building block for the construction of complex higher order architectures. Using solid phase synthesis to make carefully chosen DNA sequences such that each chain can hybridize with multiple other, research produce origami structures such as then one shown in Figure 1.6b, where each DNA chain has 4 potential binding regions, and upon addition of other chains, these systems can form trigonal, square, or pentagonal prisms. The top and bottom sides of each of these prisms are free to hybridize with DNA-polymer conjugates, and depending on the composition of these synthetic polymer chains, these DNA prisms can reorganize themselves into various micelle or cage structures that can be purified by gel electrophoresis.

In the spirit of these manipulations, Sleiman and coworkers^{87,145,146} have used similar methods to make DNA nanotubes. The building block of these tubes comes from mixing a cyclic, triangular DNA chain with the proper complementary chains. The size of these structures can be adjusted by varying the number of base pairs in the cyclic chain. Linking these triangular monomers leads to polymerization into a nanotube with well-defined dimensions. During the formation of these nanotubes, specifically sized gold nanotubes can be sieved out solution to fill the open cavities making a “nanopeapod.” By disrupting the edges of these gold nanocages with competing complementary DNA strands, the encapsulated gold nanoparticles can be released. Not only are these new structures potentially useful in nanophotonics, but also may serve as delivery scaffolds into cells.

An impressive example of manipulating primary structure to control higher order structures was reported by Guichard and coworkers.¹⁴⁷ They use the well-studied family of oligoureases, which is known to assemble into helical structures. Their short oligourea helices follow a standard helical pentad repeat similar to polypeptide alpha helices. Their understanding of the positions of the side chains allows them to intelligently design hydrophobic and charged, hydrophilic regions on these secondary structures. The combination of hydrophobic and hydrophilic interactions leads to the assembly into hexameric helical bundles with small hydrophobic cavities with volumes around 495.0 \AA^3 . Different sequences would lead to the formation of quaternary structures that supported water-filled channels of different sizes that could be used for membrane filtration purposes. By

understanding the fundamental structures and binding forces behind their super helix assemblies, they are able to adjust the quaternary structure by rational engineering.

Although there have been many examples of precise sequence leading to controllable and modular higher order structures, the study of non-natural foldamers is still limited by factors like a lack of (1) diverse backbones, (2) systems that allow for variable functionalities, (3) unique and precise topologies, and (4) longer polymers. Synthetic methodology has yet to advance far enough that it is possible to reliably create and study structures reminiscent of proteins and their properties. Despite this, strategies towards making sequence defined polymers have increased and improved a great deal over the past few decades, and polymer chemistry may one day be able to replicate the diverse functions of natural proteins.

1.6 Conclusions and Future Directions

The synthetic strategies that are exploited to make polymers have expanded at an astronomical rate. As more methods and practices are discovered that allow for the mass production of polymers, the more the market for potential applications will continue to grow. The next level of control that polymer scientists seek is the ability to control all facets of polymer structure in terms of monomer sequence, length, and stereochemistry, while combining these features with a process that possesses the quality of being scalable. Most often, methods that have complete control over the polymer structure are ones that are inherently difficult to scale, and the methods that are easily scaled are usually ones that lack complete control over the polymer structure. This inverse relationship between sequence-definition and scalability can only be overcome by discovering and developing new synthetic strategies that may lead to a diverse array of precision polymers. We believe that iterative exponential growth plus side-chain functionalization (IEG+) and flow-IEG show great promise to meet these fundamental requirements. These methods afford control over the entire polymer structure, and show potential to be a scalable multi-gram process. We believe they may eventually lead to the production of designer precision polymers that hopefully will be able to mimic the functions of biopolymers.

1.7 References

1. van Hest, J. C. M. & Tirrell, D. A. Protein-based materials, toward a new level of structural control. *Chem. Commun.* **2001**, 1897-1904.
2. Branden, C. & Tooze, J. Introduction to protein structure (Garland Publisher, Inc., New York, NY, **1999**).
3. Kuchta, R. D.; Benkovic, P.; Benkovic, S. J. Kinetic mechanism whereby DNA polymerase I (Klenow) replicates DNA with high fidelity. *Biochemistry* **1988**, *27*, 6716-6725.
4. Yonath, A. The search and its outcome: high-resolution structures of ribosomal particles from mesophilic, thermophilic, and halophilic bacteria at various functional states. *Annu. Rev. Biophys. Biomol. Struct.* **2002**, *31*, 257-273.
5. Staudinger, H. Über polymerisation. *Ber. Dtsch. Chem. Ges.* **1920**, *53*, 1073-1085.
6. Hermes, M. E. Enough for one lifetime. Wallace Carothers, inventor of nylon (Chemical Heritage Foundation, **1996**).
7. Szwarc, M. & Milkovich, L. R. Polymerization initiated by electron transfer to monomer. A new method of formation of block polymers. *J. Am. Chem. Soc.* **1956**, *78*, 2656-2657.
8. Szwarc, M. 'Living' polymers. *Nature* **1956**, *178*, 1168-1169.
9. Merrifield, R. B. Solid phase peptide synthesis. 1. Synthesis of a tetrapeptide. *J. Am. Chem. Soc.* **1963**, *85*, 2149-2154.
10. Merrifield, R. B. Solid-phase synthesis (Nobel Lecture). *Angew. Chem., Int. Ed.* **1985**, *24*, 799-810.
11. Hérisson, J. L. & Chauvin, Y. Catalyse de transformation des oléfines par les complexes du tungstène. *Makromol. Chem.* **1970**, *141*, 161-176.
12. Grubbs, R. H.; Burke, P. L. & Carr, D. D. Mechanism of the olefin metathesis reaction. *J. Am. Chem. Soc.* **1975**, *97*, 3265-3267.
13. Grubbs, R. H. Olefin-metathesis catalysts for the preparation of molecules and materials (Nobel Lecture). *Angew. Chem., Int. Ed. Engl.* **2006**, *45*, 3760-3765.
14. McLain, S. J.; Wood, C. D.; Schrock, R. R. Preparation and characterization of tantalum(III) olefin complexes and tantalum(V) metallacyclopentane complexes made from acyclic α olefins. *J. Am. Chem. Soc.* **1979**, *101*, 4558-4570.
15. Schrock, R. R. Multiple metal-carbon bonds for catalytic metathesis reactions (Nobel Lecture). *Angew. Chem., Int. Ed. Engl.* **2006**, *45*, 3748-59.
16. Higashimura, T. & Kishiro, O. Possible formation of living polymers of p-methoxystyrene by iodine. *Polym. J.* **1977**, *9*, 87-93.
17. Higashimura, T.; Mitsunashi, M.; Sawamoto, M. Synthesis of p-methoxystyrene-isobutyl vinyl ether block copolymers by living cationic polymerization with iodine. *Macromolecules* **1979**, *12*, 178-182.
18. Lutz, J.-F.; Lehn, J.-M.; Meijer, E. W.; Matyjaszewski, K. From precision polymers to complex materials and systems. *Nature Reviews Materials* **2016**, *1*, 16024.
19. Peplow, M. Fantastic plastics. *Nature* **2016**, *536*, 266-268.
20. Hibi, Y.; Ouchi, M.; Sawamoto, M. A strategy for sequence control in vinyl polymers via iterative controlled radical cyclization. *Nat. Commun.* **2016**, *7*, 11064.
21. Lutz, J.-F.; Ouchi, M.; Liu, D. R.; Sawamoto, M. Sequence-controlled polymers. *Science* **2013**, *341*, 1238149.
22. Ziegler, K. Folgen und werdegang einer erfindung Nobel-vortrag. *Angew. Chem.* **1964**, *76*, 545-553.

23. Ziegler, K.; Krupp, F.; Zosel, K. Eine einfache synthese primärer alkohole aus olefinen. *Angew. Chem.* **1955**, *67*, 425-426.
24. Bawn, C. E. H. Giulio Natta. *Nature* **1979**, *280*, 707.
25. Natta, G. Von der stereospezifischen polymerisation zur asymmetrischen autokatalytischen synthese von makromolekülen Nobel-vortrag. *Angew. Chem.* **1964**, *76*, 553-566.
26. Böhm, L. L. The ethylene polymerization with Ziegler catalysts: fifty years after the discovery. *Angew. Chem. Int. Ed.* **2003**, *42*, 5010-5030.
27. Teator, A. J.; Leibfarth, F. A. Catalyst-controlled stereoselective cationic polymerization of vinyl ethers. *Science* **2019**, *363*, 1439-1443.
28. Li, J.; Stayshich, R. M.; Meyer, T. Y. Exploiting sequence to control the hydrolysis behavior of biodegradable PLGA copolymers. *J. Am. Chem. Soc.* **2011**, *133*, 6910-6913.
29. Rosales, A. M.; Segalman, R. A.; Zuckermann, R. N. Polypeptoids: a model system to study the effect of monomer sequence on polymer properties and self-assembly. *Soft Matter* **2013**, *9*, 11713-11713.
30. Baskaran, D.; Muller, A. H. E. Anionic vinyl polymerization - 50 years after Michael Szwarc. *Prog. Polym. Sci.* **2007**, *32*, 173-219.
31. Leitgeb, A.; Wappel, J.; Slugovc, C. The ROMP toolbox upgraded. *Polymer* **2010**, *51*, 2927-2946.
32. Matyjaszewski, K.; Spanswick, J. Controlled/living radical polymerization. *Mater. Today* **2005**, *8*, 26-33.
33. Matyjaszewski, K.; Gaynor, S.; Wang, J. S. Controlled radical polymerizations: use of alky iodides in degenerative transfer. *Macromolecules* **2005**, *28*, 2093-2095.
34. Chiefari, J. et al. Living free-radical polymerization by reversible addition-fragmentation chain transfer: the RAFT process. *Macromolecules* **1998**, *31*, 5559-5562.
35. Moad, G.; Rizzardo, E. Alkoxyamine-initiated living radical polymerization: factors affecting alkoxyamine homolysis rates. *Macromolecules* **1995**, *28*, 8722-8728.
36. Gutte, B.; Merrifield, R. B. The synthesis of ribonuclease A. *J. Biol. Chem.* **1971**, *246*, 1922-1941.
37. Miyoshi, K., Arentzen, R., Huang, T. & Itakura, K. Solid-phase synthesis of polynucleotides. IV. Usage of polystyrene resins for the synthesis of polydeoxyribonucleotides by the phosphotriester method. *Nucleic Acids Res.* **1980**, *8*, 5507-5517.
38. Seeberger, P. H.; Haase, W.-C. Solid-phase oligosaccharide synthesis and combinatorial carbohydrate libraries. *Chem. Rev.* **2000**, *100*, 4349-4393.
39. Roy, R.K. et al. Design and synthesis of digitally encoded polymers that can be decoded and erased. *Nature Commun.* **2015**, *6*, 7237.
40. McGrath, K. P.; Fournier, M. J.; Mason, T. L.; Tirrell, D. A. Genetically directed syntheses of new polymeric materials. Expression of artificial genes encoding proteins with repeating - (AlaGly)₃ProGluGly- elements. *J. Am. Chem. Soc.* **1992**, *114*, 727-733.
41. Krejchi, M.T. et al. Chemical Sequence Control of Beta-Sheet Assembly in Macromolecular Crystals of Periodic Polypeptides. *Science* **1994**, *265*, 1427-1432.
42. Johnson, J. A.; Lu, Y. Y.; Van Deventer, J. A.; Tirrell, D. A. Residue-specific incorporation of non-canonical amino acids into proteins: recent developments and applications. *Current Opinion in Chemical Biology* **2010**, *14*, 774-780.
43. Zuckermann, R. N.; Kerr, J. M.; Kent, S. B. H.; Moos, W. H. Efficient method for the preparation of peptoids [oligo(N-substituted glycines)] by submonomer solid-phase synthesis. *J. Am. Chem. Soc.* **1992**, *114*, 10646-10647.

44. Simon, R. J. et al. Peptoids: a modular approach to drug discovery. *Proc. Natl. Acad. Sci.* **1992**, *89*, 9367-9371.
45. Kirshenbaum, K. et al. Sequence-specific polypeptoids: a diverse family of heteropolymers with stable secondary structure. *Proc. Natl. Acad. Sci.* **1998**, *95*, 4303-4308.
46. Zuckermann, R. N.; & Kodadek, T. Peptoids as potential therapeutics. *Curr. Opin. Mol. Ther.* **2009**, *11*, 299-307.
47. Beaucage, S. L.; Caruthers, M. H. Deoxynucleoside phosphoramidites - a new class of key intermediates for deoxypolynucleotide synthesis. *Tetrahedron Lett.* **1981**, *22*, 1859-1862.
48. Beaucage, S. L.; Iyer, R. P. Advances in the synthesis of oligonucleotides by the phosphoramidite approach. *Tetrahedron* **1992**, *48*, 2223-2311.
49. Fréchet, J.; Schuerch, C. Solid-phase synthesis of oligosaccharides. I. Preparation of the solid support. Poly[p-(1-propen-3-ol-1-yl)styrene]. *J. Am. Chem. Soc.* **1971**, *93*, 492-496.
50. Hamblin, G. D.; Rahbani, J. F.; Sleiman, H. F. Sequential growth of long DNA strands with user-defined patterns for nanostructures and scaffolds. *Nature Commun.* **2015**, *6*, 7065.
51. Edwardson, T. G. W.; Carneiro, K. M. M.; Serpell, C. J.; Sleiman, H.F. An efficient and modular route to sequence- defined polymers appended to DNA. *Angew. Chem., Int. Ed.* **2014**, *53*, 4567-4571.
52. Al Ouahabi, A.; Charles, L.; Lutz, J. F. Synthesis of non-natural sequence-encoded polymers using phosphoramidite chemistry. *J. Am. Chem. Soc.* **2015**, *137*, 5629-5635.
53. Lebedev, A. V.; Combs, D.; Hogrefe, R. I. Preactivated carboxyl linker for the rapid conjugation of alkylamines to oligonucleotides on solid support. *Bioconjugate Chem.* **2007**, *18*, 1530-1536.
54. Carthew, R. W.; Sontheimer, E. J. Origins and mechanisms of miRNAs and siRNAs. *Cell* **2009**, *136*, 642-655.
55. Seeman, N. C. Nanomaterials based on DNA. *Annu. Rev. Biochem.* **2010**, *79*, 65-87.
56. Jones, M. R.; Seeman, N. C.; Mirkin, C. A. Nanomaterials. Programmable materials and the nature of the DNA bond. *Science* **2015**, *347*, 1260901.
57. Macfarlane, R. J. et al. Nanoparticle superlattice engineering with DNA. *Science* **2011**, *334*, 204-208.
58. Sun, J.; Teran, A. A.; Liao, X.; Balsara, N. P.; Zuckermann, R. N. Crystallization in sequence-defined peptoid diblock copolymers induced by microphase separation. *J. Am. Chem. Soc.* **2014**, *136*, 2070-2077.
59. Chan-Seng, D.; Lutz, J.-F. Solid-phase synthesis as a tool for the preparation of sequence-defined oligomers based on natural amino acids and synthetic building blocks. *ACS Symposium Series* **2014**, *1170*, 103-116.
60. Bayer, E.; Mutter, M. Liquid-phase synthesis of peptides. *Nature* **1972**, *237*, 512-513.
61. Wentworth, P.; Janda, K. D. Liquid-phase chemistry: recent advances in soluble polymer-supported catalysts, reagents and synthesis. *Chem. Commun.* **1999**, 1917-1924.
62. Gravert, D. J.; Janda, K. D. Organic synthesis on soluble polymer supports: Liquid-phase methodologies. *Chem. Rev.* **1997**, *97*, 489-509.
63. Kent, S. B. Total chemical synthesis of proteins. *Chem. Soc. Rev.* **2009**, *38*, 338-351.
64. Wang, P. et al. Erythropoietin derived by chemical synthesis. *Science* **2013**, *342*, 1357-1360.
65. Bonet, A.; Odachowski, M.; Leonori, D.; Essafi, S.; Aggarwal, V. K. Enantiospecific sp(2)-sp(3) coupling of secondary and tertiary boronic esters. *Nature Chem.* **2014**, *6*, 584-589.
66. Burns, M. et al. Assembly-line synthesis of organic molecules with tailored shapes. *Nature* **2014**, *513*, 183-188.

67. Vergnaud, J.; Faugeras, P. A.; Chaleix, V.; Champavier, Y.; Zerrouki, R. Design of a new oligotriazole peptide nucleic acid analogue (oT-PNA). *Tetrahedron Lett.* **2011**, *52*, 6185-6189.
68. Derda, R.; Wherritt, D. J.; Kiessling, L. L. Solid-phase synthesis of alkanethiols for the preparation of self-assembled monolayers. *Langmuir* **2007**, *23*, 11164-11167.
69. Hartmann, L. Polymers for control freaks: sequence-defined poly(amidoamine)s and their biomedical applications. *Macromol. Chem. Phys.* **2011**, *212*, 8-13.
70. Espeel, P. et al. Multifunctionalized sequence-defined oligomers from a single building block. *Angew. Chem. Int. Ed* **2013**, *52*, 13261-13264.
71. Stutz, C.; Meszynska, A.; Lutz, J.-F.; Boerner, H. G. Convenient routes to efficiently N-PEGylated peptides. *ACS Macro Lett.* **2013**, *2*, 641-644.
72. Amrane, M. I.; Chouikhi, D.; Badi, N.; Lutz, J.-F. Synthesis of well-defined polystyrene rink amide soluble supports and their use in peptide synthesis. *Macromol. Chem. Phys.* **2014**, *215*, 1984-1990.
73. Bruckner, K.; Zitterbart, R.; Seitz, O.; Beck, S.; Linscheid, M. W. Solid phase synthesis of short peptide-based multimetal tags for biomolecule labeling. *Bioconjugate Chem.* **2014**, *25*, 1069-1077.
74. Chan-Seng, D.; Lutz, J.-F. Primary structure control of oligomers based on natural and synthetic building blocks. *ACS Macro Lett.* **2014**, *3*, 291-294.
75. Gillis, E. P.; Burke, M. D. Multistep synthesis of complex boronic acids from simple MIDA boronates. *J. Am. Chem. Soc.* **2008**, *130*, 14084-14085.
76. Woerly, E. M.; Roy, J.; Burke, M. D. Synthesis of most polyene natural product motifs using just 12 building blocks and one coupling reaction. *Nature Chem.* **2014**, *6*, 484-491.
77. Service, R.F. The synthesis machine. *Science* **2015**, *347*, 1190-1193.
78. Dömling, A.; Ugi, I. Multicomponent Reactions with Isocyanides. *Angew. Chem. Int. Ed.* **2000**, *39*, 3168-3210.
79. Banfi, L.; Riva, R. The Passerini reaction. *Org. React.* **2005**, *65*, 1-140.
80. Kreye, O.; Toth, T.; Meier, M. A. Introducing multicomponent reactions to polymer science: Passerini reactions of renewable monomers. *J. Am. Chem. Soc.* **2011**, *133*, 1790-1792.
81. Sehlinger, A.; Kreye, O.; Meier, M. A. R. Tunable Polymers Obtained from Passerini Multicomponent Reaction Derived Acrylate Monomers. *Macromolecules* **2013**, *46*, 6031-6037.
82. Solleder, S. C.; Meier, M. A. R. Sequence control in polymer chemistry through the Passerini three-component reaction. *Angew. Chem. Int. Ed.* **2014**, *53*, 711-714.
83. Arnheim, N.; Erlich, H. Polymerase chain reaction strategy. *Annu. Rev. Biochem.* **1992**, *61*, 131-156.
84. Rosenbaum, D. M.; Liu, D. R. Efficient and sequence-specific DNA-templated polymerization of peptide nucleic acid aldehydes. *J. Am. Chem. Soc.* **2003**, *125*, 13924-13925.
85. Niu, J.; Hili, R.; Liu, D. R. Enzyme-free translation of DNA into sequence-defined synthetic polymers structurally unrelated to nucleic acids. *Nature Chem.* **2013**, *5*, 282-292.
86. McKee, M. L. et al. Multistep DNA-templated reactions for the synthesis of functional sequence controlled oligomers. *Angew. Chem. Int. Ed.* **2010**, *49*, 7948-7951.
87. Serpell, C. J.; Edwardson, T. G. W.; Chidchob, P.; Carneiro, K. M. M.; Sleiman, H. F. Precision polymers and 3D DNA nanostructures: emergent assemblies from new parameter space. *J. Am. Chem. Soc.* **2014**, *136*, 15767-15774.

88. Hariri, A. A.; Hamblin, G.D.; Gidi, Y.; Sleiman, H. F.; Cosa, G. Stepwise growth of surface-grafted DNA nanotubes visualized at the single-molecule level. *Nature Chem.* **2015**, *7*, 295-300.
89. Ida, S.; Ouchi, M.; Sawamoto, M. Designer template initiator for sequence regulated polymerization: systems design for substrate-selective metal-catalyzed radical addition and living radical polymerization. *Macromol. Rapid Commun.* **2011**, *32*, 209-214.
90. Hibi, Y.; Ouchi, M.; Sawamoto, M. Sequence-regulated radical polymerization with a metal-templated monomer: repetitive ABA sequence by double cyclopolymerization. *Angew. Chem. Int. Ed.* **2011**, *50*, 7434-7437.
91. Lewandowski, B. et al. Sequence-specific peptide synthesis by an artificial small-molecule machine. *Science* **2013**, *339*, 189-193.
92. Alfrey, T.; Lavin, E. The copolymerization of styrene and maleic anhydride. *J. Am. Chem. Soc.* **1945**, *67*, 2044-2045.
93. Pfeifer, S.; Lutz, J.-F. A facile procedure for controlling monomer sequence distribution in radical chain polymerizations. *J. Am. Chem. Soc.* **2007**, *129*, 9542-9543.
94. Pfeifer, S.; Lutz, J.-F. Development of a library of N-substituted maleimides for the local functionalization of linear polymer chains. *Chem. Eur. J.* **2008**, *14*, 10949-10957.
95. Schmidt, B. V. K. J.; Fechler, N.; Falkenhagen, J.; Lutz, J.-F. Controlled folding of synthetic polymer chains through the formation of positionable covalent bridges. *Nature Chem.* **2011**, *3*, 234-238.
96. Zamfir, M.; Lutz, J.-F. Ultra-precise insertion of functional monomers in chain-growth polymerizations. *Nature Commun.* **2012**, *3*, 2151/1-2151/8.
97. Kramer, J. W. et al. Polymerization of enantiopure monomers using syndiospecific catalysts: a new approach to sequence control in polymer synthesis. *J. Am. Chem. Soc.* **2009**, *131*, 16042-16044.
98. Lienkamp, K. et al. Antimicrobial polymers prepared by ROMP with unprecedented selectivity: A molecular construction kit approach. *J. Am. Chem. Soc.* **2008**, *130*, 9836-9843.
99. Johnson, J. A. et al. Drug-loaded, bivalent-bottle-brush polymers by graft-through ROMP. *Macromolecules* **2010**, *43*, 10326-10335.
100. Burts, A. O. et al. Using EPR to compare PEG-branch-nitroxide "bivalent-brush polymers" and traditional PEG bottle-brush polymers: branching makes a difference. *Macromolecules* **2012**, *45*, 8310-8318.
101. Zhang, J.; Matta, M. E.; Hillmyer, M. A. Synthesis of sequence-specific vinyl copolymers by regioselective ROMP of multiply substituted cyclooctenes. *ACS Macro Lett.* **2012**, *1*, 1383-1387.
102. Gutekunst, W. R.; Hawker, C. J. A general approach to sequence-controlled polymers using macrocyclic ring opening metathesis polymerization. *J. Am. Chem. Soc.* **2015**, *137*, 8038-8041.
103. Xue, X. Q.; Zhu, J.; Zhang, W.; Zhang, Z. B.; Zhu, X. L. Preparation and characterization of novel main-chain azobenzene polymers via step-growth polymerization based on click chemistry. *Polymer* **2009**, *50*, 4512-4519.
104. Satoh, K.; Ozawa, S.; Mizutani, M.; Nagai, K.; Kamigaito, M. Sequence-regulated vinyl copolymers by metal-catalysed step-growth radical polymerization. *Nature Commun.* **2010**, *1*, 6.

105. Paynter, O. I.; Simmonds, D. J.; Whiting, M. C. The synthesis of long-chain unbranched aliphatic-compounds by molecular doubling. *J. Chem. Soc., Chem. Commun.* **1982**, 1165-1166.
106. Bidd, I. et al. Studies on the synthesis of linear aliphatic compounds. Part 1. Convenient syntheses of bifunctional C₁₂-acyclic compounds from cyclododecanone. *J. Chem. Soc., Perkin Trans. 1* **1983**, 1369-72.
107. Bidd, I.; Whiting, M. C. The synthesis of pure normal-paraffins with chain-lengths between one and 400. *J. Chem. Soc., Chem. Commun.* **1985**, 543-544.
108. Adegoke, E. A.; Ephraim-Bassey, H.; Kelly, D. J.; Whiting, M. C. Studies on the synthesis of linear aliphatic compounds. Part 4. An approach to long-chain paraffins with lateral side-chains. *J. Chem. Soc., Perkin Trans. 1* **1987**, 2465-2467.
109. Bidd, I.; Holdup, D. W.; Whiting, M. C. Studies on the synthesis of linear aliphatic-compounds. 3. The synthesis of paraffins with very long chains. *J. Chem. Soc., Perkin Trans. 1* **1987**, 2455-2463.
110. Igner, E.; Paynter, O. I.; Simmonds, D. J.; Whiting, M. C. Studies on the synthesis of linear aliphatic-compounds. 2. The realization of a strategy for repeated molecular doubling. *J. Chem. Soc., Perkin Trans. 1* **1987**, 2447-2454.
111. Brooke, G. M.; Burnett, S.; Mohammed, S.; Proctor, D.; Whiting, M. C. Versatile process for the syntheses of very long chain alkanes, functionalised derivatives and some branched chain hydrocarbons. *J. Chem. Soc., Perkin Trans. 1* **1996**, 1635-1645.
112. Brooke, G. M.; Mohammed, S.; Whiting, M. C. Synthesis of oligomers related to nylon 6. *J. Chem. Soc., Perkin Trans. 1* **1997**, 3371-3379.
113. Brooke, G.M., Mohammed, S. & Whiting, M.C. The synthesis of oligomers related to nylon 4 6 and nylon 6 6. *Polymer* **1999**, 40, 773-788.
114. Moore, J. S. Zhang, J. S. Efficient synthesis of nanoscale macrocyclic hydrocarbons. *Angew. Chem. Int. Ed.* **1992**, 31, 922-924.
115. Zhang, J. S.; Moore, J. S.; Xu, Z. F.; Aguirre, R. A. Nanoarchitectures. 1. Controlled synthesis of phenylacetylene sequences. *J. Am. Chem. Soc.* **1992**, 114, 2273-2274.
116. Zhang, J.S., Pesak, D.J., Ludwick, J.L. & Moore, J.S. Nanoarchitectures. 5. Geometrically-controlled and site-specifically-functionalized phenylacetylene macrocycles. *J. Am. Chem. Soc.* **1994**, 116, 4227-4239.
117. Nelson, J.C.; Saven, J. G.; Moore, J. S.; Wolynes, P. G. Solvophobic driven folding of nonbiological oligomers. *Science* **1997**, 277, 1793-1796.
118. Prince, R. B.; Okada, T.; Moore, J. S. Controlling the secondary structure of nonbiological oligomers with solvophobic and coordination interactions. *Angew. Chem. Int. Ed.* **1999**, 38, 233-236.
119. Prince, R. B.; Barnes, S. A.; Moore, J. S. Foldamer-based molecular recognition. *J. Am. Chem. Soc.* **2000**, 122, 2758-2762.
120. Pearson, D.L.; Schumm, J. S.; Tour, J. M. Iterative divergent/convergent approach to conjugated oligomers by a doubling of molecular length at each iteration. A rapid route to potential molecular wires. *Macromolecules* **1994**, 27, 2348-2350.
121. Schumm, J. S.; Pearson, D.L.; Tour, J. M. Iterative divergent/convergent approach to linear conjugated oligomers by successive doubling of the molecular length: A rapid route to a 128-angstrom-long potential molecular wire. *Angew. Chem., Int. Ed. Engl.* **1994**, 33, 1360-1363.

122. Tour, J. M. Conjugated macromolecules of precise length and constitution. Organic synthesis for the construction of nanoarchitectures. *Chem. Rev.* **1996**, *96*, 537-553.
123. Jones, L.; Schumm, J. S.; Tour, J. M. Rapid solution and solid phase syntheses of oligo(1,4-phenylene ethynylene)s with thioester termini: Molecular scale wires with alligator clips. Derivation of iterative reaction efficiencies on a polymer support. *J. Org. Chem.* **1997**, *62*, 1388-1410.
124. Pearson, D. L.; Tour, J. M. Rapid syntheses of oligo(2,5-thiophene ethynylene)s with thioester termini: Potential molecular scale wires with alligator clips. *J. Org. Chem.* **1997**, *62*, 1376-1387.
125. Huang, S. L.; Tour, J. M. Rapid solid-phase synthesis of oligo(1,4-phenylene ethynylene)s by a divergent convergent tripling strategy. *J. Am. Chem. Soc.* **1999**, *121*, 4908-4909.
126. Tour, J.M. Molecular electronics. Synthesis and testing of components. *Acc. Chem. Res.* **2000**, *33*, 791-804.
127. Lengweiler, U. D.; Fritz, M. G.; Seebach, D. Synthesis of monodisperse linear and cyclic oligo[(R)-3-hydroxybutanoates] containing up to 128 monomeric units. *Helv. Chim. Acta* **1996**, *79*, 670-701.
128. Seebach, D., Herrmann, G.F., Lengweiler, U.D. & Amrein, W. Synthesis of monodisperse macromolecular bicyclic and dendritic compounds from (R)-3-hydroxybutanoic acid and benzene-1,3,5-tricarboxylic acid and analysis by fragmenting MALDI-TOF mass spectroscopy. *Helv. Chim. Acta* **1997**, *80*, 989-1026.
129. Murer, P.; Seebach, D. Synthesis and properties of monodisperse chiral dendrimers (up to fourth generation) with doubly branched building blocks: An intriguing solvent effect. *Helv. Chim. Acta* **1998**, *81*, 603-631.
130. Seebach, D.; Fritz, M. G. Detection, synthesis, structure, and function of oligo(3-hydroxyalkanoates): contributions by synthetic organic chemists. *Int. J. Biol. Macromol.* **1999**, *25*, 217-236.
131. Wooley, K. L.; Hawker, C. J.; Frechet, J. M. J. A branched-monomer approach for the rapid synthesis of dendrimers. *Angew. Chem., Int. Ed. Engl.* **1994**, *33*, 82-85.
132. Hawker, C. J.; Malmstrom, E. E.; Frank, C. W.; Kampf, J. P. Exact linear analogs of dendritic polyether macromolecules: Design, synthesis, and unique properties. *J. Am. Chem. Soc.* **1997**, *119*, 9903-9904.
133. Miller, T. M.; Neenan, T. X. Convergent synthesis of monodisperse dendrimers based upon 1,3,5-trisubstituted benzenes. *Chem. Mater.* **1990**, *2*, 346-349.
134. Takizawa, K.; Nulwala, H.; Hu, J.; Yoshinaga, K.; Hawker, C. J. Molecularly defined (L)-lactic acid oligomers and polymers: Synthesis and characterization. *J. Polym. Sci., Part A: Polym. Chem.* **2008**, *46*, 5977-5990.
135. Takizawa, K.; Tang, C.; Hawker, C. J. Molecularly defined caprolactone oligomers and polymers: synthesis and characterization. *J. Am. Chem. Soc.* **2008**, *130*, 1718-1726.
136. Binauld, S.; Hawker, C. J.; Fleury, E.; Drockenmuller, E. A modular approach to functionalized and expanded crown ether based macrocycles using click chemistry. *Angew. Chem. Int. Ed.* **2009**, *48*, 6654-6658.
137. Binauld, S.; Damiron, D.; Connal, L. A.; Hawker, C. J.; Drockenmuller, E. Precise synthesis of molecularly defined oligomers and polymers by orthogonal iterative divergent/convergent approaches. *Macromol. Rapid Commun.* **2011**, *32*, 147-168.
138. Barnes, J. C. et al. Iterative exponential growth of sequence-controlled polymers. *Nature Chem.* **2015**, *7*, 810-815.

139. Leibfarth, F. A.; Johnson, J. A.; & Jamison, T. F. Flow-IEG: scalable synthesis of sequence and architecturally defined, unimolecular macromolecules. *Proc. Natl. Acad. Sci.* **2015**, *112*, 10617-10622.
140. Biswas, C. S. *et al.* Study of the effect of isotacticity on some physical properties of poly(N-isopropylacrylamide). *Colloid Polym. Sci.* **2015**, *293*, 1749-1757.
141. Li, J.; Rothstein, S. N.; Little, S. R.; Edenborn, H. M.; Meyer, T. Y. The effect of monomer order on the hydrolysis of biodegradable poly(lactic-co-glycolic acid) repeating sequence copolymers. *J. Am. Chem. Soc.* **2012**, *134*, 16352-16359.
142. Harada, A.; Kataoka, K. Chain length recognition: core-shell supramolecular assembly from oppositely charged block copolymers. *Science* **1999**, *283*, 65-67.
143. Li, X.; Markandeya, N.; Jonusauskas, G.; McClenaghan,; Maurizot, V.; Denisov, S. A.; Huc, I. Photoinduced electron transfer and hole migration in nanosized helical aromatic oligoamide foldamers. *J. Am. Chem. Soc.* **2016**, *138*, 13568-13578.
144. Porel, M.; Thornlow, D. N.; Phan, N. N.; Alabi, C. A. Sequence-defined bioactive macrocycles via an acid-catalyzed cascade reaction. *Nature Chem.* **2016**, *8*, 590-596.
145. Chidchob, P.; Edwardson, T. G. W.; Serpell, C. J.; Sleiman, H. F. Synergy of two assembly languages in DNA nanostructures: self-assembly of sequence-defined polymers on DNA cages. *J. Am. Chem. Soc.* **2016**, *138*, 4416-4425.
146. Lo, P. K.; Karam, P.; Aldaya, F. A.; McLaughlin, C. K.; Hamblin, G. D.; Cosa, G.; Sleiman, H. F. Loading and selective release of cargo in DNA nanotubes with longitudinal variation. *Nature Chem.* **2010**, *2*, 319-328.
147. Collie, G. W.; Pulka-Ziach, K.; Lombardo, C. M.; Fremaux, J.; Rosu, F.; Decossas, M.; Mauran, L.; Lambert, O.; Gabelica, V.; Mackereth, C. D.; Guichard, G. Shaping quaternary assemblies of water-soluble non-peptide helical foldamers by sequence manipulation. *Nature Chem.* **2015**, *7*, 871-878.

Chapter 2.
Iterative Exponential Growth Synthesis and
Assembly of Uniform Diblock Copolymers

This chapter is composed of material adapted from the following publication:

Jiang, Y.; Golder, M. R.; Nguyen, H. V. T.; Wang, Y.; Zhong, M.; Barnes, J. C.; Ehrlich, D. J. C.; Johnson, J. A. Iterative exponential growth synthesis and assembly of uniform diblock copolymers. *J. Am. Chem. Soc.* **2016**, *138*, 9369-9372.

The work in this chapter was a collaborative effort with Matthew R. Golder, Hung V. T. Nguyen, Yufeng Wang, Mingjiang Zhong, Jonathan C. Barnes, and Deborah J. C. Ehrlich. Matthew R. Golder, Jonathan C. Barnes, and Deborah J. C. Ehrlich assisted with the synthesis design and analysis of the data. Hung V. T. Nguyen performed all Transmission Electron Microscopy (TEM) imaging. Yufeng Wang guided Atomic Force Microscopy (AFM) imaging and sample preparation. Mingjiang Zhong assisted with the analysis of the Small Angle X Ray Scattering (SAXS), TEM, and AFM data. The author performed and led the design of the synthetic routes, characterized all materials, and wrote the chapter.

2.1 Introduction

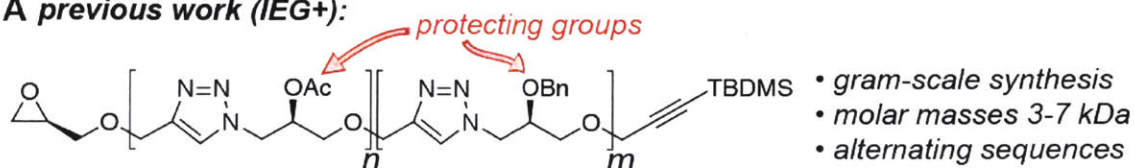
New synthetic approaches that facilitate access to precisely defined and diversely functionalized uniform macromolecules in useful quantities will enable the elucidation of structure-property relationships that will guide the design of next-generation polymeric materials.¹⁻⁷ Living statistical polymerization methods can yield polymers with precise nanoscale structures on kilogram scales, but these methods lack absolute mass-, sequence-, and stereo-control.^{8,9} Increased control has been achieved by using monomers with pre-loaded functionality,¹⁰⁻¹⁴ by taking advantage of inherent differences in the rates of propagation between monomers,¹⁵⁻¹⁷ or by templating monomer addition.^{18,19} On the opposite end of the spectrum, solid-phase syntheses provide an extremely valuable tool for the synthesis of macromolecules with absolute structural control.²⁰⁻²² However, these methods require large excesses of reagents in each step, and they are not yet amenable for the synthesis of polymers in a readily scalable way.

Iterative Exponential Growth (IEG) is an alternative synthetic strategy wherein doubly protected molecules of length l undergo cycles of orthogonal activations and couplings to yield macromolecules with length $l \cdot 2^n$ cycles.²³ Though IEG is limited to repetitive or palindromic sequences, it can provide unimolecular, fully sequence and stereo-controlled polymers in fewer reactions than solid-phase synthesis, and without the need for large excesses of reagents.²⁴⁻³⁸

Recently, our group reported³⁹ an Iterative Exponential Growth Plus Sidechain Functionalization (IEG+) strategy that allowed for the synthesis of chiral, uniform oligomers and polymers with variable sequences acetyl (Ac) and benzyl (Bn) protected alcohols (Figure 2.1A).

The key to IEG+ was the selection of extremely efficient reactions: nucleophilic opening of epoxides with azide, fluoride-mediated desilylation of alkynes, and copper-catalyzed azide-alkyne cycloaddition (CuAAC), that provided macromolecules in excellent yields and with high atom economy. Nonetheless, our previous IEG+ system only included simple sidechain protecting groups; the design of macromolecules with more advanced function requires a next-generation IEG+ strategy.

A previous work (IEG+):



B this work:

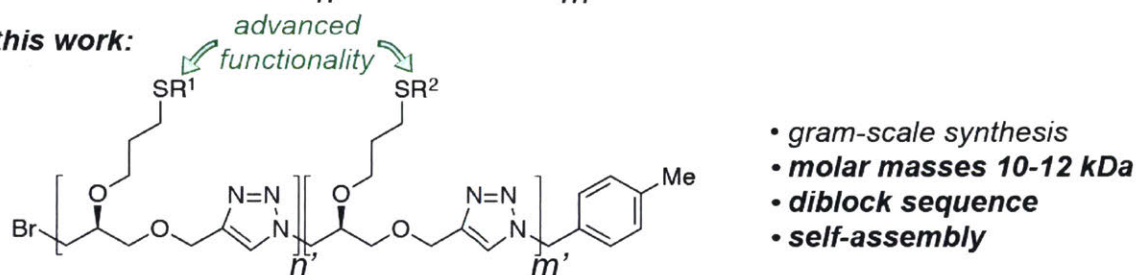


Figure 2.1. (A) Our previous IEG+ system, though efficient and high yielding, was limited to simple protecting group functionality. (B) By utilizing thiol-ene click chemistry, we can now incorporate a larger library of advanced functional groups to our IEG+ system.

Herein we report a new IEG+ strategy – allyl-IEG – that yields uniform, sequence-defined macromolecules with sidechain alkene functionalities capable of efficient post-polymerization functionalization reactions. We make use of efficient thiol-ene addition reactions to synthesize uniform BCPs (32mers) with molar masses from 9-12.1 kDa on a ~1 g scale. These BCPs undergo bulk microphase separation to form hexagonally packed cylinders with domain sizes that directly correlate with their molecular structures. Our approach offers a simple platform for studying how molecular-level details impact a broad range of polymer properties.

2.2 Results and Discussion

Figure 2.2A depicts the allyl-IEG process. First, (R)-glycidyl propargyl ether ((R)-GPE) was converted to azide **1-N₃** via triisopropylsilyl (TIPS) protection of the alkyne (i), nucleophilic opening of the epoxide with NaN₃ (ii), and allylation of the newly formed alcohol with allyl bromide (iii). Separately, alkyne **1-alkyne** was prepared from (R)-GPE by regioselective epoxide opening with tert-butyl alcohol in the presence of Mg(ClO₄)₂ (iv), followed by allylation with allyl bromide (v), acidic cleavage of the tert-butyl ether with 85% phosphoric acid (vi), tosylation of the resulting alcohol (vii), and nucleophilic substitution with LiBr (viii). Finally, **1a** and **1b** were coupled via CuAAC in the presence of 5 mol % CuBr and 10 mol % N,N,N',N'',N'''-pentamethyldiethylenetriamine (PMDETA) in DMF for 2 h to yield dimer **2** in 89% isolated yield (37.9 g).

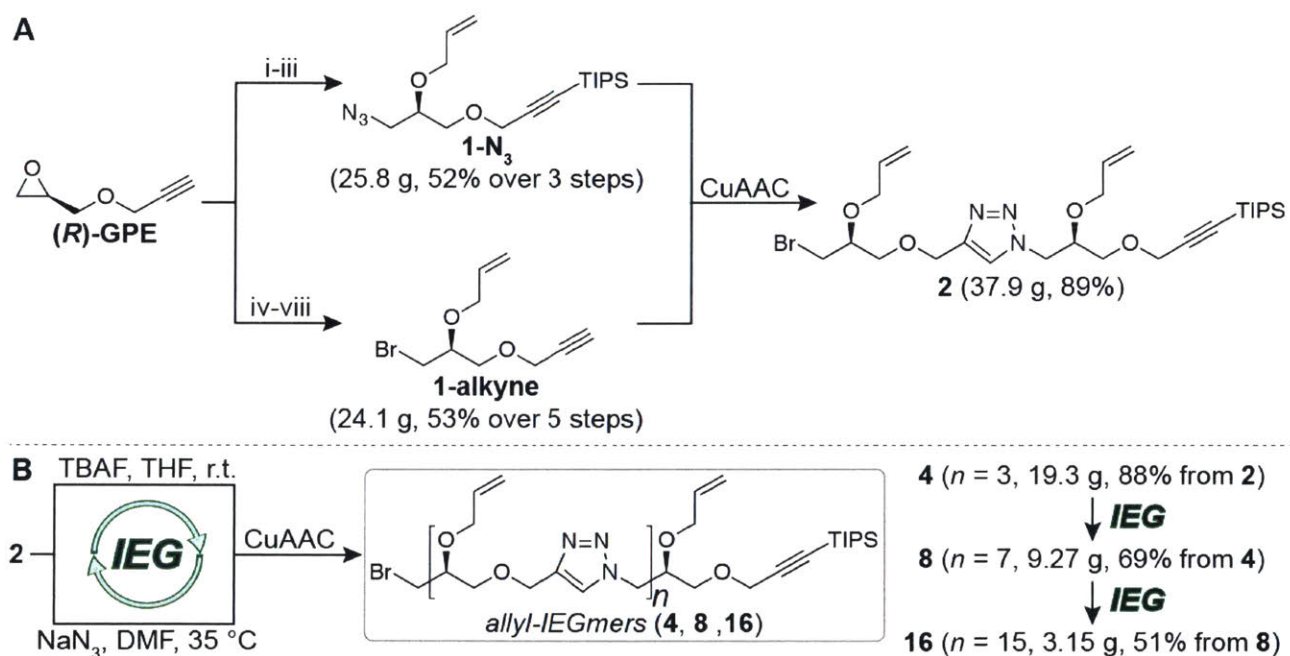


Figure 2.2. (A) Synthesis of allyl-IEG dimer **2** from (R)-GPE. (i) *n*BuLi, TIPSCl, THF, -78 °C to r.t.; (ii) NaN₃, AcOH, DMF, 65 °C; (iii) Allyl bromide, NaH, DMF, r.t.; (iv) *t*-BuOH, Mg(ClO₄)₂, r.t.; (v) Allyl bromide, NaH, DMF, r.t.; (vi) H₃PO₄, r.t.; (vii) TsCl, 4-DMAP, TEA, DCM, r.t.; (viii) LiBr, DMF, 45 °C. (B) Conditions for each IEG cycle to produce allyl-IEG tetramer **4**, octamer **8**, and hexadecamer **16**.

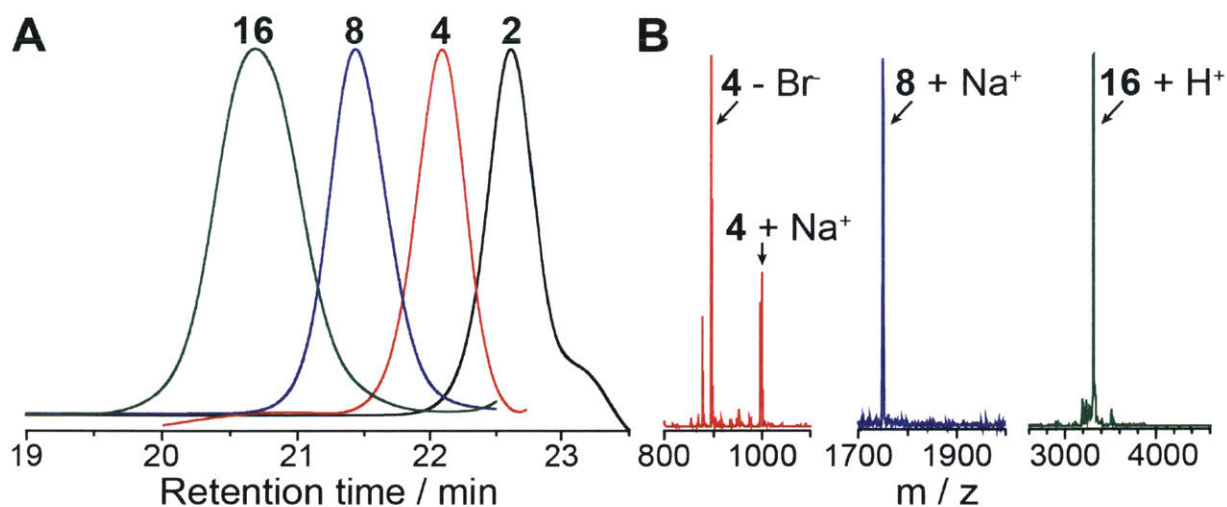


Figure 2.3 | (A) Normalized GPC traces in DMF for allylated oligomers **2**, **4**, **8**, and **16**. (B) MALDI-MS spectra for allylated oligomers **4**, **8**, and **16**.

Compound **2** is a useful starting point for subsequent IEG cycles (Figure 2.2B). Exposure of **2** to 1.0M tetrabutylammonium fluoride in THF for 15 min provided **2-alkyne**, while separate exposure of **2** to NaN₃ at 35 °C for 12 h provided **2-N₃**.⁴⁰⁻⁴² Coupling of **2-alkyne** and **2-azide** under the aforementioned CuAAC conditions gave 19.3 g of tetramer **4** (88% from **2**). Repeating this sequence with **4** as the starting material yielded octamer **8** (9.27 g, 69% from **4**) and hexadecamer **16** (3.15 g, 51% from **8**). Note that the reported yields were obtained after chromatographic purification of each oligomeric species. Furthermore, the same set of procedures was used for each coupling; the reactions were not optimized to maximize the yield for each individual allyl-IEGmer. Nonetheless, allyl-IEG enabled the production of multiple grams of **16** from **2** within 3 d.

Gel permeation chromatography (GPC) traces for **4**, **8**, and **16** were monomodal (Figure 2.3A); matrix-assisted laser desorption ionization-time-of-flight (MALDI-TOF) mass spectra (MS) for each compound displayed a major peak that corresponded to the calculated mass plus a Na⁺ or H⁺ (Figure 2.3B). ¹H NMR further validated the structures and purity (see SI).

We next turned our efforts toward leveraging these allylated oligomers for the synthesis of BCPs. Thiol-ene radical addition is a particularly useful olefin functionalization reaction that is known for its efficiency in the context of macromolecular synthesis.^{43,44} For example, Klok and coworkers demonstrated the use of thiol-ene additions for functionalization of uniform allylated oligoesters (up to octamers) prepared via an IEG strategy.⁴⁵ First, to avoid side reactions with the

TIPS-alkyne chain end, **16** was exposed to TBAF to generate **16-alkyne**. Coupling with 4-methylbenzylazide yielded **16b**, which was converted to azide **16b-N₃** via treatment with NaN₃. An N₂ sparged DMF solution of **16b-N₃**, decanethiol (8 equiv. to alkene), and 2,2-dimethoxy-2-phenylacetophenone (DMPA) (0.25 equiv.) was exposed to 365 nm light for 2 h. Dialysis in ethanol (1k MWCO tubing) provided hexadecamer **16-(C₁₀)-N₃** (Figure 2.4A). Separately, **16** was treated with TBAF to produce **16-alkyne**; the latter was coupled to **16-(C₁₀)-N₃** via CuAAC to provide 1.02 g of a 32-mer BCP (**32a**) that features 16 decane sidechains and 16 allyl groups. GPC (Figure 2.5A), MALDI-MS, (Figure 2.5B), and ¹H NMR (SI) confirmed the structure of BCP **32a**.

Irradiation of **32a** in the presence DMPA and either 1-mercapto-triethylene glycol monomethyl ether (TEG-SH) or thioglycerol (TG-SH) provided BCPs **32TEG** and **32TG**, respectively (see SI, Figure 2.4B). Figure 2.5 shows GPC and MALDI-MS data for **32TEG** and **32TG**. The GPC trace for **32TEG** features a single peak; the GPC trace of **32TG** was broad and showed shoulder peaks that arise from aggregation during GPC analysis. The MALDI spectra show a single peak that matches the calculated mass for both BCPs. Notably, **32TEG** has a mass of 12,106 Da, which we believe sets a new benchmark for non-amide or phos-phate-based uniform synthetic polymers; this mass is nearly 6 kDa greater than what was achieved in our previous IEG+ work.⁴⁰

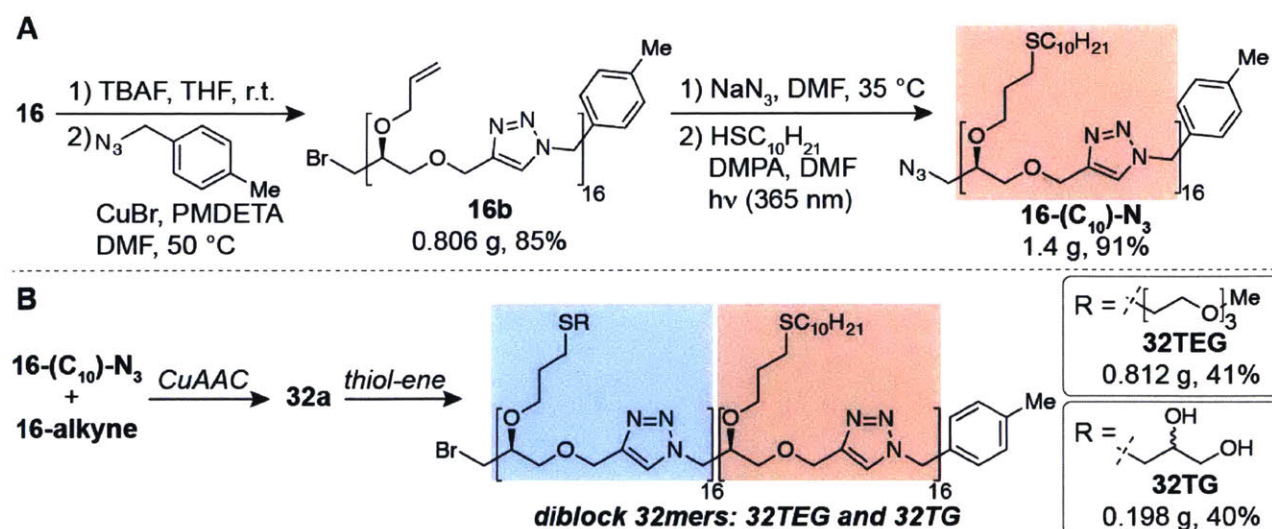


Figure 2.4. (A) Capping of the terminal alkyne and thiol-ene reaction of the allyl-IEG 16-mer. (B) Synthesis and thiol-ene functionalization of 32-mer BCPs.

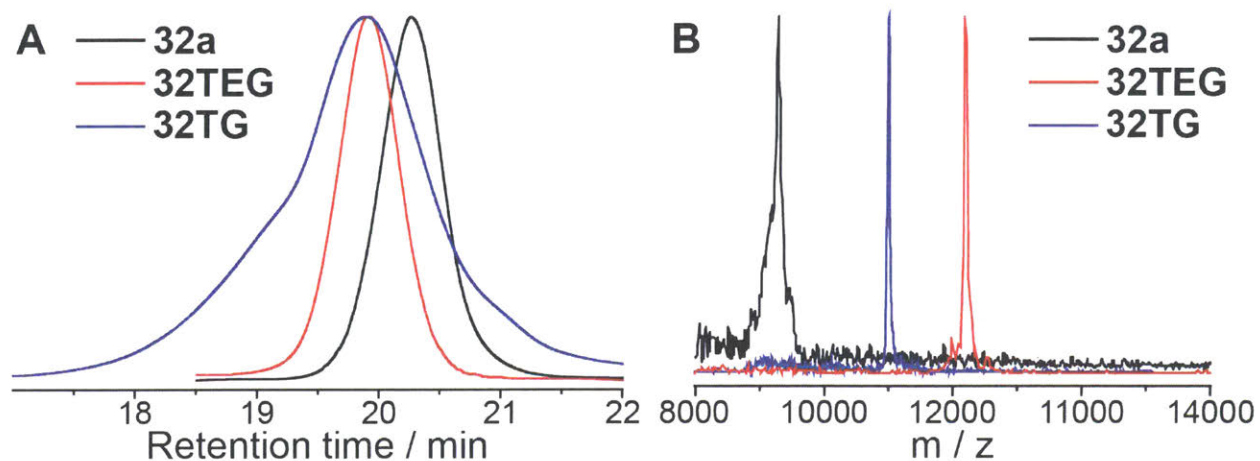


Figure 2.5. (A) Normalized GPC traces for diblock 32-mers **32a**, **32TEG**, and **32TG**. *Note:* peak broadening observed for **32TG** due to aggregation of the glycerol blocks. (B) MALDI-MS data for BCPs **32a**, **32TEG** and **32TG**.

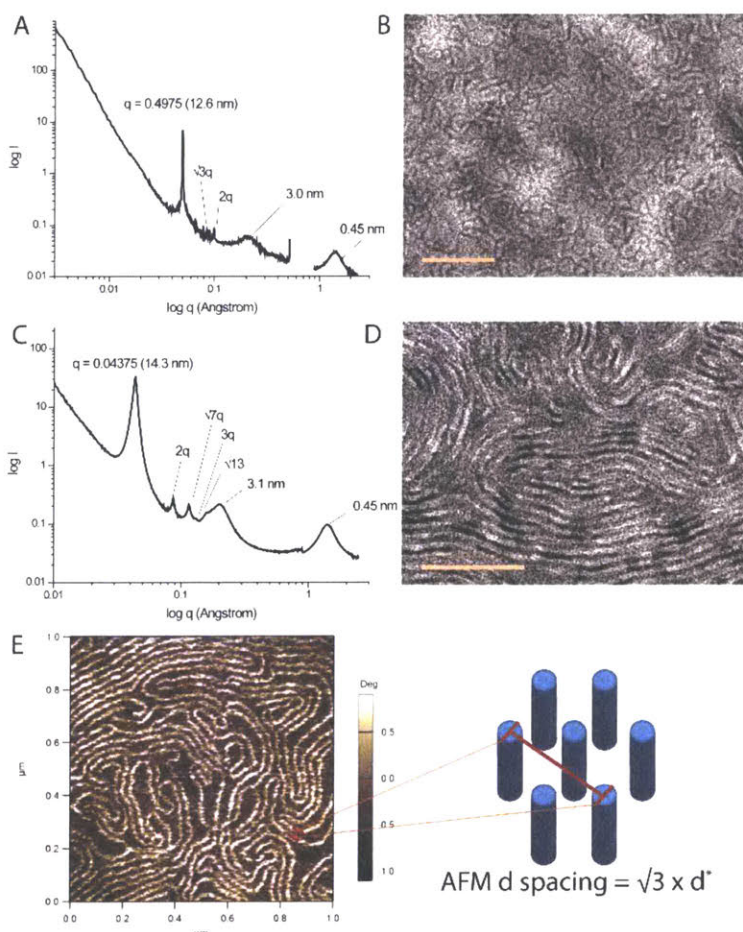


Figure 2.6. (A) SAXS data with intensity versus scattering vector q for **32TEG** and (B) TEM image (scale bar = 200 nm) of thermally annealed **32TEG**. (C) SAXS data with intensity versus scattering vector q for **32TG** and (D) TEM image (scale bar = 200 nm) of thermally annealed

32TG. (E) Tapping mode AFM phase image of **32TG**. The AFM-measured d spacing corresponds to $\sqrt{3} \times d_{\text{SAXS}}$.

We next sought to investigate the propensity of BCPs **32TEG** and **32TG** to undergo bulk self-assembly. BCP self-assembly is a rich field that has produced numerous fundamental discoveries and commercial applications.⁴⁶ Recent studies have elucidated the phase diagrams of unimolecular BCPs⁴⁷⁻⁵⁰; to our knowledge no examples of bulk self-assembly of IEG-derived polymers are known. We were particularly inspired by reports from Zuckermann and coworkers, which have shown that uniform diblock copolypeptoids with TEG and decane blocks in their sidechains form bulk lamellae.⁴⁹ In Zuckermann's system, the authors proposed that self-assembly was driven by crystallization of the decane sidechains, which enforced crystallization of the otherwise amorphous TEG side chains, and lead to lamellar phases in all cases where ordering was observed. Thus, the peptoids displayed crystallinity-driven assembly, rather than traditional amorphous BCP self-assembly,^{48,51} the latter of which is driven by the immiscibility of the two blocks scaled by the product of the chain length N and the Flory-Huggins interaction parameter χ .^{52,53} The small inter-sidechain distance (3 bonds) in peptoids likely facilitates sidechain crystallization; we wondered how the IEG backbone might behave.

Differential scanning calorimetry (DSC) for **32TEG** and **32TG** showed no observable melting transitions in the range of -55 °C to 175 °C (Figure S2.10), which indicated that these BCPs are amorphous and that the larger inter-sidechain distances in our IEG BCPs inhibit sidechain crystallization.

Small-angle X-ray scattering (SAXS) was used to characterize thermally annealed (see SI) samples of **32TEG** and **32TG**. The SAXS curve for **32TEG** (Figure 2.6A) displays a sharp and intense principal peak at $q^*=0.04975 \text{ nm}^{-1}$ and two additional reflections at $\sqrt{3}q^*$ and $2q^*$, which is indicative of a well-ordered hexagonal cylinder (HC) morphology with a domain spacing ($d^* = 2\pi/q^*$) of 12.6 nm. The SAXS curve for **32TG** (Figure 2.6B) also suggests an HC morphology with a principal peak at 0.04375 nm^{-1} , which translates to a domain spacing of 14.3 nm, and reflections at $2q^*$, $\sqrt{7}q^*$, $3q^*$, and $\sqrt{13}q^*$.

Transmission electron microscopy (TEM) images of spin-coated, thermally annealed thin films of **32TEG** and **32TG** support the HC morphologies observed by SAXS. The image for **32TEG** suggests a lack of long-range order in the film (Figure 2.6C). The d spacing measured by

TEM was $17.9 \text{ nm} \pm 0.7 \text{ nm}$, which is larger than the 12.6 nm measured by SAXS; this difference may also be due to difference in the film versus bulk morphology.⁵⁴ TEM analysis of **32TG** showed phase separation and long range order (Figure 2.6D); a d spacing of $16.2 \text{ nm} \pm 0.5 \text{ nm}$ was obtained, which agrees well with the SAXS value (14.3 nm).

Atomic force microscopy (AFM) was used to characterize the surface morphology of films of **32TEG** and **32TG**. In the case of **32TEG**, no contrast between the TEG and decane domains was observed. However, AFM analysis of **32TG** (Figure 2.6E) showed clear phase separation indicative of the HC morphology. The AFM-measured periodicity was approximately 25.0 nm , which is notably larger than the d spacing measured by SAXS and TEM. This value agrees well with the height of the HC unit cell measured by SAXS: $\sqrt{3}d_{\text{SAXS}} = 24.8 \text{ nm}$ (Figure 2.6E, right). These data suggest that the cylinders are comprised of the higher surface energy glycerol block while the lower surface energy decane blocks comprise the matrix.

As shown in Figures 2.6A and 2.6B, two broad peaks, q_α and q_β , were observed in the wide-angle X-ray scattering (WAXS) curves for both **32TEG** and **32TG**. To assign these peaks, we estimated the molecular distances in these BCPs using Chimera (see SI): the calculated length of the decane side chains was 1.76 nm and therefore the distance between polymer backbones was $\sim 3.52 \text{ nm}$. This value closely matches the experimental α values, which were 3.0 nm for **32TEG** and 3.1 nm for **32TG**. The difference between calculated and experimental values is likely due to a degree of intercalation between the side chains. Again using Chimera, we calculated that a fully extended monomer unit of our polymers would have a length of 0.95 nm , which is more than double the length of 0.45 nm represented by β . Assuming that β corresponds to the average monomer-to-monomer spacing, this finding suggests that the back-bone is not fully extended; the backbone conformation could potentially be influenced by the chirality of the units and is a subject for future study.

2.3 Conclusion

We have introduced a new allyl-IEG system that can serve as a basis for the bulk synthesis of unimolecular, chiral BCPs. So far these polymers have shown traditional self-assembly despite their short length, which is likely due to their unique, flexible, poly(ether-co-triazole) backbone. With this system in place, we seek to further explore the morphologies of these polymers beyond HCs with varying block sizes, diverse side chains, and alternating stereoconfigurations.

2.4 Supplementary Information

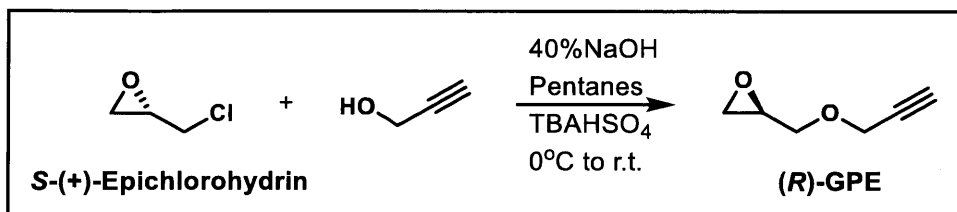
Materials / General Methods / Instrumentation

All reagents were purchased from commercial suppliers and used without further purification unless stated otherwise. Size exclusion chromatography (SEC) analyses were performed on an Agilent 1260 Infinity setup with two Shodex KD-806M columns in tandem and a 0.025 M LiBr DMF mobile phase run at 65 °C. The differential refractive index (dRI) of each compound was monitored using a Wyatt Optilab T-rEX detector. Column chromatography was carried out on silica gel 60F (EMD Millipore, 0.040–0.063 mm). 365 nm UV light for thiol-ene addition chemistry was sourced from a VWR International supplied UV-AC hand lamp with two 6-watt UV tubes, one for 254 nm and one for 365 nm wavelengths. Nuclear magnetic resonance (NMR) spectra were recorded on Varian Inova-500 spectrometers, with working frequencies of 500 (^1H) and 125 (^{13}C) MHz. Chemical shifts are reported in ppm relative to the signals corresponding to the residual non-deuterated solvents: CDCl_3 , $\delta\text{H} = 7.26$ ppm and $\delta\text{C} = 77.16$ ppm; $(\text{CD}_3)_2\text{SO}$, $\delta\text{H} = 2.50$ ppm. High-resolution mass spectra (HRMS) were measured on a Bruker Daltonics APEXIV 4.7 Tesla Fourier Transform Ion Cyclotron Resonance Mass Spectrometer (FT-ICR-MS) using an electrospray ionization (ESI) source. Matrix-assisted laser desorption/ionization-time of flight (MALDI-TOF) mass spectra were measured on a Bruker model MicroFlex instrument using α -cyano-4-hydroxycinnamic acid as the matrix. Thermal characterization of all 5th generation polytriazoles (32-mers) was carried out using thermogravimetric analysis (TGA) on a TA Instruments Discovery TGA. Samples were run in platinum TGA pans at a ramp rate of 10 °C per minute from 50 to 600 °C. Differential scanning calorimetry (DSC) was performed on a TA Instruments Discovery DSC, where each sample was run with a Tzero aluminum pan sealed with a hermetic lid. Determination of the glass transition temperature was taken from the 3rd heating cycle of a run where the sample was cycled at a rate of 10 °C per minute from –50 to 175 °C. Small angle X-ray scattering (SAXS) data were collected at beamline 12-ID-B at the Advanced Photonic Source (APS) at Argonne National Laboratory. The energy of the beam was 14 keV, which corresponds to a wavelength of 0.08857 nm. All SAXS samples were loaded into the center of Bokers aluminum washers (0.900 ± 0.005 ” OD x 0.079 ± 0.005 ” ID) with 0.40 ± 0.04 ” thickness. SAXS, TEM, and AFM samples were prepared by drop-casting by a 20 mg/mL dichloromethane (DCM) solution of the desired polymer. In all samples, the DCM was evaporated at ambient

temperature, the samples were annealed at 120 °C under vacuum for 2 h, and then all samples were allowed to cool to room temperature overnight under reduced pressure (ca. 100 mTorr).

Synthetic Protocols

1) (R)-GPE

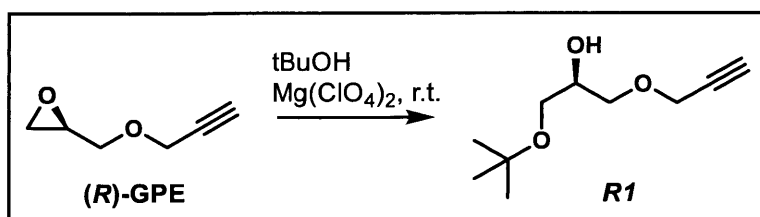


(R)-GPE: A 40% NaOH aqueous solution was prepared by dissolving 226 g of NaOH in 340 mL H₂O. Then, propargyl alcohol (30.3 mL, 540 mmol) was added to the stirring NaOH solution at 0 °C. This reaction mixture was allowed to stir for ~30 min before a solution containing tetrabutylammonium hydrogensulfate (TBAHSO₄, 9.17 g, 27.0 mmol), hexanes (360 mL), H₂O (50.0 mL) and S-(+)-epichlorohydrin (100 g, 1.08 mol) was added. The reaction was allowed to proceed for 8 hr before 500 mL of brine was added and the crude product obtained by way of chemical extraction into 3 x 500 mL DCM. The organic layers were combined, dried over Na₂SO₄, and concentrated under vacuum. Column chromatography (75% hexanes/DCM to DCM) of the crude material was used to purify the product. Residual S-(+)-epichlorohydrin was removed under reduced pressure overnight to yield product (47.3 g, 422 mmol, 78%) as a faint yellow oil with 82% ee. We have since changed this procedure to another one that yields product with >99% ee. Details for this new procedure can be found in the Supplementary Materials of Chapter 3 starting on page 104-106. HRMS-ESI for R-(-)-GPE; Calcd for C₆H₈O₂: m/z = 130.0868 [M + NH₄]⁺; Found: 130.0862 [M + NH₄]⁺. ¹H NMR (500 MHz, CDCl₃): δ(ppm) 4.19 (t, *J* = 2.4 Hz, 2H), 3.80 (dd, *J* = 11.4, 2.9 Hz, 1H), 3.46 (dd, *J* = 11.3, 5.9 Hz, 1H), 3.19–3.10 (m, 1H), 2.78 (dd, *J* = 5.2, 4.1 Hz, 1H), 2.61 (dd, *J* = 5.1, 2.6 Hz, 1H), 2.43 (t, *J* = 2.3 Hz, 1H). ¹³C NMR (125 MHz, CDCl₃): δ(ppm) 79.2, 74.8, 70.3, 58.4, 50.4, 44.2.

Note: Compounds that named with the “R#” format (e.g. R1, R2, R3, etc.) are not named in this way because they have R stereochemistry. This naming system was chosen because these compounds were made from the (R)-GPE starting material, which does have R stereochemistry.

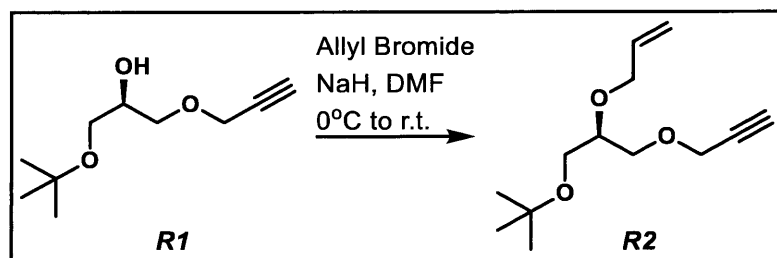
2) Monomer 1-alkyne

a) *R1*



R1: Under an N₂ atmosphere, dry, liquid tBuOH (119.0 g, 1.60 mol) was added to (***R***)-GPE (30.0 g, 268 mmol) in an oven-dried and sealed 500 mL round-bottom flask in a room temperature water bath. Next, Mg(ClO₄)₂ (15.0 g, 67.1 mmol) was added portion-wise into the stirring reaction mixture. This mixture was allowed to react for 24 hours. After completion, 500 mL of water was added to the solution followed by extraction with DCM (3 x 500 mL). The organic layers were combined, dried with Na₂SO₄, and concentrated under vacuum. Column chromatography (50% hexanes/DCM to 100% DCM) yielded product (48.3 g, 259 mmol, 97% yield). HRMS-ESI for *R1*; Calcd for C₁₀H₁₈O₃: m/z = 204.1594 [M + NH₄]⁺; Found: 204.1601 [M + NH₄]⁺. ¹H NMR (500 MHz, CDCl₃): δ(ppm) 4.20 (d, *J* = 2.3 Hz, 2H), 3.91 (ddd, *J* = 10.7, 6.2, 4.5 Hz, 1H), 3.62 (dd, *J* = 9.7, 4.5 Hz, 1H), 3.56 (dd, *J* = 9.7, 6.0 Hz, 1H), 3.44 (dd, *J* = 9.1, 4.5 Hz, 1H), 3.38 (dd, *J* = 9.0, 6.5 Hz, 1H), 2.58-2.44 (b, 1H), 2.44 (t, *J* = 2.4 Hz, 1H), 1.19 (s, 9H). ¹³C NMR (125 MHz, CDCl₃): δ(ppm) 77.2, 74.6, 73.0, 71.1, 69.5, 62.7, 58.3, 53.4, 27.3.

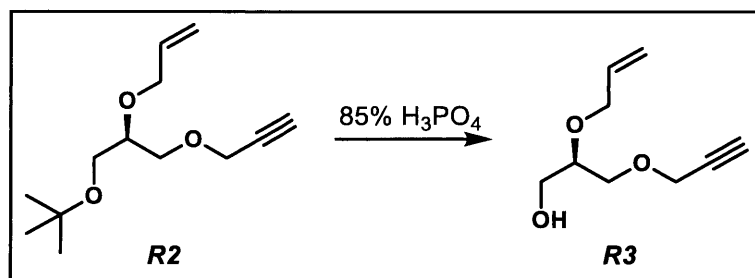
b) *R2*



R2: Under an N₂ atmosphere, dry DMF (190 mL) and allyl bromide (34.2 g, 282 mmol, 23.2 mL) were added to ***R1*** (35.0 g, 188 mmol) in an oven-dried and sealed 500 mL round-bottom flask. The reaction mixture was cooled to 0°C and 60% NaH in mineral oil (8.28 g, 207 mmol) was added portion wise into the stirring reaction mixture. The mixture was allowed to gradually warm up to room temperature and left to react overnight. After completion, DMF was removed under reduced

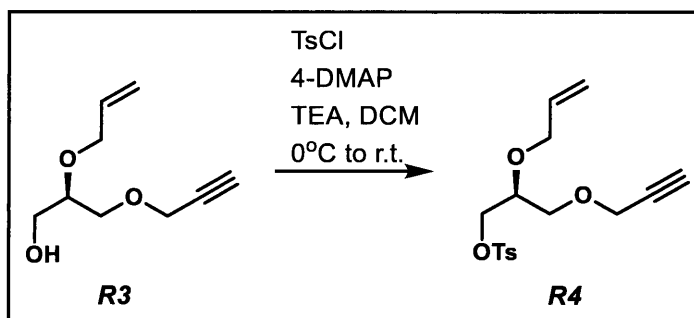
pressure. 300 mL of water was added to the solution which was extracted with DCM (3 x 500 mL). The organic layers were combined, dried with Na₂SO₄, and concentrated under vacuum. Column chromatography (80% hexanes/DCM to 50% hexanes/DCM) yielded product (40.5 g, 179 mmol, 95% yield). HRMS-ESI for *R2*; Calcd for C₁₃H₂₂O₃: m/z = 244.1907 [M + NH₄]⁺; Found: 244.1910 [M + NH₄]⁺. ¹H NMR (500 MHz, CDCl₃): δ(ppm) 5.92 (ddt, *J* = 16.1, 10.4, 5.7 Hz, 1H), 5.28 (d, *J* = 17.2 Hz, 1H), 5.15 (d, *J* = 10.4 Hz, 1H), 4.20 – 4.18 (d, *J* = 2.5 Hz, 2H), 4.16-4.14 (m, 2H), 3.69-3.66 (m, 1H), 3.63 – 3.57 (m, 2H), 3.44 (d, *J* = 5.5 Hz, 2H), 2.42 (t, *J* = 2.3 Hz, 1H), 1.18 (s, 9H). ¹³C NMR (125 MHz, CDCl₃): δ(ppm)135.1, 116.9, 94.8, 77.3, 74.6, 73.3, 71.3, 69.9, 61.5, 58.5, 25.3.

c) *R3*



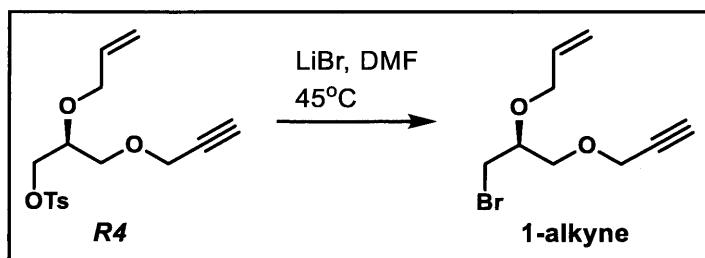
R3: Under an N₂ atmosphere, 85% H₃PO₄ (175 g, 1.78 mol) was poured onto *R2* (40.0 g, 178 mmol) in a 500 mL round-bottom flask. The reaction mixture was stirred and left to react at room temperature over 4 hours. After completion, 500 mL of water was added to the solution followed by extraction with DCM (3 x 500 mL). The organic layers were combined, dried with Na₂SO₄, and concentrated under vacuum. Column chromatography (50% hexanes/DCM to 2% MeOH/DCM) yielded product (25.6 g, 150. mmol, 84% yield). HRMS-ESI for *R3*; Calcd for C₉H₁₄O₃: m/z = 188.1281 [M + NH₄]⁺; Found: 188.1286 [M + NH₄]⁺. ¹H NMR (500 MHz, CDCl₃): δ(ppm) 5.97 – 5.88 (ddt, 16.0, 10.4, 5.6 Hz, 1H), 5.29 (dd, *J* = 17.2, 1.5 Hz, 1H), 5.19 (dd, *J* = 10.4, 1.2 Hz, 1H), 4.21-4.16 (overlap, 3H), 4.12-4.08 (m, 1H), 3.79-3.70 (m, 1H), 3.67-3.62 (overlap, 4H), 2.45 (t, *J* = 2.4 Hz, 1H), 1.99 (b, 1H). ¹³C NMR (125 MHz, CDCl₃): δ(ppm)134.7, 117.6, 94.9, 77.8, 75.0, 71.2, 69.5, 62.5, 58.7.

d) *R4*



R4: Under an N₂ atmosphere, dry DCM (500 mL), trimethylamine (16.7 g, 165.4 mmol, 22.9 mL), and 4-DMAP (9.19 g, 75.2 mmol) were added to **R3** (25.5 g, 150. mmol) in an oven-dried and sealed 1000 mL round-bottom flask. The reaction mixture was cooled to 0°C and 4-toluenesulfonyl chloride (31.5 g, 165 mmol) was added portion wise into the stirring reaction mixture. The mixture was allowed to gradually warm up to room temperature and left to react overnight. After completion, the organic solution was extracted with water (3 x 300 mL) and brine (1 x 300 mL). The organic layer was dried with Na₂SO₄ and concentrated under vacuum. Column chromatography (50% hexanes/DCM to 100% DCM) yielded product (38.2 g, 118 mmol, 78% yield). HRMS-ESI for *R4*; Calcd for C₁₆H₂₀O₅S: m/z = 342.1370 [M + NH₄]⁺; Found: 342.1372 [M + NH₄]⁺. ¹H NMR (500 MHz, CDCl₃): δ(ppm) 7.80 (d, *J* = 8.3 Hz, 2H), 7.34 (d, *J* = 8.5 Hz, 2H), 5.86-5.78 (ddt, 17.2Hz, 10.4 Hz, 4.2 Hz, 1H), 5.23 (dd, *J* = 17.2, 1.6 Hz, 1H), 5.16 (dd, *J* = 10.4Hz, 1.2 Hz, 1H), 4.17-4.02 (overlap, 6H), 3.73 (p, *J* = 4.8 Hz, 1H), 3.57 (d, *J* = 5.1 Hz, 1H), 2.45 (s, 3H), 2.43 (t, *J* = 2.4 Hz, 1H). ¹³C NMR (125 MHz, CDCl₃): δ(ppm)144.8, 134.2, 132.6, 129.8, 127.9, 117.4, 94.7, 79.1, 75.0, 71.2, 69.2, 68.1, 58.5, 21.5.

e) *1-alkyne*

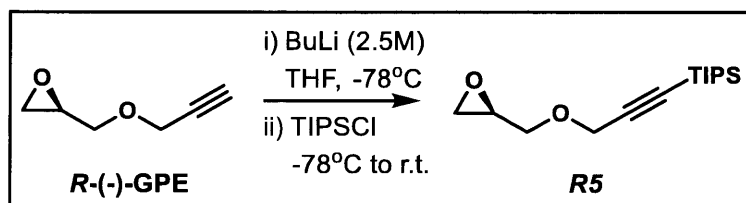


1-alkyne: DMF (250 mL) and LiBr (44.1 g, 507.5 mmol) were added to **R4** (38.0 g, 118 mmol) in a 500 mL round-bottom flask. The reaction mixture was left to stir until the LiBr was completely

dissolved, after which the mixture was placed into a 45°C oil bath and left to react overnight. DMF was then removed under reduced pressure. 300 mL of water was added to the solution followed by extraction with DCM (3 x 500 mL). The organic layers were combined, dried with Na₂SO₄, and concentrated under vacuum. Column chromatography (50% hexanes/DCM to 100% DCM) yielded product (24.1 g, 103 mmol, 88% yield). HRMS-ESI for **1-alkyne**; Calcd for C₉H₁₃BrO₂: m/z = 250.0437 [M + NH₄]⁺; Found: 250.0443 [M + NH₄]⁺. ¹H NMR (500 MHz, CDCl₃): δ(ppm) 5.97-5.89 (ddt, *J* = 17.2, 10.4, 5.8 Hz, 1H), 5.31 (dd, *J* = 17.2, 1.6 Hz, 1H), 5.21 (dd, *J* = 10.4, 1.2 Hz, 1H), 4.20 (d, *J* = 2.4 Hz, 2H), 4.15-4.12 (m, 2H), 3.75-3.66 (overlap, 3H), 3.54 (dd, *J* = 10.6, 5.3 Hz, 1H), 3.47 (dd, *J* = 10.6, 4.7 Hz, 1H), 2.45 (t, *J* = 2.4 Hz, 1H). ¹³C NMR (125 MHz, CDCl₃): δ(ppm) 134.3, 117.4, 79.2, 76.6, 74.8, 71.0, 69.5, 58.5, 32.0.

2) Monomer 1-alkyne

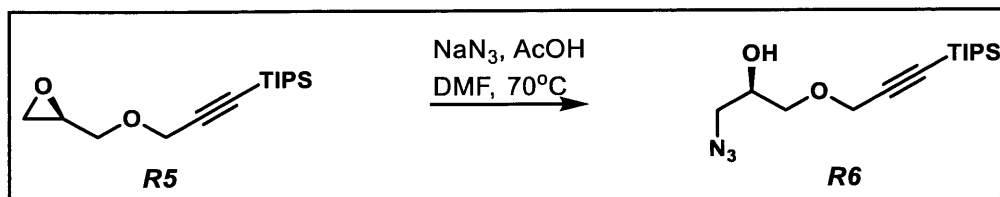
a) R5



R5: Under an N₂ atmosphere, **R-(-)-GPE** (16.0 g, 143 mmol) was added to dry THF (300 mL) in an oven-dried and sealed 500 mL two-neck round-bottom flask attached to a 150 mL addition funnel. Next, the reaction vessel was cooled to -78 °C using a dry ice/pentanes bath, followed by the dropwise addition of *n*-butyllithium (2.5 M in hexanes, 63.0 mL, 157 mmol). Once all of the *n*BuLi was added, the addition funnel was washed with ~10 mL of dry THF and the reaction mixture was allowed to stir for 30 min. Then, TIPSCl (30.3 g, 157.1 mmol, 33.6 mL) was added to the addition funnel, followed by the dropwise addition of the TIPSCl solution to the reaction mixture (still at -78 °C) over the course of 15 min. After warming to room temperature, the reaction proceeded for 3–4 h before being quenched upon addition of a cold brine solution (500 mL). The crude product was obtained by extraction into DCM (3 x 500 mL), followed by combining the organic layers, drying with Na₂SO₄, and concentrating under vacuum. Column chromatography (4% EtOAc/hexanes) of the crude material yielded product (27.4 g, 102 mmol, 71% yield) as a clear oil. HRMS-ESI for **R5**; Calcd for C₆H₈O₂: m/z = 130.0868 [M + NH₄]⁺;

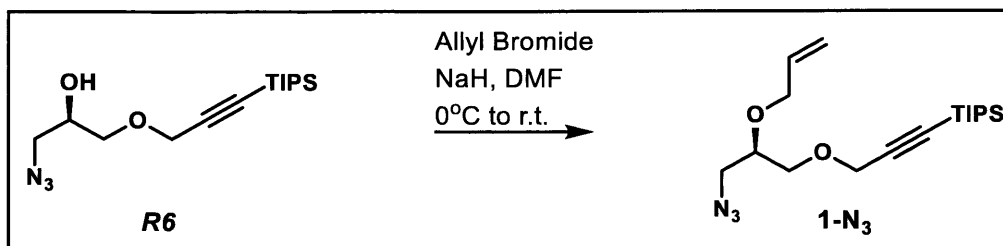
Found: 130.0862 [M + NH₄]⁺. ¹H NMR (500 MHz, CDCl₃): δ(ppm) 4.26 (d, *J* = 9.6 Hz, 2H), 3.82 (dd, *J* = 11.2, 3.3 Hz, 1H), 3.53 (dd, *J* = 11.2, 5.7 Hz, 1H), 3.18 (dq, *J* = 6.0, 3.1 Hz, 1H), 2.81 (t, *J* = 4.6 Hz, 1H), 2.64 (dd, *J* = 5.0, 2.7 Hz, 1H), 1.07 (s, 21H). ¹³C NMR (125 MHz, CDCl₃): δ(ppm) 101.6, 90.1, 70.2, 59.2, 50.6, 44.5, 18.5, 11.0.

b) R6



R6: DMF (700 mL) and acetic acid (9.20 g, 153 mmol, 8.76 mL) were added to **R5** (27.3 g, 102 mmol) in a 1000 mL round-bottom flask. NaN₃ (19.9 g, 306 mmol) was then added and the reaction mixture was heated to 70°C and allowed to stir for 24 hours. Over the course of the reaction a white gel-like precipitate formed. DMF was then removed under reduced pressure. 300 mL of water was added to the solution followed by extraction with DCM (3 x 300 mL). The organic layers were combined, dried with Na₂SO₄, and concentrated under vacuum. Column chromatography (10% EtOAc/hexanes) yielded product (26.3 g, 84.4 mmol, 83% yield). **Safety warning:** Sodium azide in the presence of acid can produce hydrazoic acid, a highly toxic and flammable gas. All of these procedures are performed in a well ventilated fume hood in order to minimize the danger. The reaction mixture can also be neutralized by addition of 50 mL of a saturated NaHCO₃ solution before removal of DMF under reduced pressure. **Note: we have also since updated this procedure and now use EtOAc instead of DCM for extraction in order to avoid undesired reaction between NaN₃ and DCM.** HRMS-ESI for **R6**; Calcd for C₁₅H₂₉N₃O₂Si: *m/z* = 329.2367 [M + NH₄]⁺; Found: 329.2367 [M + NH₄]⁺. ¹H NMR (500 MHz, CDCl₃): δ(ppm) 4.24 (s, 2H), 3.98 (p, *J* = 5.9 Hz, 1H), 3.64 (dd, *J* = 9.6, 4.1 Hz, 1H), 3.58 (dd, *J* = 9.6, 6.1 Hz, 1H), 3.39 (dd, *J* = 5.2, 0.7 Hz, 2H), 2.34 (b, 1H), 1.07 (s, 21H). ¹³C NMR (125 MHz, CDCl₃): δ(ppm) 102.6, 94.8, 88.3, 77.2, 70.8, 69.5, 59.3, 18.5, 11.1.

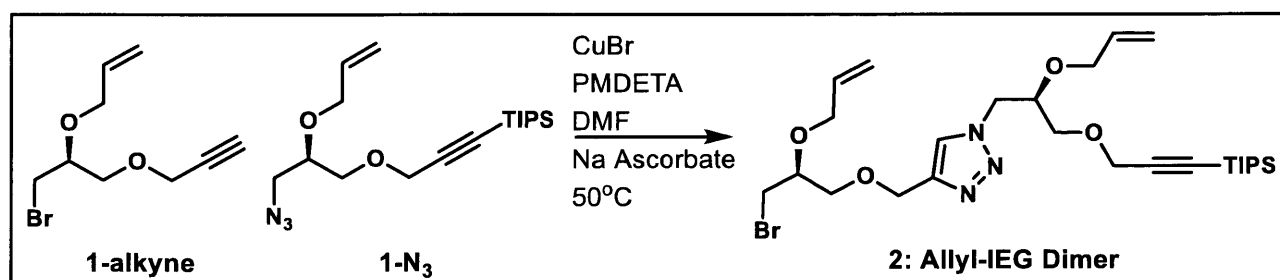
c) 1-N₃



2S: Under an N₂ atmosphere, dry DMF (250 mL) and allyl bromide (15.2 g, 126 mmol, 10.3 mL) were added to **R6** (26.0 g, 83.7 mmol) in an oven-dried and sealed 500 mL round-bottom flask. The reaction mixture was cooled to 0°C and 60% NaH in mineral oil (3.68 g, 92.1 mmol) was added portion wise into the stirring reaction mixture. The mixture was allowed to gradually warm up to room temperature and left to react overnight. After completion, DMF was removed under reduced pressure. 250 mL of water was added to the solution which was extracted with DCM (3 x 250 mL). The organic layers were combined, dried with Na₂SO₄, and concentrated under vacuum. Column chromatography (5% EtOAc/hexanes) yielded product (25.8 g, 73.4 mmol, 88% yield). HRMS-ESI for **1-N₃**; Calcd for C₁₈H₃₃N₃O₂Si: m/z = 352.2415 [M + H]⁺; Found: 352.2426 [M + H]⁺. ¹H NMR (500 MHz, CDCl₃): δ(ppm) 5.93 (ddt, *J* = 16.2, 10.8, 5.7 Hz, 1H), 5.30 (dd, *J* = 17.2, 1.5 Hz, 1H), 5.23 – 5.17 (dd, *J* = 10.4, 1.2 Hz, 1H), 4.21 (s, 3H), 4.17 (dd, *J* = 12.7, 5.7 Hz, 2H), 4.11 (dd, *J* = 12.7, 5.7 Hz, 2H), 3.69 (m, 1H), 3.64 (dd, *J* = 5.0, 2.5 Hz, 2H), 3.38 (dd, *J* = 4.8 Hz, 0.7 Hz, 2H), 1.07 (s, 21H). ¹³C NMR (125 MHz, CDCl₃): δ(ppm) 134.5, 117.6, 94.9, 75.5, 69.6, 67.0, 59.6, 52.6, 47.7, 18.7, 11.2.

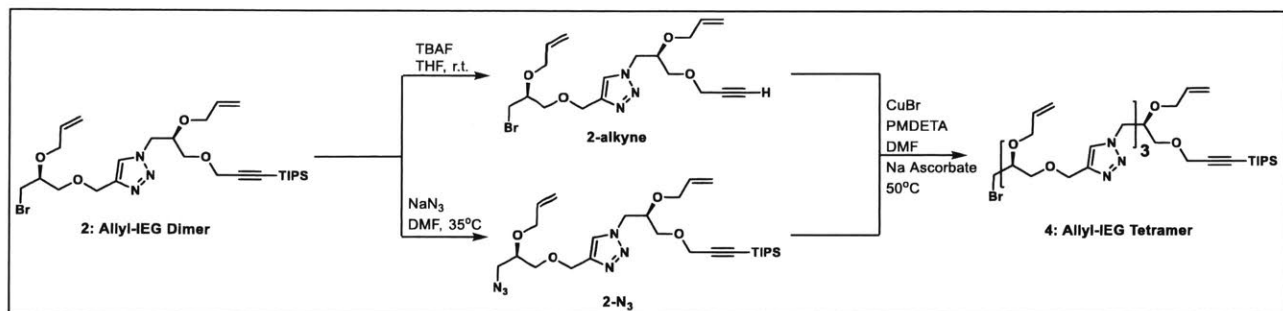
4) Allyl-IEG Generations

a) G1-Dimer (2)



2: Under an N₂ atmosphere, dry DMF (250 mL), PMDETA (1.26 g, 7.28 mmol, 1.52 mL), and Na ascorbate (1.44 g, 7.28 mmol) were added to a mixture of **1-alkyne** (17.0 g, 72.9 mmol) and **1-N₃** (25.6 g, 72.8 mmol) in an oven-dried and sealed 500 mL round-bottom flask. CuBr (522 mg, 3.64 mmol) was then added and the reaction mixture was warmed to 50°C and left to react overnight. After completion, DMF was removed under reduced pressure. 10 mL of DCM was added to the resulting viscous mixture which was then loaded carefully onto a column. Column chromatography (25% hexanes/DCM to 2% MeOH/DCM) yielded the product (37.9 g, 64.8 mmol, 89% yield) as a faint yellow oil. HRMS-ESI for **2**; Calcd for C₂₇H₄₆BrN₃O₄Si: m/z = 584.2514 [M + H]⁺; Found: 584.2490 [M + H]⁺. ¹H NMR (500 MHz, CDCl₃): δ(ppm) 7.65 (s, 1H), 5.89 (ddt, *J* = 16.3, 10.4, 5.7 Hz, 1H), 5.71 (ddt, *J* = 16.5, 10.3, 5.8 Hz, 1H), 5.28 (dd, *J* = 17.3, 1.7 Hz, 1H), 5.19 – 5.10 (overlap, 3H), 4.67 (d, *J* = 2.3 Hz, 2H), 4.60 (dd, *J* = 14.2, 3.4 Hz, 1H), 4.41 (dd, *J* = 14.2, 8.0 Hz, 1H), 4.24 (d, *J* = 2.4 Hz, 2H), 4.10 (dd, *J* = 5.8, 4.3 Hz, 2H), 4.03 (dd, *J* = 12.7, 5.7 Hz, 2H), 3.92 – 3.85 (overlap, 2H), 3.72 – 3.67 (m, 1H), 3.67 – 3.60 (overlap, 3H), 3.51 (dd, *J* = 10.6, 5.2 Hz, 1H), 3.43 (dd, *J* = 10.6, 4.7 Hz, 1H), 1.06 (s, 21H). ¹³C NMR (125 MHz, CDCl₃): δ(ppm) 144.5, 134.5, 134.0, 124.2, 117.8, 117.6, 102.6, 96.3, 94.3, 88.4, 76.3, 71.2, 70.1, 67.9, 64.9, 59.5, 51.8, 32.2, 18.6, 11.1.

b) G2-Tetramer (**4**)



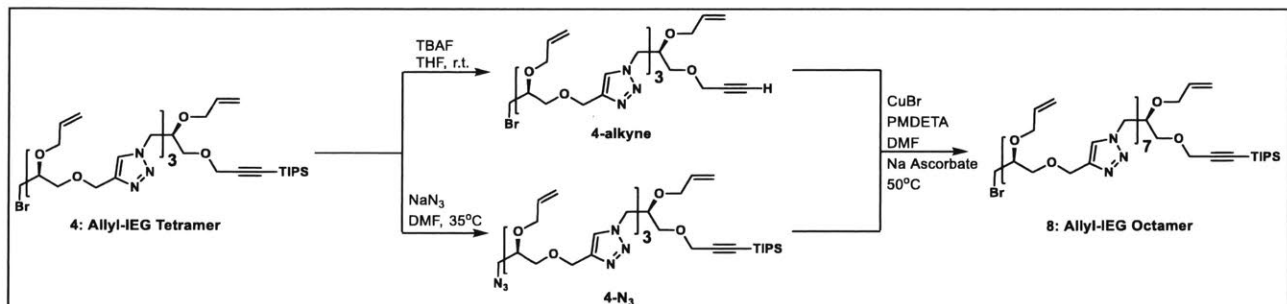
4: The **2-alkyne** precursor to **4** was prepared by dissolving **2** (13.11 g, 22.4 mmol) in THF (200 mL), followed by the slow addition of TBAF (1M in THF, 1.05 equiv, 23.55 mL). After the reaction had gone to completion, THF was removed under reduced pressure. Next, the crude product mixture was purified by column chromatography (2% MeOH/DCM) to yield **2-alkyne** (9.40 g, 21.9 mmol) as a faint yellow oil.

The **2-N₃** precursor to **4** was prepared by dissolving **2** (14.4 g, 24.6 mmol) in 300 mL DMF, followed by the addition of NaN₃ (8.00 g, 123 mmol). The reaction mixture was heated to 35 °C and allowed to stir for 12 hours before the DMF was removed via rotary evaporator at 35 °C. Heating past 35 °C was avoided as it leads to degradation of the product. Then, 500 mL of EtOAc was added to the residue and extracted with water (2 x 300 mL) and brine (1 x 300 mL). The organic layer was dried with Na₂SO₄ and concentrated under vacuum. The compound **2-N₃** was obtained (12.6 g, 23.1 mmol) as a faint yellow oil.

Under an N₂ atmosphere, dry DMF (200 mL), PMDETA (361 mg, 2.09 mmol, 0.435 mL), and Na ascorbate (826 mg, 4.17 mmol) were added to a mixture of **2-alkyne** (9.40 g, 21.9 mmol) and **2-N₃** (12.6 g, 23.1 mmol) in an oven-dried and sealed 500 mL round-bottom flask. CuBr (150. mg, 1.04 mmol) was then added and the reaction mixture was warmed to 50 °C and left to react for 2 hours. After completion, DMF was removed under reduced pressure. 10 mL of DCM was added to the resulting viscous mixture which was then loaded carefully onto a column. Column chromatography (100% DCM to 4% MeOH/DCM) yielded product (19.3 g, 19.8 mmol, 88% yield from **2**) as a yellow oil. ¹H NMR (500 MHz, CDCl₃): δ(ppm) 7.67 (s, 2H), 7.65 (s, 1H), 5.89 (ddt, *J* = 17.3, 10.3, 5.7 Hz, 1H), 5.75-5.67 (overlap, 3H), 5.28 (dq, *J* = 17.2, 1.6 Hz, 1H), 5.19-5.09 (overlap, 7H), 4.70-4.56 (overlap, 10H), 4.46-4.38 (overlap, 3H), 4.24 (d, *J* = 2.7 Hz, 2H), 4.10 (tt, *J* = 4.3, 1.4 Hz, 1H), 4.03 (overlap, 3H), 3.98-3.86 (overlap, 6H), 3.69 (dd, *J* = 9.7, 4.8 Hz,

1H), 3.66-3.61 (overlap, 3H), 3.58-3.49 (overlap, 4H), 3.51 (dd, $J = 10.7, 5.2$ Hz, 1H), 3.44 (dd, $J = 10.6, 4.7$ Hz, 1H) 1.06 (s, 21H). ^{13}C NMR (125 MHz, CDCl_3): δ (ppm) 144.0, 134.2, 133.8, 124.3, 117.5, 117.4, 101.3, 90.2, 76.5, 76.0, 70.9, 69.8, 68.6, 67.8, 64.4, 59.2, 51.5, 51.2, 32.1, 25.8, 16.2, 4.9.

c) G3-Octamer (**8**)



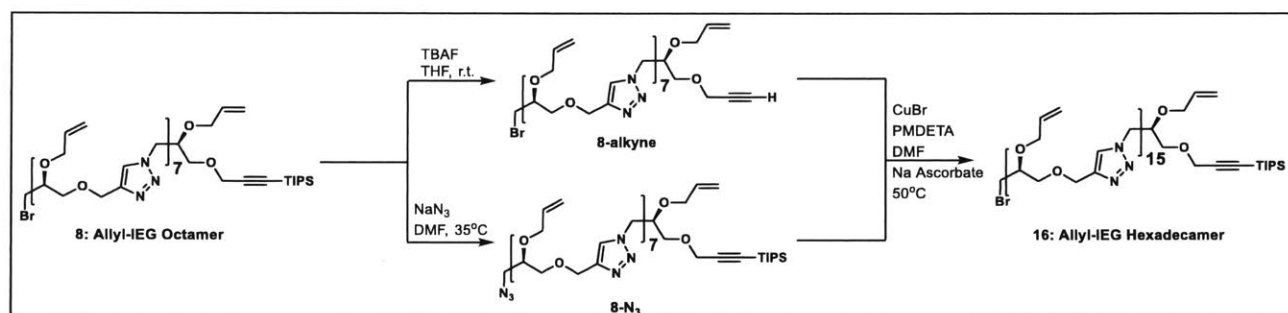
8: The **4-alkyne** precursor to **8** was prepared by dissolving **4** (7.5 g, 7.69 mmol) in THF (80 mL), followed by the slow addition of TBAF (1M in THF, 1.05 equiv, 8.07 mL). After the reaction has gone to completion, THF was removed under reduced pressure. Next, the crude product mixture was purified by column chromatography (4% MeOH/DCM) to yield **4-alkyne** (5.56 g, 6.79 mmol) as a yellow oil.

The **4-N₃** precursor to **8** was prepared by dissolving **4** (7.5 g, 7.69 mmol) in 80 mL DMF, followed by the addition of NaN₃ (3.00 g, 46.2 mmol). The reaction mixture was heated to 35 °C and allowed to stir for 12 hours before the DMF was removed via rotary evaporator. Heating past 35 °C was avoided as it leads to degradation of the product. Then, 200 mL of EtOAc was added to the residue and extracted with water (2 x 200 mL) and brine (1 x 200 mL). The organic layer was dried with Na₂SO₄ and concentrated under vacuum. The compound **4-N₃** was obtained (7.06 g, 7.53 mmol) as a yellow oil.

Under an N₂ atmosphere, dry DMF (70 mL), PMDETA (117 mg, 0.674 mmol, 0.140 mL), and Na ascorbate (267 mg, 1.348 mmol) were added to a mixture of **4-alkyne** (5.56 g, 6.79 mmol) and **4-N₃** (7.06 g, 7.53 mmol) in an oven-dried and sealed 500 mL round-bottom flask. CuBr (48.4 mg, 0.337 mmol) was then added and the reaction mixture was warmed to 50 °C and left to react for 2 hours. After completion, DMF was removed under reduced pressure. 5 mL of DCM was added to the resulting viscous mixture which was then loaded carefully onto a column. Column

chromatography (100% DCM to 6% MeOH/DCM) yielded product (9.27 g, 5.23 mmol, 69% yield from **4**) as a yellow oil. ^1H NMR (500 MHz, CDCl_3): δ (ppm) 7.68 (s, 6H), 7.65 (s, 1H), 5.91 (ddt, $J = 17.3, 10.4, 5.7$ Hz, 1H), 5.75-5.67 (overlap, 7H), 5.29 (dq, $J = 17.3$ Hz, 1.6 Hz, 1H), 5.18-5.10 (overlap, 15H), 4.70-4.56 (overlap, 22H), 4.44-4.38 (overlap, 8H), 4.26 (d, $J = 2.8$ Hz, 2H), 4.11 (ddt, $J = 5.7, 4.4, 1.4$ Hz, 1H), 4.08-3.99 (overlap, 7H), 3.92-3.86 (overlap, 14H), 3.70 (dd, $J = 9.7, 4.8$ Hz, 1H), 3.68-3.62 (overlap, 4H), 3.58-3.50 (overlap, 12H), 3.45 (dd, $J = 10.6, 4.8$, 1H), 1.06 (s, 21H). ^{13}C NMR (125 MHz, CDCl_3): δ (ppm) 143.7, 143.4, 134.0, 133.9, 133.5, 133.5, 123.9, 123.9, 116.9, 116.8, 116.8, 116.6, 116.6, 102.2, 87.5, 76.1, 75.6, 75.5, 70.5, 70.4, 70.3, 68.2, 67.4, 64.0, 58.7, 53.3, 51.0, 50.8, 50.7, 50.6, 31.9, 30.3, 30.2, 18.0, 10.4.

d) G4-Hexadecamer (**16**)



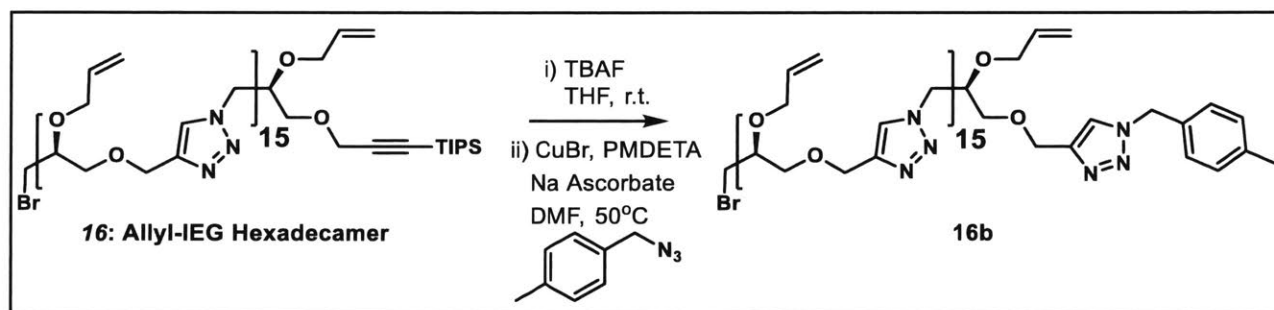
16: The **8-alkyne** precursor to **16** was prepared by dissolving **8** (3.30 g, 1.88 mmol) in THF (38 mL), followed by the slow addition of TBAF (1M in THF, 1.05 equiv, 1.97 mL). After the reaction has gone to completion, THF was removed under reduced pressure. Next, the crude product mixture was purified by column chromatography (6% MeOH/DCM) to yield **8-alkyne** (2.75 g, 1.72 mmol) as a yellow oil.

The **8-N₃** precursor to **16** was prepared by dissolving **8** (3.30 g, 1.88 mmol) in 38 mL DMF, followed by the addition of NaN_3 (611 mg, 9.40 mmol). The reaction mixture was heated to 35 °C and allowed to stir for 12 hours before the DMF was removed via rotary evaporator. Heating past 35°C was avoided as it leads to degradation of the product. Then, 150 mL of EtOAc was added to the residue and extracted with water (2 x 100 mL) and brine (1 x 100 mL). The organic layer was dried with Na_2SO_4 and concentrated under vacuum. The compound **16** was obtained (3.20 g, 1.86 mmol) as a yellow oil.

Under an N₂ atmosphere, dry DMF (38 mL), PMDETA (29.8 mg, 0.172 mmol, 0.0359 mL), and Na ascorbate (68.1 mg, 0.344 mmol) were added to a mixture of **8-alkyne** (2.75 g, 1.72 mmol) and **8-N₃** (3.20 g, 1.86 mmol) in an oven-dried and sealed 250 mL round-bottom flask. CuBr (12.3 mg, 0.086 mmol) was then added and the reaction mixture was warmed to 50°C and left to react for 2 hours. After completion, DMF was removed under reduced pressure. 5 mL of DCM was added to the resulting viscous mixture which was then loaded carefully onto a column. Column chromatography (100% DCM to 8% MeOH/DCM) yielded product (3.15 g, 0.949 mmol, 51% yield from **8**) as a yellow oil. ¹H NMR (500 MHz, CDCl₃): δ(ppm) 7.68 (s, 15H), 5.91 (ddt, *J* = 16.3, 10.9, 5.8 Hz, 1H), 5.75-5.68 (overlap, 15H), 5.34-5.23 (m, 1H), 5.19-5.11 (overlap, 31H), 4.69-4.57 (overlap, 46H), 4.44-4.40 (overlap, 16H), 4.25 (d, *J* = 1.7 Hz, 2H), 4.12-4.09 (m, 1H), 4.08-3.99 (overlap, 15H), 3.92-3.84 (overlap, 30H), 3.71-3.62 (overlap, 5H), 3.58-3.48 (m, 27H), 3.45 (dd, *J* = 10.5, 4.6 Hz, 1H), 3.35 (m, 1H), 1.07 (s, 21H). ¹³C NMR (125 MHz, CDCl₃): δ(ppm) 143.4, 133.9, 133.5, 133.4, 123.9, 116.7, 102.2, 87.5, 76.1, 75.5, 70.4, 69.4, 68.2, 67.3, 64.0, 58.7, 53.3, 51.0, 50.7, 31.9, 17.9, 10.4.

5) Thiol-ene functionalization of allyl-IEG 16-mer

a) 16b

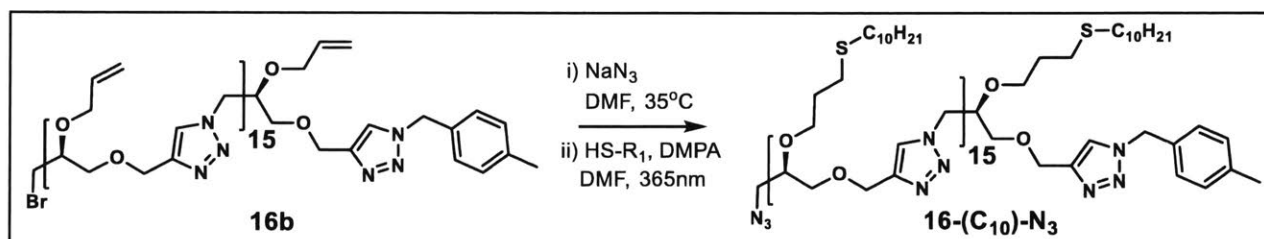


16b: 16 (2.00 g, 0.604 mmol) was dissolved in THF (12 mL), followed by the slow addition of TBAF (1M in THF, 1.05 equiv, 0.634 mL). After the reaction has gone to completion, THF was removed under reduced pressure. Next, the crude product mixture was purified by column chromatography (8% MeOH/DCM) to yield **16-alkyne** (1.80 g, 0.569 mmol) as a yellow oil.

Under an N₂ atmosphere, dry DMF (5.4 mL) and Na ascorbate (5.3 mg, 0.0269 mmol) were added to a mixture of **16-alkyne** (850 mg, 0.269 mmol) and 4-methylbenzyl azide (158 mg, 1.08 mmol) in an oven-dried and sealed 40 mL scintillation vial. A DMF solution of 0.1M CuBr and 0.2M

PMDETA (0.135 mL) was then added to the reaction mixture. The reaction was warmed to 50°C left to react for 2 hours. After completion, DMF was removed under reduced pressure. 1 mL of DCM was added to the resulting viscous mixture which was then loaded carefully onto a column. Column chromatography (100% DCM to 8% MeOH/DCM) yielded product (806 mg, 0.24 mmol, 91% yield from **16**) as a yellow oil. ¹H NMR (500 MHz, CDCl₃): δ(ppm) 7.68 (s, 14H), 7.66 (s, 1H), 7.47 (s, 1H), 7.18 (s, 4H), 5.90 (ddt, *J* = 16.1, 10.2, 5.4 Hz, 1H), 5.75-5.68 (overlap, 15H), 5.49 (s, 2H), 5.31-5.23 (m, 1H), 5.19-5.11 (overlap, 31H), 4.69-4.57 (m, 48H), 4.44-4.40 (m, 16H), 4.12 (m, 1H), 4.06-3.98 (m, 15H), 3.92-3.84 (overlap, 30H), 3.70 (dd, *J* = 9.5, 4.9 Hz, 1H), 3.67-3.62 (overlap, 2H), 3.59-3.50 (overlap, 31H), 3.45 (dd, *J* = 10.6, 4.8 Hz, 1H), 2.34 (s, 3H).

b) *16*-(C₁₀)-N₃

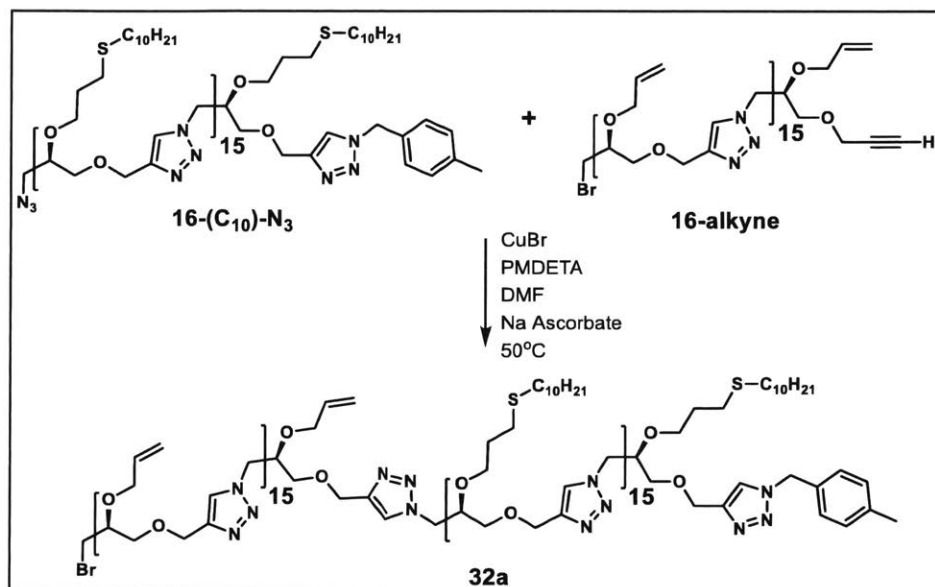


16-(C₁₀)-N₃: Under an N₂ atmosphere, dry DMF (11.2 mL) was added to **16b** (800 mg, 0.253 mmol), followed by the addition of NaN₃ (98.7 mg, 1.52 mmol). The reaction mixture was heated to 35 °C and allowed to stir for 12 hours before the DMF was removed via rotary evaporator. Then, 50 mL of EtOAc was added to the residue and extracted with water (2 x 30 mL) and brine (1 x 30 mL). The organic layer was dried with Na₂SO₄ and concentrated under vacuum yielding **16b-N₃**. **16b-N₃** (743 mg, 0.235 mmol) was dissolved in a solution of DMF (12.7 mL), 1-decanethiol (5.24 g, 30.08 mmol, 6.36 mL), and 2,2-dimethoxy-2-phenylacetophenone (241 mg, 0.94 mmol) in a 40 mL scintillation vial. The solution was sparged with N₂, and then subjected to 365 nm light for 2 hours. The solution was then dialyzed in 3.5k MWCO dialysis tubing from Spectrum Labs in EtOH (3 x 500 mL) over 12 hours. The EtOH was changed after 1 hour and 3 hours of dialysis. The dialyzed product was concentrated under vacuum and transferred to a 40 mL scintillation vial. The compound **16-(C₁₀)-N₃** was obtained (1.40 g, 0.231 mmol) from **(S)-G4-(OAllyl)₁₆-MeBz** as a yellow, waxy solid. ¹H NMR (500 MHz, CDCl₃): δ(ppm) 7.67 (s, 15H), 7.49 (s, 1H), 7.18 (s, 4H), 5.45 (s, 2H), 4.71-4.54 (overlap, 48H), 4.46-4.38 (overlap, 16H), 3.89-3.81 (overlap, 16H),

3.69-3.50 (overlap, 48H), 3.49-3.37 (overlap, 16H), 2.62-2.59 (overlap, 4H) 2.52-2.42 (b, 60H), 2.35 (s, 3H), 1.82-1.71 (overlap, 32H), 1.59-1.51 (b, 36H), 1.42-1.22 (b, 220H), 0.93-0.85 (b, 48H).

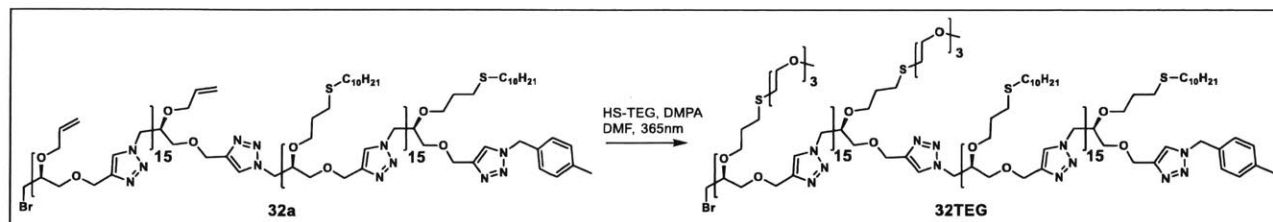
6) Synthesis of diblock copolymers

a) 32a



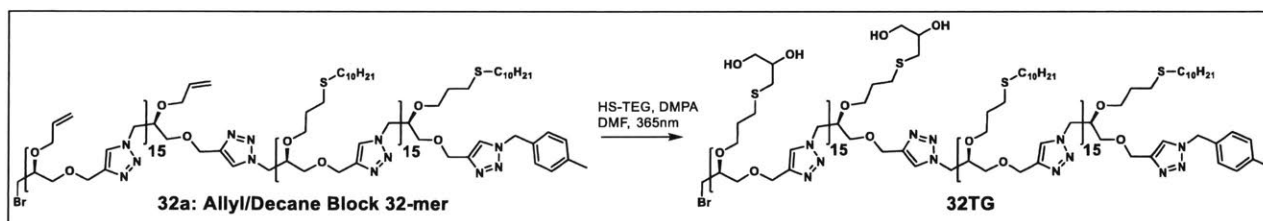
32a: Under an N₂ atmosphere, dry DMF (5 mL) and Na ascorbate (4.5 mg, 0.023 mmol) were added to a mixture of **16-(C₁₀)-N₃** (1.39 g, 0.229 mmol) and **16-alkyne** (869 mg, 0.275 mmol) in an oven-dried and sealed 40 mL scintillation vial. A DMF solution of 0.1M CuBr and 0.2M PMDETA (0.115 mL) was then added to the reaction mixture. The reaction mixture was warmed to 50 °C and left to react for 2 hours. After completion, DMF was removed under reduced pressure. 2 mL of DCM was added to the resulting viscous mixture which was then loaded carefully onto a column. Column chromatography (100% DCM to 8% MeOH/DCM) yielded product (1.0 g, 0.11 mmol, 48% yield from **16-(C₁₀)-N₃**) as a yellow solid. ¹H NMR (500 MHz, CDCl₃): δ(ppm) 7.70-7.65 (overlap, 31H), 7.48 (s, 1H), 7.19 (s, 4H), 5.90 (ddt, *J* = 16.4, 11.0, 5.7 Hz, 1H), 5.76-5.67 (overlap, 15H), 5.49 (s, 2H), 5.32-5.26 (m, 1H), 5.20-5.10 (overlap, 31H), 4.71-4.55 (overlap, 96H), 4.46-4.44 (overlap, 32H), 4.13-4.08 (m, 1H), 4.13-3.99 (overlap, 15H), 3.91-3.80 (overlap, 48H), 3.70 (dd, *J* = 9.7, 5.0 Hz, 1H), 3.72-3.50 (overlap, 79H), 3.45-3.37 (overlap, 16H), 2.68-2.55 (overlap, 4H), 2.50-2.41 (overlap, 60H), 2.35 (s, 3H), 1.99-1.92 (m, 2H), 1.79-1.70 (overlap, 32H), 1.57-1.49 (overlap, 30H), 1.38-1.15 (overlap, 224H), 0.89-0.83 (overlap, 48H).

b) **32TEG**



32TEG: **32a** (725 mg, 0.0783 mmol) was dissolved in a solution of DMF (3.6 mL), 1-mercapto-triethyleneglycol monomethyl ether¹ (1.80 g, 0.316 mmol), and 2,2-dimethoxy-2-phenylacetophenone (80.3 mg, 0.313 mmol) in a 40 mL scintillation vial. The solution was sparged with N₂ and subjected to 365 nm light for 2 hours. The solution was then dialyzed in 8k MWCO dialysis tubing from Spectrum Labs in EtOH (3 x 300 mL) over 12 hours. The product **32TEG** (810 mg, 0.067 mmol, 86% yield) was concentrated under vacuum. ¹H NMR (500 MHz, CDCl₃): δ(ppm) 7.70-7.64 (overlap, 31H), 7.47 (s, 1H), 7.17 (s, 4H), 5.49 (s, 2H), 4.70-4.56 (overlap, 96H), 4.45-4.36 (overlap, 32H), 3.87-3.80 (b, 16H), 3.69-3.51 (overlap, 288H), 3.43-3.35 (b, 64H), 2.67-2.63 (t, 32H), 2.52-2.41 (m, 64H) 2.34 (s, 3H), 1.79-1.70 (b, 32H), 1.68-1.62 (b, 36H) 1.56-1.48 (p, *J* = 7.4 Hz, 28H), 1.37-1.12 (b, 224H), 0.88-0.84 (t, 48H).

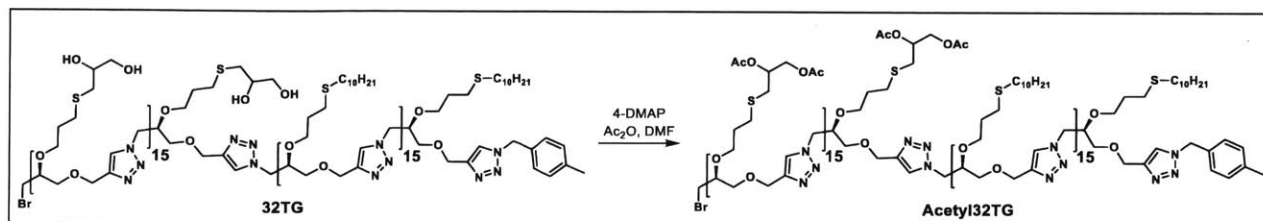
c) **32TG**



32TG: **32a** (200 mg, 0.0217 mmol) was dissolved in a solution of DMF (0.600 mL), racemic thioglycerol (300 mg, 2.78 mmol), and 2,2-dimethoxy-2-phenylacetophenone (22.2 mg, 0.0868 mmol) in a 40 mL scintillation vial. The solution was sparged with N₂ and subjected to 365 nm light for 2 hours. The solution was then dialyzed in 8k MWCO dialysis tubing from Spectrum Labs in EtOH (3 x 300 mL) over 12 hours. The product **32TG** (190 mg, 0.018 mmol, 83% yield) was concentrated under vacuum. ¹H NMR (500 MHz, (CD₃)₂SO, ppm): δH 8.08-8.00 (overlap, 32H), 7.20 (d, *J* = 7.8 Hz, 1H), 7.15 (d, 7.9 Hz, 1H), 7.21-7.13 (dd, 4H), 5.52 (s, 2H), 4.80-4.72 (m, 16H), 4.62-4.48 (overlap, 112H), 4.43-4.32 (overlap, 32H), 3.87-3.78 (b, 16H), 3.58-3.45 (overlap,

128H), 3.34-3.24 (overlap, 64H), 2.57-2.52 (overlap, 16H) 2.42-2.23 (overlap, 115H), 1.74-1.67 (m, 2H), 1.63-1.51 (overlap, 66H), 1.46-1.38 (b, 28H), 1.30-1.12 (overlap, 220H), 1.11-0.96 (b, 4H), 0.86-0.73 (b, 48H).

d) *Acetyl32TG*



Acetyl32TG: **32TG** (20 mg, 0.0018 mmol) was dissolved in DMF (2.0 mL). 4-DMAP (4.4 mg, 0.036 mmol) was added to the solution followed by acetic anhydride (0.50 mL, 5.3 mmol). The reaction was left overnight, after which the solution was pushed through silica with 10% MeOH/DCM to remove 4-DMAP. The solution was then concentrated to get the product **Acetyl32TG** (10 mg, 0.0008 mmol, 45% yield). ¹H NMR (500 MHz, CDCl₃, ppm): δH 7.73-7.67 (overlap, 32H), 7.48 (b, 1H), 7.20-7.18 (b, 4H), 5.50 (s, 2H), 5.15-5.07 (b, 16H), 4.72-4.57 (overlap, 96H), 4.46-4.32 (overlap, 48H), 4.20-4.13 (overlap, 16H), 3.90-3.82 (overlap, 32H), 3.67-3.52 (overlap, 96H), 3.45-3.37 (b, 30H), 3.25 (b, 2H), 2.08 (b, 96H), 1.96-1.87 (b, 28H), 1.78-1.72 (b, 48H), 1.57-1.50 (b, 28H), 1.39-1.15 (overlap, 220H), 0.90-0.85 (b, 48H).

Spectroscopic Characterization

^1H NMR Spectra

a) Materials leading up to **1-alkyne** and **1-N₃** and

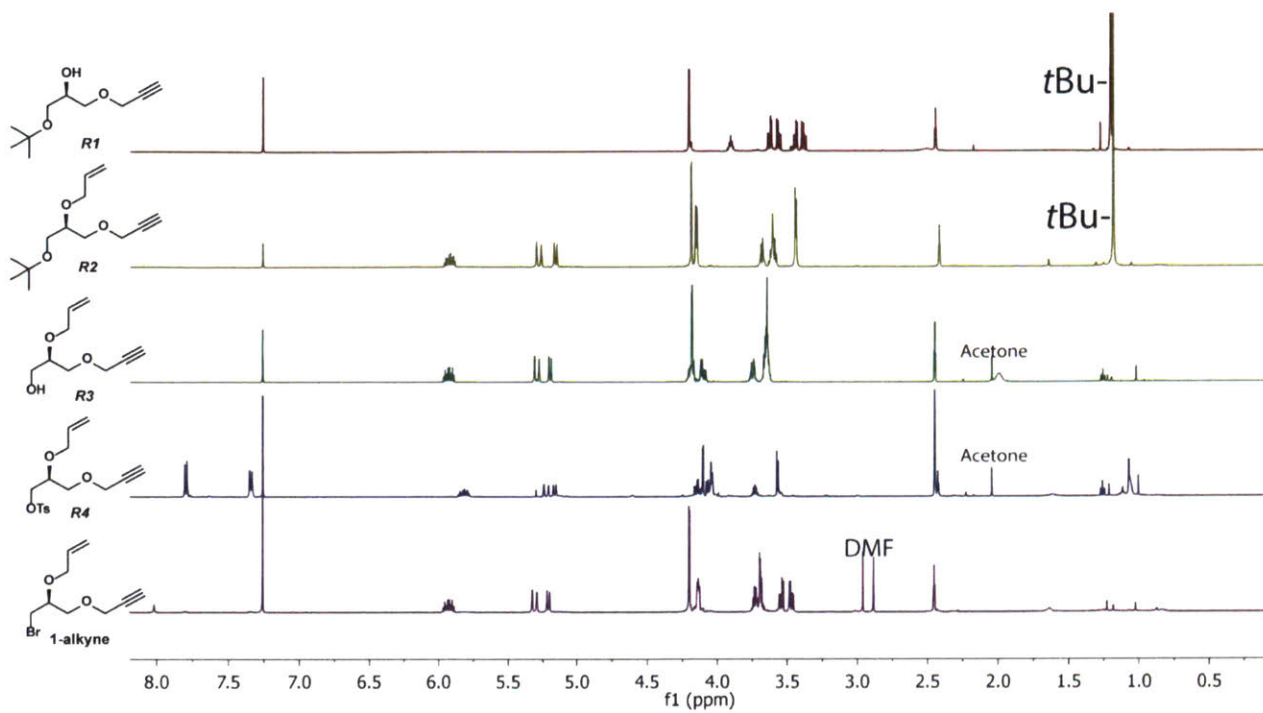


Figure S2.1. ^1H NMRs of intermediates leading to **1-alkyne**.

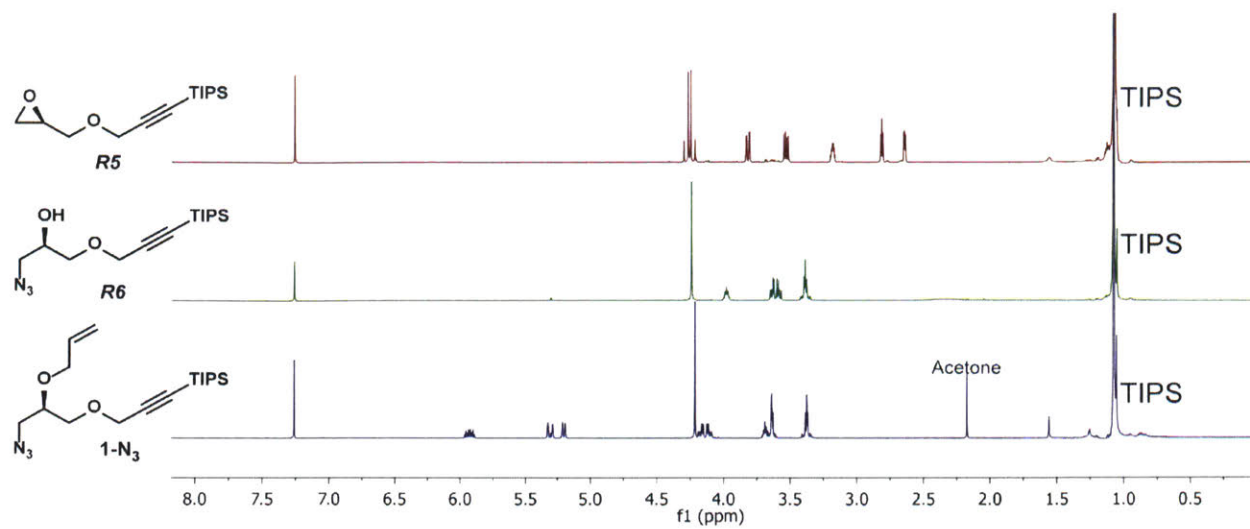


Figure S2.2. ^1H NMRs of intermediates leading to **1-N₃**.

b) Allyl-IEG Generations

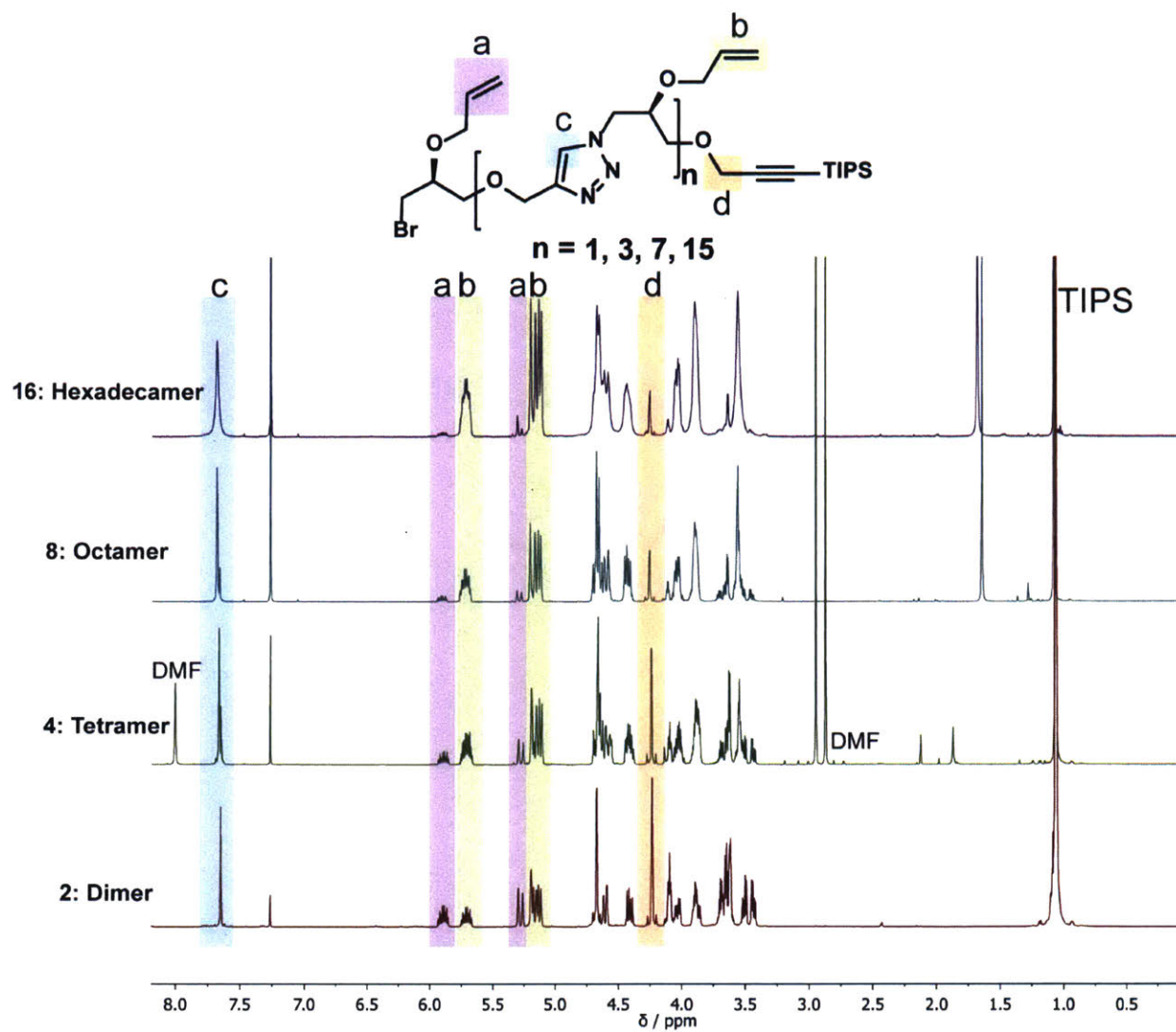


Figure S2.3. Comparison of ^1H NMR spectra of Allyl-IEG Oligomers Generations 1-4.

c) **16b** and **16-(C₁₀)-N₃**

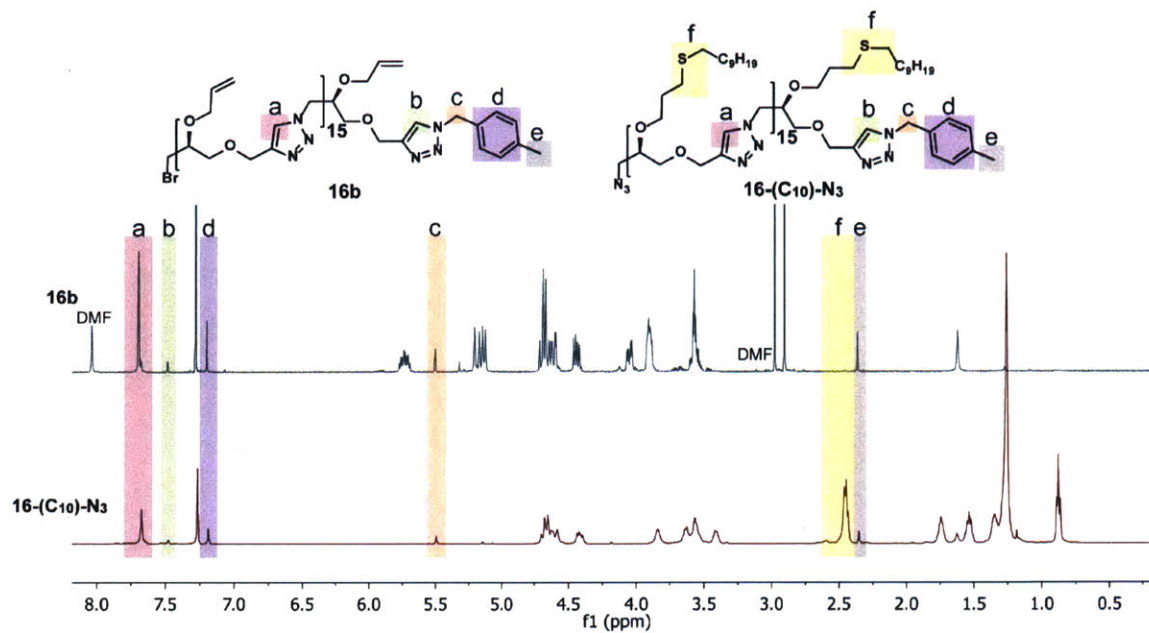


Figure S2.4. Comparison of ¹H NMR spectra of **16b** and **16-(C₁₀)-N₃**.

d) *Diblock copolymers*

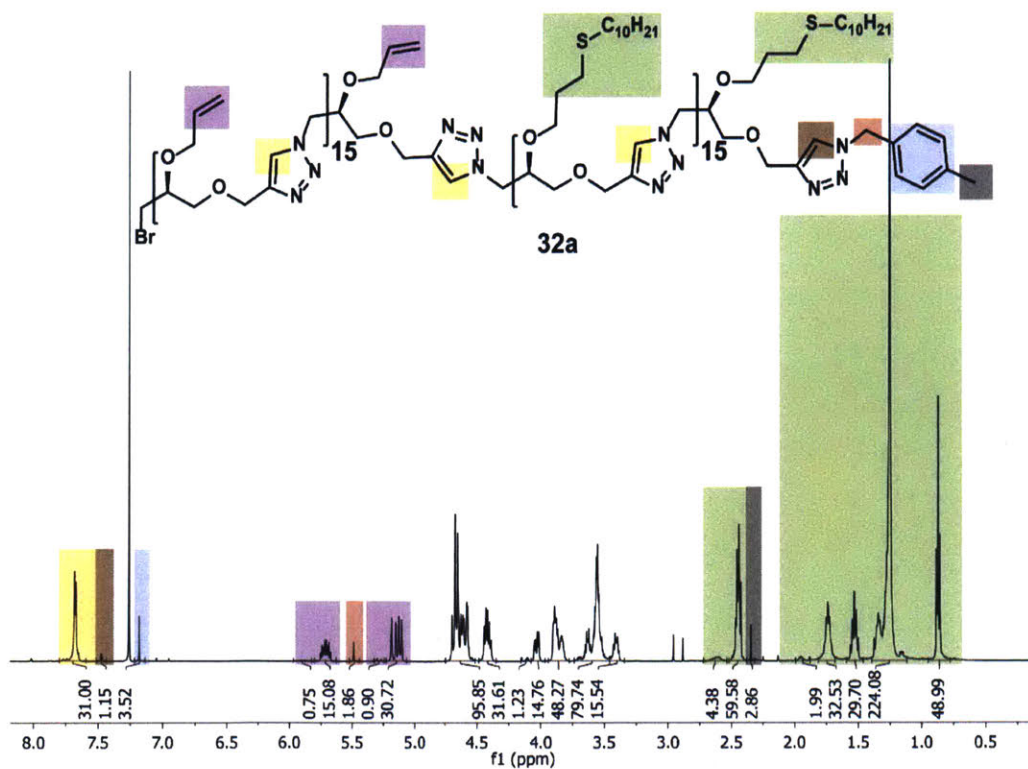


Figure S2.5. ¹H NMR spectrum of **32a**: Allyl/Decane Block 32mer in CDCl₃

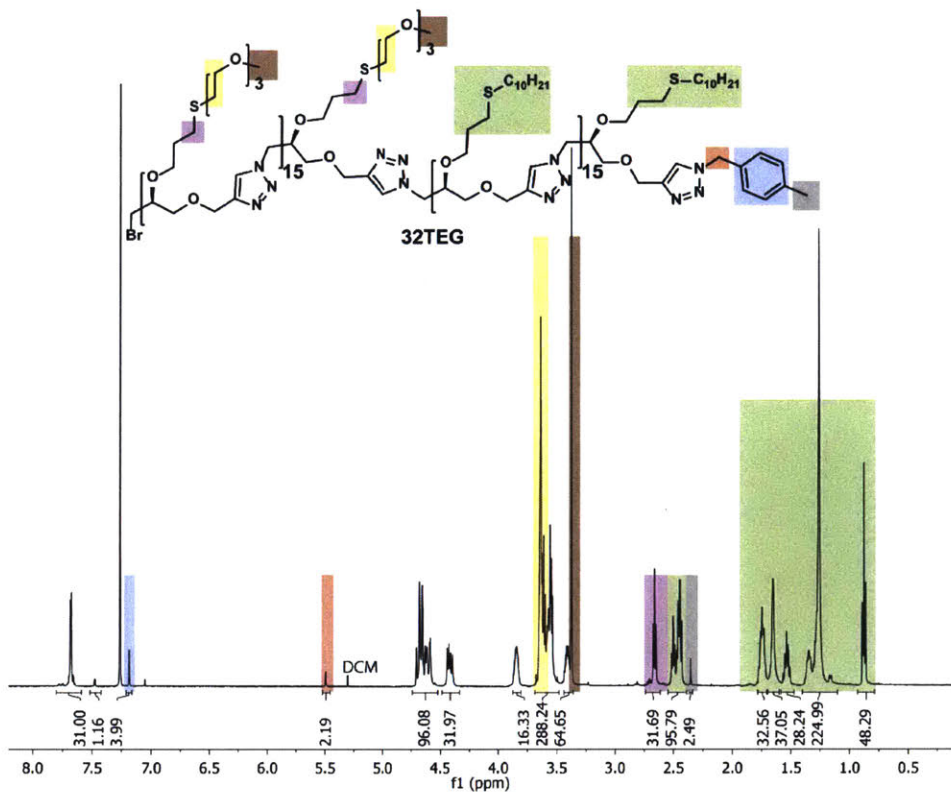


Figure S2.6. ^1H NMR spectrum of 32TEG: TEG/Decane Block 32mer in CDCl_3

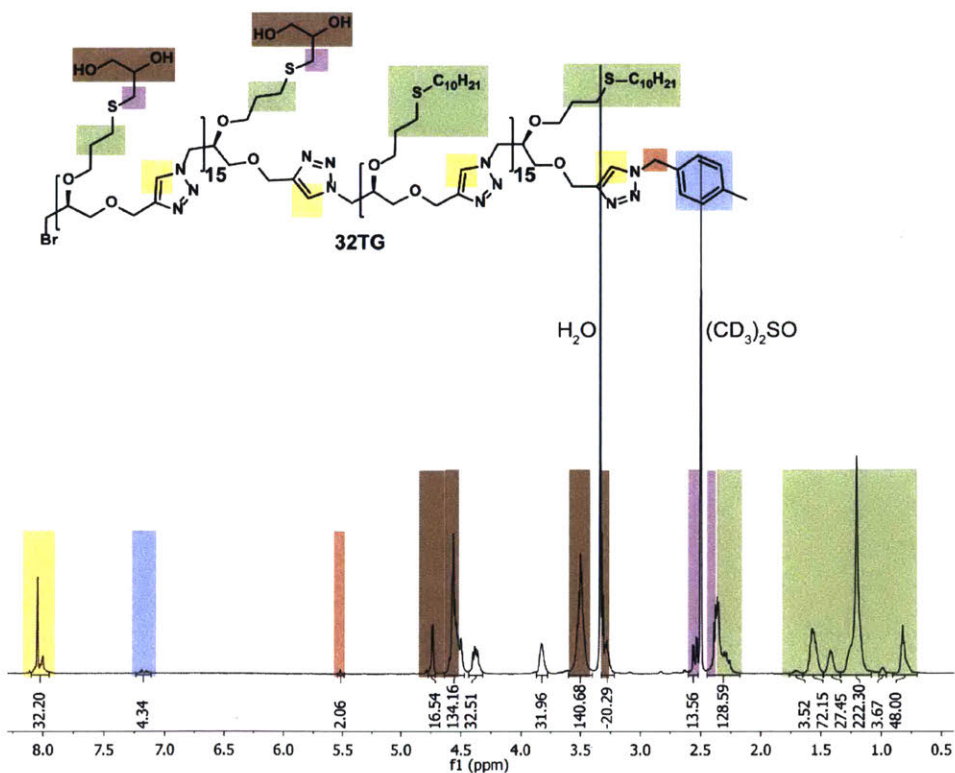


Figure S2.7. ^1H NMR spectrum of 32TG: TG/Decane Block 32mer in $(\text{CD}_3)_2\text{SO}$

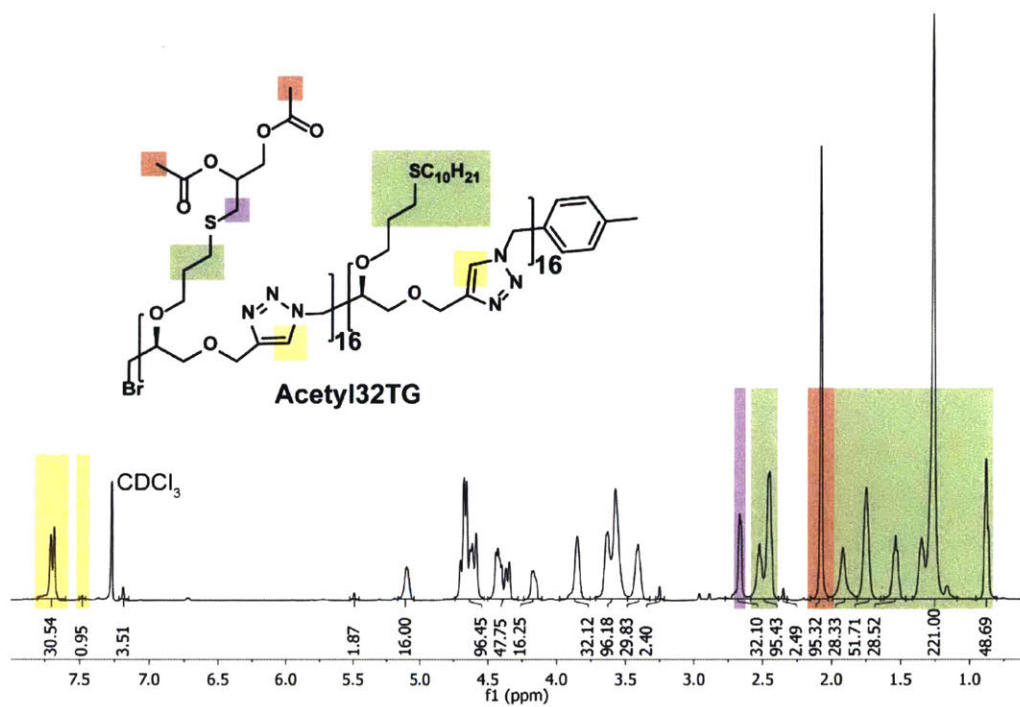


Figure S2.8. ¹H NMR spectrum of **Acetyl32TG**: Acetylated-TG/Decane Block 32mer in CDCl₃

Spectrometric Characterization

Matrix-Assisted Laser Desorption/Ionization Time-of-Flight Mass Spectrometry (MALDI-TOF-MS)

a) 4, 8, and 16

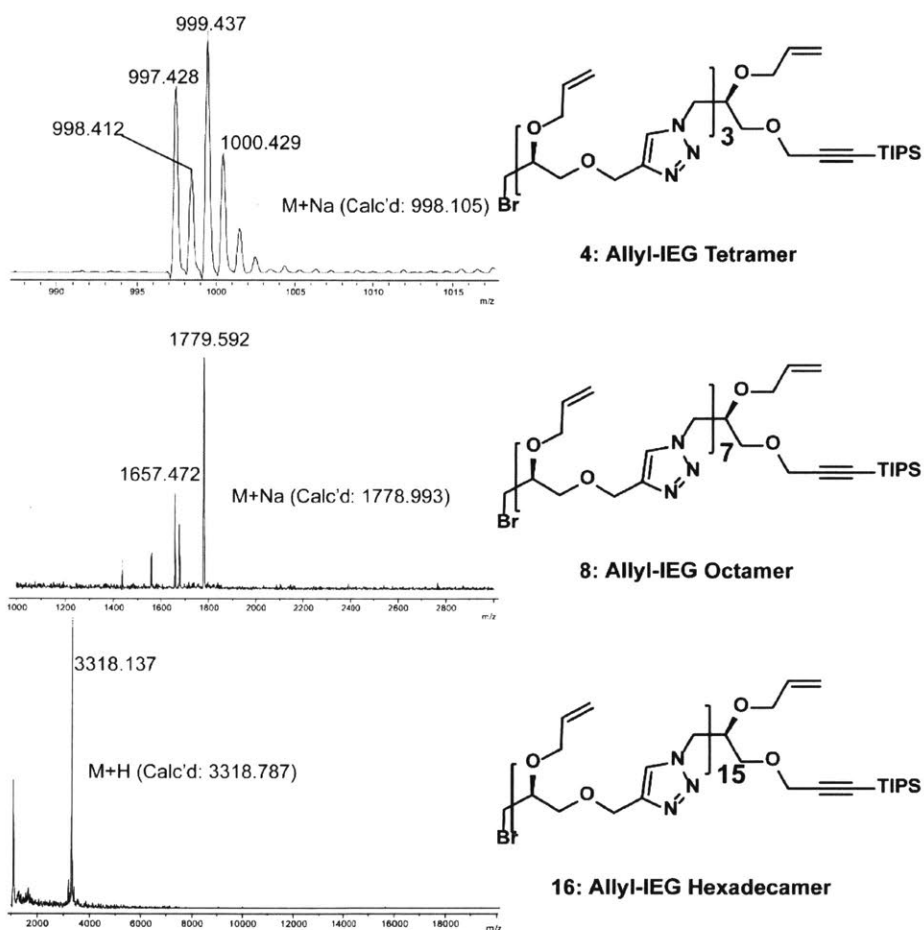


Figure S2.9. Stacked full MALDI spectra for Allyl-IEG oligomers 4, 8, and 16.

b) **32a**, **32TEG**, and **32TG**

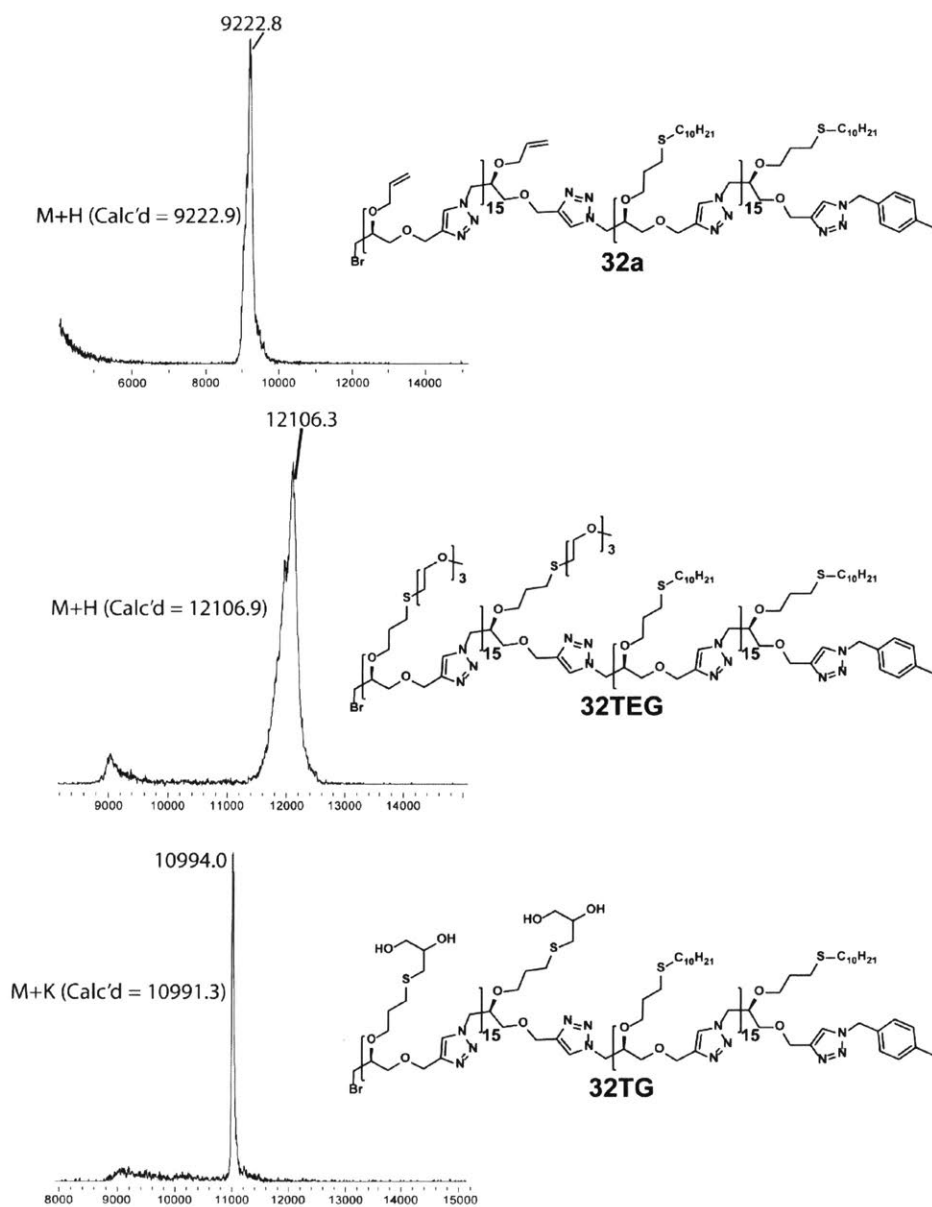


Figure S2.10. Stacked full MALDI spectra for IEG block copolymers **32a**, **32TEG**, and **32TG**.

Extended Gel Permeation Chromatography Traces

a) 2, 4, 8, and 16

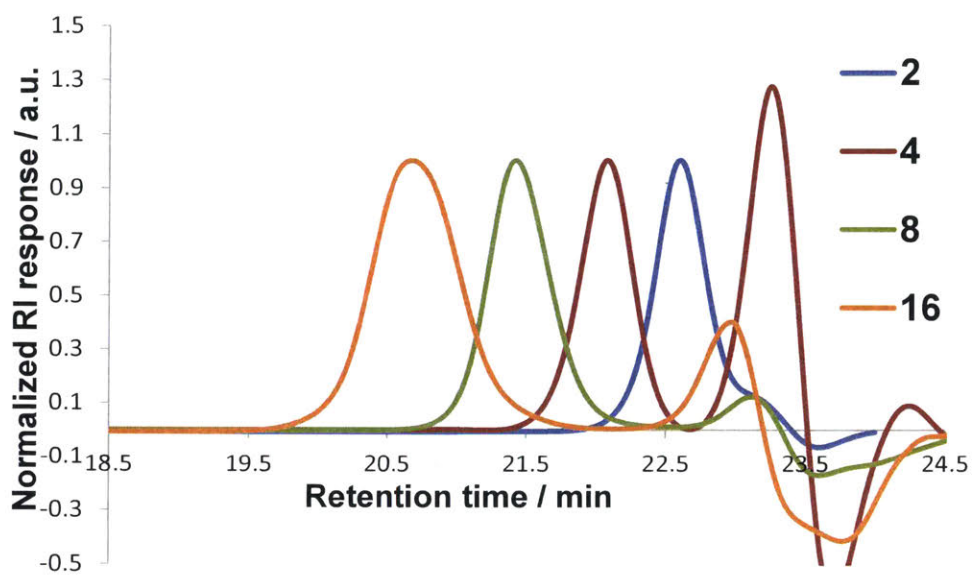


Figure S2.11. Extended GPC traces of Allyl-IEG oligomers 2, 4, 8, and 16.

b) 32a and 32TEG

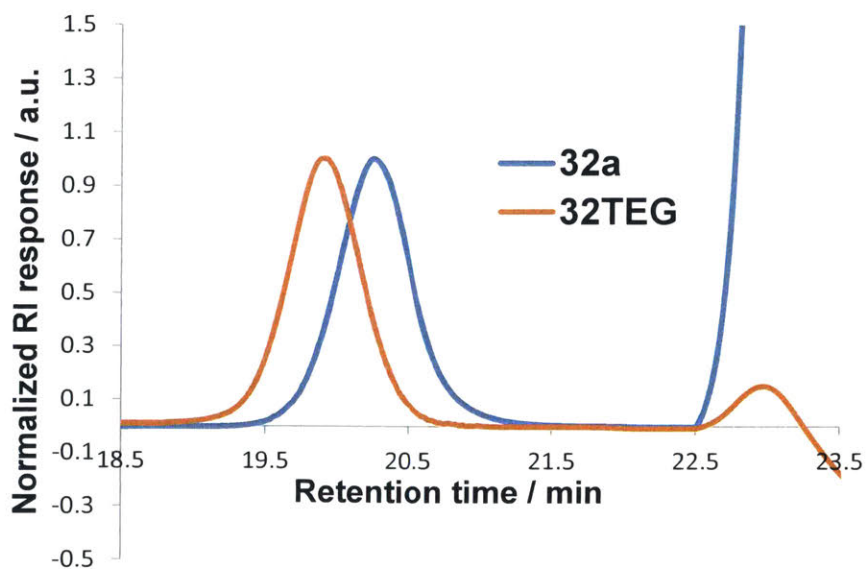


Figure S2.12. Extended GPC traces of IEG block copolymers 32a and 32TEG.

c) 32TG

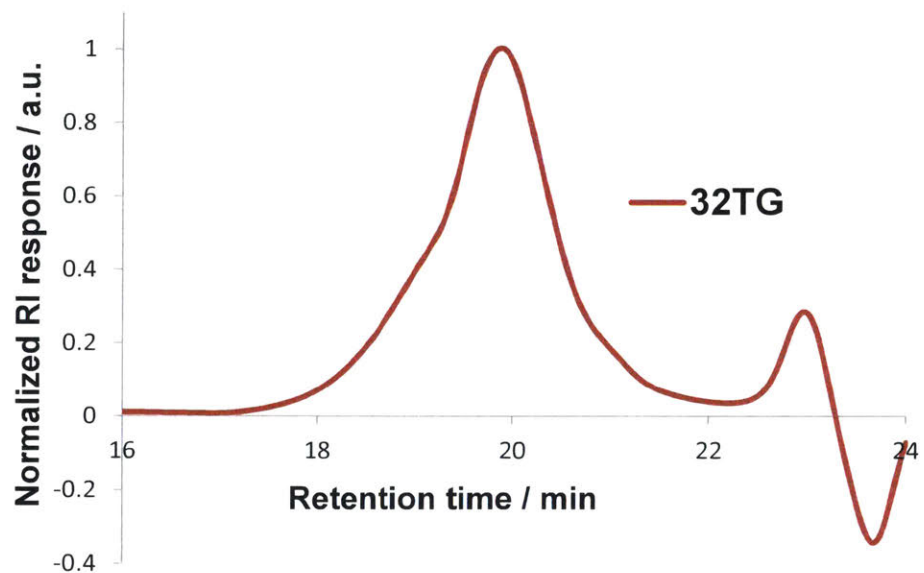


Figure S2.13. Extended GPC trace of IEG block copolymer 32TG.

d) AcetyI32TG

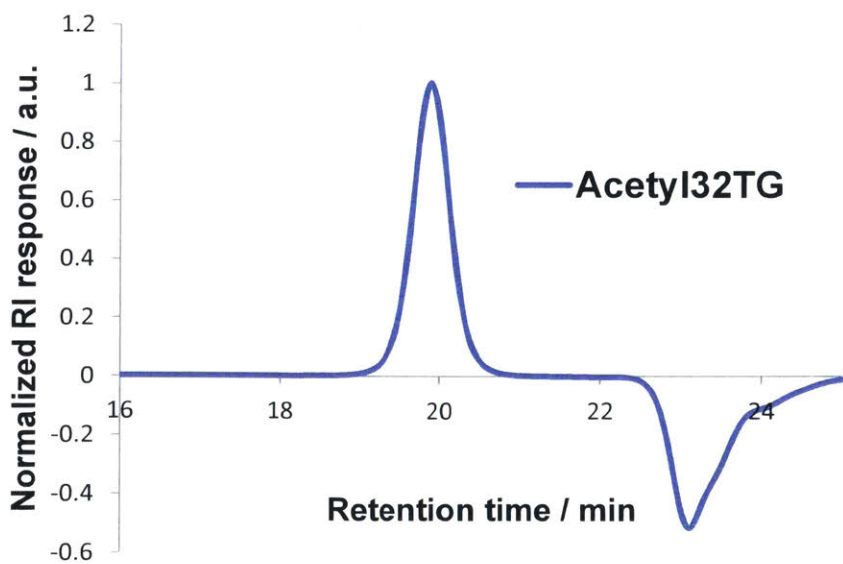


Figure S2.14. Extended GPC trace of IEG block copolymer AcetyI32TG.

Thermal Characterization

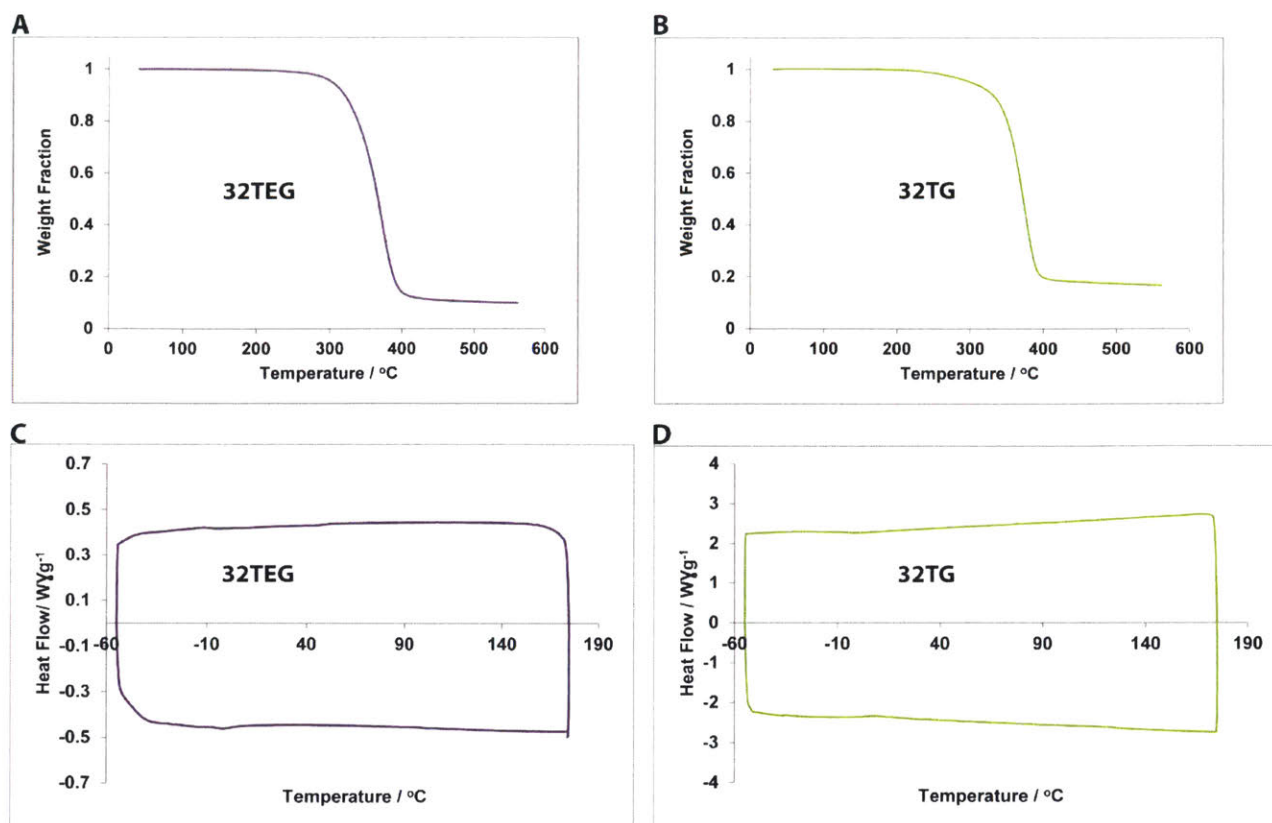


Figure S2.15. (A) TGA trace of **32TEG**. 5% weight loss occurs at 302°C. (B) TGA trace of **32TG**. 5% weight loss occurs at 301°C. (C) DSC trace of **32TEG**. A T_g can be observed at approximately 1°C. (D) DSC trace of **32TG**. A T_g can be observed at approximately 12°C.

Chimera Distance Estimation

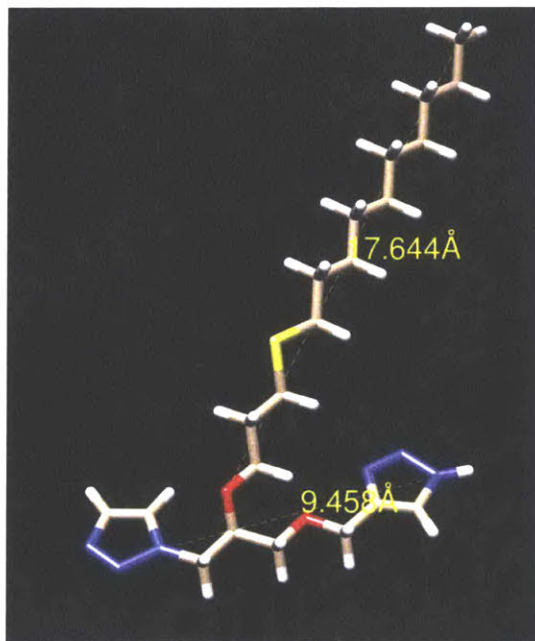


Figure S2.16. Measurements of a fully extended monomer unit in the Chimera software (Pettersen E.F.; Goddard T.D.; Huang C.C.; Couch G.S.; Greenblatt D.M.; Meng E.C.; Ferrin T.E.; J. Comput. Chem. 2004, 13, 1605.) gives a length of 9.457 angstroms for each monomer residue and a length of 17.644 angstroms for the full decane based sidechain.

2.5 References

1. Müllen, K. Molecular defects in organic materials. *Nature Reviews Materials* **2016**, *1*, 15013.
2. Lutz, J.-F.; Lehn, J.-M.; Meijer, E. W.; Matyjaszewski, K. From precision polymers to complex materials and systems. *Nature Reviews Materials* **2016**, *1*, 16024.
3. Robertson, E. J.; Battigelli, A.; Proulx, C.; Man-nige, R. V.; Haxton, T. K.; Yun, L.; Whitlam, S.; Zuckermann, R. N. Design, synthesis, assembly, and engineering of peptoid nanosheets. *Acc. Chem. Res.* **2016**, *49*, 379-389.
4. Sun, H.-J.; Zhang, S.; Percec, V. From structure to function via complex supramolecular dendrimer systems. *Chem. Soc. Rev.* **2015**, *44*, 3900-3923.
5. Percec, V.; Godde, M.; Bera, T. K.; Miura, Y.; Shiyonovskaya, I.; Singer, K. D.; Balagurusamy, V. S. K.; Heiney, P. A.; Schnell, I.; Rapp, A.; Spiess, H.-W.; Hudson, S. D.; Duan, H. Self-organization of supramolecular helical dendrimers into complex electronic materials. *Nature* **2002**, *417*, 384-387.
6. Rosen, B. M.; Wilson, C. J.; Wilson, D. A.; Peterca, M.; Imam, M. R.; Percec, V. Dendron-mediated self-assembly, disassembly, and self-organization of complex systems. *Chem. Rev.* **2009**, *109*, 6275-6540.
7. Rosen, B. M.; Percec, V. Single-electron transfer and single electron transfer degenerative chain transfer living radical polymerization. *Chem. Rev.* **2009**, *109*, 5069-5119.
8. Braunecker, W. A.; Matyjaszewski, K. Controlled/living radical polymerization: features, developments, and perspectives. *Prog. Polym. Sci.* **2007**, *32*, 93-146.
9. Bielawski, C. W.; Grubbs, R. H. Living ring-opening metathesis polymerization. *Prog. Polym. Sci.* **2007**, *32*, 1-29.
10. Lienkamp, K.; Madkour, A. E.; Musante, A.; Nelson, C. F.; Nüsslein, K.; Tew, G. N. Antimicrobial polymers prepared by ROMP with unprecedented selectivity: a molecular construction kit approach. *J. Am. Chem. Soc.* **2008**, *130*, 9836-9843.
11. Johnson, J. A.; Lu, Y. Y.; Burts, A. O.; Xia, Y.; Durrell, A. C.; Tirrell, D. A.; Grubbs, R. H. Drug-loaded, bivalent-bottle-brush polymers by graft-through ROMP. *Macromolecules* **2010**, *43*, 10326-10335.
12. Burts, A. O.; Li, Y.; Zhukhovitskiy, A. Z.; Patel, P. R.; Grubbs, R. H.; Ottaviani, M. F.; Turro, N. J.; Johnson, J. A. Using EPR to compare PEG-branch-nitroxide “bivalent-brush polymers” and traditional PEG bottle-brush polymers: branching makes a difference. *Macromolecules* **2012**, *45*, 8310-8318.
13. Zhang, J., Matta, M.E.; Hillmyer, M.A. Synthesis of sequence-specific vinyl copolymers by regioselective ROMP of multiply substituted cyclooctenes. *ACS Macro Lett.* **2012**, *1*, 1383-1387.
14. Gutekunst, W.R.; Hawker, C. J. A general approach to sequence-controlled polymers using macrocyclic ring opening metathesis polymerization. *J. Am. Chem. Soc.* **2015**, *127*, 8038-8041.
15. Schmidt, B. V. K. J.; Fechler, N.; Falkenhagen, J.; Lutz, J.-F. Controlled folding of synthetic polymer chains through the formation of positionable covalent bridges. *Nature Chem.* **2011**, *3*, 234-238.
16. Zamfir, M.; Lutz, J.-F. Ultra-precise insertion of functional monomers in chain-growth polymerizations. *Nature Commun.* **2012**, *3*, 1138.
17. Kramer, J. W.; Treitler, D. S.; Dunn, E. W.; Castro, P. M.; Roisnel, T.; Thomas, C. M.; Coates, G. W. Polymerization of enantiopure monomers using syndiospecific catalysts: a new

- approach to sequence control in polymer synthesis. *J. Am. Chem. Soc.* **2009**, *131*, 16042-16044.
18. Hibi, Y.; Ouchi, M.; Sawamoto, M. Sequence-regulated radical polymerization with a metal-templated monomer: repetitive ABA sequence by double cyclopolymerization. *Angew. Chem. Int. Ed.* **2011**, *50*, 7434-7437.
 19. Ida, S.; Ouchi, M.; Sawamoto, M. Designer template initiator for sequence regulated polymerization: systems design for substrate-selective metal-catalyzed radical addition and living radical polymerization. *Macromol. Rapid Commun.* **2011**, *32*, 209-214.
 20. Merrifield, R. B. Solid phase peptide synthesis. I. The synthesis of a tetrapeptide. *J. Am. Chem. Soc.* **1963**, *85*, 2149-2154.
 21. Wojcik, F.; Ponader, D.; Mosca, S.; Hartmann, L. Recent advances in solid phase polymer synthesis: polyamides from tailor-made building blocks. *ACS Symp. Ser.* **2014**, *1170*, 85-101.
 22. Al Ouahabi, A.; Amalian, J. A.; Charles, L.; Lutz, J. F. Mass spectrometry sequencing of long digital polymers facilitated by programmed inter-byte fragmentation. *Nature Commun.* **2017**, *8*, 967.
 23. Binauld, S.; Damiron, D.; Connal, L. A.; Hawker, C. J.; Drockenmuller, E. Precise synthesis of molecularly defined oligomers and polymers by orthogonal iterative divergent/convergent approaches. *Macromol. Rapid Comm.* **2011**, *32*, 147-168.
 24. Paynter, O. I.; Simmonds, D. J.; Whiting, M. C. The synthesis of long-chain unbranched aliphatic compounds by molecular doubling. *J. Chem. Soc. Chem. Commun.* **1982**, *20*, 1165-1166.
 25. Zhang, J. S.; Moore, J. S.; Xu, Z. F.; Aguirre, R. A. Nanoarchitectures. 1. Controlled synthesis of phenylacetylene sequences. *J. Am. Chem. Soc.* **1992**, *114*, 2273-2274.
 26. Schumm, J. S.; Pearson, D. L.; Tour, J. M. Iterative divergent/convergent doubling approach to linear conjugated oligomers. A rapid route to a 128 long potential molecular wire. *Angew. Chem. Int. Ed. Engl.* **1994**, *33*, 1360-1363.
 27. Seebach, D.; Ciceri, P. E.; Overhand, M.; Jaun, B.; Rigo, D.; Oberer, L.; Hommel, U.; Amstutz, R.; Widmer, H. Probing the helical secondary structure of short-chain β -peptides. *Helv. Chim. Acta.* **1996**, *79*, 2043-2066.
 28. Takizawa, K.; Tang, C.; Hawker, C. J. Molecularly defined caprolactone oligomers and polymers: synthesis and characterization. *J. Am. Chem. Soc.* **2008**, *130*, 1718-1726.
 29. Huang, B.; Hermes, M. E. J. Homogenous polyesters of predetermined length, composition, and sequence: Model synthesis of alternating glycolic-acid-co-(L)-lactic-acid oligomers. *Polym. Sci. A.* **1995**, *33*, 1419-1429.
 30. Cai, C. Z.; Vasella, A. Oligosaccharide analogues of polysaccharides. Part 6. Orthogonal protecting/activating groups in an improved binomial synthesis of 'acetyleno-oligosaccharides.' *Helv. Chim. Acta.* **1996**, *79*, 255-268.
 31. Liess, P.; Hensel, V.; Schluter, A. D. Oligophenylene rods: a repetitive approach. *Liebigs Annalen.* **1996**, *7*, 1037-1040.
 32. Percec, V.; Asandei, A. D. Macrocyclization overrides the polymer effect in the stabilization of liquid crystalline (LC) phases with a novel odd-even alternation. A demonstration with LC crown ethers. *Macromolecules* **1997**, *30*, 943-952.
 33. Sadighi, J. P.; Singer, R. A.; Buchwald, S. L. Palladium-catalyzed synthesis of monodisperse, controlled-length, functionalized oligoanilines. *J. Am. Chem. Soc.* **1998**, *120*, 4960-4976.

34. Louie, J.; Hartwig, J. F. Discrete high molecular weight triarylamine dendrimers prepared by palladium-catalyzed amination. *Macromolecules* **1998**, *31*, 11695-11696.
35. Williams, J. B.; Chapman, T. M.; Hercules, D. M. Synthesis of discrete mass poly(butylene glutarate) oligomers. *Macromolecules* **2003**, *36*, 3898-3908.
36. Zhou, C. Z.; Liu, T. X.; Xu, J. M.; Chen, Z. K. Synthesis, characterization, and physical properties of monodisperse oligo(p-phenyleneethynylene)s. *Macromolecules* **2003**, *36*, 1457-1464.
37. Binauld, S.; Hawker, C. J.; Fleury, E.; Drockenmuller, E. A modular approach to functionalized and expanded crown ether based macrocycles using click chemistry. *Angew. Chem. Int. Ed.* **2009**, *48*, 6654-6658.
38. Li, X.; Qi, T.; Srinivas, K.; Massip, S.; Maurizot, V.; Huc, I. Synthesis and multibromination of nanosized helical aromatic amide foldamers via segment-doubling condensation. *Org. Lett.* **2016**, *18*, 1044-1047.
39. Barnes, J. C.; Ehrlich, D. J. C.; Gao, A. X.; Leibfarth, F. A.; Jiang, Y.; Zhou, E.; Jamison, T. F.; Johnson, J. A. Iterative exponential growth of sequence-controlled polymers. *Nature Chem.* **2015**, *7*, 810-815.
40. We noticed temperatures past 35 °C led to gradual cyclization of the terminal azide with the neighboring alkene, preventing reaction in the CuAAC coupling reaction. Selected examples of this intramolecular cyclization (ref 41-43): Bennett III, R. B.; Choi, J. R.; Montgomery, W. D.; Cha, J. K. A short, enantioselective synthesis of (-)-swainsonine. *J. Am. Chem. Soc.* **1989**, *111*, 2580-2582.
41. Zhou, Y.; Murphy, P. V. New access to 1-deoxynojirimycin derivatives via azide-alkene cycloaddition. *Org. Lett.* **2008**, *10*, 3777-3780.
42. Hui, B. W.-Q.; Chiba, S. Orthogonal synthesis of isoindole and isoquinoline derivatives from organic azides. *Org. Lett.* **2009**, *11*, 729-732.
43. Campos, L. M.; Killups, K. L.; Sakai, R.; Paulesse, J. M. J.; Damiron, D.; Drockenmuller, E.; Messmore, B. W.; Hawker, C. J. Development of thermal and photochemical strategies for thiol-ene click polymer functionalization. *Macromolecules* **2008**, *41*, 7063-7070.
44. Hoyle, C. E.; Bowman, C. N. Thiol-ene click chemistry. *Angew. Chem. Int. Ed.* **2010**, *49*, 1540-1573.
45. Franz, N.; Menin, L.; Klok, H.-A. A post-modification approach to peptide foldamers. *Org. Biomol. Chem.* **2009**, *31*, 5207-5218.
46. Bates, F. S.; Hillmyer, M. A.; Lodge, T. P.; Bates, C. M.; Delaney, K. T.; Fredrickson, G. H. Multiblock polymers: panacea or Pandora's box. *Science* **2012**, *336*, 434-440.
47. van Genabeek, B.; de Waal, B. F. M.; Gosens, M. M. J.; Pitet, L. M.; Palmans, A. R.; Meijer, E. W. Synthesis and self-assembly of discrete dimethylsiloxane-lactic acid diblock copolymers: dononacotamer and its shorter homologues. *J. Am. Chem. Soc.* **2016**, *138*, 4210-4218.
48. Sun, J.; Teran, A. A.; Liao, X.; Balsara, N. P.; Zuckermann, R. N. Crystallization in sequence-defined peptoid diblock copolymers induced by microphase separation. *J. Am. Chem. Soc.* **2014**, *136*, 2070-2077.
49. Sun, J.; Jiang, X.; Lund, R.; Downing, K. H.; Balsara, N. P.; Zuckermann, R. N. Self-assembly of crystalline nanotubes from monodisperse amphiphilic diblock copoly-peptoid tiles. *Proc. Natl. Acad. Sci.* **2016**, *113*, 3954-3959.

50. Zha, R. H.; de Waal, B. F. M.; Lutz, M.; Teunissen, A. J. P.; Meijer, E. W. End groups of functionalized siloxane oligomers direct block co-polymeric or liquid-crystalline self-assembly behavior. *J. Am. Chem. Soc.* **2016**, *138*, 5693-5698.
51. Rangarajan, P.; Register, R. A.; Fetters, L. J. Morphology of semicrystalline block copolymers of ethylene-(ethylene-alt-propylene). *Macromolecules* **1993**, *26*, 4640-4645.
52. Flory, P. J. Principles of Polymer Chemistry; Cornell University Press: Ithaca, NY, **1953**.
53. Bates, F. S.; Fredrickson, G. H. Block copolymers-designer soft materials. *Physics Today* **1999**, *52*, 32-38.
54. Bang, J.; Jeong, U.; Ryu, D. Y.; Russell, T. P.; Hawker, C. Block copolymer nanolithography: translation of molecular level control to nanoscale patterns. *J. Adv. Mater.* **2009**, *21*, 4769-4792.

Chapter 3.
Stereochemical Sequence Dictates Unimolecular Diblock Copolymer Assembly

This chapter is composed of material adapted from the following publication:

Golder, M. R.†; Jiang, Y.†; Teichen, P. E.; Nguyen, H. V.-T.; Wang, W.; Milos, N.; Freedman, S. A.; Willard, A. P.; Johnson, J. A. Stereochemical sequence dictates unimolecular diblock copolymer assembly. *J. Am. Chem. Soc.* 2018, 140, 1596-1599.

The work in this chapter was a collaborative effort with Matthew R. Golder, Paul E. Teichen, Hung V. T. Nguyen, Wencong Wang, Nicole Milos, and Seth A. Freedman. Matthew R. Golder performed and analyzed the SAXS experiments. Paul E. Teichen ran simulations on the block copolymers. Hung V. T. Nguyen and Matthew R. Golder performed the TEM imaging. Wencong Wang, Nicole Milos, and Seth A. Freedman assisted in the synthesis of the materials. The author designed the synthetic routes and made all the materials. The writing of the chapter was a collaborative effort between Matthew R. Golder and the author.

3.1 Introduction

Chemistry defines stereoisomers as different compounds, and thus, macromolecules that differ by their configuration at one or more stereogenic centers will have different properties. For example, cellulose and starch are stereoisomeric polymers of glucose that have vastly disparate properties and biological functions.¹ In synthetic polymers, the advent of stereoregular α -olefin polymerizations enabled access to polymers with controlled tacticity.² These systems have found commercial utility in the production of high-value polymers such as polypropylene and polybutylene; isotactic, syndiotactic, and atactic polyolefins have varying crystallinities that dictate their mechanical and thermal properties.^{4,5} In addition, mixtures of stereodefined polymers can in some cases form stereocomplexes with unique properties.⁶

Chemists have recently focused on techniques that enable access to polymers of discrete length and/or sequence,⁷⁻¹² which are being actively investigated in energy storage¹³ and biological^{14,15} applications. Despite these advances, the role of stereochemistry in uniform macromolecular systems has received relatively little attention. For example, though the composition, sequence, and dispersity of diblock co-oligomers/polymers have been investigated recently,¹⁶⁻²¹ the role of stereochemistry in uniform block copolymer assembly has not, to our knowledge, been systematically studied. A robust strategy for the synthesis of stereo-chemically pure block copolymers with absolute structural control is a prerequisite for such an endeavor. Herein, we report iterative exponential growth (IEG) methods²²⁻²⁵ that enable the synthesis of a small library of unimolecular stereoisomeric diblock copoly(triazoles) (DPTs). X-ray scattering experiments indicate that the stereochemistry of these DPTs dictates their bulk morphology. These

results are rationalized in terms of a theoretical model system that connects stereochemical sequence to variations in the monomer packing radius. This study confirms that stereochemistry should be considered in the design, synthesis, and applications of precision polymers.

3.2 Results and Discussion

Our syntheses of DPTs via IEG²⁶ rely upon copper-catalyzed azide–alkyne cycloaddition (CuAAC) reactions²⁷ to construct the DPT backbone and thiol–ene addition reactions to install side chain functionalities. Monomers bearing either an azide or a terminal alkyne are derived from glycidyl propargyl ether (GPE) in a divergent fashion (Figure 3.1A). Following CuAAC, triazole **2** is poised for subsequent cycles of orthogonal desilylation (Figure 3.1B, top) and azidification (Figure 3.1B, bottom) before another convergent CuAAC. Repetition of this sequence provides access to 4-mers (**4**, $n = 3$), 8-mers (**8**, $n = 7$), 16-mers (**16**, $n = 15$), etc.

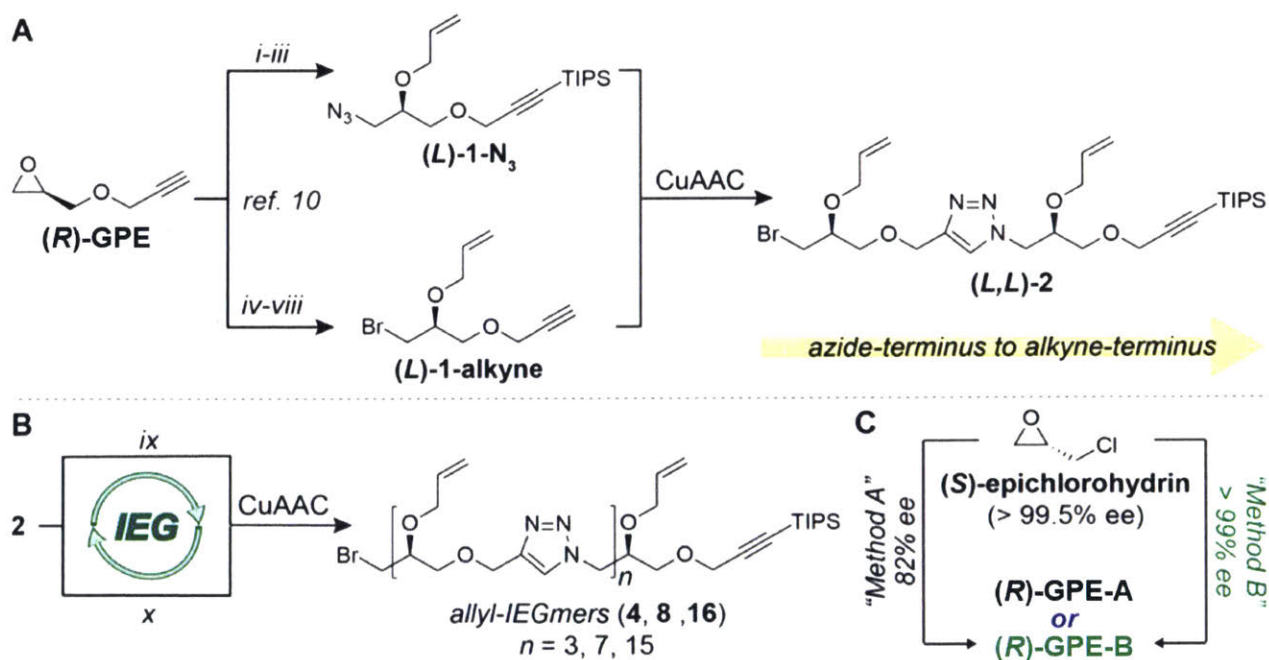


Figure 3.1. (A) IEG Synthesis of Representative Dimer L,L-2^a; (B) IEG Synthesis and Chemical Structure of Allyl-IEGmers^b; (C) Methods for GPE Synthesis^c

^a: (i) *n*-BuLi then TIPS-Cl, THF, -78 °C – rt, 4 h, 85% - 86%; (ii) NaN₃, AcOH, DMF, 70 °C, 80% - 82%; (iii) Allyl-Br, NaH, DMF, 0 °C – rt, 16 h, 70% - 80%; (iv) *t*-BuOH, Mg(ClO₄)₂, rt, 72 h, 91%; (v) Allyl-Br, NaH, DMF, 0 °C – rt, 16 h, 90% – 92%; (vi) H₃PO₄ (85%), rt, 4 h, 78% - 80%, (vii) TsCl, DMAP, Et₃N, CH₂Cl₂, 0 °C – rt, 78% - 84%, (viii) LiBr, DMF, 45 °C, 16 h, 86% - 88%.

^b: (ix) TBAF, THF, 15 min; (x) NaN₃, DMF, 35 °C, 16 h; Typical CuAAC: Cu(MeCN)₄PF₆, TBTA, sodium ascorbate, CH₂Cl₂ or CHCl₃. ^c: Method A (GPE-A). Propargyl alcohol,

TBAHSO₄, pentanes / NaOH (aq); Method B (**GPE-B**): Propargyl alcohol, BF₃·OEt₂ then NaOH, 0 °C – rt, 2 h, 71% - 74%.

The stereogenic centers propagated throughout this IEG sequence are derived from GPE; the enantiomeric excess (ee) of GPE directly impacts the diastereomeric ratio (dr) of each oligomer or polymer synthesized. Our previous route to GPE from commercially available (R)- or (S)-epichlorohydrin (>99.5% ee) using phase-transfer conditions^{24,27,28} (Figure 3.1C, Method A) provided **GPE-A** in 82% ee in our hands (Figure S3.19). This ee would preclude a detailed evaluation of the effect of tacticity on DPT self-assembly. In this work, (R)- or (S)-epichlorohydrin was treated with propargyl alcohol under Lewis acidic conditions to afford secondary alcohol **R1** (see Figure S3.1), which was then exposed to sodium hydroxide, affording GPE-B in > 99% ee in 71% - 74% yield on ca. 40 g scale (Figure 3.1C, Method B).

Chiral HPLC analysis of the four possible stereoisomeric dimers derived from a single cycle of IEG starting from **GPE-B** (**L,L-2B**, **L,D-2B**, **D,L-2B**, **L,L-2B**) and one dimer derived analogously from **GPE-A** (**L,L-2A**) further highlighted the importance of GPE ee (*Note*: in this report, DPTs are drawn from their azide (N) to alkyne (C) terminus; L and D labels are used to indicate the stereochemistry of each unit (wedge and dash bonds, respectively) akin to polypeptide nomenclature). The chromatogram for the dimer derived from **GPE-A** showed three peaks (Figure 3.2A); the dr of the major species **L,L-2A** was 84:16. In contrast, the chromatograms for all four dimers derived from **GPE-B** showed a single peak (>99:1 dr) (Figure 3.2B and Figure S3.20). These results verify the stereochemical purity of dimers derived from **GPE-B**, and suggest that the propagation of stereochemical impurity from **GPE-A** matches what is predicted by the Horeau Principle ($dr_{\text{dimer}} = (0.91)^2 = 83:17$).²⁹ Following this logic, and assuming that diastereomers are not removed during purification, then 5 cycles of IEG starting from **GPE-A** would yield a 32-mer, **32A**, with a theoretical dr for the desired diastereomer of only 4.9:95.1 (Figure S3.21).^{28,30}

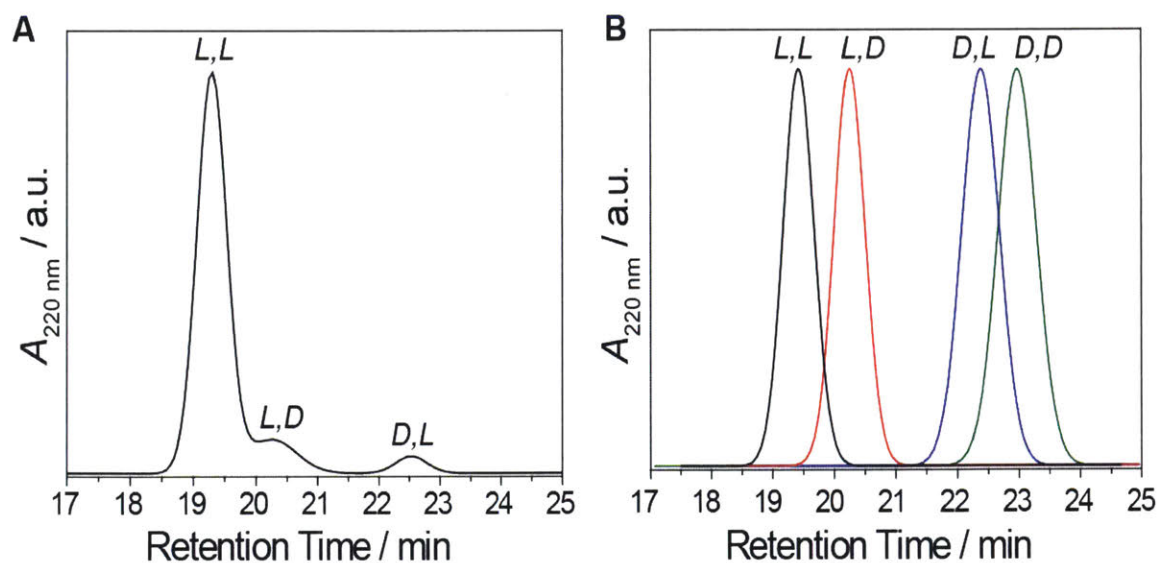


Figure 3.2. Chiral HPLC chromatograms of (A) dimer derived from **GPE-A**, (**L,L-2A**, 84:16 dr) and (B) dimers derived from **GPE-B** (**L,L-2B**, **L,D-2B**, **D,L-2B**, **D,D-2B** >99:1 dr).

With access to **GPE-B**, we synthesized four stereoisomeric DPTs: **L/L-32B**, **D/L-32B**, **alt/L-32B**, and **alt/alt-32B** (Figure 3.3). The structures of each of these compounds were confirmed by ^1H and ^{13}C NMR spectroscopy (Figures S3.2 – S3.18) as well as MALDI-TOF mass spectrometry (Figure S3.22). The thermal properties of all four polymers were analyzed by differential scanning calorimetry: no dramatic differences were observed in the T_g ($-4.8\text{ }^\circ\text{C}$ to $+1.1\text{ }^\circ\text{C}$) between the samples containing at least one homo-chiral (isotactic) block (Figure S3.27A-C). **Alt/alt-32B** displayed a T_g at $-4.1\text{ }^\circ\text{C}$ as well as T_m at $37\text{ }^\circ\text{C}$ and $69\text{ }^\circ\text{C}$ (Figure S3.27D).

The bulk morphologies of **L/L-32B**, **D/L-32B**, **alt/L-32B**, and **alt/alt-32B** were assessed by small-angle X-ray scattering (SAXS) after thermal annealing ($90\text{ }^\circ\text{C}$ for 2 h, $\sim 100\text{ mTorr}$) samples dropcast from a concentrated CH_2Cl_2 solution ($\sim 250\text{--}500\text{ mg/mL}$). Previously, we observed a hexagonal cylinder (HEX) morphology for 32A with 12.6 nm domain spacing (q) and higher-order reflections at $\sqrt{3}q$ and $2q$.²⁷ Broad structure-dependent features were also observed in the high- q region: one corresponding to 3.0 nm was attributed to the average distance between two DPT backbones (α), which reflects the extent of side chain interdigitation; another corresponding to 0.45 nm was attributed to the average monomer-to-monomer distance, which reflects the backbone conformation (β).

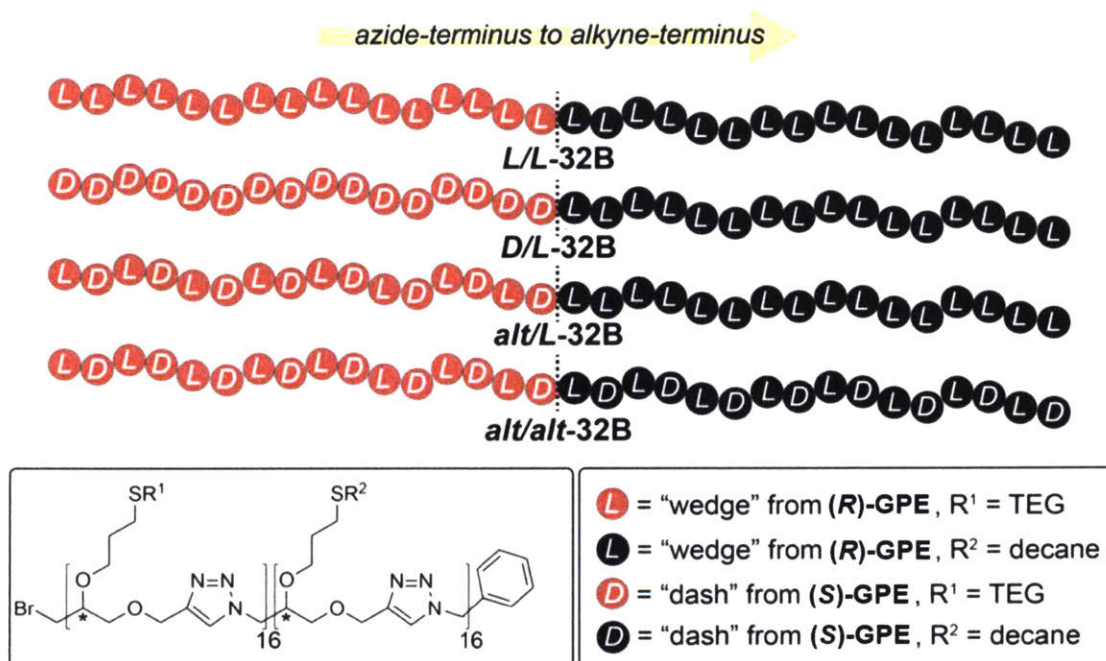


Figure 3.3. Structures of stereoisomeric 32mers accessed by IEG from GPE-B. **The stereochemistry depicted for each repeating unit refers to the stereochemistry of GPE from which that monomer was derived.** GPE = glycidal propargyl ether, TEG = tri(ethylene)glycol.

Here, we hypothesized that interactions between individual monomer units of a given chirality in the **32B** series could lead to changes in bulk morphology. Indeed, the 1D SAXS intensity plots of **L/L-32B**, **D/L-32B**, and **alt/L-32B** (Figure 3.4) were indexed to three distinct phases: double-gyroid (GYR, $d = 13.4$ nm), lamellar (LAM, $d = 13.6$ nm), and HEX ($d = 12.8$ nm), respectively (Figure 3.4A – C). Transmission electron microscopy was also used to confirm the bulk morphology of select **32B** isomers (Figures S3.28 – S3.30). Strikingly, a seemingly subtle reflection of one homochiral TEG block from L to D (i.e., **L/L-32B** to **D/L-32B**) was sufficient to switch from GYR to LAM; a single stereochemical switch at the block interface, for an otherwise completely homochiral structure, leads to a different morphology in this system. In addition, the impact of stereochemical purity is demonstrated by consideration of the effectively atactic **32A**, which produces a morphology that is more similar to **alt/L-32B** (HEX, $d = 12.6$ nm and 12.8 nm, respectively) than its target structure: **L/L-32B** (GYR, $d = 13.4$ nm). Analysis of the WAXS regions for these same three samples revealed different backbone-to-backbone spacings ($\alpha = 3.02 - 3.06$ nm) but constant monomer-to-monomer distances ($\beta = 0.44$ nm), which suggests that the

deviations observed in the domain spacings observed (12.8 – 13.6 nm) are likely due to stereochemistry-driven changes in the extent of sidechain interdigitation.

We observed a difference in the 1D SAXS/WAXS intensity plots for **alt/alt-32B** (Figure 3.4D) compared to the other **32B** DPTs, which reflects the DSC results discussed above. Rather than a sharp principle peak in the low- q region (Figure 3.4A – 3.4C), **alt/alt-32B** displayed a broad principle peak (16.3 nm domain spacing) without any higher order peaks, which is indicative of weak long-range order. In addition, sharp peaks were observed at high q values (2.28 nm domain spacing) that we attribute to crystallization of the decane sidechains. An estimation of $T_{ODT} = 50$ °C – 60 °C for **L/L-32B**, **D/L-32B**, and **alt/L-32B** (Figure S3.31), which is lower than the T_m for **alt/alt-32B** (as assessed by DSC and VT-SAXS, Figures S3.27D and S3.31), suggests that the initial onset of crystallization prevents subsequent formation of order via phase-separation. The bulk phase behavior of **alt/alt-32B** resembles recent studies from Zuckermann and coworkers on polypeptoid self-assembly where side-chain crystallization, rather than bulk phase separation, leads to lamellae with small domain spacings.^{9,16} Similarly, Meijer and co-workers recently reported on oligodimethylsiloxane-*b*-oligo(L)lactide macromolecules that crystallize and assemble into lamellae.^{19,31} Here again, our results definitively show how stereochemistry alone can lead to dramatic changes in DPT assembly, switching from crystalline to amorphous materials.

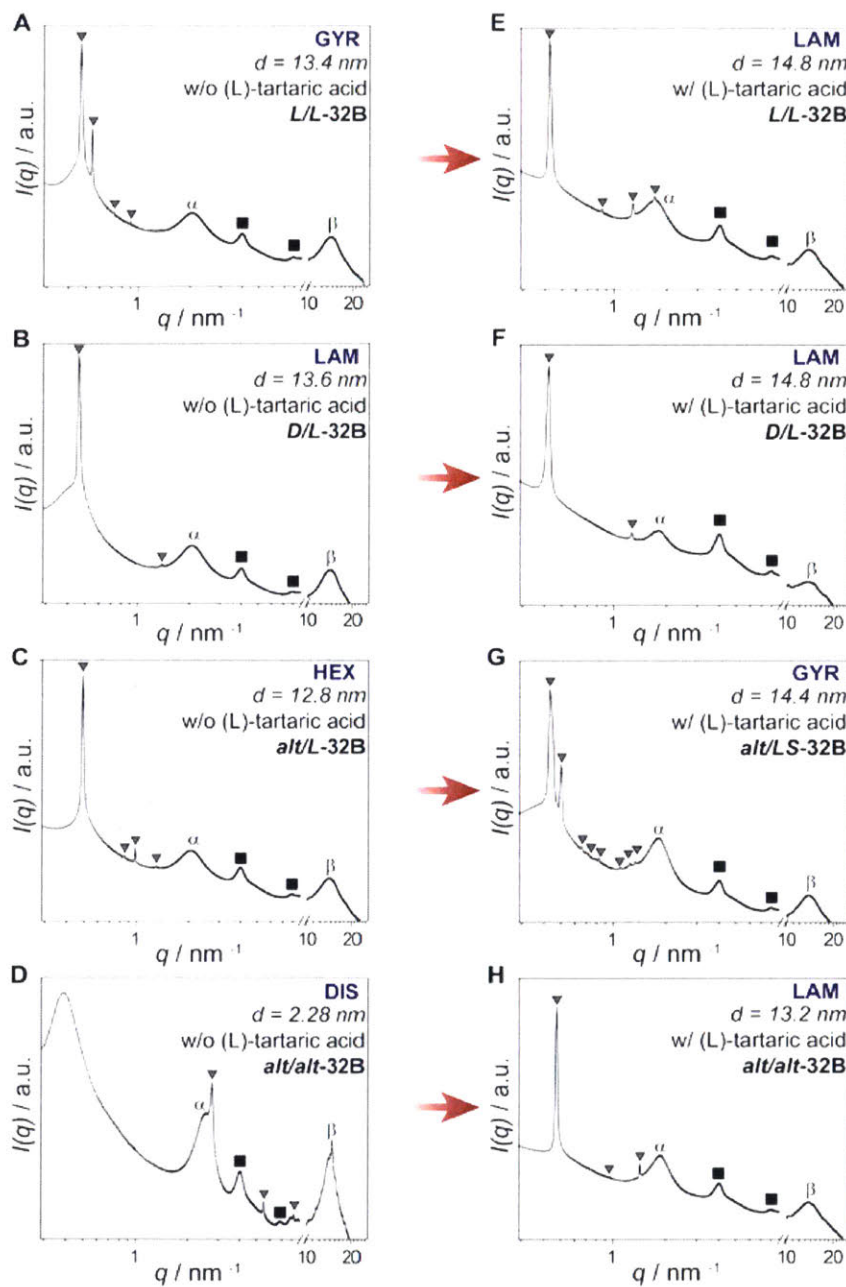


Figure 3.4. 1D intensity SAXS and WAXS plots for stereoisomeric 32Bs with or without (L)-tartaric acid addition. SAXS = small angle X-ray scattering, WAXS = wide-angle X-ray scattering, GYR = gyroid, LAM = lamellar, HEX = hexagonal cylinder. ■ = scattering from Kapton.

Small-molecule additives are often used to modulate the phase behavior of diblock copolymers.^{32,33} To investigate how chiral additives might impact the assembly of our chiral DPTs, we doped **32B** samples with super-stoichiometric quantities (16 equiv, ca. 20 wt%) of (L)-tartaric

acid in an attempt to selectively swell the hydrophilic (TEG) block and thus access new morphologies through horizontal translation across the diblock copolymer phase diagram (Figure 3.4E – G). Addition of (L)-tartaric acid induced phase transitions from GYR to LAM (**L/L-32B**) and HEX to GYR (**alt/L-32B**) with a concomitant increase in domain spacing (14.4 nm – 14.8 nm) and backbone-to-backbone spacing ($\alpha = 3.46 - 3.63$ nm) (\square remains unchanged), which suggests differing sidechain interdigitation due to the additive. These results are consistent with a small modification of volume fraction in a sensitive region of the phase diagram. Interestingly, **D/L-32B** remained lamellar (14.8 nm domain spacing, $\alpha = 3.47$ nm), presumably due to the large fraction of phase space occupied by LAM. Hence, while **L/L-32B** and **D/L-32B** assemble into different morphologies in the absence of additives, they co-occupy the largest region of phase-space upon exposure to (L)-tartaric acid. Lastly, blending of (L)-tartaric acid with **alt/alt-32B** suppressed crystallization and induced long-range order to provide a lamellar structure (13.2 nm domain spacing, $\alpha = 3.36$ nm).

The observed dependence of DPT phase morphology on stereochemical sequence indicates that stereochemistry plays a role in mediating the inter- and intramolecular interactions within these copolymers. Stereogenic centers and their sidechains occupy volumes with specific shapes that constrain their external interactions. The effect of these constraints on phase morphology can be understood in terms of a traditional diblock copolymer phase diagram, which describes how phase morphology depends on the block volume fraction, f , and χ . These parameters depend on the details of the monomer-monomer interactions and how they differ between monomers of different block type. These differences and their effect on phase morphology can be modeled with simulations of simple bead-and-spring diblock copolymers.

Herein, we have used molecular dynamics simulations of a bead-and-spring diblock copolymer model to explore the effect of chirality on phase morphology.^{34,35} The simulations include a condensed phase melt of model polymers that each consist of 32 individual monomers organized into two blocks, with 16 A-type monomers (representing the decane sidechains in our DPTs) and 16 B-type monomers (representing the TEG sidechains in our DPTs). Along with its chemical identity (i.e., A or B), each monomer is assigned a chirality, either **L** or **D**, which results in four distinct monomer types, i.e., (**L**)-A, (**D**)-A, (**L**)-B, and (**D**)-B. The non-bonded monomer-monomer interactions are described using a Lennard-Jones-like pair potential characterized by an interaction diameter, σ , and an interaction energy, ϵ . The values of these model parameters depend

on the identity of the monomers involved in the interaction. To describe the interaction energy, we use a standard symmetric diblock copolymer model for which $\epsilon_{AA} = \epsilon_{BB} = 1$ (in reduced units) and $\epsilon_{AB} = \epsilon_{BA} = 1 + \gamma$, indicating that AB interactions are less favorable than AA or BB interactions. In our model, γ denotes the extent of disruptive forces between chemically dissimilar blocks.

We simulated the phase behavior of diblock copolymer melts with a variety of different stereochemical sequences; Figure 3.4 contains the results of simulations carried out on six different A/B diblock copolymer melts: isotactic/syndiotactic (i.e. **alt/L-32B**), isotactic/di-syndiotactic (iso/disyn), isotactic/atactic (iso/ran), syndiotactic/di-syndiotactic (syn/disyn), syndiotactic/syndiotactic (i.e. **alt/alt-32B**), and (di-syndiotactic/di-syndiotactic (disyn/disyn). We differentiate phase morphologies based on the radial distribution function, $g(r)$, computed for monomers of the same block-type. The length scale over which $g(r)$ decays to unity roughly indicates the size of block domains within the melt.

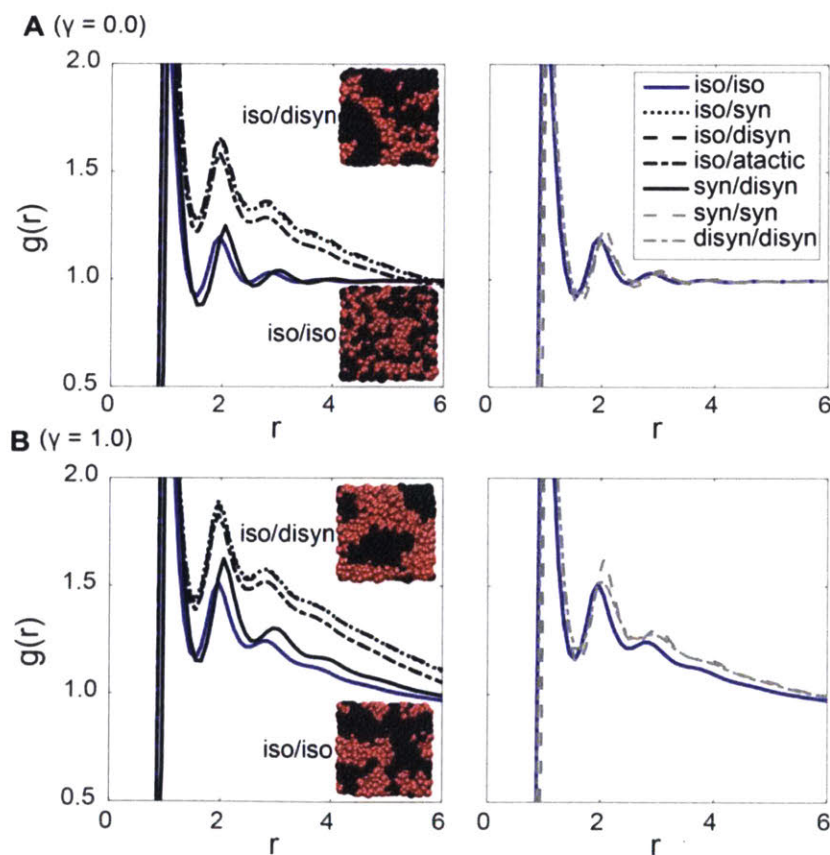


Figure 3.5. The radial distribution function, $g(r)$, as a function of length (r) computed for monomers of similar block type, from simulations of model A/B diblock copolymers with different stereochemical characteristics. Panels on the right-hand side contains simulation snapshots

of A/B copolymer melts, with black and red beads representing the positions of A-type and B-type monomers, respectively. These snapshots serve to illustrate qualitative differences in the morphology of the simulated systems.

As Figure 3.5 illustrates, the phase behavior of our simulated systems depends on stereochemical sequence. We observe that systems with one isotactic block and one block of mixed stereochemistry tend to form phases with block domains that are more extended than those in systems with both blocks isotactic or syndiotactic. We observe these differences for the case where monomer interaction energies are block independent ($\gamma = 0$), and also when A-B interactions are directly penalized ($\gamma = 1$).

The results in Figure 3.5 suggest that effective variations in interaction radius arising from stereochemical mismatch can affect phase morphology across a range of different diblock copolymer compositions. In systems with relatively low degrees of polymerization that are located in a region of the phase diagram that includes several nearby morphologies, stereochemistry can significantly influence bulk properties. The equilibrium phases of mismatched stereochemistries are significantly different than those of purely isotactic copolymers, but matched stereochemistries do not exhibit the same shift in the order-disorder transition.

3.3 Conclusion

Despite the fact that biological polymers are chiral and that tacticity has an overwhelming impact on the physical properties of synthetic polymers, little effort has been made to elucidate the underpinnings of stereochemistry in unimolecular synthetic polymers. This work highlights the utility of unimolecular DPT synthesis via IEG and conclusively demonstrates how chirality impacts self-assembly in this emerging class of polymers. To our knowledge, this work provides the first empirical and theoretical accounts of the importance of diastereomeric interactions in unimolecular diblock copolymer self-assembly, proving that it is possible to modulate bulk self-assembly solely through careful stereochemical manipulations. In turn, these results outline the requisite framework for the rationale design of even more elaborate unimolecular systems for specific advanced applications.

3.4 Supplementary Information

General Considerations

Unless otherwise noted, all reagents were purchased from commercial suppliers and used as supplied. Degassed, anhydrous tetrahydrofuran (THF) and dichloromethane (DCM) were obtained by filtration through alumina according to the methods described by Grubbs (JC Meyer) (Pangborn, A. B.; Giardello, M. A.; Grubbs, R. H.; Rosen, R. K.; Timmers, F. J. *Organometallics* 1996, 15, 1518.). Anhydrous dimethylformamide (DMF) and *tert*-butyl alcohol (*t*-BuOH) were purchased from Sigma Aldrich and was used as received. All moisture sensitive reactions were carried out under an inert atmosphere of nitrogen using standard syringe/septa techniques. Column chromatography was carried out using ZEOprep 60 HYD silica gel (40-63 μm). Automated flash chromatography was conducted using a Biotage Isolera One. 365 nm UV light for thiol-ene addition chemistry was sourced from a VWR International supplied UV-AC hand lamp with two 6-watt UV tubes, one for 254 nm and one for 365 nm wavelengths.

GPC-MALLS characterization was performed on an Agilent 1260 LC system equipped with a Wyatt T-rEX refractive index (dRI) detector and Wyatt DAWN HELEOS 18 angle light scattering detector. Samples were run on two Agilent PLgel 5 μm MIXED-C GPC columns in series at a temperature of 60 $^{\circ}\text{C}$ and flow rate of 1 mL/min with dimethyl formamide (DMF) containing 0.025 M LiBr as the eluent.

^1H nuclear magnetic resonance (^1H -NMR) and ^{13}C nuclear magnetic resonance (^{13}C -NMR) spectra were recorded on a Bruker AVANCE-400 MHz NMR spectrometer, VARIAN Inova-500 MHz NMR spectrometer, or a JEOL 500MHz NMR spectrometer. Spectra were analyzed on MestReNova NMR software. Chemical shifts are expressed in parts per million (ppm); splitting patterns are designated as s (singlet), d (doublet), t (triplet), m (multiplet), and br (broad); and coupling constants, J , are reported in hertz (Hz).

High-resolution mass spectra (HRMS) were obtained on a Bruker Daltonics APEXIV 4.7 Tesla Fourier Transform Ion Cyclotron Resonance Mass Spectrometer (FT-ICR-MS) using an electrospray ionization source (ESI) at the MIT Department of Chemistry Instrumentation Facility (DCIF).

Chiral high-performance liquid chromatography (HPLC) was performed on an Agilent 1260 or an Agilent 1290 Infinity II system using a mixture of hexanes and isopropanol.

Matrix-assisted laser desorption ionization time-of-flight (MALDI-TOF) mass spectra were obtained at the MIT Koch Institute Biopolymers and Proteomics Core Facility on a Bruker MicroFlex using sinapinic acid as the matrix.

Preparative gel-permeation chromatography (prep-GPC) was performed on a JAI Preparative Recycling HPLC (LaboACE-LC-5060) system equipped with either 2.5HR and 2HR columns in series (20 mm ID x 600 mm length) or 2.5H and 2H columns in series (40 mm ID x 600 mm length) using CHCl_3 as the eluent.

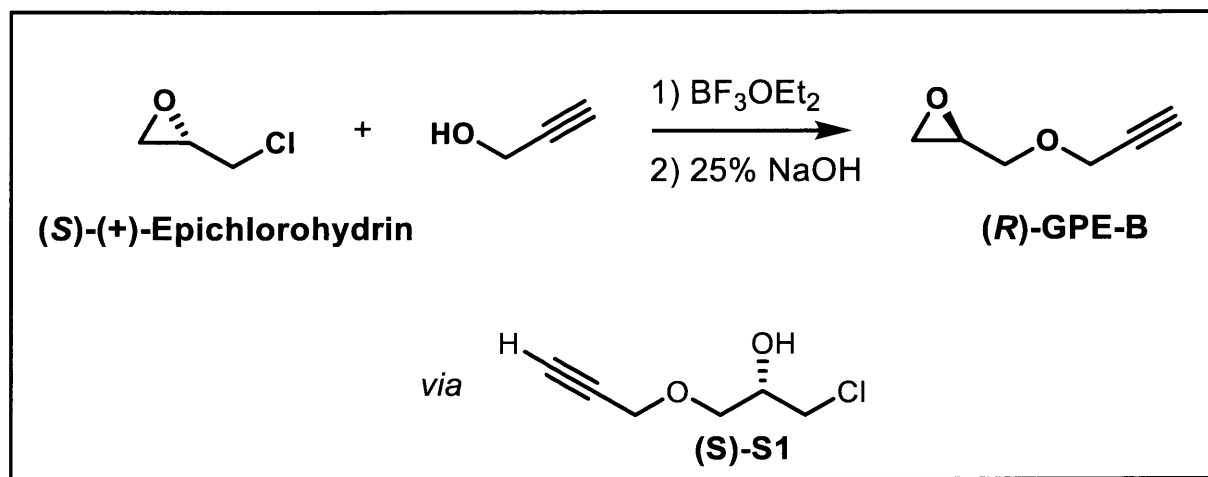
Differential scanning calorimetry (DSC) was performed on a TA Instruments Discovery DSC, where each sample was run with a Tzero aluminum pan sealed with a hermetic lid. Determination of the glass transition temperature, with the exception of sample *L/alt-32B*, was taken from the 3rd heating cycle of a run where the sample was cycled at a rate of 10 °C per minute from -40 °C to 150 °C. Sample *L/alt-32B* was heated to 90 °C (~ 100 mbar), cooled overnight to room temperature in a vacuum oven, and left to sit for 3 days before DSC measurement. The 1st heating cycle of the DSC run was evaluated where the sample was heated at a rate of 10 °C per minute from -30 °C to 160 °C.

Small angle X-ray scattering (SAXS) data were collected at beamline 12-ID-B at the Advanced Photonic Source (APS) at Argonne National Laboratory. The energy of the beam was 14 keV, which corresponds to a wavelength of 0.08857 nm. All SAXS samples were loaded into the center of Bokers aluminum washers (0.900 ± 0.005 " OD x 0.079 ± 0.005 " ID) with 0.40 ± 0.04 " thickness. SAXS samples were prepared by drop-casting by a 250 mg/mL – 500 mg/mL dichloromethane (DCM) solution of the desired polymer. For all samples, the DCM was allowed to evaporate at ambient temperature, annealed at 90 °C under vacuum for 2 h, and were allowed to cool to room temperature overnight under reduced pressure (~ 100 mTorr).

TEM images were acquired using a FEI Tecnai Multipurpose TEM (G2 Spirit TWIN, 120 kV) at the MIT Center for Materials Science and Engineering. A solution (5 μL) of polymer (ca. 20 mg/mL in DMF) was dropped onto a carbon film-coated 200-mesh copper grid (Electronic Microscopy Sciences) placed on a piece of parafilm. The sample was allowed to dry at room temperature for 2 d. Then, the samples were negatively stained by dropping 5 μL of 2 wt% uranyl acetate (Electronic Microscopy Sciences) onto the grid. After 10 minutes, the residual uranyl acetate solution was carefully wicked away using the edge of a Kimwipe. The samples were allowed to fully dry (ca. 1 d) before analysis.

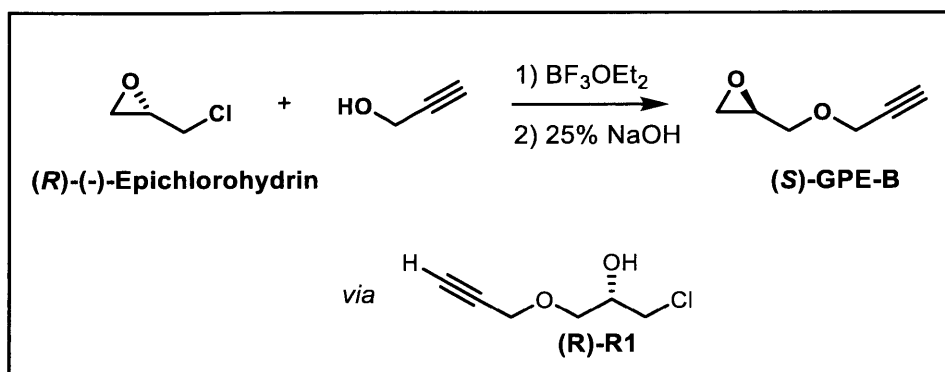
Synthetic Procedures

1. (R)-GPE-B and (S)-GPE-B



(R)-GPE-B: BF₃·OEt₂ (3.83 g, 3.33 mL, 27.0 mmol) was added to propargyl alcohol (93.5 mL, 1620 mmol) in a 500 mL RBF. The solution was cooled to 0 °C in an ice bath. (S)-epichlorohydrin (50.0 g, 42.4 mL, 540 mmol) was added dropwise by addition funnel. Care was taken to keep the solution from heating up excessively. After complete addition of (S)-epichlorohydrin, the reaction was warmed to room temperature and left to react for 2 hours. Afterwards, DCM (400 mL) was added to the reaction mixture which was extracted with distilled water (4 x 200 mL) to remove BF₃·OEt₂ and the remaining propargyl alcohol. DCM was removed by rotary evaporation. A 25% NaOH solution (44 g of NaOH in 130 mL water) was prepared and cooled to room temperature. This solution was added to the concentrated crude secondary alcohol (**S1**, see Figure S3.1) and stirred for 15 minutes. Water (200 mL) was added followed by 400 mL of DCM. The organic layer was separated and extracted with water (200 mL). The organic layer was dried over sodium sulfate and concentrated to yield a yellowish liquid. The product was purified by distillation to yield **(R)-GPE-B** as a colorless liquid (45 g, 0.40 mmol, 74% yield). HRMS-ESI for **(R)-GPE-B**; Calcd for C₆H₈O₂: m/z = 130.0868 [M + NH₄]⁺; Found: 130.0862 [M + NH₄]⁺. ¹H NMR (500 MHz, CDCl₃):

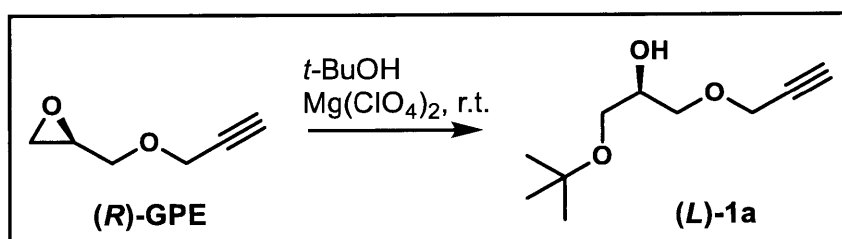
δ (ppm) 4.19 (t, $J = 2.4$ Hz, 2H), 3.80 (dd, $J = 11.4, 2.9$ Hz, 1H), 3.46 (dd, $J = 11.3, 5.9$ Hz, 1H), 3.19–3.10 (m, 1H), 2.78 (dd, $J = 5.2, 4.1$ Hz, 1H), 2.61 (dd, $J = 5.1, 2.6$ Hz, 1H), 2.43 (t, $J = 2.3$ Hz, 1H). ^{13}C NMR (125 MHz, CDCl_3): δ (ppm) 79.2, 74.8, 70.3, 58.4, 50.4, 44.2.



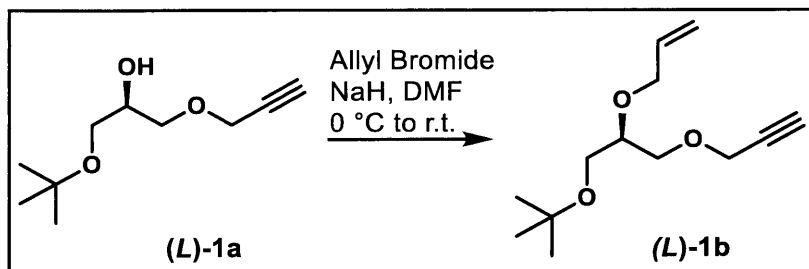
(S)-GPE-B: $\text{BF}_3 \cdot \text{OEt}_2$ (3.83 g, 3.33 mL, 27.0 mmol) was added to propargyl alcohol (93.5 mL, 1620 mmol) in a 500 mL RBF. The solution was cooled to 0 °C in an ice bath. (R)-epichlorohydrin (50.0 g, 42.4 mL, 540 mmol) was added slowly dropwise by addition funnel. Care was taken to keep the solution from heating up excessively. After complete addition of (R)-epichlorohydrin, the reaction was warmed to room temperature and left to react for 2 hours. Afterwards, DCM (400 mL) was added to the reaction mixture which was extracted with distilled water (4 x 200 mL) to remove $\text{BF}_3 \cdot \text{OEt}_2$ and the remaining propargyl alcohol. DCM was removed by rotary evaporation. A 25% NaOH solution (44 g of NaOH in 130 mL water) was prepared and cooled to room temperature. This solution was added to the concentrated crude secondary alcohol (**S1**, see Figure S3.1) and stirred for 15 minutes. Water (200 mL) was added followed by DCM (400 mL). The organic layer was isolated and extracted with another water (200 mL). The organic layer was dried over sodium sulfate and concentrated to yield a yellowish liquid. The product was purified by distillation to yield (S)-GPE-B as a colorless liquid (43 g, 0.38 mmol, 71% yield). HRMS-ESI

for **(S)-GPE-B**; Calcd for C₆H₈O₂: m/z = 130.0868 [M + NH₄]⁺; Found: 130.0861 [M + NH₄]⁺. ¹H NMR (500 MHz, CDCl₃): δ(ppm) 4.19 (t, *J* = 2.4 Hz, 2H), 3.80 (dd, *J* = 11.4, 2.9 Hz, 1H), 3.46 (dd, *J* = 11.3, 5.9 Hz, 1H), 3.19–3.10 (m, 1H), 2.78 (dd, *J* = 5.2, 4.1 Hz, 1H), 2.61 (dd, *J* = 5.1, 2.6 Hz, 1H), 2.43 (t, *J* = 2.3 Hz, 1H). ¹³C NMR (125 MHz, CDCl₃): δ(ppm) 79.2, 74.7, 70.3, 58.4, 50.5, 44.2.

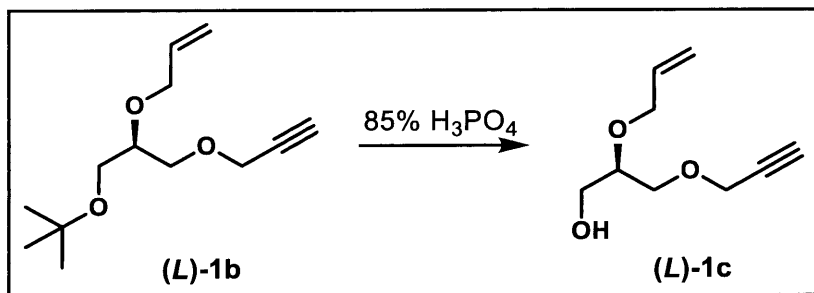
2. (*L*)- and (*D*)-1-alkyne



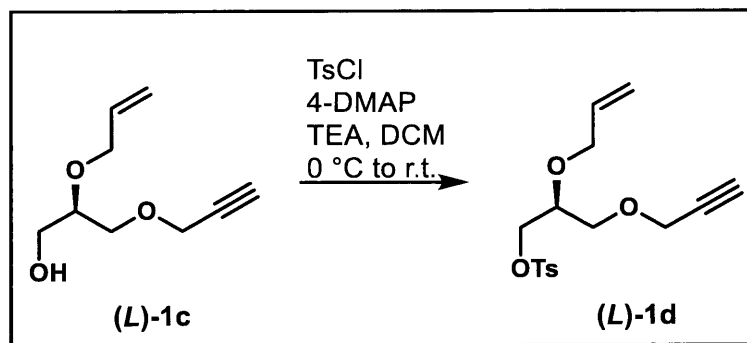
(L)-1a: Under an N₂ atmosphere, dry *t*-BuOH (198 g, 2.68 mol) was added to **(R)-GPE-B** (60.0 g, 536 mmol) in an oven-dried 500 mL RBF that was immersed in a room temperature water bath. Next, Mg(ClO₄)₂ (12.0 g, 53.6 mmol) was added portion-wise into the stirring reaction mixture. This mixture was allowed to react for 72 h. After completion, water (500 mL) was added to the solution followed by extraction with DCM (3 x 1000 mL). The organic layers were combined, extracted with water (500 mL), dried over Na₂SO₄, and concentrated under vacuum. Column chromatography (50% hexanes/DCM to 100% DCM) yielded the product (91 g, 490 mmol, 91% yield). HRMS-ESI for **(L)-1-tBu**; Calcd for C₁₀H₁₈O₃: m/z = 204.1594 [M + NH₄]⁺; Found: 204.1603 [M + NH₄]⁺. ¹H NMR (500 MHz, CDCl₃): δ(ppm) 4.20 (d, *J* = 2.3 Hz, 2H), 3.91 (ddd, *J* = 10.7, 6.2, 4.5 Hz, 1H), 3.62 (dd, *J* = 9.7, 4.5 Hz, 1H), 3.56 (dd, *J* = 9.7, 6.0 Hz, 1H), 3.44 (dd, *J* = 9.1, 4.5 Hz, 1H), 3.38 (dd, *J* = 9.0, 6.5 Hz, 1H), 2.51 (d, 1H), 2.44 (t, *J* = 2.4 Hz, 1H), 1.20 (s, 9H). ¹³C NMR (125 MHz, CDCl₃): δ(ppm) 79.2, 74.5, 72.6, 70.8, 69.1, 62.5, 58.0, 27.0.



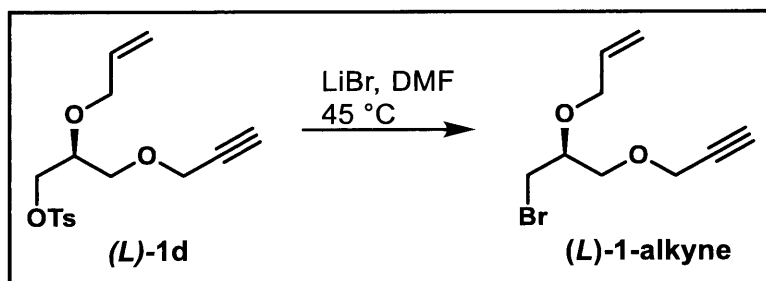
(L)-1b: Under an N₂ atmosphere, dry DMF (500 mL) and allyl bromide (48.6 g, 402 mmol, 33.1 mL) were added to **(L)-1a** (49.9 g, 268 mmol) in an oven-dried 1000 mL RBF. The reaction mixture was cooled to 0 °C and NaH (11.8 g, 295 mmol, 60% dispersion in mineral oil) was added portion-wise into the stirring reaction mixture. The mixture was allowed to gradually warm to room temperature and left to react overnight. After completion, DMF was removed under reduced pressure. Water (300 mL) was added to the solution which was extracted with DCM (3 x 400 mL). The organic layers were combined, dried over Na₂SO₄, and concentrated under vacuum. Column chromatography (80% hexanes/DCM to 50% hexanes/DCM) yielded the product (54 g, 24 mmol, 90% yield). HRMS-ESI for **(L)-1b**; Calcd for C₁₃H₂₂O₃: m/z = 244.1907 [M + NH₄]⁺; Found: 244.1908 [M + NH₄]⁺. ¹H NMR (500 MHz, CDCl₃): δ(ppm) 5.93 (ddt, *J* = 16.1, 10.4, 5.7 Hz, 1H), 5.30 (d, *J* = 17.1 Hz, 1H), 5.15 (d, *J* = 10.4 Hz, 1H), 4.19 (d, *J* = 2.6 Hz, 2H), 4.15 (m, 2H), 3.68 (m, 1H), 3.60 (m, 2H), 3.44 (d, *J* = 5.0 Hz, 2H), 2.41 (t, *J* = 2.2 Hz, 1H), 1.18 (s, 9H). ¹³C NMR (125 MHz, CDCl₃): δ(ppm) 135.1, 116.4, 79.6, 77.2, 74.4, 72.7, 71.0, 69.8, 62.5, 58.3, 27.3.



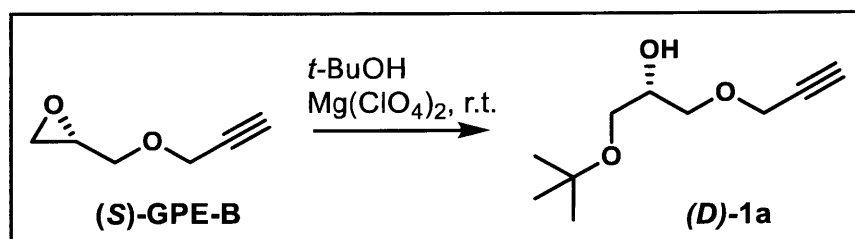
(L)-1c: Under an N₂ atmosphere, 85% H₃PO₄ (200. g, 2.04 mol) was poured onto **(L)-1b** (52.0 g, 230. mmol) in a 500 mL RBF. The reaction mixture was stirred and left to react at room temperature for 4 h. After completion, water (500 mL) was added to the solution followed by extraction with DCM (3 x 500 mL). The organic layers were combined, dried with Na₂SO₄, and concentrated under vacuum. Column chromatography (50% hexanes/DCM to 2% MeOH/DCM) yielded the product (31 g, 180 mmol, 80% yield). HRMS-ESI for **(L)-1c**; Calcd for C₉H₁₄O₃: m/z = 188.1281 [M + NH₄]⁺; Found: 188.1284 [M + NH₄]⁺. ¹H NMR (500 MHz, CDCl₃): δ(ppm) 5.94 (ddt, 16.1, 10.4, 5.5 Hz, 1H), 5.29 (dd, *J* = 17.5, 1.5 Hz, 1H), 5.20 (dd, *J* = 10.3, 1.2 Hz, 1H), 4.19 (overlap, 3H), 4.11 (dd, *J* = 12.5, 5.5 Hz, 1H), 3.74 (m, 1H), 3.64 (overlap, 4H), 2.44 (t, *J* = 2.3 Hz, 1H), 1.96 (bt, *J* = 6.0 Hz, 1H). ¹³C NMR (125 MHz, CDCl₃): δ(ppm) 134.7, 117.3, 79.4, 77.9, 74.8, 71.1, 69.4, 62.3, 58.6.



(L)-1d: Under an N₂ atmosphere, dry DCM (500 mL), triethylamine (21.5 g, 212 mmol, 29.4 mL), and 4-dimethylaminopyridine (4-DMAP) (4.32 g, 35.4 mmol) were added to **(L)-1c** (30.1 g, 177 mmol) in an oven-dried 1000 mL RBF. The reaction mixture was cooled to 0 °C and 4-toluenesulfonyl chloride (37.1 g, 195 mmol) was added portion-wise into the stirring reaction mixture. The mixture was allowed to gradually warm up to room temperature and left to react overnight. After completion, the organic solution was extracted with water (3 x 300 mL) and brine (1 x 300 mL). The organic layer was dried over Na₂SO₄ and concentrated under vacuum. Column chromatography (50% hexanes/DCM to 100% DCM) yielded the product (50 g, 15 mmol, 78% yield). HRMS-ESI for **(L)-1d**; Calcd for C₁₆H₂₀O₅S: m/z = 342.1370 [M + NH₄]⁺; Found: 342.1373 [M + NH₄]⁺. ¹H NMR (500 MHz, CDCl₃): δ(ppm) 7.79 (d, *J* = 8.2 Hz, 2H), 7.34 (d, *J* = 8.4 Hz, 2H), 5.82 (ddt, 17.1 Hz, 10.5 Hz, 4.4 Hz, 1H), 5.23 (dd, *J* = 17.3, 1.6 Hz, 1H), 5.16 (dd, *J* = 10.4 Hz, 1.3 Hz, 1H), 4.17-4.03 (overlap, 6H), 3.73 (p, *J* = 4.7 Hz, 1H), 3.58 (d, *J* = 5.1 Hz, 1H), 2.45 (overlap, 4H). ¹³C NMR (125 MHz, CDCl₃): δ(ppm) 144.9, 134.2, 132.6, 129.8, 127.9, 117.4, 79.1, 75.0, 71.3, 69.2, 68.2, 58.5, 21.6.

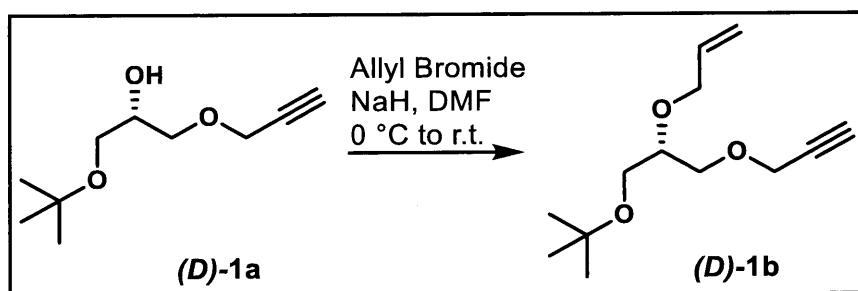


(L)-1-alkyne: DMF (150 mL) and LiBr (54.5 g, 604 mmol) were added to **(L)-1d** (49.2 g, 152 mmol) in a 500 mL RBF. The reaction mixture was left to stir until the LiBr was completely dissolved, after which the mixture was placed into a 70 °C oil bath and left to react overnight. DMF was then removed under reduced pressure. Water (300 mL) was added to the solution followed by extraction with DCM (3 x 500 mL). The organic layers were combined, dried over Na₂SO₄, and concentrated under vacuum. Column chromatography (50% hexanes/DCM to 100% DCM) yielded the product (31 g, 130 mmol, 88% yield). HRMS-ESI for **(L)-1-alkyne**; Calcd for C₉H₁₃BrO₂: m/z = 250.0437 [M + NH₄]⁺; Found: 250.0440 [M + NH₄]⁺. ¹H NMR (500 MHz, CDCl₃): δ(ppm) 5.94 (ddt, *J* = 16.9, 10.0, 5.4 Hz, 1H), 5.31 (dd, *J* = 17.0, 1.5 Hz, 1H), 5.21 (dd, *J* = 10.4, 1.1 Hz, 1H), 4.21 (d, *J* = 2.2 Hz, 2H), 4.14 (m, 2H), 3.76-3.67 (overlap, 3H), 3.55 (dd, *J* = 10.3, 5.1 Hz, 1H), 3.47 (dd, *J* = 10.3, 4.5 Hz, 1H), 2.47 (t, *J* = 2.5 Hz, 1H). ¹³C NMR (125 MHz, CDCl₃): δ(ppm) 134.4, 117.5, 79.3, 76.6, 74.9, 71.1, 69.6, 58.6, 32.0.



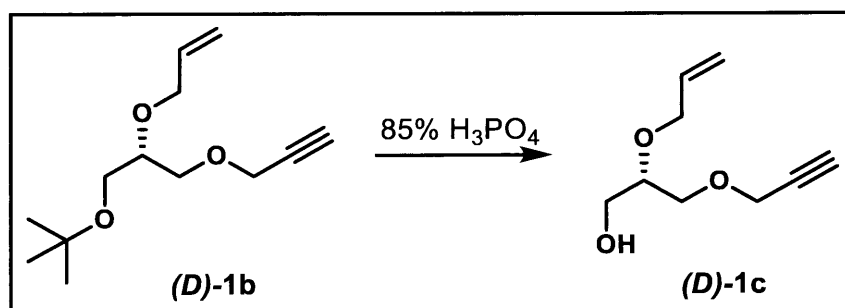
(D)-1a: Under an N₂ atmosphere, dry *t*-BuOH (165 g, 2.23 mol) was added to **(S)-GPE-B** (50.0 g, 446 mmol) in an oven-dried 500 mL RBF immersed in a room temperature water bath. Next,

Mg(ClO₄)₂ (10.0 g, 44.6 mmol) was added portion-wise into the stirring reaction mixture. This mixture was allowed to react for 72 h. After completion, water (500 mL) was added to the solution followed by extraction with DCM (3 x 1000 mL). The organic layers were combined, extracted with water (500 mL), dried over Na₂SO₄, and concentrated under vacuum. Column chromatography (50% hexanes/DCM to 100% DCM) yielded the product (75.6 g, 406 mmol, 91% yield). HRMS-ESI for **(D)-1a**; Calcd for C₁₀H₁₈O₃: m/z = 204.1594 [M + NH₄]⁺; Found: 204.1598 [M + NH₄]⁺. ¹H NMR (500 MHz, CDCl₃): δ(ppm) 4.20 (d, *J* = 2.3 Hz, 2H), 3.91 (ddd, *J* = 10.7, 6.2, 4.5 Hz, 1H), 3.62 (dd, *J* = 9.7, 4.5 Hz, 1H), 3.56 (dd, *J* = 9.7, 6.0 Hz, 1H), 3.44 (dd, *J* = 9.1, 4.5 Hz, 1H), 3.38 (dd, *J* = 9.0, 6.5 Hz, 1H), 2.58-2.44 (br, 1H), 2.44 (t, *J* = 2.4 Hz, 1H), 1.19 (s, 9H). ¹³C NMR (125 MHz, CDCl₃): δ(ppm) 79.3, 74.6, 72.7, 70.9, 69.2, 62.6, 58.1, 27.1.

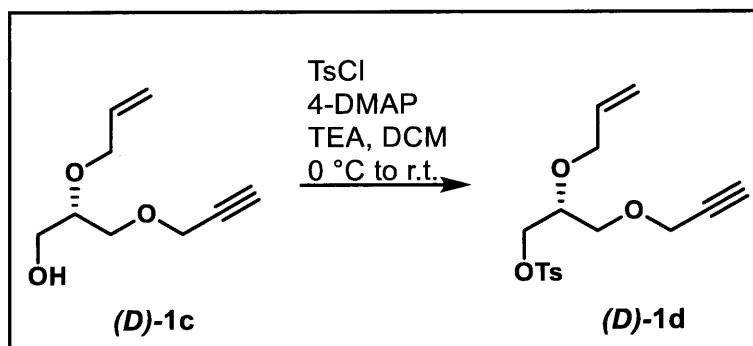


(D)-1b: Under an N₂ atmosphere, dry DMF (400 mL) and allyl bromide (39.2 g, 324 mmol, 28.0 mL) were added to **(D)-1a** (40.3 g, 216 mmol) in an oven-dried 1000 mL RBF. The reaction mixture was cooled to 0 °C and NaH (9.50 g, 238 mmol, 60% dispersion in mineral oil) was added portion-wise into the stirring reaction mixture. The mixture was allowed to gradually warm to room temperature and left to react overnight. After completion, DMF was removed under reduced pressure. Water (300 mL) was added to the solution which was extracted with DCM (3 x 300 mL). The organic layers were combined, dried over Na₂SO₄, and concentrated under vacuum. Column chromatography (80% hexanes/DCM to 50% hexanes/DCM) yielded the product (44 g, 200 mmol,

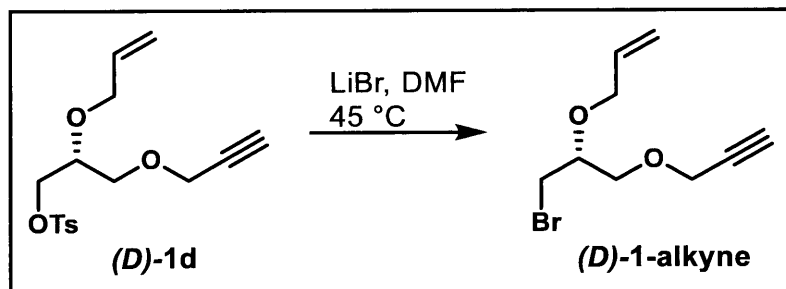
92% yield). HRMS-ESI for **(D)-1b**; Calcd for C₁₃H₂₂O₃: m/z = 244.1907 [M + NH₄]⁺; Found: 244.1911 [M + NH₄]⁺. ¹H NMR (500 MHz, CDCl₃): δ(ppm) 5.92 (ddt, *J* = 16.1, 10.4, 5.7 Hz, 1H), 5.28 (d, *J* = 17.2 Hz, 1H), 5.15 (d, *J* = 10.4 Hz, 1H), 4.20 – 4.18 (d, *J* = 2.5 Hz, 2H), 4.16-4.14 (m, 2H), 3.69-3.66 (m, 1H), 3.63 – 3.57 (m, 2H), 3.44 (d, *J* = 5.5 Hz, 2H), 2.42 (t, *J* = 2.3 Hz, 1H), 1.18 (s, 9H). ¹³C NMR (125 MHz, CDCl₃): δ(ppm) 135.2, 116.6, 79.7, 77.3, 74.4, 72.9, 71.2, 69.9, 61.4, 58.4, 27.4.



(D)-1c: Under an N₂ atmosphere, 85% H₃PO₄ (150 g, 1.51 mol) was poured onto **(D)-1b** (40.1 g, 177 mmol) in a 500 mL RBF. The reaction mixture was stirred and left to react at room temperature for 4 h. After completion, water (500 mL) was added to the solution followed by extraction with DCM (3 x 400 mL). The organic layers were combined, dried over Na₂SO₄, and concentrated under vacuum. Column chromatography (50% hexanes/DCM to 2% MeOH/DCM) yielded the product (24 g, 140 mmol, 78% yield). HRMS-ESI for **(D)-1c**; Calcd for C₉H₁₄O₃: m/z = 188.1281 [M + NH₄]⁺; Found: 188.1283 [M + NH₄]⁺. ¹H NMR (500 MHz, CDCl₃): δ(ppm) 5.97 – 5.88 (ddt, 16.0, 10.4, 5.6 Hz, 1H), 5.29 (dd, *J* = 17.2, 1.5 Hz, 1H), 5.19 (dd, *J* = 10.4, 1.2 Hz, 1H), 4.21-4.16 (overlap, 3H), 4.12-4.08 (m, 1H), 3.79-3.70 (m, 1H), 3.67-3.62 (overlap, 4H), 2.45 (t, *J* = 2.4 Hz, 1H), 1.99 (br, 1H). ¹³C NMR (125 MHz, CDCl₃): δ(ppm) 134.8, 117.4, 79.5, 77.9, 74.8, 71.2, 69.5, 62.5, 58.7.

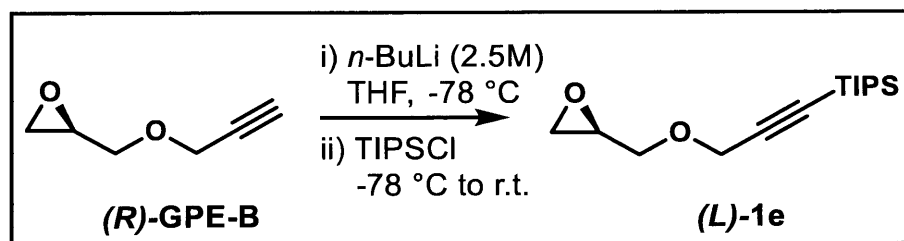


(D)-1d: Under an N_2 atmosphere, dry DCM (500 mL), triethylamine (16.4 g, 162 mmol, 22.4 mL), and 4-dimethylaminopyridine (4-DMAP) (6.06 g, 54.0 mmol) were added to **(D)-1c** (23.0 g, 135 mmol) in an oven-dried 1000 mL RBF. The reaction mixture was cooled to 0 °C and 4-toluenesulfonyl chloride (28.3 g, 149 mmol) was added portion-wise into the stirring reaction mixture. The mixture was allowed to gradually warm up to room temperature and left to react overnight. After completion, the organic solution was extracted with water (3 x 300 mL) and brine (1 x 300 mL). The organic layer was dried over Na_2SO_4 and concentrated under vacuum. Column chromatography (50% hexanes/DCM to 100% DCM) yielded the product (37 g, 110 mmol, 84% yield). HRMS-ESI for **(D)-1d**; Calcd for $\text{C}_{16}\text{H}_{20}\text{O}_5\text{S}$: $m/z = 342.1370$ $[\text{M} + \text{NH}_4]^+$; Found: 342.1374 $[\text{M} + \text{NH}_4]^+$. ^1H NMR (500 MHz, CDCl_3): δ (ppm) 7.80 (d, $J = 8.3$ Hz, 2H), 7.34 (d, $J = 8.5$ Hz, 2H), 5.86-5.78 (ddt, 17.2 Hz, 10.4 Hz, 4.2 Hz, 1H), 5.23 (dd, $J = 17.2, 1.6$ Hz, 1H), 5.16 (dd, $J = 10.4$ Hz, 1.2 Hz, 1H), 4.17-4.02 (overlap, 6H), 3.73 (p, $J = 4.8$ Hz, 1H), 3.57 (d, $J = 5.1$ Hz, 1H), 2.45 (s, 3H), 2.43 (t, $J = 2.4$ Hz, 1H). ^{13}C NMR (125 MHz, CDCl_3): δ (ppm) 144.9, 134.3, 132.7, 129.9, 128.0, 117.6, 79.2, 75.1, 75.0, 71.4, 69.3, 68.3, 58.6, 21.7.

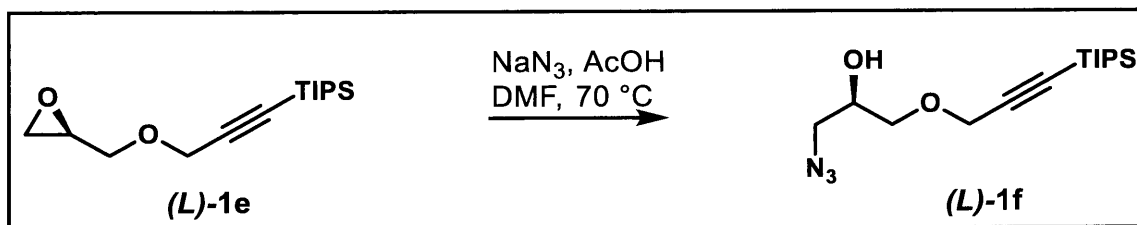


(D)-1-alkyne: DMF (110 mL) and LiBr (39.4 g, 454 mmol) were added to **(D)-1d** (36.7 g, 113 mmol) in a 500 mL RBF. The reaction mixture was left to stir until the LiBr was completely dissolved, after which the mixture was placed into a 70 °C oil bath and left to react overnight. DMF was then removed under reduced pressure. Water (300 mL) was added to the solution followed by extraction with DCM (3 x 500 mL). The organic layers were combined, dried over Na₂SO₄, and concentrated under vacuum. Column chromatography (50% hexanes/DCM to 100% DCM) yielded the product (23 g, 97 mmol, 86% yield). HRMS-ESI for **(D)-1-alkyne**; Calcd for C₉H₁₃BrO₂: m/z = 250.0437 [M + NH₄]⁺; Found: 250.0445 [M + NH₄]⁺. ¹H NMR (500 MHz, CDCl₃): δ(ppm) 5.97-5.89 (ddt, *J* = 17.2, 10.4, 5.8 Hz, 1H), 5.31 (dd, *J* = 17.2, 1.6 Hz, 1H), 5.21 (dd, *J* = 10.4, 1.2 Hz, 1H), 4.20 (d, *J* = 2.4 Hz, 2H), 4.15-4.12 (m, 2H), 3.75-3.66 (overlap, 3H), 3.54 (dd, *J* = 10.6, 5.3 Hz, 1H), 3.47 (dd, *J* = 10.6, 4.7 Hz, 1H), 2.45 (t, *J* = 2.4 Hz, 1H). ¹³C NMR (125 MHz, CDCl₃): δ(ppm) 134.4, 117.7, 79.3, 76.8, 74.9, 71.2, 69.7, 58.7, 32.0.

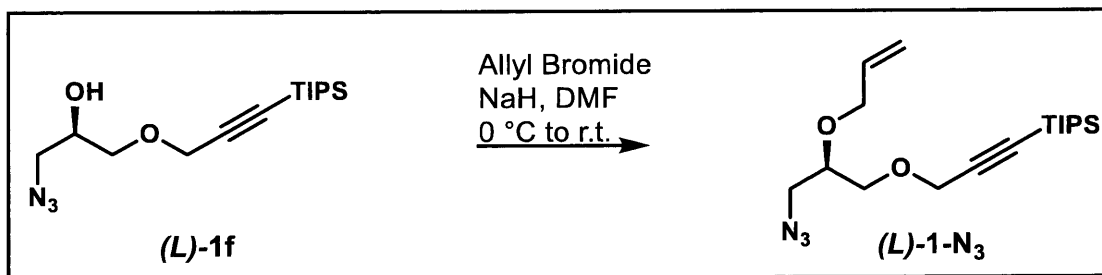
3. (*L*)- and (*D*)-1-N₃



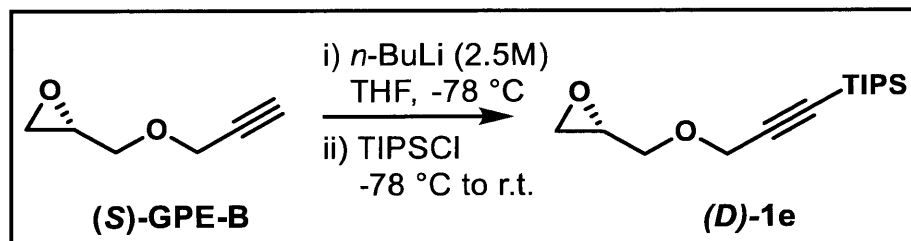
(L)-1e: Under an N₂ atmosphere, **(R)-GPE-B** (30.0 g, 268 mmol) was added to dry THF (600 mL) in an oven-dried 1000 mL two-neck RBF attached to a 150 mL addition funnel. Next, the reaction vessel was cooled to -78 °C, followed by dropwise addition of *n*-butyllithium (*n*-BuLi) (118 mL, 295 mmol, 2.5 M in hexanes). Once all of the *n*-BuLi was added, the addition funnel was washed with ~10 mL of dry THF and the reaction mixture was allowed to stir for 30 min. Then, triisopropylsilyl chloride (TIPSCI) (62.0 g, 321 mmol, 68.8 mL) was added to the addition funnel, followed by the dropwise addition of the TIPSCI to the reaction mixture (still at -78 °C) over the course of 15 min. After warming to room temperature, the reaction proceeded for 3 – 4 h before being quenched upon addition of a cold brine solution (500 mL). The crude product was obtained by extraction into DCM (3 x 500 mL), followed by combining the organic layers, drying over Na₂SO₄, and concentrating under vacuum. Column chromatography (4% EtOAc/hexanes) yielded the product (61 g, 230 mmol, 85% yield) as a colorless oil. HRMS-ESI for **(L)-1e**; Calcd for C₆H₈O₂: *m/z* = 130.0868 [M + NH₄]⁺; Found: 130.0860 [M + NH₄]⁺. ¹H NMR (500 MHz, CDCl₃): δ(ppm) 4.26 (d, *J* = 9.5 Hz, 2H), 3.82 (dd, *J* = 11.1, 3.2 Hz, 1H), 3.53 (dd, *J* = 11.1, 5.7 Hz, 1H), 3.18 (m, 1H), 2.82 (t, *J* = 4.5 Hz, 1H), 2.64 (dd, *J* = 5.1, 2.9 Hz, 1H), 1.07 (s, 21H). ¹³C NMR (125 MHz, CDCl₃): δ(ppm) 102.8, 88.2, 70.0, 59.3, 50.5, 44.5, 18.6, 11.2.



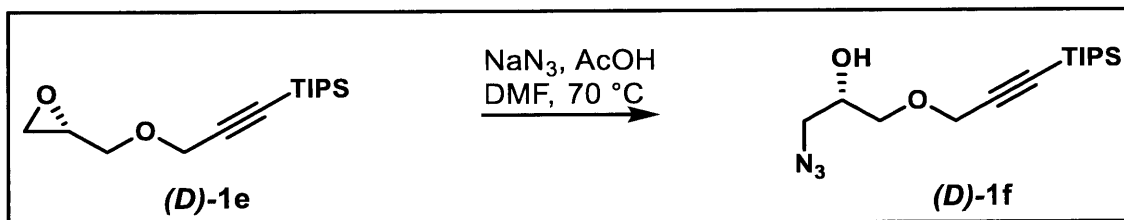
(L)-1f: DMF (800 mL) and acetic acid (19.5 g, 324 mmol, 18.5 mL) were added to **(L)-1e** (58.0 g, 216 mmol) in a 1000 mL RBF. NaN₃ (42.1 g, 648 mmol) was then added and the reaction mixture was heated to 70 °C and allowed to stir for 24 h. Over the course of the reaction a white gel-like precipitate formed. **Safety warning:** Sodium azide in the presence of acid can produce hydrazoic acid, a highly toxic and flammable gas. All of these procedures are performed in a well ventilated fume hood in order to minimize the danger. The reaction mixture was neutralized by addition of 100 mL of a saturated NaHCO₃ solution to neutralize any remaining acid. Water and DMF were then removed under reduced pressure. 500 mL of water was added to the solution followed by extraction with DCM (3 x 400 mL). The organic layers were combined, dried over Na₂SO₄, and concentrated under vacuum. **Note: we have since updated this procedure and now use EtOAc and not DCM for extraction to avoid any undesired reaction between DCM and NaN₃.** Column chromatography (10% EtOAc/hexanes) yielded the product (55 g, 180 mmol, 82% yield). HRMS-ESI for **(L)-1e**; Calcd for C₁₅H₂₉N₃O₂Si: m/z = 329.2367 [M + NH₄]⁺; Found: 329.2368 [M + NH₄]⁺. ¹H NMR (500 MHz, CDCl₃): δ(ppm) 4.24 (s, 2H), 3.98 (p, *J* = 6.0 Hz, 1H), 3.63 (dd, *J* = 9.5, 4.0 Hz, 1H), 3.59 (dd, *J* = 9.7, 6.1 Hz, 1H), 3.39 (dd, *J* = 5.2, 0.7 Hz, 2H), 2.38 (d, *J* = 5.0 Hz, 1H), 1.08 (s, 21H). ¹³C NMR (125 MHz, CDCl₃): δ(ppm) 102.6, 94.8, 88.3, 77.2, 70.8, 69.5, 59.3, 18.5, 11.1.



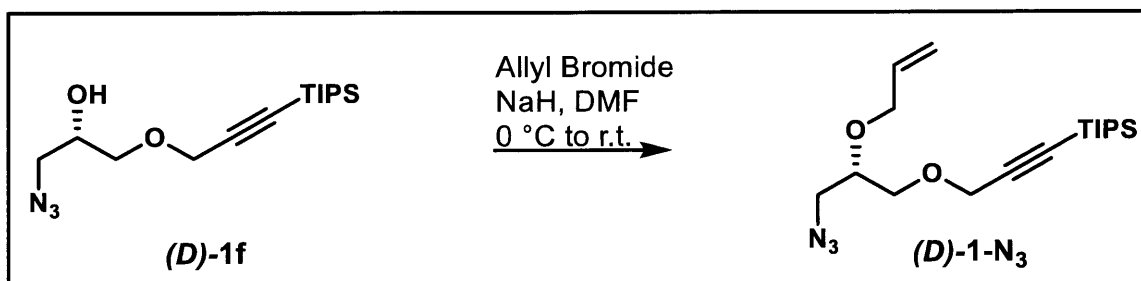
(L)-1-N₃: Under an N₂ atmosphere, dry DMF (500 mL) and allyl bromide (36.7 g, 303 mmol, 25.0 mL) were added to **(L)-1f** (55.0 g, 177 mmol) in an oven-dried 1000 mL RBF. The reaction mixture was cooled to 0 °C and NaH (8.90 g, 222 mmol, 60% dispersion in mineral oil) was added portion-wise into the stirring reaction mixture. The mixture was allowed to gradually warm up to room temperature and left to react overnight. After completion, DMF was removed under reduced pressure. 500 mL of water was added to the solution which was extracted with DCM (3 x 400 mL). The organic layers were combined, dried over Na₂SO₄, and concentrated under vacuum. Column chromatography (5% EtOAc/hexanes) yielded the product (50 g, 140 mmol, 80% yield). HRMS-ESI for **(L)-1-N₃**; Calcd for C₁₈H₃₃N₃O₂Si: m/z = 352.2415 [M + H]⁺; Found: 352.2423 [M + H]⁺. ¹H NMR (500 MHz, CDCl₃): δ(ppm) 5.93 (ddt, *J* = 16.3, 10.8, 5.9 Hz, 1H), 5.31 (dd, *J* = 17.0, 1.6 Hz, 1H), 5.20 (dd, *J* = 10.5, 1.4 Hz, 1H), 4.22 (s, 3H), 4.17 (dd, *J* = 12.5, 5.5 Hz, 2H), 4.11 (dd, *J* = 12.6, 5.7 Hz, 2H), 3.68 (m, 1H), 3.64 (dd, *J* = 5.2, 2.8 Hz, 2H), 3.37 (dd, *J* = 4.8 Hz, 0.6 Hz, 2H), 1.08 (s, 21H). ¹³C NMR (125 MHz, CDCl₃): δ(ppm) 134.5, 117.6, 102.9, 88.3, 77.0, 71.4, 68.7, 59.4, 52.2, 18.7, 11.2.



(D)-1e: Under an N_2 atmosphere, **(S)-GPE-B** (25.0 g, 223 mmol) was added to dry THF (500 mL) in an oven-dried and sealed 1000 mL two-neck round-bottom flask attached to a 150 mL addition funnel. Next, the reaction vessel was cooled to $-78\text{ }^\circ\text{C}$ using a dry ice/acetone bath, followed by the dropwise addition of *n*-butyllithium (*n*-BuLi) (2.5 M in hexanes, 98 mL, 245 mmol). Once all of the *n*-BuLi was added, the addition funnel was washed with ~ 10 mL of dry THF and the reaction mixture was allowed to stir for 30 min. Then, triisopropylsilyl chloride (TIPSCl) (51.7 g, 268 mmol, 57.3 mL) was added to the addition funnel, followed by the dropwise addition of the TIPSCl to the reaction mixture (still at $-78\text{ }^\circ\text{C}$) over the course of 15 min. After warming to room temperature, the reaction proceeded for 3–4 h before being quenched upon addition of a cold brine solution (500 mL). The crude product was obtained by extraction into DCM (3 x 500 mL), followed by combining the organic layers, drying with Na_2SO_4 , and concentrating under vacuum. Column chromatography (4% EtOAc/hexanes) of the crude material yielded the product (51 g, 190 mmol, 86% yield) as a clear oil. HRMS-ESI for **(D)-1e**; Calcd for $\text{C}_6\text{H}_8\text{O}_2$: $m/z = 130.0868$ [$\text{M} + \text{NH}_4$] $^+$; Found: 130.0864 [$\text{M} + \text{NH}_4$] $^+$. ^1H NMR (500 MHz, CDCl_3): δ (ppm) 4.26 (d, $J = 9.5$ Hz, 2H), 3.82 (dd, $J = 11.2, 3.2$ Hz, 1H), 3.53 (dd, $J = 11.3, 5.7$ Hz, 1H), 3.18 (m, 1H), 2.81 (t, $J = 4.7$ Hz, 1H), 2.64 (dd, $J = 5.1, 2.7$ Hz, 1H), 1.07 (s, 21H). ^{13}C NMR (125 MHz, CDCl_3): δ (ppm) 101.6, 90.1, 70.2, 59.2, 50.6, 44.5, 18.5, 11.0.

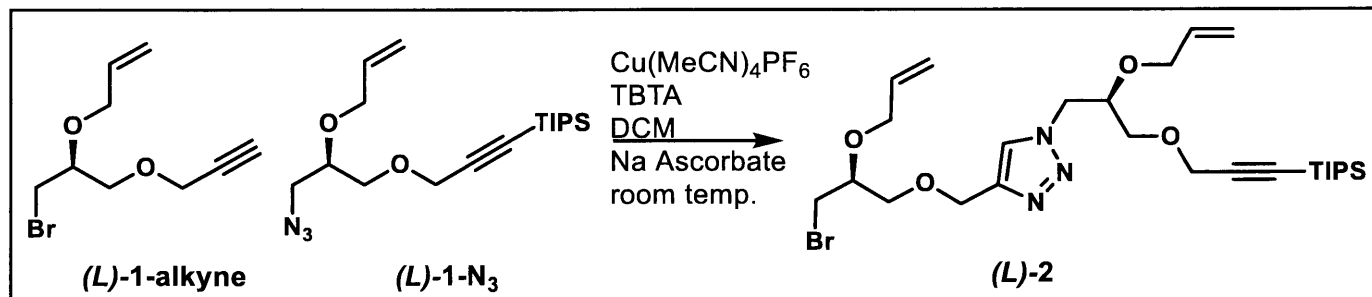


(D)-1f: DMF (800 mL) and acetic acid (16.8 g, 280 mmol, 16.0 mL) were added to **(D)-1e** (50.0 g, 187 mmol) in a 1000 mL RBF. NaN_3 (36.4 g, 560 mmol) was then added and the reaction mixture was heated to 70 °C and allowed to stir for 24 h. Over the course of the reaction a white gel-like precipitate formed. **Safety warning:** Sodium azide in the presence of acid can produce hydrazoic acid, a highly toxic and flammable gas. All of these procedures are performed in a well ventilated fume hood in order to minimize the danger. The reaction mixture was neutralized by addition of 100 mL of a saturated NaHCO_3 solution to neutralize any remaining acid. Water and DMF were then removed under reduced pressure. 500 mL of water was added to the solution followed by extraction with DCM (3 x 400 mL). The organic layers were combined, dried over Na_2SO_4 , and concentrated under vacuum. **Note: we have since updated this procedure and now use EtOAc and not DCM for extraction to avoid any undesired reaction between DCM and NaN_3 .** Column chromatography (10% EtOAc/hexanes) yielded the product (46 g, 150 mmol, 80% yield). HRMS-ESI for **(D)-1f**; Calcd for $\text{C}_{15}\text{H}_{29}\text{N}_3\text{O}_2\text{Si}$: $m/z = 329.2367$ [$\text{M} + \text{NH}_4$] $^+$; Found: 329.2368 [$\text{M} + \text{NH}_4$] $^+$. ^1H NMR (500 MHz, CDCl_3): δ (ppm) 4.24 (s, 2H), 3.98 (p, $J = 5.9$ Hz, 1H), 3.64 (dd, $J = 9.6, 4.1$ Hz, 1H), 3.58 (dd, $J = 9.6, 6.1$ Hz, 1H), 3.39 (dd, $J = 5.2, 0.7$ Hz, 2H), 2.39 (d, $J = 5.0$ Hz, 1H), 1.08 (s, 21H). ^{13}C NMR (125 MHz, CDCl_3): δ (ppm) 102.6, 88.6, 70.8, 69.7, 59.5, 53.6, 18.6, 11.2.



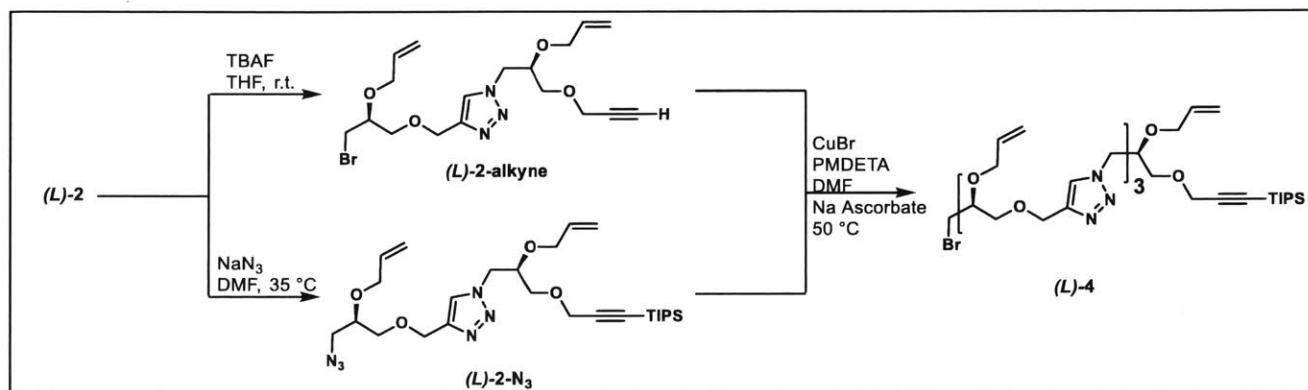
(D)-1-N₃: Under an N₂ atmosphere, dry DMF (400 mL) and allyl bromide (35.0 g, 289 mmol, 25.0 mL) were added to **(D)-1f** (45.0 g, 145 mmol) in an oven-dried 1000 mL RBF. The reaction mixture was cooled to 0 °C and NaH (7.50 g, 189 mmol, 60% in mineral oil) was added portion-wise into the stirring reaction mixture. The mixture was allowed to gradually warm up to room temperature and left to react overnight. After completion, DMF was removed under reduced pressure. Water (500 mL) was added to the solution which was extracted with DCM (3 x 400 mL). The organic layers were combined, dried over Na₂SO₄, and concentrated under vacuum. Column chromatography (5% EtOAc/hexanes) yielded the product (36 g, 100 mmol, 70% yield). HRMS-ESI for **(D)-1-N₃**; Calcd for C₁₈H₃₃N₃O₂Si: m/z = 352.2415 [M + H]⁺; Found: 352.2415 [M + H]⁺. ¹H NMR (500 MHz, CDCl₃): δ(ppm) 5.93 (ddt, *J* = 16.2, 10.5, 5.8 Hz, 1H), 5.30 (dd, *J* = 17.1, 1.4 Hz, 1H), 5.20 (dd, *J* = 10.5, 1.0 Hz, 1H), 4.21 (s, 2H), 4.17 (dd, *J* = 12.8, 5.6 Hz, 2H), 4.11 (dd, *J* = 12.8, 5.7 Hz, 2H), 3.68 (m, 1H), 3.63 (dd, *J* = 5.1, 2.5 Hz, 2H), 3.37 (dd, *J* = 5.0 Hz, 0.9 Hz, 2H), 1.07 (s, 21H). ¹³C NMR (125 MHz, CDCl₃): δ(ppm) 134.5, 117.6, 102.9, 88.3, 77.0, 71.4, 67.1, 59.5, 52.2, 18.7, 11.2.

4. IEG Oligomers



(L)-2: Under an N₂ atmosphere, DCM (250 mL), tetrakis(acetonitrile)copper(I) hexafluorophosphate (Cu(MeCN)₄PF₆) (2.42 g, 6.50 mmol) tris(benzyltriazolylmethyl)amine (TBTA) (6.90 g, 13.0 mmol), and sodium ascorbate (2.58 g, 13.0 mmol) were added to **(L)-1-N₃** (45.4 g, 129 mmol) in an oven-dried 500 mL RBF. The mixture was stirred and sonicated until the (Cu(MeCN)₄PF₆) and TBTA dissolved. A solution of **(L)-1-alkyne** (30.4 g, 130 mmol) in of DCM (50 mL) was then added slowly to the above solution. The reaction mixture was left to react overnight after which DCM was removed under reduced pressure. 10 mL of DCM was added to the resulting viscous mixture, which was then loaded carefully onto a column. Column chromatography (25% hexanes/DCM to 1% MeOH/DCM) yielded the product (59 g, 100 mmol, 79% yield) as a pale yellow oil. HRMS-ESI for **(L)-2**; Calcd for C₂₇H₄₆BrN₃O₄Si: m/z = 584.2514 [M + H]⁺; Found: 584.2501 [M + H]⁺. ¹H NMR (500 MHz, CDCl₃): δ(ppm) 7.66 (s, 1H), 5.90 (ddt, *J* = 16.3, 10.4, 5.7 Hz, 1H), 5.72 (ddt, *J* = 16.5, 10.3, 5.8 Hz, 1H), 5.29 (dd, *J* = 17.3, 1.7 Hz, 1H), 5.16 (overlap, 3H), 4.69 (d, *J* = 2.2 Hz, 2H), 4.61 (dd, *J* = 14.2, 3.4 Hz, 1H), 4.42 (dd, *J* = 14.2, 8.0 Hz, 1H), 4.25 (d, *J* = 2.4 Hz, 2H), 4.12 (overlap, 2H), 4.04 (dd, *J* = 12.7, 5.7 Hz, 2H), 3.90 (overlap, 2H), 3.70 (m, 1H), 3.67 – 3.60 (overlap, 3H), 3.52 (dd, *J* = 10.6, 5.1 Hz, 1H), 3.44 (dd, *J* = 10.6, 4.5 Hz, 1H), 1.07 (s, 21H). ¹³C NMR (125 MHz, CDCl₃): δ(ppm) 144.5, 134.5,

134.0, 124.2, 117.8, 117.6, 102.6, 96.3, 94.3, 88.4, 76.3, 71.2, 70.1, 67.9, 64.9, 59.5, 51.8, 32.2, 18.6, 11.1.

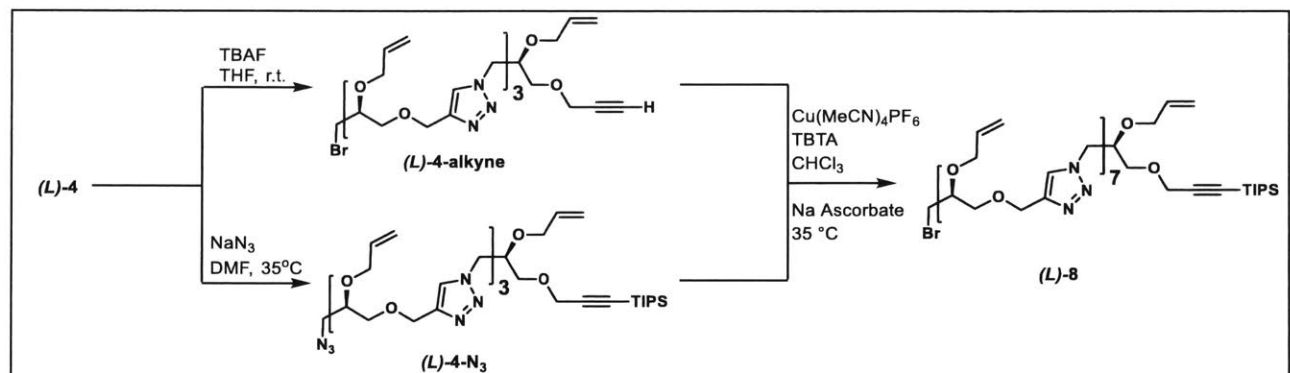


(L)-4: The **(L)-2-alkyne** precursor to **(L)-4** was prepared by dissolving **(L)-2** (24.4 g, 41.6 mmol) in THF (400 mL) in a 1L RBF, followed by slow addition of tetrabutylammonium fluoride (TBAF) (1.05 equiv, 43.7 mL, 1M in THF,). After 15 minutes, the reaction mixture was concentrated under reduced pressure. The crude mixture was then dissolved in EtOAc (500 mL) and extracted with deionized water (500 mL x 3). The organic layer was dried over Na₂SO₄ and concentrated under vacuum. The resulting yellow oil, which contains **(L)-2-alkyne** and TIPS-F impurity, was used directly in the next step.

The **(L)-2-N₃** precursor to **(L)-4** was prepared by dissolving **(L)-2** (24.4 g, 41.6 mmol) in DMF (400 mL), followed by the addition of NaN₃ (16.3 g, 250 mmol). The reaction mixture was heated to 35 °C and allowed to stir for 12 h before the DMF was removed via rotary evaporator at 35 °C. *Heating past 35 °C was avoided as it leads to degradation of the product.* Then, EtOAc (500 mL) was added to the residue, which was extracted with water (2 x 300 mL) and brine (1 x 300 mL).

The organic layer was dried over Na₂SO₄ and concentrated under vacuum. The resulting **(L)-2-N₃** was obtained as a faint yellow oil and used in the next step without further purification.

Under an N₂ atmosphere, dry DMF (100 mL), PMDETA (721 mg, 4.16 mmol, 0.869 mL), CuBr (298 mg, 2.08 mmol), and sodium ascorbate (824 mg, 4.16 mmol) were added to **(L)-2-N₃** in an oven-dried 500 mL RBF. *Note that the (Cu(MeCN)₄PF₆)/TBTA click conditions used to generate **(L)-2** were not used here as it is difficult to separate TBTA from **(L)-4**. **(L)-2-alkyne** in dry DMF (10 mL) was then added to the solution and the reaction mixture was warmed to 50 °C for 2 h. After completion, DMF was removed under reduced pressure. 10 mL of DCM was added to the resulting viscous mixture which was then loaded carefully onto a column. Column chromatography (100% DCM to 1.25% MeOH/DCM then 3% MeOH/DCM) yielded the product (32 g, 33 mmol) in 79% yield from **(L)-2** as a yellow oil. ¹H NMR (500 MHz, CDCl₃): δ(ppm) 7.68 (s, 2H), 7.66 (s, 1H), 5.89 (ddt, *J* = 17.3, 10.3, 5.7 Hz, 1H), 5.76-5.67 (overlap, 3H), 5.28 (dq, *J* = 16.8, 0.9 Hz, 1H), 5.20-5.10 (overlap, 7H), 4.71-4.55 (overlap, 10H), 4.46-4.38 (overlap, 3H), 4.25 (d, *J* = 2.7 Hz, 2H), 4.10 (m, 1H), 4.03 (overlap, 3H), 3.95-3.85 (overlap, 6H), 3.70 (dd, *J* = 9.5, 4.9 Hz, 1H), 3.67-3.61 (overlap, 3H), 3.58-3.48 (overlap, 4H), 3.51 (dd, *J* = 10.8, 5.2 Hz, 1H), 3.44 (dd, *J* = 10.6, 4.7 Hz, 1H) 1.07 (s, 21H).*

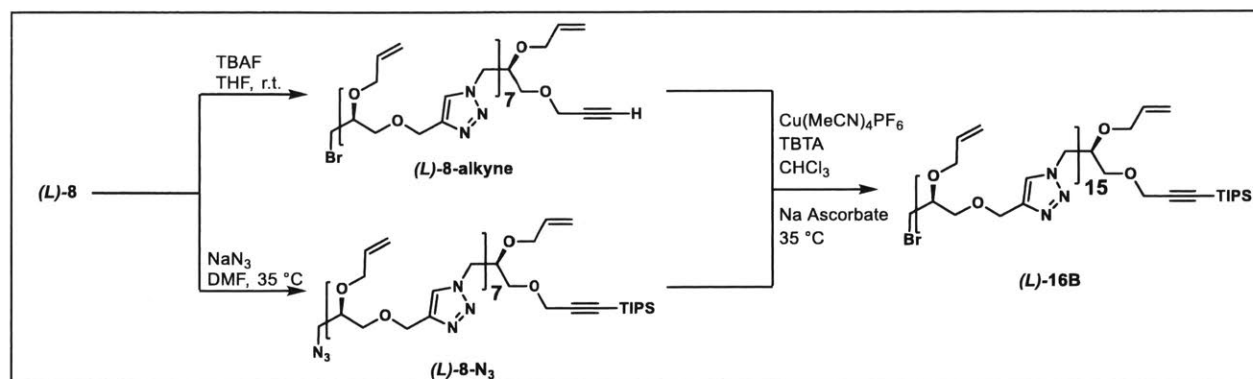


(L)-8: The **(L)-4-alkyne** precursor to **(L)-8** was prepared by dissolving **(L)-4** (12.4 g, 12.7 mmol) in THF (120 mL) in a 1L flask, followed by the slow addition of tetrabutylammonium fluoride (TBAF) (1.05 equiv, 13.3 mL, 1M in THF). After 15 minutes, the reaction mixture was concentrated under reduced pressure. The crude mixture was then dissolved in EtOAc (500 mL) and extracted with deionized water (500 mL x 3). The organic layer was dried over Na₂SO₄ and concentrated under vacuum. The resulting yellow oil containing **(L)-4-alkyne** and TIPS-F was used directly in the next step.

The **(L)-4-N₃** precursor to **(L)-8** was prepared by dissolving **(L)-4** (12.4 g, 12.7 mmol) in DMF (400 mL), followed by the addition of NaN₃ (4.95 g, 76.2 mmol). The reaction mixture was heated to 35 °C and allowed to stir for 12 h before the DMF was removed via rotary evaporator at 35 °C. *Heating past 35 °C was avoided as it leads to degradation of the product.* Then, EtOAc (500 mL) was added to the residue which was extracted with water (2 x 300 mL) and brine (1 x 300 mL). The organic layer was dried over Na₂SO₄ and concentrated under vacuum. The resulting **(L)-4-N₃** was obtained as a faint yellow oil and was used in the next step without further purification.

Under an N₂ atmosphere, chloroform (100 mL), Cu(MeCN)₄PF₆ (473 mg, 1.27 mmol) tris(benzyltriazolylmethyl)amine (TBTA) (1.35 g, 2.54 mmol), and sodium ascorbate (0.503 g, 2.54 mmol) were added to **(L)-4-N₃** in an oven-dried 500 mL RBF. The mixture was stirred and

sonicated until the $(\text{Cu}(\text{MeCN})_4\text{PF}_6)$ and TBTA dissolved. A solution of **(L)-4-alkyne** in chloroform (10 mL) was then added slowly to the above solution. The reaction mixture was warmed to 35 °C overnight and then concentrated under reduced pressure. DCM (10 mL) was added to the resulting viscous mixture, which was then loaded carefully onto a column. Column chromatography (100% DCM to 2.5% MeOH/DCM then 5% MeOH/DCM) yielded the product (19 g, 11 mmol) in 86% yield from **(L)-4** as a yellow oil. ^1H NMR (500 MHz, CDCl_3): δ (ppm) 7.67 (s, 6H), 7.66 (s, 1H), 5.90 (ddt, $J = 17.2, 10.4, 5.6$ Hz, 1H), 5.76-5.67 (overlap, 7H), 5.29 (dq, $J = 17.3$ Hz, 1.5 Hz, 1H), 5.18-5.09 (overlap, 15H), 4.70-4.56 (overlap, 22H), 4.46-4.38 (overlap, 8H), 4.25 (d, $J = 2.7$ Hz, 2H), 4.11 (ddt, $J = 5.6, 4.4, 1.3$ Hz, 1H), 4.08-4.00 (overlap, 7H), 3.93-3.85 (overlap, 14H), 3.69 (dd, $J = 9.7, 4.8$ Hz, 1H), 3.67-3.61 (overlap, 4H), 3.58-3.48 (overlap, 12H), 3.44 (dd, $J = 10.7, 4.7$, 1H), 1.07 (s, 21H).

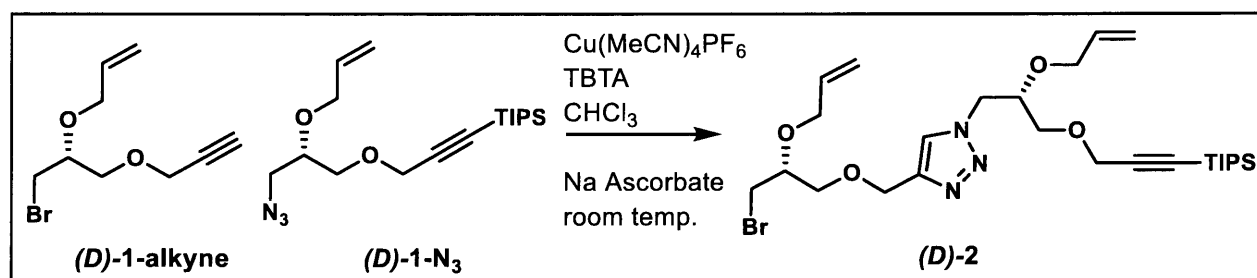


(L)-16B: The **(L)-8-alkyne** precursor to **(L)-16B** was prepared by dissolving **(L)-8** (8.83 g, 5.0 mmol) in THF (50 mL) in a 250 mL flask, followed by the slow addition of tetrabutylammonium fluoride (TBAF) (1.05 equiv, 5.25 mL, 1M in THF). After 15 minutes, the reaction mixture was concentrated under reduced pressure. The crude mixture was then dissolved in EtOAc (200 mL) and extracted with deionized water (300 mL x 3). The organic layer was dried over Na₂SO₄ and concentrated under vacuum. The resulting yellow oil containing **(L)-8-alkyne** and TIPS-F was used directly in the next step.

The **(L)-8-N₃** precursor to **(L)-16B** was prepared by dissolving **(L)-8** (8.83 g, 5.00 mmol) in DMF (100 mL), followed by the addition of NaN₃ (1.95 g, 30.0 mmol). The reaction mixture was heated to 35 °C and allowed to stir for 12 h before the DMF was removed via rotary evaporator at 35 °C. *Heating past 35 °C was avoided as it leads to degradation of the product.* Then, EtOAc (250 mL) was added to the residue and extracted with water (2 x 300 mL) and brine (1 x 300 mL). The organic layer was dried with Na₂SO₄ and concentrated under vacuum. The resulting **(L)-8-N₃** was obtained as a faint yellow oil that was used in the next step without further purification.

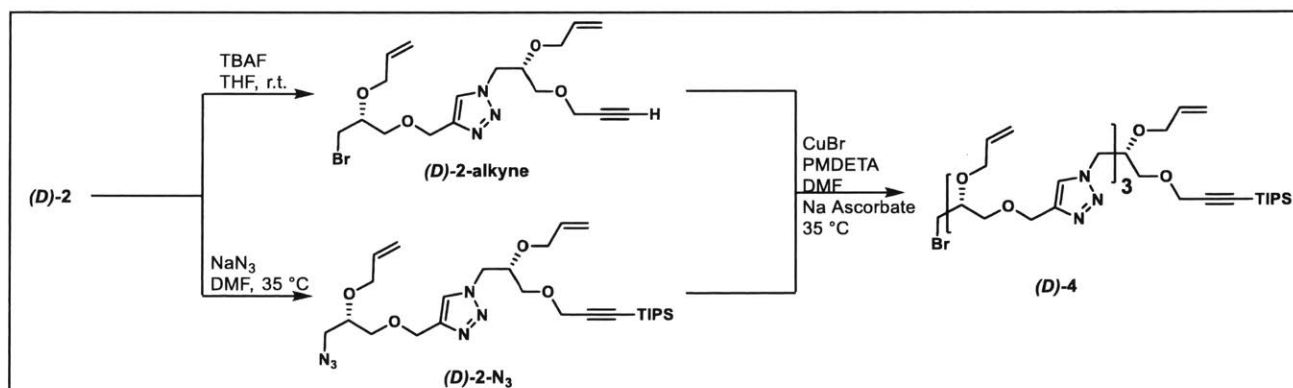
Under an N₂ atmosphere, chloroform (100 mL), Cu(MeCN)₄PF₆ (373 mg, 1.00 mmol) tris(benzyltriazolylmethyl)amine (TBTA) (1.06 g, 2.00 mmol), and sodium ascorbate (0.396 g, 2.00 mmol) were added to **(L)-8-N₃** in an oven-dried 250 mL RBF. The mixture was stirred and sonicated until the (Cu(MeCN)₄PF₆) and TBTA dissolved. A solution of **(L)-8-alkyne** in

chloroform (10 mL) was then added slowly to the above solution. The reaction mixture was warmed to 35 °C overnight then concentrated under reduced pressure. DCM (10 mL) was added to the resulting viscous mixture, which was then loaded carefully onto a column. Column chromatography (100% DCM to 3.5% MeOH/DCM then 6% MeOH/DCM) yielded the product (9.1 g, 2.7 mmol) in 55% yield from **(L)-8** as a yellow oil. ¹H NMR (500 MHz, CDCl₃): δ(ppm) 7.68 (s, 14H), 7.66 (s, 1H), 5.91 (ddt, *J* = 16.3, 10.8, 5.8 Hz, 1H), 5.77-5.68 (overlap, 15H), 5.29 (m, 1H), 5.21-5.08 (overlap, 31H), 4.71-4.56 (overlap, 46H), 4.46-4.38 (overlap, 16H), 4.25 (d, *J* = 1.7 Hz, 2H), 4.11 (m, 1H), 4.08-3.99 (overlap, 15H), 3.93-3.85 (overlap, 30H), 3.72-3.62 (overlap, 5H), 3.60-3.49 (m, 27H), 3.45 (dd, *J* = 10.5, 4.6 Hz, 1H), 1.07 (s, 21H).



(D)-2: Under an N₂ atmosphere, DCM (100 mL), tetrakis(acetonitrile)copper(I) hexafluorophosphate ($\text{Cu}(\text{MeCN})_4\text{PF}_6$) (596 mg, 1.60 mmol) tris(benzyltriazolylmethyl)amine (TBTA) (1.70 g, 3.20 mmol), and sodium ascorbate (634 mg, 3.2 mmol) were added to **(D)-1-N₃** (11.2 g, 31.8 mmol) in an oven-dried 500 mL RBF. The mixture was stirred and sonicated until the $\text{Cu}(\text{MeCN})_4\text{PF}_6$ and TBTA dissolved. A DCM (10 mL) solution of **(D)-1-alkyne** (7.40 g, 31.8 mmol) was then added slowly to the above solution. The reaction mixture was left to react overnight before concentrating under reduced pressure. DCM (5 mL) was added to the resulting viscous mixture, which was then loaded carefully onto a column. Column chromatography (25%

hexanes/DCM to 1% MeOH/DCM) yielded the product (16 g, 28 mmol, 88% yield) as a faint yellow oil. HRMS-ESI for **(D)-2**; Calcd for C₂₇H₄₆BrN₃O₄Si: m/z = 584.2514 [M + H]⁺; Found: 584.2488 [M + H]⁺. ¹H NMR (500 MHz, CDCl₃): δ(ppm) 7.65 (s, 1H), 5.90 (ddt, *J* = 16.3, 10.4, 5.7 Hz, 1H), 5.72 (ddt, *J* = 16.5, 10.3, 5.8 Hz, 1H), 5.29 (dd, *J* = 17.3, 1.7 Hz, 1H), 5.20 – 5.10 (overlap, 3H), 4.68 (b, 2H), 4.64 (dd, *J* = 14.2, 3.4 Hz, 1H), 4.44 (dd, *J* = 14.2, 8.0 Hz, 1H), 4.24 (d, *J* = 2.4 Hz, 2H), 4.12 (dd, *J* = 5.8, 4.3 Hz, 2H), 4.05 (dd, *J* = 12.7, 5.7 Hz, 2H), 3.94 – 3.85 (overlap, 2H), 3.74 – 3.67 (m, 1H), 3.67 – 3.61 (overlap, 3H), 3.51 (dd, *J* = 10.6, 5.2 Hz, 1H), 3.44 (dd, *J* = 10.6, 4.7 Hz, 1H), 1.07 (s, 21H). ¹³C NMR (125 MHz, CDCl₃): δ(ppm) 144.5, 134.5, 134.0, 124.2, 117.8, 117.6, 102.6, 96.3, 94.3, 88.4, 76.3, 71.2, 70.1, 67.9, 64.9, 59.5, 51.8, 32.2, 18.6, 11.1.

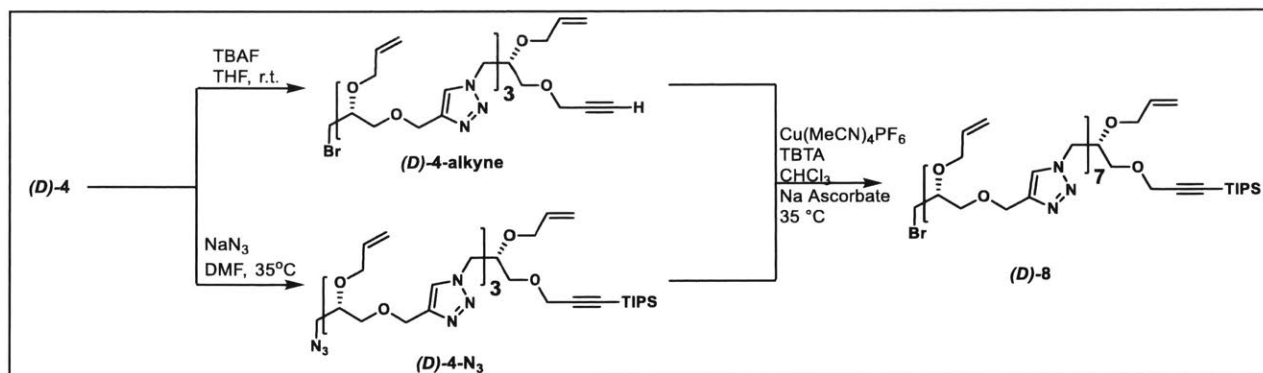


(D)-4: The **(D)-2-alkyne** precursor to **(D)-4** was prepared by dissolving **(D)-2** (7.50 g, 12.8 mmol) in THF (120 mL) in a 500 mL flask, followed by the slow addition of tetrabutylammonium fluoride (TBAF) (1.05 equiv, 13.5 mL, 1M in THF). After 15 minutes, the reaction mixture was concentrated under reduced pressure. The crude mixture was then dissolved in EtOAc (200 mL) and extracted with deionized water (200 mL x 3). The organic layer was dried over Na₂SO₄ and

concentrated under vacuum. The resulting yellow oil containing **(D)-2-alkyne** and TIPS-F was used directly in the next step.

The **(D)-2-N₃** precursor to **(D)-4** was prepared by dissolving **(D)-2** (7.50 g, 12.8 mmol) in DMF (130 mL), followed by the addition of NaN₃ (5.00 g, 76.9 mmol). The reaction mixture was heated to 35 °C and allowed to stir for 12 h before the DMF was removed via rotary evaporator at 35 °C. *Heating past 35 °C was avoided as it leads to degradation of the product.* Then, EtOAc (300 mL) was added to the residue which was extracted with water (2 x 200 mL) and brine (1 x 200 mL). The organic layer was dried over Na₂SO₄ and concentrated under vacuum. The resulting **(D)-2-N₃** was obtained as a faint yellow oil that was used in the next step without further purification.

Under an N₂ atmosphere, dry DMF (50 mL), PMDETA (222 mg, 1.28 mmol, 0.267 mL), CuBr (92.0 mg, 0.640 mmol), and sodium ascorbate (254 mg, 1.28 mmol) were added to **(D)-2-N₃** in an oven-dried 500 mL RBF. *The (Cu(MeCN)₄PF₆)/TBTA click conditions used for the synthesis of (D)-2 were not used here as it is difficult to separate TBTA from (D)-4.* **(D)-2-alkyne** in dry DMF (5 mL) was then added to the solution and the reaction mixture was warmed to 50 °C for 2 h. After completion, DMF was removed under reduced pressure. DCM (5 mL) was added to the resulting viscous mixture which was then loaded carefully onto a column. Column chromatography (100% DCM to 1.25% MeOH/DCM then 3% MeOH/DCM) yielded the product (9.0 g, 9.2 mmol) in 72% yield from **(D)-2** as a yellow oil. ¹H NMR (500 MHz, CDCl₃): δ(ppm) 7.67 (s, 2H), 7.66 (s, 1H), 5.91 (ddt, *J* = 17.4, 10.3, 5.8 Hz, 1H), 5.78-5.68 (overlap, 3H), 5.28 (dq, *J* = 17.2, 1.3 Hz, 1H), 5.21-5.10 (overlap, 7H), 4.70-4.55 (overlap, 10H), 4.46-4.37 (overlap, 3H), 4.24 (d, *J* = 2.7 Hz, 2H), 4.11 (m, 1H), 4.08-3.98 (overlap, 3H), 3.94-3.85 (overlap, 6H), 3.67 (dd, *J* = 9.7, 4.8 Hz, 1H), 3.67-3.61 (overlap, 3H), 3.59-3.47 (overlap, 4H), 3.45 (dd, *J* = 10.7, 5.2 Hz, 1H), 1.07 (s, 21H).

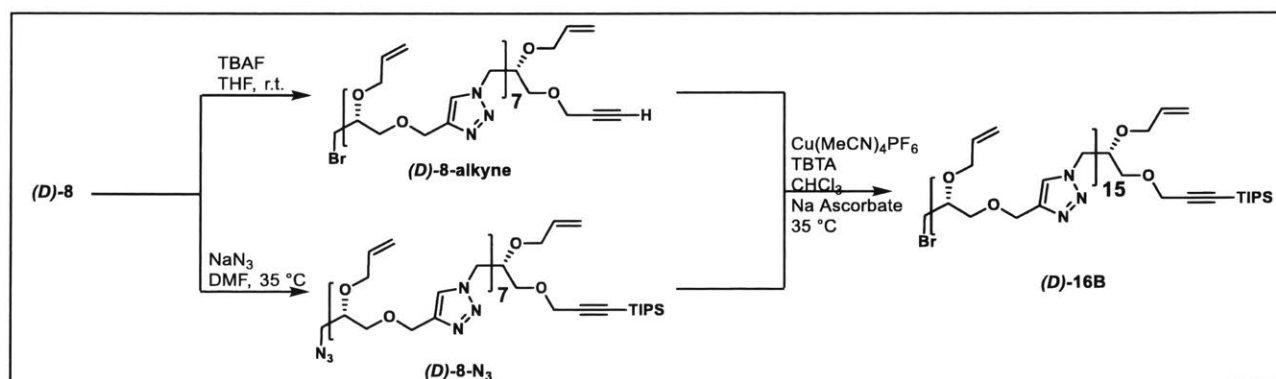


(D)-8: The **(D)-4-alkyne** precursor to **(D)-8** was prepared by dissolving **(D)-4** (3.50 g, 3.60 mmol) in THF (35 mL) in a 250 mL flask, followed by the slow addition of tetrabutylammonium fluoride (TBAF) (1.05 equiv, 3.8 mL, 1M in THF). After 15 minutes, the reaction mixture was concentrated under reduced pressure. The crude mixture was then dissolved in EtOAc (100 mL) and extracted with deionized water (100 mL x 3). The organic layer was dried over Na₂SO₄ and concentrated under vacuum. The resulting yellow oil containing **(D)-4-alkyne** and TIPS-F was used directly in the next step.

The **(D)-4-N₃** precursor to **(D)-8** was prepared by dissolving **(D)-4** (3.50 g, 3.60 mmol) in DMF (40 mL), followed by the addition of NaN₃ (1.40 g, 21.5 mmol). The reaction mixture was heated to 35 °C and allowed to stir for 12 h before the DMF was removed via rotary evaporator at 35 °C. *Heating past 35 °C was avoided as it leads to degradation of the product.* Then, EtOAc (100 mL) was added to the residue which was extracted with water (2 x 100 mL) and brine (1 x 100 mL). The organic layer was dried over Na₂SO₄ and concentrated under vacuum. The resulting **(D)-4-N₃** was obtained as a faint yellow oil that was used in the next step without further purification.

Under an N₂ atmosphere, chloroform (25 mL), Cu(MeCN)₄PF₆ (134 mg, 0.360 mmol) tris(benzyltriazolylmethyl)amine (TBTA) (382 mg, 0.720 mmol), and sodium ascorbate (143 mg, 0.720 mmol) were added to **(D)-4-N₃** in an oven-dried 500 mL RBF. The mixture was stirred and sonicated until the (Cu(MeCN)₄PF₆) and TBTA dissolved. A chloroform (5 mL) solution of **(D)-**

4-alkyne was then added slowly to the above solution. The reaction mixture was warmed to 35 °C overnight then concentrated under reduced pressure. DCM (5 mL) was added to the resulting viscous mixture, which was then loaded carefully onto a column. Column chromatography (100% DCM to 2.5% MeOH/DCM then 5% MeOH/DCM) yielded the product (4.4 g, 2.5 mmol) in 69% yield from **(D)-4** as a yellow oil. ¹H NMR (500 MHz, CDCl₃): δ(ppm) 7.67 (s, 6H), 7.66 (s, 1H), 5.91 (ddt, *J* = 17.3, 10.4, 5.7 Hz, 1H), 5.75-5.67 (overlap, 7H), 5.29 (dq, *J* = 17.3 Hz, 1.6 Hz, 1H), 5.18-5.10 (overlap, 15H), 4.70-4.56 (overlap, 22H), 4.44-4.38 (overlap, 8H), 4.26 (d, *J* = 2.8 Hz, 2H), 4.11 (ddt, *J* = 5.7, 4.4, 1.4 Hz, 1H), 4.08-3.99 (overlap, 7H), 3.92-3.86 (overlap, 14H), 3.70 (dd, *J* = 9.7, 4.8 Hz, 1H), 3.68-3.62 (overlap, 4H), 3.58-3.50 (overlap, 12H), 3.45 (dd, *J* = 10.6, 4.8, 1H), 1.06 (s, 21H).

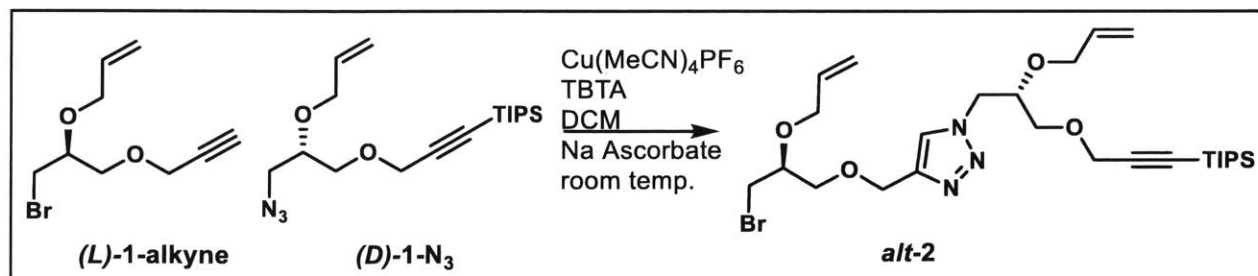


(D)-16B: The **(D)-8-alkyne** precursor to **(D)-16** was prepared by dissolving **(D)-8** (1.50 g, 0.850 mmol) in THF (10 mL) in a 40 mL scintillation vial, followed by the slow addition of tetrabutylammonium fluoride (TBAF) (1.05 equiv, 0.889 mL, 1M in THF). After 15 minutes, the reaction mixture was concentrated under reduced pressure. The crude mixture was then dissolved in EtOAc (100 mL) and extracted with deionized water (100 mL x 3). The organic layer was dried

over Na₂SO₄ and concentrated under vacuum. The resulting yellow oil containing **(D)-8-alkyne** and TIPS-F was used directly in the next step.

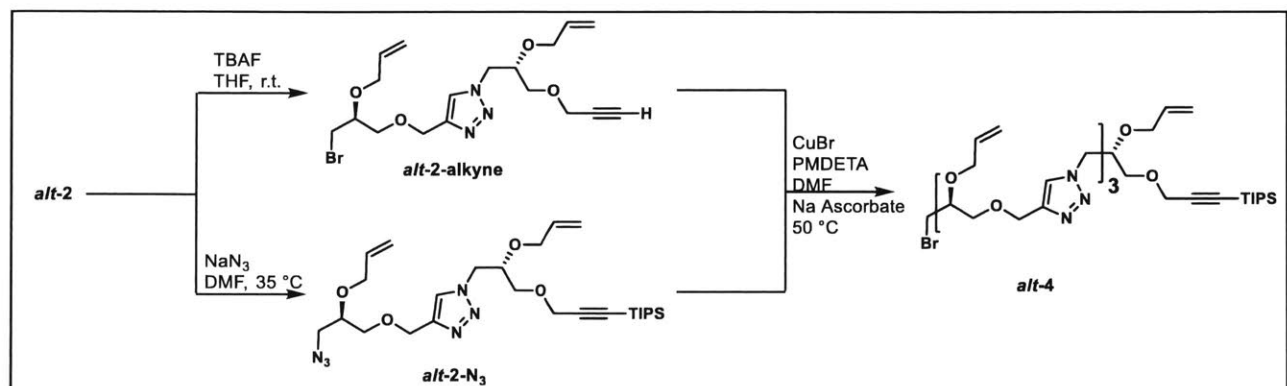
The **(D)-8-N₃** precursor to **(D)-16B** was prepared by dissolving **(D)-8** (1.50 g, 0.850 mmol) in DMF (100 mL), followed by the addition of NaN₃ (330 mg, 5.10 mmol). The reaction mixture was heated to 35 °C and allowed to stir for 12 h before the DMF was removed via rotary evaporator at 35 °C. *Heating past 35 °C was avoided as it leads to degradation of the product.* Then, EtOAc (100 mL) was added to the residue which was extracted with water (2 x 100 mL) and brine (1 x 100 mL). The organic layer was dried over Na₂SO₄ and concentrated under vacuum. The resulting **(D)-8-N₃** was obtained as a faint yellow oil that was used in the next step without further purification.

Under an N₂ atmosphere, chloroform (20 mL), Cu(MeCN)₄PF₆ (63.4 mg, 0.170 mmol) tris(benzyltriazolylmethyl)amine (TBTA) (180 mg, 0.340 mmol), and sodium ascorbate (67.4 mg, 0.340 mmol) were added to **(D)-8-N₃** in an oven-dried 250 mL RBF. The mixture was stirred and sonicated until the (Cu(MeCN)₄PF₆) and TBTA dissolved. A chloroform (3 mL) solution of **(D)-8-alkyne** was then added slowly to the above solution. The reaction mixture was warmed to 35 °C and left to react overnight before concentrating under reduced pressure. DCM (3 mL) was added to the resulting viscous mixture, which was then loaded carefully onto a column. Column chromatography (100% DCM to 3.5% MeOH/DCM then 6% MeOH/DCM) yielded the product (1.2 g, 0.36 mmol) in 42% yield from **(D)-16B** as a yellow oil. ¹H NMR (500 MHz, CDCl₃): δ(ppm) 7.68 (s, 14H), 7.66 (s, 1H), 5.90 (m, 1H), 5.75-5.67 (overlap, 15H), 5.29 (m, 1H), 5.19-5.08 (overlap, 31H), 4.69-4.56 (overlap, 46H), 4.46-4.38 (overlap, 16H), 4.24 (d, *J* = 1.5 Hz, 2H), 4.10 (m, 1H), 4.07-3.98 (overlap, 15H), 3.93-3.85 (overlap, 30H), 3.72-3.62 (overlap, 5H), 3.58-3.48 (overlap, 27H), 3.45 (dd, *J* = 10.5, 4.6 Hz, 1H), 1.07 (s, 21H).



alt-2: Under an N₂ atmosphere, DCM (150 mL), tetrakis(acetonitrile)copper(I) hexafluorophosphate (Cu(MeCN)₄PF₆) (1.27 g, 3.40 mmol) tris(benzyltriazolylmethyl)amine (TBTA) (3.61 g, 6.80 mmol), and Na ascorbate (1.35 g, 6.8 mmol) were added to **(D)-1-N₃** (23.8 g, 67.5 mmol) in an oven-dried 500 mL RBF. The mixture was stirred and sonicated until the (Cu(MeCN)₄PF₆) and TBTA dissolved. A DCM (50 mL) solution of **(L)-1-alkyne** (15.8 g, 67.5 mmol) was then added slowly to the above solution. The reaction mixture was left to react overnight after which DCM was removed under reduced pressure. DCM (10 mL) was added to the resulting viscous mixture, which was then loaded carefully onto a column. Column chromatography (25% hexanes/DCM to 1% MeOH/DCM) yielded the product (32 g, 55 mmol, 81% yield) as a faint yellow oil. HRMS-ESI for **alt-2**; Calcd for C₂₇H₄₆BrN₃O₄Si: m/z = 584.2514 [M + H]⁺; Found: 584.2520 [M + H]⁺. ¹H NMR (500 MHz, CDCl₃): δ(ppm) 7.66 (s, 1H), 5.90 (ddt, *J* = 16.3, 10.4, 5.7 Hz, 1H), 5.72 (ddt, *J* = 16.5, 10.3, 5.8 Hz, 1H), 5.29 (dd, *J* = 17.3, 1.7 Hz, 1H), 5.16 (overlap, 3H), 4.70 (d, *J* = 2.2 Hz, 2H), 4.61 (dd, *J* = 14.2, 3.4 Hz, 1H), 4.42 (dd, *J* = 14.2, 8.0 Hz, 1H), 4.25 (d, *J* = 2.4 Hz, 2H), 4.13 (overlap, 2H), 4.03 (dd, *J* = 12.7, 5.7 Hz, 2H), 3.90 (overlap, 2H), 3.70 (m, 1H), 3.67 – 3.57 (overlap, 3H), 3.53 (dd, *J* = 10.6, 5.1 Hz, 1H), 3.44 (dd, *J* = 10.6, 4.5 Hz, 1H), 1.07 (s, 21H). ¹³C NMR (125 MHz, CDCl₃): δ(ppm) 144.5, 134.5,

134.0, 124.2, 117.8, 117.6, 102.6, 96.3, 94.3, 88.4, 76.3, 71.2, 70.1, 67.9, 64.9, 59.5, 51.8, 32.2, 18.6, 11.1.

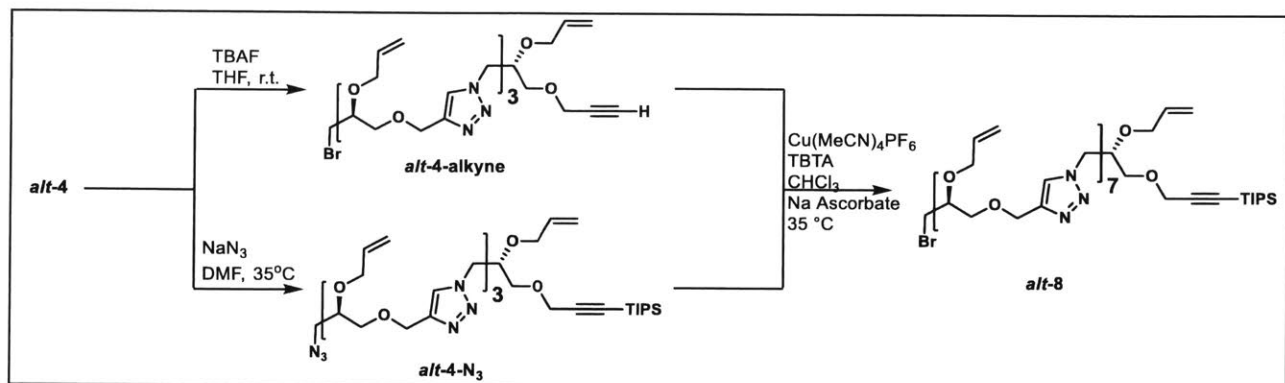


alt-4: The **alt-2-alkyne** precursor to **alt-4** was prepared by dissolving **alt-2** (13.0 g, 22.2 mmol) in THF (200 mL) in a 1L flask, followed by the slow addition of tetrabutylammonium fluoride (TBAF) (1.05 equiv, 23.3 mL, 1M in THF). After 15 minutes, the reaction mixture was concentrated under reduced pressure. The crude mixture was then dissolved in EtOAc (500 mL) and extracted with deionized water (500 mL x 3). The organic layer was dried with Na₂SO₄ and concentrated under vacuum. The resulting yellow oil containing **alt-2-alkyne** and TIPS-F was used directly in the next step.

The **alt-2-N₃** precursor to **alt-4** was prepared by dissolving **alt-2** (13.0 g, 22.2 mmol) in DMF (220 mL), followed by the addition of NaN₃ (8.66 g, 133 mmol). The reaction mixture was heated to 35 °C and allowed to stir for 12 h before the DMF was removed via rotary evaporator at 35 °C. *Heating past 35 °C was avoided as it leads to degradation of the product.* Then, EtOAc (500 mL) was added to the residue which was extracted with water (2 x 300 mL) and brine (1 x 300 mL).

The organic layer was dried over Na₂SO₄ and concentrated under vacuum. The resulting **alt-2-N₃** was obtained as a faint yellow oil that was used in the next step without further purification.

Under an N₂ atmosphere, dry DMF (50 mL), PMDETA (381 mg, 2.20 mmol, 0.459 mL), CuBr (158 mg, 1.10 mmol), and sodium ascorbate (436 mg, 2.20 mmol) were added to **alt-2-N₃** in an oven-dried 500 mL RBF. *The (Cu(MeCN)₄PF₆)/TBTA click conditions used for the alt-2 were not used here as it is difficult to separate TBTA from alt-4.* **alt-2-alkyne** in dry DMF (5 mL) was then added to the solution and the reaction mixture was warmed to 50 °C for 2 h. After completion, DMF was removed under reduced pressure. DCM (10 mL) was added to the resulting viscous mixture which was then loaded carefully onto a column. Column chromatography (100% DCM to 1.25% MeOH/DCM then 3% MeOH/DCM) yielded the product (16 g, 16 mmol) in 74% yield from **alt-2** as a yellow oil. ¹H NMR (500 MHz, CDCl₃): δ(ppm) 7.68 (s, 2H), 7.66 (s, 1H), 5.89 (ddt, *J* = 17.3, 10.3, 5.7 Hz, 1H), 5.76-5.67 (overlap, 3H), 5.28 (dq, *J* = 16.8, 0.9 Hz, 1H), 5.20-5.10 (overlap, 7H), 4.71-4.55 (overlap, 10H), 4.46-4.38 (overlap, 3H), 4.25 (d, *J* = 2.7 Hz, 2H), 4.10 (m, 1H), 4.03 (overlap, 3H), 3.95-3.85 (overlap, 6H), 3.70 (dd, *J* = 9.5, 4.9 Hz, 1H), 3.67-3.61 (overlap, 3H), 3.58-3.50 (overlap, 4H), 3.45 (dd, *J* = 10.8, 5.2 Hz, 1H), 3.44 (dd, *J* = 10.6, 4.7 Hz, 1H) 1.07 (s, 21H). ¹³C NMR (100 MHz, CDCl₃): δ(ppm) 144.6, 144.3, 134.6, 134.1, 134.0, 123.4, 124.3, 117.9, 117.8, 117.6, 101.5, 90.6, 77.4, 77.0, 76.4, 71.4, 71.3, 70.2, 69.0, 68.2, 64.8, 59.5, 51.8, 51.6, 32.3, 26.1, 16.5, -4.6.

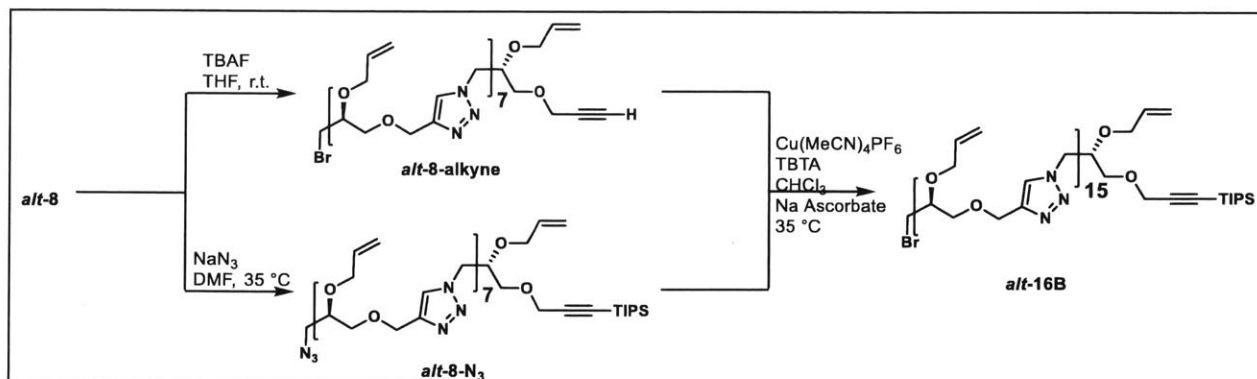


alt-8: The **alt-4-alkyne** precursor to **alt-8** was prepared by dissolving **alt-4** (6.00 g, 6.20 mmol) in THF (60 mL) in a 1L flask, followed by the slow addition of tetrabutylammonium fluoride (TBAF) (1.05 equiv, 6.5 mL, 1M in THF). After 15 minutes, the reaction mixture was concentrated under reduced pressure. The crude mixture was then dissolved in EtOAc (200 mL) and extracted with deionized water (3 x 200 mL). The organic layer was dried over Na₂SO₄ and concentrated under vacuum. The resulting yellow oil containing **alt-4-alkyne** and TIPS-F was used directly in the next step.

The **alt-4-N₃** precursor to **alt-8** was prepared by dissolving **alt-4** (6.00 g, 6.20 mmol) in DMF (400 mL), followed by the addition of NaN₃ (2.42 g, 37.2 mmol). The reaction mixture was heated to 35 °C and allowed to stir for 12 h before concentration via rotary evaporator at 35 °C. *Heating past 35 °C was avoided as it leads to degradation of the product.* Then, EtOAc (300 mL) was added to the residue which was extracted with water (2 x 200 mL) and brine (1 x 200 mL). The organic layer was dried over Na₂SO₄ and concentrated under vacuum. The resulting **alt-4-N₃** was obtained as a faint yellow oil that was used in the next step without further purification.

Under an N₂ atmosphere, chloroform (60 mL), Cu(MeCN)₄PF₆ (231 mg, 0.620 mmol) tris(benzyltriazolylmethyl)amine (TBTA) (658 mg, 1.24 mmol), and sodium ascorbate (246 mg,

1.24 mmol) were added to **alt-4-N₃** in an oven-dried 500 mL RBF. The mixture was stirred and sonicated until the (Cu(MeCN)₄PF₆) and TBTA dissolved. A chloroform (5 mL) solution of **alt-4-alkyne** was then added slowly to the above solution. The reaction mixture was warmed to 35 °C and left to react overnight whereupon chloroform was removed under reduced pressure. DCM (5 mL) was added to the resulting viscous mixture which was then loaded carefully onto a column. Column chromatography (100% DCM to 2.5% MeOH/DCM then 5% MeOH/DCM) yielded the product (7.6 g, 4.3 mmol) in 70% yield from **alt-4** as a yellow oil. ¹H NMR (500 MHz, CDCl₃): δ(ppm) 7.67 (s, 6H), 7.66 (s, 1H), 5.91 (ddt, *J* = 17.3, 10.4, 5.7 Hz, 1H), 5.75-5.67 (overlap, 7H), 5.27 (dq, *J* = 17.3 Hz, 1.6 Hz, 1H), 5.18-5.10 (overlap, 15H), 4.70-4.56 (overlap, 22H), 4.44-4.38 (overlap, 8H), 4.26 (d, *J* = 2.8 Hz, 2H), 4.11 (ddt, *J* = 5.7, 4.4, 1.4 Hz, 1H), 4.08-3.99 (overlap, 7H), 3.92-3.86 (overlap, 14H), 3.70 (dd, *J* = 9.7, 4.8 Hz, 1H), 3.68-3.62 (overlap, 4H), 3.58-3.50 (overlap, 12H), 3.45 (dd, *J* = 10.6, 4.8, 1H), 1.06 (s, 21H). ¹³C NMR (100 MHz, CDCl₃): δ(ppm) 144.6, 144.2, 134.5, 134.0, 124.4, 124.2, 117.8, 117.7, 117.6, 101.5, 90.6, 77.4, 76.9, 76.4, 76.3, 71.3, 70.2, 69.0, 68.1, 64.9, 64.8, 59.5, 51.8, 51.6, 32.3, 26.1, 16.5, -4.6.



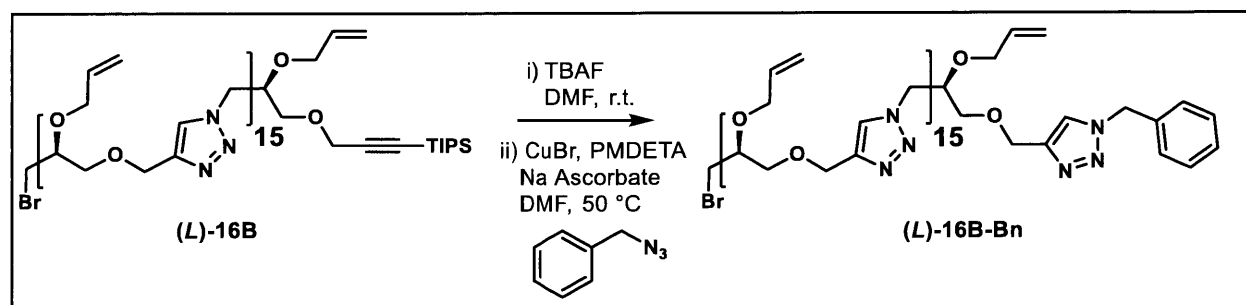
alt-16B: The **alt-8-alkyne** precursor to **alt-16** was prepared by dissolving **alt-8** (2.50 g, 1.40 mmol) in THF (50 mL) in a 250 mL flask, followed by the slow addition of tetrabutylammonium fluoride (TBAF) (1.05 equiv, 1.50 mL, 1M in THF). After 15 minutes, the reaction mixture was concentrated under reduced pressure. The crude mixture was then dissolved in EtOAc (100 mL) and extracted with deionized water (3 x 100 mL). The organic layer was dried over Na₂SO₄ and concentrated under vacuum. The resulting yellow oil containing **alt-8-alkyne** and TIPS-F was used directly in the next step.

The **alt-8-N₃** precursor to **alt-16B** was prepared by dissolving **alt-8** (2.50 g, 1.40 mmol) in DMF (100 mL), followed by the addition of NaN₃ (550 mg, 8.50 mmol). The reaction mixture was heated to 35 °C and allowed to stir for 12 h before the DMF was removed via rotary evaporator at 35 °C. *Heating past 35 °C was avoided as it leads to degradation of the product.* Then, EtOAc (250 mL) was added to the residue and extracted with water (2 x 100 mL) and brine (1 x 100 mL). The organic layer was dried over Na₂SO₄ and concentrated under vacuum. The resulting **alt-8-N₃** was obtained as a faint yellow oil and used in the next step without further purification.

Under an N₂ atmosphere, chloroform (15 mL), Cu(MeCN)₄PF₆ (104 mg, 0.280 mmol) tris(benzyltriazolylmethyl)amine (TBTA) (297 mg, 0.560 mmol), and sodium ascorbate (111 mg,

0.560 mmol) were added to **alt-8-N₃** in an oven-dried 250 mL RBF. The mixture was stirred and sonicated until the (Cu(MeCN)₄PF₆) and TBTA dissolved. A chloroform (5 mL) solution of **alt-8-alkyne** was then added slowly to the above solution. The reaction mixture was warmed to 35 °C and left to react overnight whereupon chloroform was removed under reduced pressure. DCM (10 mL) was added to the resulting viscous mixture, which was then loaded carefully onto a column. Column chromatography (100% DCM to 3.5% MeOH/DCM then 6% MeOH/DCM) yielded the product (2.2 g, 0.67 mmol) in 48% yield from **alt-8** as an off-white solid. ¹H NMR (500 MHz, CDCl₃): δ(ppm) 7.68 (s, 14H), 7.66 (s, 1H), 5.91 (ddt, *J* = 16.3, 10.8, 5.8 Hz, 1H), 5.77-5.68 (overlap, 15H), 5.29 (m, 1H), 5.21-5.08 (overlap, 31H), 4.71-4.56 (overlap, 46H), 4.46-4.38 (overlap, 16H), 4.25 (d, *J* = 1.7 Hz, 2H), 4.11 (m, 1H), 4.08-3.99 (overlap, 15H), 3.93-3.85 (overlap, 30H), 3.72-3.62 (overlap, 5H), 3.60-3.49 (m, 27H), 3.45 (dd, *J* = 10.5, 4.6 Hz, 1H), 1.07 (s, 21H). ¹³C NMR (100 MHz, CDCl₃): δ(ppm) 144.6, 144.2, 134.5, 134.0, 124.5, 124.3, 117.8, 117.6, 102.6, 88.6, 77.4, 76.9, 76.4, 76.3, 71.4, 71.3, 70.6, 70.2, 69.0, 68.0, 64.9, 64.8, 59.5, 51.9, 51.6, 32.3, 18.7, 11.2.

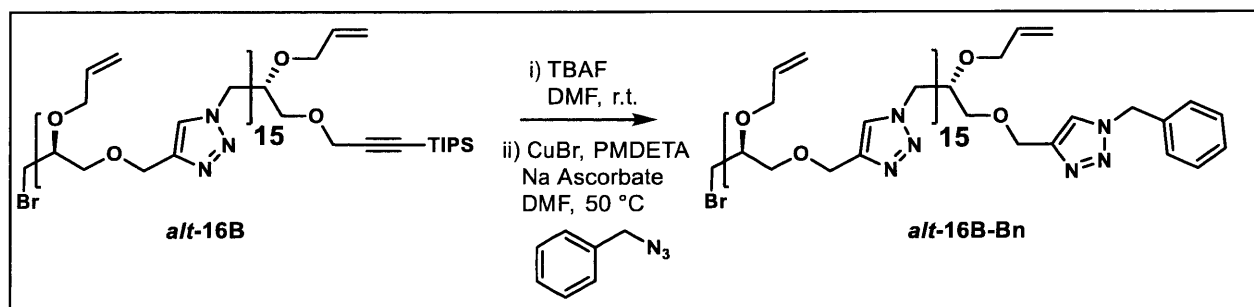
5. Thiol-ene functionalization of 16mer allyl ethers



(L)-16B-Bn: **(L)-16** (200 mg, 0.0603 mmol) was dissolved in DMF (0.600 mL), followed by the slow addition of TBAF (1.05 equiv, 0.0634 mL, 1M in THF). After 15 minutes, the reaction

mixture was concentrated under reduced pressure. The product was then purified by preparatory GPC (chloroform) to yield **(L)-16B-alkyne** (169 mg, 0.0537 mmol, 89% yield) as a yellow oil.

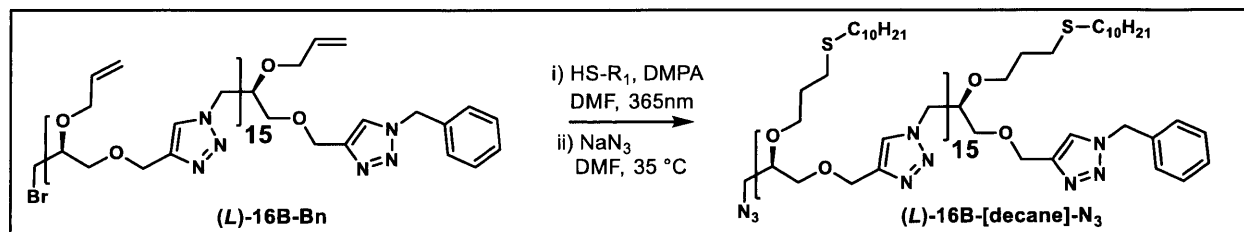
Under an N₂ atmosphere, dry DMF (0.500 mL) and sodium ascorbate (15.1 mg, 0.0762 mmol) were added to a mixture of **(L)-16B-alkyne** (120 mg, 0.038 mmol) and 4-methylbenzyl azide (55.6 mg, 0.380 mmol) in an oven-dried 40 mL scintillation vial. A DMF solution of 0.1 M CuBr and 0.2 M PMDETA (0.381 mL) was then added to the reaction mixture. The reaction was warmed to 50 °C for 2 h. After completion, DMF was removed under reduced pressure. DCM (1 mL) was added to the resulting viscous mixture which was then loaded carefully onto a column. Column chromatography (100% DCM to 8% MeOH/DCM) yielded the product (100 mg, 0.031 mmol) in 83% yield from **(L)-16** as a yellow oil. ¹H NMR (500 MHz, CDCl₃): δ(ppm) 7.70 (s, 14H), 7.69 (s, 1H), 7.52 (s, 1H), 7.39 (overlap, 3H), 7.29 (overlap, 1H), 5.92 (ddt, *J* = 16.1, 10.2, 5.4 Hz, 1H), 5.77-5.68 (overlap, 15H), 5.55 (s, 2H), 5.33-5.29 (m, 1H), 5.19-5.11 (overlap, 31H), 4.69-4.57 (m, 48H), 4.47-4.40 (m, 16H), 4.12 (m, 1H), 4.06-3.99 (m, 15H), 3.94-3.83 (overlap, 30H), 3.73 (dd, *J* = 9.6, 4.9 Hz, 1H), 3.67-3.63 (overlap, 2H), 3.61-3.48 (overlap, 31H), 3.47 (dd, *J* = 10.5, 4.7 Hz, 1H).



alt-16B-Bn: **alt-16B** (300 mg, 0.0904 mmol) was dissolved in DMF (0.900 mL), followed by the slow addition of TBAF (1.05 equiv, 0.095 mL, 1M in THF). After 15 minutes, the crude reaction

mixture was concentrated under reduced pressure. The product was then purified by preparatory GPC (chloroform) to yield **alt-16B-alkyne** (262 mg, 0.0832 mmol, 92% yield) as an off-white solid.

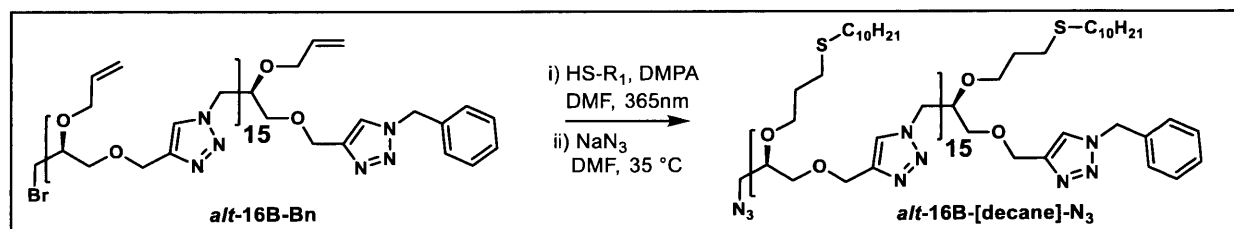
Under an N₂ atmosphere, dry DMF (0.500 mL) and sodium ascorbate (15.1 mg, 0.0762 mmol) were added to a mixture of **alt-16B-alkyne** (120 mg, 0.038 mmol) and 4-methylbenzyl azide (55.6 mg, 0.38 mmol) in an oven-dried 40 mL scintillation vial. A DMF solution of 0.1 M CuBr and 0.2 M PMDETA (0.381 mL) was then added to the reaction mixture. The reaction was warmed to 50 °C left to react for 2 h. After completion, DMF was removed under reduced pressure. DCM (1 mL) was added to the resulting viscous mixture which was then loaded carefully onto a column. Column chromatography (100% DCM to 8% MeOH/DCM) yielded the product (110 mg, 0.033 mmol) in 87% yield from **alt-16B** as an off-white solid. ¹H NMR (500 MHz, CDCl₃): δ(ppm) 7.70 (s, 14H), 7.68 (s, 1H), 7.51 (s, 1H), 7.38 (overlap, 3H), 7.30 (overlap, 2H), 5.91 (ddt, *J* = 16.4, 10.0, 5.2 Hz, 1H), 5.77-5.90 (overlap, 15H), 5.55 (s, 2H), 5.33-5.25 (m, 1H), 5.20-5.11 (overlap, 31H), 4.69-4.58 (m, 48H), 4.46-4.42 (m, 16H), 4.11 (m, 1H), 4.06-3.98 (m, 15H), 3.92-3.84 (overlap, 30H), 3.72 (dd, *J* = 9.5, 5.0 Hz, 1H), 3.67-3.62 (overlap, 2H), 3.59-3.51 (overlap, 31H), 3.46 (dd, *J* = 10.7, 4.6 Hz, 1H).



(L)-16B-[decane]-N₃: **(L)-16B-Bn** (104 mg, 0.0315 mmol) was dissolved in a solution of CDCl₃ (0.853 mL), 1-decanethiol (0.703 g, 4.03 mmol, 0.853 mL), and 2,2-dimethoxy-2-

phenylacetophenone (258 mg, 1.01 mmol) in a 20 mL scintillation vial. The solution was sparged for 2 min with N₂ and then irradiated with 365 nm light for 2 h. The crude mixture was checked for completion by ¹ NMR spectroscopy. The desired product was purified by preparatory GPC (chloroform). **(L)-16B-[decane]** was obtained (0.172 g, 0.284 mmol, 90% yield) as a yellow, waxy solid.

DMF (0.568 mL) was added to **(L)-16B-[decane]** (172 mg, 0.0284 mmol) followed by the addition of NaN₃ (11.1 mg, 0.170 mmol). The reaction mixture was heated to 65 °C and allowed to stir for 12 h whereupon DMF was removed via rotary evaporator. Then, EtOAc (50 mL) was added to the residue which was extracted with water (2 x 30 mL) and brine (1 x 30 mL). The organic layer was dried over Na₂SO₄ and concentrated under vacuum yielding **(L)-16B-[decane]-N₃** (160 mg, 0.027 mmol, 96% yield). ¹H NMR (500 MHz, CDCl₃): δ(ppm) 7.69 (s, 14H), 7.66 (s, 1H), 7.52 (s, 1H), 7.38 (overlap, 3H), 7.28 (overlap, 2H), 5.55 (s, 2H), 4.71-4.55 (overlap, 48H), 4.46-4.39 (overlap, 16H), 3.90-3.82 (overlap, 16H), 3.69-3.50 (overlap, 48H), 3.50-3.38 (overlap, 16H), 2.63-2.60 (overlap, 4H) 2.52-2.42 (br, 60H), 1.82-1.72 (overlap, 32H), 1.59-1.50 (br, 36H), 1.42-1.22 (br, 220H), 0.92-0.87 (br, 48H).

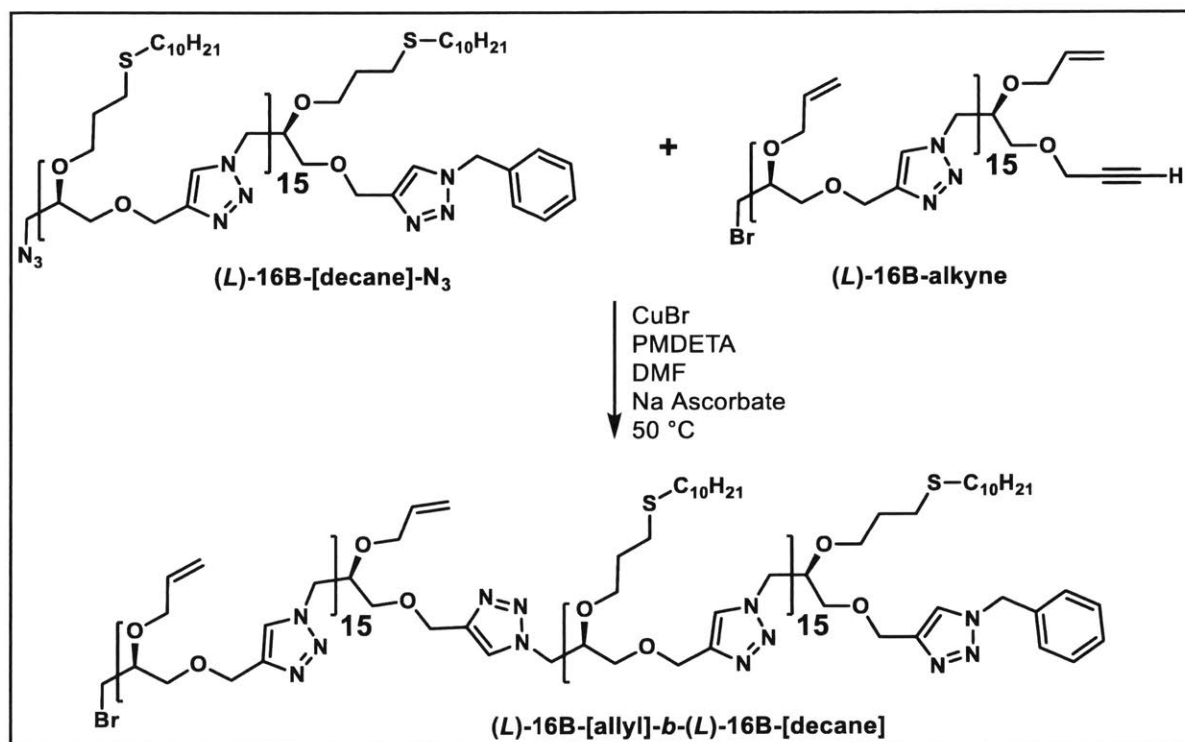


alt-16B-[decane]-N₃: *alt*-(L)-16B-[decane]-Bn (109 mg, 0.0328 mmol) was dissolved in a solution of CDCl₃ (0.889 mL), 1-decanethiol (0.733 g, 4.20 mmol, 0.889 mL), and 2,2-dimethoxy-2-phenylacetophenone (269 mg, 1.05 mmol) in a 20 mL scintillation vial. The solution was sparged for 2 min with N₂ and then irradiated with 365 nm light for 2 h. The crude mixture was checked

for completion by ^1H NMR spectroscopy. The desired product was purified by preparatory GPC (chloroform). ***alt-16B-[decane]*** was obtained (0.179 g, 0.0295 mmol, 90% yield) as a yellow, waxy solid.

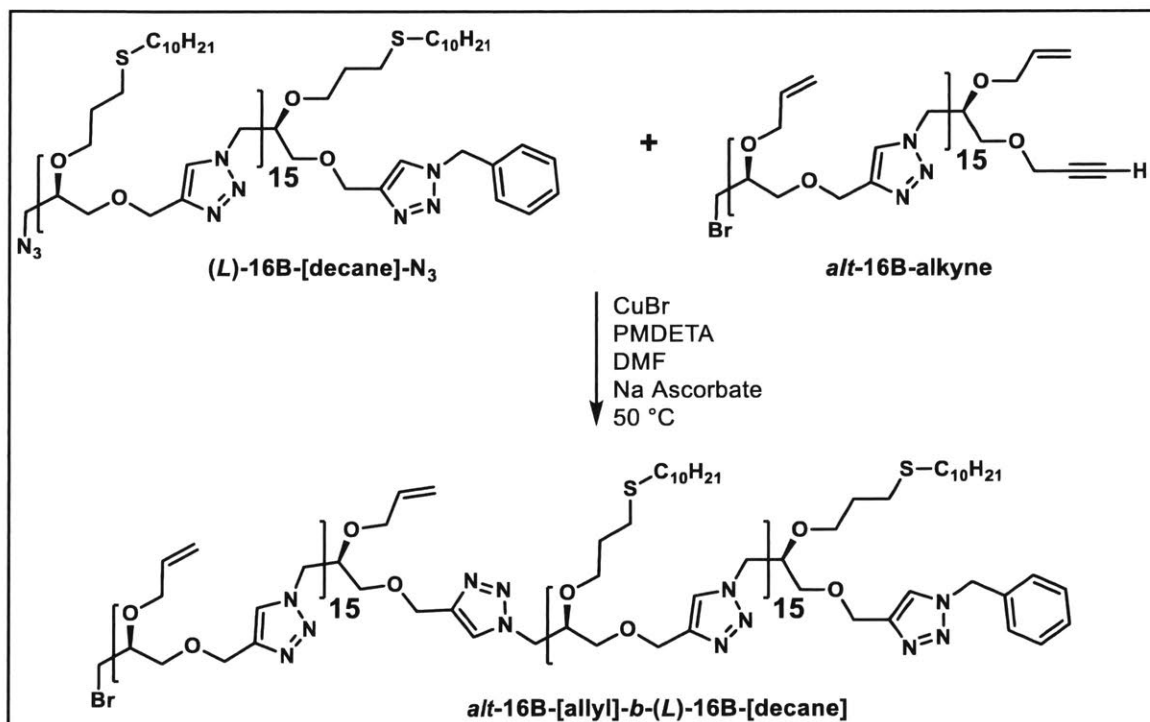
DMF (0.568 mL) was added to ***alt-16B-[decane]*** (179 mg, 0.0295 mmol), followed by the addition of NaN_3 (11.5 mg, 0.177 mmol). The reaction mixture was heated to $65\text{ }^\circ\text{C}$ and allowed to stir for 12 h whereupon DMF was removed via rotary evaporator. Then, EtOAc (50 mL) was added to the residue which was extracted with water (2 x 30 mL) and brine (1 x 30 mL). The organic layer was dried over Na_2SO_4 and concentrated under vacuum yielding ***alt-16-[decane]-N₃*** (170 mg, 0.028 mmol, 94% yield) as a yellow, waxy solid. ^1H NMR (500 MHz, CDCl_3): δ (ppm) 7.68 (s, 14H), 7.63 (s, 1H), 7.50 (s, 1H), 7.37 (overlap, 3H), 7.28 (overlap, 2H), 5.54 (s, 2H), 4.72-4.54 (overlap, 48H), 4.46-4.38 (overlap, 16H), 3.90-3.81 (overlap, 16H), 3.69-3.50 (overlap, 48H), 3.49-3.38 (overlap, 16H), 2.62-2.59 (overlap, 4H) 2.52-2.42 (br, 60H), 1.82-1.71 (overlap, 32H), 1.60-1.51 (br, 36H), 1.42-1.22 (br, 220H), 0.90-0.85 (br, 48H).

6. Synthesis of diblock copolymers



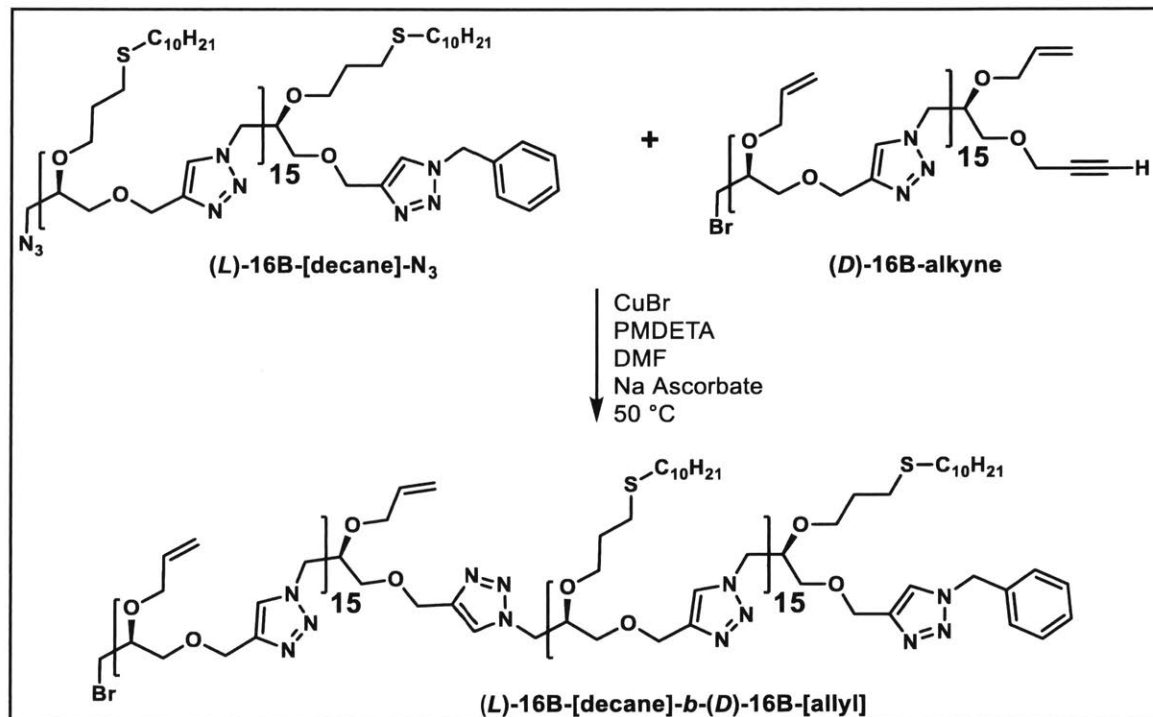
(L)-16B-[allyl]-b-(L)-16B-[decane]: Under an N₂ atmosphere, dry DMF (0.100 mL), sodium ascorbate (7.92 mg, 0.040 mmol), CuBr (2.80 mg, 0.02 mmol), and PMDTA (7.00 mg, 0.040 mmol, 8.40 μ L) were added to (L)-16B-[decane]-N₃ (50.0 mg, 0.00820 mmol). A mixture of DMF (0.100 mL) and (L)-16B-alkyne (51 mg, 0.0164 mmol) was added to the above solution. The reaction mixture was warmed to 50 °C overnight. After completion, the reaction mixture was concentrated under reduced pressure. DCM (3 mL) was added to the resulting viscous mixture that was passed through a plug of neutral alumina (8% MeOH/DCM). The filtrate was concentrated under vacuum. The crude product was purified by preparatory GPC (chloroform). (L)-16B-[allyl]-b-(L)-16B-[decane] (15 mg, 0.0016 mmol, 20% yield) was obtained as a yellow solid. ¹H NMR (500 MHz, CDCl₃): δ (ppm) 7.70-7.66 (overlap, 31H), 7.51 (s, 1H), 7.37 (overlap, 3H), 7.28 (overlap, 2H), 5.91 (ddt, J =16.2, 10.9, 5.5 Hz, 1H), 5.77-5.67 (overlap, 15H), 5.48 (s, 2H), 5.32-

5.26 (m, 1H), 5.21-5.10 (overlap, 31H), 4.72-4.55 (overlap, 96H), 4.46-4.43 (overlap, 32H), 4.13-4.08 (m, 1H), 4.14-3.98 (overlap, 15H), 3.91-3.79 (overlap, 48H), 3.72 (dd, $J = 9.5, 5.0$ Hz, 1H), 3.72-3.50 (overlap, 79H), 3.46-3.37 (overlap, 16H), 2.68-2.52 (overlap, 4H), 2.50-2.41 (overlap, 60H), 1.99-1.92 (m, 2H), 1.79-1.70 (overlap, 32H), 1.57-1.50 (overlap, 30H), 1.38-1.16 (overlap, 224H), 0.89-0.84 (overlap, 48H).



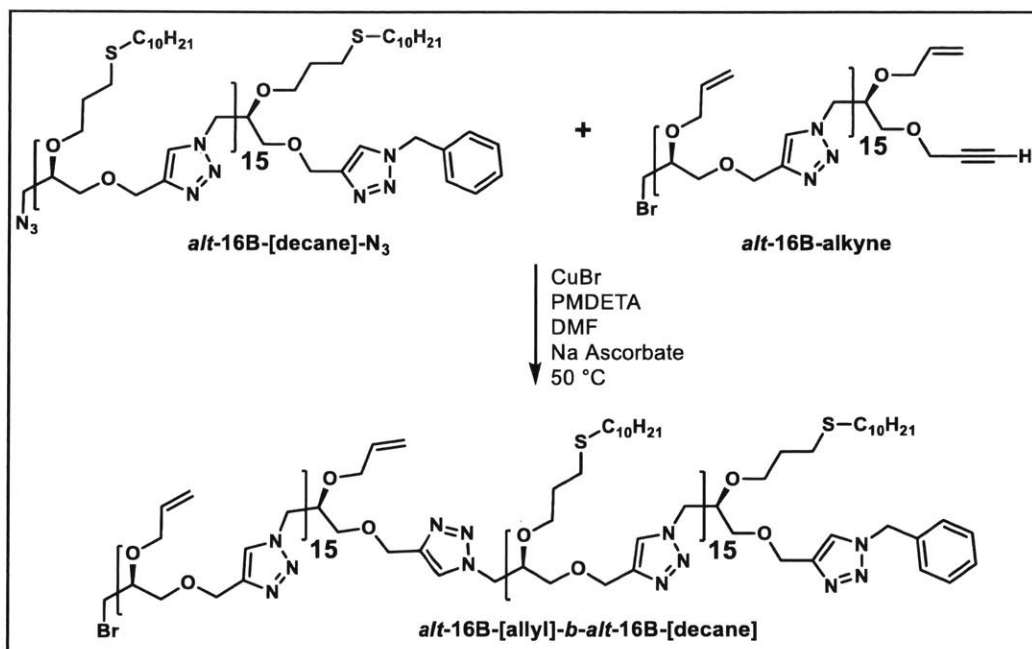
alt-16B-[allyl]-b-(L)-16B-[decane]: Under an N₂ atmosphere, dry DMF (0.100 mL), sodium ascorbate (7.92 mg, 0.0400 mmol), CuBr (2.80 mg, 0.0200 mmol), and PMDTA (7.00 mg, 0.040 mmol, 8.40 μ L) were added to **(L)-16B-[decane]-N₃** (50 mg, 0.0082 mmol). A mixture of DMF (0.100 mL) and **alt-16-alkyne** (51.0 mg, 0.0164 mmol) was added to the above solution. The reaction mixture was warmed to 50 °C overnight. After completion, DMF was removed under reduced pressure. DCM (3 mL) was added to the resulting viscous mixture that was passed through a plug of neutral alumina (8% MeOH/DCM). The filtrate was concentrated under vacuum. The crude product was purified by preparatory GPC (chloroform). **alt-16B-[allyl]-b-(L)-16B-[decane]**

(19 mg, 0.0021 mmol, 25% yield) was obtained as a yellow solid. ^1H NMR (500 MHz, CDCl_3): δ (ppm) 7.71-7.64 (overlap, 31H), 7.51 (s, 1H), 7.37 (overlap, 3H), 7.27 (overlap, 2H), 5.89 (ddt, $J = 16.5, 11.0, 5.5$ Hz, 1H), 5.76-5.67 (overlap, 15H), 5.54 (s, 2H), 5.31-5.25 (m, 1H), 5.21-5.10 (overlap, 31H), 4.72-4.55 (overlap, 96H), 4.46-4.44 (overlap, 32H), 4.14-4.07 (m, 1H), 4.14-3.98 (overlap, 15H), 3.91-3.80 (overlap, 48H), 3.70 (dd, $J = 9.7, 5.0$ Hz, 1H), 3.72-3.50 (overlap, 79H), 3.45-3.37 (overlap, 16H), 2.67-2.54 (overlap, 4H), 2.50-2.41 (overlap, 60H), 2.01-1.93 (m, 2H), 1.78-1.68 (overlap, 32H), 1.57-1.49 (overlap, 30H), 1.38-1.15 (overlap, 224H), 0.90-0.82 (overlap, 48H).



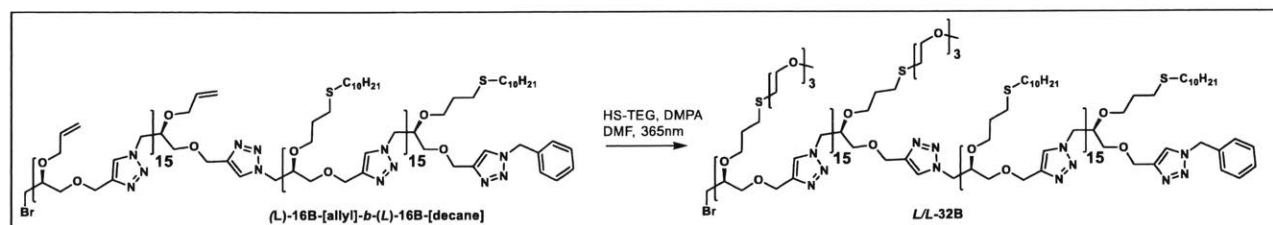
(D)-16B-[allyl]-*b*-(L)-16B-[decane]: (D)-16 (100 mg, 0.0302 mmol) was dissolved in DMF (0.300 mL), followed by the slow addition of TBAF (1.05 equiv, 0.0317 mL, 1M in THF). After 15 minutes, DMF was removed under reduced pressure. The crude product was then purified by preparatory GPC (chloroform) to yield (D)-16B-alkyne (85 mg, 0.0269 mmol, 89% yield) as an off-white solid.

Under an N₂ atmosphere, dry DMF (0.100 mL), sodium ascorbate (7.92 mg, 0.040 mmol), CuBr (2.80 mg, 0.020 mmol), and PMDTA (7.00 mg, 0.040 mmol, 8.40 μL) were added to **(L)-16B-[decane]-N₃** (50.0 mg, 0.00820 mmol). A mixture of DMF (0.100 mL) and **(D)-16B-alkyne** (51.0 mg, 0.0164 mmol) was added to the above solution. The reaction mixture was warmed to 50 °C overnight. After completion, DMF was removed under reduced pressure. DCM (3 mL) was added to the resulting viscous mixture that was passed through a plug of neutral alumina (8% MeOH/DCM). The filtrate was concentrated under vacuum. Purification by preparatory GPC (chloroform) afforded the desired product **(D)-16B-[allyl]-b-(L)-16B-[decane]** (13 mg, 0.0014 mmol, 17% yield) as a yellow solid. ¹H NMR (500 MHz, CDCl₃): δ(ppm) 7.72-7.67 (overlap, 31H), 7.52 (s, 1H), 7.37 (overlap, 3H), 7.30 (overlap, 2H), 5.90 (ddt, *J*=16.4, 11.0, 5.7 Hz, 1H), 5.76-5.67 (overlap, 15H), 5.54 (s, 2H), 5.30-5.24 (m, 1H), 5.20-5.10 (overlap, 31H), 4.71-4.57 (overlap, 96H), 4.46-4.44 (overlap, 32H), 4.11 (m, 1H), 4.13-4.01 (overlap, 15H), 3.91-3.80 (overlap, 48H), 3.70 (m, 1H), 3.72-3.50 (overlap, 79H), 3.45-3.36 (overlap, 16H), 2.68-2.55 (overlap, 4H), 2.50-2.41 (overlap, 60H), 1.99-1.93 (m, 2H), 1.79-1.72 (overlap, 32H), 1.60-1.49 (overlap, 30H), 1.39-1.18 (overlap, 224H), 0.90-0.84 (overlap, 48H).

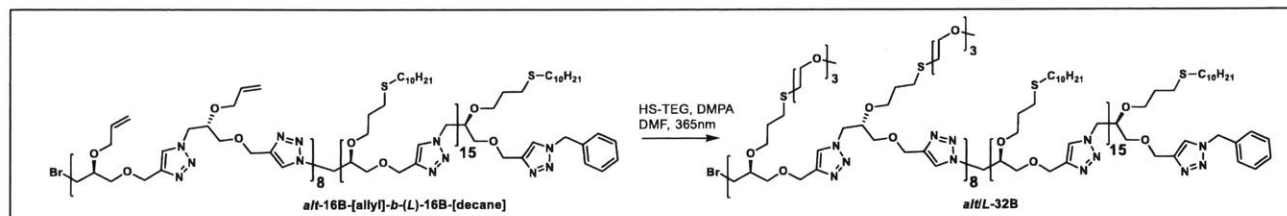


***alt*-16B-[allyl]-*b*-*alt*-16B-[decane]**: Under an N₂ atmosphere, dry DMF (0.100 mL), sodium ascorbate (22.0 mg, 0.111 mmol), CuBr (7.90 mg, 0.0554 mmol), and PMDTA (19.2 mg, 0.111 mmol, 23.1 μ L) were added to *alt*-16B-[decane]-N₃ (168 mg, 0.0277 mmol). A mixture of DMF (0.100 mL) and *alt*-16B-[allyl]-alkyne (90.0 mg, 0.0286 mmol) was added to the above solution. The reaction mixture was warmed to 50 °C overnight. After completion, DMF was removed under reduced pressure. DCM (3 mL) was added to the resulting viscous mixture that was passed through a plug of neutral alumina plug (8% MeOH/DCM). The filtrate was concentrated under vacuum. Purification by preparatory GPC (chloroform) afforded the desired product ***alt*-16B-[allyl]-*b*-*alt*-16B-[decane]** (76 mg, 0.0083 mmol, 29% yield) as a yellow solid. ¹H NMR (500 MHz, CDCl₃): δ (ppm) 7.72-7.64 (overlap, 31H), 7.50 (s, 1H), 7.36 (overlap, 3H), 7.27 (overlap, 2H), 5.89 (ddt, J =16.3, 11.0, 5.5 Hz, 1H), 5.76-5.66 (overlap, 15H), 5.53 (s, 2H), 5.31-5.24 (m, 1H), 5.21-5.09 (overlap, 31H), 4.73-4.30 (overlap, 128H), 4.13-4.06 (m, 1H), 4.06-3.99 (overlap, 15H), 3.96-3.79 (overlap, 48H), 3.74-3.48 (overlap, 80H), 3.44-3.36 (overlap, 16H), 2.69-2.36 (overlap, 64H),

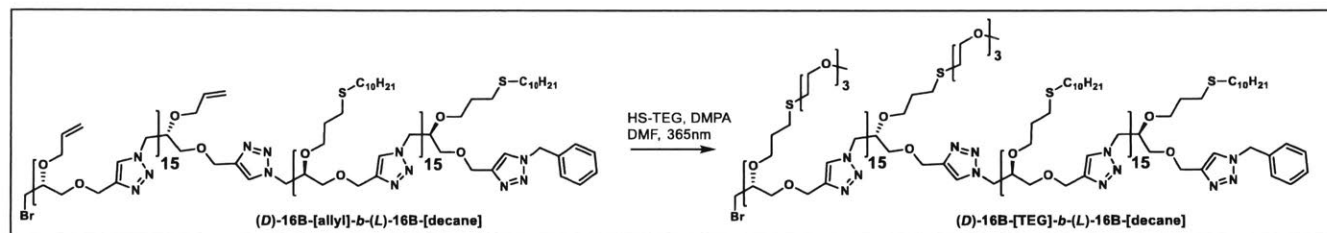
1.99-1.92 (m, 2H), 1.81-1.62 (overlap, 32H), 1.57-1.49 (overlap, 30H), 1.38-1.18 (overlap, 224H), 0.89-0.82 (overlap, 48H).



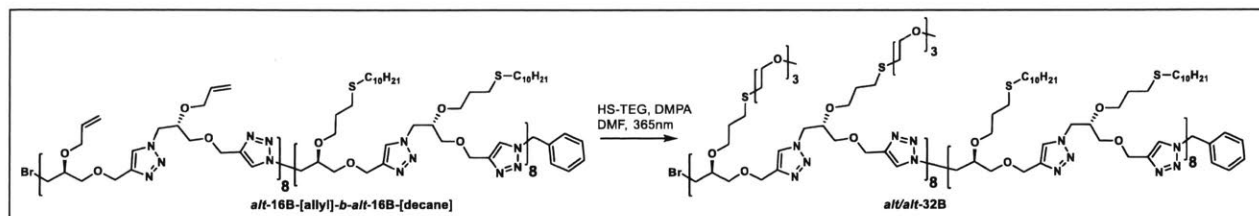
L/L-32B (i.e. **(L)-16B-[TEG]-b-(L)-16B-[decane]**): **(L)-16B-[allyl]-b-(L)-16B-[decane]** (15.0 mg, 0.00163 mmol) was dissolved in a solution of CDCl_3 (0.075 mL), 1-mercapto-triethyleneglycol monomethyl ether² (75.1 mg, 0.416 mmol), and 2,2-dimethoxy-2-phenylacetophenone (13.4 mg, 0.0521 mmol) in a 20 mL scintillation vial. The solution was sparged with N_2 for 30 s and irradiated with 365 nm light for 2 h. After checking for completion of the reaction by ^1H NMR spectroscopy, the reaction mixture was purified by preparatory GPC (chloroform). After purification, the collected fractions were concentrated under vacuum. The product **L/L-32B** (11 mg, 0.00090 mmol, 56% yield) was obtained as an off-white solid. ^1H NMR (500 MHz, CDCl_3): δ (ppm) 7.71-7.63 (overlap, 31H), 7.51 (s, 1H), 7.36 (overlap, 3H), 7.28 (overlap, 2H), 5.54 (s, 2H), 4.72-4.55 (overlap, 96H), 4.46-4.37 (overlap, 32H), 3.89-3.79 (overlap, 16H), 3.71-3.48 (overlap, 288H), 3.43-3.35 (overlap, 64H), 2.67-2.61 (overlap, 32H), 2.54-2.41 (overlap, 96H), 1.85-1.70 (br, 32H), 1.68-1.48 (overlap, 28H), 1.37-1.14 (br, 224H), 0.88-0.84 (t, 48H).



alt/L-32B (i.e. **alt-16B-[TEG]-b-(L)-16B-[decane]**): **alt-16B-[allyl]-b-(L)-16B-[decane]** (19.0 mg, 0.00206 mmol) was dissolved in a solution of CDCl_3 (0.0950 mL), 1-mercapto-triethyleneglycol monomethyl ether² (95.2 mg, 0.528 mmol), and 2,2-dimethoxy-2-phenylacetophenone (17.0 mg, 0.0660 mmol) in a 20 mL scintillation vial. The solution was sparged with N_2 for 30 s and irradiated with 365 nm light for 2 h. After checking for completion of the reaction by ^1H NMR spectroscopy, the reaction mixture was purified by preparatory GPC (chloroform). After purification, the collected fractions were concentrated under vacuum. The product **alt/L-32B** (13 mg, 0.0011 mmol, 52% yield) was obtained as an off-white solid. ^1H NMR (500 MHz, CDCl_3): δ (ppm) 7.72-7.64 (overlap, 31H), 7.50 (s, 1H), 7.37 (overlap, 3H), 7.29 (overlap, 2H), 5.53 (s, 2H), 4.70-4.55 (overlap, 96H), 4.46-4.36 (overlap, 32H), 3.90-3.81 (overlap, 16H), 3.71-3.50 (overlap, 288H), 3.44-3.35 (overlap, 64H), 2.73-2.55 (overlap, 32H), 2.54-2.41 (overlap, 96H), 1.95 (br, 2H), 1.84 (br, 2H), 1.78-1.69 (br, 28H), 1.68-1.62 (br, 36H), 1.57-1.48 (overlap, 28H), 1.39-1.12 (br, 224H), 0.88-0.85 (t, 48H).



D/L-32B (i.e. **(D)-16B-[TEG]-b-(L)-16B-[decane]**): **(D)-16B-[allyl]-b-(L)-16B-[decane]** (13.0 mg, 0.00141 mmol) was dissolved in a solution of CDCl_3 (0.0650 mL), 1-mercapto-triethyleneglycol monomethyl ether¹ (65.1 mg, 0.361 mmol), and 2,2-dimethoxy-2-phenylacetophenone (11.6 mg, 0.0452 mmol) in a 20 mL scintillation vial. The solution was sparged with N_2 for 30 s and irradiated with 365 nm light for 2 h. After checking for completion of the reaction by ^1H NMR spectroscopy, the reaction mixture was purified by preparatory GPC (chloroform). After purification, the collected fractions were concentrated under vacuum. The product **D/L-32B** (11 mg, 0.00090 mmol, 64% yield) was obtained as an off-white solid. ^1H NMR (500 MHz, CDCl_3): δ (ppm) 7.69-7.64 (overlap, 31H), 7.50 (s, 1H), 7.36 (overlap, 3H), 7.27 (overlap, 2H), 5.53 (s, 2H), 4.71-4.54 (overlap, 96H), 4.45-4.37 (overlap, 32H), 3.90-3.80 (br, 16H), 3.67-3.50 (overlap, 288H), 3.43-3.34 (overlap, 64H), 2.71-2.63 (overlap, 32H), 2.53-2.40 (overlap, 96H), 1.94 (br, 2H), 1.83 (br, 2H), 1.78-1.68 (br, 28H), 1.56-1.47 (overlap, 36H) 1.36-1.14 (overlap, 252H), 0.87-0.83 (t, 48H).



alt/alt-32B (i.e. *alt-16B-[TEG]-b-alt-16B-[decane]*): *alt-16B-[allyl]-b-alt-16B-[decane]* (40.0 mg, 0.00434 mmol) was dissolved in a solution of CDCl_3 (0.200 mL), 1-mercapto-triethyleneglycol monomethyl ether¹ (200 mg, 1.11 mmol), and 2,2-dimethoxy-2-phenylacetophenone (35.6 mg, 0.139 mmol) in a 20 mL scintillation vial. The solution was sparged with N_2 for 30 s and irradiated with 365 nm light for 2 h. After checking for completion of the reaction by ^1H NMR spectroscopy, the reaction mixture was purified by preparatory GPC (chloroform). After purification, the collected fractions were concentrated under vacuum. The product ***alt/alt-32B*** (37 mg, 0.0031 mmol, 70% yield) was obtained as an off-white solid. ^1H NMR (500 MHz, CDCl_3): δ (ppm) 7.71-7.66 (overlap, 31H), 7.51 (s, 1H), 7.36 (overlap, 3H), 7.27 (overlap, 2H), 5.54 (s, 2H), 4.70-4.55 (overlap, 96H), 4.46-4.37 (overlap, 32H), 3.90-3.80 (br, 16H), 3.66-3.52 (overlap, 288H), 3.43-3.36 (overlap, 64H), 2.70-2.63 (t, 32H), 2.52-2.42 (overlap, 96H), 1.78-1.65 (overlap, 32H), 1.57-1.49 (overlap, 36H), 1.37-1.12 (overlap, 252H), 0.88-0.84 (t, 48H).

NMR Spectroscopic Characterization

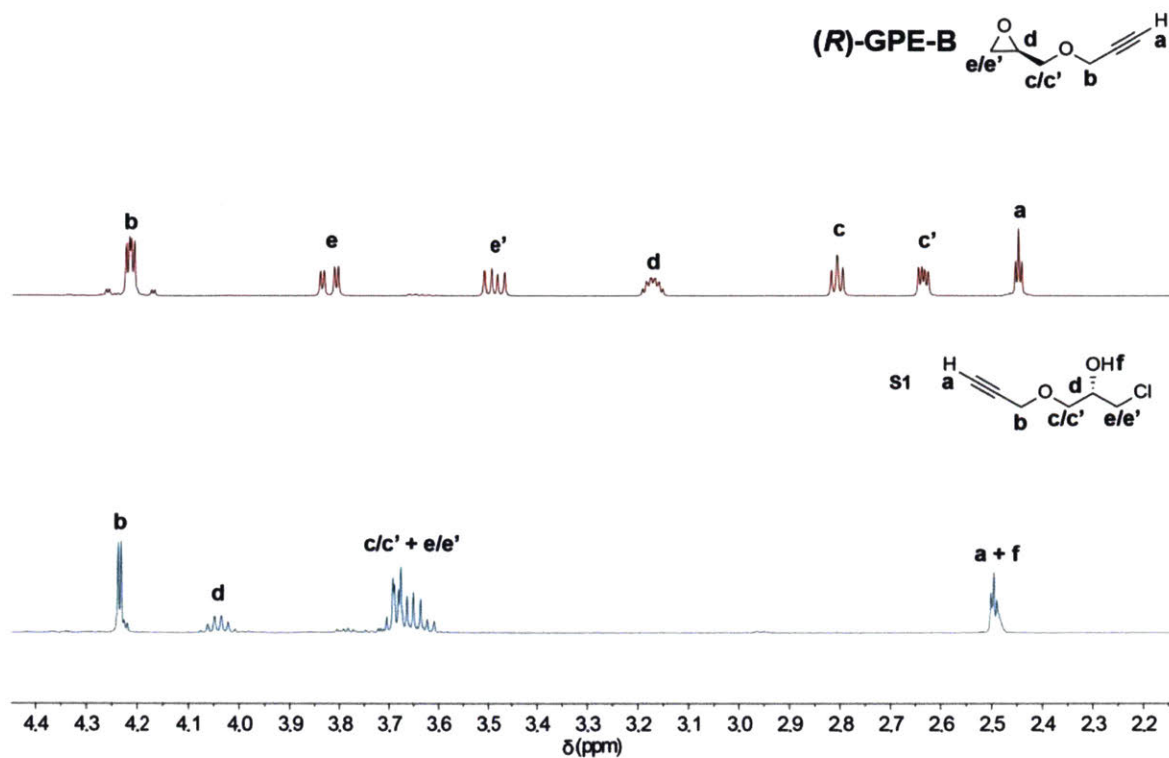


Figure S3.1. ¹H NMR spectra of secondary alcohol **S1** (bottom) and **GPE-B** (top). **S1** is formed upon treatment of epichlorohydrin with propargyl alcohol under Lewis acidic (BF₃·OEt₂) conditions; epoxide **GPE-B** is formed when **S1** is deprotonated under basic conditions.

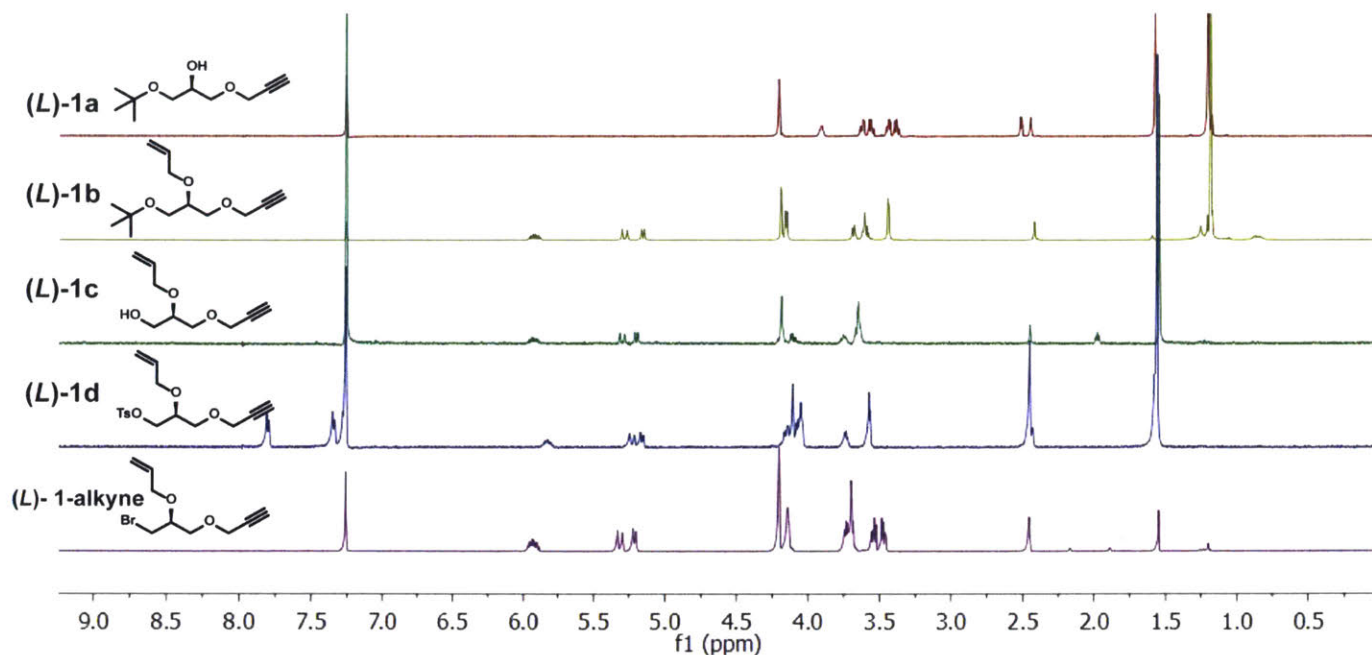


Figure S3.2. ^1H NMR spectra of intermediates ((L) -1a to (L) -1d) leading to (L) -1-alkyne.

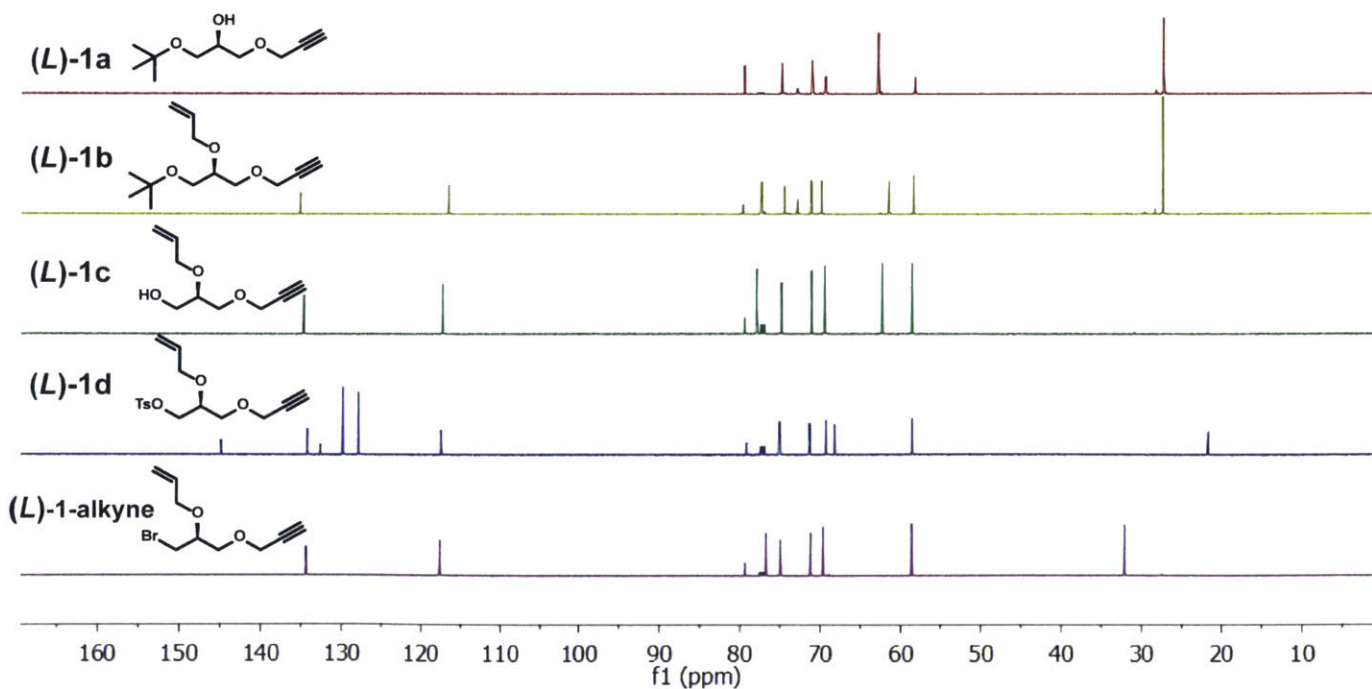


Figure S3.3. ^{13}C NMR spectra of intermediates ((L) -1a to (L) -1d) leading to (L) -1-alkyne.

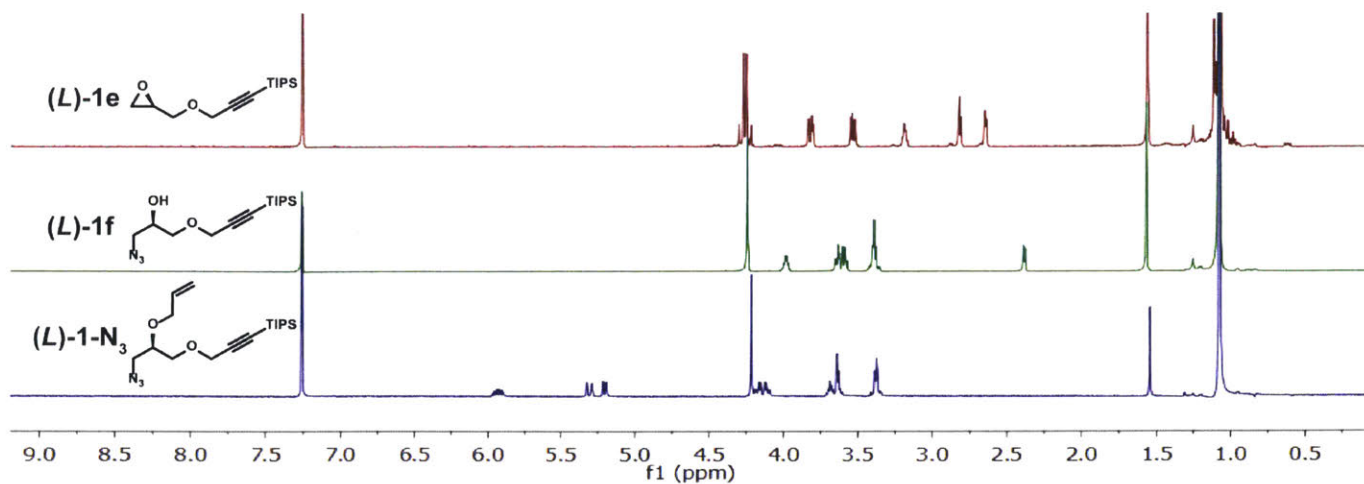


Figure S3.4. ^1H NMR spectra of intermediates ((*L*)-**1e** to (*L*)-**1f**) leading to (*L*)-**1-N₃**.

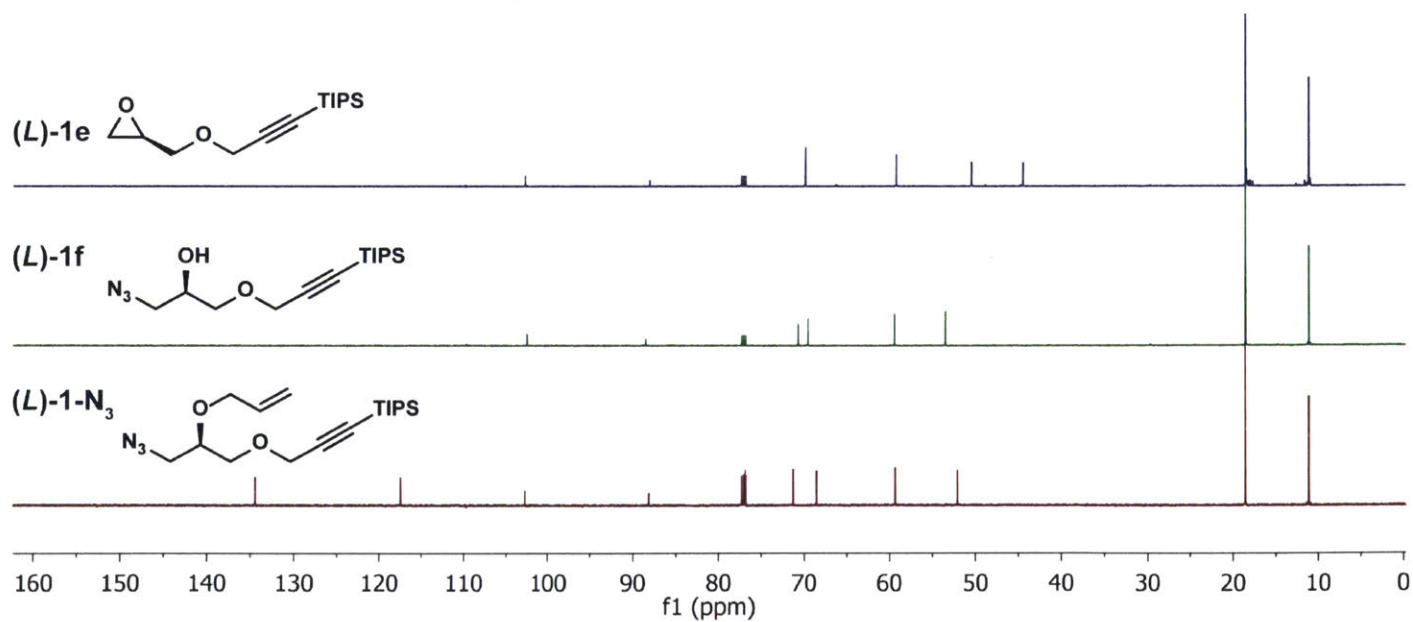


Figure S3.5. ^{13}C NMR spectra of intermediates ((*L*)-**1e** to (*L*)-**1f**) leading to (*L*)-**1-N₃**.

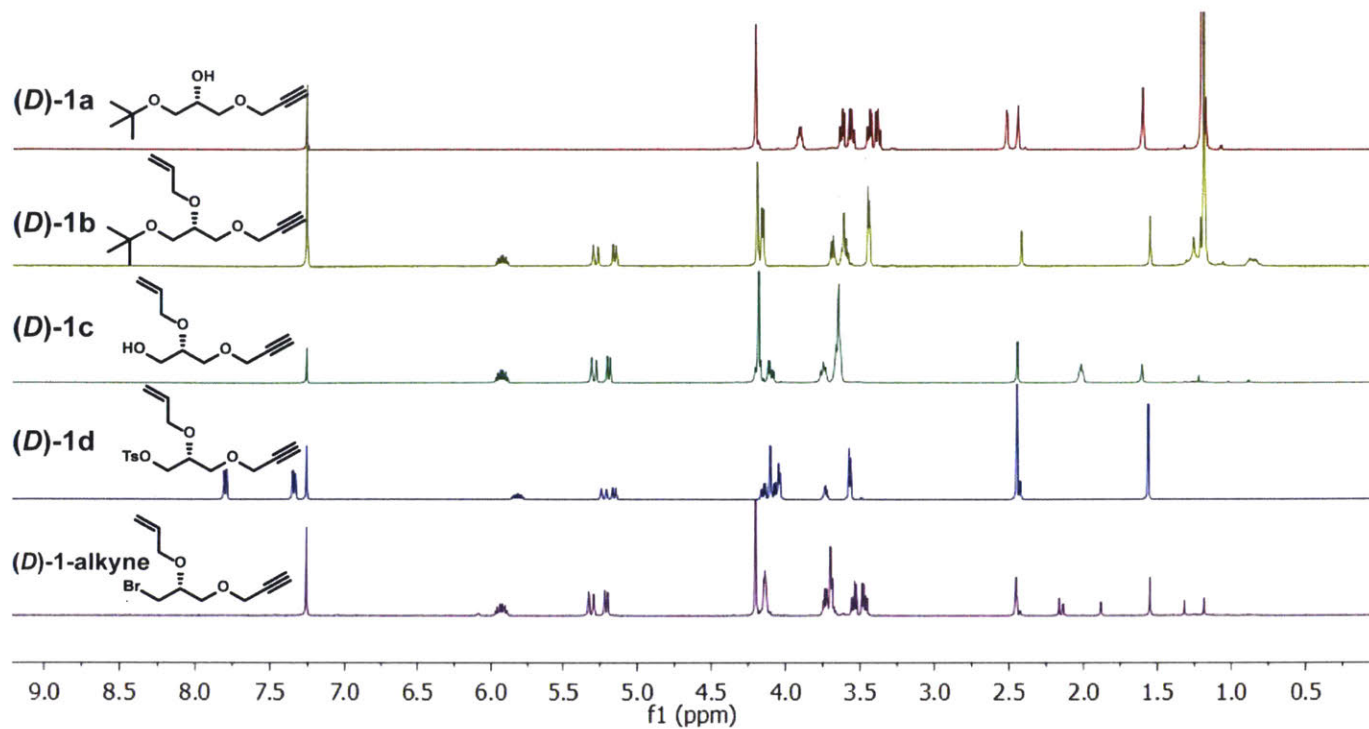


Figure S3.6. ^1H NMR spectra of intermediates (**(D)-1a** to **(D)-1d**) leading to **(D)-1-alkyne**.

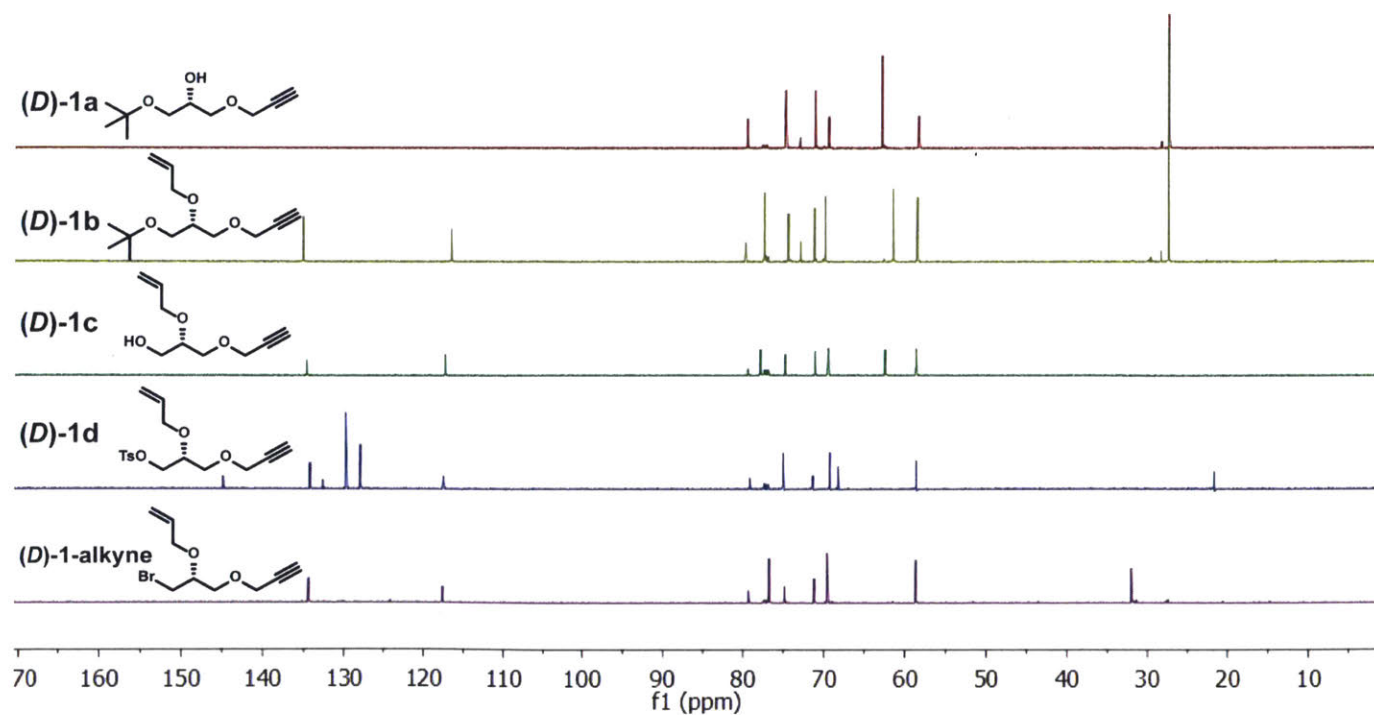


Figure S3.7. ^{13}C NMR spectra of intermediates (**(D)-1a** to **(D)-1d**) leading to **(D)-1-alkyne**.

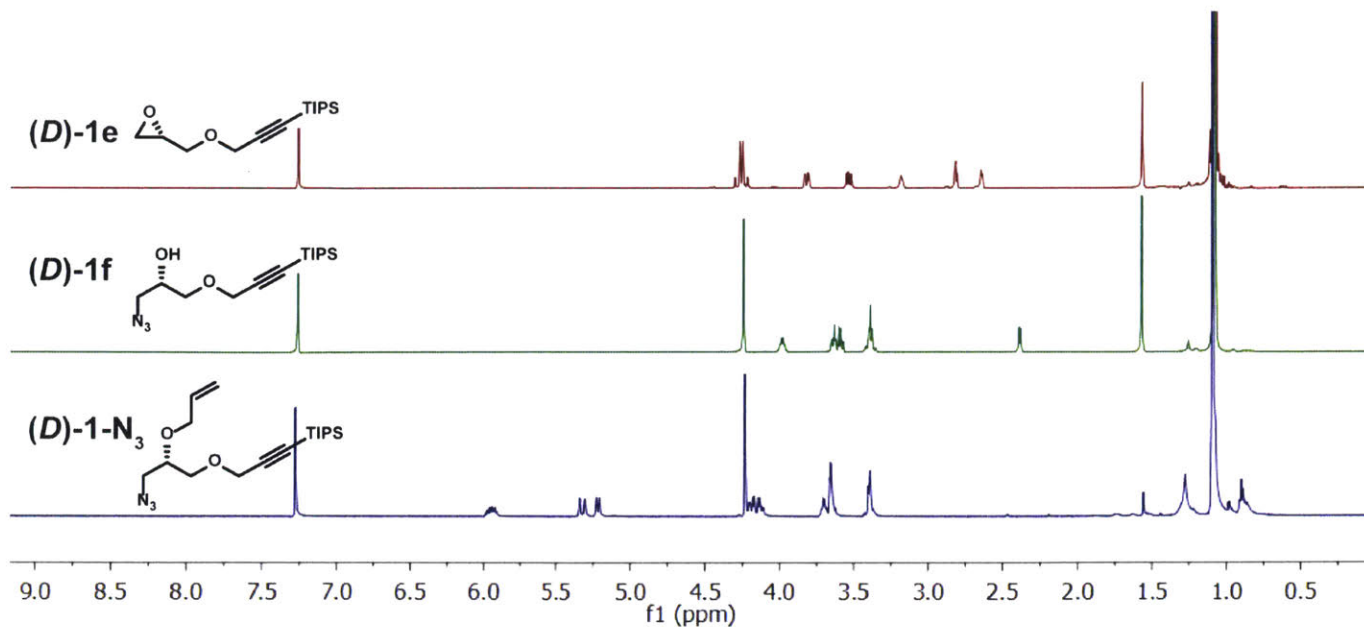


Figure S3.8. ^1H NMR spectra of intermediates (**(D)-1e** to **(D)-1f**) leading to **(D)-1-N₃**.

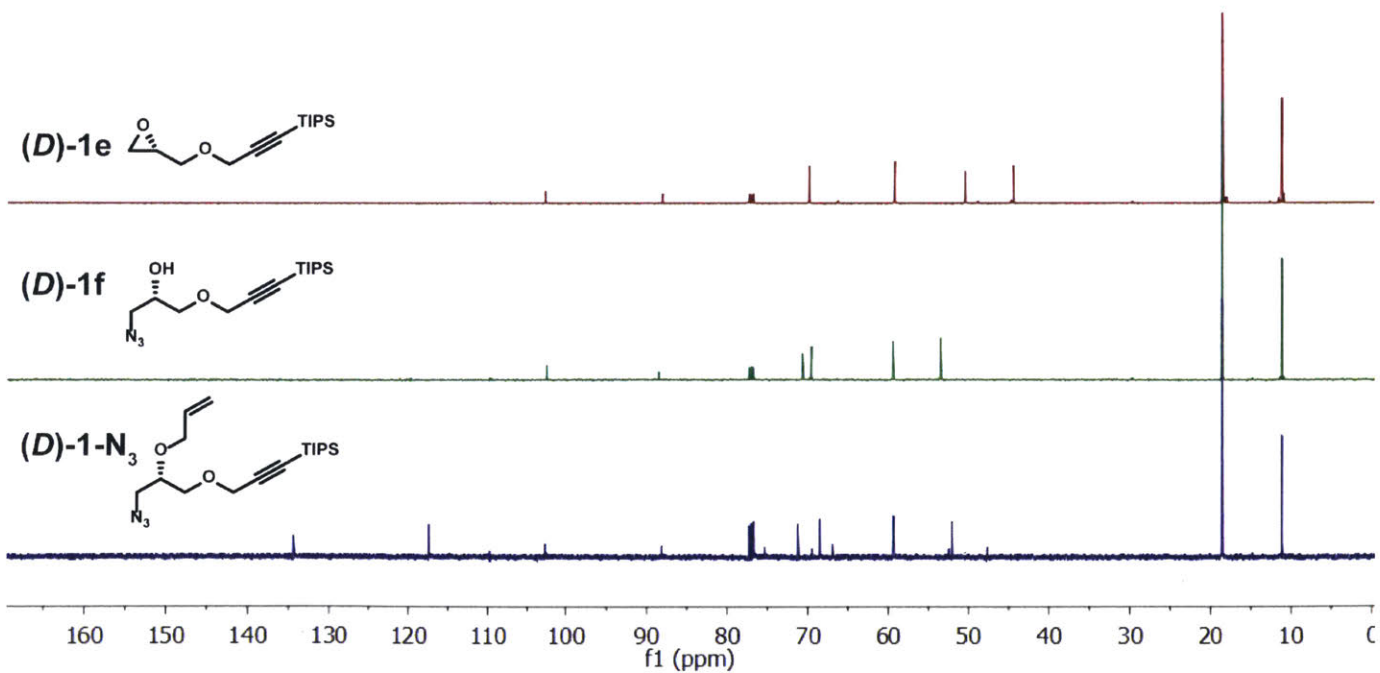


Figure S3.9. ^{13}C NMR spectra of intermediates (**(D)-1e** to **(D)-1f**) leading to **(D)-1-N₃**.

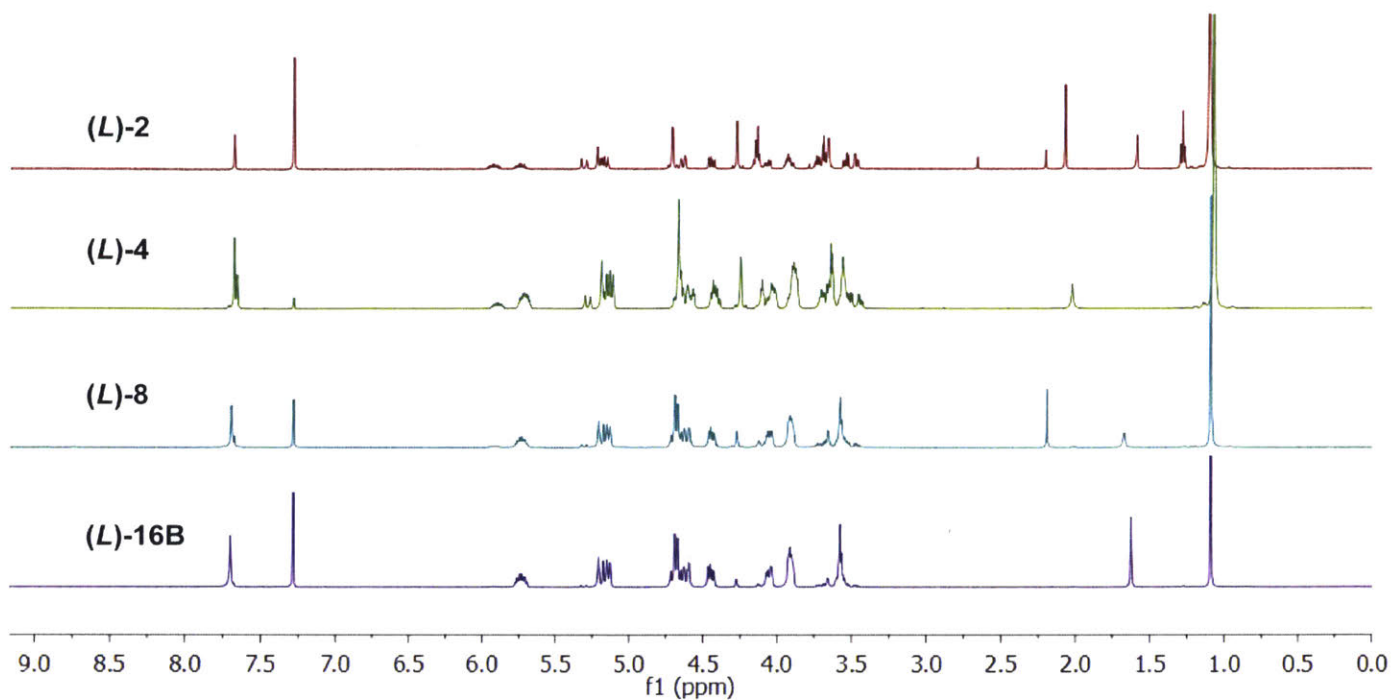


Figure S3.10. ¹H NMR spectra of (*L*)-allyl IEGmers ((*L*)-2, (*L*)-4, (*L*)-8, and (*L*)-16B)

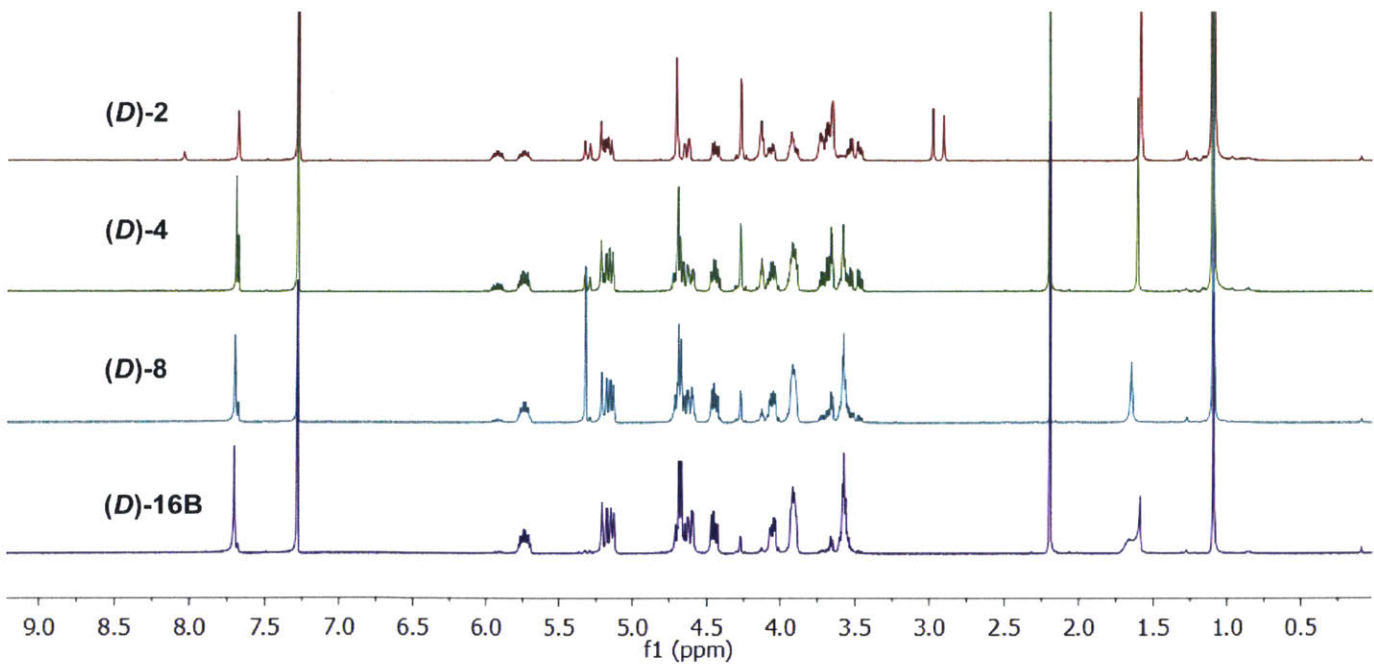


Figure S3.11. ¹H NMR spectra of (*D*)-allyl IEGmers ((*D*)-2, (*D*)-4, (*D*)-8, and (*D*)-16B)

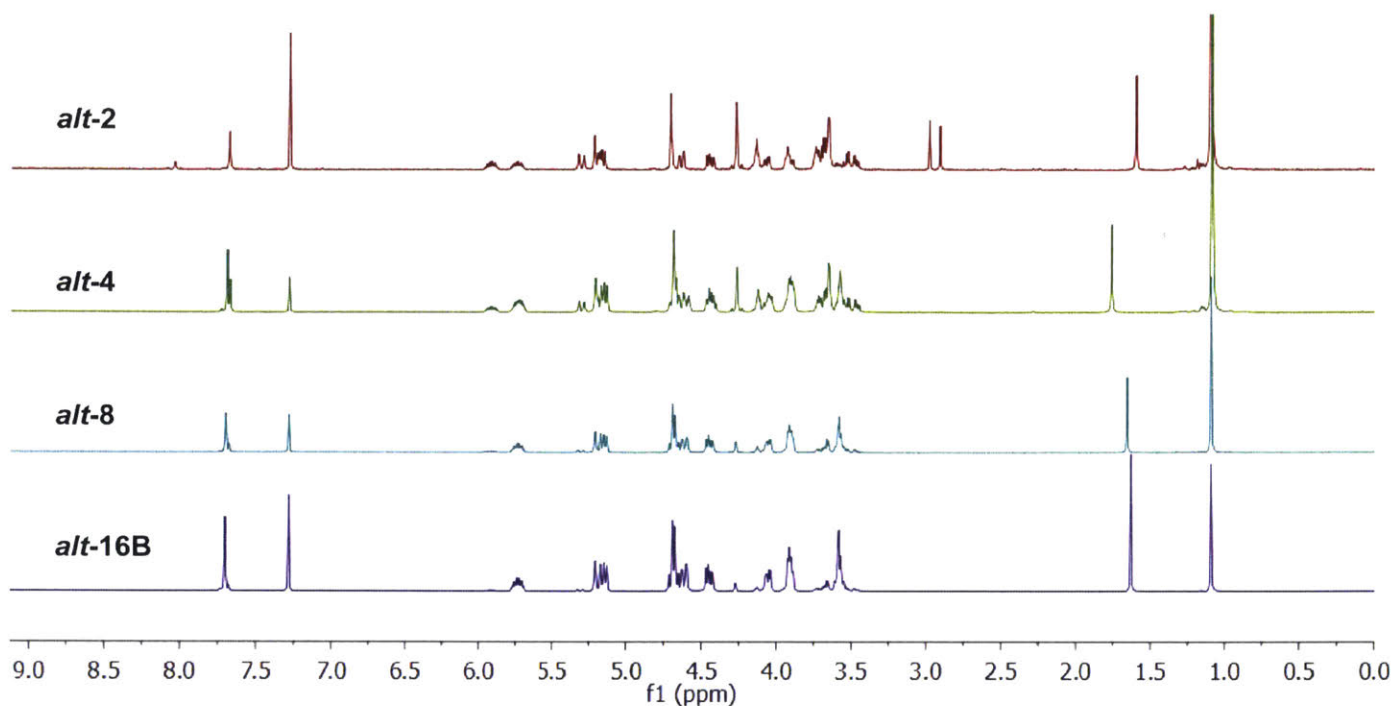


Figure S3.12. ^1H NMR spectra of *alt* (i.e. (*L,D*))-allyl IEGmers (*alt-2*, *alt-4*, *alt-8*, and *alt-16B*).

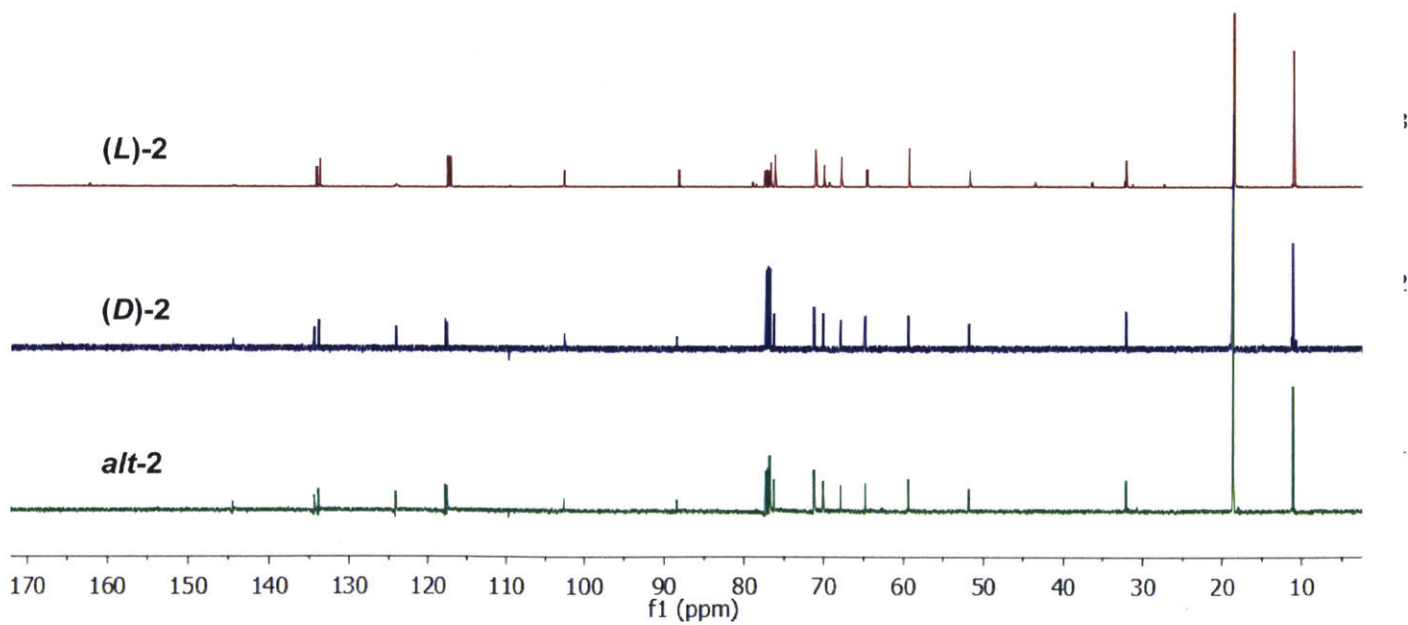


Figure S3.13. ^{13}C NMR spectra of (*L*)-2, (*D*)-2, and *alt-2*.

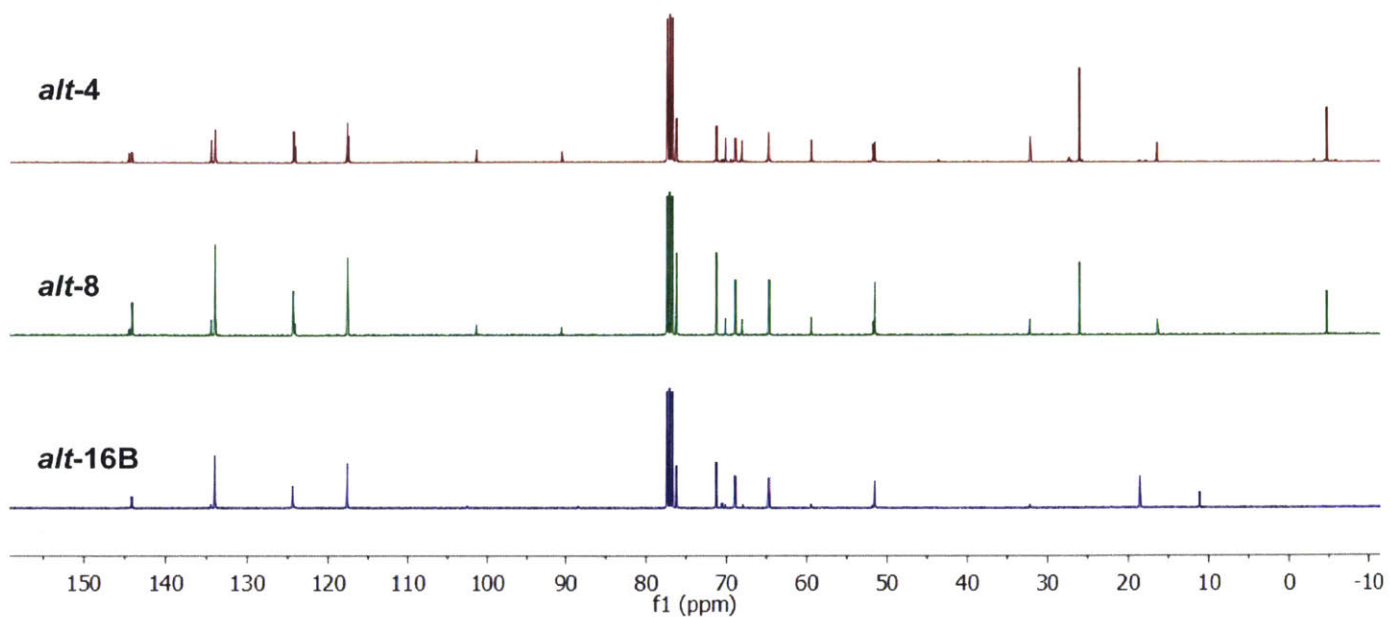


Figure S3.14. ^{13}C NMR spectra of *alt*- IEGmers (*alt-4*, *alt-8*, *alt-16B*)

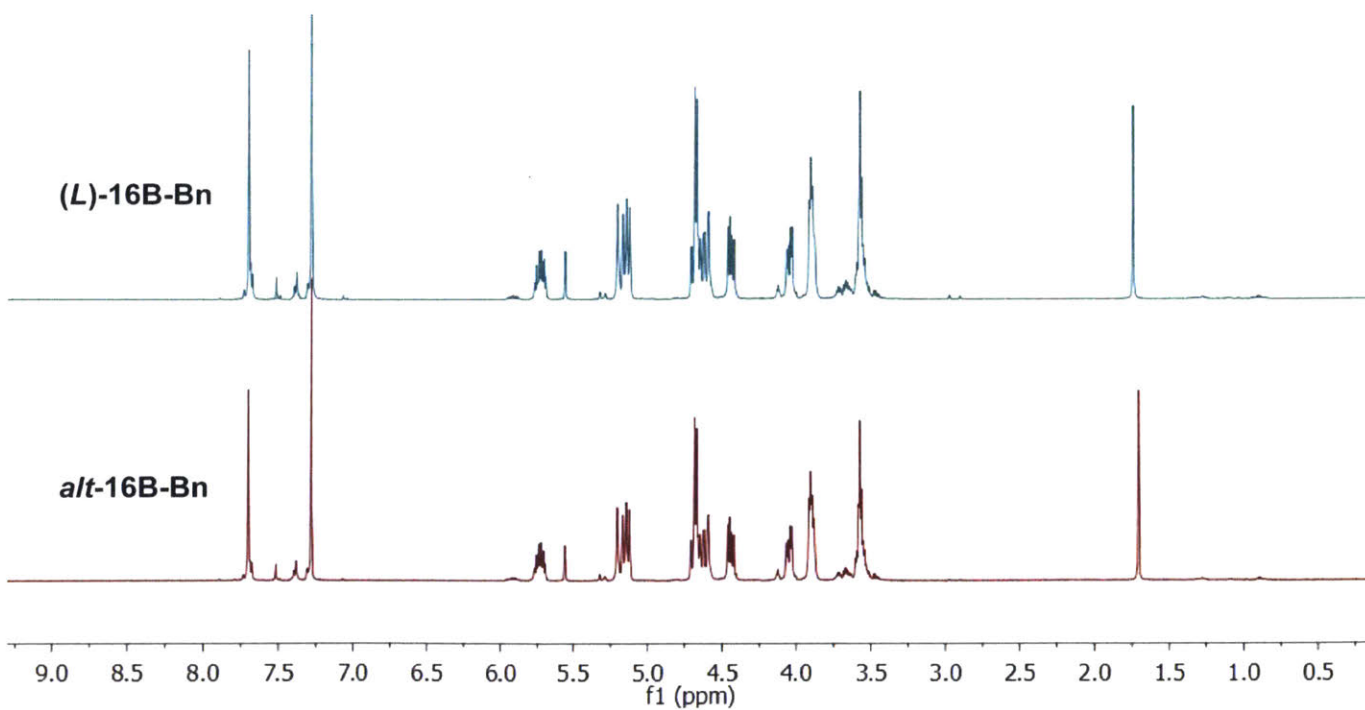


Figure S3.15. ^1H NMR spectra of *(L)-16B-Bn* and *alt-16B-Bn*.

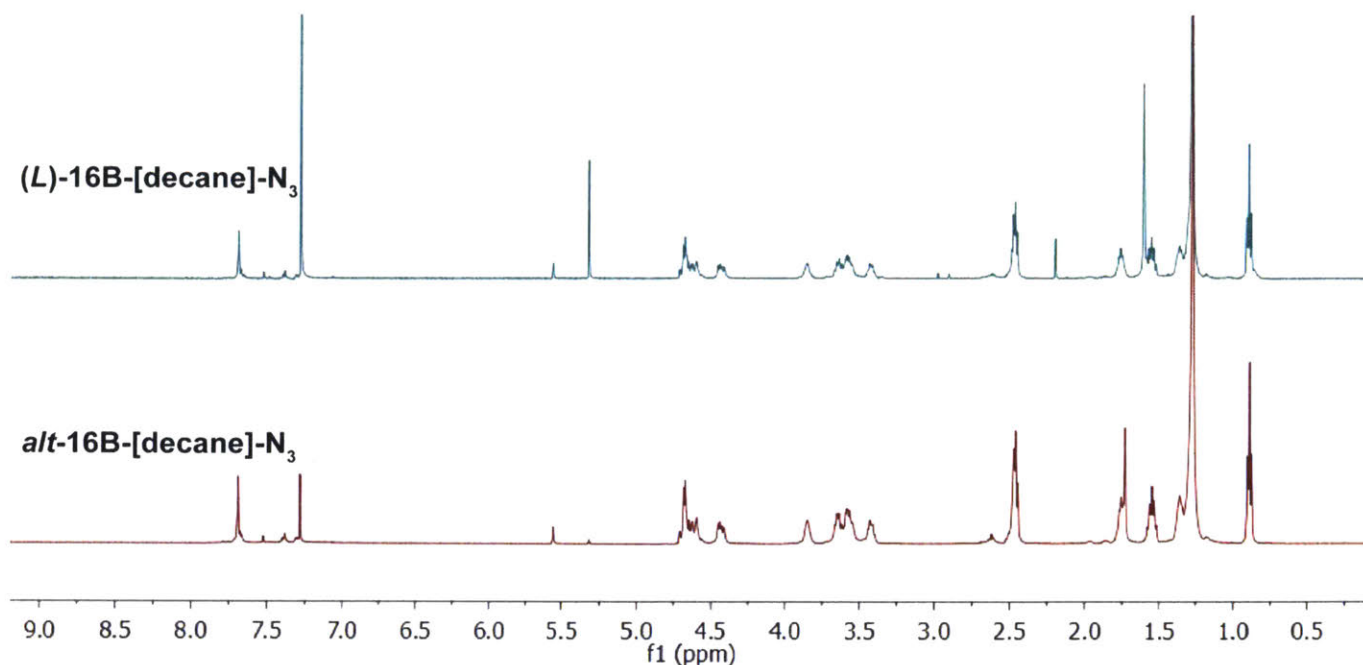


Figure S3.16. ^1H NMR spectra of **(L)-16B-[decane]-N₃** and **alt-16B-[decane]-N₃**.

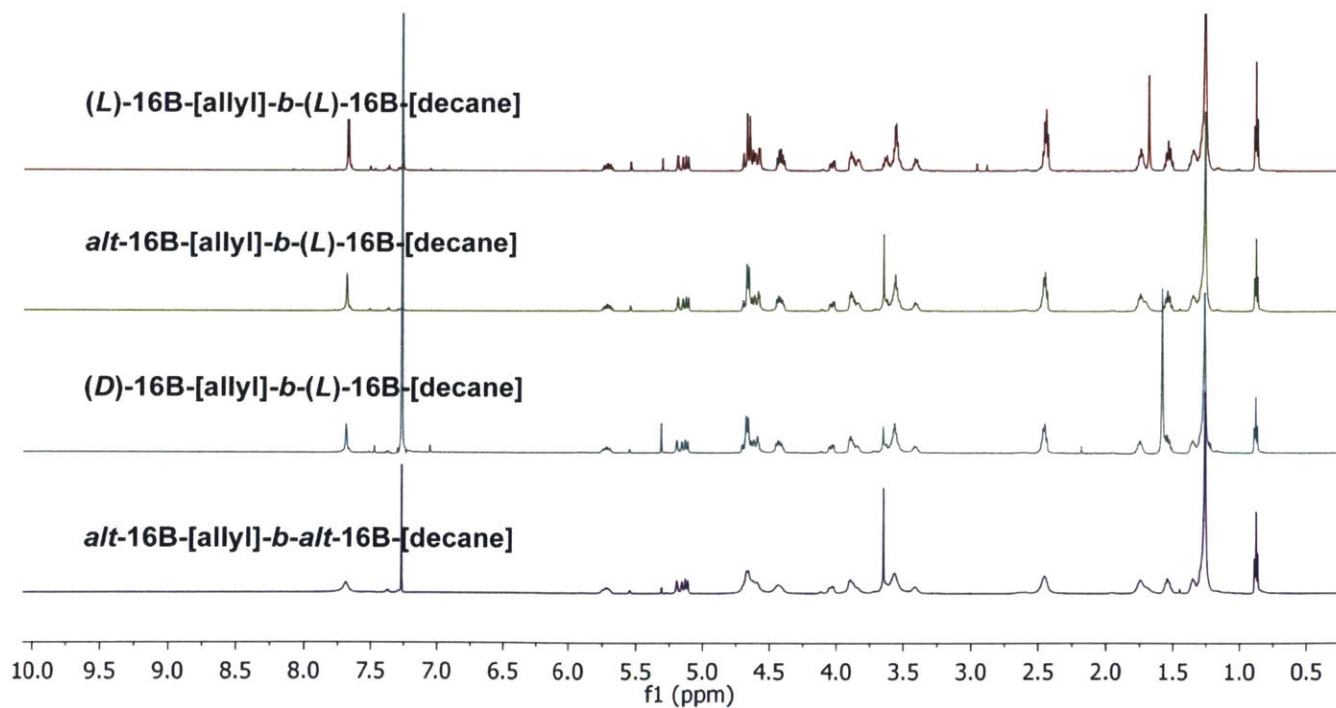


Figure S3.17. ^1H NMR spectra of **(L)-16B-[allyl]-b-(L)-16B-[decane]**, **alt-16B-[allyl]-b-(L)-16B-[decane]**, **(D)-16B-[allyl]-b-(L)-16B-[decane]**, and **alt-16B-[allyl]-b-alt-16B-[decane]**

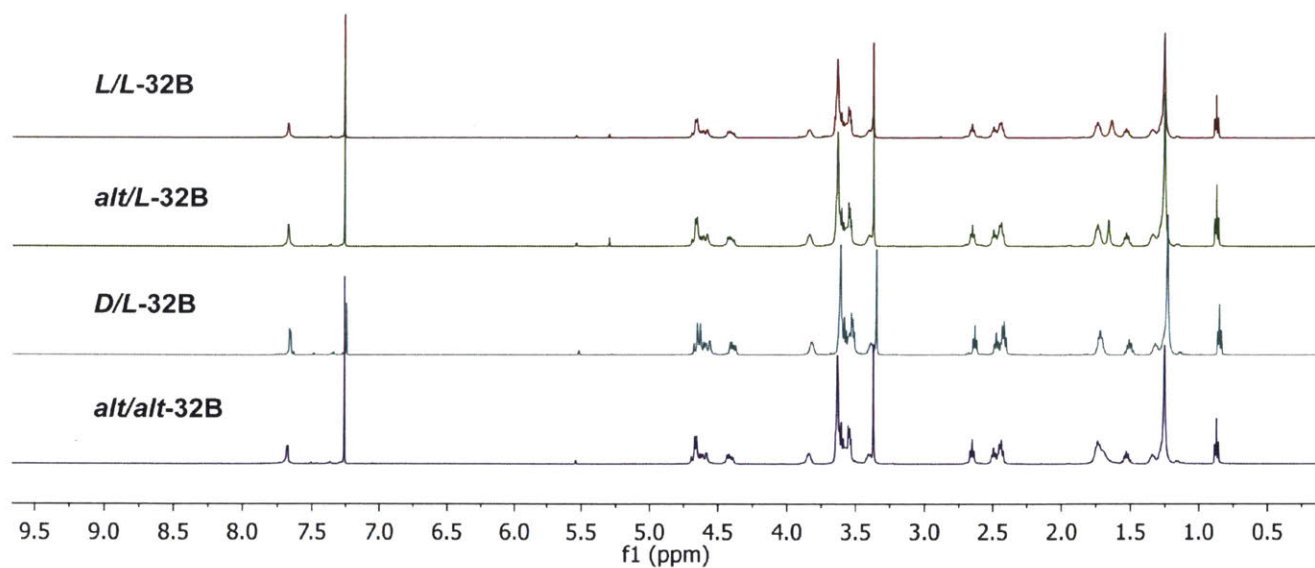
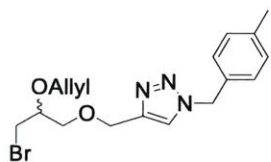


Figure S3.18. ^1H NMR spectra of *L/L-32B* (i.e. (*L*)-16B-[TEG]-*b*-(*L*)-16B-[decane]), *D/L-32B* (i.e. (*D*)-16B-[TEG]-*b*-(*L*)-16B-[decane]), *alt/L-32B*, (i.e. *alt*-16B-[TEG]-*b*-(*L*)-16B-[decane]), and *alt/alt-32B* (i.e. *alt*-16B-[TEG]-*b*-*alt*-16B-[decane]).

Chiral HPLC

Figure S3.19: Analysis of monomers derived from either (*L*)-1-alkyne or (*D*)-1-alkyne.

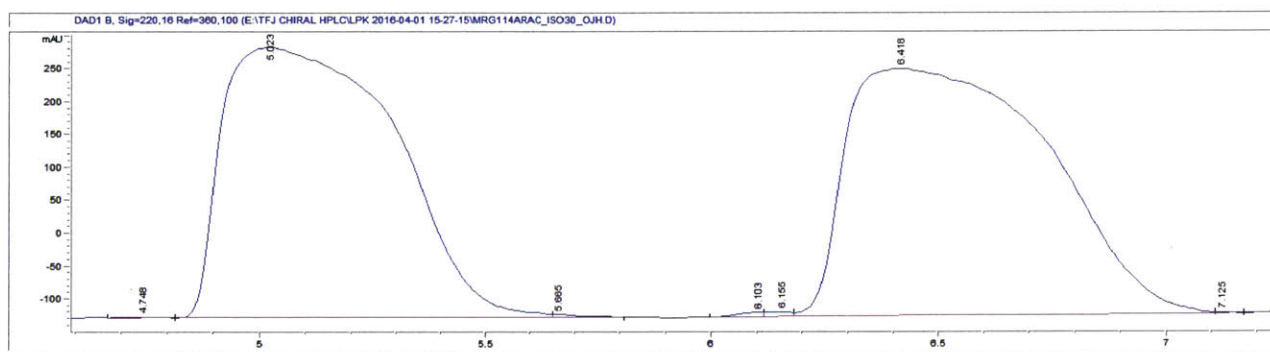


Column (wavelength): CHIRALCEL OJ-H (220 nm)

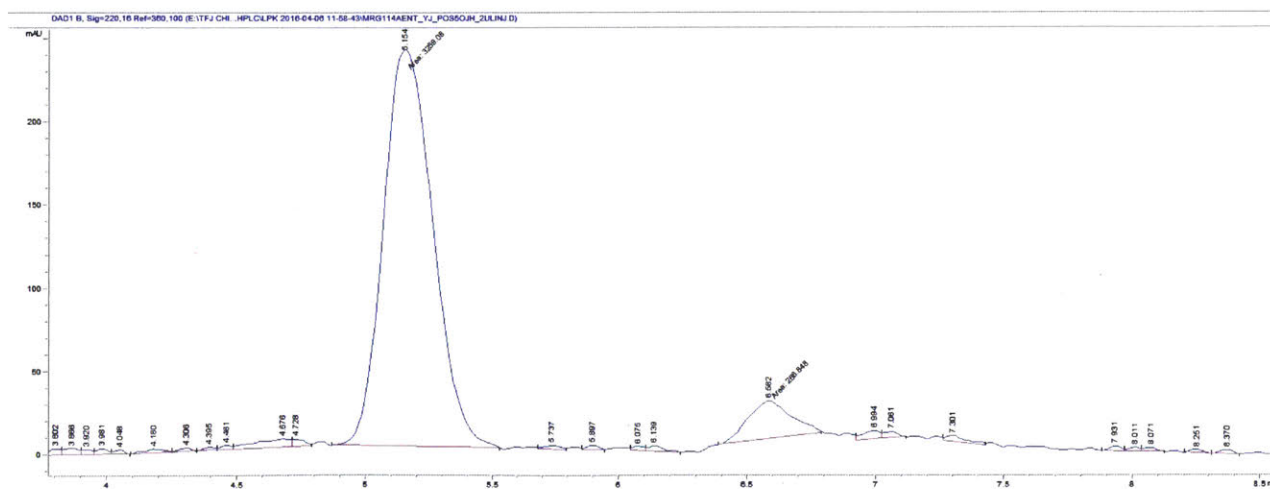
Temperature: 23 °C

Mobile Phase: 30% isopropanol/hexanes, 1 mL/min

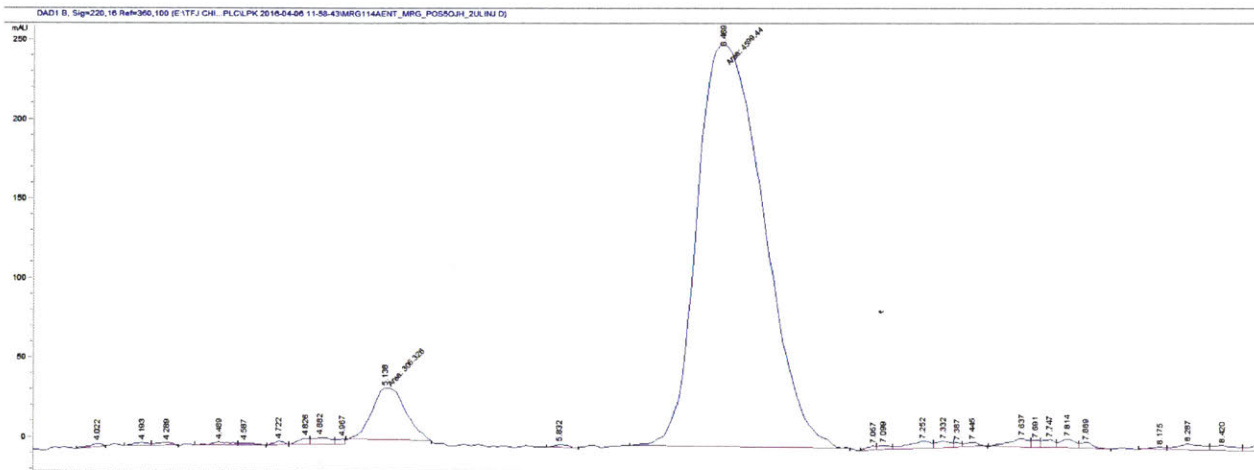
Pseudo-racemate:



Method A, (*L*)-1-alkyne (from *R*-epichlorohydrin), 84% *ee*:



Method A, (*D*)-1-alkyne (from *S*-epichlorohydrin), 82% ee:



Method B, (*L*)-1-alkyne (from *R*-epichlorohydrin), >99% ee:

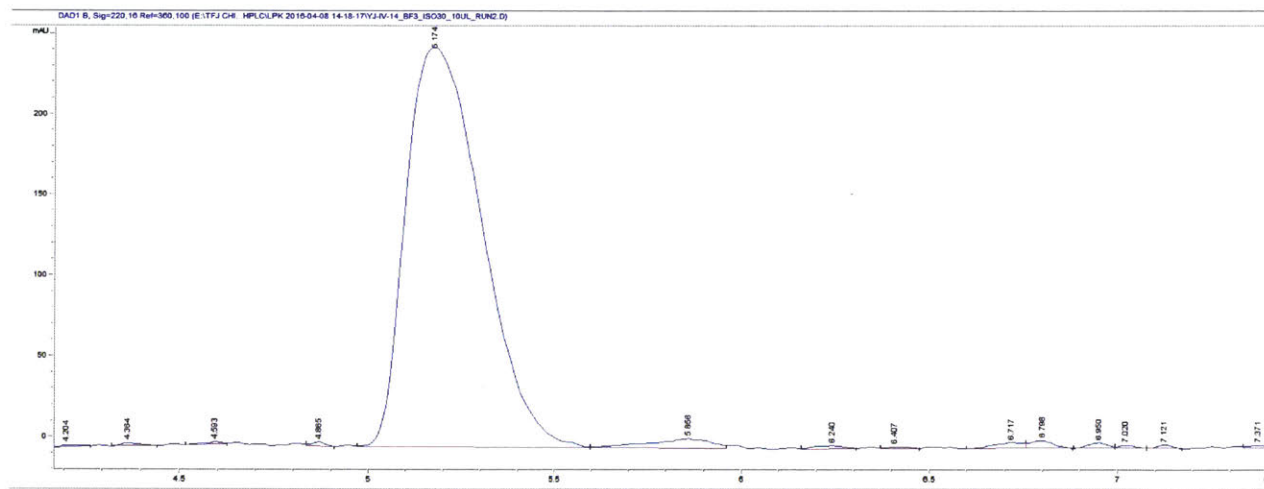


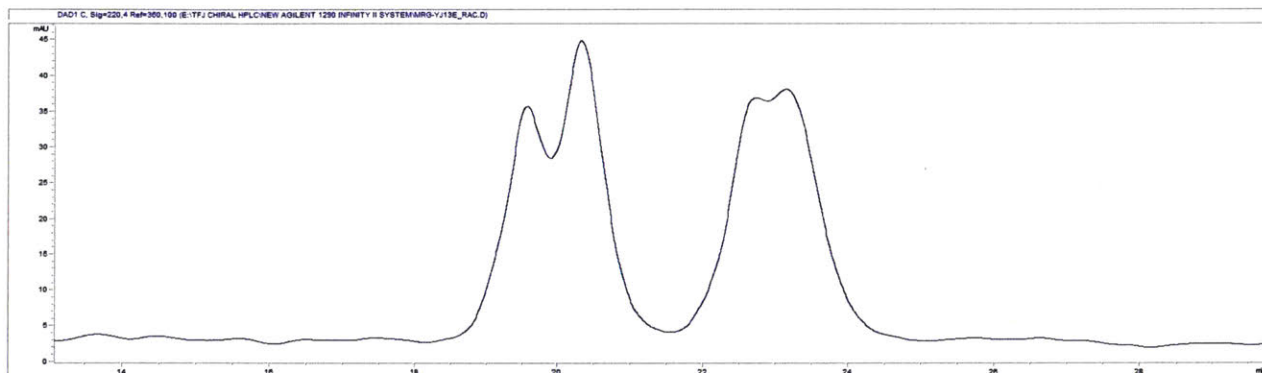
Figure S3.20: Analysis of dimers

Column (wavelength): CHIRALPAK IA-3 (220 nm)

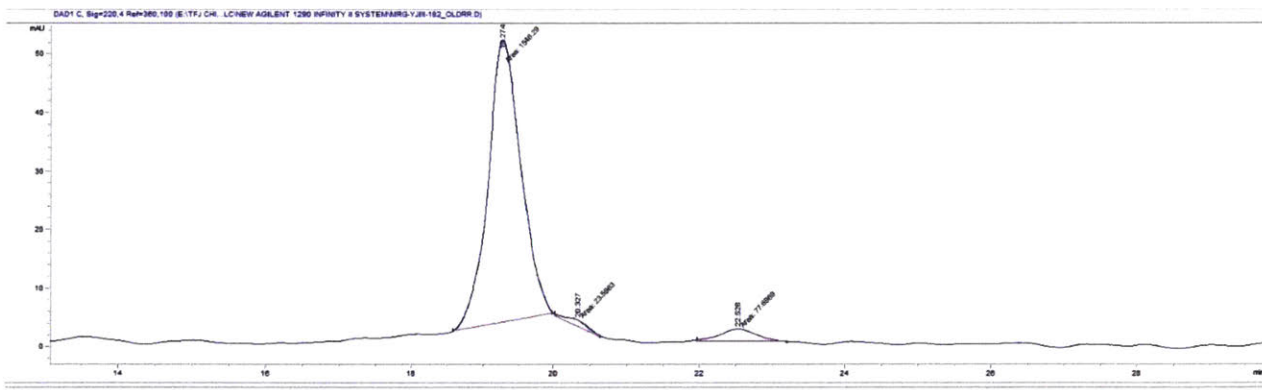
Temperature: 23 °C

Mobile Phase: 1.5% isopropanol/hexanes, 0.5 mL/min

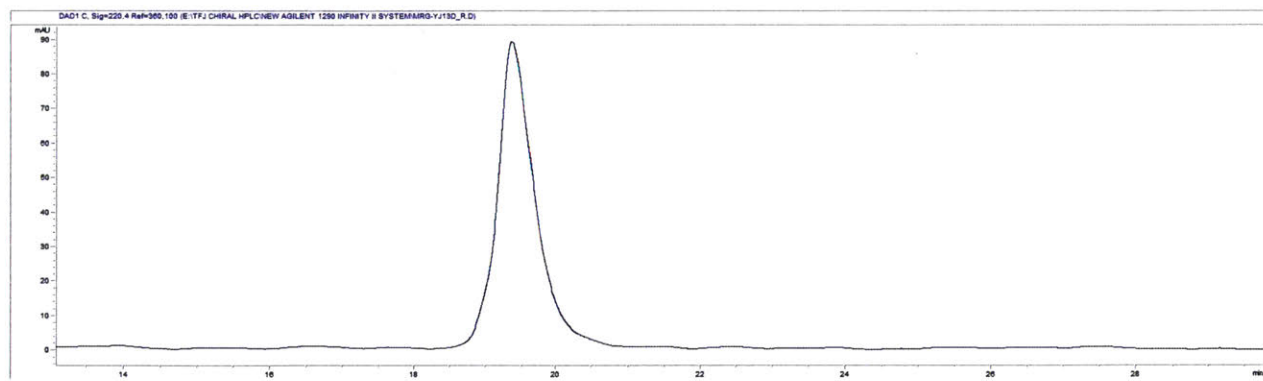
Four possible diastereomers (two racemic pairs):



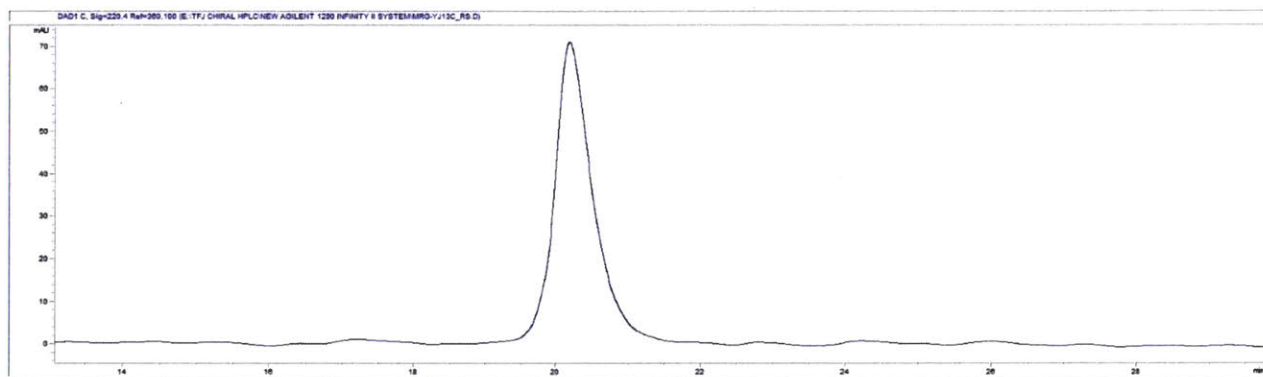
L,L-2A (Dimer via Method A GPE), 84:16 dr:



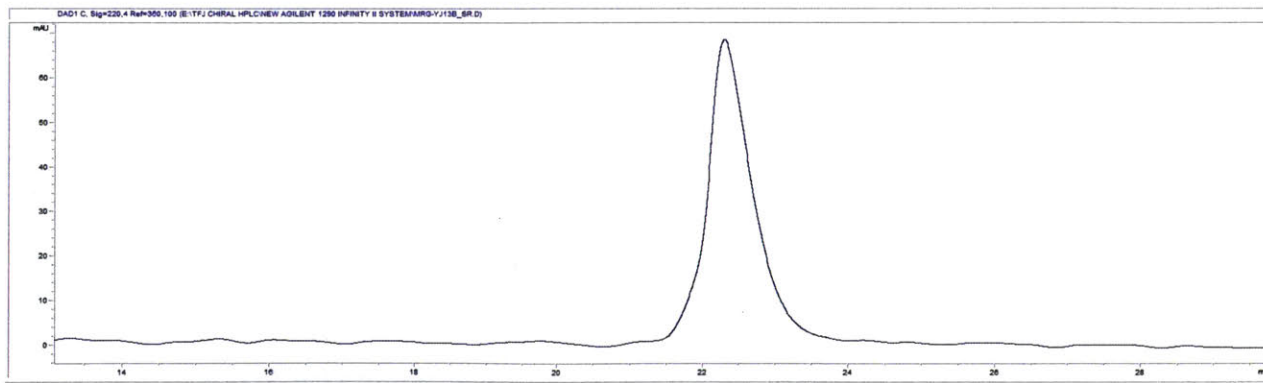
L,L-2B (Dimer via Method B GPE), >99:1 dr:



L,D-2B (Dimer via Method B GPE), >99:1 dr:



D,L-2B (Dimer via Method B GPE), >99:1 dr:



D,D-2B (Dimer via Method B GPE), >99:1 dr:

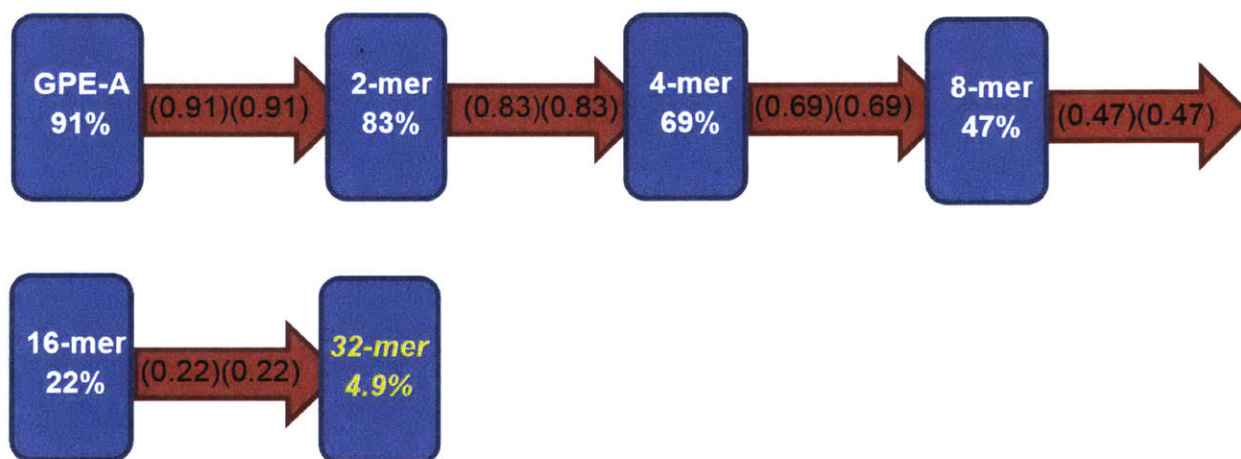
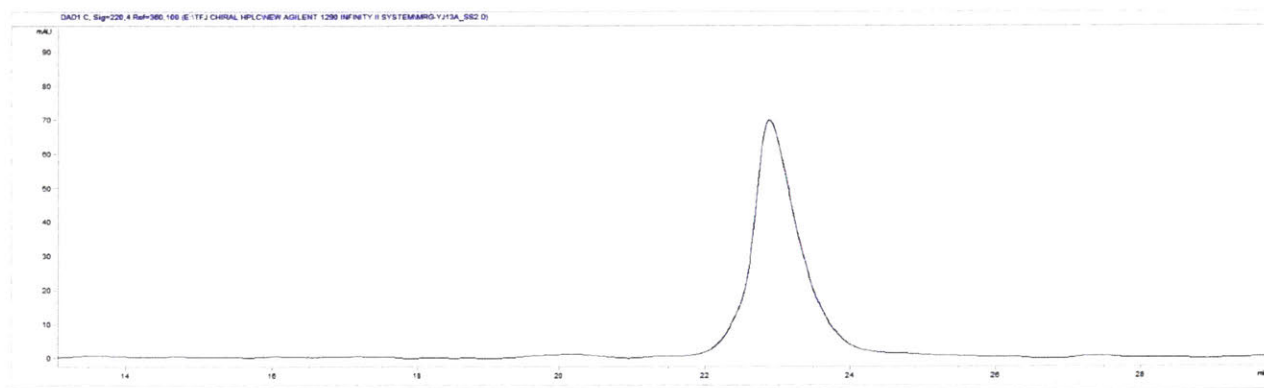


Figure S3.21. Explanation for the origin of stereochemical degradation during IEG cycles beginning with **GPE-A** (82% ee)

MALDI-TOF Mass Spectrometric Characterization

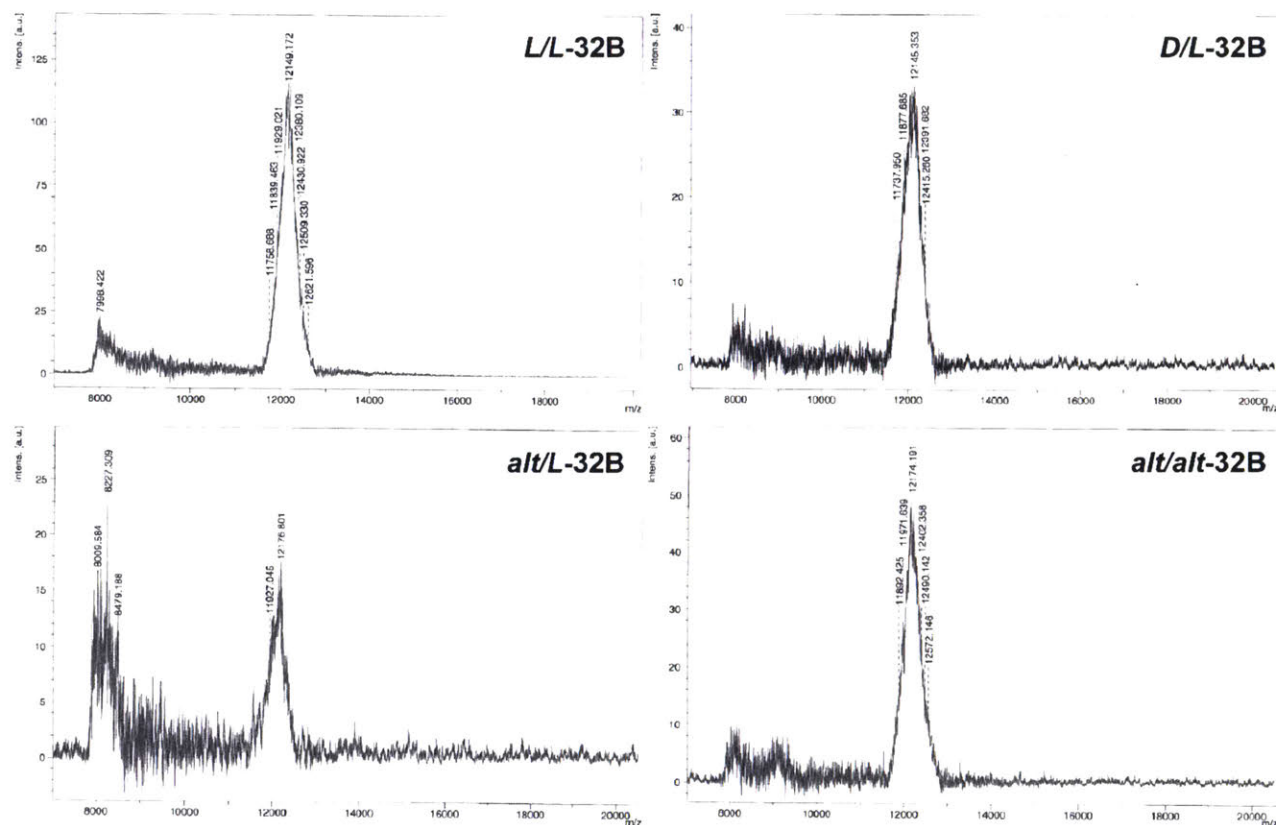


Figure S3.22. Full MALDI spectra for IEG block copolymers *L/L-32B* (i.e. (*L*)-16B-[TEG]-*b*-(*L*)-16B-[decane]), *D/L-32B* (i.e. (*D*)-16B-[TEG]-*b*-(*L*)-16B-[decane]), *alt/L-32B*, (i.e. *alt*-16B-[TEG]-*b*-(*L*)-16B-[decane]), and *alt/alt-32B* (i.e. *alt*-16B-[TEG]-*b*-*alt*-16B-[decane]).

Size Exclusion Chromatography

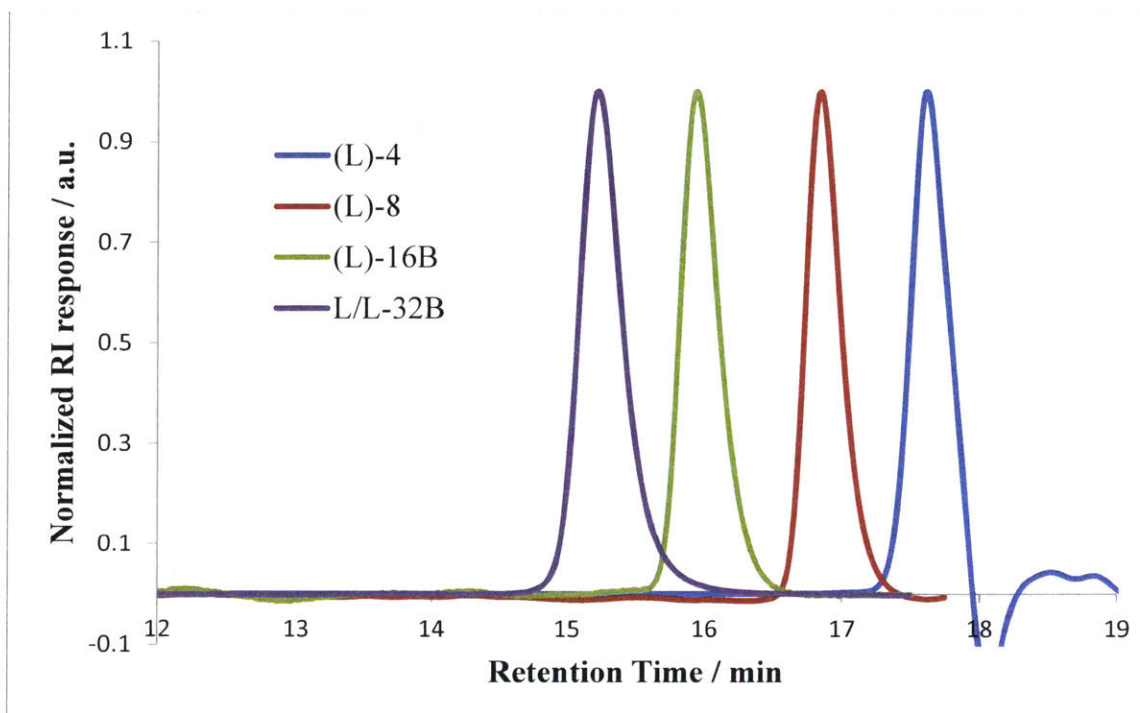


Figure S3.23. GPC traces for isotactic (*L*)-allyl IEGmers ((*L*)-4, (*L*)-8, and (*L*)-16B) and *L/L*-32B.

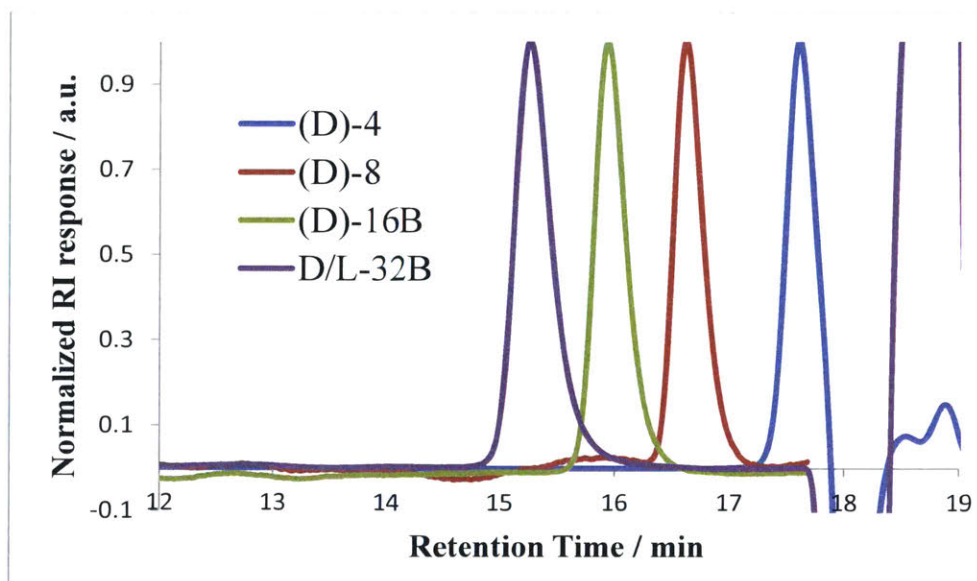


Figure S3.24. GPC traces for isotactic (*D*)-allyl IEGmers ((*D*)-4, (*D*)-8, and (*D*)-16B) and *D/L*-32B.

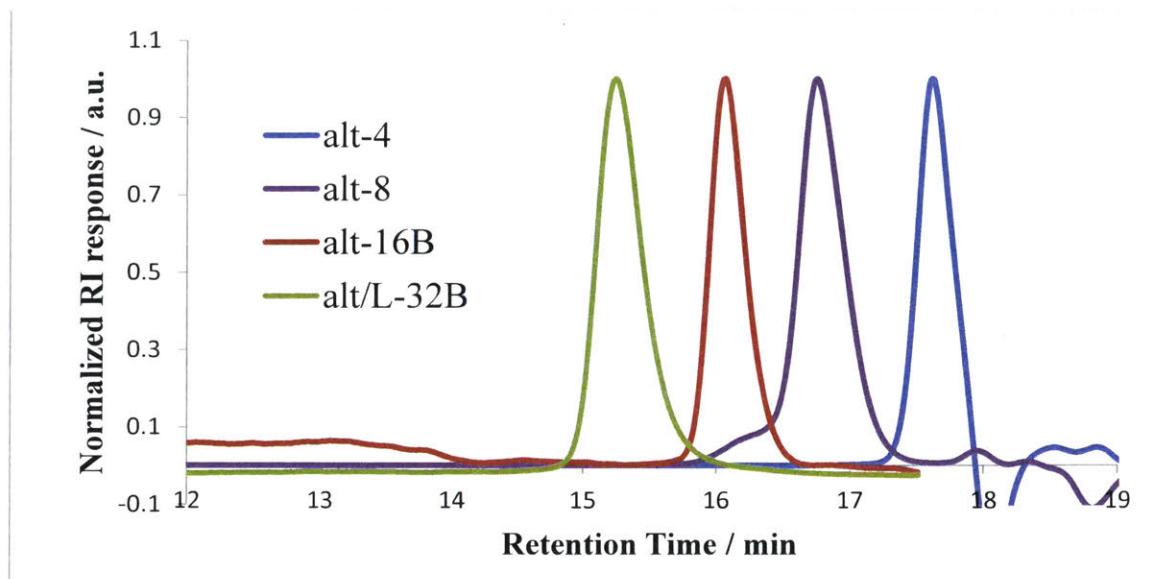


Figure S3.25. GPC spectra for syndiotactic *alt*-allyl IEGmers (*alt-4*, *alt-8*, and *alt-16B*) and *alt/L-32B*.

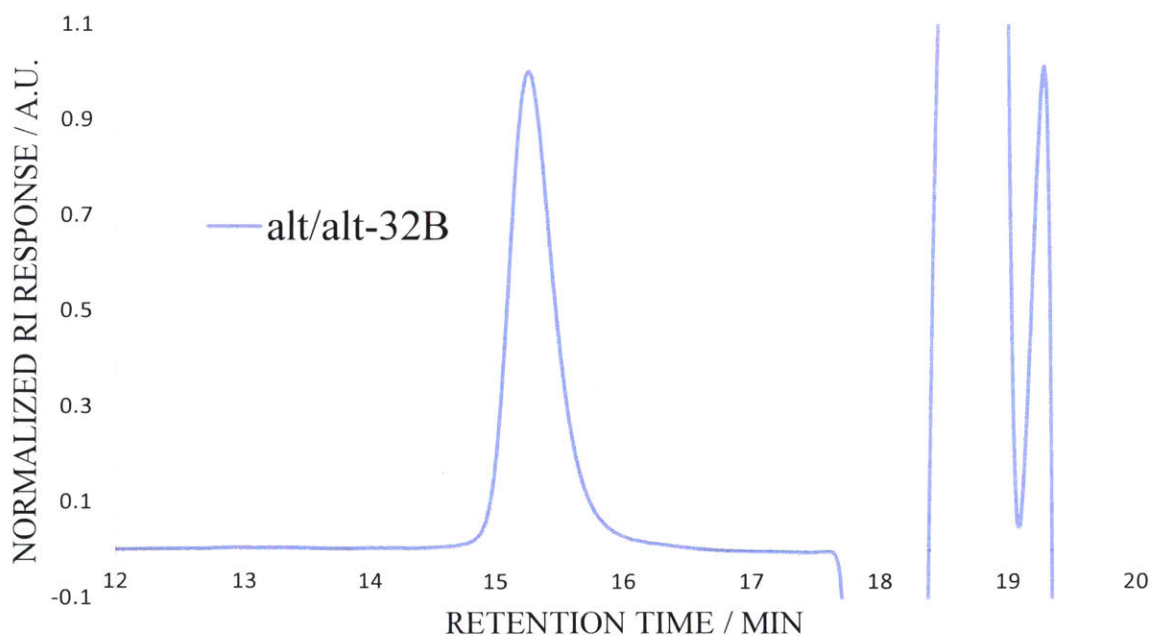


Figure S3.26. GPC trace for *alt/alt-32B*.

Thermal Characterization

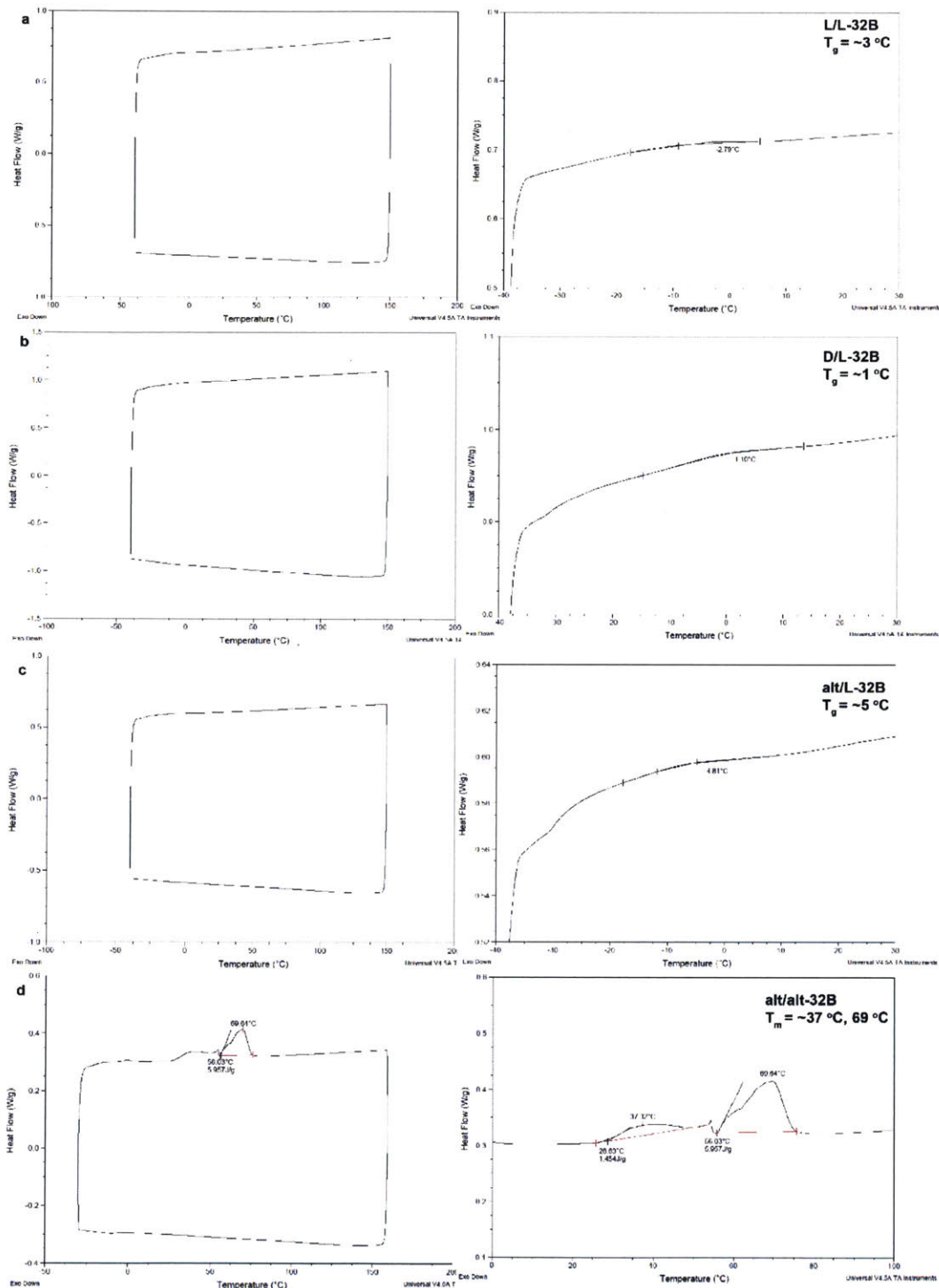


Figure S3.27. a. DSC trace of **L/L-32B**. A T_g can be observed at approximately 3 °C. **b.** DSC trace of **D/L-32B**. A T_g can be observed at approximately 1 °C. **c.** DSC trace of **alt/L**. A T_g can be observed at approximately 5 °C. **d.** DSC trace of **alt/alt-32B**. A T_g can be observed at

approximately -4°C . Two T_m peaks are also observed. The first peak is at 37°C with an enthalpy of melting of approximately 1.5 J/g and the second is at 69°C with an enthalpy of melting of approximately 6.0 J/g . The decane side chains make up 18.7% of the total molecular weight. This translates to an approximate decane enthalpy of 31.8 J/g . Prior work by Sun et al.³ on a peptoid homopolymer where decane side chains made up 71.6% of the total molecular weight found an enthalpy of melting of 21.7 J/g . This translates to an approximate decane enthalpy of 30.3 J/g which matches closely to our experimental results.

Transmission Electron Microscopy

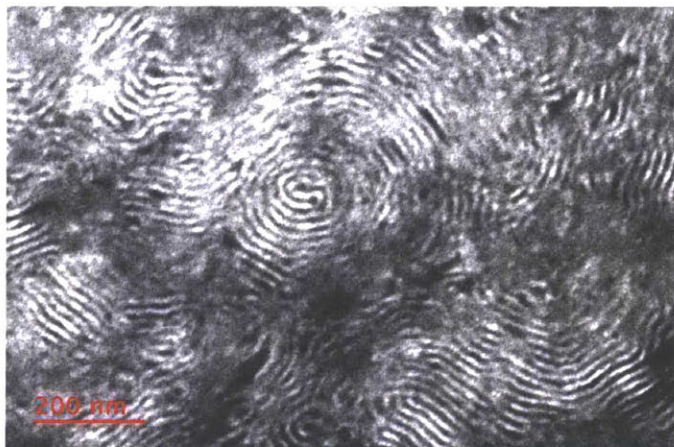


Figure S3.28. Micrograph of **D/L-32B**

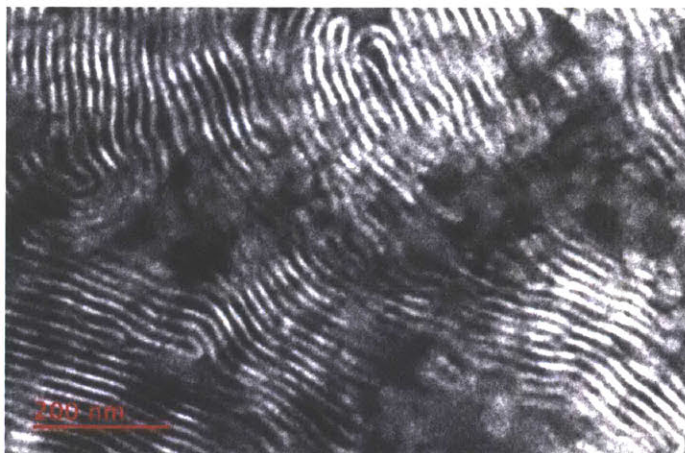


Figure S3.29. Micrograph of *alt/L-32B*

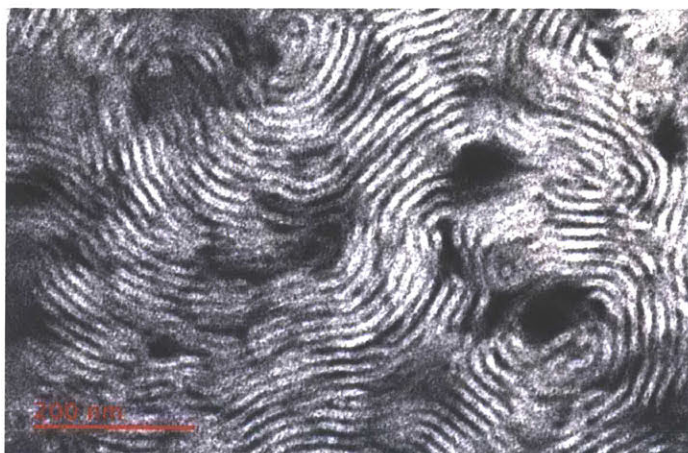


Figure S3.30. Micrograph of *alt/alt-32B* + tartaric acid.

Small-angle X-ray Scattering

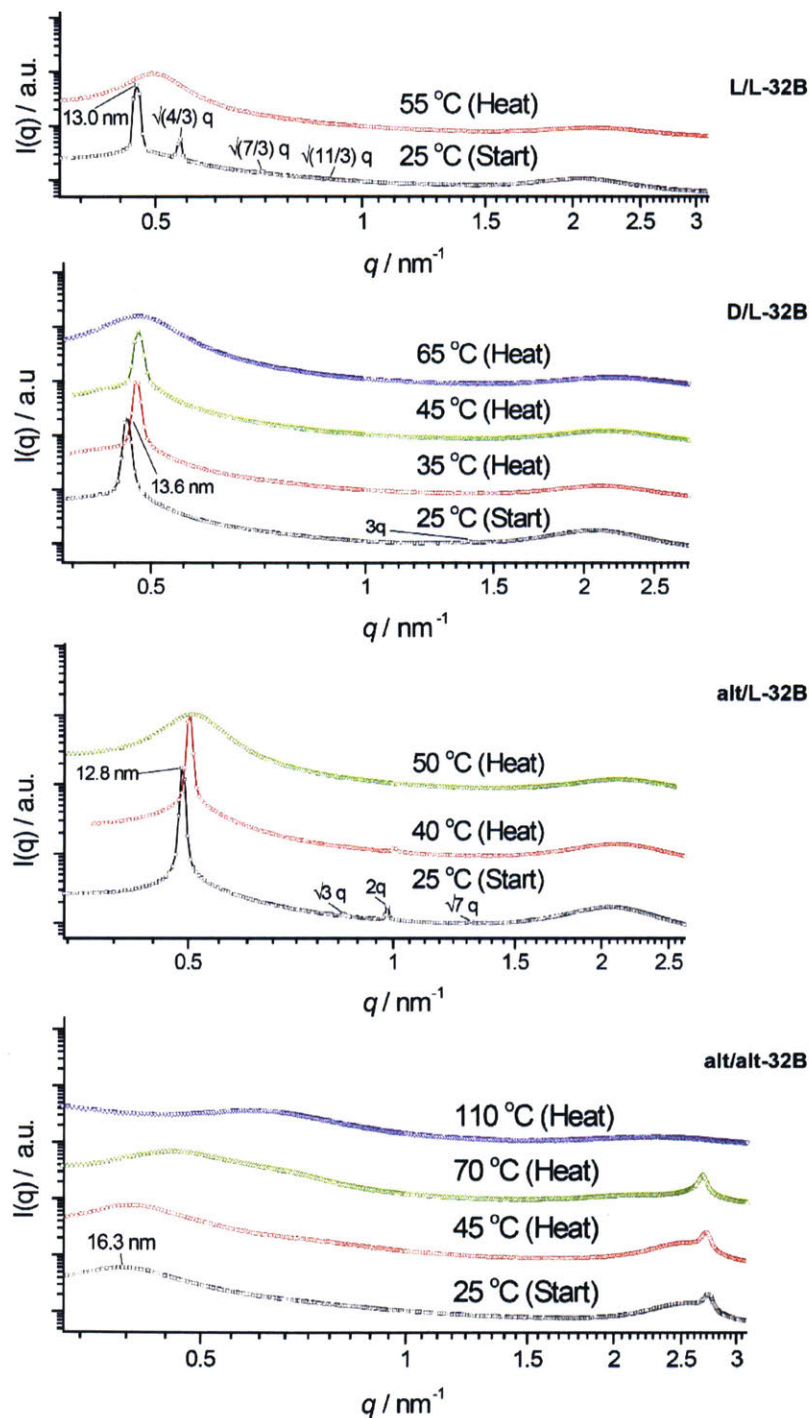


Figure S3.31. Variable temperature 1D-SAXS plots provide an estimate of T_{ODT} for **L/L-32B**, **D/L-32B**, and **alt/L-32B** (50 °C – 60 °C).

Molecular Dynamics

Chiral monomers and their sidechains fluctuate at room temperature such that the volume they occupy (exclusively) resembles an ellipsoidal blob that is offset from the backbone of the copolymer chain. To understand how chirality affects the equilibrium phase behavior of copolymer melts we simulate coarse grained molecular dynamics using linear chains of spheres where each sphere represents a chiral monomer and its sidechain (Murat, M.; Grest, G. S.; Kremer, K. *Macromolecules* **1999**, *32*, 595.). We approximate the excluded volume interaction with the Weeks-Chandler-Andersen (WCA) pair potential, $U(r)$, fixing the energy scale by $E_{ij} = E$ for $i = j$ and the length scale $\sigma_{ij} = \sigma$. The interaction of mismatched sidechains defines an excess interaction, $E_{AB}/E = 1 + E$, and the chiral mismatch elongates the model copolymer chain through the range of the WCA potential,

$$\sigma_{AA} / \sigma = 1 + \lambda \quad , \quad (1)$$

$$\sigma_{BB} / \sigma = 1 + \lambda \quad , \quad (2)$$

$$\sigma_{AB} / \sigma = 1 + \lambda \quad . \quad (3)$$

Each coarse grained sphere is bonded to its neighbors with a finitely extensible nonlinear elastic (FENE) bonding potential with a spring constant of $k = 30.0E/\sigma^2$ and a maximum extension of $R_0 = 1.5\sigma$.

Copolymer melts are equilibrated starting from a dilute and disordered melt of density $\rho = 0.5/\sigma^3$. We integrate the equations of motion using the velocity-Verlet algorithm with a time step $\Delta t = 0.005\tau$ where $\tau = \sigma \sqrt{m/E}$. A cubic simulation cell of length $L = (MN/\rho)^{1/3}$ is filled with $M = 500$ model copolymer chains that obey periodic boundary conditions. Nosé-Hoover barostat and thermostat fix the pressure and temperature at $P = 5.0E/\sigma^3$ and $T = 1.0E/k_B$, respectively. The fluctuations in all three dimensions of the simulation cell are coupled for $5 \times 10^6 \tau$ of total equilibration time. We obtain similar results when starting the system in the lamellar phase by first compressing graft planes with copolymer halves to a density of roughly $\rho = 0.85/\sigma^3$ then equilibrating four lamellae at fixed pressure $P = 5.0E/\sigma^3$ where fluctuations of simulation dimensions that are parallel and perpendicular to the grafting planes are decoupled. (Grest, G. S.;

Lacasse, M. D. *The Journal of Chemical Physics* **1996**, *105*, 10583.) Equilibrium statistics are sampled every 1000τ for $10^5\tau$ using the open-source LAMMPS program.

Elongation shifts the effective Flory-Huggins parameter, χ , for chiral copolymers. A lower bound for χ can be calculated directly in the one-fluid approximation from simulation of the homopolymer pair distribution function, $g(r)$. Using linear regression across $0.0 \leq \epsilon \leq 3.5$ we estimate that $\chi = 0.8, 1.1$, and $2.0E$ for $\lambda = 0.00, \lambda = 0.05$, and $\lambda = 0.10$, respectively. Elongating a single block brings about order where the increased range of the chiral mismatch repulsion increases χ , and the short-range structure in the pair distribution function grows simultaneous with larger deviations from ideality at large distances. A random shuffling of a chiral sequence leads to a modest reduction of order whereas the equilibrium phases of copolymers with alternating chirality in both the A and B blocks closely resemble those of isotactic-isotactic stereochemistry. These trends are also observed in the maximum density of A+A' type monomers contained in a sphere of radius r/σ drawn anywhere in the simulation volume, $d(r)$. We abbreviate E with E in the discussion.

3.5 References

1. North, M. Principles and Applications of Stereochemistry; CRC Press, **1998**.
2. Ziegler, K.; Holzkamp, E.; Breil, H.; Martin, H. Polymerisation von Äthylen und anderen Olefinen. *Angew. Chem.* **1955**, *67*, 426.
3. Natta, G.J. Une nouvelle classe de polymeres d' α -olefines ayant une régularité de structure exceptionnelle. *Polym. Sci.* **1955**, *16*, 143–154.
4. Coates, G. W.; Waymouth, R. M. Oscillating stereocontrol: a strategy for the synthesis of thermoplastic elastomeric polypropylene. *Science* **1995**, *267*, 217–219.
5. Hotta, A.; Cochran, E.; Ruokolainen, J.; Khanna, V.; Fredrickson, G.H.; Kramer, E. J.; Shin, Y.-W.; Shimizu, F.; Cherian, A. E.; Hustad, P. D.; Rose, J. M.; Coates, G. W. Semicrystalline thermoplastic elastomeric polyolefins: Advances through catalyst development and macromolecular design. *Proc. Natl. Acad. Sci.* **2006**, *103*, 15327–15332.
6. Bertin, A. Emergence of Polymer Stereocomplexes for Biomedical Applications. *Macromol. Chem. Phys.* **2012**, *213*, 2329–2352.
7. Badi, N.; Lutz, J.-F. Sequence control in polymer synthesis. *Chem. Soc. Rev.* **2009**, *38*, 3383–3390.
8. Lutz, J.-F.; Ouchi, M.; Liu, D. R.; Sawamoto, M. Sequence-controlled polymers. *Science* **2013**, *341*, 1238149.
9. Knight, A. S.; Zhou, E. Y.; Francis, M. B.; Zuckermann, R. N. Sequence Programmable Peptoid Polymers for Diverse Materials Applications. *Adv. Mater.* **2015**, *27*, 5665–5691.
10. Lutz, J.-F.; Lehn, J.-M.; Meijer, E. W.; Matyjaszewski, K. From precision polymers to complex materials and systems. *Nature Reviews Materials* **2016**, *1*, 16024.
11. Müllen, K. Molecular defects in organic materials. *Nature Reviews Materials* **2016**, *1*, 15013.
12. Grayson, S. M.; Fréchet, J. M. J. Convergent Dendrons and Dendrimers: from Synthesis to Applications. *Chem. Rev.* **2001**, *101*, 3819–3868.
13. Sun, J.; Liao, X.; Minor, A. M.; Balsara, N. P.; Zuckermann, R. N. Morphology-Conductivity Relationship in Crystalline and Amorphous Sequence-Defined Peptoid Block Copolymer Electrolytes. *J. Am. Chem. Soc.* **2014**, *136*, 14990–14997.
14. Washington, M. A.; Swiner, D. J.; Bell, K. R.; Fedorchak, M. V.; Little, S. R.; Meyer, T. Y. Stereochemical Sequence Dictates Unimolecular Diblock Copolymer Assembly. *Biomaterials* **2017**, *117*, 66–76.
15. Iwamoto, N.; Butler, D. C. D.; Svrzikapa, N.; Mohapatra, S.; Zlatev, I.; Sah, D. W. Y.; Meena; Standley, S. M.; Lu, G.; Apponi, L. H.; Frank-Kamenetsky, M.; Zhang, J. J.; Vargeese, C.; Verdine, G. L. Control of phosphorothioate stereochemistry substantially increases the efficacy of antisense oligonucleotides. *Nat. Biotechnol.* **2017**, *35*, 845–851.
16. Sun, J.; Teran, A. A.; Liao, X. X.; Balsara, N. P.; Zuckermann, R. N. Nanoscale phase separation in sequence-defined peptoid diblock copolymers. *J. Am. Chem. Soc.* **2013**, *135*, 14119–14124.
17. Rosales, A. M.; Segalman, R. A.; Zuckermann, R. N. Polypeptoids: a model system to study the effect of monomer sequence on polymer properties and self-assembly. *Soft Matter* **2013**, *9*, 8400–8414.
18. Lawrence, J.; Goto, E.; Ren, J. M.; McDearmon, B.; Kim, D. S.; Ochiai, Y.; Clark, P. G.; Laitar, D. S.; Higashihara, T.; Hawker, C. J. A Versatile and Efficient Strategy to Discrete Conjugated Oligomers. *J. Am. Chem. Soc.* **2017**, *139*, 13735–13739.

19. Van Genabeek, B.; de Waal, B. F. M.; Gosens, M. M. J.; Pitet, L. M.; Palmans, A. R. A.; Meijer, E. W. Amplifying (im)perfection: The Impact of Crystallinity in Discrete and Disperse Block Co-oligomers. *J. Am. Chem. Soc.* **2016**, *138*, 4210–4218.
20. Van Genabeek, B.; De Waal, B. F. M.; Ligt, B.; Palmans, A. R. A.; Meijer, E. W. Dispersity under Scrutiny: Phase Behavior Differences between Disperse and Discrete Low Molecular Weight Block Co-Oligomers. *ACS Macro Lett.* **2017**, *6*, 674–678.
21. Oschmann, B.; Lawrence, J.; Schulze, M. W.; Ren, J. M.; Anastasaki, A.; Luo, Y.; Nothling, M. D.; Pester, C. W.; Delaney, K. T.; Connal, L. A.; McGrath, A. J.; Clark, P. G.; Bates, C. M.; Hawker, C. J. Effects of Tailored Dispersity on the Self-Assembly of Dimethylsiloxane–Methyl Methacrylate Block Co-Oligomers. *ACS Macro Lett.* **2017**, *6*, 668–673.
22. Binauld, S.; Damiron, D.; Connal, L. A.; Hawker, C. J.; Drockenmuller, E. Precise synthesis of molecularly defined oligomers and polymers by orthogonal iterative divergent/convergent approaches. *Macromol. Rapid Commun.* **2011**, *32*, 147–68.
23. Barnes, J. C.; Ehrlich, D. J. C.; Gao, A. X.; Leibfarth, F. A.; Jiang, Y.; Zhou, E.; Jamison, T. F.; Johnson, J. A. Iterative exponential growth of sequence-controlled polymers. *Nature Chem.* **2015**, *7*, 810–815.
24. Leibfarth, F. A.; Johnson, J. A.; Jamison, T. F. Scalable synthesis of sequence-defined, unimolecular macromolecules by Flow-IEG. *Proc. Natl. Acad. Sci.* **2015**, *112*, 10617–10622.
25. Wicker, A. C.; Leibfarth, F. A.; Jamison, T. F. Flow-IEG enables programmable thermodynamic properties in sequence-defined unimolecular macromolecules. *Polym. Chem.* **2017**, *8*, 5786–5794.
26. Jiang, Y.; Golder, M. R.; Nguyen, H. V. T.; Wang, Y.; Zhong, M.; Barnes, J. C.; Ehrlich, D. J. C.; Johnson, J. A. Iterative exponential growth synthesis and assembly of uniform diblock copolymers. *J. Am. Chem. Soc.* **2016**, *138*, 9369–9372.
27. Martens, S.; Holloway, J. O.; Du Prez, F. E. Click and Click-Inspired Chemistry for the Design of Sequence-Controlled Polymers. *Macromol. Rapid Commun.* **2017**, *38*, 1700469.
28. Beaver, M. G.; Jamison, T. F. Ni(II) Salts and 2-Propanol Effect Catalytic Reductive Coupling of Epoxides and Alkynes. *Org. Lett.* **2011**, *13*, 4140–4143.
29. Vigneron, J. P.; Dhaenens, M.; Horeau, A. Nouvelle methode pour porter au maximum la purete optique d'un produit partiellement dedouble sans l'aide d'aucune substance chirale. *Tetrahedron* **1973**, *29*, 1055–1059.
30. Heller, D.; Drexler, H.-J.; Fischer, C.; Buschmann, H.; Baumann, W.; Heller, B. How long have nonlinear effects been known in the field of catalysis? *Angew. Chem. Int. Ed.* **2000**, *39*, 495–499.
31. van Genabeek, B.; Lamers, B. A. G.; de Waal, B. F. M.; van Son, M.H. C.; Palmans, A. R. A.; Meijer, E. W. Amplifying (Im)perfection: The Impact of Crystallinity in Discrete and Disperse Block Co-oligomers. *J. Am. Chem. Soc.* **2017**, *139*, 14869–14872.
32. Yao, L.; Lu, X.; Chen, S.; Watkins, J. J. Formation of Helical Phases in Achiral Block Copolymers by Simple Addition of Small Chiral Additives. *Macromolecules* **2014**, *47*, 6547–6553.
33. Luo, Y.; Kim, B.; Montarnal, D.; Mester, Z.; Pester, C. W.; McGrath, A. J.; Hill, G.; Kramer, E. J.; Fredrickson, G. H.; Hawker, C. J. Improved self-assembly of poly(dimethylsiloxane-*b*-ethylene oxide) using a hydrogen-bonding additive. *J. Polym. Sci., Part A: Polym. Chem.* **2016**, *54*, 2200–2208.

34. Grest, G. S.; Lacasse, M. D. Efficient continuum model for simulating polymer blends and copolymers. *J. Chem. Phys.* **1996**, *105*, 10583–10594.
35. Murat, M.; Grest, G. S.; Kremer, K. Statics and Dynamics of Symmetric Diblock Copolymers: A Molecular Dynamics Study. *Macromolecules* **1999**, *32*, 595–609.

Chapter 4.
Uniform Glycopolymers with Stereo-defined Microstructure
for Selective Lectin Binding Performance

This chapter is composed of material adapted from the following publication:

Hartweg, M. †; Jiang, Y. †; Yilmaz, G.; Jarvis, C.; Nguyen, H. V.-T.; Primo, G. A.; Monaco, A.; Beyer, V. P.; Mata, A.; Chen, K.; Kiessling, L. L.; Johnson, J. A.; Becer, C. R. Unimolecular chiral glycopolymers for selective lectin binding performance. 2019. *In preparation*.

The work in this chapter was a collaborative effort with Manuel Hartweg, Gökhan Yilmaz, Cassie Jarvis, Hung V. T. Nguyen, Gastón A. Primo, Alessandra Monaco, Valentin P. Beyer, Alvaro Mata, and Kathleen Chen. Manuel Hartweg designed and performed the synthesis of the thiomannose sodium salt and its addition onto the allyl-IEG compounds. Manuel Hartweg, Gökhan Yilmaz, Gastón A. Primo, Alessandra Monaco, Valentin P. Beyer, and Alvaro Mata ran the Surface Plasmon Resonance (SPR) and the cell viability studies. Cassie Jarvis performed the imaging and analysis of the endocytosis of the TAMRA functionalized glycopolymers into Raji B-cells in different conditions. Hung V. T. Nguyen performed all of the TEM and Dynamic Light Scattering (DLS) experiments. Kathleen Chen assisted in the synthesis of the allyl-IEG polymers. The author synthesized all allyl-IEG polymers. The writing of the chapter was a collaborative effort between Manuel Hartweg and the author.

4.1 Introduction

Since their discovery in 1897 by Emil Fischer, lectins have been found to be key biological units that are responsible for signal transmission and local intercellular communication.¹ Lectins accomplish these tasks through recognition of oligosaccharides that are either solubilized or embedded on the surfaces of bacteria, plant cells, animal cells, and viruses.²⁻⁶ Many of the precise mechanisms and signaling pathways that lectins control are directly related to different diseases and triggers in the immune system; thus, there is a great desire to specifically stimulate therapeutic lectins for targeted therapy.^{7,8} This targeting is unfortunately complicated to accomplish without unintentionally triggering other undesired lectin signaling pathways. Oligosaccharides, the natural lectin substrates, accomplish this through their extremely nuanced structures: each saccharide monomer alone has countless variations in anomeric centers, ring sizes, linkages, site specific substitutions, and branch points.^{9,10} To take control over the vast biological functions of lectins and use them in the therapeutic setting, we need to better understand the important structural parameters of their sugar-based molecule substrates.

To tease out the subtle effects of substrate structure, there need to be reliable, versatile, and scalable methods to make them. Currently, there exist no easily accessible biological expression systems or amplification methods that are able to make sufficient quantities of pure oligosaccharides.¹¹ The only proven methods are strenuous, often requiring complex protecting

groups, huge excesses of reagents, and difficult purifications.¹²⁻¹⁸ Given the intrinsic difficulty of making natural oligosaccharide structures, polymer chemists have developed glycopolymers, which are much more easily synthesized alternatives to their natural counterparts. Glycopolymers are generally composed of a non-natural, designed polymer backbone with pendant saccharide functionalized side chains. Glycopolymers have been made on large scale with solid-phase chemistry,^{19,20} graft-through polymerizations,^{21,22} dendrimer chemistry,²³ and supramolecular assembly.²⁴

Though the individual saccharide side chains of glycopolymers generally have weaker binding to lectins than their natural counterparts, the combined effect of the many saccharides on each glycopolymer imparts unique benefits.²⁵ Lectins have multiple saccharide binding sites or carbohydrate-recognition domains (CRDs),²⁶ and by taking advantage of “bind-and-slide” effects²⁷ and receptor-clustering, each multivalent glycopolymer binds to multiple CRDs on both individual lectins and clusters of lectins, effectively increasing its lectin-binding constant.²⁸⁻³⁰ These factors have helped glycopolymers show potential therapeutic use in treating multiple diseases, for example, by blocking hemagglutinin on influenza A,³¹⁻³⁴ inhibiting HIV’s binding to DC-SIGN,³⁵⁻⁴⁰ and triggering immunological function for vaccine development.⁴¹ Importantly, the studied glycopolymers have randomly arranged structures and thus have limited capability to target therapeutically relevant lectins that all have clearly defined, precise structures. To advance glycopolymers as a field, there is need for scalable methods of synthesizing these polymers with as much structural control over sequence, stereochemistry, and architecture as their natural protein counterparts.⁴²⁻⁴⁷

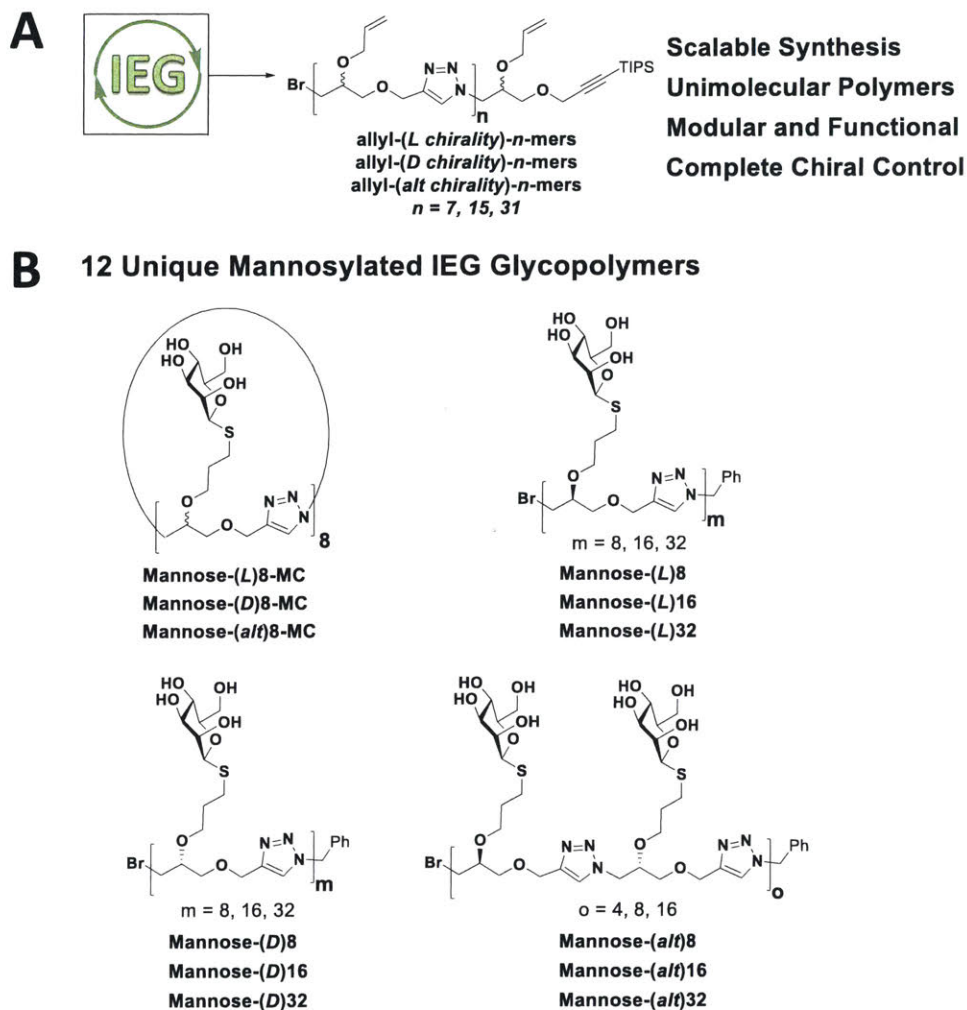


Figure 4.1. (A) Our allyl- functionalized, unimolecular, chiral polymer platform made through IEG. *Note:* in this report, all polymers are drawn from their azide (N) to alkyne (C) terminus; *L* and *D* labels are used to indicate the stereochemistry of each unit (wedge and dash bonds, respectively) akin to polypeptide nomenclature. Polymers with alternating *L* and *D* stereocenters are termed as “alt” for simplicity. (B) 12 uniquely designed mannosylated polymers that vary in cyclic vs. linear morphology, chirality, and length.

For decades, methods have been proposed to make functional unimolecular polymers,⁴⁸⁻⁶⁰ and over the past few years, we have developed a unimolecular polytriazole system that has addressed this goal.⁶¹⁻⁶⁴ As shown in Figure 4.1, we use Iterative Exponential Growth (IEG)⁶⁵⁻⁶⁷ to make allyl-functional polytriazoles with absolute control over topology, monomer sequence, and backbone chiralities. IEG is a synthetic methodology wherein orthogonally α,ω -diprotected molecules undergo cycles of deprotections and coupling reactions to yield macromolecules that

grow exponentially in length. Through synthetic modification of the base monomers, we can install a variety of functionalities like alcohols, amines, and alkenes.^{61,62,63,64}

4.2 Results and Discussion

We used thiol-ene postpolymerization functionalization with anomerically pure β -thiomannose under UV light to modify our allyl-functionalized polytriazoles with mannose sidechains. As shown in Figure 4.1B, we created a library of 12 different, unimolecular glycopolymers that can be used to test various structural parameters for lectin binding. To study the effect of topology, we compared linear and macrocyclic morphologies of our Mannosylated 8mers. To see the effects of increasing multivalency, we compared glycopolymers with lengths of 8, 16, and 32 units. Finally, we varied the effect of chirality by creating polymers that have all (*L*) isotactic, (*alt*) syndiotactic, or all (*D*) isotactic stereochemical variations. *Note*: in this report, all polymers are drawn from their azide (N) to alkyne (C) terminus; *L* and *D* labels are used to indicate the stereochemistry of each unit (wedge and dash bonds, respectively) akin to polypeptide nomenclature. Polymers with alternating *L* and *D* stereocenters are termed as “*alt*” for simplicity.

Through circular dichroism, we found that glycopolymers in our library generally exhibited chiral secondary structures that changed with varying topologies, lengths, stereochemistries, and pH environments (Figure S4.32). We assessed the biocompatibility of our glycopolymers via a live/dead assay of NIH 3T3 fibroblast cells with calcein and ethidium homodimer staining. 3T3 fibroblast cells treated with 5% solutions of each glycopolymer at 24 hour and 48 hour time points showed no amount of cell death. (Figure S4.29). Also, an Alamar Blue Assay demonstrated the glycopolymers have minimal influence on cell metabolic activity when added to 1×10^4 (Figure S4.30) and 5×10^4 (Figure S4.31) fibroblast monolayers. All glycopolymers regardless of chain length, stereochemistry, and architecture proved themselves to have low cytotoxicity and little to no effect on relative cell metabolic activity. Having characterized the structural features of our glycopolymers and their biocompatibility we next used real time surface plasmon resonance (SPR) measurements to evaluate the binding of these mannosylated glycopolymers against 8 different therapeutically relevant lectins.

Generally, past evaluations on glycopolymer lectin binding have been limited to evaluation of only a single species of lectin, usually a choice of ConA, DC-SIGN, DC-SIGNR, or Langerin. To our knowledge there have been no comparative studies where glycopolymers have been

evaluated for specificity towards certain lectins over others. Thus, the glycopolymer field has limited understanding of how structural parameters that can dictate selective interactions with human lectins. To demonstrate the biological effect that our glycopolymers' structural parameters of topology, length, and chirality would have on lectin binding, we measured their kinetic binding data against immobilized C-type lectins DC-SIGN, DC-SIGNR, MBL, SP-D, Langerin, Dectin-2, Mincle and DEC-205 (Chap. XXX, ESI). For every glycopolymer at different mannose side chain concentrations (16, 8, 4, 2 and 1 μM), real time SPR measurements with each of the lectins were carried out. Association rate constants (k_a), dissociation rate constants (k_d), binding affinity constants (K_A), and maximum binding responses (R_{max}) were determined.

Ligand		DC-SIGN	DC-SIGNR	MBL	SP-D	Langerin	Dectin-2	Mincle	DEC-205
32mer	(L)	187	68.1	112	90.7	87.3	85.1	50.8	330
	(alt)	113	126	103	73.7	41.5	167	52.3	248
	(D)	56	85.7	83.9	60.5	134.7	33.9	61.7	113
16mer	(L)	172	27.8	185	277	48.4	49.7	97.2	67.9
	(alt)	139	19.7	144	147	41.3	61.2	147	40.2
	(D)	96.2	32.3	102.7	96.7	147.7	32.1	161	51.4
8mer	(L)	68.9	23.9	11.3	2.39	11.5	13.3	3.27	31.3
	(alt)	40.6	17.4	4.9	1.59	3.85	18.2	5.99	19.7
	(D)	20.9	22.6	5.1	2.6	20.3	9.9	6.12	13.1
8mer MC	(L)	29.4	10.8	49	7.78	25.7	8.31	5.79	18
	(alt)	37.7	22.2	97.8	41.7	19.1	63.8	29.4	23.8
	(D)	14.4	2.76	34.5	3.22	8.39	4.77	1.82	12.3

Table 4.1. Summary of k_a -values ($\text{M}^{-1} \text{s}^{-1}$) between every glycopolymer vs. eight lectins, color coded according to relative k_a -values. Red and orange domains display binding minima within the respective lectin series, yellow domains display average binding, and green domains display binding maxima.

As expected, SPR reveals a relatively strong dependency of number of mannose units, i.e. length of polymer, on the association rate (k_a) (Table 1) for each lectin. 8-mers, whether linear or cyclic, generally display significantly lower k_a values than 16-mers and 32-mers. The absolute stereochemistry also impacts k_a , but does not follow any specific trend; however, subtle tendencies in terms of k_a can be identified. **Mannose-(alt)8-MC** for instance shows a faster association rate than **Mannose-(L)8-MC** or **Mannose-(D)8-MC** for almost all the lectins tested. In case of DC-SIGN, MBL SP-D, and DEC-205, linear **Mannose-(L)-nmers** associate faster than polymers of

other chiralities. For Langerin and Mincle, linear **Mannose-(D)-nmers** associate faster. For Dectin-2, **Mannose-(alt)-nmers** and **Mannose-8-MC**'s show faster association than than their isotactic (*L*) and (*D*) counterparts.

Ligand		DC-SIGN	DC-SIGNR	MBL	SP-D	Langerin	Dectin-2	Mincle	DEC-205
32mer	(<i>L</i>)	5.66×10^{-5}	2.67×10^{-5}	2.39×10^{-6}	3.01×10^{-6}	2.06×10^{-6}	3.29×10^{-7}	5.63×10^{-6}	1.47×10^{-7}
	(<i>alt</i>)	1.98×10^{-5}	8.66×10^{-4}	1.44×10^{-6}	1.80×10^{-6}	5.38×10^{-6}	4.92×10^{-7}	9.77×10^{-6}	1.56×10^{-7}
	(<i>D</i>)	1.49×10^{-5}	2.69×10^{-4}	1.61×10^{-6}	3.07×10^{-6}	3.79×10^{-6}	1.25×10^{-7}	6.41×10^{-6}	2.06×10^{-7}
16mer	(<i>L</i>)	1.26×10^{-6}	1.26×10^{-5}	9.81×10^{-6}	4.03×10^{-6}	8.01×10^{-6}	9.17×10^{-6}	7.46×10^{-6}	3.90×10^{-6}
	(<i>alt</i>)	3.89×10^{-6}	4.59×10^{-5}	1.60×10^{-6}	3.71×10^{-5}	6.82×10^{-5}	1.83×10^{-7}	3.71×10^{-5}	7.77×10^{-7}
	(<i>D</i>)	6.93×10^{-6}	1.09×10^{-4}	1.02×10^{-5}	1.86×10^{-5}	3.71×10^{-5}	3.07×10^{-6}	1.55×10^{-6}	7.45×10^{-7}
8mers	(<i>L</i>)	1.71×10^{-4}	5.74×10^{-5}	2.42×10^{-6}	5.74×10^{-5}	1.03×10^{-5}	1.03×10^{-5}	5.84×10^{-5}	9.12×10^{-7}
	(<i>alt</i>)	1.55×10^{-4}	3.25×10^{-5}	2.63×10^{-6}	7.22×10^{-6}	2.09×10^{-6}	4.58×10^{-5}	1.94×10^{-5}	2.17×10^{-7}
	(<i>D</i>)	9.45×10^{-4}	9.66×10^{-5}	9.66×10^{-5}	9.66×10^{-5}	4.37×10^{-7}	7.21×10^{-5}	4.12×10^{-5}	3.89×10^{-7}
8mer MCs	(<i>L</i>)	4.65×10^{-5}	9.83×10^{-4}	6.23×10^{-6}	5.78×10^{-6}	7.55×10^{-6}	3.05×10^{-7}	4.31×10^{-6}	8.62×10^{-6}
	(<i>alt</i>)	1.68×10^{-6}	2.99×10^{-5}	4.56×10^{-6}	6.27×10^{-6}	2.94×10^{-6}	5.45×10^{-7}	3.18×10^{-6}	7.33×10^{-6}
	(<i>D</i>)	1.84×10^{-4}	7.25×10^{-5}	1.82×10^{-6}	3.99×10^{-6}	4.76×10^{-6}	2.13×10^{-7}	1.12×10^{-6}	2.31×10^{-6}

Table 4.2. Summary table of k_d -values (s^{-1}) between every glycopolymer vs. eight lectins, colour coded according to relative k_d -values. Red and orange domains display binding minima within the respective lectin series, yellow domains display average binding, and green domains display binding maxima.

Equilibrium dissociation constants (k_d) (Table 2) of the investigated glycopolymers are intrinsically different for every lectin and generally depend on the glycopolymers' multivalent binding with the proteins. In the case of DC-SIGN, the k_d values of cyclic **Mannose-8-MC**'s are an order of magnitude higher than the k_d value of linear **Mannose-32mers** and two orders of magnitude higher than the k_d value of linear **Mannose-16mers**. Among the **Mannose-8-MC**'s, the k_d of **Mannose-(alt)8-MC** is two orders of magnitude lower than the dissociation constant of **Mannose-(D)8-MC** and one order of magnitude lower than **Mannose-(L)8-MC** for DC-SIGN. In the cases of MBL, SP-D, Langerin, Dectin-2 and Mincle, linear **Mannose-8**'s showed the highest k_d value. Typically, the respective **Mannose-8-MC**'s k_d values are an order of magnitude lower than their linear **Mannose-8** equivalents. Furthermore, particularly low dissociation constants were observed for **Mannose-(D)8** with Langerin; all **Mannose-32**'s, **Mannose-8-MC**'s, and **Mannose-(alt)16** with Dectin-2; and all linear glycopolymers with DEC-205.

Ligand		DC-SIGN	DC-SIGNR	MBL	SP-D	Langerin	Dectin-2	Mincle	DEC-205
32mer	(L)	3.31×10 ⁶	2.55×10 ⁶	4.67×10 ⁷	3.01×10 ⁷	4.23×10 ⁷	2.59×10 ⁸	9.02×10 ⁶	2.24×10 ⁸
	(alt)	5.71×10 ⁶	1.46×10 ⁵	7.15×10 ⁷	4.09×10 ⁷	7.72×10 ⁶	3.39×10 ⁸	5.54×10 ⁶	1.39×10 ⁹
	(D)	3.76×10 ⁶	3.19×10 ⁵	5.21×10 ⁷	1.97×10 ⁷	3.55×10 ⁷	2.68×10 ⁸	9.63×10 ⁶	5.50×10 ⁸
16mer	(L)	1.37×10 ⁸	2.21×10 ⁶	1.89×10 ⁷	6.87×10 ⁷	6.05×10 ⁶	5.51×10 ⁶	1.30×10 ⁷	1.74×10 ⁷
	(alt)	3.37×10 ⁷	4.29×10 ⁵	9.00×10 ⁷	3.96×10 ⁶	6.05×10 ⁵	3.34×10 ⁸	3.96×10 ⁶	5.17×10 ⁷
	(D)	1.39×10 ⁷	2.95×10 ⁵	1.01×10 ⁷	5.19×10 ⁶	3.96×10 ⁶	1.05×10 ⁷	1.03×10 ⁸	6.90×10 ⁷
8mers	(L)	4.04×10 ⁵	4.17×10 ⁵	4.69×10 ⁶	4.17×10 ⁴	1.14×10 ⁶	4.17×10 ⁴	0.56×10 ⁵	3.43×10 ⁷
	(alt)	2.62×10 ⁵	5.35×10 ⁵	1.86×10 ⁶	2.21×10 ⁵	1.84×10 ⁶	1.29×10 ⁶	3.08×10 ⁵	9.08×10 ⁷
	(D)	2.21×10 ⁴	2.34×10 ⁵	0.53×10 ⁵	0.27×10 ⁵	4.65×10 ⁷	1.37×10 ⁵	1.48×10 ⁵	3.37×10 ⁷
8mer MCs	(L)	6.32×10 ⁵	1.1×10 ⁴	7.86×10 ⁶	1.34×10 ⁶	3.40×10 ⁶	2.73×10 ⁷	1.34×10 ⁶	2.09×10 ⁶
	(alt)	2.24×10 ⁶	7.41×10 ⁵	2.14×10 ⁷	6.65×10 ⁶	6.50×10 ⁶	1.17×10 ⁸	9.24×10 ⁶	3.25×10 ⁶
	(D)	7.83×10 ⁴	3.81×10 ⁴	1.89×10 ⁷	0.80×10 ⁶	1.76×10 ⁶	2.24×10 ⁷	1.63×10 ⁶	5.32×10 ⁶

Table 4.3. Summary table of K_A -values (M^{-1}) between every glycopolymer vs. eight lectins, colour coded according to relative K_A -values (M^{-1}). Red and orange domains display binding minima within the respective lectin series, yellow domains display average binding, and green domains display binding maxima.

Ligand		DC-SIGN	DC-SIGNR	MBL	SP-D	Langerin	Dectin-2	Mincle	DEC-205
32mer	(L)	970	380	5575	1140	825	1140	510	235
	(alt)	740	340	5340	790	795	2085	535	180
	(D)	590	305	4210	730	925	830	555	175
16mer	(L)	495	270	2790	360	550	600	210	160
	(alt)	415	210	1885	220	360	710	240	135
	(D)	380	145	725	190	695	450	290	102
8mers	(L)	300	110	470	170	270	150	100	85
	(alt)	230	80	235	145	260	250	155	70
	(D)	190	65	175	110	350	125	190	45
8mer MCs	(L)	700	100	2005	675	615	640	250	340
	(alt)	865	380	5320	1340	500	1430	335	395
	(D)	475	60	1080	270	190	260	90	300

Table 4.4. Summary table of R_{max} (RU)-values between every glycopolymer vs. eight lectins, colour coded according to relative R_{max} values. Red and orange domains display binding minima within the respective lectin series, yellow domains display average binding, and green domains display binding maxima.

As expected, we found that the binding affinity constants K_A (Table 3), the ratio of k_a/k_d , was generally higher for longer polymers, due to their higher k_a value. Additionally, it was observed that **Mannose-(alt)8-MC** displays higher K_A than **Mannose-(D)8-MC** and **Mannose-(L)8-MC**. Moreover, K_A of the **Mannose-8-MC**'s against Dectin-2 were remarkably high. In the

case of DC-SIGN, all **Mannose-16**'s showed K_A that were at least an order of magnitude higher than **Mannose-32**'s and **Mannose-8-MC**'s. K_A 's for **Mannose-32**'s against Dectin-2 and DEC-205, **Mannose-(L)16** against DC-SIGN, and **Mannose-(alt)16** for Dectin-2 were particularly high.

Last, extracting R_{\max} values (Table 4) from the kinetic SPR data allows us to quantify the overall strength the binding between our glycopolymers and the 8 different C-type lectins. From these results, we can confirm a few consistent features. First, longer chain lengths generally increase lectin binding strength when backbone chirality is controlled, and some individual lectins are more effected by glycopolymer length than other lectins. For example with SP-D, **Mannose-32**'s bind almost 3 or 4 fold stronger than **Mannose-16**'s, and **Mannose-16**'s bind at most 2-fold more strongly than **Mannose-8**'s. Second, macrocyclic topologies lead to far stronger lectin binding: **Mannose-8-MC**'s generally bind more strongly than linear **Mannose-8**'s, **Mannose-16**'s, and in some cases **Mannose-32**'s. We expected this effect as macrocyclic oligomers have more constrained structures and consequently, less entropic penalty. **Mannose-(alt)8-MC** has a similar or greater R_{\max} values to the **Mannose-32**'s in the cases of DC-SIGN, DC-SIGNR, MBL, and SP-D. All chiralities of the **Mannose-8-MC**'s bind DEC-205 far better than the linear examples. Third, stereochemistry has a major impact on all glycopolymer lengths. In the cases of DC-SIGN, DC-SIGNR, MBL, SP-D and DEC-20, linear **Mannose-(L)-nmers** bind stronger than linear **Mannose-(alt)-nmers** which bind stronger than their linear **Mannose-(D)-nmers** counterparts. Despite this general binding preference for **Mannose-(L)-nmers**, Langerin and Mincle both have a mild preference for the S chirality. Among the macrocycles, **Mannose-(alt)8-MC** generally binds stronger than both **Mannose-(D)8-MC** and **Mannose-(L)8-MC**.

In addition to evaluating the effects of topology, length, and chirality on the lectin binding, we wanted to demonstrate that side chain variation could also greatly change the biological properties of our glycopolymers. To do so, we compared two glycopolymers functionalized with a TAMRA fluorescent dye and two different side chains shown in **Figure 4.2A: Mannose-(L)32-TAMRA** and **PhMannose-(L)32-TAMRA**. **Mannose-(L)32-TAMRA** differs from the other previously tested glycopolymers with its fluorescent end group. It has high solubility in water and does not aggregate into larger particles. The PhMannose side chain conveys several different properties compared to its Mannose counterpart due largely to its tendency to aggregate into larger particles when put onto a polymer platform. This aggregation effect can be seen in Figure S4.33 where **PhMannose-(L)32-TAMRA** glycopolymers are shown to form particles between 100 nm

and 150 nm in diameter. **PhMannose-(L)32-TAMRA** is sparingly soluble in water, so we were unable to perform SPR studies on it.

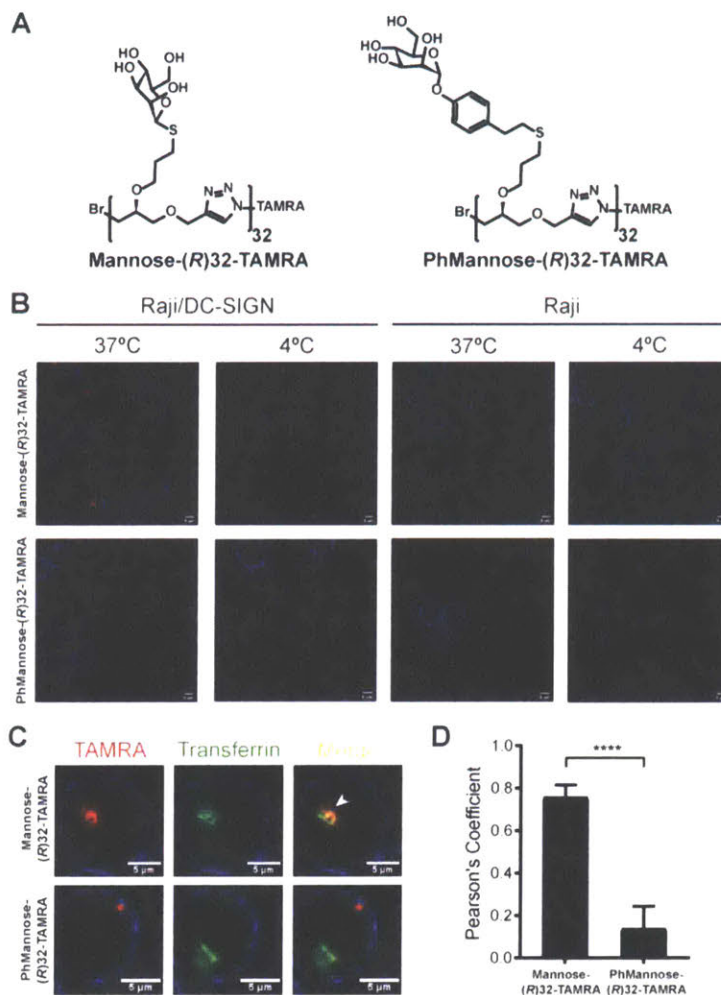


Figure 4.2. (A) Structures of **Mannose-(L)32-TAMRA** and **PhMannose-(L)32-TAMRA** used to study the effect of side chains into cells. (B) Fluorescence spectroscopy to visualize presence of TAMRA functionalized polymers with DC-SIGN positive Raji B-cells and DC-SIGN negative Raji B-cells at either 37 °C or 4 °C. Both polymers localize in or on the DC-SIGN positive Raji B-cells at 37 °C, but not in other conditions. (C) Fluorescence spectroscopy of TAMRA dye, Transferrin, and merged images in DC-SIGN positive Raji B-cells incubated at 37 °C. **Mannose-(L)32-TAMRA** localizes in primarily in endosomes, while **PhMannose-(L)32-TAMRA** localizes separately from the endosomes and on the surface of the cell membrane. (D) Quantified Pearson's coefficient demonstrating strong association between TAMRA and Transferrin fluorescence for **Mannose-(L)32-TAMRA** and weak association for **PhMannose-(L)32-TAMRA**.

As shown in **Figure 4.2B**, when both **Mannose-(L)32-TAMRA** and **PhMannose-(L)32-TAMRA** are incubated with DC-SIGN positive Raji B-cells and DC-SIGN negative Raji B-cells at either 37 °C or 4 °C, they both only bind to the cells when the lectin DC-SIGN is present at metabolic temperatures. Neither can properly associate with lectins at low temperatures, and neither associate well with cells without lectins. We then imaged the TAMRA dye to locate the glycopolymers and transferrin to locate the endosomes in the DC-SIGN positive Raji B-cells. **Figure 4.2C and 4.2D** demonstrate that **Mannose-(L)32-TAMRA**, as expected, is endocytosed into the Raji cells and localized inside endosomes. While **PhMannose-(L)32-TAMRA** has affinity to DC-SIGN, it does not localize inside the endosomes like its mannose counterpart, and instead sits on the outside of the cellular membrane. Potentially the large size of the **PhMannose-(L)32-TAMRA** nanoparticles prevent endocytosis into the cells and consequently push the glycopolymer through a different trafficking mechanism.

4.3 Conclusion

Herein, we report a biocompatible, unimolecular glycopolymer platform that can be manipulated to preferentially bind specific lectins. In addition to confirming increased valency increases overall binding strength of our glycopolymers to lectins, we have found that different stereoconfigurations and macromolecular architecture (linear vs. cyclic) bias glycopolymers towards binding different lectins. Finally, by changing the mannose side chain to a phenylmannose side chain, we are able to further change the physical properties of our glycopolymer system and the resulting biological effects. These initial proofs of concept demonstrate the structural versatility of our IEG synthesized polytriazole platforms, and with our reported findings, we aim to further develop the glycopolymer field and eventually create novel, efficacious lectin targeting pharmaceuticals.

4.4 Supplemental Information

Methods and Materials

All reagents were purchased from commercial suppliers and used without further purification unless stated otherwise. 365 nm UV light for thiol-ene addition chemistry was sourced from a VWR International supplied UV-AC hand lamp with two 6-watt UV tubes, one for 254 nm and one for 365 nm wavelengths. Gel permeation chromatography (GPC) analyses were performed on an Agilent 1260 Infinity setup with two Shodex KD-806M columns in tandem and a 0.025 M LiBr DMF mobile phase run at 60 °C. The differential refractive index (dRI) of each compound was monitored using a Wyatt Optilab T-rEX detector. Column chromatography was carried out on silica gel 60F (EMD Millipore, 0.040–0.063 mm). ¹H and ¹³C Nuclear magnetic resonance (NMR) spectra were recorded on a Bruker AVANCE-400 MHz NMR spectrometer and a Varian Inova-500 spectrometer. Chemical shifts are reported in ppm relative to the signals corresponding to the residual non-deuterated solvents: CDCl₃, δH = 7.26 ppm and δC = 77.16 ppm; (CD₃)₂SO, δH = 2.50 ppm. High-resolution mass spectra (HRMS) were measured on a Bruker Daltonics APEXIV 4.7 Tesla Fourier Transform Ion Cyclotron Resonance Mass Spectrometer (FT-ICR-MS) using an electrospray ionization (ESI) source. Matrix-assisted laser desorption/ionization-time of flight (MALDI-TOF) mass spectra were obtained on a Bruker model MicroFlex instrument using α-cyano-4-hydroxycinnamic acid as the matrix.

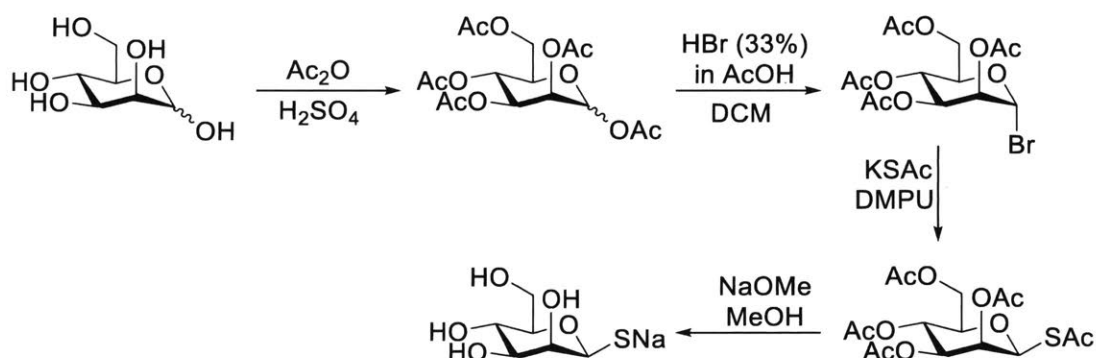
Surface Plasmon Resonance (SPR) was used for interaction analysis through all lectins. The extent of interaction between the glycopolymers and lectins were performed on a BIAcore 2000 system (GE Healthcare). The lectins (0.005 mg/ml) were immobilized *via* a standard amino coupling protocol onto a CM5 sensor chip that was activated by flowing a 1:1 mixture of 0.1 M *N*-hydroxysuccinimide and 0.1 M *N*-ethyl-*N'*-(dimethylaminopropyl)carbodiimide over the chip for 5 min at 25 °C at a flow rate of 5 μ L/min after the system equilibration with HEPES filtered buffer (10 mM HEPES pH 7.4, 150 mM NaCl, 5 mM CaCl₂). Subsequently, channels 1 (blank), 2, 3 and 4 were blocked by following a solution of ethanolamine (1 M pH 8.5) for 10 min at 5 μ L/min to remove remaining reactive groups on the channels. Sample solutions were prepared at varying concentrations (16 μ M-1 μ M) in the same HEPES buffer to calculate the binding kinetics. Sensorgrams for each glycopolymer concentration were recorded with a 300 seconds injection of polymer solution (on period) followed by 150 seconds of buffer alone (off period). Regeneration of the sensor chip surfaces was performed using 10 mM HEPES pH 7.4, 150 mM NaCl, 10 mM EDTA, 0.01% P20 surfactant solution. Kinetic data was evaluated using a single set of sites (1:1 Langmuir Binding) model in the BIAevaluation 3.1 software.

Cytotoxicity Assays. Two main assays were used to test the cytotoxicity of MH chemicals. Live/Dead (L/D) assay allows the detection and distinction between live (green) and dead (red) cells by means of fluorescent microscopy. On the other hand, Alamar Blue (AB) was used to test the mitochondrial activity of the cells. **General Procedure:** Prepare cells monolayer accordingly. Then, weight each compound and prepare solutions of 1 mg.mL⁻¹ with filtered PBS 1X. Sterilize the solutions by 15 min under UV. For inoculating the cells monolayers with the chemicals, add 475 μ L of DMEM and 25 μ L of each compound respectively. Leave the chemicals for the desire time of the experiment. Finally, add either L/D reagents or AM and then quantify. **Live/Dead Assay:** NIH 3T3 Fibroblasts cells were used. Monolayers of 10K cells were prepared. For this, after seeding, the cells were left for 4 hs to allow attachment. Passed this time, the monolayers were thoroughly washed with HBBS and each chemical was seeded at 5% w.v⁻¹ (considering a final volume of 500 μ L and chemicals of 1 mg.mL⁻¹). Four different time points were taken: 6, 12, 24 and 48 hs. Calcein and Ethidium Bromide solutions at 1 μ L.mL⁻¹ were prepared and add to each monolayer. A Leica... microscope was used for acquiring the images. Fiji-ImageJ software (NIH, USA) was used for image analysis. **Alamar Blue Assay:** NIH 3T3 Fibroblasts cells were used.

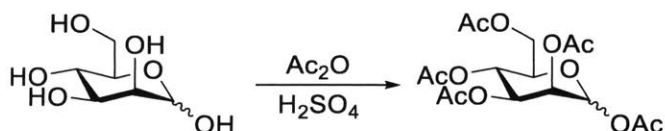
Monolayers of 10K cells were prepared. For this, after seeding, the cells were left for 4 hs to allow attachment. Passed this time, the monolayers were thoroughly washed with HBBS and each chemical was seeded at 5% w.v⁻¹ (considering a final volume of 500 μ L and chemicals of 1 mg.mL⁻¹). Four different time points were taken: 6, 12, 24 and 48 hs. After each time point, the monolayers were washed with fresh DMEM and incubated with a 10% AB solution for 2.5 hs. The supernatants were collected and quantify at 570 and 640 nm, respectively. Each monolayer was inoculated again with its respective chemical and the same procedure was repeated after the next time point.

Synthetic procedures

Synthesis route towards β -D-thiomannose sodium salt (All work to make this compound from D-(+)-Mannose was performed by Manuel Hartweg. Procedures included here for completeness.)



Synthesis of 1,2,3,4,6-Penta-O-acetyl-mannopyranoside



D-(+)-Mannose (20.0 g, 111 mmol) and acetic anhydride (200 mL) was cooled to 0 °C and a few drops of conc. H₂SO₄ is added. The suspension was gradually warmed to room temperature and stirred at room temperature for 18 h, whereby it turned into a solution. The solution was poured onto ice (200 g) and it was stirred for 30 min. DCM (3 x 200 mL) were added and the phases were separated. The combined organic layers were washed with sat. NaHCO₃ (200 mL) and brine (200 mL), and dried over MgSO₄. After filtration and removal of the solvent at reduced pressure

1,2,3,4,6-penta-*O*-acetyl-mannopyranoside was obtained as colourless sticky material (97%). ¹H NMR (400 MHz, CDCl₃) δ (ppm) = 6.05 (d, J = 1.9 Hz, 1H), 5.33 – 5.29 (m, 2H), 5.24 – 5.20 (m, 1H), 4.24 (dd, J = 12.4, 4.9 Hz, 1H), 4.07 (dd, J = 12.4, 2.5 Hz, 1H), 4.04 – 3.97 (m, 1H), 2.17, 2.16, 2.04, 2.04, 2.00 (s, 5 x 3H, COCH₃). ¹³C NMR (100 MHz, CDCl₃) δ (ppm) = 170.8 (COCH₃), 170.1 (COCH₃), 169.9 (COCH₃), 169.7 (COCH₃), 168.2 (COCH₃), 90.8 (C¹), 70.8 (C²), 68.9 (C⁵), 68.5 (C³), 65. (C⁴), 62.3, (C⁶) 21.0 (COCH₃), 20.9 (COCH₃), 20.9 (COCH₃), 20.8 (COCH₃), 20.8 (COCH₃).

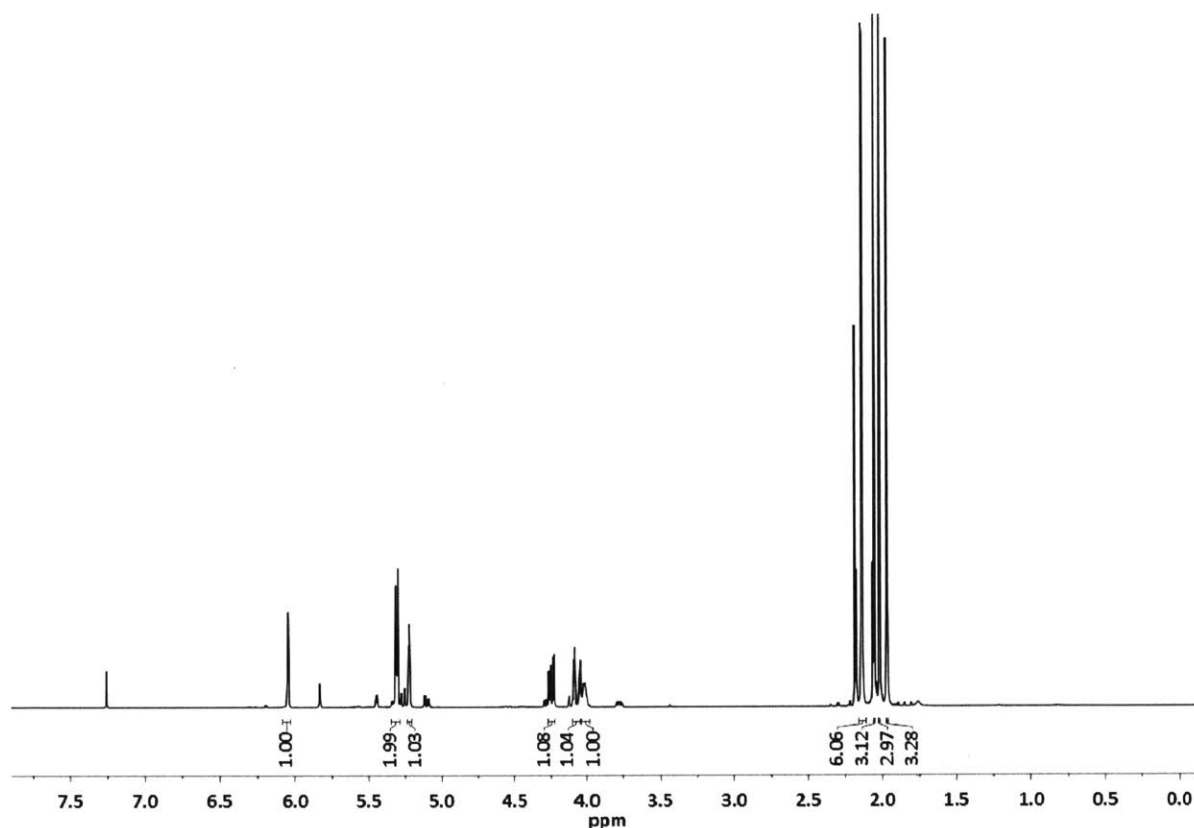


Figure S4.1. ¹H NMR spectrum of (400 MHz, CDCl₃, 25 °C) of *1,2,3,4,6*-penta-*O*-acetyl-mannopyranoside.

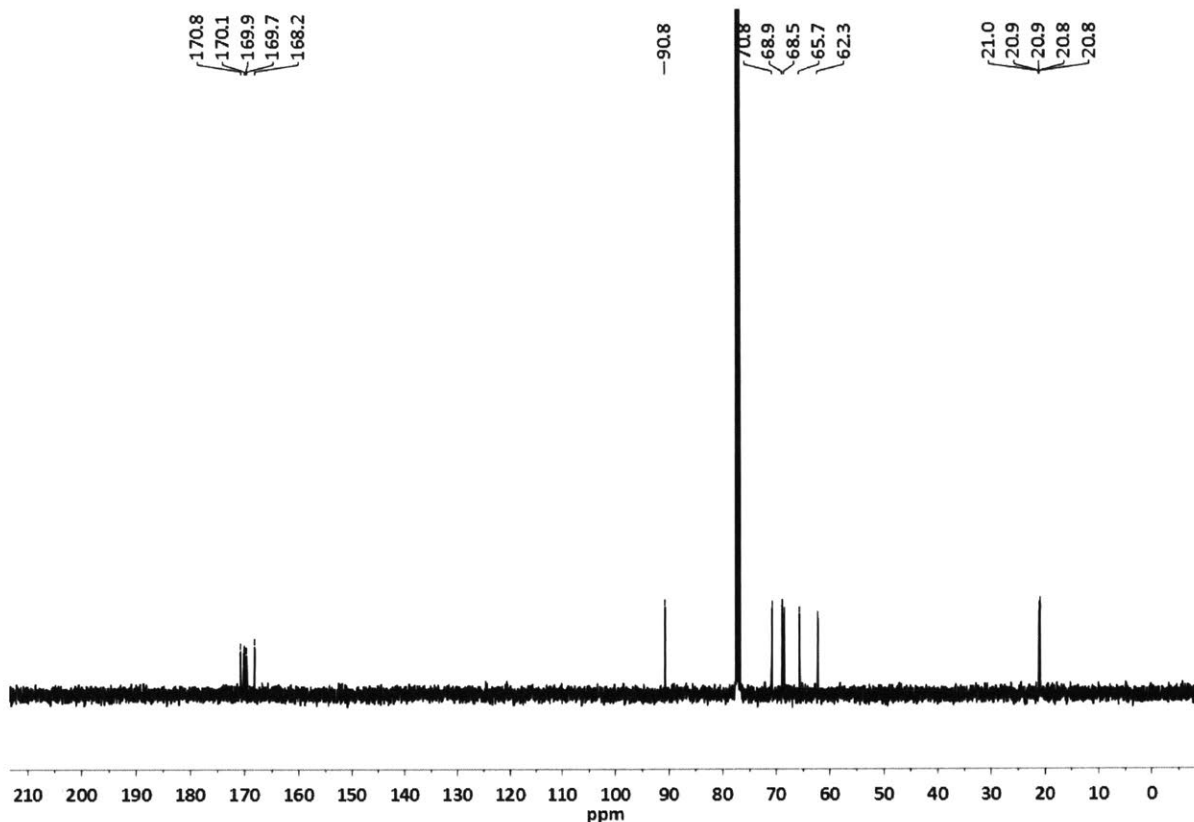
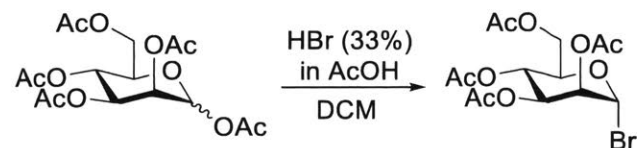


Figure S4.2. ^{13}C NMR spectrum of (400 MHz, CDCl_3 , 25 °C) of 1,2,3,4,6-penta-*O*-acetyl-mannopyranoside.

Synthesis of 2,3,4,6-Tetra-*O*-acetyl- α -*D*-mannopyranosyl bromide



1,2,3,4,6-Penta-*O*-acetyl-mannopyranoside (42.0 g, 12.8 mmol) was dissolved in DCM (400 mL) and hydrogen bromide (33% in acetic acid, 240 mL) was added and it was stirred at room temperature for 4 – 12 h (until TLC showed full consumption of the starting material). The solution was poured into water (400 mL), DCM (250 mL) and the phases were separated and the aqueous phase was re-extracted with DCM (2 x 200 mL). The combined organic layers were washed water (500 mL). Sat. NaHCO_3 solution was added until pH = 8 was obtained, then the phases were separated and the organic phase was washed with brine (500 mL), dried over MgSO_4 and filtered. The solvent was removed under reduced pressure and 2,3,4,6-tetra-*O*-acetyl- α -*D*-mannopyranosyl bromide was obtained as pale yellow sticky material (39 g, 88%), that turned brown after a few

days. ^1H NMR (400 MHz, CDCl_3) δ (ppm) = 6.28 (dd, $J_{1,2} = 1.7$, $J_{1,5} = 0.7$ Hz, 1H, H^1), 5.70 (dd, $J_{3,4} = 10.2$, $J_{3,2} = 3.4$ Hz, 1H, H^3), 5.43 (dd, $J_{2,3} = 3.4$, $J_{2,1} = 1.6$ Hz, 1H, H^2), 5.35 (t, $J_{4,3} = 10.2$ Hz, 1H, H^4), 4.31 (dd, $J_{6a,6b} = 12.5$, $J_{6a,5} = 4.9$ Hz, 1H, H^{6a}), 4.20 (dddd, $J_{5,4} = 10.2$, $J_{5,6a} = 4.9$, $J_{5,6b} = 2.2$, $J_{5,1} = 0.8$ Hz, 1H, H^5), 4.12 (dd, $J_{6b,6a} = 12.4$, $J_{6b,5} = 2.2$ Hz, 1H, H^{6b}), 2.16 (s, 3H, COCH_3), 2.09 (s, 3H, COCH_3), 2.06 (s, 3H, COCH_3), 1.99 (s, 3H, COCH_3). ^{13}C NMR (100 MHz, CDCl_3) δ (ppm) = 170.6 (COCH_3), 169.8 (COCH_3), 169.6 (d, 2 x COCH_3), 83.2 (C^1), 73.0 (C^2), 72.2 (C^5), 68.0 (C^3), 65.4 (C^4), 61.6 (CHCH_2CO , C^6), 20.9 (COCH_3), 20.8 (COCH_3), 20.7 (COCH_3), 20.7 (COCH_3).

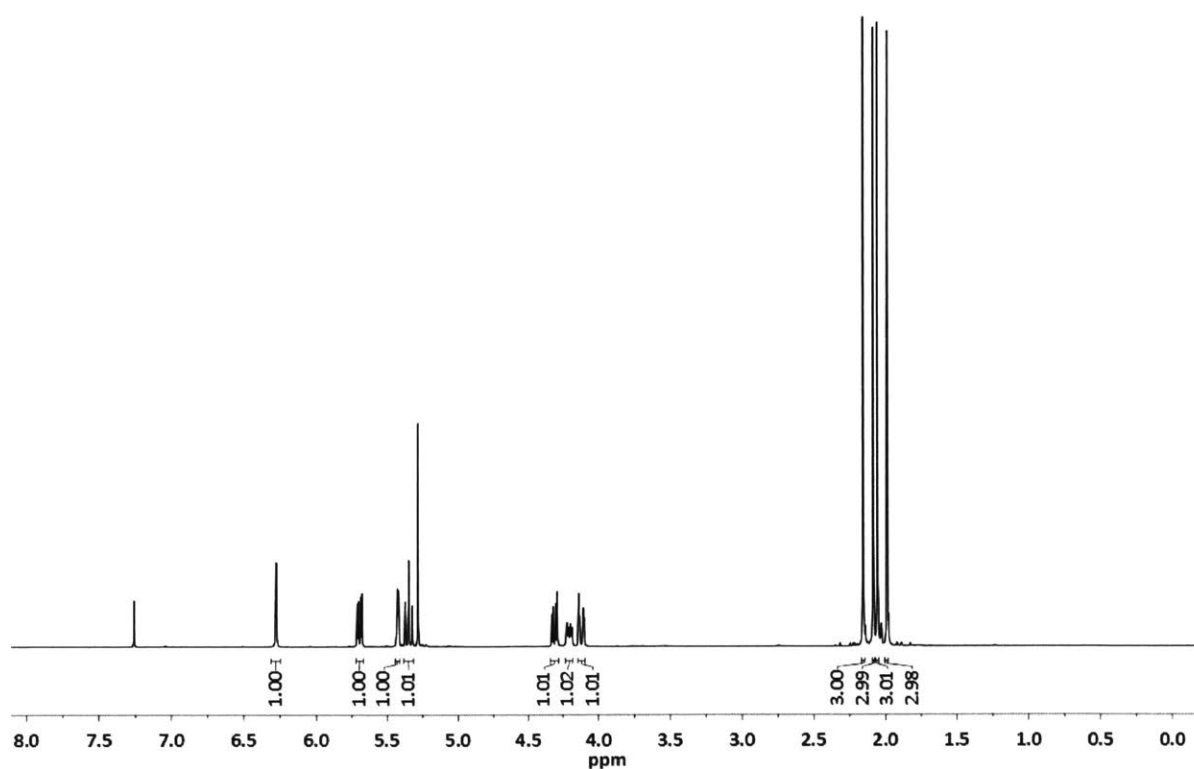


Figure S4.3. ^1H NMR spectrum of (400 MHz, CDCl_3 , 25 $^\circ\text{C}$) of 2,3,4,6-tetra-*O*-acetyl- α -*D*-mannopyranosyl bromide

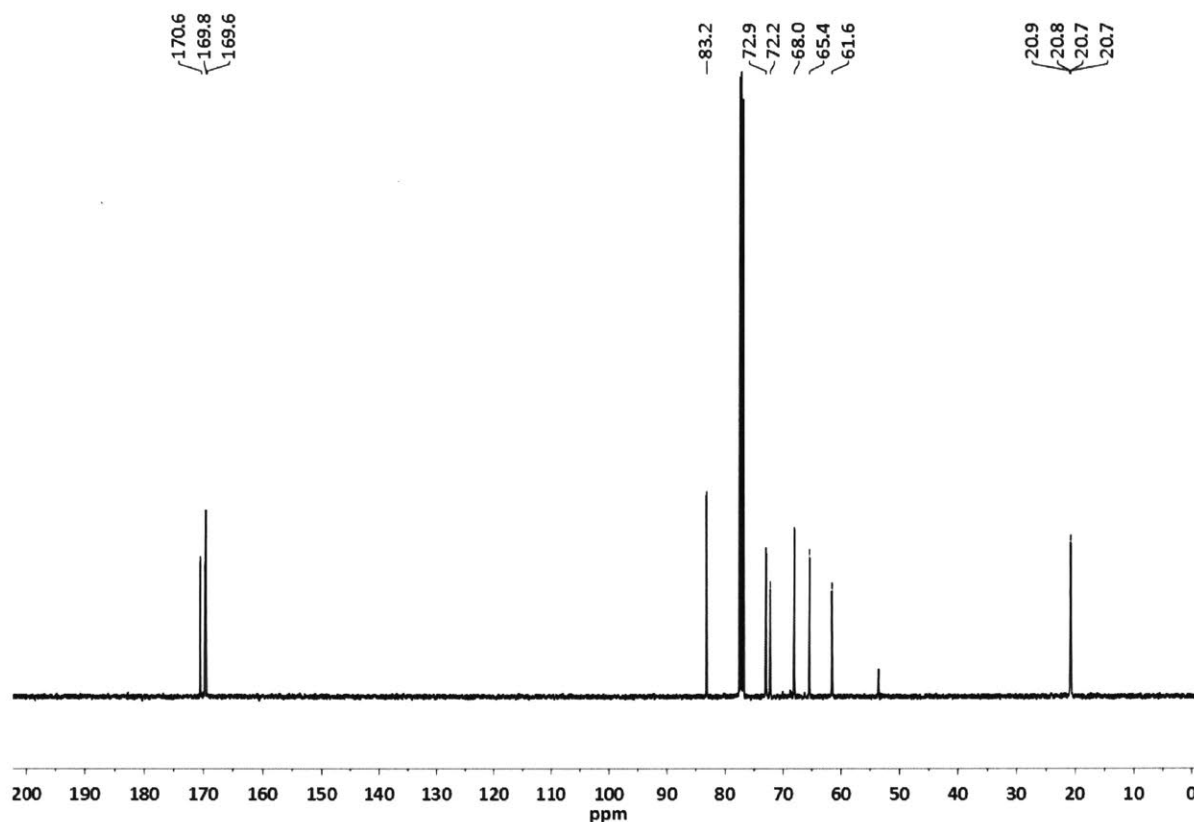
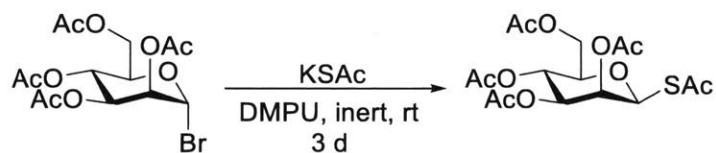


Figure S4.4. ^{13}C NMR spectrum of (400 MHz, CDCl_3 , 25 $^\circ\text{C}$) of 2,3,4,6-*tetra-O*-acetyl- α -*D*-mannopyranosyl bromide

Synthesis of 2,3,4,6-Tetra-*O*-acetyl-1-*S*-acetyl-1-thio- β -*D*-mannopyranose



2,3,4,6-*Tetra-O*-acetyl- α -*D*-mannopyranosyl bromide (33.0 g, 80.3 mmol, 1 eq) was dissolved in DMPU (150 mL) and the solution was degassed for 30 min. Under inert atmosphere, potassium thioacetate (10.1 g, 88.5 mmol, 1.1 eq) were added and the solution was stirred at room temperature for 2 d. EtOAc (400 mL) and water (400 mL) were added, the phases were separated and the aqueous phase was re-extracted with EtOAc (2 x 200 mL). The combined organic layers were washed with brine (500 mL), dried over MgSO_4 , filtered and the solvent was removed under reduced pressure. The residue was dissolved in a minimum amount of DCM/MeOH ($v/v = 1/1$, approx. 100 $v\%$). To the solution, petrol ether was added (1.2 L), whereby a precipitate formed. It

was cooled to 5 oC for 18 h, the formed precipitate was filtered off and dried under high vacuum to afford 2,3,4,6-tetra-*O*-acetyl-1-*S*-acetyl-1-thio- β -*D*-mannopyranose as yellow solid (20. g, 62%). ^1H NMR (400 MHz, CDCl_3) δ (ppm) = 5.51 – 5.46 (m, 2H, H^1 , H^2), 5.25 (t, $J = 10.0$ Hz, 1H, H^4), 5.14 (dd, $J_{3,4} = 10.1$, 3.4 Hz, 1H, H^3), 4.26 (dd, $J_{6a,6b} = 12.5$, $J_{6b,5} = 5.3$ Hz, 1H, H^{6a}), 4.11 (dd, $J_{6b,6a} = 12.4$, $J_{6b,5} = 2.3$ Hz, 1H, H^{6b}), 3.81 (ddd, $J_{5,4} = 10.0$, $J_{5,6a} = 5.3$, $J_{5,6b} = 2.3$ Hz, 1H, H^5), 2.36 (s, 3H, $\text{SC}(\text{O})\text{CH}_3$), 2.18 (s, 3H, COCH_3), 2.08 (s, 3H, COCH_3), 2.04 (s, 3H, COCH_3), 1.97 (s, 3H, COCH_3). ^{13}C NMR (100 MHz, CDCl_3) δ (ppm) = 191.8 ($\text{SC}(\text{O})\text{CH}_3$), 170.9 (COCH_3), 170.1 (COCH_3), 170.1 (COCH_3), 169.8 (COCH_3), 79.5 (C^1), 77.0 (C^5), 71.9 (C^3), 70.7 (C^2), 65.4 (C^4), 62.5 (C^6), 30.8 ($\text{SC}(\text{O})\text{CH}_3$), 20.9 (COCH_3), 20.8 (COCH_3), 20.8 (COCH_3), 20.7 (COCH_3).

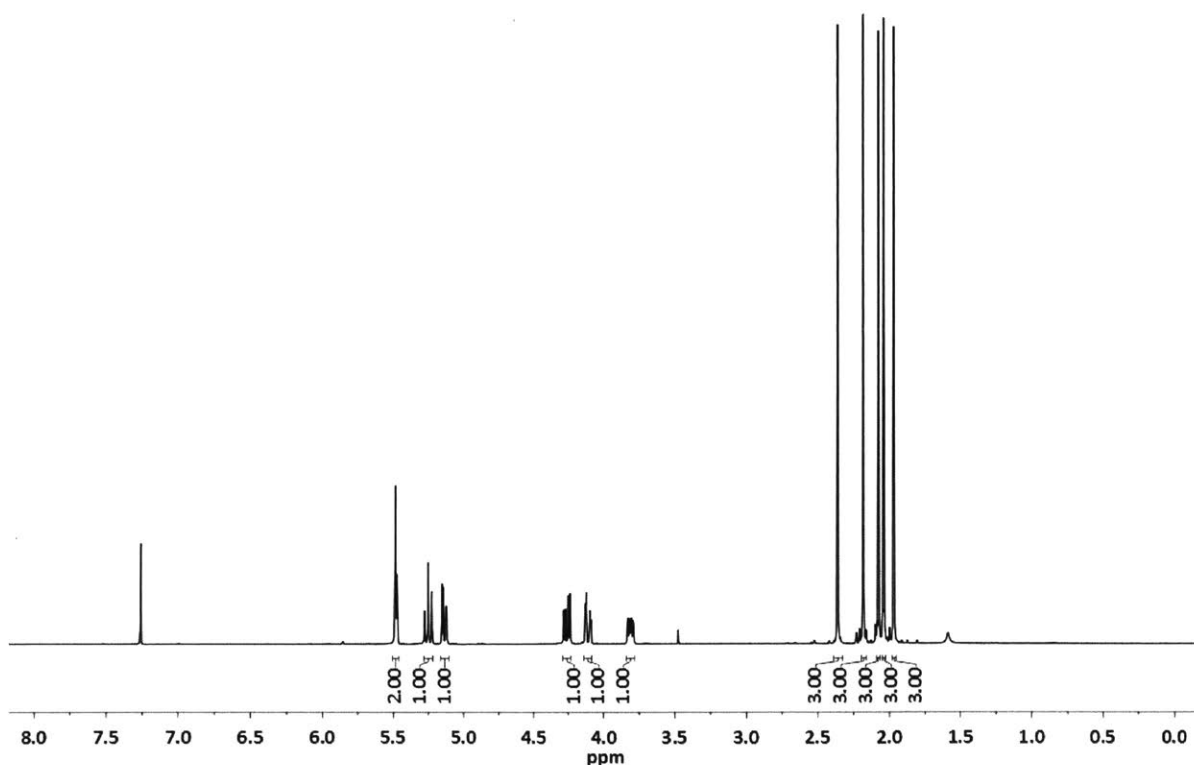


Figure S4.5. ^1H NMR spectrum of (400 MHz, CDCl_3 , 25 $^\circ\text{C}$) of 2,3,4,6-tetra-*O*-acetyl-1-*S*-acetyl-1-thio- β -*D*-mannopyranose.

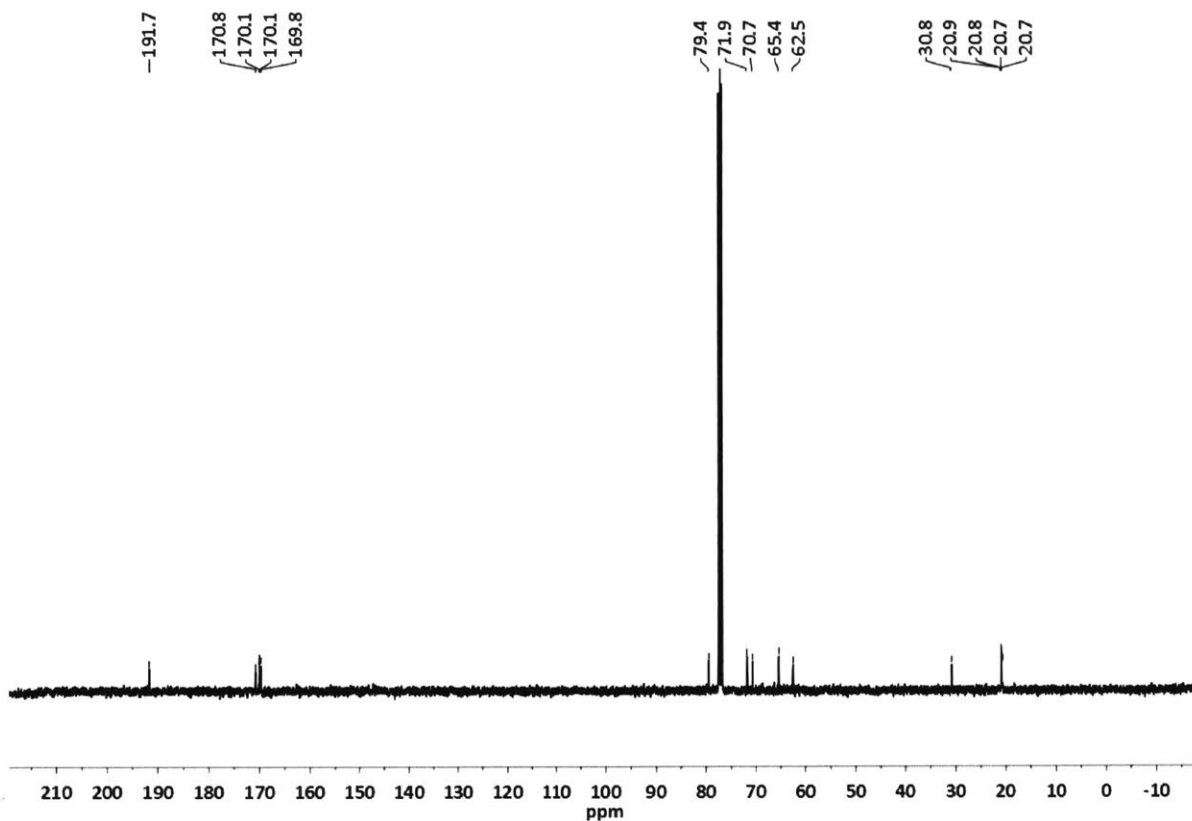
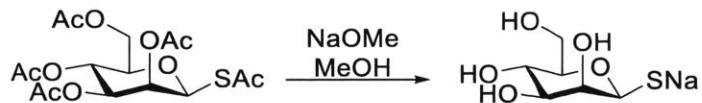


Figure S4.6. ^{13}C NMR spectrum (400 MHz, CDCl_3 , 25 $^\circ\text{C}$) of 2,3,4,6-tetra-*O*-acetyl-1-*S*-acetyl-1-thio- β -*D*-mannopyranose.

Synthesis of 1-Thio- β -*D*-Mannose sodium salt (ManSNa)



2,3,4,6-*Tetra-O*-acetyl-1-*S*-acetyl-1-thio- β -*D*-mannopyranose (19.0 g, 46.8 mmol, 1 eq) was dissolved in MeOH (400 mL) and NaOMe (3.78 g, 70.1 mmol, 1.5 eq) was added. After 3 h, the resulting precipitate was filtered off and dried under high vacuum. 1-Thio- β -*D*-mannose sodium salt was obtained as white solid (9.00 g, 88%). *CAUTION: when not stored as sodium salt, ManSH starts decomposing within hours as a solid and minutes in solution. ManSNa however, can be stored long term (>>6 month) at -20 $^\circ\text{C}$ easily without decomposition.* ^1H NMR (400 MHz, D_2O) δ (ppm) = 5.01 (d, $J_{1,2} = 1.0$ Hz, 1H, H^1), 3.86 (dd, $J_{2,3} = 12.2$, $J_{2,1} = 2.4$ Hz, 1H, H^2), 3.73 – 3.55

(m, 4H, H^3 , H^4 , H^{6a} , H^{6b}), 3.39 – 3.32 (m, 1H, H^5). ^{13}C NMR (100 MHz, D_2O) δ (ppm) = 82.2 (C^1), 80.1 (C^3), 75.0 (C^5), 74.7 (C^2), 66.7 (C^4), 61.4 (C^6).

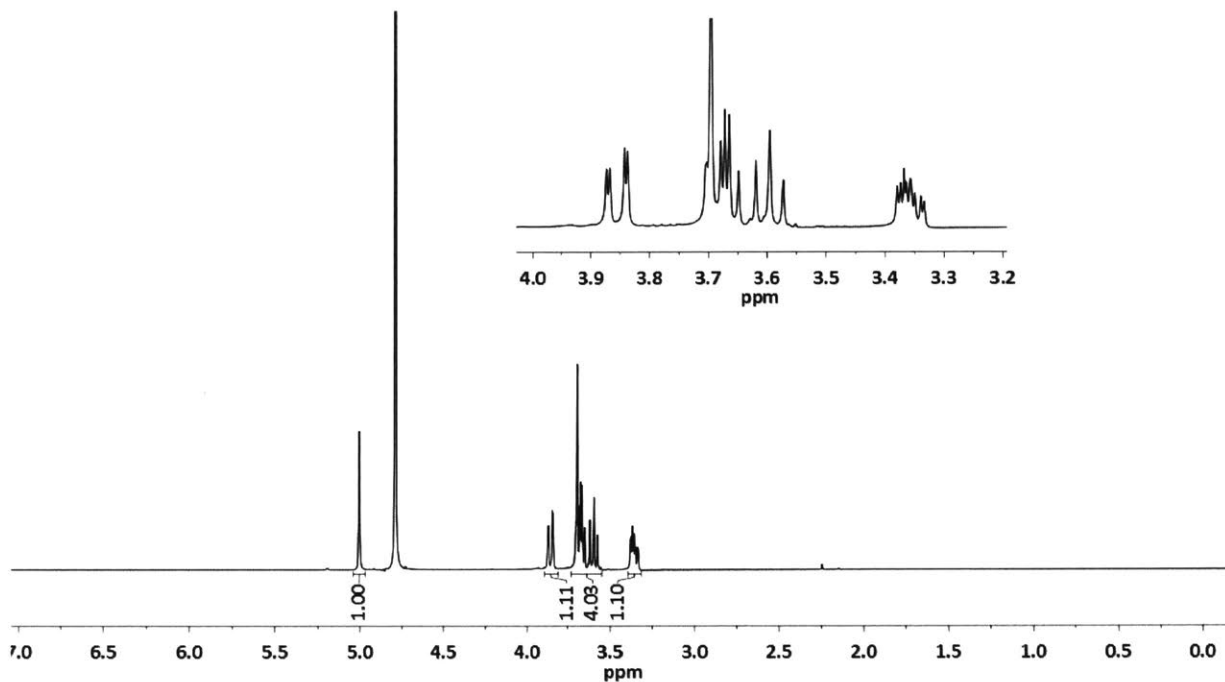


Figure S4.7. ^1H NMR spectrum (400 MHz, D_2O , 25 $^\circ\text{C}$) of 1-thio- β -D-Mannose sodium salt.

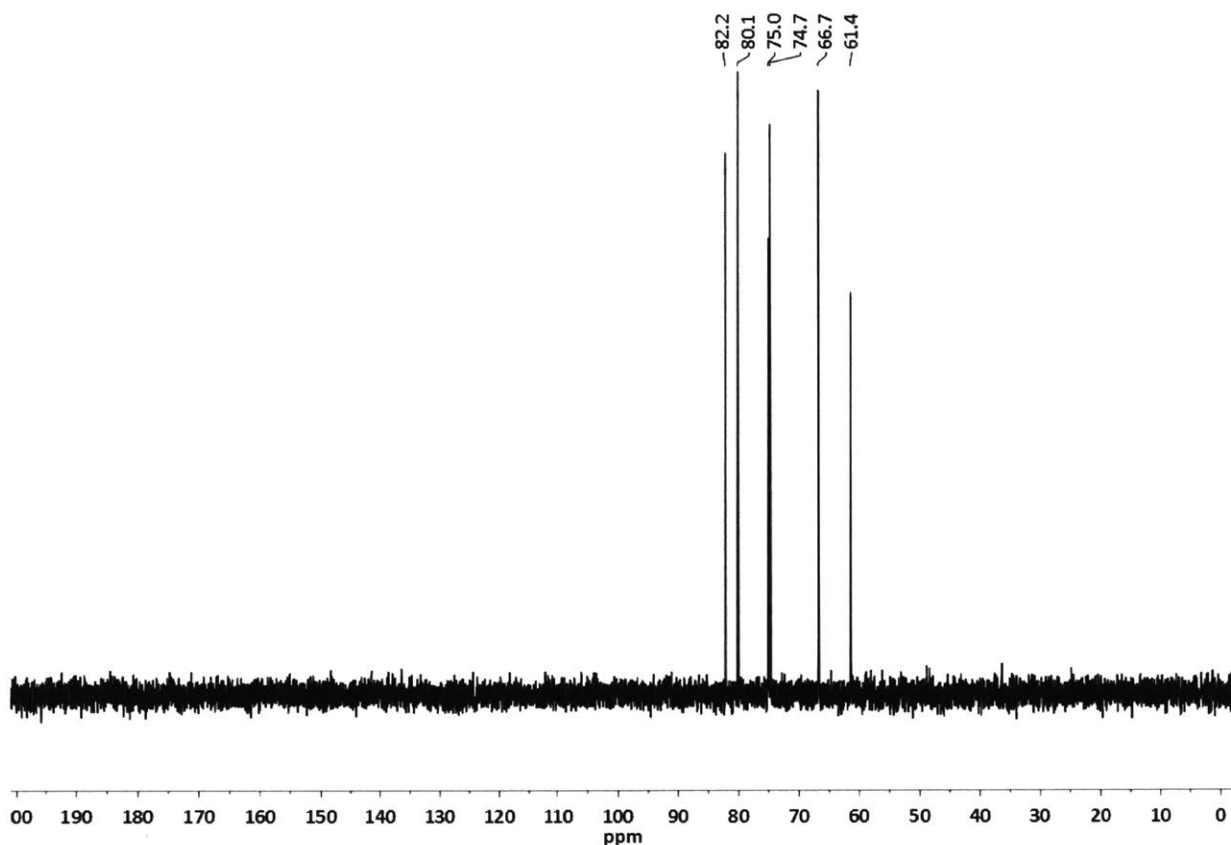
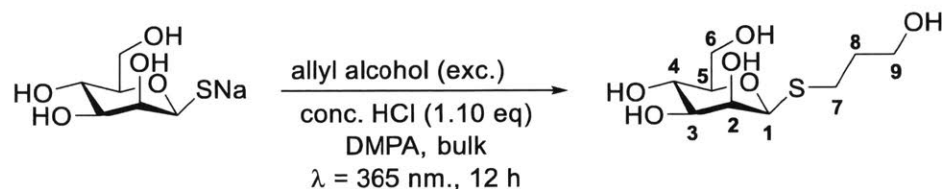


Figure S4.8. ^{13}C NMR spectrum (400 MHz, D_2O , 25 °C) of 1-thio- β -*D*-Mannose sodium salt.

Synthesis of 1-thiopropen-1-ol- β -*D*-mannose



1-Thio- β -*D*-mannose sodium salt (121 mg, 555 μmol , 1.0 eq) and DMPA (28 mg, 110 μmol , 20 mol%) were added to allyl alcohol (1.00 mL). Conc. HCl (37%, 60 μL , 610 μmol , 1.10 eq) was added and the solution was stirred under UV radiation ($\lambda = 365 \text{ nm}$) at room temperature for 12 h. A mixture of chloroform and hexane (1/1, v/v, 80 mL) was added and the solution was cooled to $-20 \text{ }^\circ\text{C}$ for 18 h for crystallization. The solution was decanted off and the resulting colourless crystals were recrystallized again using the same procedure (106 mg, 416 μmol , 75%). ^1H NMR (Methanol- d_4 , 400 MHz) $\delta = 4.76$ (d, $J_{1,2} = 1.1 \text{ Hz}$, 1H, H^1), 3.92 (dd, $J_{2,3} = 3.4$, $J_{2,1} = 1.1 \text{ Hz}$, 1H, H^2), 3.89 (dd, $J_{6b,6a} = 11.8$, $J_{6,5} = 2.4 \text{ Hz}$, 1H, H^{6b}), 3.76 – 3.66 (m, 3H, H^9 , H^{6a}), 3.60 (t, $J_{4,5} = 9.5$

Hz, 1H, H^4), 3.50 (dd, $J = 9.4$, $J_{3,2} = 3.4$ Hz, 1H, H^3), 3.28 (ddd, $J_{5,4} = 9.6$, $J_{5,6a} = 5.8$, $J_{5,6b} = 2.4$ Hz, 1H, H^5), 2.89 – 2.76 (m, 2H, H^7), 1.92 – 1.82 (m, 2H, H^8). ^{13}C NMR (Methanol- d_4 , 400 MHz) $\delta = 86.4$ (C^1), 82.4 (C^3), 76.3 (C^5), 74.0 (C^2), 68.4 (C^4), 63.0 (C^6), 61.3 (C^9), 33.9 (C^8), 28.7 (C^7).

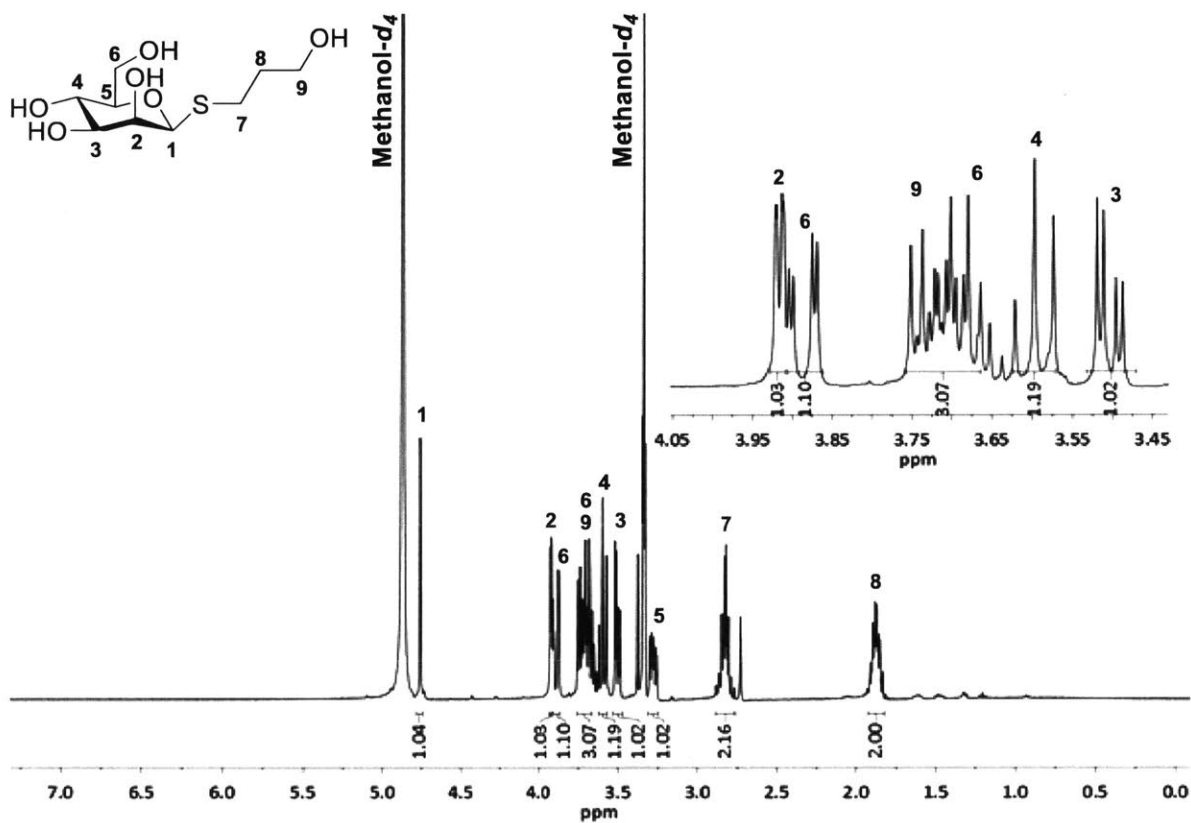


Figure S4.9. ^1H NMR spectrum of (400 MHz, MeOD, 25 $^\circ\text{C}$) of 1-thiopropan-1-ol- β -D-mannose.

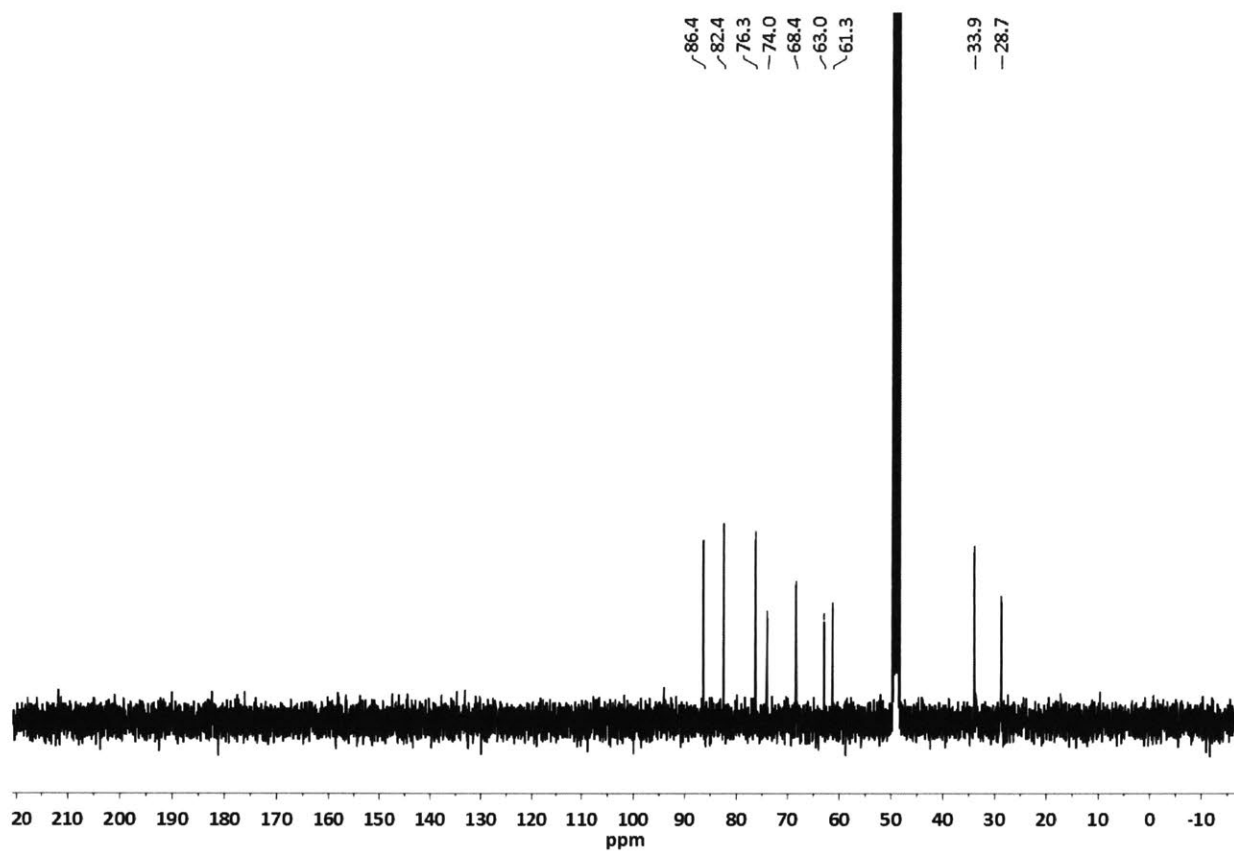


Figure S4.10. ^{13}C NMR spectrum of (100 MHz, MeOD, 25 °C) of 1-thioprop-1-ol- β -*D*-mannose.

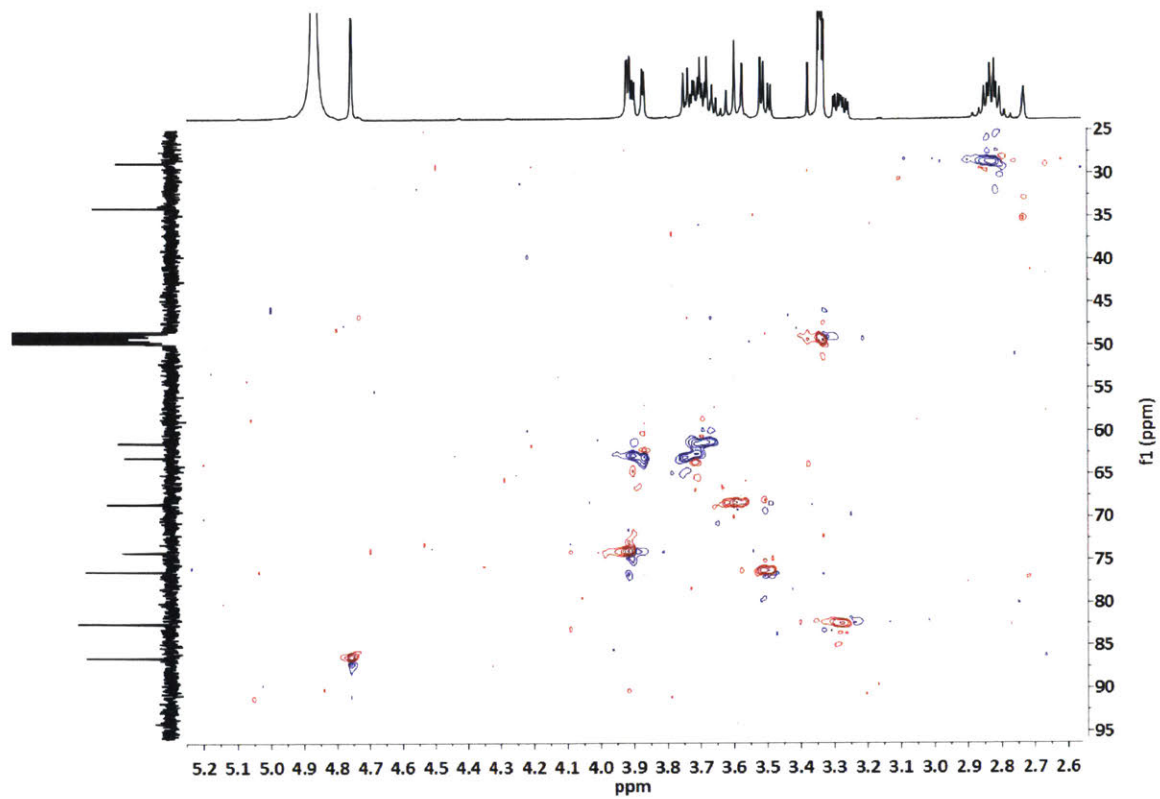


Figure S4.11. 2D HMBC (^1H ^{13}C) spectrum of (400 MHz, MeOD, 25 $^\circ\text{C}$) of 1-thiopropyl- β -D-mannose.

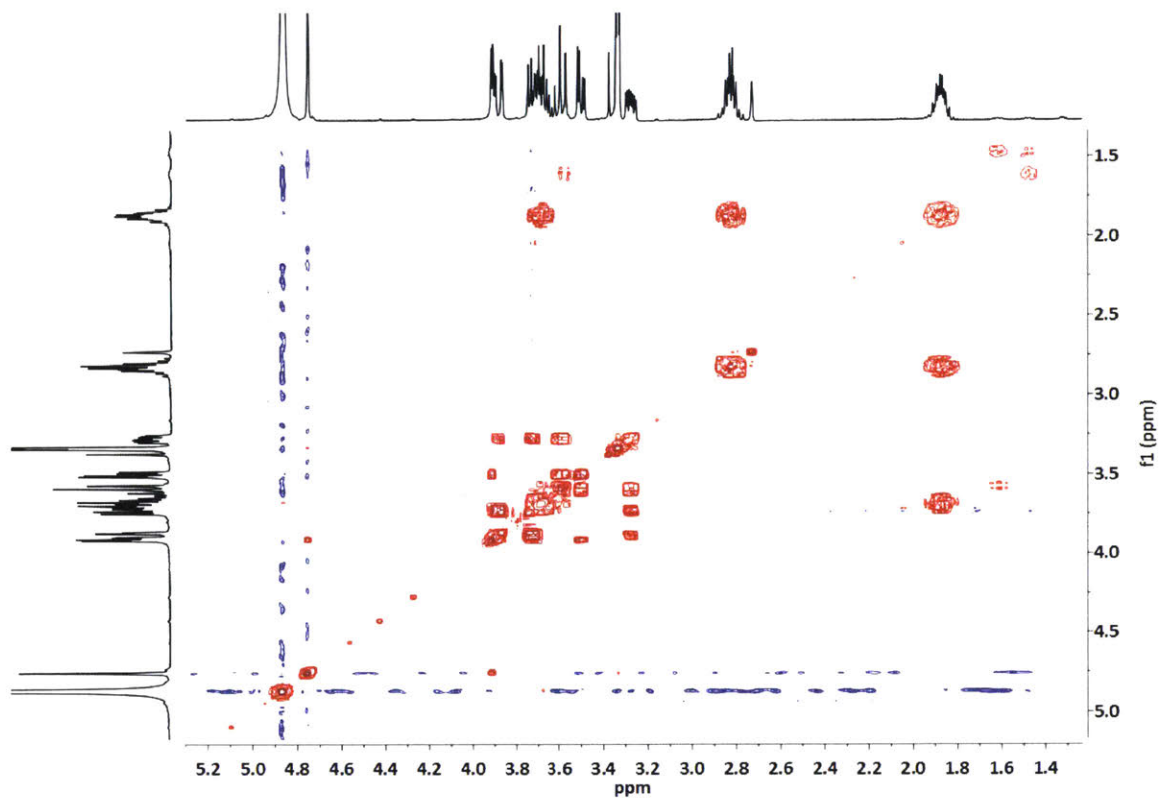


Figure S4.12. 2D HSQC (^1H ^{13}C) spectrum of (400 MHz, MeOD, 25 °C) of 1-thioprop-1-ol- β -*D*-mannose.

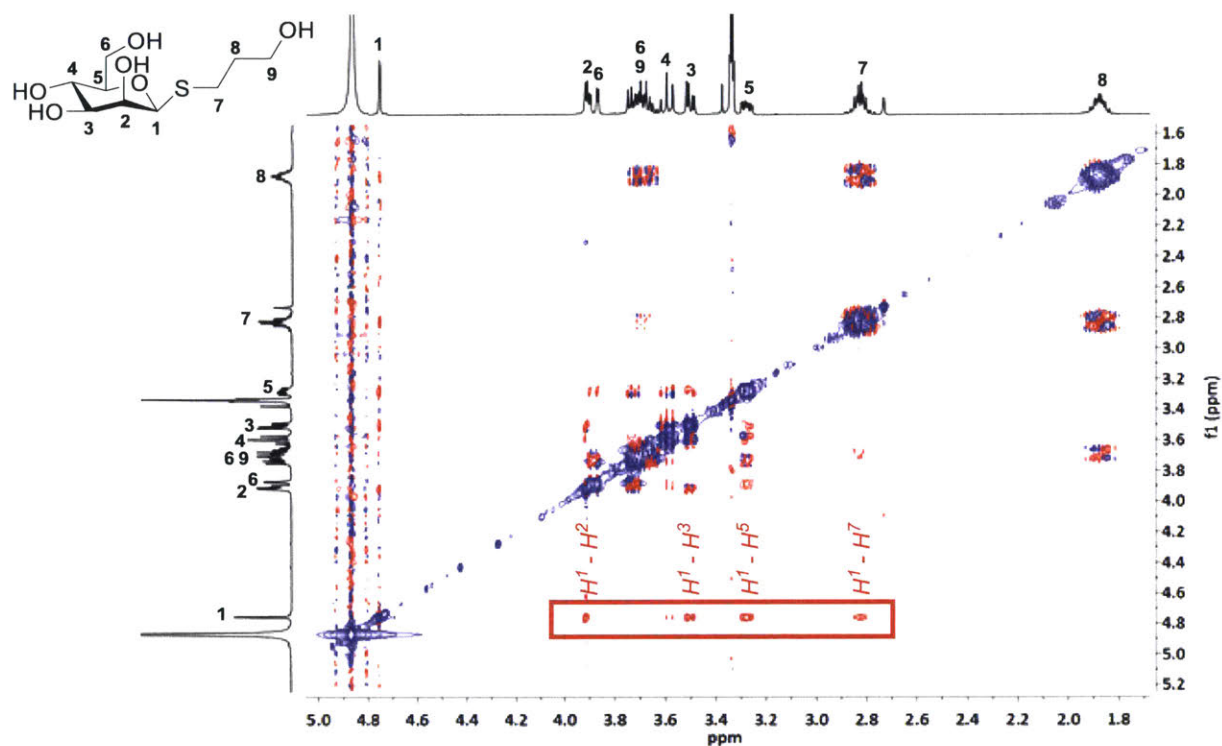
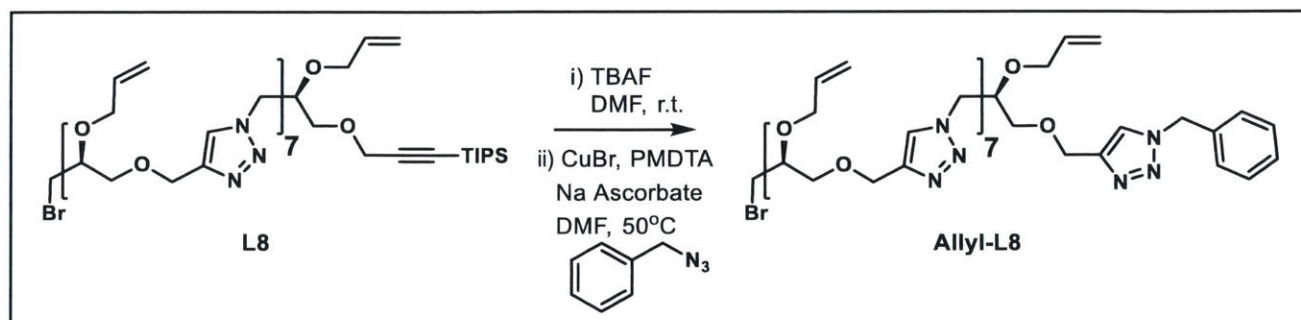
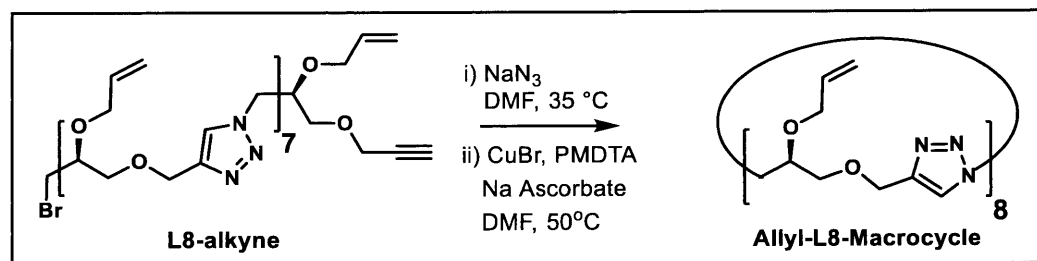


Figure S4.13. 2D NEOSY (^1H ^1H) spectrum (400 MHz, MeOD, 25 °C) of 1-thiopropyl- β -D-mannose. Emphasized cross signals of the anomeric proton H^1 with H^2 , H^3 and H^5 indicate exclusively β -conformation of the mannosyl-thioether.

Synthesis of Allyl Functional IEGmers of all (*L*), (*alt*), and all (*D*) stereochemistries. *Note:* in this report, all polymers are drawn from their azide (*N*) to alkyne (*C*) terminus; *L* and *D* labels are used to indicate the stereochemistry of each unit (wedge and dash bonds, respectively) akin to polypeptide nomenclature. Polymers with alternating *L* and *D* stereocenters are termed as “*alt*” for simplicity.



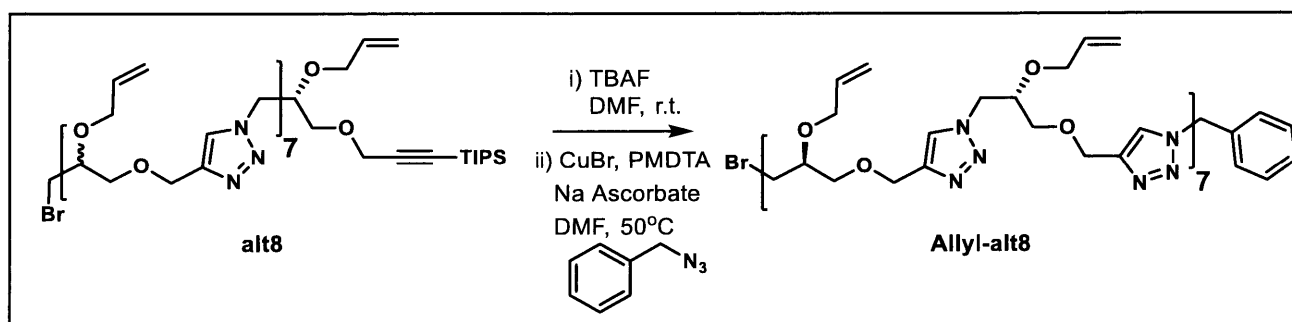
Allyl-L8: **L8** (200 mg, 0.11 mmol) was dissolved in DMF (10 mL), followed by the slow addition of TBAF (1.05equiv, 0.12 mL, 1M in THF). After 15 minutes, 100 mL of EtOAc was added and the organic solution was extracted 3x with 100 mL of 1% LiCl solution. The organic layer was concentrated to yield **L8-alkyne** (180 mg, 0.10 mmol) which was used without further purification. Under an N₂ atmosphere, dry DMF (0.200 mL) and sodium ascorbate (3.2 mg, 0.016 mmol) were added to a mixture of **L8-alkyne** (26 mg, 0.016 mmol) and benzyl azide (21 mg, 0.16 mmol) in an oven-dried 40 mL scintillation vial. A DMF solution of 0.1 M CuBr and 0.2 M PMDETA (0.080 mL) was then added to the reaction mixture. The reaction was warmed to 50 °C for 2 h. After completion, DMF was removed under reduced pressure. DCM (0.5 mL) was added to the resulting viscous mixture which was then loaded carefully onto a column. Column chromatography (100% DCM to 3.5% MeOH/DCM) yielded the product (18 mg, 0.010 mmol) in 56% yield from **L8**. ¹H NMR (500 MHz, CDCl₃): δ(ppm) 7.67 (overlap, 5H), 7.66 (s, 1H), 7.65 (s, 1H), 7.49 (s, 1H), 7.39-7.37 (overlap, 3H), 7.29 (overlap, 2H), 5.90 (ddt, 1H), 5.77-5.67 (overlap, 7H), 5.53 (s, 2H), 5.30-5.27 (m, 1H), 5.18-5.11 (overlap, 14H), 4.69-4.55 (overlap, 24H), 4.44-4.39 (overlap, 8H), 4.10 (m, 2H), 4.05-3.99 (m, 8H), 3.91-3.84 (overlap, 16H), 3.73-3.62 (overlap, 3H), 3.59-3.50 (overlap, 17H), 3.45 (dd, 1H).



Allyl-L8-macrocycle: NaN₃ (18 mg, 0.28 mmol) was added to a solution of **L8-alkyne** (150 mg, 0.094 mmol) in DMF (10 mL). The reaction was heated to 35 °C for 24 hours. After completion, 100 mL of EtOAc was added and the organic solution was extracted 3x with 100 mL of 5% LiCl solution. The organic layer was concentrated to yield **N₃-L8-alkyne** (140 mg, 0.089 mmol) which was used without further purification.

Under an N₂ atmosphere, dry DMF (8.9 mL) and sodium ascorbate (52 mg, 0.27 mmol) were added to a mixture of **N₃-L8-alkyne** (140 mg, 0.089 mmol) in an oven-dried 40 mL scintillation vial. A DMF solution of 0.1 M CuBr and 0.2 M PMDETA (2.7 mL) was then added to the reaction mixture. The reaction was warmed to 50 °C for 2 days. DMF was removed under reduced pressure. DCM (1 mL) was added to the resulting viscous mixture which was pushed through a neutral

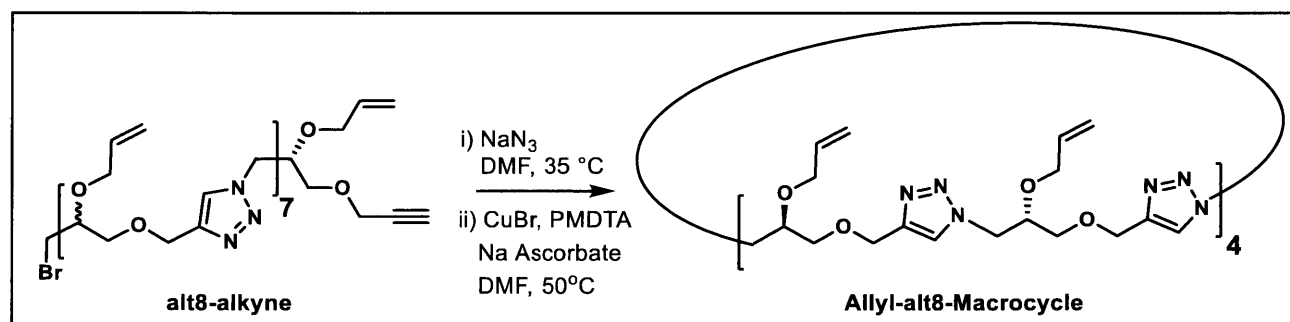
alumina column with 5% MeOH/DCM to remove precipitates and copper. The collected solution was concentrated by reduced pressure. 3 mL of Chloroform stabilized by ethanol was added to the crude product and the solution was filtered. The compound was then purified through recycling preparatory GPC yielding **Allyl-L8-macrocycle** (21 mg, 0.013 mmol) in 13% yield from **L8**. ^1H NMR (500 MHz, CDCl_3): δ (ppm) 7.69 (s, 8H), 5.76-5.69 (overlap, 8H), 5.19-5.10 (overlap, 16H), 4.68-4.56 (overlap, 24H), 4.46-4.42 (overlap, 8H), 4.05-4.02 (overlap, 8H), 3.92-3.89 (overlap, 16H), 3.59-3.50 (overlap, 16H).



Allyl-alt8: **alt8** (250 mg, 0.14 mmol) was dissolved in DMF (10 mL), followed by the slow addition of TBAF (1.05equiv, 0.15 mL, 1M in THF). After 15 minutes, 100 mL of EtOAc was added and the organic solution was extracted 3x with 100 mL of 1% LiCl solution. The organic layer was concentrated to yield **alt8-alkyne** (190 mg, 0.11 mmol) which was used without further purification.

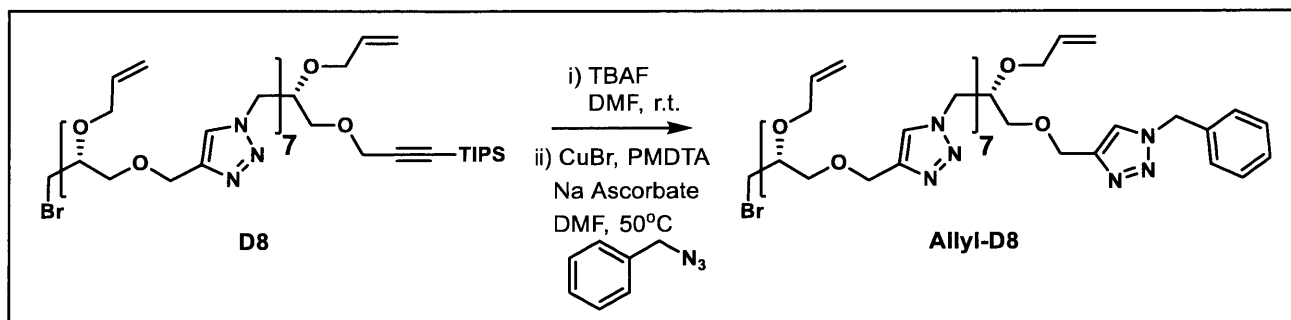
Under an N_2 atmosphere, dry DMF (0.200 mL) and sodium ascorbate (3.2 mg, 0.016 mmol) were added to a mixture of **alt8-alkyne** (26 mg, 0.016 mmol) and benzyl azide (21 mg, 0.16 mmol) in an oven-dried 40 mL scintillation vial. A DMF solution of 0.1 M CuBr and 0.2 M PMDETA (0.080 mL) was then added to the reaction mixture. The reaction was warmed to 50 °C for 2 h. After completion, DMF was removed under reduced pressure. DCM (0.5 mL) was added to the resulting viscous mixture which was then loaded carefully onto a column. Column chromatography (100% DCM to 3.5% MeOH/DCM) yielded the product (20 mg, 0.012 mmol) in 59% yield from **alt8**. ^1H NMR (500 MHz, CDCl_3): δ (ppm) 7.67 (overlap, 5H), 7.66 (s, 1H), 7.65 (s, 1H), 7.49 (s, 1H), 7.39-7.37 (overlap, 3H), 7.29 (overlap, 2H), 5.90 (ddt, 1H), 5.77-5.67 (overlap, 7H), 5.53 (s, 2H), 5.30-5.27 (m, 1H), 5.18-5.11 (overlap, 14H), 4.69-4.55 (overlap, 24H), 4.44-4.39 (overlap, 8H),

4.10 (m, 2H), 4.05-3.99 (m, 8H), 3.91-3.84 (overlap, 16H), 3.73-3.62 (overlap, 3H), 3.59-3.50 (overlap, 17H), 3.45 (dd, 1H).



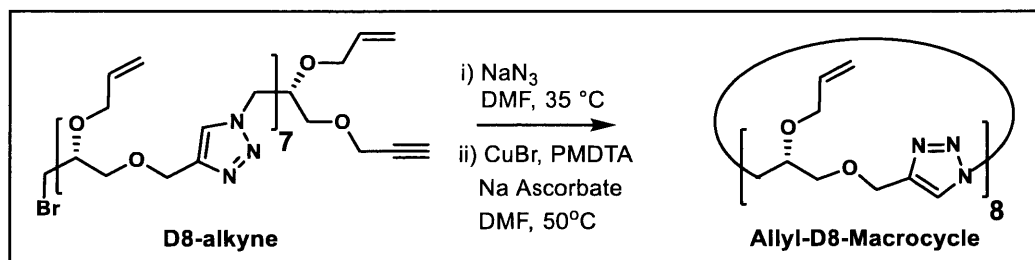
Allyl-alt8-macrocycle: NaN_3 (21 mg, 0.32 mmol) was added to a solution of **alt8-alkyne** (160 mg, 0.10 mmol) in DMF (10 mL). The reaction was heated to 35°C for 24 hours. After completion, 100 mL of EtOAc was added and the organic solution was extracted 3x with 100 mL of 5% LiCl solution. The organic layer was concentrated to yield **N₃-alt8-alkyne** (150 mg, 0.094 mmol) which was used without further purification.

Under an N_2 atmosphere, dry DMF (9.4 mL) and sodium ascorbate (56 mg, 0.28 mmol) were added to a mixture of **N₃-alt8-alkyne** (148 mg, 0.094 mmol) in an oven-dried 40 mL scintillation vial. A DMF solution of 0.1 M CuBr and 0.2 M PMDETA (2.8 mL) was then added to the reaction mixture. The reaction was warmed to 50°C for 2 days. DMF was removed under reduced pressure. DCM (1 mL) was added to the resulting viscous mixture which was pushed through a neutral alumina column with 5% MeOH/DCM to remove precipitates and copper. The collected solution was concentrated by reduced pressure. 3 mL of Chloroform stabilized by ethanol was added to the crude product and the solution was filtered. The compound was then purified through recycling preparatory GPC yielding **Allyl-alt8-macrocycle** (19 mg, 0.012 mmol) in 10% yield from **alt8**. ^1H NMR (500 MHz, CDCl_3): δ (ppm) 7.68 (s, 8H), 5.75-5.69 (overlap, 8H), 5.19-5.10 (overlap, 16H), 4.68-4.56 (overlap, 24H), 4.47-4.42 (overlap, 8H), 4.05-4.02 (overlap, 8H), 3.92-3.89 (overlap, 16H), 3.60-3.51 (overlap, 16H).



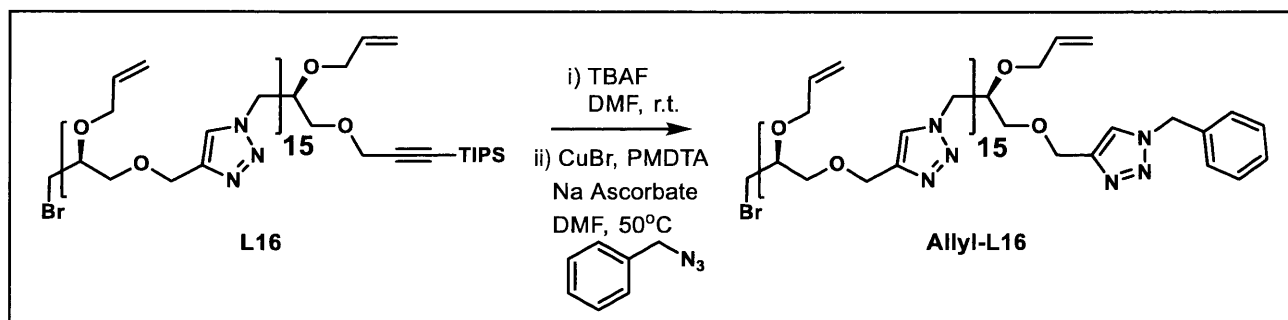
Allyl-D8: **D8** (200 mg, 0.11 mmol) was dissolved in DMF (10 mL), followed by the slow addition of TBAF (1.05equiv, 0.12 mL, 1M in THF). After 15 minutes, 100 mL of EtOAc was added and the organic solution was extracted 3x with 100 mL of 1% LiCl solution. The organic layer was concentrated to yield **D8-alkyne** (180 mg, 0.11 mmol) which was used without further purification.

Under an N₂ atmosphere, dry DMF (0.200 mL) and sodium ascorbate (3.6 mg, 0.018 mmol) were added to a mixture of **D8-alkyne** (29 mg, 0.018 mmol) and benzyl azide (24 mg, 0.18 mmol) in an oven-dried 40 mL scintillation vial. A DMF solution of 0.1 M CuBr and 0.2 M PMDETA (0.090 mL) was then added to the reaction mixture. The reaction was warmed to 50 °C for 2 h. After completion, DMF was removed under reduced pressure. DCM (0.5 mL) was added to the resulting viscous mixture which was then loaded carefully onto a column. Column chromatography (100% DCM to 3.5% MeOH/DCM) yielded the product (22 mg, 0.013 mmol) in 69% yield from **D8**. ¹H NMR (500 MHz, CDCl₃): δ(ppm) 7.67 (overlap, 5H), 7.66 (s, 1H), 7.65 (s, 1H), 7.49 (s, 1H), 7.39-7.37 (overlap, 3H), 7.29 (overlap, 2H), 5.90 (ddt, 1H), 5.77-5.67 (overlap, 7H), 5.53 (s, 2H), 5.30-5.27 (m, 1H), 5.18-5.11 (overlap, 14H), 4.69-4.55 (overlap, 24H), 4.44-4.39 (overlap, 8H), 4.10 (m, 2H), 4.05-3.99 (m, 8H), 3.91-3.84 (overlap, 16H), 3.73-3.62 (overlap, 3H), 3.59-3.50 (overlap, 17H), 3.45 (dd, 1H).



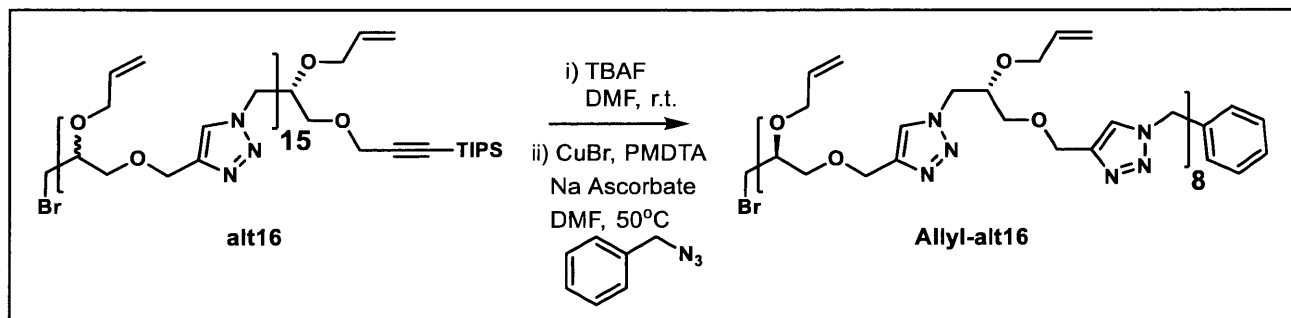
Allyl-D8-macrocyle: NaN_3 (18 mg, 0.28 mmol) was added to a solution of **D8-alkyne** (150 mg, 0.094 mmol) in DMF (10 mL). The reaction was heated to 35 °C for 24 hours. After completion, 100 mL of EtOAc was added and the organic solution was extracted 3x with 100 mL of 5% LiCl solution. The organic layer was concentrated to yield **N₃-D8-alkyne** (140 mg, 0.089 mmol) which was used without further purification.

Under an N_2 atmosphere, dry DMF (8.9 mL) and sodium ascorbate (52 mg, 0.27 mmol) were added to a mixture of **N₃-D8-alkyne** (140 mg, 0.089 mmol) in an oven-dried 40 mL scintillation vial. A DMF solution of 0.1 M CuBr and 0.2 M PMDETA (2.7 mL) was then added to the reaction mixture. The reaction was warmed to 50 °C for 2 days. DMF was removed under reduced pressure. DCM (1 mL) was added to the resulting viscous mixture which was pushed through a neutral alumina column with 5% MeOH/DCM to remove precipitates and copper. The collected solution was concentrated by reduced pressure. 3 mL of Chloroform stabilized by ethanol was added to the crude product and the solution was filtered. The compound was then purified through recycling preparatory GPC yielding **Allyl-D8-macrocyle** (20 mg, 0.013 mmol) in 13% yield from **D8**. ^1H NMR (500 MHz, CDCl_3): δ (ppm) 7.69 (s, 8H), 5.76-5.69 (overlap, 8H), 5.19-5.10 (overlap, 16H), 4.68-4.56 (overlap, 24H), 4.46-4.42 (overlap, 8H), 4.05-4.02 (overlap, 8H), 3.92-3.89 (overlap, 16H), 3.59-3.50 (overlap, 16H).



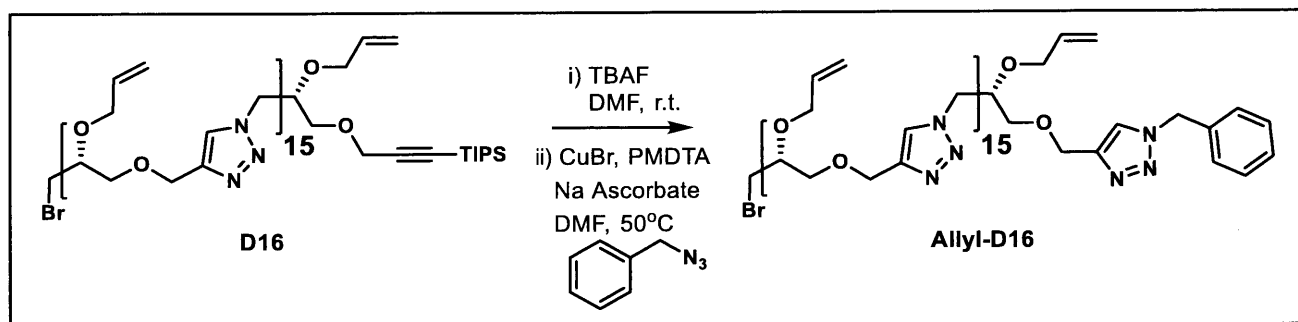
Allyl-L16: **L16** (200 mg, 0.0603 mmol) was dissolved in DMF (0.600 mL), followed by the slow addition of TBAF (1.05 equiv, 0.0634 mL, 1M in THF). After 15 minutes, the reaction mixture was concentrated under reduced pressure. The product was then purified by preparatory GPC (chloroform) to yield **L16-alkyne** (170 mg, 0.054 mmol, 90% yield).

Under an N₂ atmosphere, dry DMF (0.500 mL) and sodium ascorbate (15.1 mg, 0.0762 mmol) were added to a mixture of **L16-alkyne** (120 mg, 0.038 mmol) and benzyl azide (55.6 mg, 0.380 mmol) in an oven-dried 40 mL scintillation vial. A DMF solution of 0.1 M CuBr and 0.2 M PMDETA (0.381 mL) was then added to the reaction mixture. The reaction was warmed to 50 °C for 2 h. After completion, DMF was removed under reduced pressure. DCM (1 mL) was added to the resulting viscous mixture which was then loaded carefully onto a column. Column chromatography (100% DCM to 8% MeOH/DCM) yielded the product (90 mg, 0.027 mmol) in 65% yield from **L16**. ¹H NMR (500 MHz, CDCl₃): δ(ppm) 7.67 (overlap, 13H), 7.66 (s, 1H), 7.65 (s, 1H), 7.49 (s, 1H), 7.37-7.35 (overlap, 3H), 7.29-7.27 (overlap, 2H), 5.92-5.86 (ddt, J = 16.1, 10.2, 5.4 Hz, 1H), 5.75-5.68 (overlap, 15H), 5.53 (s, 2H), 5.30-5.27 (m, 1H), 5.18-5.10 (overlap, 31H), 4.69-4.55 (m, 48H), 4.44-4.40 (m, 16H), 4.10 (m, 2H), 4.05-3.98 (m, 14H), 3.92-3.85 (overlap, 30H), 3.73-3.62 (overlap, 3H), 3.58-3.49 (overlap, 31H), 3.45 (dd, 1H).



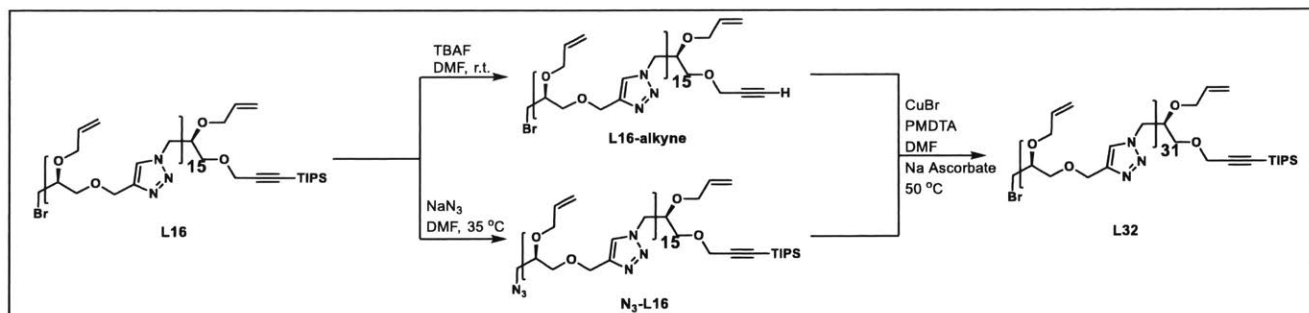
Allyl-alt16: **alt16** (200 mg, 0.0603 mmol) was dissolved in DMF (0.600 mL), followed by the slow addition of TBAF (1.05 equiv, 0.0634 mL, 1M in THF). After 15 minutes, the reaction mixture was concentrated under reduced pressure. The product was then purified by preparatory GPC (chloroform) to yield **alt16-alkyne** (160 mg, 0.050 mmol).

Under an N₂ atmosphere, dry DMF (0.500 mL) and sodium ascorbate (15.1 mg, 0.0762 mmol) were added to a mixture of **alt16-alkyne** (120 mg, 0.038 mmol) and benzyl azide (55.6 mg, 0.380 mmol) in an oven-dried 40 mL scintillation vial. A DMF solution of 0.1 M CuBr and 0.2 M PMDETA (0.381 mL) was then added to the reaction mixture. The reaction was warmed to 50 °C for 2 h. After completion, DMF was removed under reduced pressure. DCM (1 mL) was added to the resulting viscous mixture which was then loaded carefully onto a column. Column chromatography (100% DCM to 8% MeOH/DCM) yielded the product (81 mg, 0.025 mmol) in 54% yield from **alt16**. ¹H NMR (500 MHz, CDCl₃): δ(ppm) 7.68 (overlap, 13H), 7.67 (s, 1H), 7.64 (s, 1H), 7.49 (s, 1H), 7.38-7.35 (overlap, 3H), 7.29-7.27 (overlap, 2H), 5.92-5.86 (ddt, J = 16.1, 10.2, 5.4 Hz, 1H), 5.76-5.68 (overlap, 15H), 5.54 (s, 2H), 5.30-5.27 (m, 1H), 5.18-5.10 (overlap, 31H), 4.70-4.54 (m, 48H), 4.44-4.39 (m, 16H), 4.10 (m, 2H), 4.05-3.98 (m, 14H), 3.92-3.85 (overlap, 30H), 3.74-3.61 (overlap, 3H), 3.58-3.49 (overlap, 31H), 3.45 (dd, 1H).



Allyl-D16: **B16** (200 mg, 0.0603 mmol) was dissolved in DMF (0.600 mL), followed by the slow addition of TBAF (1.05 equiv, 0.0634 mL, 1M in THF). After 15 minutes, the reaction mixture was concentrated under reduced pressure. The product was then purified by preparatory GPC (chloroform) to yield **D16-alkyne** (170 mg, 0.056 mmol).

Under an N₂ atmosphere, dry DMF (0.500 mL) and sodium ascorbate (15.1 mg, 0.0762 mmol) were added to a mixture of **D16-alkyne** (120 mg, 0.038 mmol) and benzyl azide (55.6 mg, 0.380 mmol) in an oven-dried 40 mL scintillation vial. A DMF solution of 0.1 M CuBr and 0.2 M PMDETA (0.381 mL) was then added to the reaction mixture. The reaction was warmed to 50 °C for 2 h. After completion, DMF was removed under reduced pressure. DCM (1 mL) was added to the resulting viscous mixture which was then loaded carefully onto a column. Column chromatography (100% DCM to 8% MeOH/DCM) yielded the product (92 mg, 0.028 mmol) in 68% yield from **D16**. ¹H NMR (500 MHz, CDCl₃): δ(ppm) 7.67 (overlap, 13H), 7.66 (s, 1H), 7.65 (s, 1H), 7.49 (s, 1H), 7.37-7.35 (overlap, 3H), 7.29-7.27 (overlap, 2H), 5.93-5.86 (ddt, J = 16.1, 10.2, 5.4 Hz, 1H), 5.75-5.68 (overlap, 15H), 5.54 (s, 2H), 5.30-5.27 (m, 1H), 5.18-5.10 (overlap, 31H), 4.69-4.55 (m, 48H), 4.44-4.40 (m, 16H), 4.10 (m, 2H), 4.05-3.99 (m, 14H), 3.92-3.85 (overlap, 30H), 3.73-3.62 (overlap, 3H), 3.58-3.49 (overlap, 28H), 3.44 (dd, 1H).

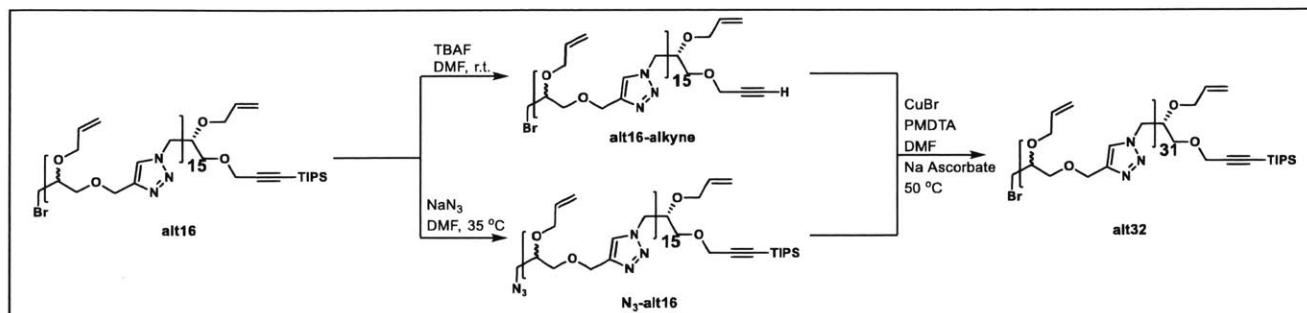


L32: The **L16-alkyne** precursor to **L32** was prepared by dissolving **L16** (500 mg, 0.15 mmol) in DMF (5 mL), followed by the slow addition of TBAF (1.05 equiv, 0.160 mL, 1M in THF). After 1 hour, DMF was removed under reduced pressure. 3 mL of CHCl₃ stabilized with ethanol was added to the crude mixture, which was then purified by recycling preparatory GPC to yield **L16-alkyne** (440 mg, 0.14 mmol) as a yellow oil.

The **N₃-L16** precursor to **L32** was prepared by dissolving **L16** (500 mg, 0.15 mmol) in 10 mL DMF, followed by the addition of NaN₃ (58.5 mg, 0.90 mmol). The reaction mixture was heated to 35 °C and allowed to stir for 24 hours before the DMF was removed via rotary evaporator. Heating past 35 °C was avoided as it leads to degradation of the product. Then, 200 mL of DCM was added to the residue and extracted with water (2 x 200 mL) and brine (1 x 200 mL). **Note: we have since updated this procedure and now use EtOAc instead of DCM for this extraction in order to avoid undesired reaction between NaN₃ and DCM.** The organic layer was dried with Na₂SO₄ and concentrated under vacuum. **N₃-L16** was obtained (420 mg, 0.13 mmol).

Under an N₂ atmosphere, dry DMF (10 mL) and sodium ascorbate (27.7 mg, 0.14 mmol) were added to a mixture of **L16-alkyne** (440 mg, 0.14 mmol) and **N₃-L16** (420 mg, 0.13 mmol) in an oven-dried 40 mL scintillation vial. A DMF solution of 0.1 M CuBr and 0.2 M PMDETA (0.065 mL) was then added and the reaction mixture was warmed to 50 °C and left to react for 24 hours. After completion, DMF was removed under reduced pressure. DCM (1 mL) was added to the resulting viscous mixture which was pushed through a neutral alumina column with 8% MeOH/DCM to remove precipitates and copper. The collected solution was concentrated by reduced pressure. 3 mL of Chloroform stabilized by ethanol was added to the crude product and the solution was filtered. The compound was then purified through recycling preparatory GPC yielding the product **L32** (310 mg, 0.048 mmol) in 32% yield from **L16**. ¹H NMR (500 MHz, CDCl₃): δ(ppm) 7.67 (overlap, 31H), 5.93-5.86 (ddt, 1H), 5.74-5.68 (overlap, 31H), 5.29-5.26 (m,

1H), 5.18-5.10 (overlap, 63H), 4.68-4.57 (overlap, 96H), 4.44-4.40 (overlap, 16H), 4.22 (m, 2H), 4.06-3.98 (m, 30H), 3.91-3.87 (overlap, 60H), 3.70-3.62 (overlap, 3H), 3.58-3.49 (overlap, 60H), 3.44 (dd, 1H), 1.07 (s, 21H).

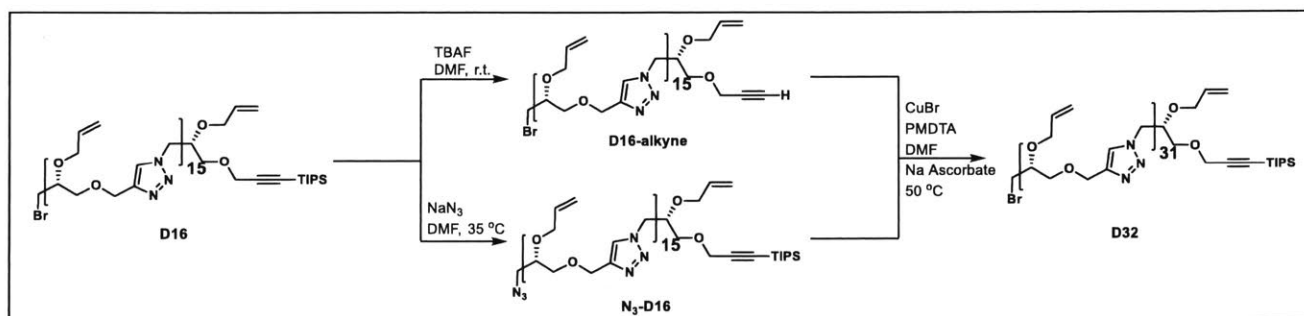


alt32: The **alt16-alkyne** precursor to **alt32** was prepared by dissolving **alt16** (500 mg, 0.15 mmol) in DMF (5 mL), followed by the slow addition of TBAF (1.05 equiv, 0.160 mL, 1M in THF). After 1 hour, DMF was removed under reduced pressure. 3 mL of CHCl₃ stabilized with ethanol was added to the crude mixture, which was then purified by recycling preparatory GPC to yield **alt16-alkyne** (395 mg, 0.125 mmol).

The **N₃-alt16** precursor to **alt32** was prepared by dissolving **alt16** (500 mg, 0.15 mmol) in 10 mL DMF, followed by the addition of NaN₃ (58.5 mg, 0.90 mmol). The reaction mixture was heated to 35 °C and allowed to stir for 24 hours before the DMF was removed via rotary evaporator. Heating past 35 °C was avoided as it leads to degradation of the product. Then, 200 mL of DCM was added to the residue and extracted with water (2 x 200 mL) and brine (1 x 200 mL). **Note: we have since updated this procedure and now use EtOAc instead of DCM for this extraction in order to avoid undesired reaction between NaN₃ and DCM.** The organic layer was dried with Na₂SO₄ and concentrated under vacuum. **N₃-alt16** was obtained (390 mg, 0.12 mmol).

Under an N₂ atmosphere, dry DMF (10 mL) and sodium ascorbate (23.8 mg, 0.12 mmol) were added to a mixture of **alt16-alkyne** (440 mg, 0.125 mmol) and **N₃-alt16** (420 mg, 0.12 mmol) in an oven-dried 40 mL scintillation vial. A DMF solution of 0.1 M CuBr and 0.2 M PMDETA (0.060 mL) was then added and the reaction mixture was warmed to 50 °C and left to react for 24 hours. After completion, DMF was removed under reduced pressure. DCM (1 mL) was added to the resulting viscous mixture which was pushed through a neutral alumina column with 8% MeOH/DCM to remove precipitates and copper. The collected solution was concentrated by

reduced pressure. 3 mL of Chloroform stabilized by ethanol was added to the crude product and the solution was filtered. The compound was then purified through recycling preparatory GPC yielding the product **alt32** (270 mg, 0.042 mmol) in 28% yield from **alt16**. ¹H NMR (500 MHz, CDCl₃): δ(ppm) 7.69 (overlap, 31H), 5.93-5.86 (ddt, 1H), 5.75-5.68 (overlap, 31H), 5.29-5.26 (m, 1H), 5.20-5.10 (overlap, 63H), 4.69-4.58 (overlap, 96H), 4.44-4.40 (overlap, 16H), 4.24 (m, 2H), 4.07-3.97 (m, 30H), 3.91-3.87 (overlap, 60H), 3.70-3.48 (overlap, 63H), 3.44 (dd, 1H), 1.06 (s, 21H).

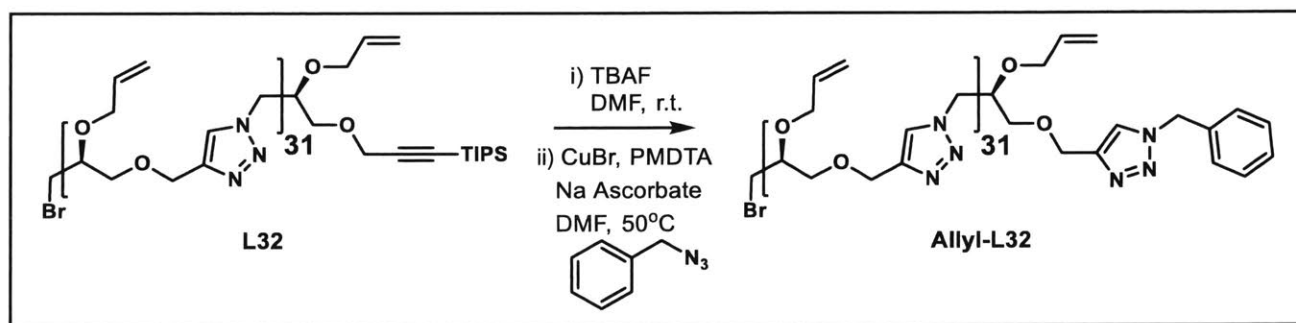


D32: The **D16-alkyne** precursor to **D32** was prepared by dissolving **D16** (500 mg, 0.15 mmol) in DMF (5 mL), followed by the slow addition of TBAF (1.05 equiv, 0.160 mL, 1M in THF). After 1 hour, DMF was removed under reduced pressure. 3 mL of CHCl₃ stabilized with ethanol was added to the crude mixture, which was then purified by recycling preparatory GPC to yield **D16-alkyne** (450 mg, 0.14 mmol).

The **N₃-D16** precursor to **D32** was prepared by dissolving **D16** (500 mg, 0.15 mmol) in 10 mL DMF, followed by the addition of NaN₃ (58.5 mg, 0.90 mmol). The reaction mixture was heated to 35 °C and allowed to stir for 24 hours before the DMF was removed via rotary evaporator. Heating past 35 °C was avoided as it leads to degradation of the product. Then, 200 mL of DCM was added to the residue and extracted with water (2 x 200 mL) and brine (1 x 200 mL). **Note: we have since updated this procedure and now use EtOAc instead of DCM for this extraction in order to avoid undesired reaction between NaN₃ and DCM.** The organic layer was dried with Na₂SO₄ and concentrated under vacuum. **N₃-D16** was obtained (450 mg, 0.14 mmol).

Under an N₂ atmosphere, dry DMF (10 mL) and sodium ascorbate (27.7 mg, 0.14 mmol) were added to a mixture of **D16-alkyne** (450 mg, 0.14 mmol) and **N₃-D16** (450 mg, 0.14 mmol) in an oven-dried 40 mL scintillation vial. A DMF solution of 0.1 M CuBr and 0.2 M PMDETA (0.070

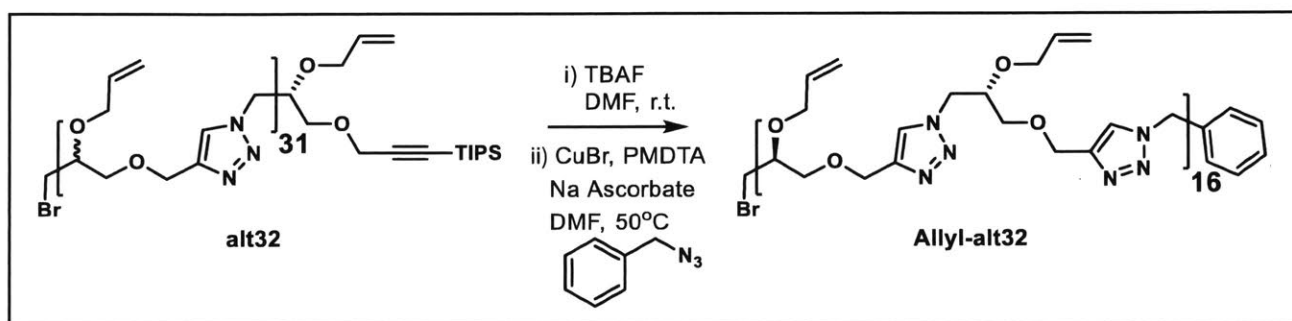
mL) was then added and the reaction mixture was warmed to 50 °C and left to react for 24 hours. After completion, DMF was removed under reduced pressure. DCM (1 mL) was added to the resulting viscous mixture which was pushed through a neutral alumina column with 8% MeOH/DCM to remove precipitates and copper. The collected solution was concentrated by reduced pressure. 3 mL of Chloroform stabilized by ethanol was added to the crude product and the solution was filtered. The compound was then purified through recycling preparatory GPC yielding the product **D32** (330 mg, 0.051 mmol) in 34% yield from **D16**. ¹H NMR (500 MHz, CDCl₃): δ(ppm) 7.67 (overlap, 31H), 5.93-5.86 (ddt, 1H), 5.74-5.68 (overlap, 31H), 5.29-5.26 (m, 1H), 5.18-5.10 (overlap, 63H), 4.68-4.57 (overlap, 96H), 4.44-4.40 (overlap, 16H), 4.24 (m, 2H), 4.06-3.98 (m, 30H), 3.91-3.87 (overlap, 60H), 3.70-3.62 (overlap, 3H), 3.58-3.49 (overlap, 60H), 3.44 (dd, 1H), 1.07 (s, 21H).



Allyl-L32: **L32** (30 mg, 0.0047 mmol) was dissolved in DMF (0.200 mL), followed by the slow addition of TBAF (1.05 equiv, 0.0049 mL, 1M in THF). After 1 hour, the reaction mixture was concentrated under reduced pressure. The product was then purified by preparatory GPC (chloroform) to yield **L32-alkyne** (25 mg, 0.0040 mmol).

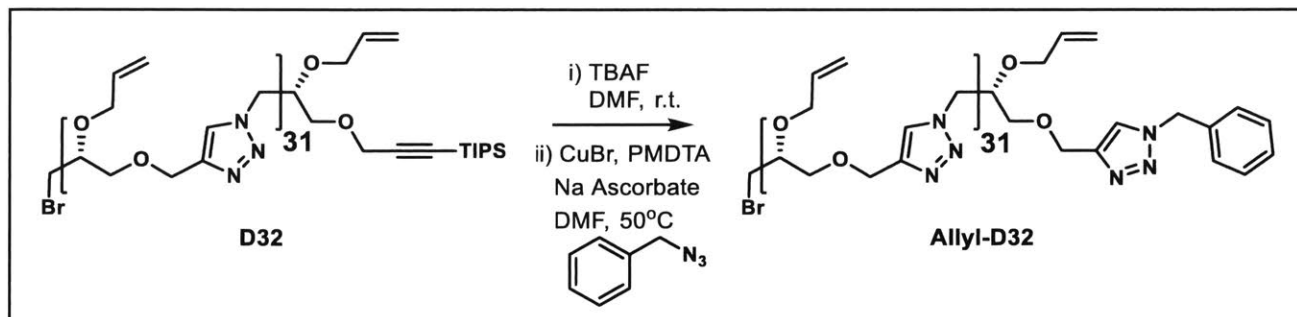
Under an N₂ atmosphere, dry DMF (0.200 mL) and sodium ascorbate (4.0 mg, 0.020 mmol) were added to a mixture of **L32-alkyne** (25 mg, 0.0040 mmol) and benzyl azide (5.3 mg, 0.040 mmol) in an oven-dried 40 mL scintillation vial. A DMF solution of 0.1 M CuBr and 0.2 M PMDETA (0.040 mL) was then added to the reaction mixture. The reaction was warmed to 50 °C for 2 h. After completion, DMF was removed under reduced pressure. DCM (1 mL) was added to the resulting viscous mixture which was pushed through a neutral alumina column with 8% MeOH/DCM to remove precipitates and copper. The collected solution was concentrated by reduced pressure. 3 mL of Chloroform stabilized by ethanol was added to the crude product and

the solution was filtered. The compound was then purified through recycling preparatory GPC yielding the product (19 mg, 0.0030 mmol) in 63% yield from **L32**. $^1\text{H NMR}$ (500 MHz, CDCl_3): δ (ppm) 7.67 (overlap, 31H), 7.49 (s, 1H), 7.38-7.34 (overlap, 3H), 7.28-7.26 (overlap, 2H), 5.93-5.86 (ddt, 1H), 5.74-5.68 (overlap, 31H), 5.53 (s, 2H), 5.29-5.26 (m, 1H), 5.18-5.10 (overlap, 63H), 4.68-4.57 (overlap, 96H), 4.44-4.40 (overlap, 16H), 4.10 (m, 2H), 4.06-3.98 (m, 30H), 3.91-3.87 (overlap, 60H), 3.70-3.62 (overlap, 3H), 3.58-3.49 (overlap, 60H), 3.44 (dd, 1H).



Allyl-alt32: **alt32** (30 mg, 0.0047 mmol) was dissolved in DMF (0.200 mL), followed by the slow addition of TBAF (1.05 equiv, 0.0049 mL, 1M in THF). After 15 minutes, the reaction mixture was concentrated under reduced pressure. The product was then purified by preparatory GPC (chloroform) to yield **alt32-alkyne** (22 mg, 0.0036 mmol).

Under an N_2 atmosphere, dry DMF (0.200 mL) and sodium ascorbate (3.6 mg, 0.018 mmol) were added to a mixture of **alt32-alkyne** (22 mg, 0.0036 mmol) and benzyl azide (4.8 mg, 0.036 mmol) in an oven-dried 40 mL scintillation vial. A DMF solution of 0.1 M CuBr and 0.2 M PMDETA (0.036 mL) was then added to the reaction mixture. The reaction was warmed to 50 °C for 2 h. After completion, DMF was removed under reduced pressure. DCM (1 mL) was added to the resulting viscous mixture which was pushed through a neutral alumina column with 8% MeOH/DCM to remove precipitates and copper. The collected solution was concentrated by reduced pressure. 3 mL of Chloroform stabilized by ethanol was added to the crude product and the solution was filtered. The compound was then purified through recycling preparatory GPC yielding the product (20 mg, 0.0031 mmol) in 66% yield from **alt32**. $^1\text{H NMR}$ (500 MHz, CDCl_3): δ (ppm) 7.69 (overlap, 31H), 7.51 (s, 1H), 7.38-7.34 (overlap, 3H), 7.28-7.26 (overlap, 2H), 5.93-5.86 (ddt, 1H), 5.75-5.68 (overlap, 31H), 5.53 (s, 2H), 5.29-5.26 (m, 1H), 5.20-5.10 (overlap, 63H), 4.69-4.58 (overlap, 96H), 4.44-4.40 (overlap, 16H), 4.10 (m, 2H), 4.07-3.97 (m, 30H), 3.91-3.87 (overlap, 60H), 3.70-3.48 (overlap, 63H), 3.44 (dd, 1H).



Allyl-D32: **D32** (30 mg, 0.0047 mmol) was dissolved in DMF (0.200 mL), followed by the slow addition of TBAF (1.05 equiv, 0.0049 mL, 1M in THF). After 15 minutes, the reaction mixture was concentrated under reduced pressure. The product was then purified by preparatory GPC (chloroform) to yield **D32-alkyne** (25 mg, 0.0040 mmol).

Under an N₂ atmosphere, dry DMF (0.200 mL) and sodium ascorbate (4.0 mg, 0.020 mmol) were added to a mixture of **D32-alkyne** (25 mg, 0.0040 mmol) and benzyl azide (5.3 mg, 0.040 mmol) in an oven-dried 40 mL scintillation vial. A DMF solution of 0.1 M CuBr and 0.2 M PMDETA (0.040 mL) was then added to the reaction mixture. The reaction was warmed to 50 °C for 2 h. After completion, DMF was removed under reduced pressure. DCM (1 mL) was added to the resulting viscous mixture which was pushed through a neutral alumina column with 8% MeOH/DCM to remove precipitates and copper. The collected solution was concentrated by reduced pressure. 3 mL of Chloroform stabilized by ethanol was added to the crude product and the solution was filtered. The compound was then purified through recycling preparatory GPC yielding the product (22 mg, 0.034 mmol) in 73% yield from **D32**. ¹H NMR (500 MHz, CDCl₃): δ(ppm) 7.67 (overlap, 31H), 7.49 (s, 1H), 7.38-7.34 (overlap, 3H), 7.28-7.26 (overlap, 2H), 5.93-5.86 (ddt, 1H), 5.74-5.68 (overlap, 31H), 5.53 (s, 2H), 5.29-5.26 (m, 1H), 5.18-5.10 (overlap, 63H), 4.68-4.57 (overlap, 96H), 4.44-4.40 (overlap, 16H), 4.10 (m, 2H), 4.06-3.98 (m, 30H), 3.91-3.87 (overlap, 60H), 3.70-3.62 (overlap, 3H), 3.58-3.49 (overlap, 60H), 3.44 (dd, 1H).

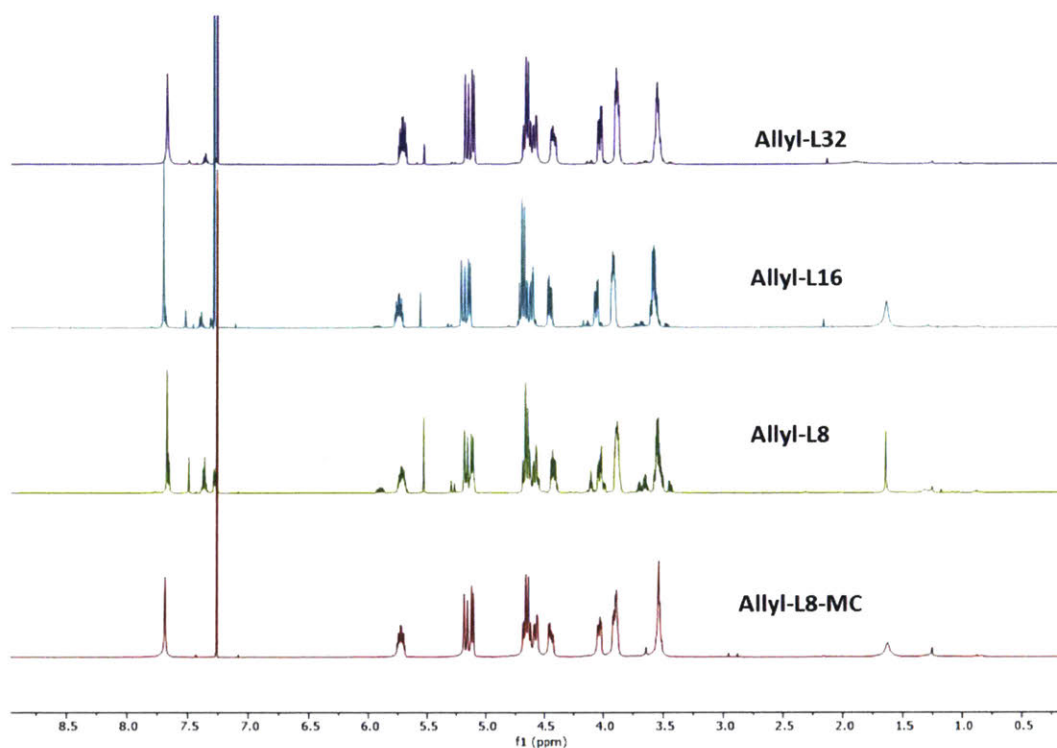


Figure S4.14. ¹H NMR spectra (500 MHz, CDCl₃, 25 °C) of Allyl-L8-macrocycle, Allyl-L8, Allyl-L16, Allyl-L32.

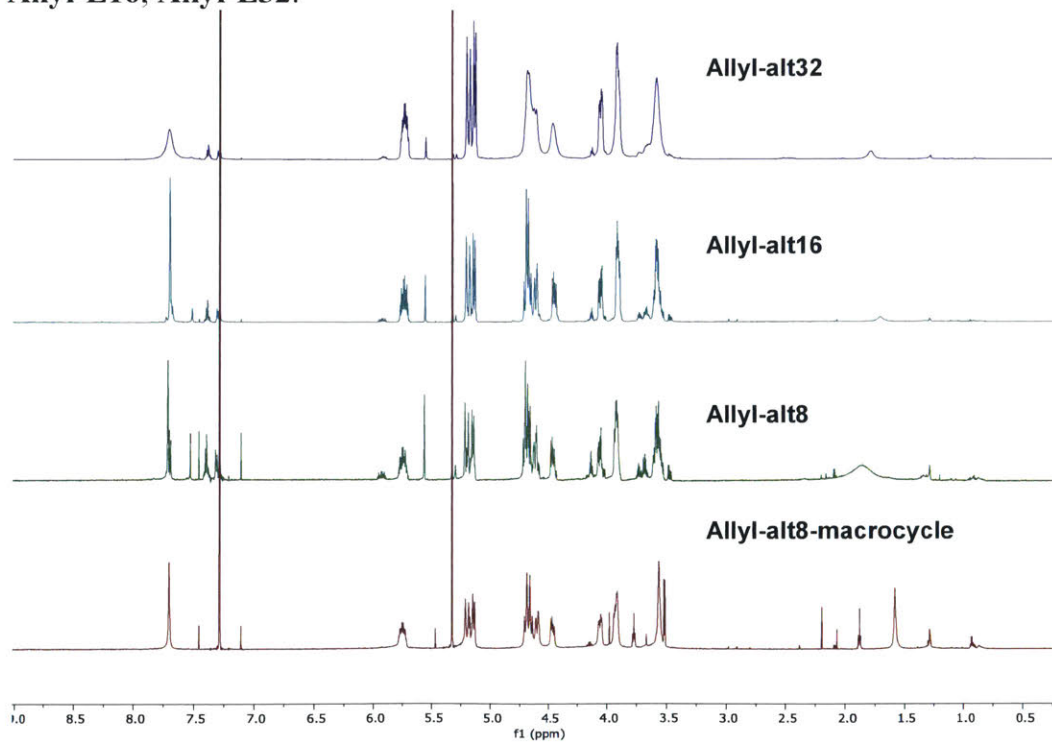


Figure S4.15. ¹H NMR spectra (500 MHz, CDCl₃, 25 °C) of Allyl-alt8-macrocycle, Allyl-alt8, Allyl-alt16, Allyl-alt32.

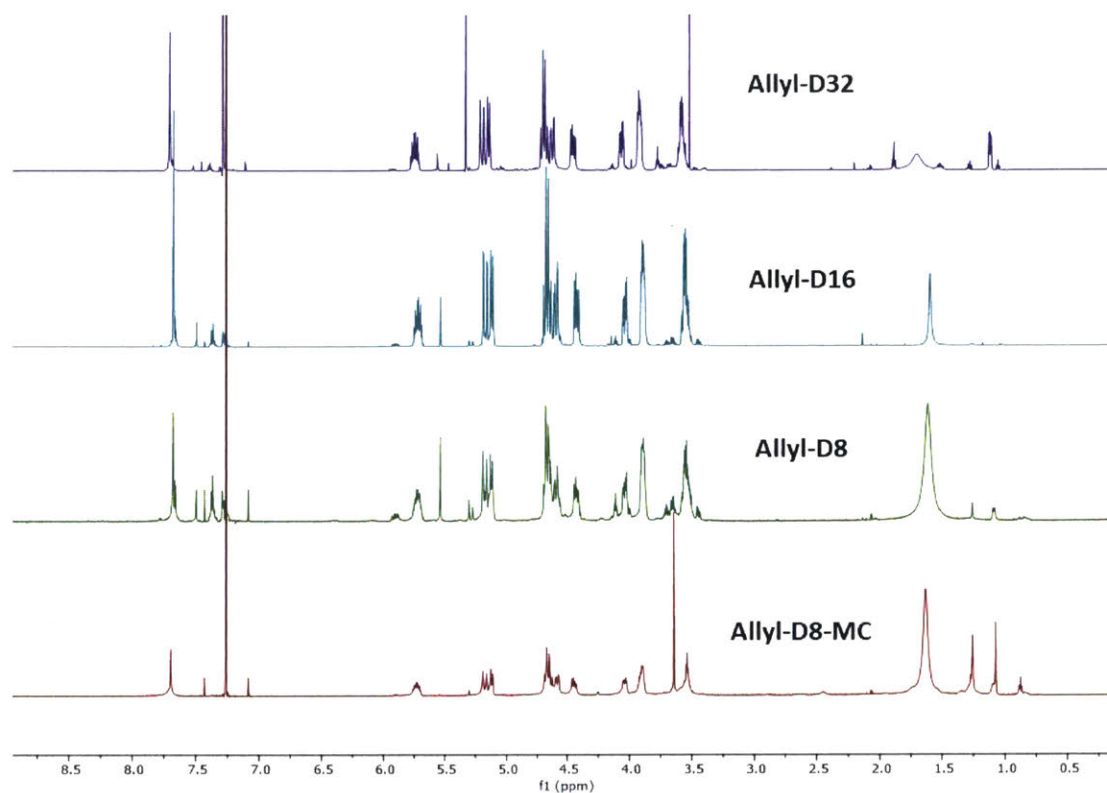
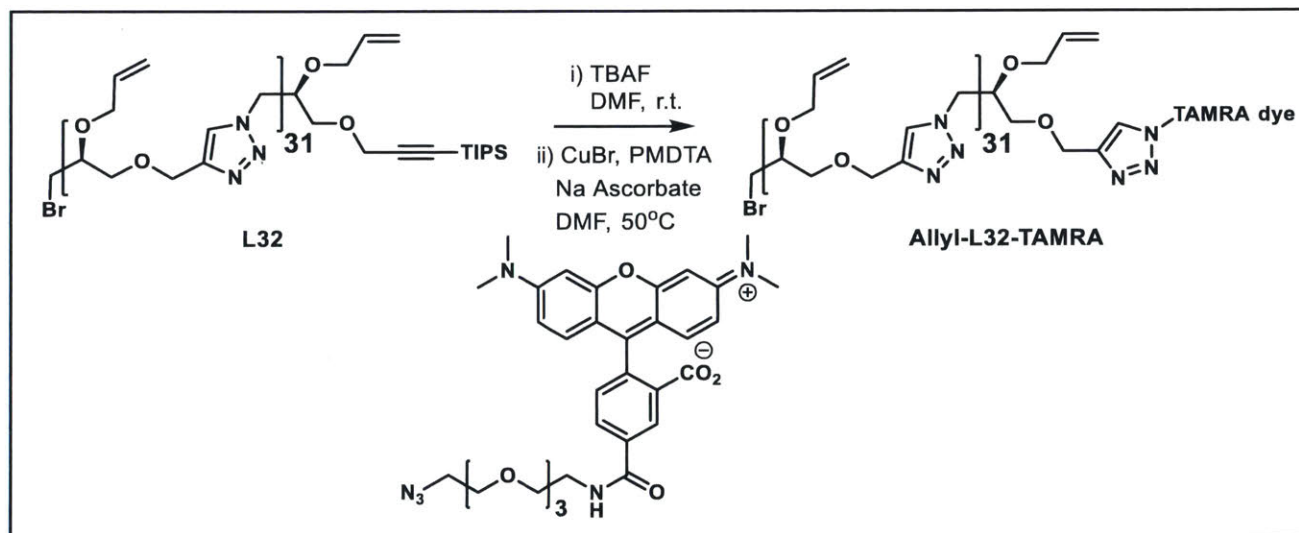


Figure S4.16. ^1H NMR spectra (500 MHz, CDCl_3 , 25 $^\circ\text{C}$) of Allyl-D8-macrocycle, Allyl-D8, Allyl-D16, Allyl-D32.

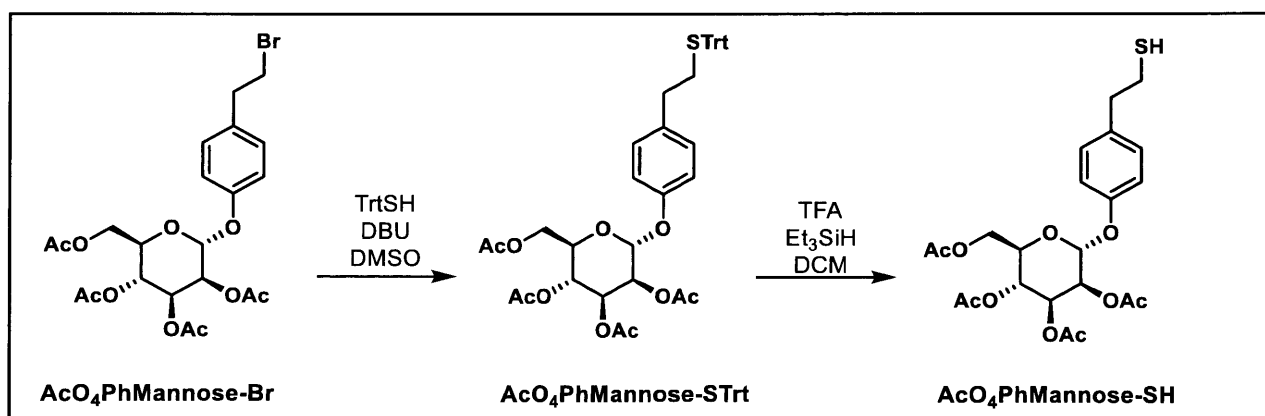
Synthesis of PhMannose Functional A32mer



Allyl-L32-TAMRA: L32 (150 mg, 0.023 mmol) was dissolved in DMF (1 mL), followed by the slow addition of TBAF (1.05 equiv, 0.024 mL, 1M in THF). After 1 hour, the reaction mixture

was concentrated under reduced pressure. The product was then purified by preparatory GPC (chloroform) to yield **L32-alkyne** (110 mg, 0.017 mmol).

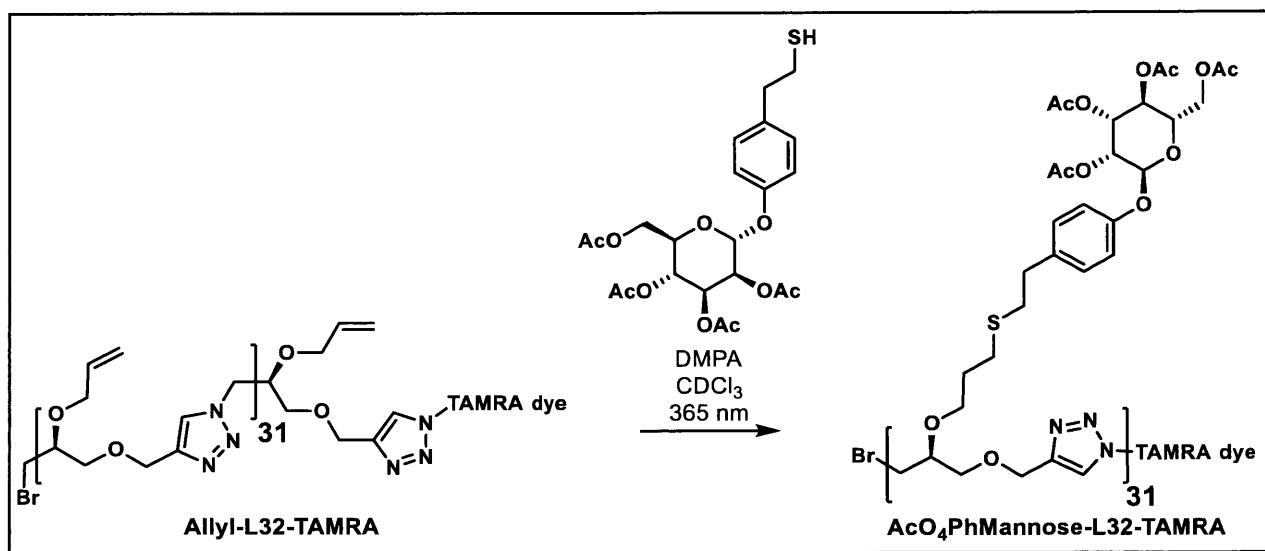
Under an N₂ atmosphere, dry DMF (1 mL) and sodium ascorbate (7.1 mg, 0.036 mmol) were added to a mixture of **L32-alkyne** (108 mg, 0.018 mmol) and TAMRA azide (15 mg, 0.027 mmol) in an oven-dried 40 mL scintillation vial. A DMF solution of 0.1 M CuBr and 0.2 M PMDETA (0.018 mL) was then added to the reaction mixture. The reaction was warmed to 50 °C overnight. After completion, DMF was removed under reduced pressure. DCM (1 mL) was added to the resulting viscous mixture which was pushed through a neutral alumina column with 8% MeOH/DCM to remove precipitates and copper. The collected solution was concentrated by reduced pressure. 3 mL of Chloroform stabilized by ethanol was added to the crude product and the solution was filtered. The compound was then purified through recycling preparatory GPC yielding the product (100 mg, 0.015 mmol) in 67% yield from **L32**. ¹H NMR (500 MHz, CDCl₃): δ(ppm) 7.69 (overlap, 32H), 5.93-5.86 (ddt, 1H), 5.75-5.68 (overlap, 31H), 5.53 (s, 2H), 5.29-5.26 (m, 1H), 5.20-5.10 (overlap, 63H), 4.69-4.58 (overlap, 96H), 4.44-4.40 (overlap, 16H), 4.15-4.10 (overlap, 4H), 4.07-3.97 (m, 30H), 3.91-3.87 (overlap, 60H), 3.70-3.48 (overlap, 63H), 3.44 (dd, 1H), 3.32-3.18 (overlap, 16H), 3.02 (s, 9H).



AcO₄PhMannose-STrt: **AcO₄PhMannose-Br** (400 mg, 0.753 mmol) was dissolved in DMSO (0.753 mL). Ph₃MeSH (229 mg, 0.828 mmol) was added and then DBU (149 mg, 0.979 mmol) was added dropwise to the reaction mixture. The solution was left to react overnight. 100 mL of EtOAc was added to the solution and the organic mixture was extracted 2x with 100 mL of 5% LiCl solution. The organic layer was concentrated under reduced pressure. DCM (0.5 mL) was

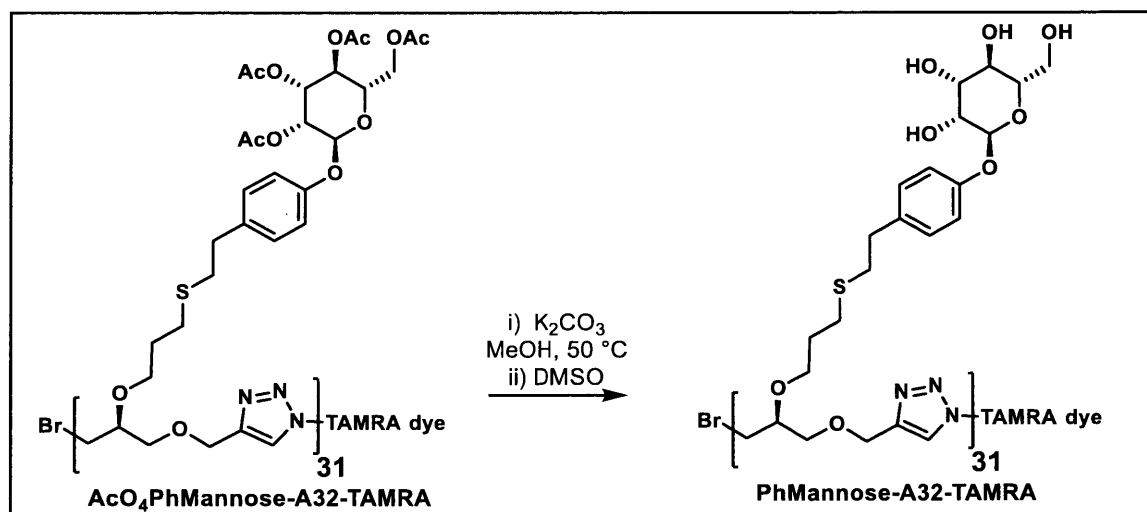
added to the resulting mixture which was then loaded carefully onto a column. Column chromatography (100% hexanes to 50% EtOAc/hexanes) yielded the product (530 mg, 0.72 mmol) in 96% yield. $^1\text{H NMR}$ (500 MHz, CDCl_3): δ (ppm) 7.39 (dd, 6H), 7.27 (overlap, 6H), 7.20 (dd, 3H), 6.92 (dd, 4H), 5.53 (dd, 1H), 5.45 (d, 1H), 5.41 (dd, 1H), 5.35 (dd, 1H), 4.27 (dd, 1H), 4.09-4.03 (overlap, 2H), 2.51 (t, 2H), 2.39 (t, 2H), 2.19 (s, 3H), 2.05 (s, 3H), 2.03 (s, 3H), 1.99 (s, 3H).

AcO₄PhMannose-SH: **AcO₄PhMannose-STrt** (100 mg, 0.136 mmol) was dissolved in DCM (2.5 mL) and Et_3SiH (0.250 mL). TFA (0.250 mL) was added dropwise and the reaction was left to react at room temperature for 1 hour. The solution was then concentrated under reduced pressure and 3 mL of chloroform stabilized with ethanol was added to the crude mixture. The mixture was filtered and purified through recycling preparatory GPC to obtain **AcO₄PhMannose-SH** (60 mg, 0.12 mmol) in 91% yield. $^1\text{H NMR}$ (500 MHz, CDCl_3): δ (ppm) 7.12 (d, 2H), 7.02 (d, 2H), 5.54 (dd, 1H), 5.50 (d, 1H), 5.43 (dd, 1H), 5.36 (dd, 1H), 4.28 (dd, 1H), 4.11-4.05 (overlap, 2H), 2.87 (t, 2H), 2.75 (t, 2H), 2.19 (s, 3H), 2.05 (s, 3H), 2.04 (s, 3H), 2.03 (s, 3H), 1.35 (t, 1H).



AcO₄PhMannose-L32-TAMRA: **AcO₄PhMannose-SH** (65 mg, 0.136 mmol) and **Allyl-L32-TAMRA** (5 mg, 0.00077 mmol) were mixed with 2,2-dimethoxy-2-phenylacetophenone (8.7 mg, 0.034 mmol) and CDCl_3 (0.200 mL) in a small 2 mL scintillation vial. The solution was degassed with N_2 until approximately half of the CDCl_3 had evaporated. The homogenous reaction mixture was treated with 365 nm UV light for 2 hours after which full reaction of the alkene peaks with the thiol was confirmed through $^1\text{H NMR}$. 3 mL of chloroform stabilized with ethanol was added

to the crude mixture. The mixture was filtered and purified through recycling preparatory GPC to obtain **AcO₄PhMannose-L32-TAMRA** (14 mg, 0.00064 mmol) in 84% yield. ¹H NMR (500 MHz, CDCl₃): δ(ppm) 7.69 (overlap, 32H), 7.50 (d, 1H), 7.24 (d, 1H), 7.13 (d, 64H), 7.06 (overlap, 2H), 7.02 (d, 64H), 6.94 (dd, 1H), 6.81 (dd, 1H), 5.56 (overlap, 32H), 5.50 (overlap, 32H), 5.44 (overlap, 32H), 5.38 (overlap, 32H), 4.70-4.56 (overlap, 96H), 4.44-4.40 (overlap, 16H), 4.28 (overlap, 32H), 4.12-4.04 (overlap, 64H), 3.91-3.82 (overlap, 32H), 3.66-3.51 (overlap, 112H), 3.45-3.37 (overlap, 32H), 2.81 (t, 64H), 2.69 (t, 64H), 2.50 (t, 64H), 2.21 (s, 96H), 2.06 (s, 96H), 2.05 (s, 96H), 2.04 (s, 96H), 1.78-1.72 (overlap, 64H).



PhMannose-L32-TAMRA: **AcO₄PhMannose-L32-TAMRA** (10 mg, 0.00045 mmol) was dissolved in MeOH (1 mL) and K₂CO₃ (100 mg) was added to the solution. The reaction was stirred for 4 hours at 50 °C after which an additional 20 mL of DMSO was added to the reaction mixture. The reaction was allowed to stir for another 24 hours at 50 °C. The solution was then transferred into 500 MWCO regenerated cellulose dialysis tubing and it was dialyzed for 2 days against water. Water was changed periodically every 12 hours. A good portion of the polymer precipitates in the dialysis tubing as a magenta solid. After dialysis, the pink water solution and the precipitated magenta solid in the dialysis tubing are isolated and water is removed under reduced pressure to yield **PhMannose-L32-TAMRA** (7.0 mg, 0.00042 mmol) in 92% yield. ¹H NMR (500 MHz,

(CD₃)₂SO): δ(ppm) 8.13-7.97 (overlap, 32H), 7.24-7.06 (overlap, 68H), 7.01-6.90 (overlap, 64H), 6.66 (br, 2H), 6.51-6.47 (overlap, 2H), 5.69-5.61 (overlap, 4H), 5.33-5.30 (overlap, 32H), 5.12-4.70 (overlap, 72H), 4.54-4.27 (overlap, 166H), 4.14-4.07 (overlap, 3H), 3.98-3.94 (overlap, 4H), 3.89-3.77 (overlap, 64H), 3.67-3.64 (overlap, 32H), 3.59-3.44 (overlap, 168H), 3.41-3.21 (overlap with H₂O peak), 3.16 (overlap, 32H), 2.93-2.79 (overlap, 32H), 2.68-2.58 (overlap, 100H), 2.36-2.28 (overlap, 64H), 1.73-1.64 (overlap, 8H), 1.59-1.52 (overlap, 56H).

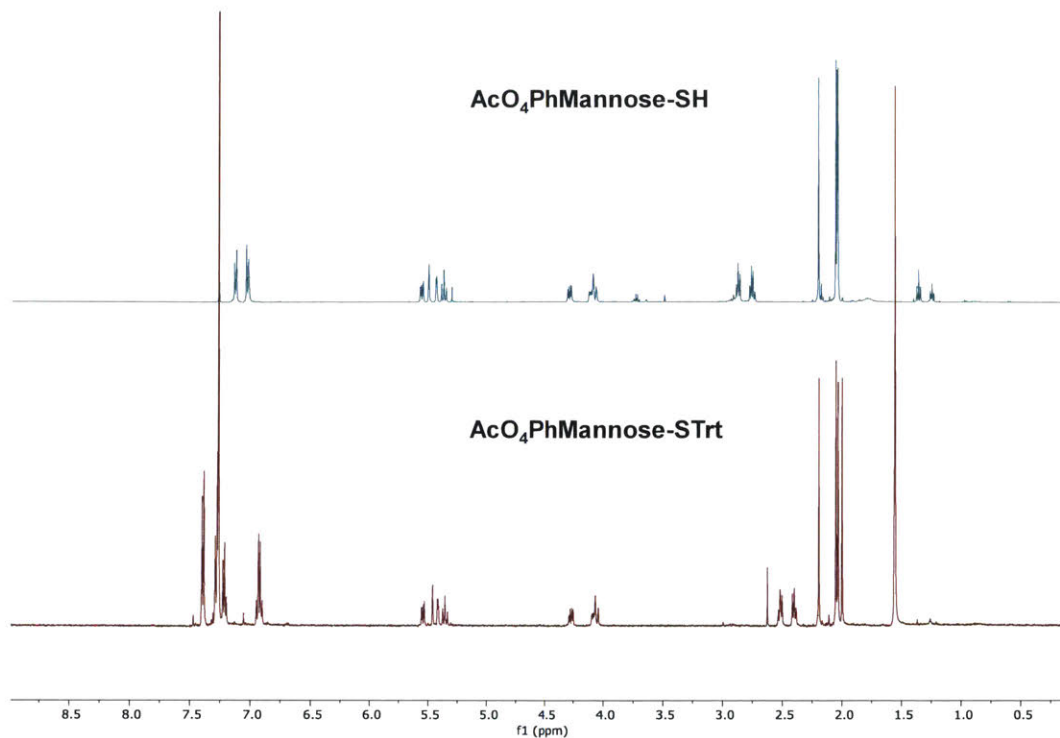


Figure S4.17. ^1H NMR spectra of (500 MHz, CDCl_3 , 25 $^\circ\text{C}$) of **AcO₄PhMannose-STrt** and **AcO₄PhMannose-SH**.

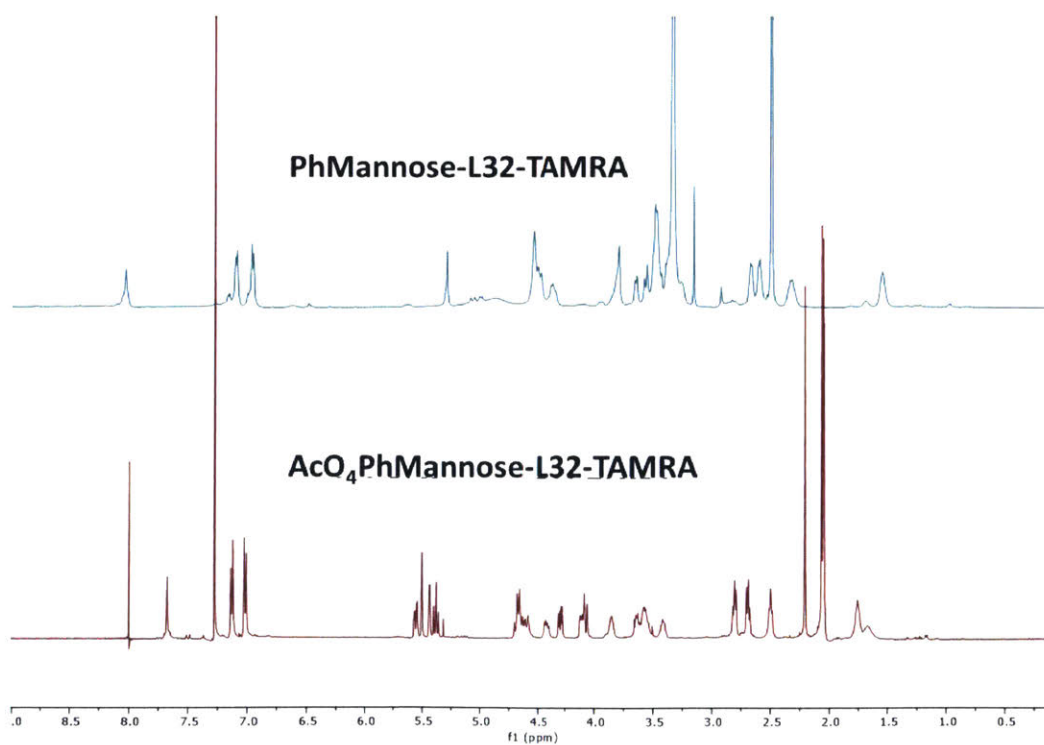
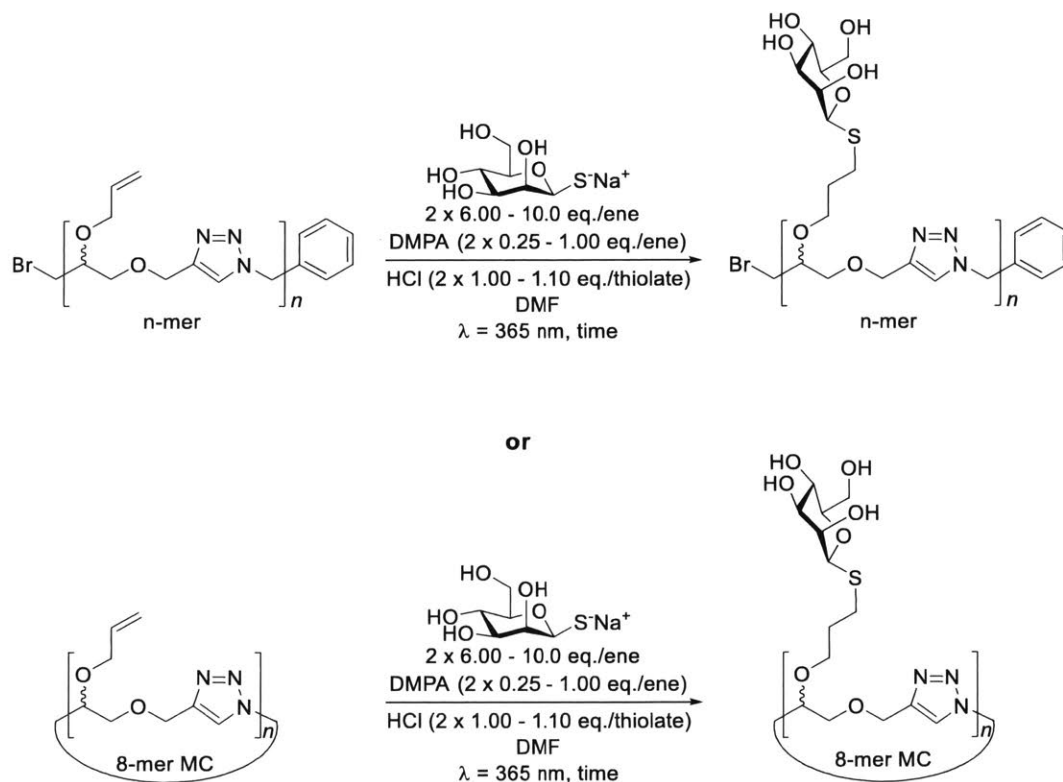


Figure S4.18. ^1H NMR spectra of (500 MHz, CDCl_3 , 25 $^\circ\text{C}$) of **AcO₄PhMannose-L32-TAMRA** and **PhMannose-L32-TAMRA**.

Thiol-ene reactions of allyl-IEG polymers and 1-thio- β -D-mannose sodium salt (these reaction procedures were completed by Manuel Hartweg and included for completion)



Synthesis of mannosylated (*L*)-8mer

1-Thio- β -D-mannose sodium salt (194 mg, 887 μ mol, 6 eq/ene), allyl-IEG-(*L*)-8mer (32.0 mg, 18.5 μ mol), DMPA (9.0 mg, 37 μ mol, 0.25 eq/ene) were suspended in DMF (320 mL) and the suspension was degassed for 10 min. Thereafter, conc. hydrochloric acid (37%, 73 μ L, 880 μ mol, 1 eq/thiolate) in DMF (320 mL) was added to the suspension. The heterogeneous mixture was irradiated with UV light ($\lambda = 365$ nm) under heavy stirring for 6 h. Another batch of 1-thio- β -D-mannose sodium salt (194 mg, 887 μ mol, 6 eq/ene), DMPA (9.0 mg, 37 μ mol, 0.25 eq/ene), DMF (320 μ L) and conc. hydrochloric acid (37%, 73 μ L, 887 μ mol, 1 eq/thiolate) in DMF (320 μ L) was added and the heterogeneous mixture was irradiated UV light ($\lambda = 365$ nm) under heavy stirring for another 12 h. The crude reaction mixture was dialysed against MeOH, MeOH/H₂O (1/1) (x2), and H₂O (800 mL each). The product was obtained after lyophilisation as white solid (23 mg, 38%). ¹H NMR (400 MHz, D₂O) δ (ppm) = 8.04 – 7.91 (m, 8H, *H*^{Ar}), 7.34 – 7.19 (m, 5H, *H*^{Ar}),

4.66 – 4.57 (m, 24H, H^1 , OCH_2C), 4.57 – 4.51 (m, 8H, $C(O)CH_2O^A$), 4.48 – 4.41 (m, 8H, $CH(O)CH_2O^B$), 3.93 – 3.87 (m, 16H, H^2 , $CH_2CH(O)CH_2$), 3.81 – 3.77 (m, 8H, H^{6A}), 3.65 – 3.53 (m, 32H, H^{6B} , $OCH_2^A CH$, NCH_2CH), 3.53 – 3.44 (m, 16H, H^4 , H^3), 3.39 – 3.33 (m, 8H, $OCH_2^B CH$), 3.31 – 3.26 (m, 8H, H^5), 2.56 – 2.48 (m, 8H, S $SCH_2^A CH$), 2.45 – 2.36 (m, 8H, S $SCH_2^B CH$), 1.71 – 1.57 (m, 16H, $CH_2CH_2CH_2$).

Synthesis of mannosylated (L)-16mer

1-Thio- β -D-mannose sodium salt (527 mg, 2.62 mmol, 6 eq/ene), allyl-IEG-(R)-16mer (90.0 mg, 27.3 μ mol), DMPA (28.0 mg, 109 μ mol, 2 eq/ene) were suspended in DMF (900 mL) and the suspension was degassed for 10 min. Thereafter, conc. hydrochloric acid (37%, 217 μ L, 2.62 mmol, 1 eq/thiolate) in DMF (900 mL) was added to the suspension. The heterogeneous mixture was irradiated with UV light ($\lambda = 365$ nm) under heavy stirring for 6 h. Another batch of 1-thio- β -D-mannose sodium salt (527 mg, 2.62 mmol, 6 eq/ene), DMPA (28.0 mg, 109 μ mol, 2 eq/ene), DMF (900 μ L) and conc. hydrochloric acid (37%, 217 μ L, 2.62 mmol, 1 eq/thiolate) in DMF (900 μ L) was added and the heterogeneous mixture was irradiated UV light ($\lambda = 365$ nm) under heavy stirring for another 12 h. The crude reaction mixture was dialysed against MeOH, MeOH/H₂O (1/1) (x2), and H₂O (800 mL each). The product was obtained after lyophilisation as white solid (62 mg, 35%). ¹H NMR (400 MHz, D₂O) δ (ppm) = 8.04 – 7.93 (m, 16H, H^{Ar}), 7.33 – 7.16 (m, 5H, H^{Ar}), 4.66 – 4.57 (m, 48H, H^1 , OCH_2C), 4.57 – 4.51 (m, 16H, $C(O)CH_2O^A$), 4.48 – 4.41 (m, 16H, $CH(O)CH_2O^B$), 3.93 – 3.87 (m, 32H, H^2 , $CH_2CH(O)CH_2$), 3.81 – 3.77 (m, 16H, H^{6A}), 3.65 – 3.53 (m, 64H, H^{6B} , $OCH_2^A CH$, NCH_2CH), 3.53 – 3.44 (m, 32H, H^4 , H^3), 3.39 – 3.33 (m, 16H, $OCH_2^B CH$), 3.31 – 3.26 (m, 16H, H^5), 2.56 – 2.48 (m, 16H, S $SCH_2^A CH$), 2.45 – 2.36 (m, 16H, S $SCH_2^B CH$), 1.71 – 1.57 (m, 32H, $CH_2CH_2CH_2$).

Synthesis of mannosylated (L)-32mer

1-Thio- β -D-mannose sodium salt (196 mg, 897 μ mol, 6 eq/ene), allyl-IEG-(R)-32mer (30.0 mg, 4.67 μ mol), DMPA (10 mg, 37.4 μ mol, 0.25 eq/ene) were suspended in DMF (300 mL) and the suspension was degassed for 10 min. Thereafter, conc. hydrochloric acid (37%, 74 μ L, 890 μ mol, 1 eq/thiolate) in DMF (300 mL) was added to the suspension. The heterogeneous mixture was irradiated with UV light ($\lambda = 365$ nm) under heavy stirring for 6 h. Another batch of 1-thio- β -D-mannose sodium salt (196 mg, 897 μ mol, 6 eq/ene), DMPA (10 mg, 37 μ mol, 0.25 eq/ene), DMF

(300 μL) and conc. hydrochloric acid (37%, 74 μL , 890 μmol , 1 eq/thiolate) in DMF (300 μL) was added and the heterogeneous mixture was irradiated UV light ($\lambda = 365 \text{ nm}$) under heavy stirring for another 12 h. The crude reaction mixture was dialysed against MeOH, MeOH/H₂O (1/1) (x2), and H₂O (800 mL each). The product was obtained after lyophilisation as white solid (36 mg, 61%). ¹H NMR (400 MHz, D₂O) δ (ppm) = 8.04 – 7.95 (m, 32H, H^{Ar}), 7.34 – 7.19 (m, 5H, H^{Ar}), 4.66 – 4.57 (m, 96H, H^{I} , OCH₂C), 4.57 – 4.51 (m, 32H, C(O)CH₂O^A), 4.48 – 4.41 (m, 32H, CH(O)CH₂O^B), 3.93 – 3.87 (m, 64H, H^{2} , CH₂CH(O)CH₂), 3.81 – 3.77 (m, 32H, H^{6A}), 3.65 – 3.53 (m, 128H, H^{6B} , OCH₂^ACH, NCH₂CH), 3.53 – 3.44 (m, 64H, H^{4} , H^{3}), 3.39 – 3.33 (m, 32H, OCH₂^BCH), 3.31 – 3.26 (m, 32H, H^{5}), 2.56 – 2.48 (m, 32H, S SCH₂^ACH), 2.45 – 2.36 (m, 32H, S SCH₂^BCH), 1.71 – 1.57 (m, 64H, CH₂CH₂CH₂).

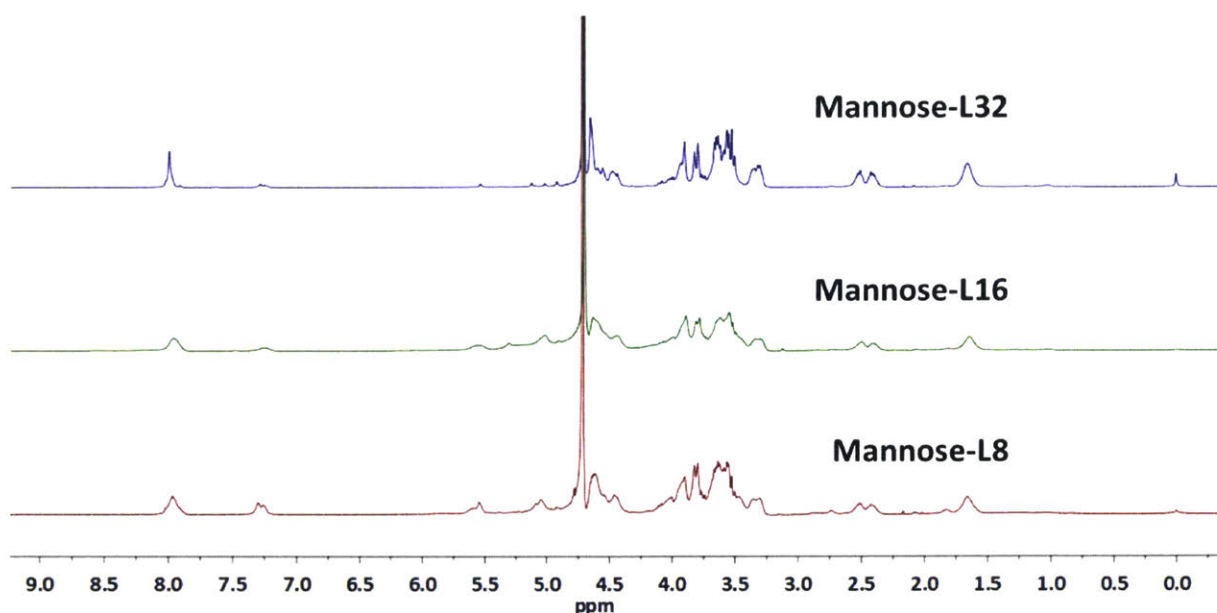


Figure S4.19. ¹H NMR spectrum (500 MHz, CDCl₃, 25 °C) of **Mannose-(L)32**, **Mannose-(L)16**, and **Mannose-(L)8**.

Synthesis of TAMRA-tagged mannosylated (L)-32mer

1-Thio- β -D-mannose sodium salt (188 mg, 862 μmol , 10 eq/ene), TAMRA tagged allyl-IEG-(R)-32mer (16.0 mg, 2.34 μmol), DMPA (22 mg, 86.2 μmol , 1 eq/ene) were suspended in DMF (300 mL) and the suspension was degassed for 10 min. Thereafter, conc. hydrochloric acid (37%, 71 μL , 860 μmol , 1 eq/thiolate) in DMF (400 mL) was added to the suspension. The heterogeneous mixture was irradiated with UV light ($\lambda = 365 \text{ nm}$) under heavy stirring for 6 h. Another batch of

1-thio- β -*D*-mannose sodium salt (188 mg, 862 μ mol, 10 eq/ene), DMPA (22 mg, 86 μ mol, 1 eq/ene), DMF (300 μ L) and conc. hydrochloric acid (37%, 71 μ L, 860 μ mol, 1 eq/thiolate) in DMF (300 μ L) was added and the heterogeneous mixture was irradiated UV light ($\lambda = 365$ nm) under heavy stirring for another 12 h. The crude reaction mixture was dialysed against MeOH, MeOH/H₂O (1/1) (x2), and H₂O (800 mL each). The product was obtained after lyophilisation as pink solid (24 mg, 77%). ¹H NMR (600 MHz, D₂O) δ (ppm) = 8.04 – 7.95 (m, 32H, *H*^{A_r}), 4.74 – 4.50 (m, 160H, *H*¹, OCH₂C, C(O)CH₂O^A, C(O)CH₂O^A), 4.03 – 3.94 (m, 64H, *H*², CH₂CH(O)CH₂), 3.78 – 3.52 (m, 224H, *H*^{6A}, *H*^{6B}, OCH₂^ACH, NCH₂CH, *H*⁴, *H*³), 3.45 – 3.35 (m, 64H), 3.46 – 3.34 (m, 64H, OCH₂^BCH, *H*⁵), 2.63 – 2.53 (m, 32H, S SCH₂^ACH), 2.52 – 2.42 (m, 32H, S SCH₂^BCH), 1.80 – 1.63 (m, 64H, CH₂CH₂CH₂).

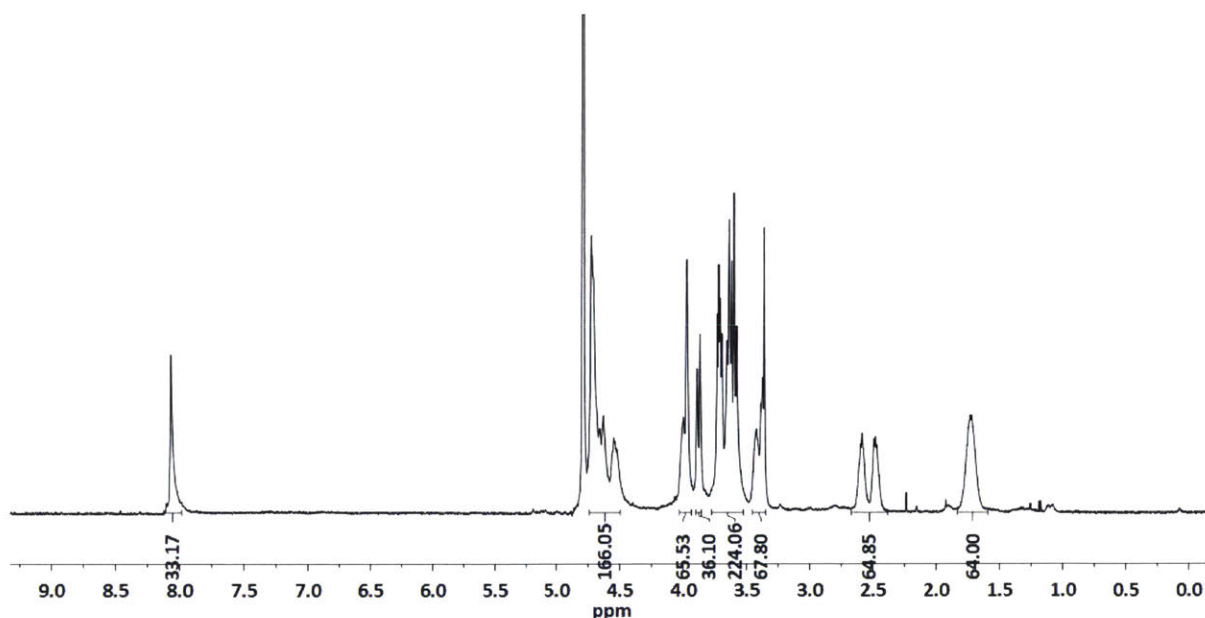


Figure S4.20. ¹H NMR spectrum of (500 MHz, CDCl₃, 25 °C) of **Mannose-(L)32-TAMRA**.

Synthesis of mannosylated (*D*)-8mer

1-Thio- β -*D*-mannose sodium salt (194 mg, 887 μ mol, 6 eq/ene), allyl-IEG-(*D*)-8mer (32.0 mg, 18.5 μ mol), DMPA (9.0 mg, 37 μ mol, 0.25 eq/ene) were suspended in DMF (320 mL) and the suspension was degassed for 10 min. Thereafter, conc. hydrochloric acid (37%, 73 μ L, 880 μ mol, 1 eq/thiolate) in DMF (320 mL) was added to the suspension. The heterogeneous mixture was irradiated with UV light ($\lambda = 365$ nm) under heavy stirring for 6 h. Another batch of 1-thio- β -*D*-mannose sodium salt (194 mg, 887 μ mol, 6 eq/ene), DMPA (9.0 mg, 37 μ mol, 0.25 eq/ene), DMF

(320 μL) and conc. hydrochloric acid (37%, 73 μL , 880 μmol , 1 eq/thiolate) in DMF (320 μL) was added and the heterogeneous mixture was irradiated UV light ($\lambda = 365 \text{ nm}$) under heavy stirring for another 12 h. The crude reaction mixture was dialysed against MeOH, MeOH/H₂O (1/1) (x2), and H₂O (800 mL each). The product was obtained after lyophilisation as white solid (23 mg, 38%). ¹H NMR (400 MHz, MeOD-*d*₄) δ (ppm) = 8.20 – 8.04 (m, 8H, *H*^{A_r}), 7.50 – 7.35 (m, 5H, *H*^{A_r}), 4.87 – 4.55 (m, 40H, *H*¹, OCH₂C, C(O)CH₂O^A, CH(O)CH₂O^B), 4.11 – 4.02 (m, 16H, *H*², CH₂CH(O)CH₂), 4.00 – 3.92 (m, 8H, *H*^{6A}), 3.86 – 3.62 (m, 48H, *H*^{6B}, OCH₂^ACH, NCH₂CH, *H*⁴, *H*³), 3.56 – 3.40 (m, 16H, OCH₂^BCH, *H*⁵), 2.71 – 2.54 (m, 16H, S SCH₂CH), 1.90 – 1.67 (m, 16H, CH₂CH₂CH₂).

Synthesis of mannosylated (*D*)-16mer

1-Thio- β -*D*-mannose sodium salt (423 mg, 1.94 mmol, 10 eq/ene), allyl-IEG-(*D*)-16mer (40 mg, 12 μmol), DMPA (50. mg, 190 μmol , 1 eq/ene) were suspended in DMF (500 mL) and the suspension was degassed for 10 min. Thereafter, conc. hydrochloric acid (37%, 180 μL , 2.1 mmol, 1.10 eq/thiolate) in DMF (1.00 mL) was added to the suspension. The heterogeneous mixture was irradiated with UV light ($\lambda = 365 \text{ nm}$) under heavy stirring for 6 h. Another batch of 1-thio- β -*D*-mannose sodium salt (423 mg, 1.94 mmol, 10 eq/ene), DMPA (49.7 mg, 194 μmol , 1 eq/ene), DMF (400 μL) and conc. hydrochloric acid (37%, 178 μL , 2.13 mmol, 1.10 eq/thiolate) in DMF (400 μL) was added and the heterogeneous mixture was irradiated UV light ($\lambda = 365 \text{ nm}$) under heavy stirring for another 12 h. The crude reaction mixture was dialysed against MeOH, MeOH/H₂O (1/1) (x2), and H₂O (800 mL each). The product was obtained after lyophilisation as white solid (49 mg, 63%). ¹H NMR (400 MHz, MeOD-*d*₄) δ (ppm) = 8.20 – 8.04 (m, 16H, *H*^{A_r}), 7.50 – 7.34 (m, 5H, *H*^{A_r}), 4.87 – 4.55 (m, 80H, *H*¹, OCH₂C, C(O)CH₂O^A, CH(O)CH₂O^B), 4.11 – 4.02 (m, 32H, *H*², CH₂CH(O)CH₂), 4.00 – 3.92 (m, 16H, *H*^{6A}), 3.86 – 3.62 (m, 96H, *H*^{6B}, OCH₂^ACH, NCH₂CH, *H*⁴, *H*³), 3.56 – 3.40 (m, 32H, OCH₂^BCH, *H*⁵), 2.71 – 2.54 (m, 32H, S SCH₂CH), 1.90 – 1.67 (m, 32H, CH₂CH₂CH₂).

Synthesis of mannosylated (*D*)-32mer

1-Thio- β -*D*-mannose sodium salt (196 mg, 897 μmol , 10 eq/ene), allyl-IEG-(*D*)-32mer (18 mg, 2.8 μmol), DMPA (23 mg, 90. μmol , 1 eq/ene) were suspended in DMF (200 mL) and the suspension was degassed for 10 min. Thereafter, conc. hydrochloric acid (37%, 83 μL , 990 μmol , 1.10 eq/thiolate) in DMF (200 mL) was added to the suspension. The heterogeneous mixture was irradiated with UV light ($\lambda = 365 \text{ nm}$) under heavy stirring for 6 h. Another batch of 1-thio- β -*D*-

mannose sodium salt (196 mg, 897 μmol , 10 eq/ene), DMPA (23.0 mg, 89.7 μmol , 1 eq/ene), DMF (200 μL) and conc. hydrochloric acid (37%, 83 μL , 988 μmol , 1.10 eq/thiolate) in DMF (200 μL) was added and the heterogeneous mixture was irradiated UV light ($\lambda = 365 \text{ nm}$) under heavy stirring for another 12 h. The crude reaction mixture was dialysed against MeOH, MeOH/H₂O (1/1) (x2), and H₂O (800 mL each). The product was obtained after lyophilisation as white solid (21 mg, 72%).

¹H NMR (400 MHz, MeOD-*d*₄) δ (ppm) = 8.20 – 8.04 (m, 32H, H^{Ar}), 7.50 – 7.34 (m, 5H, H^{Ar}), 4.87 – 4.55 (m, 160H, H^{I} , OCH₂C, C(O)CH₂O^A, CH(O)CH₂O^B), 4.11 – 4.02 (m, 64H, H^{2} , CH₂CH(O)CH₂), 4.00 – 3.92 (m, 32H, H^{6A}), 3.86 – 3.62 (m, 192H, H^{6B} , OCH₂^ACH, NCH₂CH, H^{4} , H^{3}), 3.56 – 3.40 (m, 64H, OCH₂^BCH, H^{5}), 2.71 – 2.54 (m, 64H, S SCH₂CH), 1.90 – 1.67 (m, 64H, CH₂CH₂CH₂).

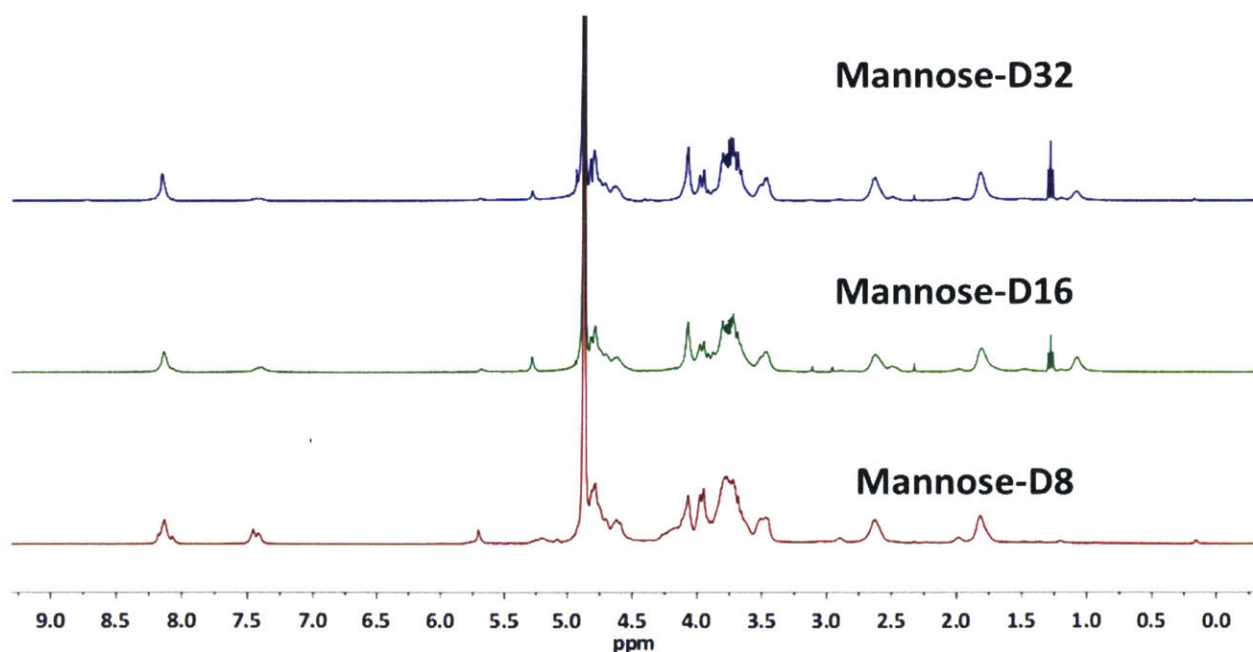


Figure S4.21. ¹H NMR spectra of (500 MHz, CDCl₃, 25 °C) of **Mannose-(D)32**, **Mannose-(D)16**, and **Mannose-(D)8**.

Synthesis of mannosylated (alt)-8mer

1-Thio- β -D-mannose sodium salt (145 mg, 666 μmol , 6 eq/ene), allyl-IEG-(*alt*)-8mer (24.0 mg, 13.9 μmol), DMPA (7.0 mg, 27 μmol , 0.25 eq/ene) were suspended in DMF (240 mL) and the suspension was degassed for 10 min. Thereafter, conc. hydrochloric acid (37%, 55 μL , 660 μmol ,

1 eq/thiolate) in DMF (240 mL) was added to the suspension. The heterogeneous mixture was irradiated with UV light ($\lambda = 365$ nm) under heavy stirring for 6 h. Another batch of 1-thio- β -*D*-mannose sodium salt (423 mg, 1.94 mmol, 6.00 eq/ene), DMPA (145 mg, 666 μ mol, 0.25 eq/ene), DMF (240 μ L) and conc. hydrochloric acid (37%, 55 μ L, 666 μ mol, 1 eq/thiolate) in DMF (240 μ L) was added and the heterogeneous mixture was irradiated UV light ($\lambda = 365$ nm) under heavy stirring for another 12 h. The crude reaction mixture was dialysed against MeOH, MeOH/H₂O (1/1) (x2), and H₂O (800 mL each). The product was obtained after lyophilisation as white solid (24 mg, 53%). ¹H NMR (400 MHz, MeOD-*d*₄) δ (ppm) = 8.21 – 8.05 (m, 8H, *H*^{Ar}), 7.52 – 7.37 (m, 5H, *H*^{Ar}), 4.88 – 4.57 (m, 40H, *H*¹, OCH₂C, C(O)CH₂O^A, CH(O)CH₂O^B), 4.13 – 4.04 (m, 16H, *H*², CH₂CH(O)CH₂), 4.01 – 3.93 (m, 8H, *H*^{6A}), 3.88 – 3.60 (m, 48H, *H*^{6B}, OCH₂^ACH, NCH₂CH, *H*⁴, *H*³), 3.56 – 3.40 (m, 16H, OCH₂^BCH, *H*⁵), 2.74 – 2.52 (m, 16H, S SCH₂CH), 1.90 – 1.71 (m, 16H, CH₂CH₂CH₂).

Synthesis of mannosylated (alt)-16mer

1-Thio- β -*D*-mannose sodium salt (268 mg, 1.22 mmol, 10 eq/ene), allyl-IEG-(*alt*)-8mer (24.0 mg, 7.28 μ mol), DMPA (32 mg, 120 μ mol, 1 eq/ene) were suspended in DMF (300 mL) and the suspension was degassed for 10 min. Thereafter, conc. hydrochloric acid (37%, 75 μ L, 1.3 mmol, 1.1 eq/thiolate) in DMF (250 mL) was added to the suspension. The heterogeneous mixture was irradiated with UV light ($\lambda = 365$ nm) under heavy stirring for 6 h. Another batch of 1-thio- β -*D*-mannose sodium salt (268 mg, 1.22 mmol, 10 eq/ene), DMPA (32 mg, 120 μ mol, 1 eq/ene), DMF (250 μ L) and conc. hydrochloric acid (37%, 75 μ L, 1.3 mmol, 1.1 eq/thiolate) in DMF (250 μ L) was added and the heterogeneous mixture was irradiated UV light ($\lambda = 365$ nm) under heavy stirring for another 12 h. The crude reaction mixture was dialysed against MeOH, MeOH/H₂O (1/1) (x2), and H₂O (800 mL each). The product was obtained after lyophilisation as white solid (20 mg, 46%). ¹H NMR (400 MHz, MeOD-*d*₄) δ (ppm) = 8.21 – 8.05 (m, 16H, *H*^{Ar}), 7.50 – 7.34 (m, 5H, *H*^{Ar}), 4.88 – 4.57 (m, 80H, *H*¹, OCH₂C, C(O)CH₂O^A, CH(O)CH₂O^B), 4.13 – 4.04 (m, 32H, *H*², CH₂CH(O)CH₂), 4.01 – 3.93 (m, 16H, *H*^{6A}), 3.88 – 3.60 (m, 96H, *H*^{6B}, OCH₂^ACH, NCH₂CH, *H*⁴, *H*³), 3.56 – 3.40 (m, 32H, OCH₂^BCH, *H*⁵), 2.74 – 2.52 (m, 32H, S SCH₂CH), 1.90 – 1.71 (m, 32H, CH₂CH₂CH₂).

Synthesis of mannosylated (alt)-32mer

1-Thio- β -D-mannose sodium salt (196 mg, 897 μ mol, 10 eq/ene), allyl-IEG-(alt)-32mer (18 mg, 2.8 μ mol), DMPA (46 mg, 180 μ mol, 2 eq/ene) were suspended in DMF (200 mL) and the suspension was degassed for 10 min. Thereafter, conc. hydrochloric acid (37%, 83 μ L, 990 μ mol, 1.1 eq/thiolate) in DMF (200 mL) was added to the suspension. The heterogeneous mixture was irradiated with UV light ($\lambda = 365$ nm) under heavy stirring for 6 h. Another batch of 1-thio- β -D-mannose sodium salt (196 mg, 897 μ mol, 10 eq/ene), DMPA (46.0 mg, 179 μ mol, 2 eq/ene), DMF (200 μ L) and conc. hydrochloric acid (37%, 83 μ L, 990 μ mol, 1.1 eq/thiolate) in DMF (200 μ L) was added and the heterogeneous mixture was irradiated UV light ($\lambda = 365$ nm) under heavy stirring for another 12 h. The crude reaction mixture was dialysed against MeOH, MeOH/H₂O (1/1) (x2), and H₂O (800 mL each). The product was obtained after lyophilisation as white solid (22 mg, 62%). ¹H NMR (400 MHz, MeOD-*d*₄) δ (ppm) = 8.21 – 8.05 (m, 32H, H^{Ar}), 7.50 – 7.34 (m, 5H, H^{Ar}), 4.88 – 4.57 (m, 160H, H¹, OCH₂C, C(O)CH₂O^A, CH(O)CH₂O^B), 4.13 – 4.04 (m, 64H, H², CH₂CH(O)CH₂), 4.01 – 3.93 (m, 32H, H^{6A}), 3.88 – 3.60 (m, 192H, H^{6B}, OCH₂^ACH, NCH₂CH, H⁴, H³), 3.56 – 3.40 (m, 64H, OCH₂^BCH, H⁵), 2.74 – 2.52 (m, 64H, S SCH₂CH), 1.90 – 1.71 (m, 64H, CH₂CH₂CH₂).

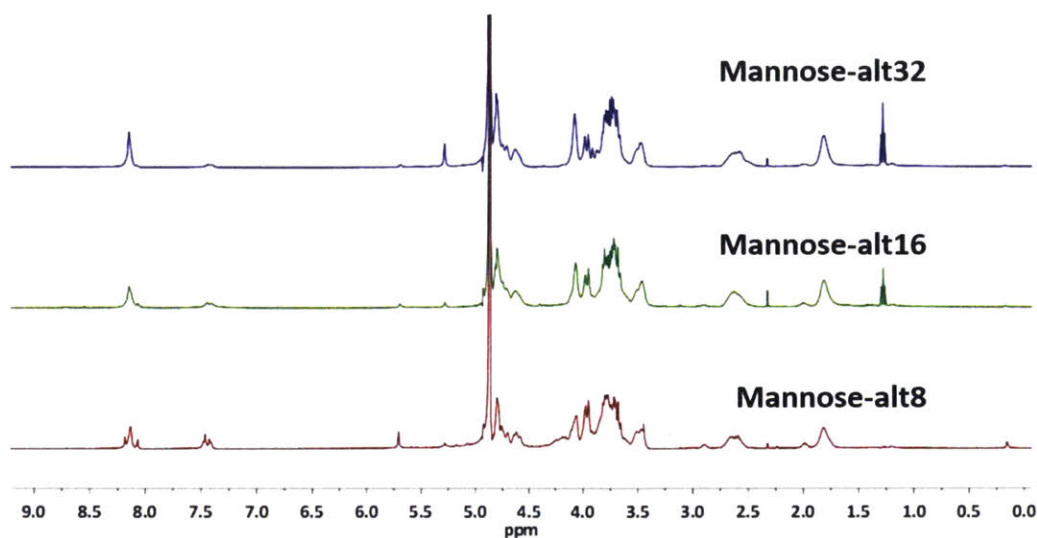


Figure S4.22. ^1H NMR spectra of (500 MHz, CDCl_3 , 25 $^\circ\text{C}$) of **Mannose-(alt)32**, **Mannose-(alt)16**, and **Mannose-(alt)8**.

Synthesis of mannosylated (*L*)-8mer macrocycle

1-Thio- β -*D*-mannose sodium salt (268 mg, 1.22 mmol, 10 eq/ene), allyl-IEG-(*L*)-8mer macrocycle (24.0 mg, 15.3 μmol), DMPA (32 mg, 120 μmol , 1 eq/ene) were suspended in DMF (250 mL) and the suspension was degassed for 10 min. Thereafter, conc. hydrochloric acid (37%, 68 μL , 1.2 mmol, 1 eq/thiolate) in DMF (250 mL) was added to the suspension. The heterogeneous mixture was irradiated with UV light ($\lambda = 365$ nm) under heavy stirring for 6 h. Another batch of 1-thio- β -*D*-mannose sodium salt (268 mg, 1.22 mmol, 10 eq/ene), DMPA (32 mg, 122 μmol , 1 eq/ene), DMF (250 μL) and conc. hydrochloric acid (37%, 68 μL , 1.2 mmol, 1 eq/thiolate) in DMF (250 μL) was added and the heterogeneous mixture was irradiated UV light ($\lambda = 365$ nm) under heavy stirring for another 12 h. The crude reaction mixture was dialysed against MeOH, MeOH/ H_2O (1/1) (x2), and H_2O (800 mL each). The product was obtained after lyophilisation as white solid (26 mg, 64%). ^1H NMR (600 MHz, D_2O) δ (ppm) = 7.96 (s, 8H, H^{Ar}), 4.66 – 4.57 (m, 24H, H^1 , OCH_2C), 4.57 – 4.51 (m, 8H, $\text{C}(\text{O})\text{CH}_2\text{O}^{\text{A}}$), 4.48 – 4.41 (m, 8H, $\text{CH}(\text{O})\text{CH}_2\text{O}^{\text{B}}$), 3.93 – 3.87 (m, 16H, H^2 , $\text{CH}_2\text{CH}(\text{O})\text{CH}_2$), 3.81 – 3.77 (m, 8H, $H^{6\text{A}}$), 3.65 – 3.53 (m, 32H, $H^{6\text{B}}$, $\text{OCH}_2^{\text{A}}\text{CH}$, NCH_2CH), 3.53 – 3.44 (m, 16H, H^4 , H^3), 3.39 – 3.33 (m, 8H, $\text{OCH}_2^{\text{B}}\text{CH}$), 3.31 – 3.26 (m, 8H, H^5), 2.56 – 2.48 (m, 8H, S $\text{SCH}_2^{\text{A}}\text{CH}$), 2.45 – 2.36 (m, 8H, S $\text{SCH}_2^{\text{B}}\text{CH}$), 1.71 – 1.57 (m, 16H, $\text{CH}_2\text{CH}_2\text{CH}_2$).

Synthesis of mannosylated (*D*)-8mer macrocycle

1-Thio- β -*D*-mannose sodium salt (123 mg, 563 μ mol, 10 eq/ene), allyl-IEG-(*D*)-8mer macrocycle (11.0 mg, 7.04 μ mol), DMPA (14 mg, 560 μ mol, 1 eq/ene) were suspended in DMF (200 mL) and the suspension was degassed for 10 min. Thereafter, conc. hydrochloric acid (37%, 31 μ L, 560 μ mol, 1 eq/thiolate) in DMF (250 mL) was added to the suspension. The heterogeneous mixture was irradiated with UV light ($\lambda = 365$ nm) under heavy stirring for 6 h. Another batch of 1-thio- β -*D*-mannose sodium salt (123 mg, 563 μ mol, 10 eq/ene), DMPA (14 mg, 560 μ mol, 1 eq/ene), DMF (250 μ L) and conc. hydrochloric acid (37%, 31 μ L, 560 μ mol, 1 eq/thiolate) in DMF (250 μ L) was added and the heterogeneous mixture was irradiated UV light ($\lambda = 365$ nm) under heavy stirring for another 12 h. The crude reaction mixture was dialysed against MeOH, MeOH/H₂O (1/1) (x2), and H₂O (800 mL each). The product was obtained after lyophilisation as white solid (12 mg, 52%). ¹H NMR (600 MHz, D₂O) δ (ppm) = 7.96 (s, 8H, *H*^{A1}), 4.66 – 4.57 (m, 24H, *H*¹, OCH₂C), 4.57 – 4.51 (m, 8H, C(O)CH₂O^A), 4.48 – 4.41 (m, 8H, CH(O)CH₂O^B), 3.93 – 3.87 (m, 16H, *H*², CH₂CH(O)CH₂), 3.81 – 3.77 (m, 8H, *H*^{6A}), 3.65 – 3.53 (m, 32H, *H*^{6B}, OCH₂^ACH, NCH₂CH), 3.53 – 3.44 (m, 16H, *H*⁴, *H*³), 3.39 – 3.33 (m, 8H, OCH₂^BCH), 3.31 – 3.26 (m, 8H, *H*⁵), 2.52 – 2.40 (m, 16H, S SCH₂CH), 1.71 – 1.57 (m, 16H, CH₂CH₂CH₂).

Synthesis of mannosylated (alt)-8mer macrocycle

1-Thio- β -*D*-mannose sodium salt (101 mg, 461 μ mol, 10 eq/ene), allyl-IEG-(alt)-8mer macrocycle (9.0 mg, 5.8 μ mol), DMPA (12 mg, 46 μ mol, 1 eq/ene) were suspended in DMF (200 mL) and the suspension was degassed for 10 min. Thereafter, conc. hydrochloric acid (37%, 26 μ L, 461 μ mol, 1 eq/thiolate) in DMF (250 mL) was added to the suspension. The heterogeneous mixture was irradiated with UV light ($\lambda = 365$ nm) under heavy stirring for 6 h. Another batch of 1-thio- β -*D*-mannose sodium salt (101 mg, 461 μ mol, 10 eq/ene), DMPA (12 mg, 46 μ mol, 1 eq/ene), DMF (250 μ L) and conc. hydrochloric acid (37%, 26 μ L, 460 μ mol, 1 eq/thiolate) in DMF (250 μ L) was added and the heterogeneous mixture was irradiated UV light ($\lambda = 365$ nm) under heavy stirring for another 12 h. The crude reaction mixture was dialysed against MeOH, MeOH/H₂O (1/1) (x2), and H₂O (800 mL each). The product was obtained after lyophilisation as white solid (8.0 mg, 42%). ¹H NMR (600 MHz, D₂O) δ (ppm) = 7.96 (s, 8H, *H*^{Ar}), 4.66 – 4.57 (m, 24H, *H*¹, OCH₂C), 4.57 – 4.51 (m, 8H, C(O)CH₂O^A), 4.48 – 4.41 (m, 8H, CH(O)CH₂O^B), 3.93 – 3.87 (m, 16H, *H*², CH₂CH(O)CH₂), 3.81 – 3.77 (m, 8H, *H*^{6A}), 3.65 – 3.53 (m, 32H, *H*^{6B}, OCH₂^ACH, NCH₂CH), 3.53 – 3.44 (m, 16H, *H*⁴, *H*³), 3.39 – 3.33 (m, 8H, OCH₂^BCH), 3.31 – 3.26 (m, 8H, *H*⁵), 2.56 – 2.36 (m, 16H, S SCH₂CH), 1.72 – 1.57 (m, 16H, CH₂CH₂CH₂).

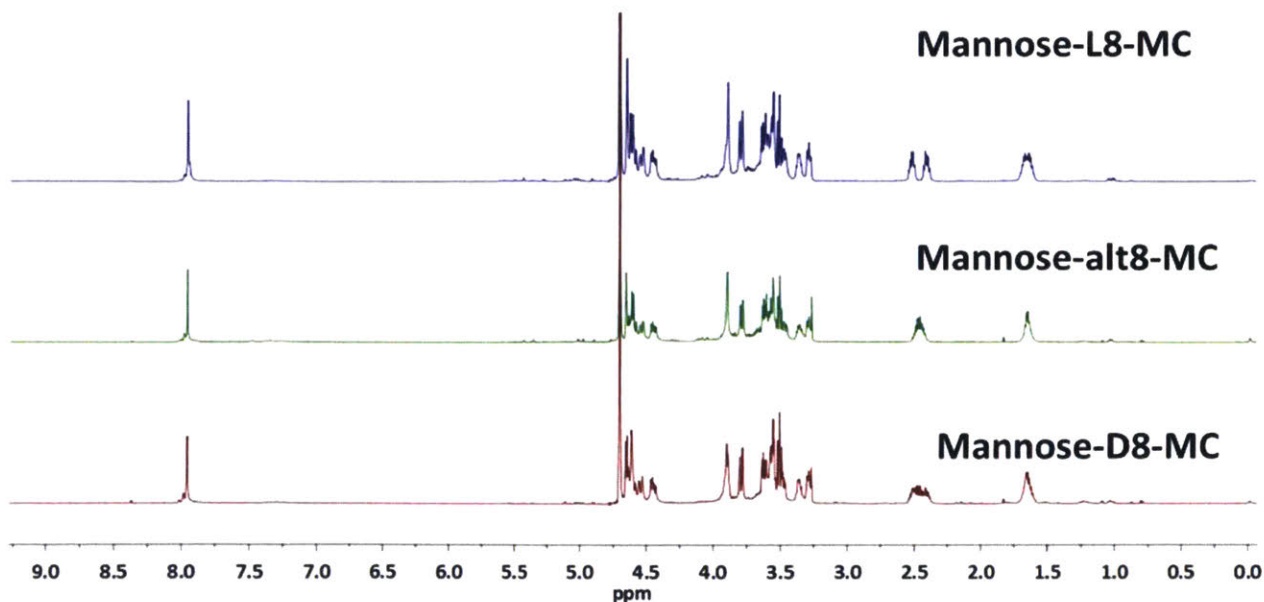


Figure S4.23. ¹H NMR spectrum (500 MHz, CDCl₃, 25 °C) of Mannose-(*L*)8-MC, Mannose-(*D*)8-MC, and Mannose-(*alt*)8-MC.

GPC analysis data of mannosylated IEG-oligomers

Alternating (*alt*) polymers

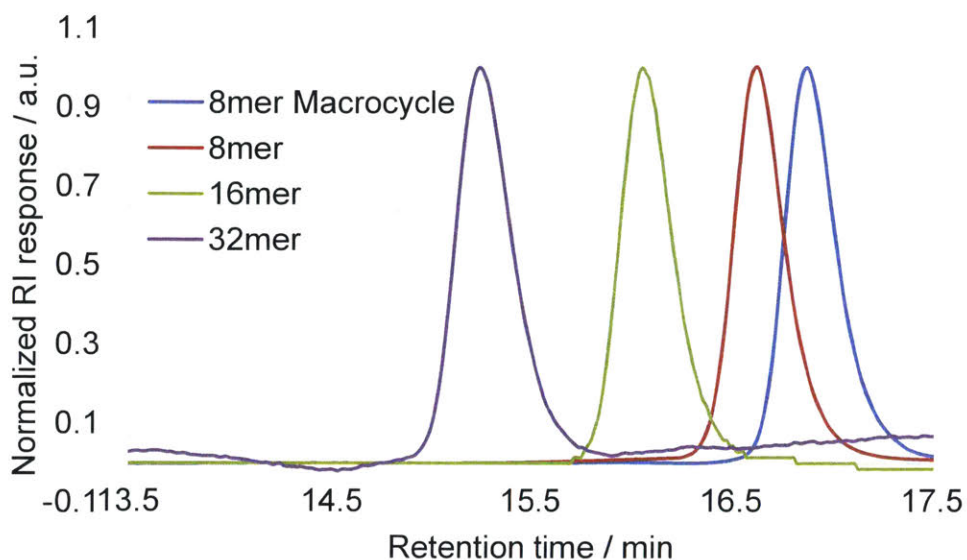


Figure S4.24. GPC traces for **Mannose-(*alt*)32**, **Mannose-(*alt*)16**, **Mannose-(*alt*)8**, and **Mannose-(*alt*)8-MC**.

(*L*) polymers

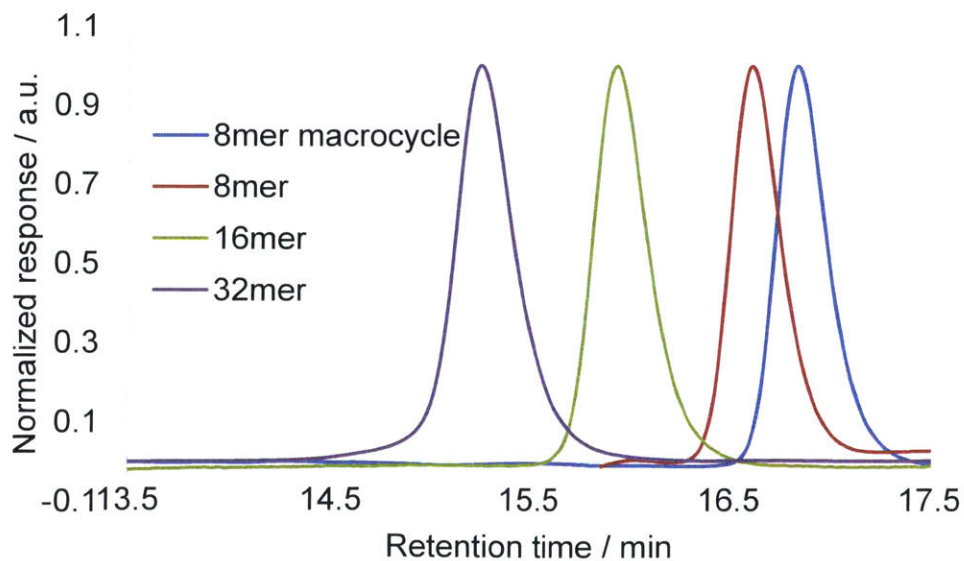


Figure S4.25. GPC traces for **Mannose-(*L*)32**, **Mannose-(*L*)16**, **Mannose-(*L*)8**, and **Mannose-(*L*)8-MC**.

(D) Polymers

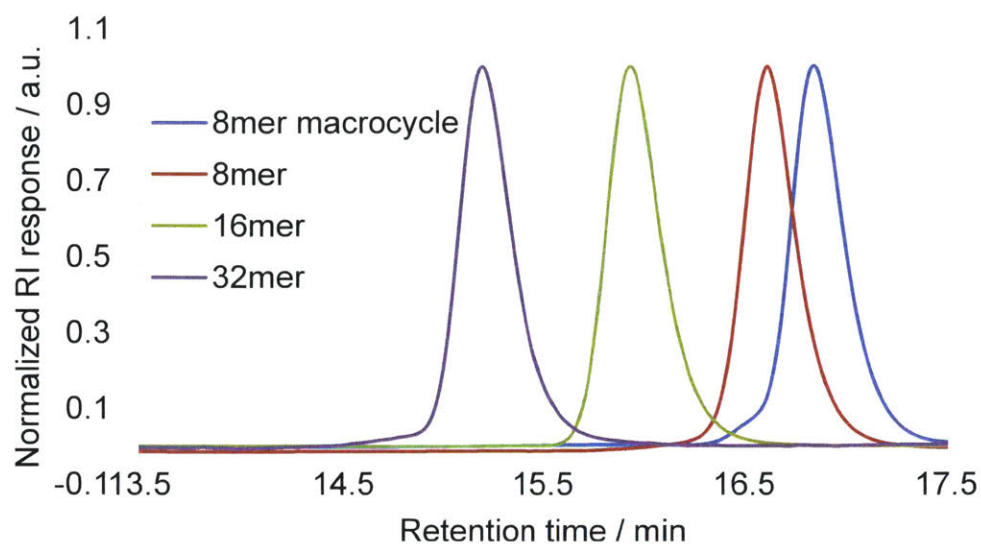


Figure S4.26. GPC traces for **Mannose-(D)32**, **Mannose-(D)16**, **Mannose-(D)8**, and **Mannose-(D)8-MC**.

AcO₄PhMannose-L32-TAMRA

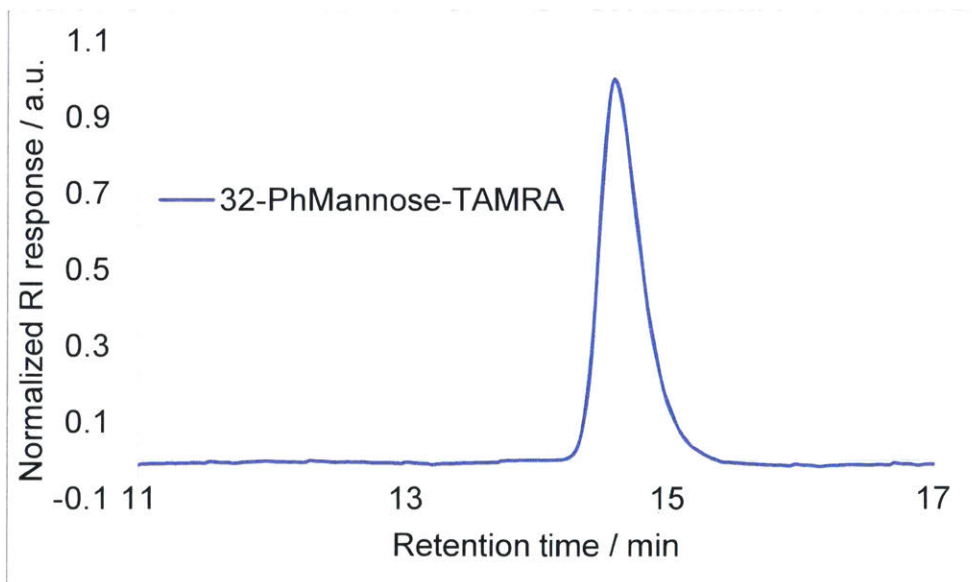


Figure S4.27. GPC trace for **AcO₄PhMannose-L32-TAMRA**.

Live/Dead Assay

Table 4.1. Different compounds tested, quantity used and position on the well plates.

Position #	Compound	Weight (mg)
1	(L)-32mer	1.3
2	(D)-16mer	1.4
3	(L)-16mer	1.3
4	(D)-32mer	1.4
5	(alt)-8mer	1.0
6	(D)-8mer	1.0
7	(L)-8mer	1.0
8	(alt)-16mer	1.4
9	(alt)-32mer	1.0
10	MH533	1.1

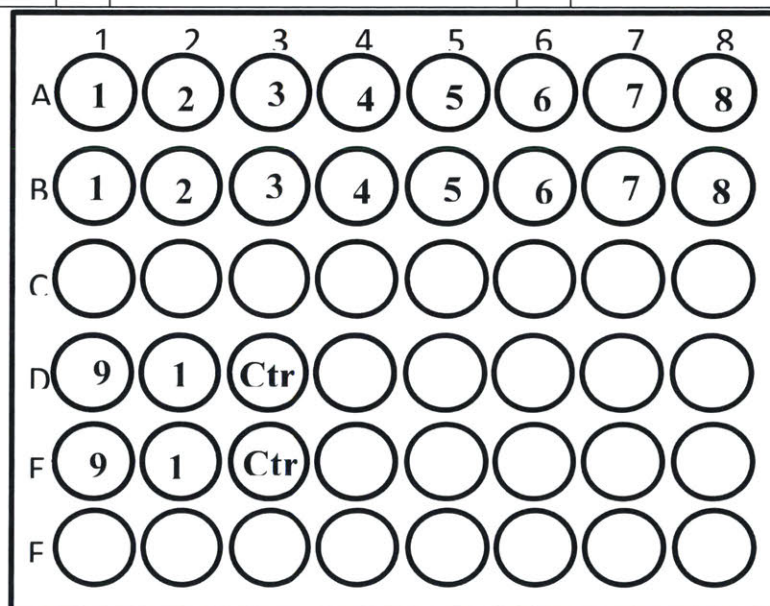


Figure S4.28. Tissue Culture Plate (TCP) layout. Refer to this for linking raw images with samples. Each sample was done by duplicate for each time point.

3T3 fibroblasts were exposed to 5% w/v⁻¹ solutions of the different chemicals synthesized (**Table 4.1**). After 6 h of incubation and until 48 h, no apparent negative effect was observed (**Figure 4.2**). A low density of dead cells was detected at all times and conditions, not showing a significant

difference with the control. However, a decrease on growth rate was observed for all compounds. While the control monolayer reached the confluence at almost 6 h, compounds 1 to 10 reached the confluence by 48 h.

Summary of the live/dead assay:

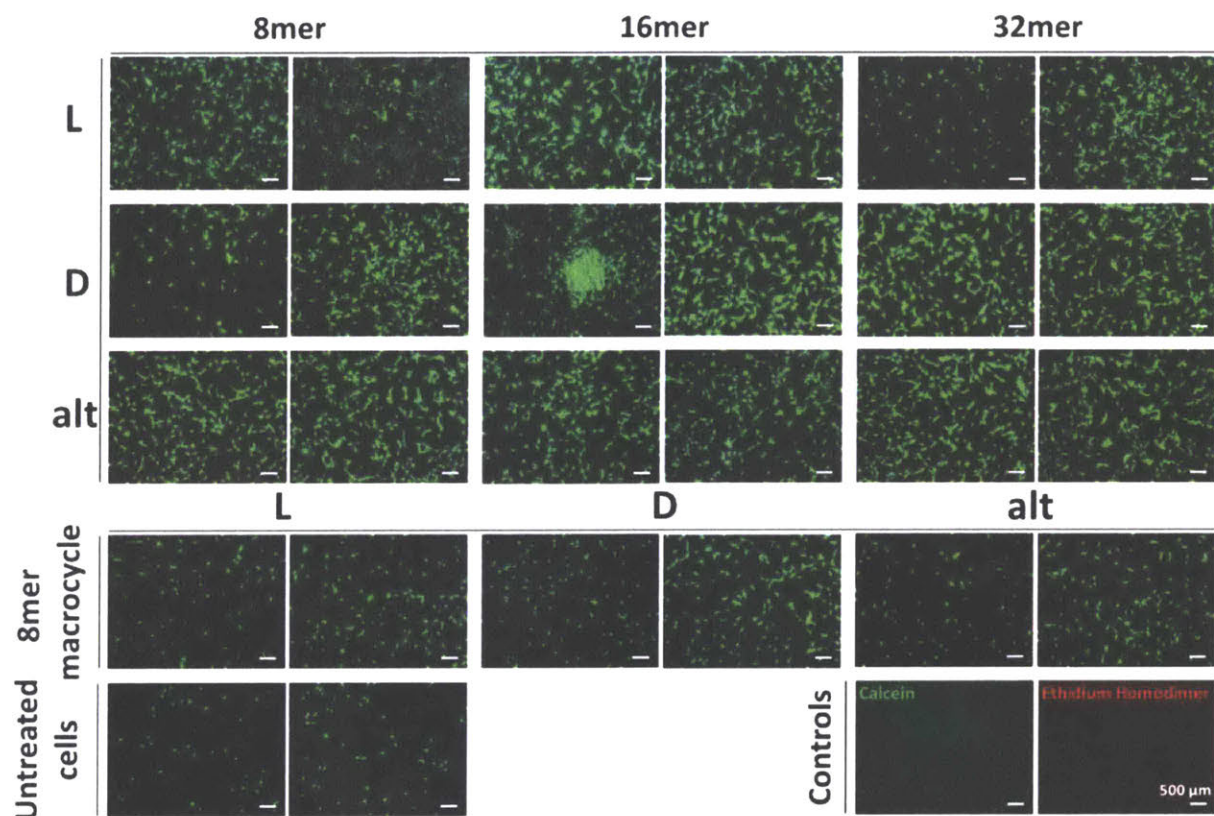


Figure S4.29. Live/Dead assay of NIH 3T3 fibroblasts inoculated with 5% solutions of different chemically modified glycans after 6 h (left) and 12 h (right).

Alamar Blue Assay

To study the cytotoxicity of the synthesised oligomers/polymers, the metabolic activity of NIH 3T3 Fibroblasts was measured by the Alamar Blue (AB) assay. Two cell densities were studied. As shown in Figures S4.30 and S4.31, none of the components display apparent cytotoxicity. For either cell density of 1×10^4 or 5×10^4 cells, there is no significant difference on the percentage of Alamar Blue reduced. It must be noted that after 48 h, the metabolic activity increases due to an increase on the number of cells. However, for a 5×10^4 cells per well (Figure S4.31) the difference on reduction of AB for both time points is not that marked, starting appearing some cell death after 2 d. The percentage of AB reduced for MH557, MH551 RSMC, MH551 RMC, MH442, MH445, MH446 and MH549A not only proves that these compounds are not toxic, but that when they are present in the culture media fibroblasts have an enhance of their metabolic activity.

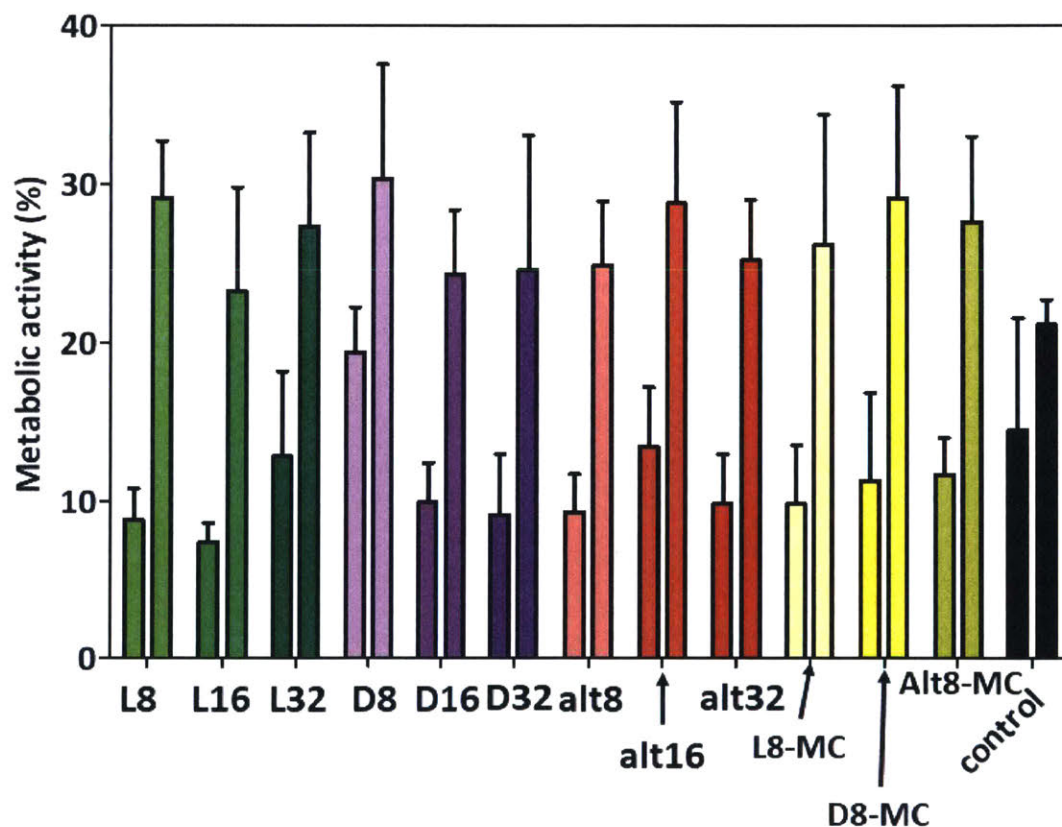


Figure S4.30. Alamar Blue reduction of a monolayer of 1×10^4 NIH 3T3 Fibroblasts. For each compound, measurements after 24 and 48 h of exposition were acquired.

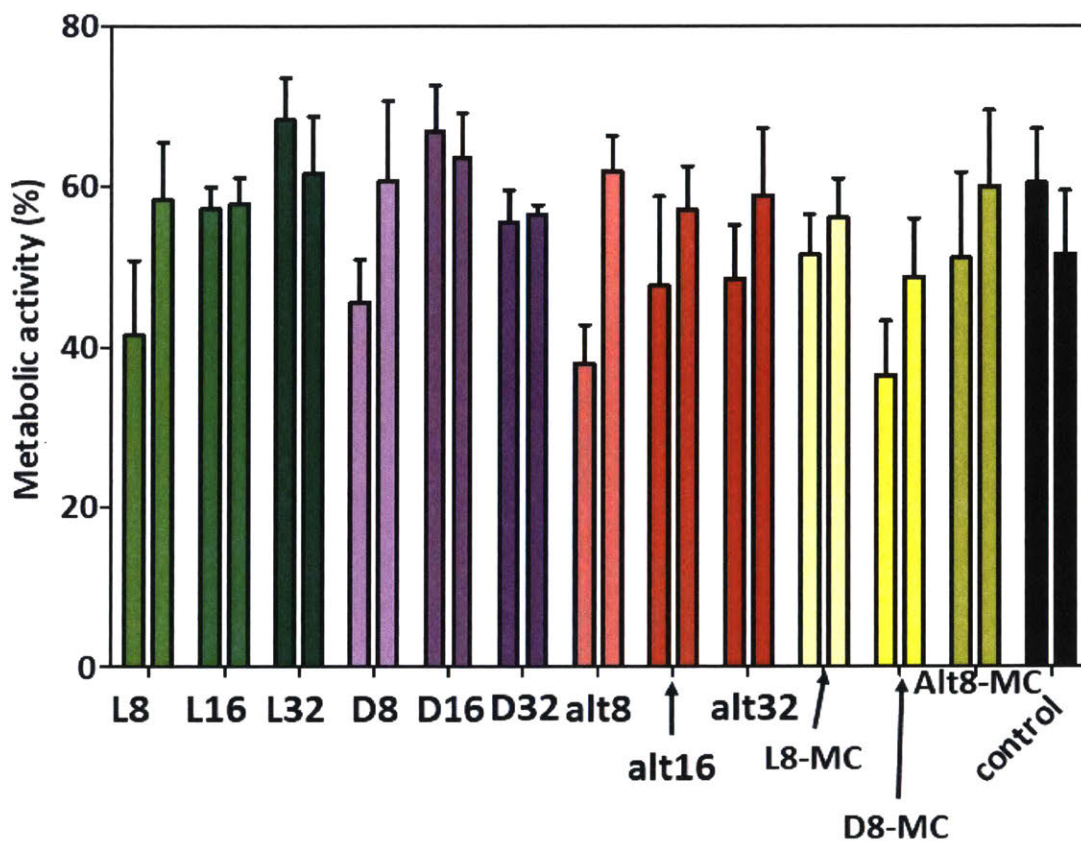


Figure S4.31. Alamar Blue reduction of a monolayer of 5×10^4 NIH 3T3 Fibroblasts. For each compound, measurements after 24 and 48 h of exposition were acquired.

Circular Dichronism measurements of glycosylated IEG polymers

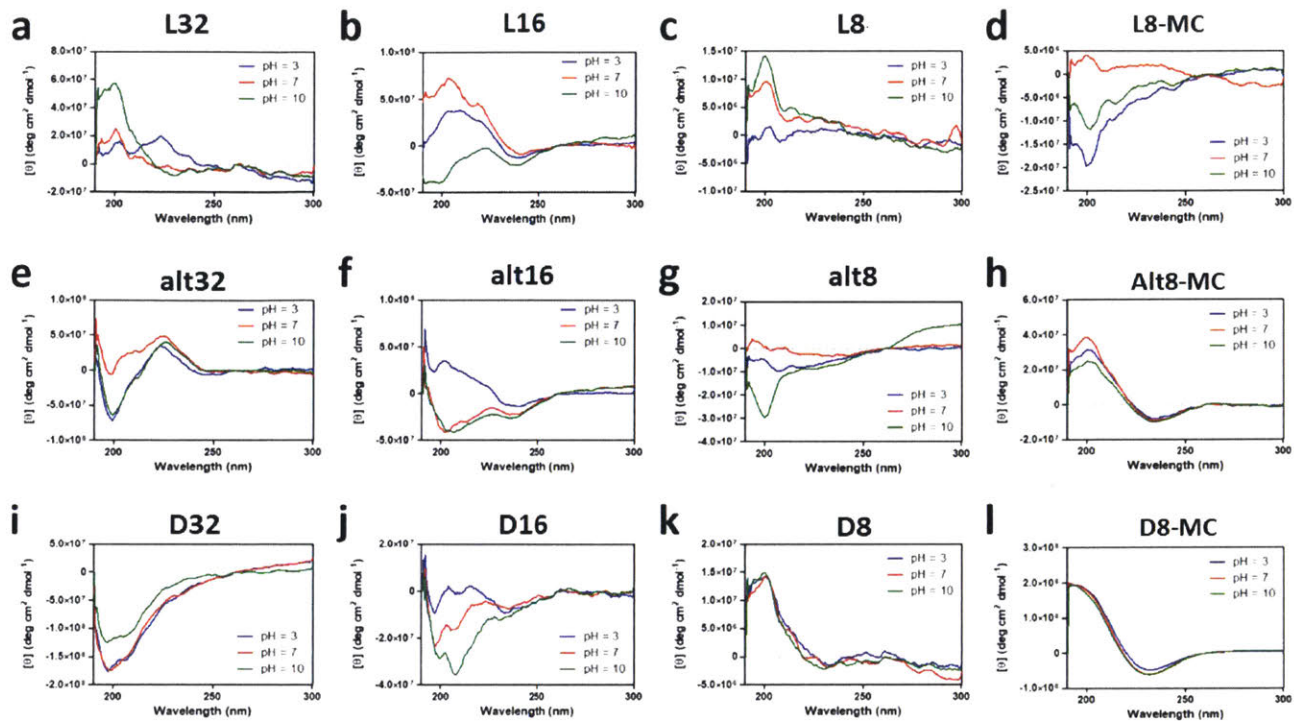


Figure S4.32. **a, d, i.** CD spectra for 32mers; **b, f, j.** CD spectra for 16mers; **c, g, k.** CD spectra for 8mers; **d, h, l.** CD spectra for 8mer macrocycles.

Lectin binding studies results

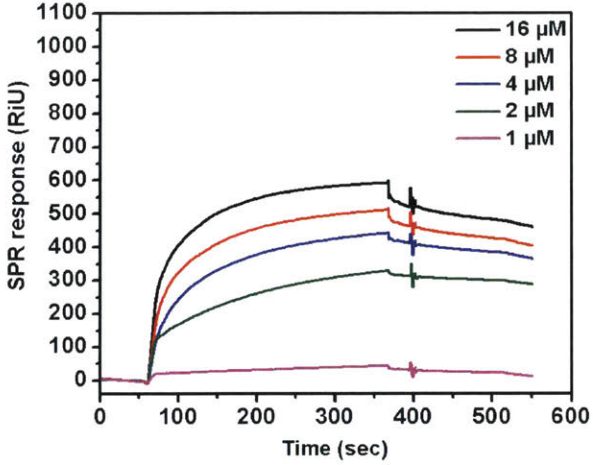
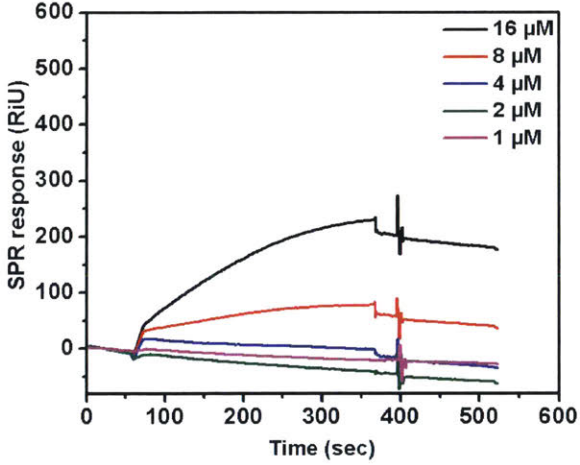
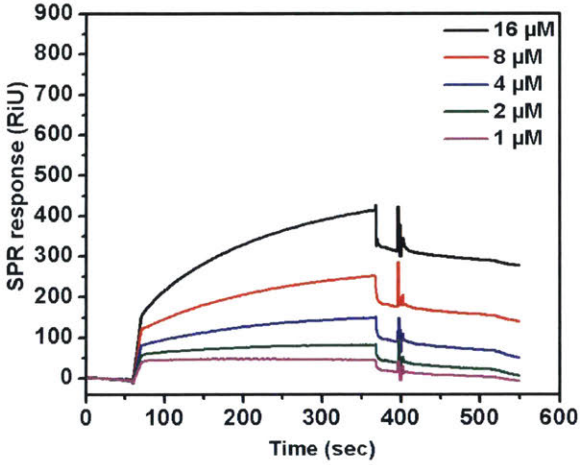
DC-SIGN

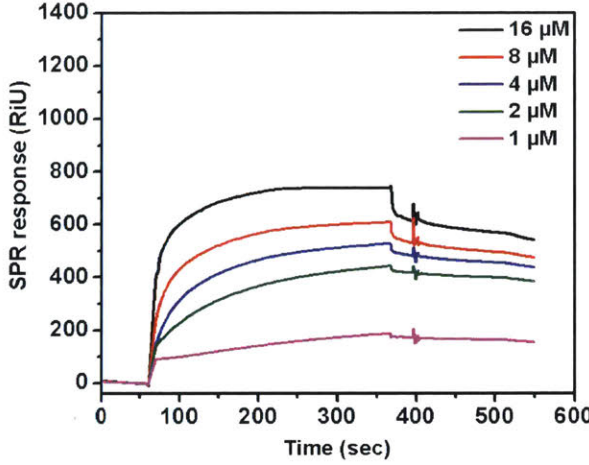
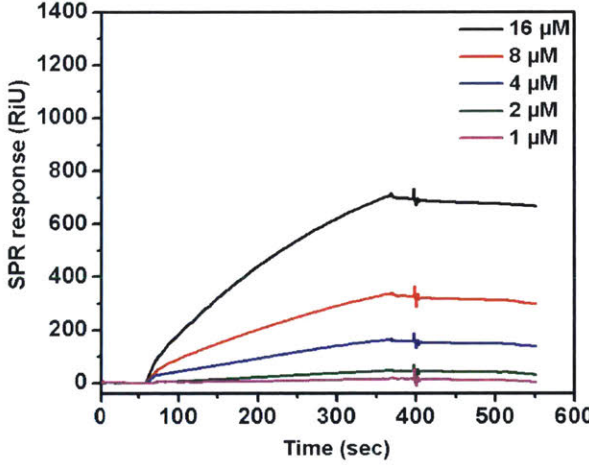
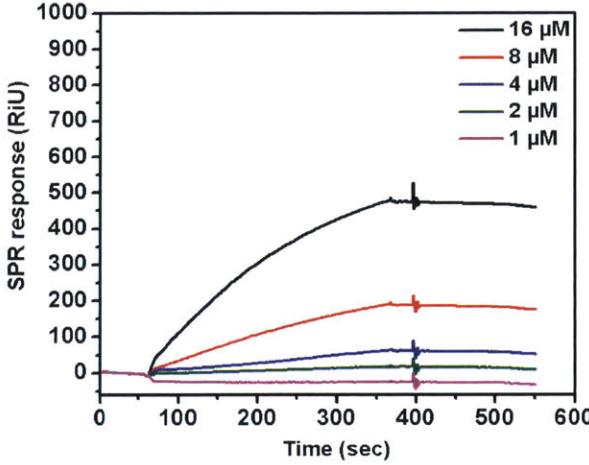
Table S4.1. Kinetic data of binding between glycopolymers and DC-SIGN as calculated by SPR.

Ligand	k_a ($M^{-1} s^{-1}$)	k_d (s^{-1})	K_D (M^{-1})	R_{max} (RU)
<i>(L)</i> -32mer	187	5.66×10^{-5}	3.31×10^6	970
(alt)-32mer	113	1.98×10^{-5}	5.71×10^6	740
<i>(D)</i> -32mer	56	1.49×10^{-5}	3.76×10^6	590
<i>(L)</i> -16mer	172	1.26×10^{-6}	1.37×10^8	495
(alt)-16mer	139	3.89×10^{-6}	3.37×10^7	415
<i>(D)</i> -16mer	96.2	6.93×10^{-6}	1.39×10^7	380
<i>(L)</i> -8mer	68.9	1.71×10^{-4}	4.04×10^5	300
(alt)-8mer	40.6	1.55×10^{-4}	2.62×10^5	230
<i>(D)</i> -8mer	20.9	9.45×10^{-4}	2.21×10^4	190
<i>(L)</i> -8mer macrocycle	29.4	4.65×10^{-5}	6.32×10^5	700
(alt)-8mer macrocycle	37.7	1.68×10^{-6}	2.24×10^6	865
<i>(D)</i> -8mer macrocycle	14.4	1.84×10^{-4}	7.83×10^4	475

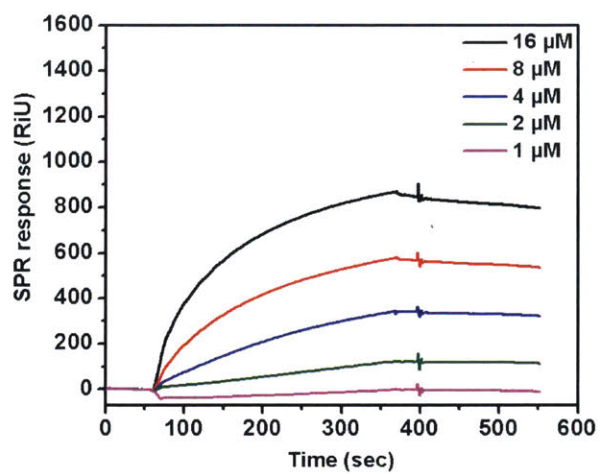
Ligand	
<i>(L)</i> -8mer	<p>SPR sensorgrams for <i>(L)</i>-8mer. The y-axis represents SPR response (RIU) from 0 to 800, and the x-axis represents Time (sec) from 0 to 600. Five curves are shown for different concentrations: 16 μM (black), 8 μM (red), 4 μM (blue), 2 μM (green), and 1 μM (magenta). The response increases over time and plateaus around 350 seconds. The 16 μM curve reaches the highest response of approximately 300 RIU, while the 1 μM curve reaches the lowest response of approximately 30 RIU. All curves exhibit a sharp dip at approximately 380 seconds, likely due to a buffer change.</p>
<i>(L)</i> -16mer	<p>SPR sensorgrams for <i>(L)</i>-16mer. The y-axis represents SPR response (RIU) from 0 to 1000, and the x-axis represents Time (sec) from 0 to 600. Five curves are shown for different concentrations: 16 μM (black), 8 μM (red), 4 μM (blue), 2 μM (green), and 1 μM (magenta). The response increases over time and plateaus around 350 seconds. The 16 μM curve reaches the highest response of approximately 500 RIU, while the 1 μM curve reaches the lowest response of approximately 50 RIU. All curves exhibit a sharp dip at approximately 380 seconds, likely due to a buffer change.</p>

<p>(L)-32mer</p>	
<p>(D)-8mer</p>	
<p>(D)-16mer</p>	

<p>(D)-32mer</p>	 <p>SPR response (RiU) vs Time (sec) for (D)-32mer. The graph shows five curves for concentrations of 16 μM (black), 8 μM (red), 4 μM (blue), 2 μM (green), and 1 μM (magenta). The 16 μM curve reaches a plateau of approximately 580 RiU, while the 1 μM curve remains near 0 RiU. All curves show a sharp drop at 400 seconds.</p>
<p>(alt)-8mer</p>	 <p>SPR response (RiU) vs Time (sec) for (alt)-8mer. The graph shows five curves for concentrations of 16 μM (black), 8 μM (red), 4 μM (blue), 2 μM (green), and 1 μM (magenta). The 16 μM curve reaches a plateau of approximately 220 RiU, while the 1 μM curve reaches approximately -50 RiU. All curves show a sharp drop at 400 seconds.</p>
<p>(alt)-16mer</p>	 <p>SPR response (RiU) vs Time (sec) for (alt)-16mer. The graph shows five curves for concentrations of 16 μM (black), 8 μM (red), 4 μM (blue), 2 μM (green), and 1 μM (magenta). The 16 μM curve reaches a plateau of approximately 400 RiU, while the 1 μM curve reaches approximately 20 RiU. All curves show a sharp drop at 400 seconds.</p>

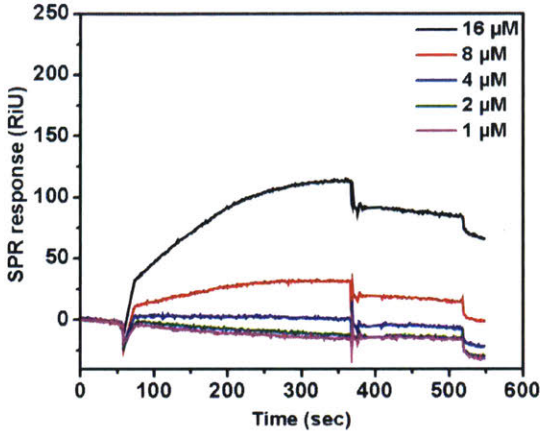
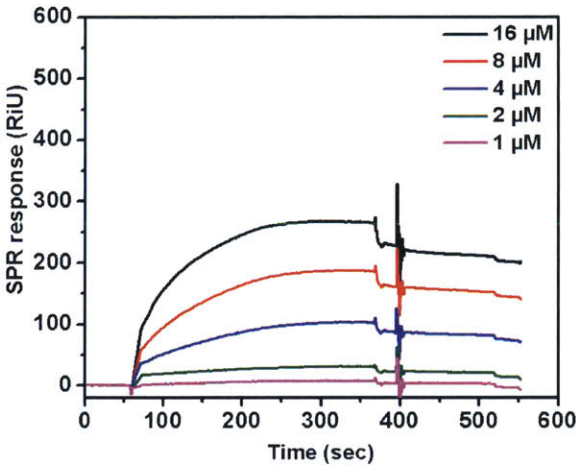
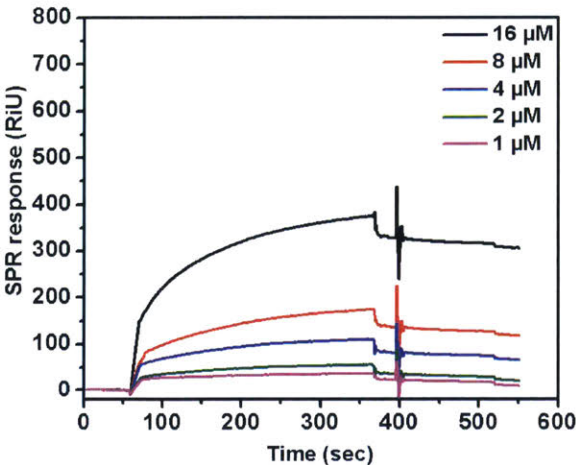
<p>(alt)- 32mer</p>	 <p>SPR response (RIU) vs Time (sec) for (alt)-32mer. The y-axis ranges from 0 to 1400 RIU, and the x-axis ranges from 0 to 600 sec. Five curves are shown for concentrations: 16 μM (black), 8 μM (red), 4 μM (blue), 2 μM (green), and 1 μM (magenta). All curves show an initial rise to a plateau, followed by a sharp drop at approximately 380 seconds, and then a slight recovery. The 16 μM curve reaches the highest plateau at ~700 RIU.</p>
<p>(L)-8mer macrocycle</p>	 <p>SPR response (RIU) vs Time (sec) for (L)-8mer macrocycle. The y-axis ranges from 0 to 1400 RIU, and the x-axis ranges from 0 to 600 sec. Five curves are shown for concentrations: 16 μM (black), 8 μM (red), 4 μM (blue), 2 μM (green), and 1 μM (magenta). The curves show a rise to a plateau, a sharp drop at ~380 seconds, and a slight recovery. The 16 μM curve reaches the highest plateau at ~700 RIU.</p>
<p>(D)-8mer macrocycle</p>	 <p>SPR response (RIU) vs Time (sec) for (D)-8mer macrocycle. The y-axis ranges from 0 to 1000 RIU, and the x-axis ranges from 0 to 600 sec. Five curves are shown for concentrations: 16 μM (black), 8 μM (red), 4 μM (blue), 2 μM (green), and 1 μM (magenta). The curves show a rise to a plateau, a sharp drop at ~380 seconds, and a slight recovery. The 16 μM curve reaches the highest plateau at ~480 RIU.</p>

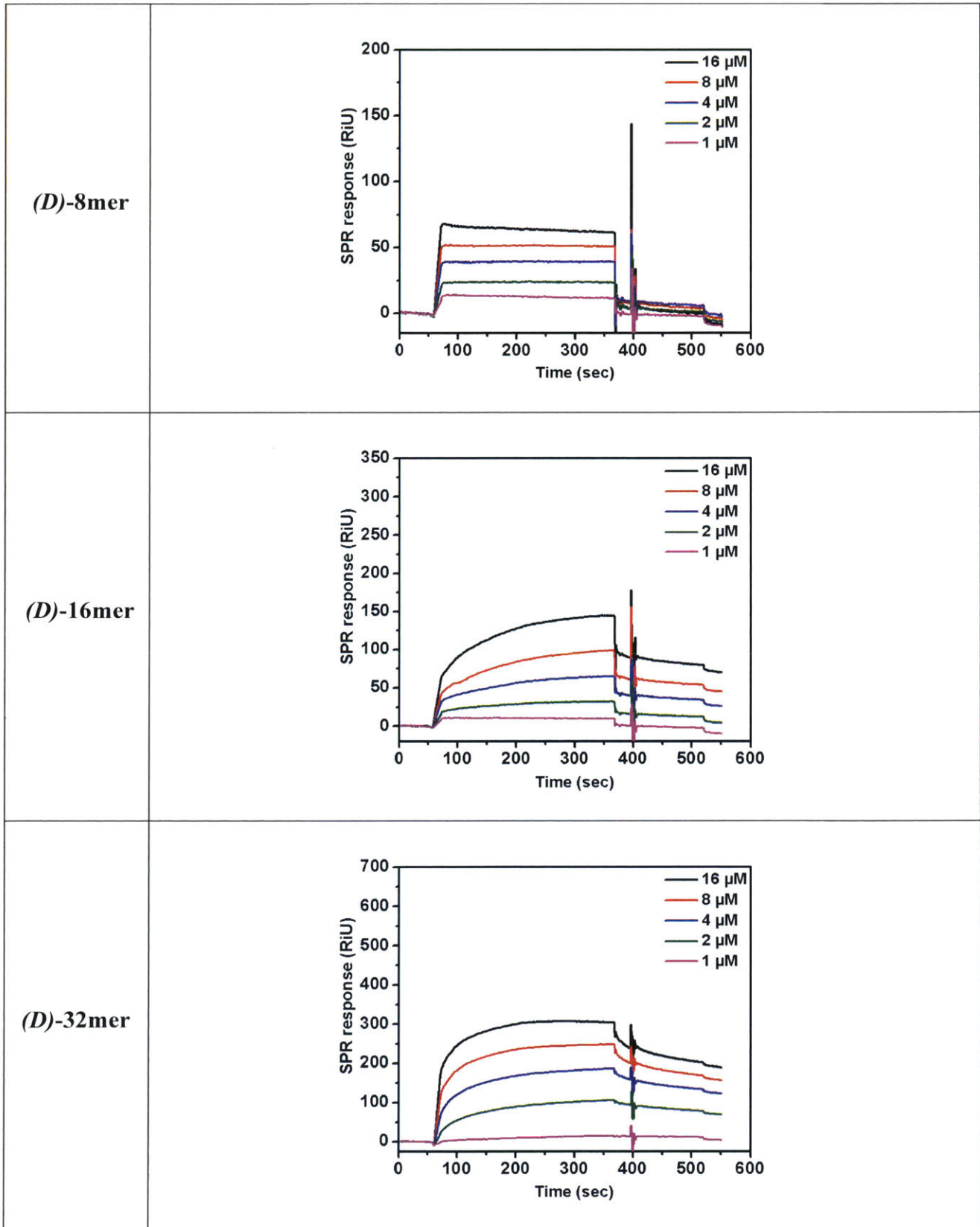
**(alt)-8mer
macrocycle**



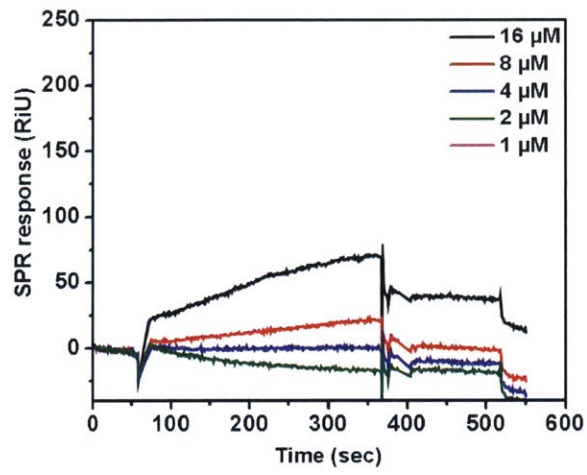
DC-SIGNR

Table S4.2. Kinetic data of binding between glycopolymers and DC-SIGNR as calculated by SPR.				
Ligand	k_a ($M^{-1} s^{-1}$)	k_d (s^{-1})	K_D (M^{-1})	R_{max} (RU)
(L)-32mer	68.1	2.67×10^{-5}	2.55×10^6	380
(alt)-32mer	126	8.66×10^{-4}	1.46×10^5	340
(D)-32mer	85.7	2.69×10^{-4}	3.19×10^5	305
(L)-16mer	27.8	1.26×10^{-5}	2.21×10^6	270
(alt)-16mer	19.7	4.59×10^{-5}	4.29×10^5	210
(D)-16mer	32.3	1.09×10^{-4}	2.95×10^5	145
(L)-8mer	23.9	5.74×10^{-5}	4.17×10^5	110
(alt)-8mer	17.4	3.25×10^{-5}	5.35×10^5	80
(D)-8mer	22.6	9.66×10^{-5}	2.34×10^5	65
(L)-8mer macrocycle	10.8	9.83×10^{-4}	1.1×10^4	100
(alt)-8mer macrocycle	22.2	2.99×10^{-5}	7.41×10^5	380
(D)-8mer macrocycle	2.76	7.25×10^{-5}	3.81×10^4	60

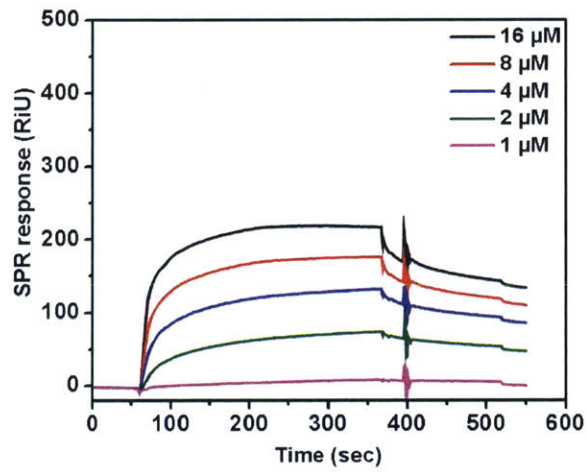
Ligand	
<i>(L)</i> -8mer	 <p>SPR sensorgrams for <i>(L)</i>-8mer ligand at concentrations of 16 μM, 8 μM, 4 μM, 2 μM, and 1 μM. The y-axis is SPR response (RIU) from 0 to 250, and the x-axis is Time (sec) from 0 to 600. The 16 μM curve reaches a maximum response of approximately 110 RIU.</p>
<i>(L)</i> -16mer	 <p>SPR sensorgrams for <i>(L)</i>-16mer ligand at concentrations of 16 μM, 8 μM, 4 μM, 2 μM, and 1 μM. The y-axis is SPR response (RIU) from 0 to 600, and the x-axis is Time (sec) from 0 to 600. The 16 μM curve reaches a maximum response of approximately 260 RIU.</p>
<i>(L)</i> -32mer	 <p>SPR sensorgrams for <i>(L)</i>-32mer ligand at concentrations of 16 μM, 8 μM, 4 μM, 2 μM, and 1 μM. The y-axis is SPR response (RIU) from 0 to 800, and the x-axis is Time (sec) from 0 to 600. The 16 μM curve reaches a maximum response of approximately 360 RIU.</p>



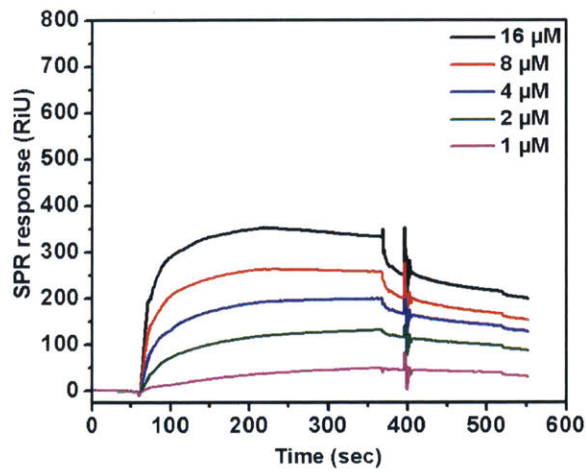
(alt)-8mer

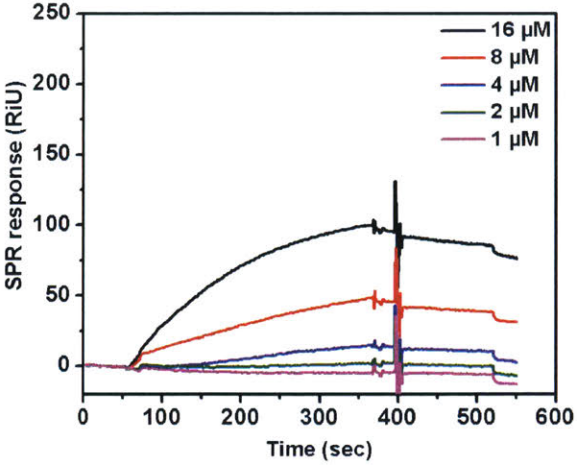
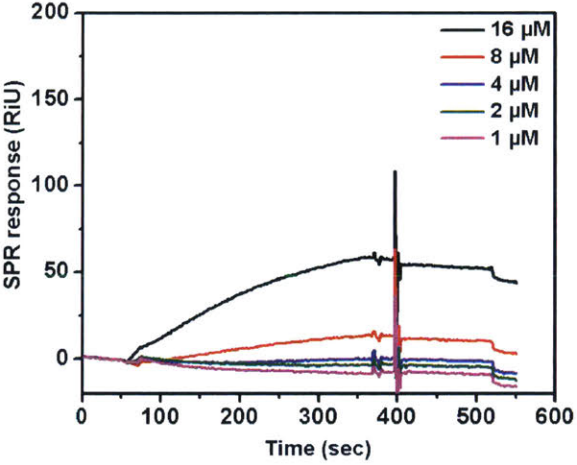
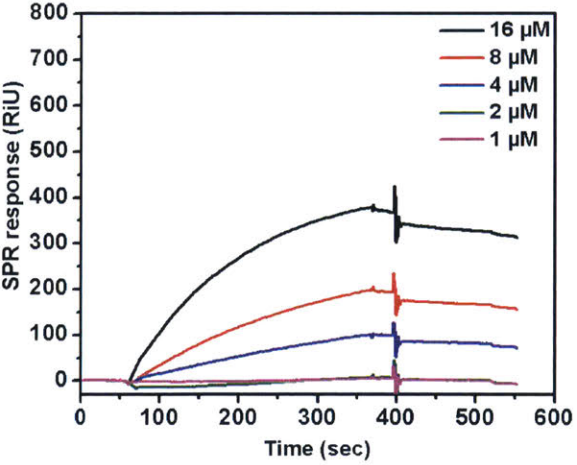


**(alt)-
16mer**



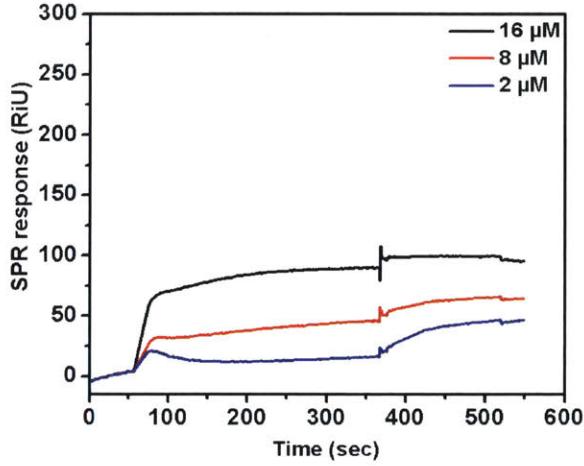
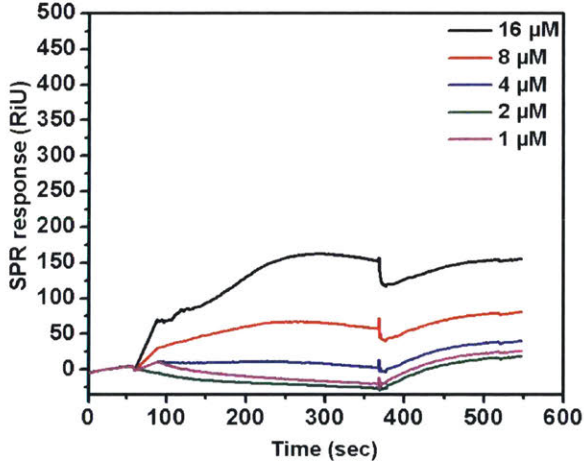
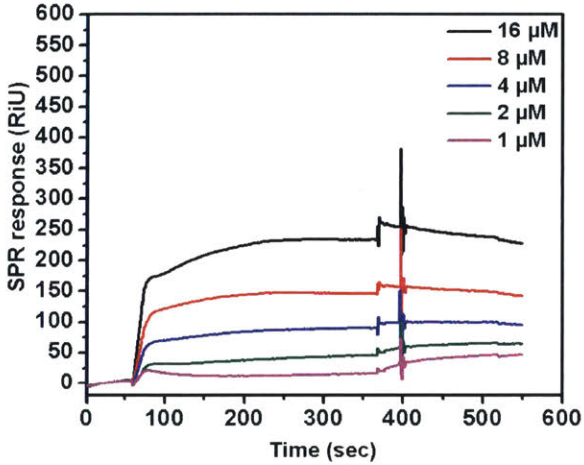
**(alt)-
32mer**

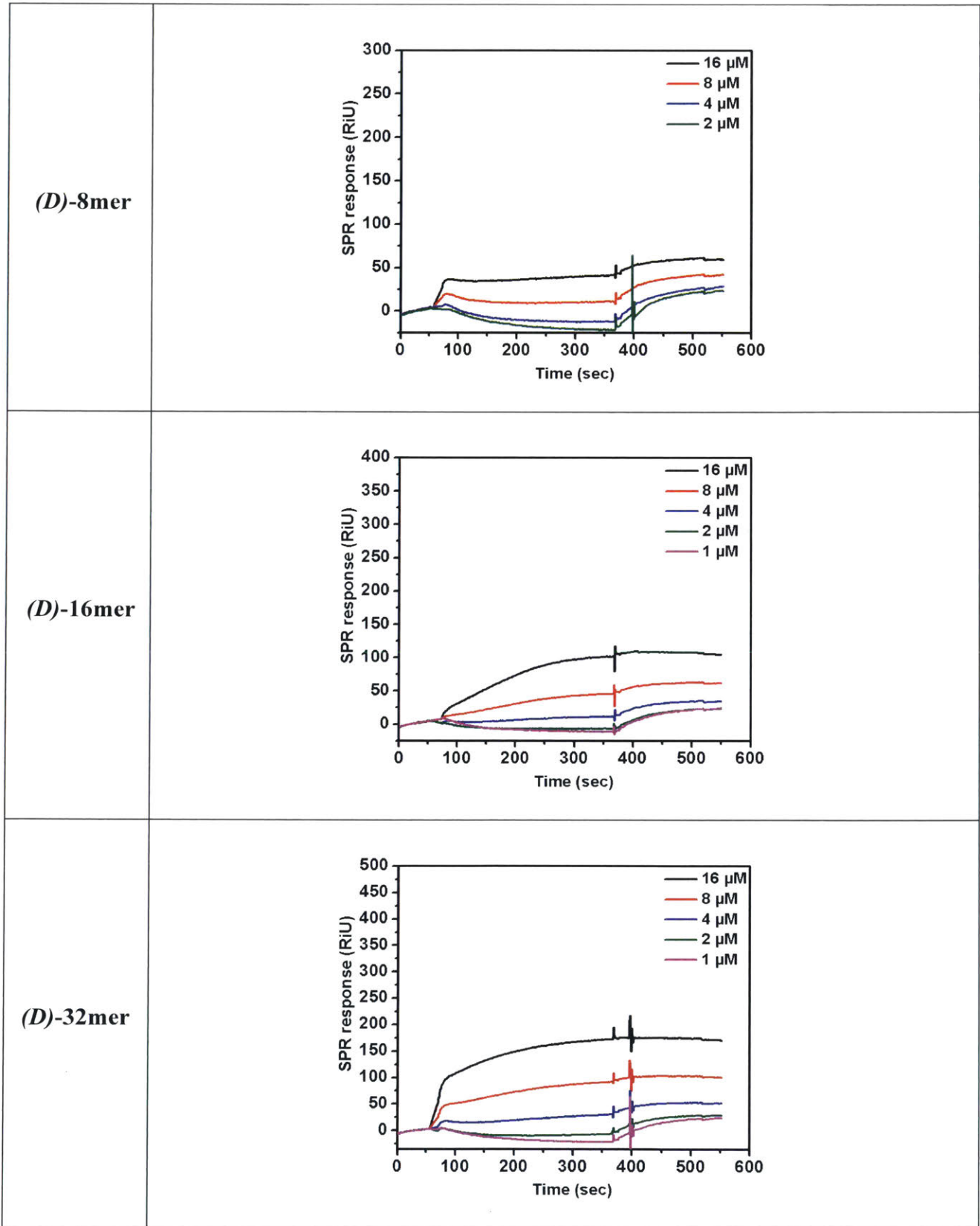


<p>(L)-8mer macrocycle</p>	 <p>SPR response (RiU) vs Time (sec) for (L)-8mer macrocycle. The y-axis ranges from 0 to 250 RiU, and the x-axis ranges from 0 to 600 sec. Five curves are shown for concentrations: 16 μM (black), 8 μM (red), 4 μM (blue), 2 μM (green), and 1 μM (magenta). All curves show an increase in response over time, with a sharp drop at approximately 400 seconds. The 16 μM curve reaches the highest response of approximately 100 RiU.</p>
<p>(D)-8mer macrocycle</p>	 <p>SPR response (RiU) vs Time (sec) for (D)-8mer macrocycle. The y-axis ranges from 0 to 200 RiU, and the x-axis ranges from 0 to 600 sec. Five curves are shown for concentrations: 16 μM (black), 8 μM (red), 4 μM (blue), 2 μM (green), and 1 μM (magenta). All curves show an increase in response over time, with a sharp drop at approximately 400 seconds. The 16 μM curve reaches the highest response of approximately 60 RiU.</p>
<p>(alt)-8mer macrocycle</p>	 <p>SPR response (RiU) vs Time (sec) for (alt)-8mer macrocycle. The y-axis ranges from 0 to 800 RiU, and the x-axis ranges from 0 to 600 sec. Five curves are shown for concentrations: 16 μM (black), 8 μM (red), 4 μM (blue), 2 μM (green), and 1 μM (magenta). All curves show an increase in response over time, with a sharp drop at approximately 400 seconds. The 16 μM curve reaches the highest response of approximately 380 RiU.</p>

DEC-205

Table S4.3. Kinetic data of binding between glycopolymers and DEC-205 as calculated by SPR.				
Ligand	k_a ($M^{-1} s^{-1}$)	k_d (s^{-1})	K_D (M^{-1})	R_{max} (RU)
(L)-32mer	330	1.47×10^{-7}	2.24×10^9	235
(alt)-32mer	248	1.56×10^{-7}	1.59×10^9	180
(D)-32mer	113	2.06×10^{-7}	5.5×10^8	175
(L)-16mer	67.9	3.9×10^{-6}	1.74×10^7	160
(alt)-16mer	40.2	7.77×10^{-7}	5.17×10^7	135
(D)-16mer	51.4	7.45×10^{-7}	6.90×10^7	102
(L)-8mer	31.3	9.12×10^{-7}	3.43×10^7	85
(alt)-8mer	19.7	2.17×10^{-7}	9.08×10^7	70
(D)-8mer	13.1	3.89×10^{-7}	3.37×10^7	45
(L)-8mer macrocycle	18	8.62×10^{-6}	2.09×10^6	340
(alt)-8mer macrocycle	23.8	7.33×10^{-6}	3.25×10^6	395
(D)-8mer macrocycle	12.3	2.31×10^{-6}	5.32×10^6	300

Ligand	
(L)-8mer	 <p>SPR response (RIU) vs Time (sec) for (L)-8mer. The plot shows three curves corresponding to different concentrations: 16 μM (black), 8 μM (red), and 2 μM (blue). The y-axis ranges from 0 to 300 RIU, and the x-axis ranges from 0 to 600 seconds. All curves show an initial rapid increase in response, followed by a slower approach to a steady-state plateau. The 16 μM curve reaches the highest plateau at approximately 90 RIU, the 8 μM curve reaches approximately 60 RIU, and the 2 μM curve reaches approximately 45 RIU. A small step change is visible at approximately 380 seconds.</p>
(L)-16mer	 <p>SPR response (RIU) vs Time (sec) for (L)-16mer. The plot shows five curves corresponding to different concentrations: 16 μM (black), 8 μM (red), 4 μM (blue), 2 μM (green), and 1 μM (magenta). The y-axis ranges from 0 to 500 RIU, and the x-axis ranges from 0 to 600 seconds. All curves show an initial rapid increase in response, followed by a slower approach to a steady-state plateau. The 16 μM curve reaches the highest plateau at approximately 150 RIU, the 8 μM curve reaches approximately 75 RIU, the 4 μM curve reaches approximately 35 RIU, the 2 μM curve reaches approximately 20 RIU, and the 1 μM curve reaches approximately 10 RIU. A small step change is visible at approximately 380 seconds.</p>
(L)-32mer	 <p>SPR response (RIU) vs Time (sec) for (L)-32mer. The plot shows five curves corresponding to different concentrations: 16 μM (black), 8 μM (red), 4 μM (blue), 2 μM (green), and 1 μM (magenta). The y-axis ranges from 0 to 600 RIU, and the x-axis ranges from 0 to 600 seconds. All curves show an initial rapid increase in response, followed by a slower approach to a steady-state plateau. The 16 μM curve reaches the highest plateau at approximately 230 RIU, the 8 μM curve reaches approximately 140 RIU, the 4 μM curve reaches approximately 80 RIU, the 2 μM curve reaches approximately 50 RIU, and the 1 μM curve reaches approximately 30 RIU. A small step change is visible at approximately 380 seconds.</p>



<p>(alt)-8mer</p>	
<p>(alt)-16mer</p>	
<p>(alt)-32mer</p>	

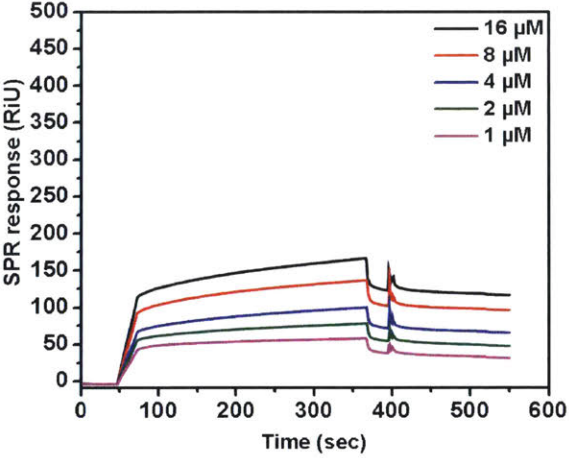
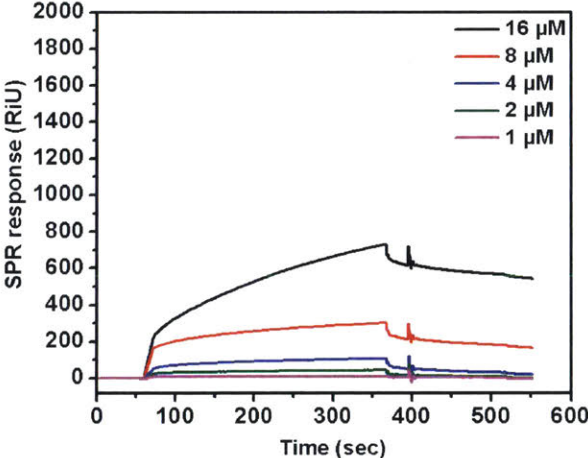
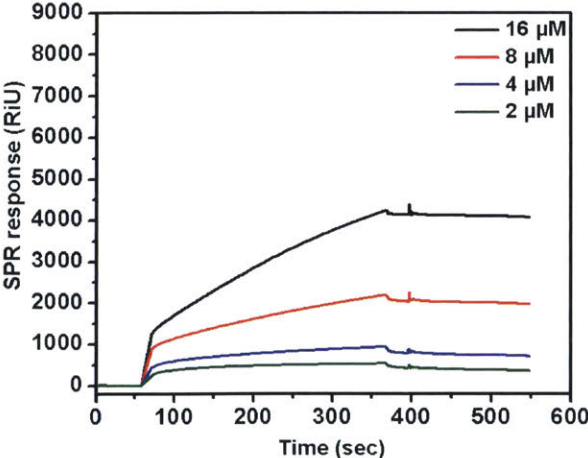
<p>(L)-8mer macrocycle</p>	<p>SPR response (RiU)</p> <p>Time (sec)</p> <p>16 μM 8 μM 2 μM</p>
<p>(D)-8mer macrocycle</p>	<p>SPR response (RiU)</p> <p>Time (sec)</p> <p>16 μM 8 μM 2 μM</p>
<p>(alt)-8mer macrocycle</p>	<p>SPR response (RiU)</p> <p>Time (sec)</p> <p>16 μM 8 μM 4 μM 2 μM 1 μM</p>

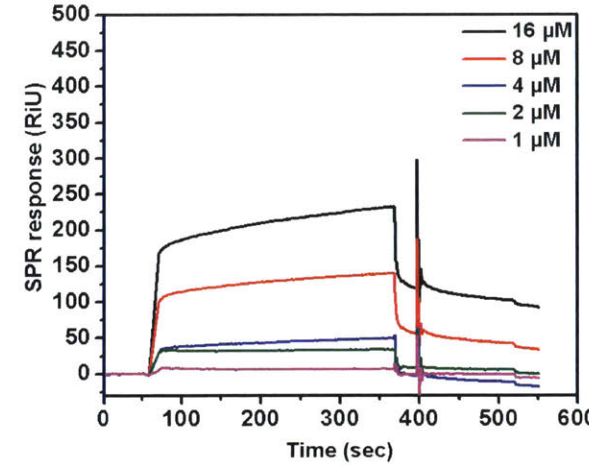
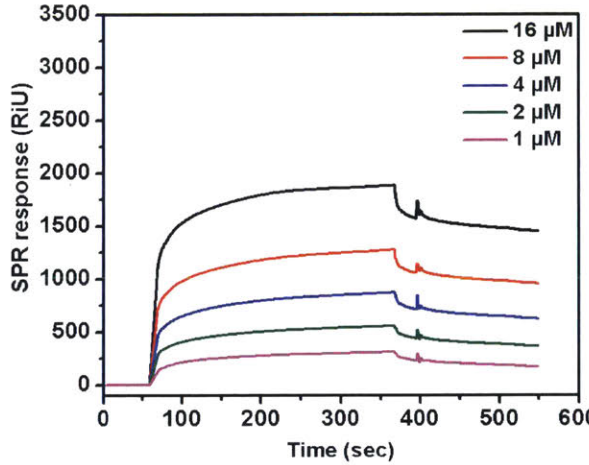
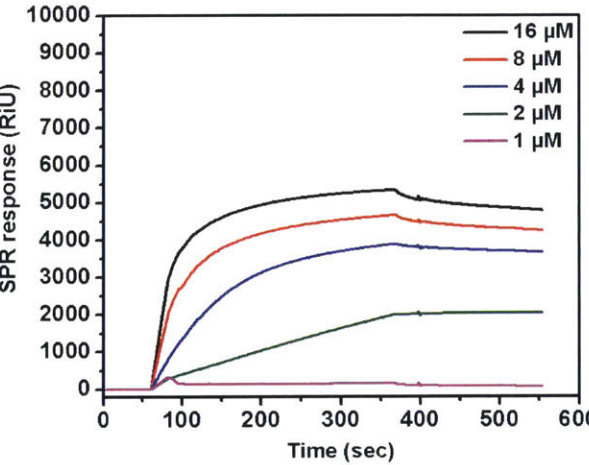
MBL

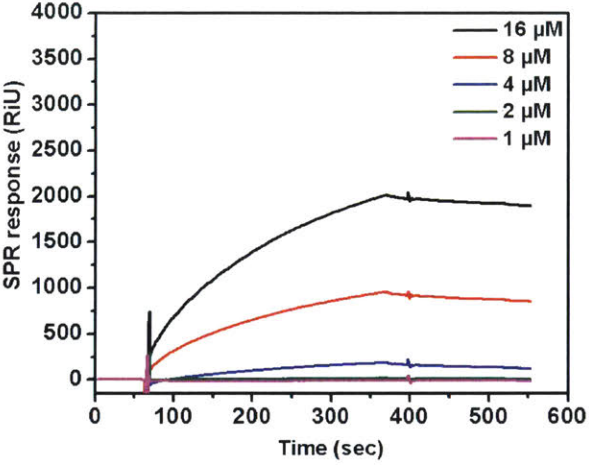
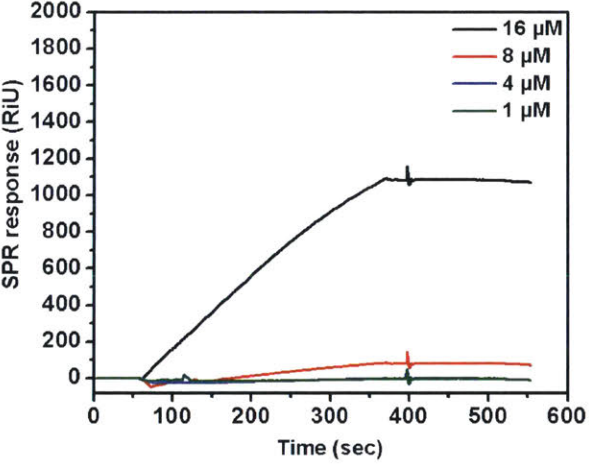
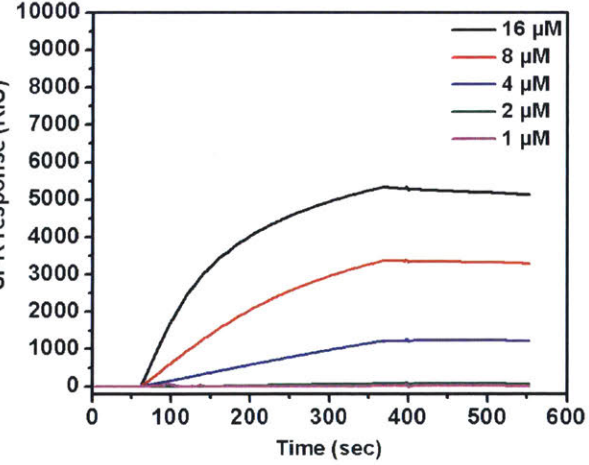
Table S4.4. Kinetic data of binding between glycopolymers and MBL as calculated by SPR.

Ligand	k_a ($M^{-1} s^{-1}$)	k_d (s^{-1})	K_D (M^{-1})	R_{max} (RU)
(L)-32mer	112	2.39×10^{-6}	4.67×10^7	5575
(alt)-32mer	103	1.44×10^{-6}	7.15×10^7	5340
(D)-32mer	83.9	1.61×10^{-6}	5.21×10^7	4210
(L)-16mer	185	9.81×10^{-6}	1.89×10^7	2790
(alt)-16mer	144	1.6×10^{-6}	9.00×10^7	1885
(D)-16mer	102.7	1.02×10^{-5}	1.01×10^7	725
(L)-8mer	11.3	2.42×10^{-6}	4.69×10^6	470
(alt)-8mer	4.9	2.63×10^{-6}	1.86×10^6	235
(D)-8mer	5.1	9.66×10^{-5}	0.53×10^5	175
(L)-8mer macrocycle	49	6.23×10^{-6}	7.86×10^6	2005
(alt)-8mer macrocycle	97.8	4.56×10^{-6}	2.14×10^7	5320
(D)-8mer macrocycle	34.5	1.82×10^{-6}	1.89×10^7	1080

Ligand	
(L)-8mer	
(L)-16mer	
(L)-32mer	

<p>(D)-8mer</p>	 <p>SPR response (RiU) vs Time (sec) for (D)-8mer. The y-axis ranges from 0 to 500 RiU, and the x-axis ranges from 0 to 600 sec. Five curves are shown for concentrations: 16 μM (black), 8 μM (red), 4 μM (blue), 2 μM (green), and 1 μM (magenta). All curves show a sharp increase in response starting around 50 seconds, reaching a plateau between 300 and 400 seconds. The 16 μM curve reaches the highest plateau at approximately 160 RiU, while the 1 μM curve reaches the lowest at approximately 40 RiU. A small dip in response is observed at approximately 380 seconds for all curves, likely due to buffer exchange.</p>
<p>(D)-16mer</p>	 <p>SPR response (RiU) vs Time (sec) for (D)-16mer. The y-axis ranges from 0 to 2000 RiU, and the x-axis ranges from 0 to 600 sec. Five curves are shown for concentrations: 16 μM (black), 8 μM (red), 4 μM (blue), 2 μM (green), and 1 μM (magenta). The 16 μM curve shows the highest response, reaching a plateau of approximately 700 RiU. The 8 μM curve reaches approximately 300 RiU, 4 μM reaches approximately 100 RiU, 2 μM reaches approximately 50 RiU, and 1 μM reaches approximately 20 RiU. A dip in response is visible at approximately 380 seconds.</p>
<p>(D)-32mer</p>	 <p>SPR response (RiU) vs Time (sec) for (D)-32mer. The y-axis ranges from 0 to 9000 RiU, and the x-axis ranges from 0 to 600 sec. Four curves are shown for concentrations: 16 μM (black), 8 μM (red), 4 μM (blue), and 2 μM (green). The 16 μM curve reaches the highest response, peaking at approximately 4200 RiU. The 8 μM curve reaches approximately 2000 RiU, 4 μM reaches approximately 800 RiU, and 2 μM reaches approximately 400 RiU. A dip in response is visible at approximately 380 seconds.</p>

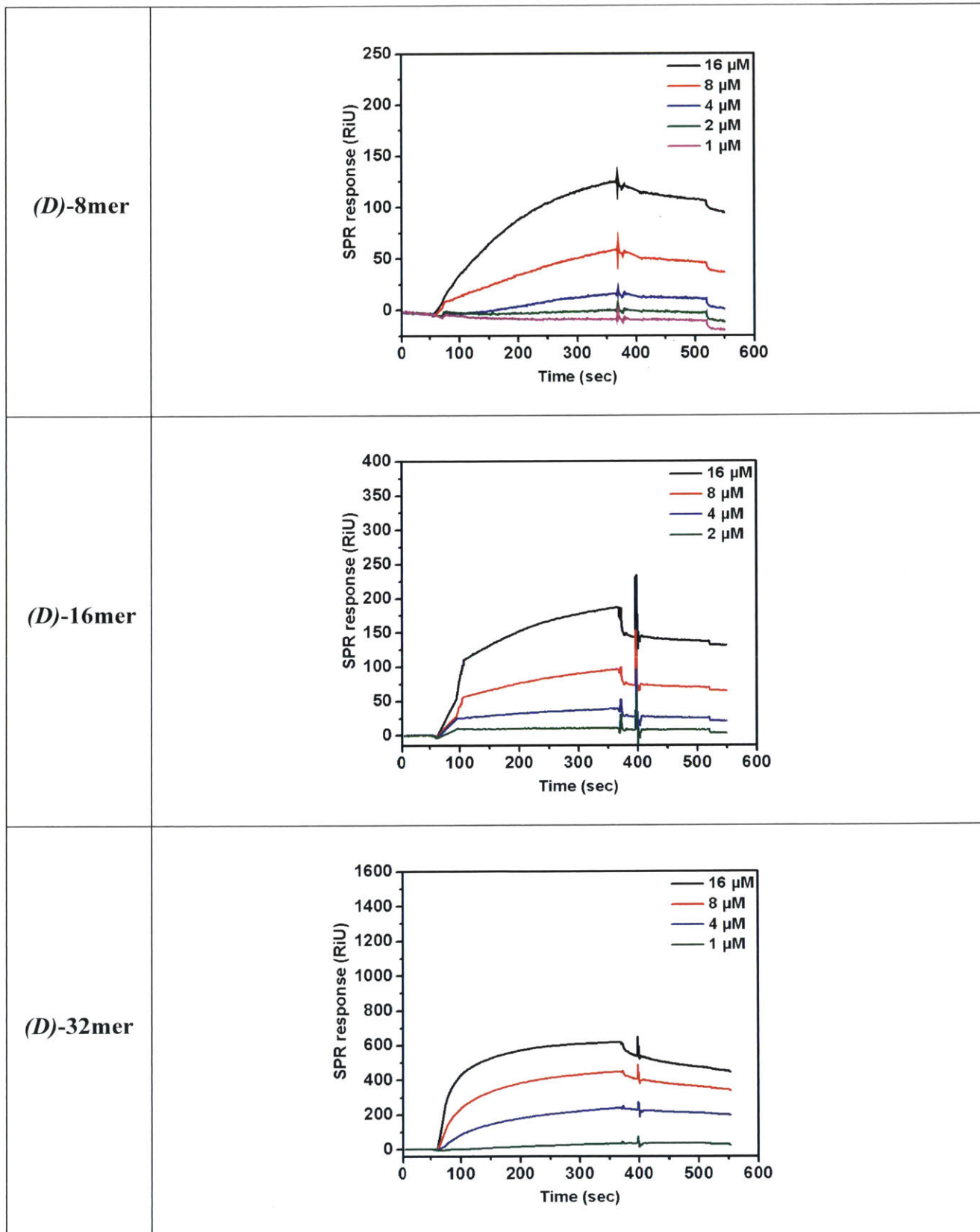
<p>(alt)-8mer</p>	 <p>SPR response (RiU) vs Time (sec) for (alt)-8mer. The y-axis ranges from 0 to 500 RiU, and the x-axis ranges from 0 to 600 sec. Five curves are shown for concentrations: 16 μM (black), 8 μM (red), 4 μM (blue), 2 μM (green), and 1 μM (magenta). All curves show a sharp increase in response starting around 50 seconds, reaching a plateau between 100 and 250 RiU by 100 seconds. At approximately 380 seconds, there is a sharp drop in response for all concentrations, followed by a partial recovery to a lower baseline level.</p>
<p>(alt)-16mer</p>	 <p>SPR response (RiU) vs Time (sec) for (alt)-16mer. The y-axis ranges from 0 to 3500 RiU, and the x-axis ranges from 0 to 600 sec. Five curves are shown for concentrations: 16 μM (black), 8 μM (red), 4 μM (blue), 2 μM (green), and 1 μM (magenta). The curves show a sharp increase in response starting around 50 seconds, reaching a plateau between 200 and 1800 RiU by 100 seconds. At approximately 380 seconds, there is a sharp drop in response, followed by a partial recovery to a lower baseline level.</p>
<p>(alt)-32mer</p>	 <p>SPR response (RiU) vs Time (sec) for (alt)-32mer. The y-axis ranges from 0 to 10000 RiU, and the x-axis ranges from 0 to 600 sec. Five curves are shown for concentrations: 16 μM (black), 8 μM (red), 4 μM (blue), 2 μM (green), and 1 μM (magenta). The curves show a sharp increase in response starting around 50 seconds, reaching a plateau between 2000 and 5000 RiU by 100 seconds. At approximately 380 seconds, there is a sharp drop in response, followed by a partial recovery to a lower baseline level.</p>

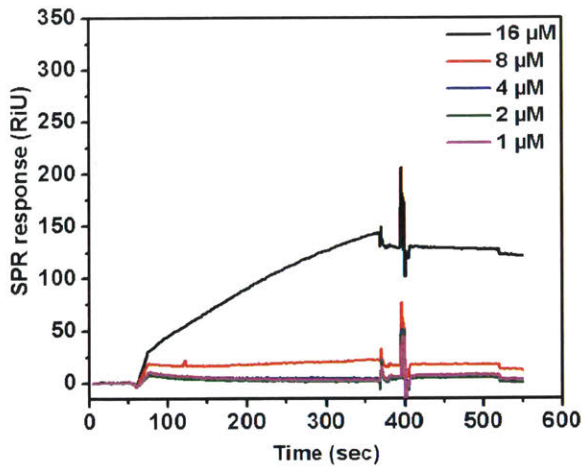
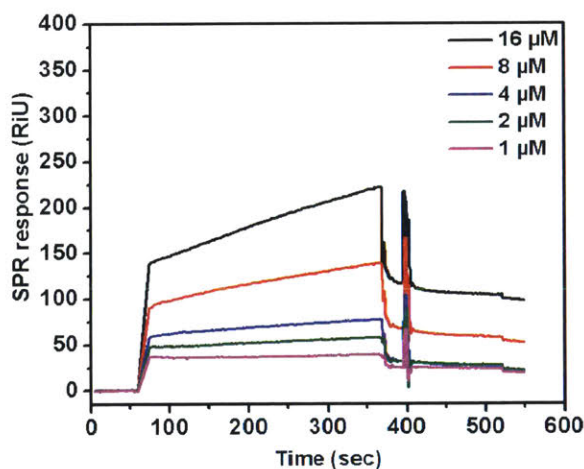
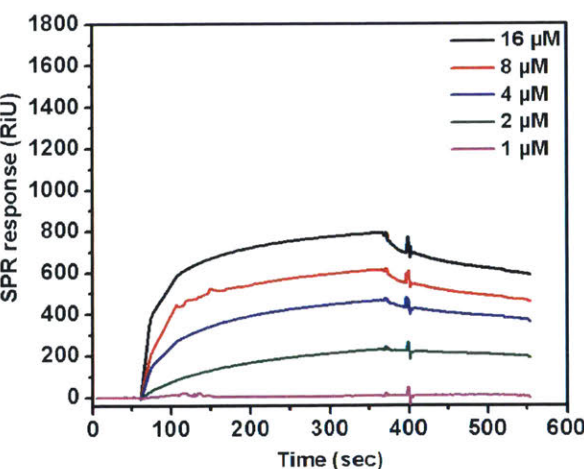
<p>(L)-8mer macrocycle</p>	 <p>SPR response (RIU) vs Time (sec) for (L)-8mer macrocycle. The graph shows five curves for concentrations of 16 μM (black), 8 μM (red), 4 μM (blue), 2 μM (grey), and 1 μM (pink). The 16 μM curve reaches a plateau of approximately 1900 RIU, while the 1 μM curve remains near 0 RIU.</p>
<p>(D)-8mer macrocycle</p>	 <p>SPR response (RIU) vs Time (sec) for (D)-8mer macrocycle. The graph shows four curves for concentrations of 16 μM (black), 8 μM (red), 4 μM (blue), and 1 μM (grey). The 16 μM curve reaches a plateau of approximately 1050 RIU, while the 1 μM curve remains near 0 RIU.</p>
<p>(alt)-8mer macrocycle</p>	 <p>SPR response (RIU) vs Time (sec) for (alt)-8mer macrocycle. The graph shows five curves for concentrations of 16 μM (black), 8 μM (red), 4 μM (blue), 2 μM (grey), and 1 μM (pink). The 16 μM curve reaches a plateau of approximately 5000 RIU, while the 1 μM curve remains near 0 RIU.</p>

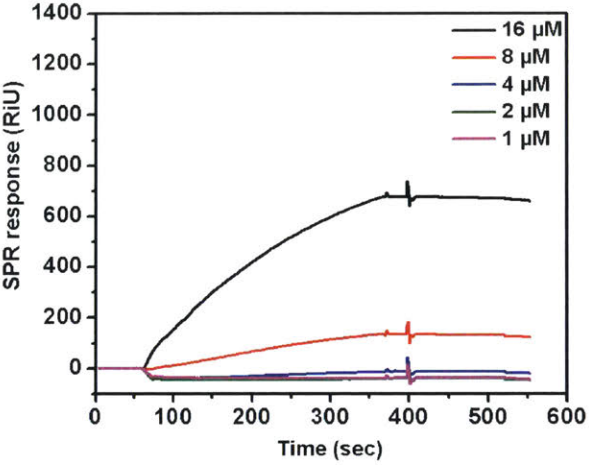
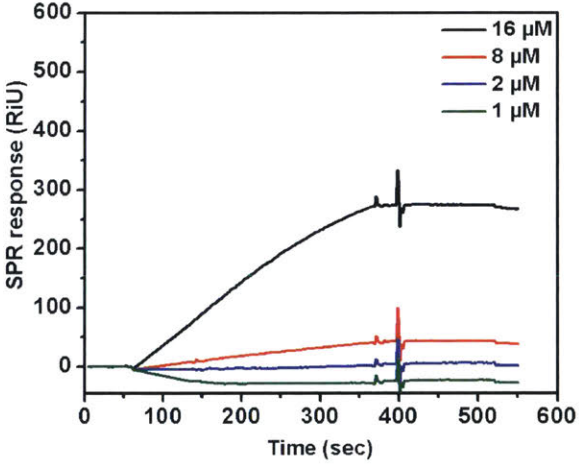
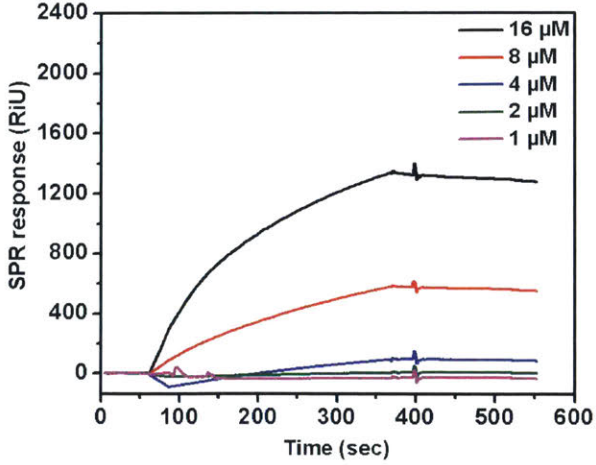
SP-D

Table S4.5. Kinetic data of binding between glycopolymers and SPD as calculated by SPR.				
Ligand	k_a ($M^{-1} s^{-1}$)	k_d (s^{-1})	K_D (M^{-1})	R_{max} (RU)
(L)-32mer	90.7	3.01×10^{-6}	3.01×10^7	1140
(alt)-32mer	73.7	1.8×10^{-6}	4.09×10^7	790
(D)-32mer	60.5	3.07×10^{-6}	1.97×10^7	730
(L)-16mer	277	4.03×10^{-6}	6.87×10^7	360
(alt)-16mer	147	3.71×10^{-5}	3.96×10^6	220
(D)-16mer	96.7	1.86×10^{-5}	5.19×10^6	190
(L)-8mer	2.39	5.74×10^{-5}	4.17×10^4	170
(alt)-8mer	1.59	7.22×10^{-6}	2.21×10^5	145
(D)-8mer	2.6	9.66×10^{-5}	0.27×10^5	110
(L)-8mer macrocycle	7.78	5.78×10^{-6}	1.34×10^6	675
(alt)-8mer macrocycle	41.7	6.27×10^{-6}	6.65×10^6	1340
(D)-8mer macrocycle	3.22	3.99×10^{-6}	0.80×10^6	270

Ligand	
(L)-8mer	<p>SPR sensorgrams for (L)-8mer ligand at concentrations of 16 μM, 8 μM, 4 μM, 2 μM, and 1 μM. The y-axis is SPR response (RIU) from 0 to 400, and the x-axis is Time (sec) from 0 to 600. The 16 μM curve reaches a plateau of ~160 RIU, while the 1 μM curve remains near 0.</p>
(L)-16mer	<p>SPR sensorgrams for (L)-16mer ligand at concentrations of 16 μM, 8 μM, 4 μM, 2 μM, and 1 μM. The y-axis is SPR response (RIU) from 0 to 900, and the x-axis is Time (sec) from 0 to 600. The 16 μM curve reaches a plateau of ~350 RIU, while the 1 μM curve remains near 0.</p>
(L)-32mer	<p>SPR sensorgrams for (L)-32mer ligand at concentrations of 16 μM, 8 μM, 4 μM, and 2 μM. The y-axis is SPR response (RIU) from 0 to 2000, and the x-axis is Time (sec) from 0 to 600. The 16 μM curve reaches a plateau of ~1100 RIU, while the 2 μM curve reaches ~100 RIU.</p>



<p>(alt)-8mer</p>	 <p>SPR response (RIU) vs Time (sec) for (alt)-8mer. The graph shows five curves for concentrations 16 μM (black), 8 μM (red), 4 μM (blue), 2 μM (green), and 1 μM (purple). The 16 μM curve reaches a maximum response of approximately 140 RIU at 350 seconds. All curves show a sharp dip at 400 seconds, likely due to a buffer change.</p>
<p>(alt)-16mer</p>	 <p>SPR response (RIU) vs Time (sec) for (alt)-16mer. The graph shows five curves for concentrations 16 μM (black), 8 μM (red), 4 μM (blue), 2 μM (green), and 1 μM (purple). The 16 μM curve reaches a maximum response of approximately 220 RIU at 350 seconds. All curves show a sharp dip at 400 seconds.</p>
<p>(alt)-32mer</p>	 <p>SPR response (RIU) vs Time (sec) for (alt)-32mer. The graph shows five curves for concentrations 16 μM (black), 8 μM (red), 4 μM (blue), 2 μM (green), and 1 μM (purple). The 16 μM curve reaches a maximum response of approximately 750 RIU at 350 seconds. All curves show a sharp dip at 400 seconds.</p>

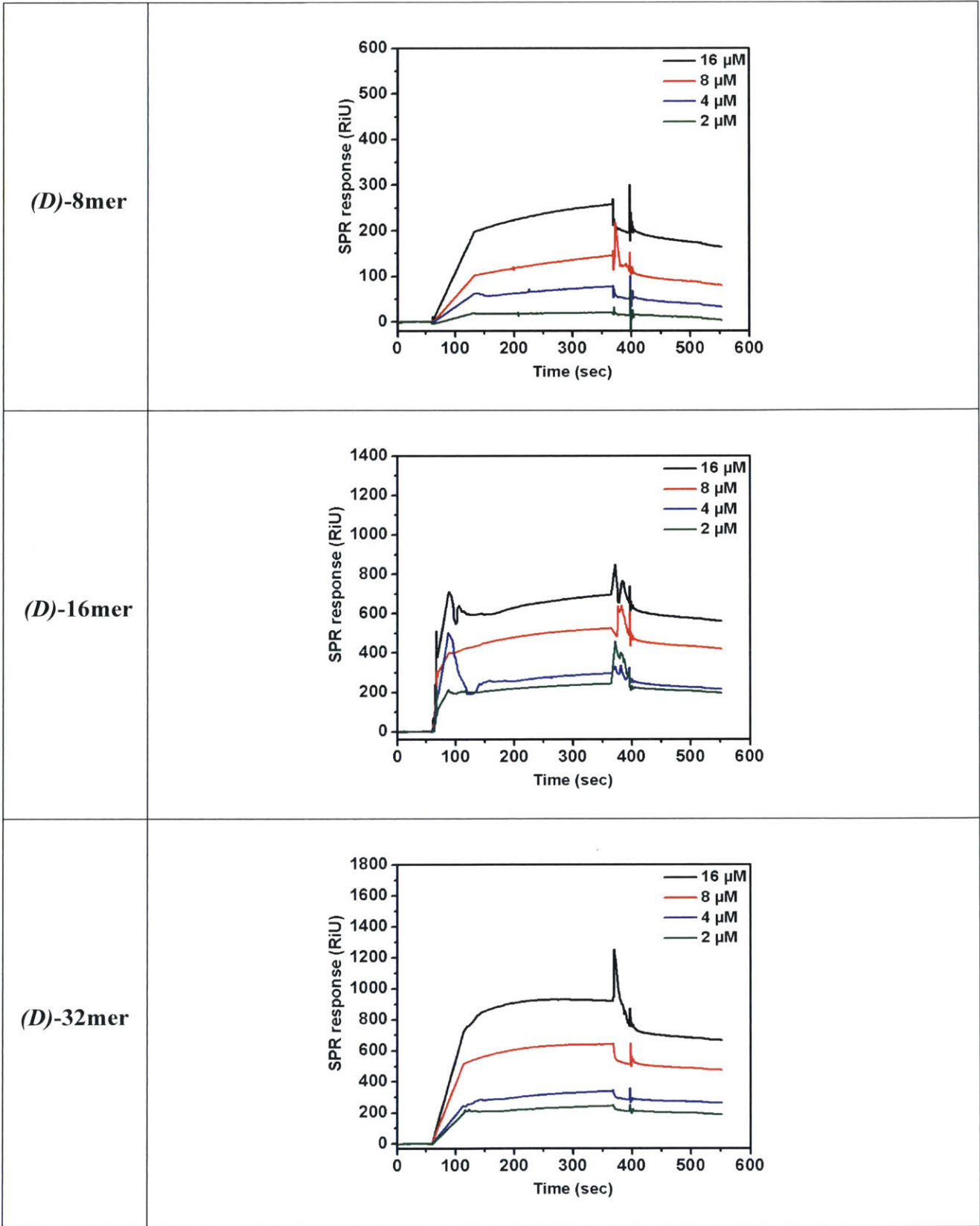
<p>(L)-8mer macrocycle</p>	 <p>SPR response (RiU) vs Time (sec) for (L)-8mer macrocycle. The graph shows five curves for concentrations: 16 μM (black), 8 μM (red), 4 μM (blue), 2 μM (grey), and 1 μM (magenta). The 16 μM curve reaches a plateau of approximately 680 RiU. The 8 μM curve reaches approximately 150 RiU. The other three curves remain near 0 RiU.</p>
<p>(D)-8mer macrocycle</p>	 <p>SPR response (RiU) vs Time (sec) for (D)-8mer macrocycle. The graph shows four curves for concentrations: 16 μM (black), 8 μM (red), 2 μM (blue), and 1 μM (grey). The 16 μM curve reaches a plateau of approximately 280 RiU. The 8 μM curve reaches approximately 50 RiU. The 2 μM and 1 μM curves remain near 0 RiU.</p>
<p>(alt)-8mer macrocycle</p>	 <p>SPR response (RiU) vs Time (sec) for (alt)-8mer macrocycle. The graph shows five curves for concentrations: 16 μM (black), 8 μM (red), 4 μM (blue), 2 μM (grey), and 1 μM (magenta). The 16 μM curve reaches a plateau of approximately 1350 RiU. The 8 μM curve reaches approximately 550 RiU. The 4 μM curve reaches approximately 100 RiU. The 2 μM and 1 μM curves remain near 0 RiU.</p>

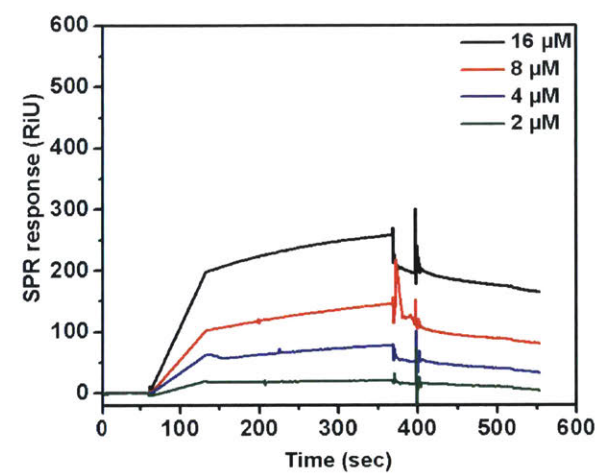
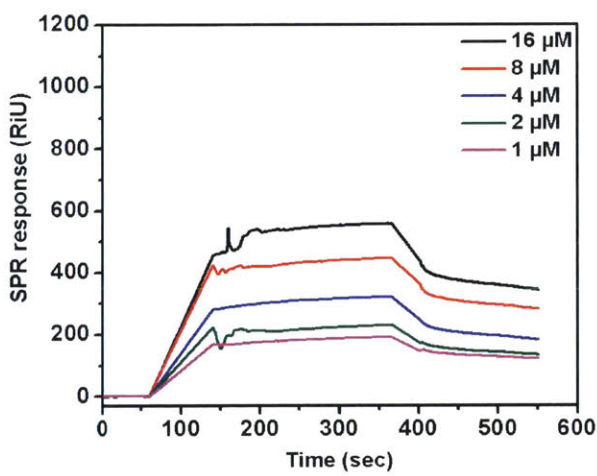
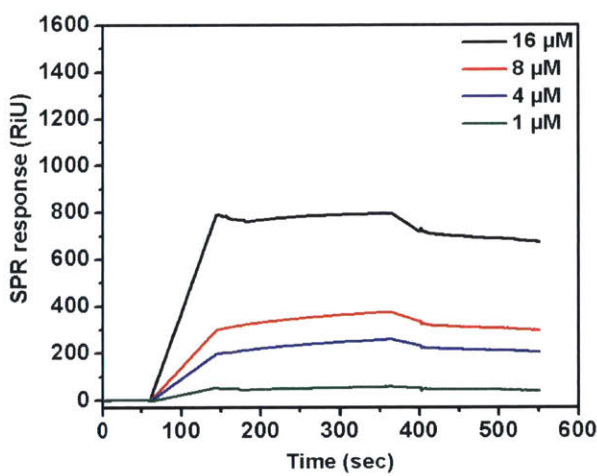
Langerin

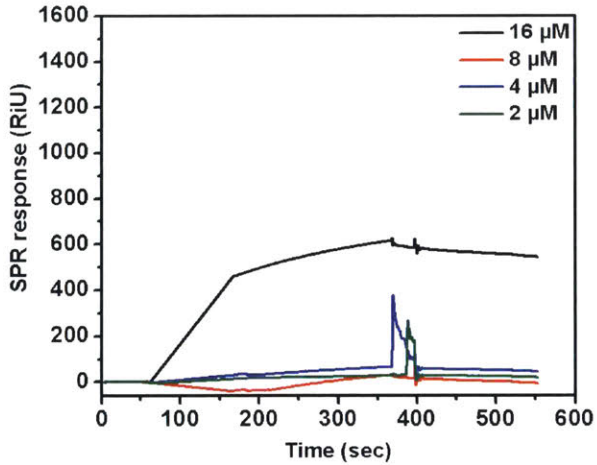
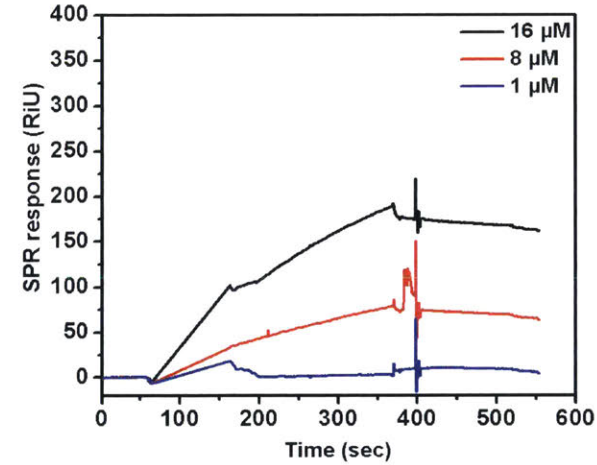
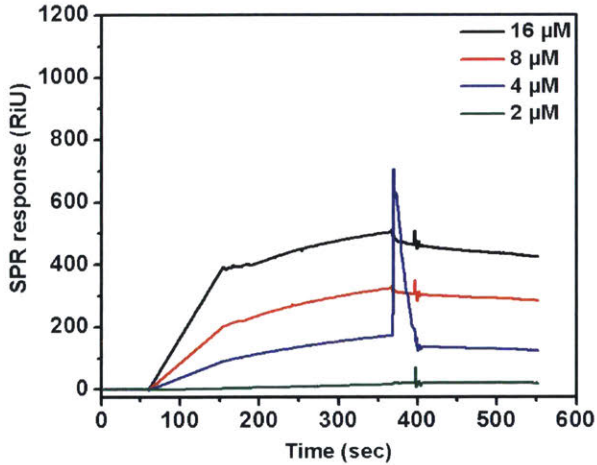
Table S4.6. Kinetic data of binding between glycopolymers and Langerin as calculated by SPR.

Ligand	k_a ($M^{-1} s^{-1}$)	k_d (s^{-1})	K_D (M^{-1})	R_{max} (RU)
(L)-32mer	87.3	2.06×10^{-6}	4.23×10^7	825
(alt)-32mer	41.5	5.38×10^{-6}	7.72×10^6	795
(D)-32mer	134.7	3.79×10^{-6}	3.55×10^7	925
(L)-16mer	48.4	8.01×10^{-6}	6.05×10^6	550
(alt)-16mer	41.3	6.82×10^{-5}	6.05×10^5	360
(D)-16mer	147.7	3.71×10^{-5}	3.96×10^6	695
(L)-8mer	11.5	1.03×10^{-5}	1.14×10^6	270
(alt)-8mer	3.85	2.09×10^{-6}	1.84×10^6	260
(D)-8mer	20.3	4.37×10^{-7}	4.65×10^7	350
(L)-8mer macrocycle	25.7	7.55×10^{-6}	3.4×10^6	615
(alt)-8mer macrocycle	19.1	2.94×10^{-6}	6.50×10^6	500
(D)-8mer macrocycle	8.39	4.76×10^{-6}	1.76×10^6	190

Ligand	
<i>(L)</i> -8mer	
<i>(L)</i> -16mer	
<i>(L)</i> -32mer	

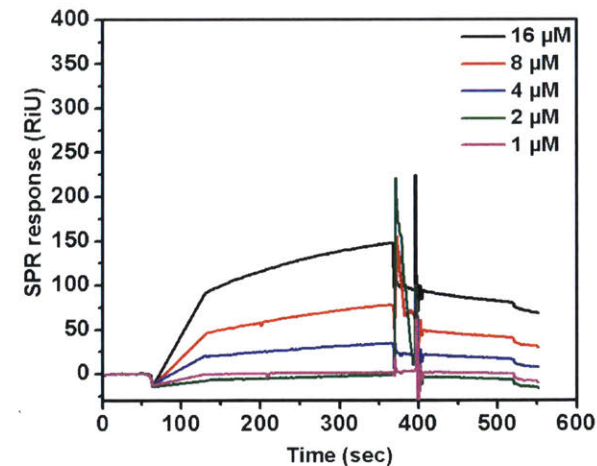
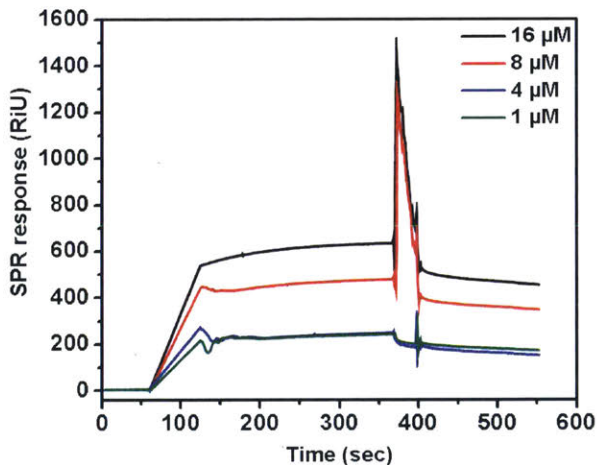
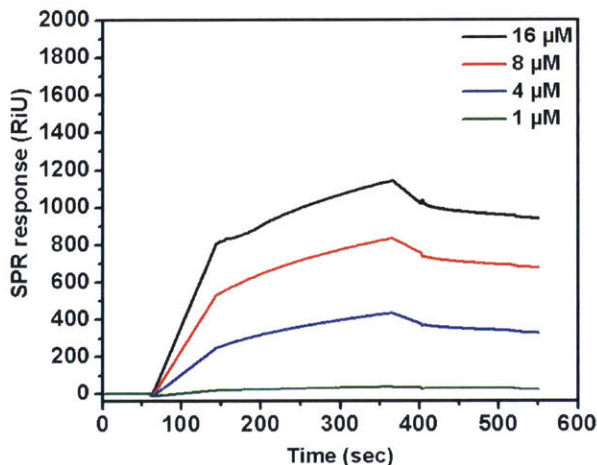


<p>(alt)-8mer</p>	 <p>SPR response (RiU) vs Time (sec) for (alt)-8mer. The graph shows four curves for concentrations of 16 μM (black), 8 μM (red), 4 μM (blue), and 2 μM (green). The 16 μM curve reaches the highest response of approximately 250 RiU. All curves show a sharp dip at approximately 380 seconds.</p>
<p>(alt)-16mer</p>	 <p>SPR response (RiU) vs Time (sec) for (alt)-16mer. The graph shows five curves for concentrations of 16 μM (black), 8 μM (red), 4 μM (blue), 2 μM (green), and 1 μM (magenta). The 16 μM curve reaches the highest response of approximately 550 RiU. All curves show a sharp dip at approximately 380 seconds.</p>
<p>(alt)-32mer</p>	 <p>SPR response (RiU) vs Time (sec) for (alt)-32mer. The graph shows four curves for concentrations of 16 μM (black), 8 μM (red), 4 μM (blue), and 1 μM (green). The 16 μM curve reaches the highest response of approximately 750 RiU. All curves show a sharp dip at approximately 380 seconds.</p>

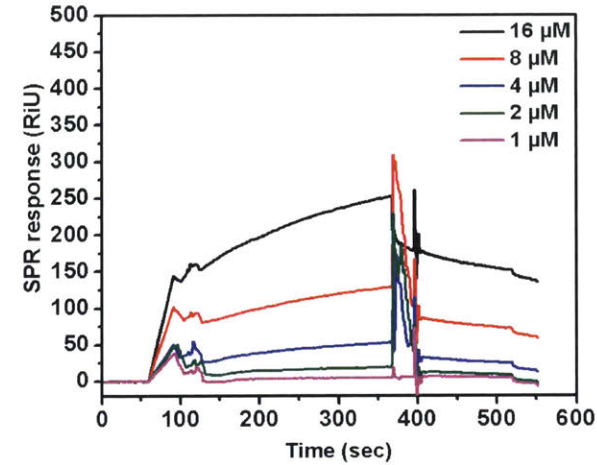
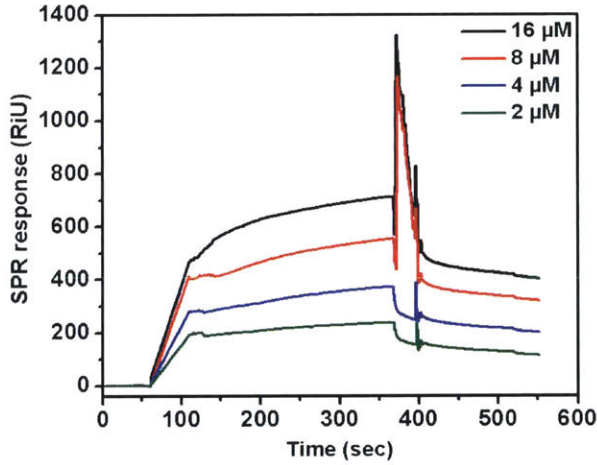
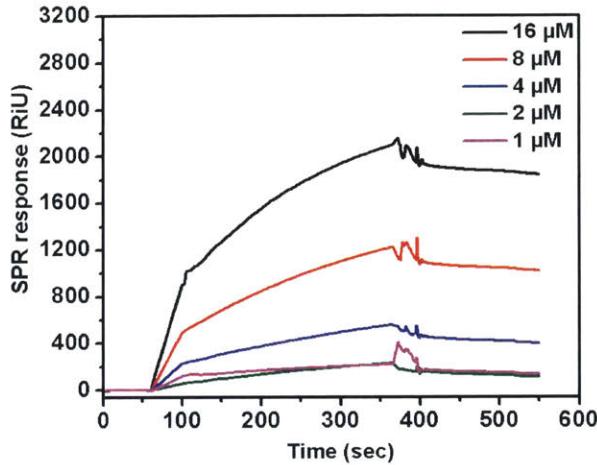
<p>(L)-8mer macrocycle</p>	 <p>SPR response (RIU) vs Time (sec) for (L)-8mer macrocycle. The graph shows four curves for concentrations of 16 μM (black), 8 μM (red), 4 μM (blue), and 2 μM (grey). The 16 μM curve shows the highest response, reaching approximately 600 RIU. The 4 μM curve shows a sharp peak at approximately 380 seconds, reaching about 400 RIU. The 8 μM and 2 μM curves show much lower responses, around 100 and 50 RIU respectively.</p>
<p>(D)-8mer macrocycle</p>	 <p>SPR response (RIU) vs Time (sec) for (D)-8mer macrocycle. The graph shows three curves for concentrations of 16 μM (black), 8 μM (red), and 1 μM (blue). The 16 μM curve reaches a steady-state response of about 170 RIU. The 8 μM curve reaches about 70 RIU. The 1 μM curve shows a very low response, around 10 RIU.</p>
<p>(alt)-8mer macrocycle</p>	 <p>SPR response (RIU) vs Time (sec) for (alt)-8mer macrocycle. The graph shows four curves for concentrations of 16 μM (black), 8 μM (red), 4 μM (blue), and 2 μM (grey). The 16 μM curve reaches about 450 RIU. The 8 μM curve reaches about 300 RIU. The 4 μM curve shows a sharp peak at approximately 380 seconds, reaching about 700 RIU. The 2 μM curve shows a very low response, around 20 RIU.</p>

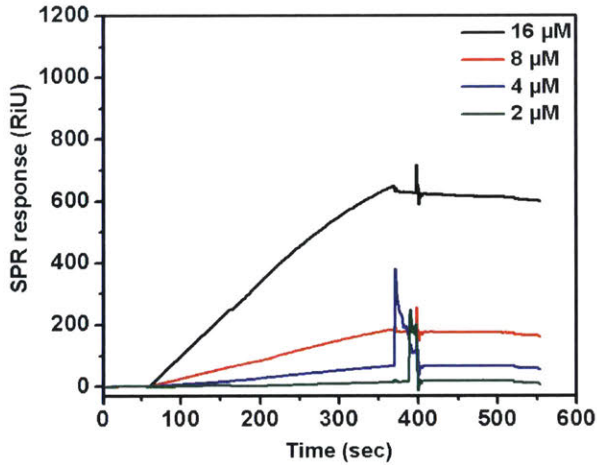
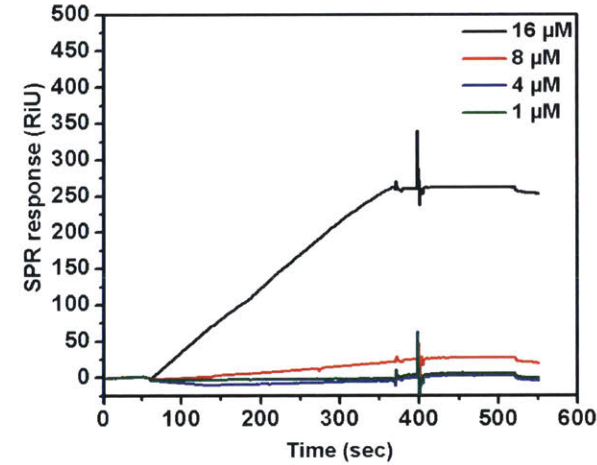
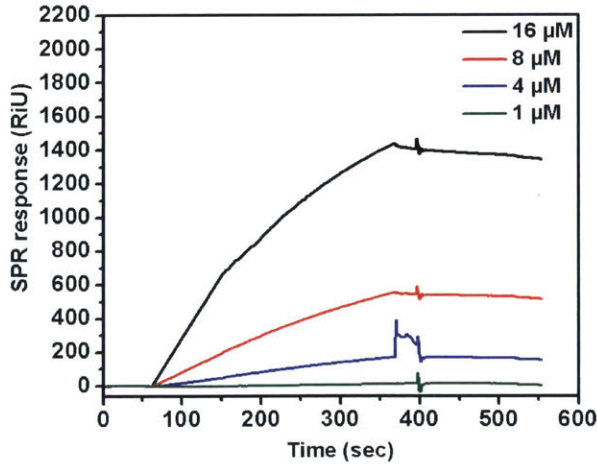
Dectin-2

Ligand	k_a ($M^{-1} s^{-1}$)	k_d (s^{-1})	K_D (M^{-1})	R_{max} (RU)
(L)-32mer	85.1	3.29×10^{-7}	2.59×10^8	1140
(alt)-32mer	167	4.92×10^{-7}	3.39×10^8	2085
(D)-32mer	33.9	1.25×10^{-7}	2.68×10^8	830
(L)-16mer	49.7	9.17×10^{-6}	5.51×10^6	600
(alt)-16mer	61.2	1.83×10^{-7}	3.34×10^8	710
(D)-16mer	32.1	3.07×10^{-6}	1.05×10^7	450
(L)-8mer	13.3	1.03×10^{-5}	4.17×10^4	150
(alt)-8mer	18.2	4.58×10^{-5}	1.29×10^6	250
(D)-8mer	9.9	7.21×10^{-5}	1.37×10^5	125
(L)-8mer macrocycle	8.31	3.05×10^{-7}	2.73×10^7	640
(alt)-8mer macrocycle	63.8	5.45×10^{-7}	1.17×10^8	1430
(D)-8mer macrocycle	4.77	2.13×10^{-7}	2.24×10^7	260

Ligand	
(L)-8mer	
(L)-16mer	
(L)-32mer	

<p>(D)-8mer</p>	
<p>(D)-16mer</p>	
<p>(D)-32mer</p>	

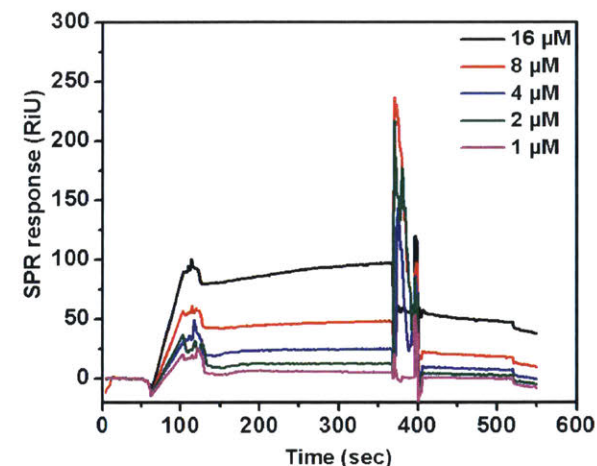
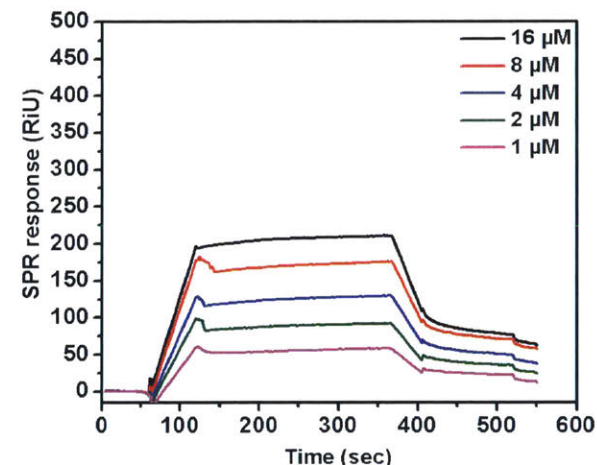
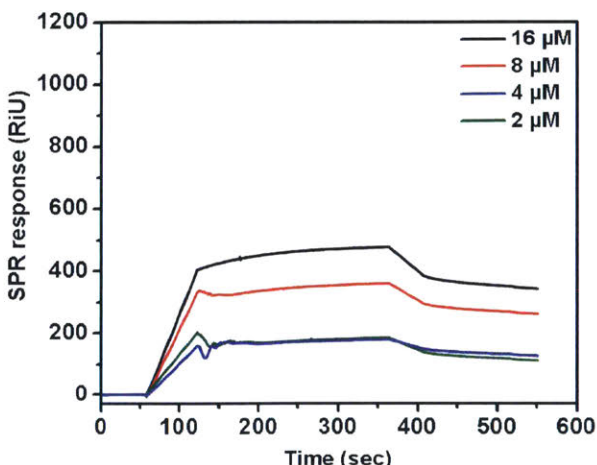
<p>(alt)-8mer</p>	 <p>SPR response (RiU) vs Time (sec) for (alt)-8mer. The y-axis ranges from 0 to 500 RiU, and the x-axis ranges from 0 to 600 sec. Five curves are shown for concentrations: 16 μM (black), 8 μM (red), 4 μM (blue), 2 μM (green), and 1 μM (magenta). All curves show an initial rise to a steady state, followed by a sharp peak at approximately 380 seconds, and then a gradual decay. The peak height increases with concentration, reaching about 300 RiU for 16 μM.</p>
<p>(alt)-16mer</p>	 <p>SPR response (RiU) vs Time (sec) for (alt)-16mer. The y-axis ranges from 0 to 1400 RiU, and the x-axis ranges from 0 to 600 sec. Four curves are shown for concentrations: 16 μM (black), 8 μM (red), 4 μM (blue), and 2 μM (green). The curves show a similar trend to the 8mer, with a sharp peak at approximately 380 seconds. The peak height for 16 μM reaches about 1300 RiU.</p>
<p>(alt)-32mer</p>	 <p>SPR response (RiU) vs Time (sec) for (alt)-32mer. The y-axis ranges from 0 to 3200 RiU, and the x-axis ranges from 0 to 600 sec. Five curves are shown for concentrations: 16 μM (black), 8 μM (red), 4 μM (blue), 2 μM (green), and 1 μM (magenta). The curves show a similar trend, with a sharp peak at approximately 380 seconds. The peak height for 16 μM reaches about 2100 RiU.</p>

<p>(L)-8mer macrocycle</p>	 <p>SPR response (RiU) vs Time (sec) for (L)-8mer macrocycle. The graph shows four curves for concentrations of 16 μM (black), 8 μM (red), 4 μM (blue), and 2 μM (grey). All curves show an increase in response over time, with a sharp spike at approximately 380 seconds. The 16 μM curve reaches the highest response of about 650 RiU.</p>
<p>(D)-8mer macrocycle</p>	 <p>SPR response (RiU) vs Time (sec) for (D)-8mer macrocycle. The graph shows four curves for concentrations of 16 μM (black), 8 μM (red), 4 μM (blue), and 1 μM (grey). All curves show an increase in response over time, with a sharp spike at approximately 380 seconds. The 16 μM curve reaches the highest response of about 260 RiU.</p>
<p>(alt)-8mer macrocycle</p>	 <p>SPR response (RiU) vs Time (sec) for (alt)-8mer macrocycle. The graph shows four curves for concentrations of 16 μM (black), 8 μM (red), 4 μM (blue), and 1 μM (grey). All curves show an increase in response over time, with a sharp spike at approximately 380 seconds. The 16 μM curve reaches the highest response of about 1400 RiU.</p>

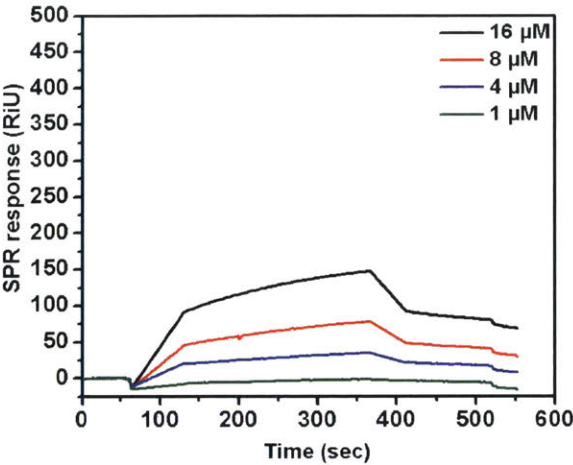
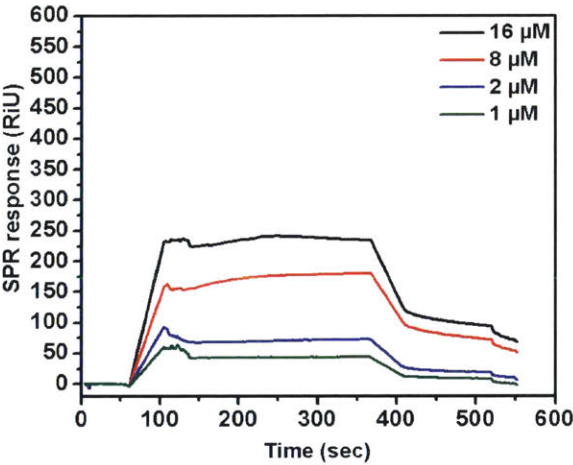
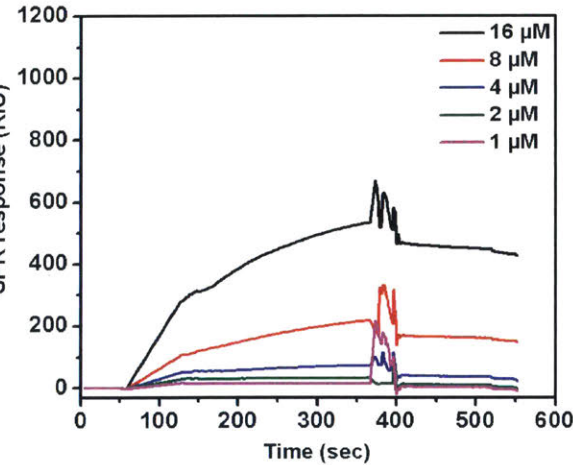
Mincle

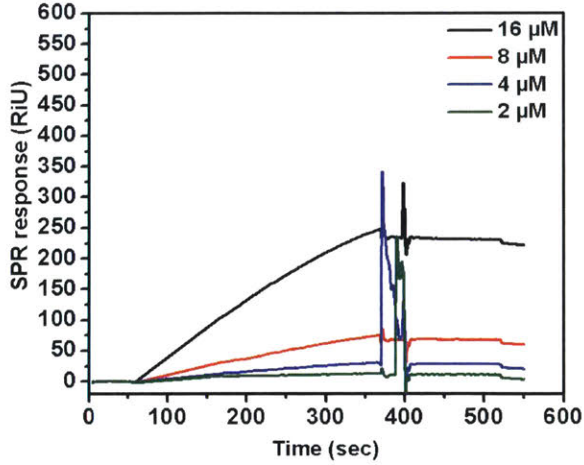
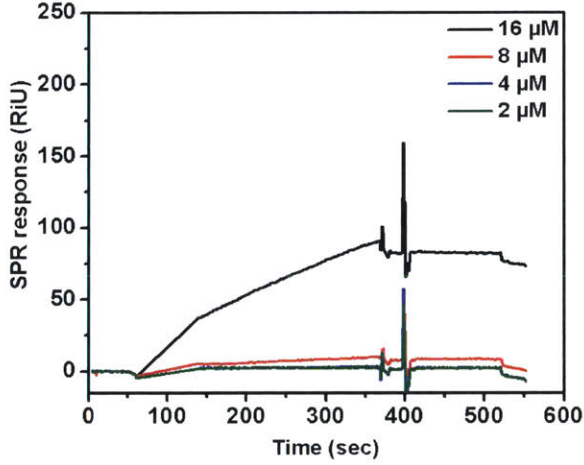
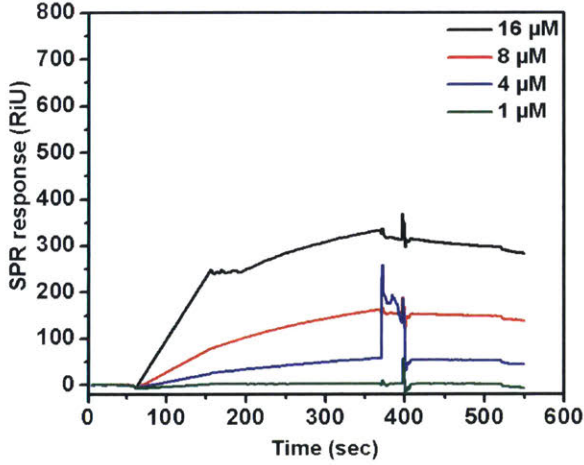
Table S4.8. Kinetic data of binding between glycopolymers and Mincle as calculated by SPR.

Ligand	k_a ($M^{-1} s^{-1}$)	k_d (s^{-1})	K_D (M^{-1})	R_{max} (RU)
(L)-32mer	50.8	5.63×10^{-6}	9.02×10^6	510
(alt)-32mer	52.3	9.77×10^{-6}	5.54×10^6	535
(D)-32mer	61.7	6.41×10^{-6}	9.63×10^6	555
(L)-16mer	97.2	7.46×10^{-6}	1.3×10^7	210
(alt)-16mer	147	3.71×10^{-5}	3.96×10^6	240
(D)-16mer	161	1.55×10^{-6}	1.03×10^8	290
(L)-8mer	3.27	5.84×10^{-5}	0.56×10^5	100
(alt)-8mer	5.99	1.94×10^{-5}	3.08×10^5	155
(D)-8mer	6.12	4.12×10^{-5}	1.48×10^5	190
(L)-8mer macrocycle	5.79	4.31×10^{-6}	1.34×10^6	250
(alt)-8mer macrocycle	29.4	3.18×10^{-6}	9.24×10^6	335
(D)-8mer macrocycle	1.82	1.12×10^{-6}	1.63×10^6	90

Ligand	
<i>(L)</i> -8mer	
<i>(L)</i> -16mer	
<i>(L)</i> -32mer	

<p>(D)-8mer</p>	
<p>(D)-16mer</p>	
<p>(D)-32mer</p>	

<p>(alt)-8mer</p>	 <p>SPR response (RIU) vs Time (sec) for (alt)-8mer. The y-axis ranges from 0 to 500 RIU, and the x-axis ranges from 0 to 600 sec. Four curves are shown for concentrations of 16 μM (black), 8 μM (red), 4 μM (blue), and 1 μM (green). All curves show an increase in response starting around 75 seconds, peaking between 350 and 400 seconds, and then gradually decreasing. The 16 μM curve reaches the highest peak of approximately 145 RIU.</p>
<p>(alt)-16mer</p>	 <p>SPR response (RIU) vs Time (sec) for (alt)-16mer. The y-axis ranges from 0 to 600 RIU, and the x-axis ranges from 0 to 600 sec. Four curves are shown for concentrations of 16 μM (black), 8 μM (red), 2 μM (blue), and 1 μM (green). The curves show a sharp initial increase starting around 75 seconds, reaching a plateau between 100 and 400 seconds, and then decreasing. The 16 μM curve reaches the highest peak of approximately 230 RIU.</p>
<p>(alt)-32mer</p>	 <p>SPR response (RIU) vs Time (sec) for (alt)-32mer. The y-axis ranges from 0 to 1200 RIU, and the x-axis ranges from 0 to 600 sec. Five curves are shown for concentrations of 16 μM (black), 8 μM (red), 4 μM (blue), 2 μM (grey), and 1 μM (pink). The curves show a steady increase in response starting around 75 seconds, with a notable peak or oscillation around 380 seconds. The 16 μM curve reaches the highest peak of approximately 650 RIU.</p>

<p>(L)-8mer macrocycle</p>	 <p>SPR response (RiU) vs Time (sec) for (L)-8mer macrocycle. The graph shows four curves for concentrations of 16 μM (black), 8 μM (red), 4 μM (blue), and 2 μM (green). All curves show an increase in response over time, with a sharp spike at approximately 380 seconds. The 16 μM curve reaches the highest response of approximately 250 RiU.</p>
<p>(D)-8mer macrocycle</p>	 <p>SPR response (RiU) vs Time (sec) for (D)-8mer macrocycle. The graph shows four curves for concentrations of 16 μM (black), 8 μM (red), 4 μM (blue), and 2 μM (green). All curves show an increase in response over time, with a sharp spike at approximately 380 seconds. The 16 μM curve reaches a response of approximately 90 RiU.</p>
<p>(alt)-8mer macrocycle</p>	 <p>SPR response (RiU) vs Time (sec) for (alt)-8mer macrocycle. The graph shows four curves for concentrations of 16 μM (black), 8 μM (red), 4 μM (blue), and 1 μM (green). All curves show an increase in response over time, with a sharp spike at approximately 380 seconds. The 16 μM curve reaches a response of approximately 350 RiU.</p>

TEM and DLS analysis of PhMannose-A32-TAMRA aggregates

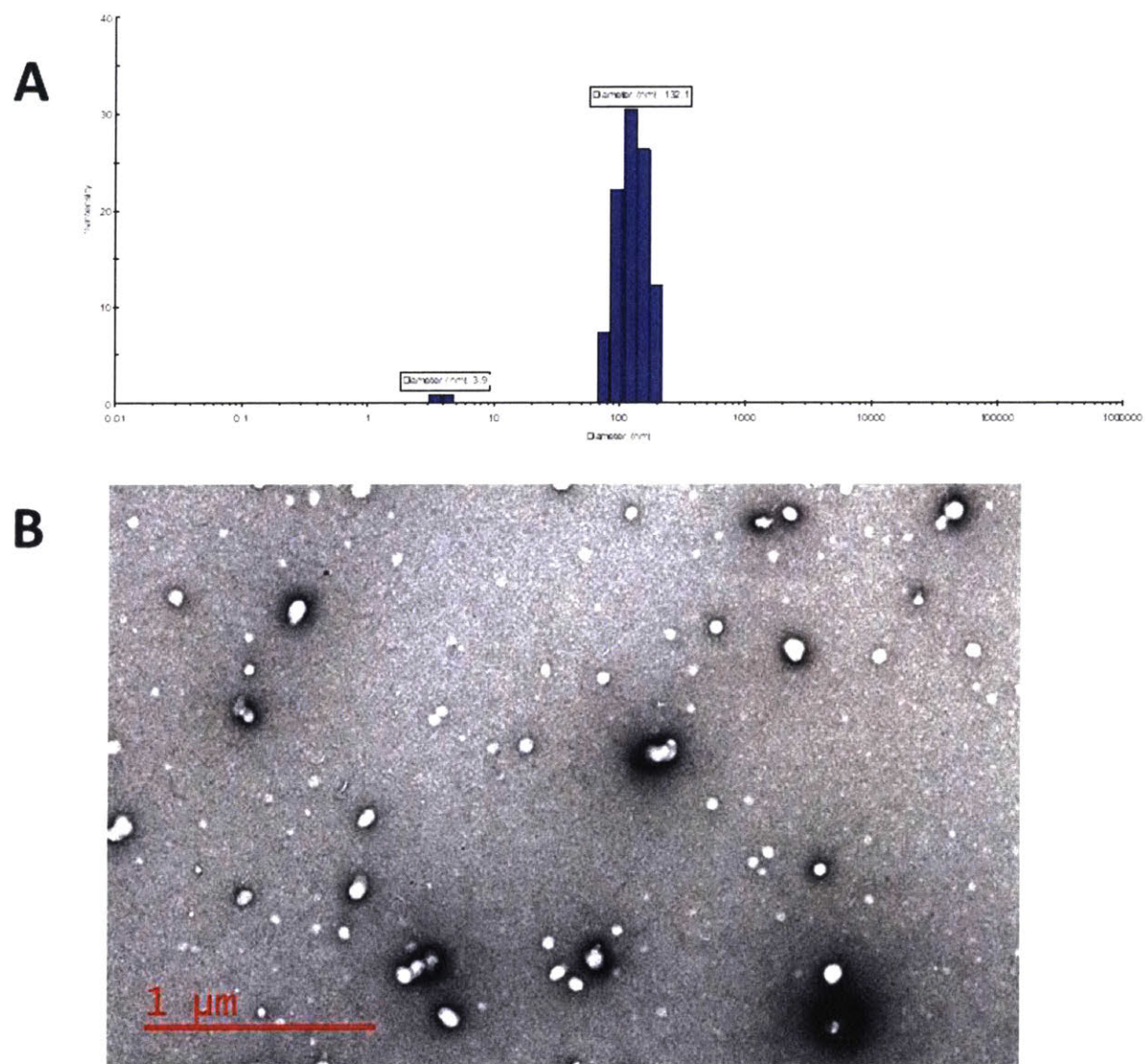


Figure S4.33. (A) DLS of dilute 0.01 mg/mL solution of **PhMannose-A32-TAMRA**. Particles show average diameter of 132 nm. (B) TEM of **PhMannose-A32-TAMRA** aggregates.

4.5 References

1. Figdor, C. G.; van Kooyk, Y.; Adema, G. J. C-type lectin receptors on dendritic cells and langerhans cells. *Nat. Rev. Immunol.* **2002**, *2*, 77-84.
2. Sharon, N.; Lis, H. Lectins as cell recognition molecules. *Science* **1989**, *246*, 227-246.
3. Weis, W. I.; Drickamer, K. Structural basis of lectin-carbohydrate recognition. *Annu. Rev. Biochem.* **1996**, *65*, 441-473.
4. Rüdiger, H.; Gabius, H. J. Plant lectins: occurrence, biochemistry, functions and applications. *Glycoconj. J.* **2001**, *18*, 589.
5. Liener, I. E.; Sharon, N.; Goldstein, I. J. The Lectins. Properties, Functions, and Applications in Biology and Medicine; Academic Press, Orlando, **1986**
6. Gabius, H. J. Animal Lectins. *Eur. J. Biochem.* **1997**, *243*, 543-576.
7. Delbianco, M.; Kononov, A.; Poveda, A.; Yu, Y.; Diercks, T.; Jiménez-Barbero, J.; Seeberger, P. H. Well-defined oligo- and polysaccharides as ideal probes for structural studies. *J. Am. Chem. Soc.* **2018**, *140*, 5421-5426.
8. Shivatare, V. S.; Shivatare, S. S.; Lee, C.-C. D.; Liang, C.-H.; Liao, K.-S.; Cheng, Y.-Y.; Saidachary, G.; Wu, C.-Y.; Lin, N.-H.; Kwong, P. D.; Burton, D. R.; Wu, C.-Y.; Wong, C.-H. Unprecedented Role of Hybrid N-Glycans as Ligands for HIV-1 Broadly Neutralizing Antibodies. *J. Am. Chem. Soc.* **2018**, *140*, 5202-5210.
9. Vyas, N. K. Atomic features of protein-carbohydrate interactions. *Curr. Opin. Struct. Biol.* **1991**, *1*, 732-740.
10. Kiessling, L. L.; Splain, R. A. Chemical approaches to glycobiology. *Annu. Rev. Biochem.* **2010**, *79*, 619-653.
11. Nycholat, C. M.; Peng, W.; McBride, R.; Antonopoulos, A.; De Vries, R. P.; Polonskaya, Z.; Finn, M. G.; Dell, A.; Haslam, S. M.; Paulson, J. C. Synthesis of biologically active N- and O-linked glycans with multisialylated poly-N-acetylglucosamine extensions using P. damsela α 2-6 sialyltransferase. *J. Am. Chem. Soc.* **2013**, *135*, 18280-18283.
12. Danishefsky, S. J.; McClure, K. F.; Randolph, J. T.; Ruggeri, R. B. A strategy for the Solid-phase synthesis of oligosaccharides. *Science* **1993**, *260*, 1307-1309.
13. Seeberger, P. H. The logic of automated glycan assembly. *Acc. Chem. Res.* **2015**, *48*, 1450-1463.
14. Iskratsch, T.; Braun, A.; Paschinger, K.; Wilson, I. B. H. Specificity analysis of lectins and antibodies using remodeled glycoproteins. *Anal. Biochem.* **2009**, *386*, 133-146.
15. Hahm, H. S.; Schlegel, M. K.; Hurevich, M.; Eller, S.; Schuhmacher, F.; Hofmann, J.; Pagel, K.; Seeberger, P. H. Automated glycan assembly using the glyconeer 2.1 synthesizer. *Proc. Natl. Acad. Sci.* **2017**, *114*, 3385-3389.
16. Naresh, K.; Schumacher, F.; Hahm, H. S.; Seeberger, P. H. Pushing the limits of automated glycan assembly: synthesis of a 50mer polymannoside. *Chem. Commun.* **2017**, *53*, 9085-9088.
17. Hahm, H. S.; Broecker, F.; Kawasaki, F.; Mietzsch, M.; Heilbronn, R.; Fukuda, M.; Seeberger, P. H. Automated glycan assembly of oligo-N-acetylglucosamine and keratan surface probes to study virus-glycan interactions. *Chem* **2017**, *2*, 114-124.
18. Plante, O. J.; Palmacci, E. R.; Seeberger, P. H. Automated solid-phase synthesis of oligosaccharides. *Science* **2001**, *291*, 1523-1527.
19. Gerke, C.; Ebbesen, M. F.; Jansen, D.; Boden, S.; Freichel, T.; Hartmann, L. Sequence-controlled glycopolymers via step-growth polymerization of precision

glycomacromolecules for lectin receptor clustering. *Biomacromolecules* **2017**, *18*, 787-796.

20. Jacobi, F.; de la Calle, A. C.; Boden, S.; Grafmüller, A.; Hartmann, L.; Schmidt, S. Multivalent binding of precision glycooligomers on soft glycocalyx mimicking hydrogels. *Biomacromolecules* **2018**, *19*, 3479-3488.
21. Ambrosi, M.; Cameron, N. R.; Davis, B. G.; Stolnik, S. Investigation of the interaction between peanut agglutinin and synthetic glycopolymeric multivalent ligands. *Org. Biomol. Chem.* **2005**, *3*, 1476-1480.
22. Mortell, K. H.; Weatherman, R. V.; Kiessling, L. L. Recognition Specificity of Neoglycopolymers Prepared by Ring-Opening Metathesis Polymerization. *J. Am. Chem. Soc.* **1996**, *118*, 2297-2298.
23. Lepenies, B.; Lee, J.; Sonkaria, S. Targeting C-type lectin receptors with multivalent carbohydrate ligands. *Adv. Drug Deliv. Rev.* **2013**, *65*, 1271-1281.
24. Geng, J.; Biedermann, F.; Zayed, J. M.; Tian, F.; Scherman, O. A. Supramolecular Glycopolymers in Water: A Reversible Route Toward Multivalent Carbohydrate–Lectin Conjugates Using Cucurbit[8]uril. *Macromolecules* **2011**, *44*, 4276-4281.
25. Miura, Y.; Hoshino, Y.; Seto, H. Glycopolymer nanobiotechnology. *Chem. Rev.* **2016**, *116*, 1673-1692.
26. Lis, H.; Sharon, N. Lectins: carbohydrate-specific proteins that mediate cellular recognition. *Chem. Rev.* **1998**, *98*, 637-674.
27. Dam, T. K.; Brewer, C. F. Effects of clustered epitopes in multivalent ligand–receptor interactions. *Biochemistry* **2008**, *47*, 8470–8476.
28. Ting, S. R. S.; Chen, G.; Stenzel, M. H. Synthesis of glycopolymers and their multivalent recognitions with lectins. *Polym. Chem.* **2010**, *1*, 1392-1412.
29. Kiessling, L. L.; Grim, J. C. Glycopolymer probes of signal transduction. *Chem. Soc. Rev.* **2013**, *42*, 4476-4491.
30. Pieters, R. J. Maximizing multivalency effects in protein-carbohydrate interactions. *Org. Biomol. Chem.* **2009**, *7*, 2013-2025.
31. Nagao, M.; Fujiwara, Y.; Matsubara, T.; Hoshino, Y.; Sato, T.; Miura, Y. Design of glycopolymers carrying sialyl oligosaccharides for controlling the interaction with the influenza virus. *Biomacromolecules* **2017**, *18*, 4385-4392.
32. Mochalova, L. V.; Tuzikov, A. B.; Marinina, V. P.; Gambaryan, A.S.; Byramova, N.E.; Bovin, N.V.; Matrosovich, M.N. Synthetic polymeric inhibitors of influenza virus receptor-binding activity suppress virus replication. *Antiviral Research* **1994**, *23*, 179-190.
33. Matrosovich, M.N.; Mochalova, L.V.; Marinina, V.P.; Byramova, N.E.; Bovin, N.V. Synthetic polymeric sialoside inhibitors of influenza virus receptor-binding activity. *FEBS* **1990**, *272*, 209-212.
34. Haldar, J.; de Cienfuegos, L. A.; Tumpey, T. M.; Gubareva, L. V.; Chen, J.; Klibanov, A. M. Bifunctional polymeric inhibitors of human influenza A Viruses. *Pharm. Res.* **2010**, *27*, 259-263.
35. Zhang, Q.; Collins, J.; Anastasaki, A.; Wallis, R.; Mitchell, D. A.; Becer, C. R.; Haddleton, D. M. Sequence-controlled multi-block glycopolymers to inhibit DC-SIGN-gp120 binding. *Angew. Chem. Int. Ed.* **2013**, *52*, 4435-4439.

36. Zhang, Q.; Su, L.; Collins, J.; Chen, G.; Wallis, R.; Mitchell, D. A.; Haddleton, D. M.; Becer, C. R. Dendritic cell lectin-targeting sentinel-like unimolecular glycoconjugates to release an anti-HIV drug. *J. Am. Chem. Soc.* **2014**, *136*, 4325-4332.
37. Mitchell, D. A.; Zhang, Q.; Voorhaar, L.; Haddleton, D. M.; Herath, S.; Gleinich, A. S.; Randeve, H. S.; Crispin, M.; Lehnert, H.; Wallis, R.; Patterson, S.; Becer, C. R. Manipulation of cytokine secretion in human dendritic cells using glycopolymers with picomolar affinity for DC-SIGN. *Chem. Sci.* **2017**, *8*, 6974-6980.
38. Yilmaz, G.; Uzunova, V.; Hartweg, M.; Beyer, V.; Napier, R.; Becer, C. R. The effect of linker length on ConA and DC-SIGN binding of S-glucosyl functionalized poly(2-oxazoline)s. *Polym. Chem.* **2018**, *9*, 611-618.
39. Becer, C. R.; Gibson, M. I.; Geng, J.; Ilyas, R.; Wallis, R.; Mitchell, D. A.; Haddleton, D. M. High-Affinity Glycopolymer Binding to Human DC-SIGN and Disruption of DC-SIGN Interactions with HIV Envelope Glycoprotein. *J. Am. Chem. Soc.* **2010**, *132*, 15130-15132.
40. McReynolds, K. D.; Gervay-Hague, J. Chemotherapeutic interventions targeting HIV interactions with host-associated carbohydrates. *Chem. Rev.* **2007**, *107*, 1533-1522.
41. Geng, J.; Mantovani, G.; Tao, L.; Nicolas, J.; Chen, G.; Wallis, R.; Mitchell, D. A.; Johnson, B. R. G.; Evans, S. D.; Haddleton, D. M. Site-directed conjugation of "clicked" glycopolymers to form glycoprotein mimics: binding to mammalian lectin and induction of immunological function. *J. Am. Chem. Soc.* **2007**, *129*, 15156-15163.
42. Becer, C. R. The glycopolymer code: synthesis of glycopolymers and multivalent carbohydrate-lectin interactions. *Macromol. Rapid Commun.* **2012**, *33*, 742-752.
43. Zanini, D.; Roy, R. Chemoenzymatic Synthesis and Lectin Binding Properties of Dendritic N-Acetyllactosamine. *Bioconjug. Chem.* **1997**, *8*, 187-192.
44. Ponader, D.; Wojcik, F.; Beceren-Braun, F.; Dervede, J.; Hartmann, L. Sequence-defined glycopolymer segments presenting mannose: synthesis and lectin binding affinity. *Biomacromolecules* **2012**, *13*, 1845-1852.
45. Ponader, D.; Maffre, P.; Aretz, J.; Pussak, D.; Ninnemann, N. M.; Schmidt, S.; Seeberger, P. H.; Rademacher, C.; Nienhaus, G. U.; Hartmann, L. Carbohydrate-lectin recognition of sequence-defined heteromultivalent glycooligomers. *J. Am. Chem. Soc.* **2014**, *136*, 2008-2016.
46. Lavilla, C.; Yilmaz, G.; Uzunova, V.; Napier, R.; Becer, C. R.; Heise, A. Block-sequence-specific glycopolypeptides with selective lectin binding properties. *Biomacromolecules* **2017**, *18*, 1928-1936.
47. Yilmaz, G.; Becer, C. R. Glycopolymer code based on well-defined glycopolymers or glyconanomaterials and their biomolecular recognition. *Front. Bioeng. Biotechnol.* **2014**, *2*, 1-18.
48. Lutz, J.-F. Sequence-controlled polymerizations: the next Holy Grail in polymer science? *Polym. Chem.* **2010**, *1*, 55-62.
49. Lutz, J. F.; Lehn, J. M.; Meijer, E. W.; Matyjaszewski, K. From precision polymers to complex materials and systems. *Nature Reviews Materials* **2016**, *1*, 16024.
50. Merrifield, R. B. Solid phase peptide synthesis. I. the synthesis of a tetrapeptide. *J. Am. Chem. Soc.* **1963**, *85*, 2149-2154.
51. Zuckermann, R. N.; Kerr, J. M.; Moosf, W. H.; Kent, S. B. H. Efficient method for the preparation of peptoids [oligo(N-substituted glycines)] by submonomer solid-phase synthesis. *J. Am. Chem. Soc.* **1992**, *114*, 10646-10647.

52. Espeel, P.; Carrette, L. L. G.; Bury, K.; Capenberghs, S.; Martins, J. C.; Duprez, F. E.; Madder, A. Multifunctional sequence-defined oligomers from a single building block. *Angew. Chem. Int. Ed.* **2013**, *52*, 13261-13264.
53. Roy, R. K.; Meszynska, A.; Laure, C.; Charles, L.; Verchin, C.; Lutz, J.-F. Design and synthesis of digitally encoded polymers that can be decoded and erased. *Nat. Commun.* **2015**, *6*, 7237.
54. Hartweg, M.; Edwards-Gayle, C. J. C.; Radvar, E.; Collis, D.; Reza, M.; Kaupp, M.; Steinkoenig, J.; Ruokolainen, J.; Rambo, R.; Barner-Kowollik, C.; Hamley, I. W.; Azevedo, H. S.; Becer, C. R. Ugi multicomponent reaction to prepare peptide-peptoid hybrid structures with diverse chemical functionalities. *Polym. Chem.* **2018**, *9*, 482-489.
55. Porel, M.; Alabi, C. A. Sequence-Defined Polymers via Orthogonal Alkyl Acrylamide Building Blocks. *J. Am. Chem. Soc.* **2014**, *136*, 13162-13165.
56. Porel, M.; Thornlow, D. N.; Phan, N. N.; Alabi, C. A. Sequence-defined bioactive macrocycles via an acid-catalysed cascade reaction. *Nature Chem.* **2016**, *8*, 590-596.
57. Solleder, S. C.; Meier, M. A. R. Sequence control in polymer chemistry through the passerini three-component reaction. *Angew. Chem. Int. Ed.* **2014**, *53*, 711-714.
58. Solleder, S. C.; Zengel, D.; Wetzl, K. S.; Meier, M. A. R. A scalable and high-yield strategy for the synthesis of sequence-defined macromolecules. *Angew. Chem. Int. Ed.* **2016**, *55*, 1204-1207.
59. Zydzia, N.; Konrad, W.; Feist, F.; Afonin, S.; Weidner, S.; Barner-Kowollik, C. Coding and decoding libraries of sequence-defined functional copolymers synthesized via photoligation. *Nat. Commun.* **2016**, *7*, 13672.
60. Percec, V.; Asandei, A. D. Macrocyclization overrides the polymer effect in the stabilization of liquid crystalline (LC) phases with a novel odd-even alternation. A demonstration with LC crown ethers. *Macromolecules* **1997**, *30*, 943-952.
61. Leibfarth, F. A.; Johnson, J. A.; Jamison, T. F. Scalable synthesis of sequence-defined, unimolecular macromolecules by Flow-IEG. *Proc. Natl. Acad. Sci.* **2015**, *112*, 10617-10622.
62. Barnes, J. C.; Ehrlich, D. J. C.; Gao, A. X.; Leibfarth, F. A.; Jiang, Y.; Zhou, E.; Jamison, T. F.; Johnson, J. A. Iterative exponential growth of stereo- and sequence-controlled polymers. *Nature Chem.* **2015**, *7*, 810-815.
63. Jiang, Y.; Golder, M. R.; Nguyen, H. V. T.; Wang, Y.; Zhong, M.; Barnes, J. C.; Ehrlich, D. J. C.; Johnson, J. A. Iterative exponential growth synthesis and assembly of uniform diblock copolymers. *J. Am. Chem. Soc.* **2016**, *138*, 9369-9372.
64. Golder, M. R.; Jiang, Y.; Teichen, P. E.; Nguyen, H. V. T.; Wang, W.; Milos, N.; Freedman, S. A.; Willard, A. P.; Johnson, J. A. Stereochemical sequence dictates unimolecular diblock copolymer assembly. *J. Am. Chem. Soc.* **2018**, *140*, 1596-1599.
65. Binauld, S.; Damiron, D.; Connal, L. A.; Hawker, C. J.; Drockenmuller, E. Precise synthesis of molecularly defined oligomers and polymers by orthogonal iterative divergent/convergent approaches. *Macromol. Rapid Commun.* **2011**, *32*, 147-168.
66. Cai, C.; Vasella, A. Oligosaccharide analogues of polysaccharides. part 6. orthogonal protecting/activating groups in an improved binomial synthesis of acetyleno-oligosaccharides. *Helv. Chim. Acta.* **1996**, *79*, 255-268.
67. Takizawa, K.; Tang, C.; Hawker, C. J. Molecularly defined caprolactone oligomers and polymers: synthesis and characterization. *J. Am. Chem. Soc.* **2008**, *130*, 1718-1726.

Chapter 5.
Chiral Unimolecular-armed Bottlebrush Polymers as Biological Probes

This chapter is composed of material adapted from the following publication:

Nguyen, H. V.-T. †; Jiang, Y.†; Barnes, J. C.; Oldenhuis, N. J.; Huang, Z.; Wang, W.; Chen, K.; Chen, Q.; Golder, M. R.; Young, K.; Johnson, J. A. Chiral unimolecular-armed bottlebrush polymers as biological probes. 2019. *In preparation*.

The work in this chapter was a collaborative effort with Hung V.-T. Nguyen, Jonathan C. Barnes, Nathan J. Oldenhuis, Zhihao Huang, Wencong Wang, Kathleen Chen, Qixian Chen, Matthew R. Golder, and Katherine Young. Jonathan C. Barnes, Hung V.-T. Nguyen, and the author designed the study. Hung V.-T. Nguyen, Jonathan C. Barnes, Zhihao Huang, and the author synthesized, characterized, and prepared materials and samples for these studies. Hung V.-T. Nguyen, Nathan J. Oldenhuis, and Jonathan C. Barnes performed in vitro studies. H.V.-T.N., J.C.B., and the author performed in vivo studies.

5.1 Introduction

Life is built upon complex homochiral building blocks, such as polynucleic acids, polysaccharides, and polypeptides. These polymeric components rely on the innate tetrahedral geometry of the carbon atom, which naturally leads to chirality in all of biology.¹ The central doctrine of the biological world depends on delicate molecular recognition processes that involve precise spatial and directional orientation of its chiral structures.¹⁻³ Reactive binding pockets on enzymes for example owe their defined forms to the rigidity and interactions within their chiral polypeptide sequences, which stabilize their secondary, tertiary, and quaternary structures.⁴ Their shapes allow for extreme substrate specificity and the resulting processes are crucial for a multitude of cellular processes such as sugar binding, cellular trafficking, and host defense. Over millennia of evolution, specific stereo-configurations have become essential to nature's chiral machinery: all natural peptides have *L* conformations and all natural sugars have *D* conformations.^{1,4,5}

Despite the importance of chirality to structure in nature, scientists have long used artificial macromolecules that lack complex chirality and consequently structural definition to probe and influence biological processes. These macromolecules are often simple and achiral, random and atactic.^{1,4,5} While these artificial macromonomers have been used in a plethora of biological fields, they rarely have any greater responsibility than simply working as carriers for bioactive moieties.⁶⁻⁸ For example, in drug delivery, simple polymer chains like poly(ethylene)glycol (PEG) are used as vehicles to bring biologically active small molecule cargo to targeted areas in the body.⁹⁻¹² Most polymeric systems have no innate ability to interact with delicate biological systems. To give them this power, it is often necessary to functionalize them with biological molecules, such as in the

glycopolymer field. Here, atactic polymer chains are functionalized with sugar side chains, and the resulting multivalency increase the binding strength of the sugars to their corresponding lectin substrates. This simple method has had great success and led to many proof-of-concept applications across multiple fields of research such as biosensing, nanomedicine, and biomaterials.¹³⁻¹⁷ We believe the application of polymers on complex biological systems can be further accelerated by using polymers that allow for more nuanced control over chemical sequence and consequently structure.

In attempts to improve structural control, many strategies have been attempted. In some fields of research, polymers with atactic backbones are functionalized with chiral side chains to impart some higher order structure. In one case, polyacrylates were functionalized with valine side chains of either *R* or *S* chirality, which have been used as nanoparticle (NP) or surface coatings for protein adsorption, cellular interactions, and tumor ablation. Despite a random backbone, the activity of these polymers was influenced by the valine's chirality.¹⁸⁻²¹ Other researchers have aimed to take advantage of the natural polypeptide structure by designing artificial versions and applying them to applications such as transfection agents. Sequence-definition is of utmost importance to these cell-penetrating peptides (CPPs) if they are to effectively hijack a cell's molecular recognition processes.²²⁻²⁵ Unfortunately because CPPs' are polypeptides, they are highly susceptible to proteases or opsonization processes in the body.²⁶⁻²⁹ To attempt to address this drawback, achiral peptoids have been tried as alternatives to CPPs due to their greater stability from their non-natural structures. However, peptoids are very "floppy" due to rotamers and a lack of chiral handles, and this greatly reduce a peptoids' effectiveness in comparison to polypeptides.²⁶⁻³¹ β -peptoids attempt to solve this issue by including chiral side chains and eliminating tertiary amides. They can form elegant secondary structures and be used as therapeutic agents, but they are almost as limited as polypeptides because their secondary amides are still susceptible to proteases.³²⁻³⁵

We aim to create a precise, non-natural polymer platform with absolute control over chirality and high *in vivo* stability that can be applied to biological systems. Using our previously developed synthetic strategy 'iterative exponential growth plus side-chain functionalization' (IEG+), we can prepare scalable quantities of unimolecular polymers with precise control over their sequence stereochemistry.³⁶ Briefly, the original strategy involves an IEG+ monomer containing a silyl-protected alkyne and an epoxide that can be regioselectively and

stereospecifically opened to afford an azide. Complementary deprotections of this monomer reveal the respective alkyne and azide (plus side-chain), which can then be coupled via the efficient copper-catalysed azide-alkyne cycloaddition (CuAAC) ‘click reaction.’ This constitutes an IEG+ cycle, which increases the degree of polymerization (DP) exponentially, yielding a dimer after 1 cycle, a 4mer after 2 cycles, an 8mer after 3 cycles, and so on. To date, we have deployed IEG+ to prepare precise polymers with up to 32 repeat units (molecular weights of up to ~12k Da) and subsequently decorated them with varying functional groups via a graft-to approach.^{37,38} These encouraging results motivated us to adopt this strategy for the creation of precise polymers towards biological applications.

As shown in Figure 5.1a, a polypeptide generally has a single carbon atom with a chiral side chain separating each secondary amide unit. Also shown in figure 5.1a are our 5 atom IEG (5AIEG) and 2 atom IEG (2AIEG) systems where we have substituted the biodegradable amide with a nondegradable triazole. Separating each of these triazoles is a connective unit of either 5 atoms or 2 atoms in length, each with a chiral side chain. The 5AIEG system has many degrees of freedom and chiral centers that interact little with one another. The 2AIEG platform, on the other hand, is far more rigid, and consequently we hypothesized would assume some higher level secondary structure. We aimed to directly compare these two analogous artificial polymers that have different backbone rigidity with the purpose of evaluating the importance of having rigid, chiral structures for non-natural polymers in natural biological systems.

In order to evaluate these chiral structures *in vivo*, it was necessary to synthesize polymers with high MW and nanoparticle sizes to improve their pharmacokinetics. It would not be feasible to make long, linear polymer chains of the size necessary through IEG due to synthetic limitations. Consequently, to accomplish this, we used the fundamental 5AIEG and 2AIEG structures to design norbornene macromonomers (Figure 5.1b) that could be polymerized via ring-opening metathesis polymerization (ROMP) to make chiral unimolecular-armed bottlebrush (CUBP) nanoarchitectures (Figure 5.1c). In addition to size, the design of these CUBPs has the added advantages of having a potentially lower critical micelle concentration, an extended backbone that further exposes the chiral hydroxyl groups, and most importantly a significantly higher localized density of the hydroxyl groups.³⁹⁻⁴¹ We believed this would facilitate strong hydroxyl-based multivalency interactions. Also, inherent to ROMP is high functional group tolerance and high polymerization efficiency, which would be beneficial in future studies where we install functional groups more biologically relevant than simple hydroxyls.^{42,43}

Herein, we describe the synthesis of our novel CUBPs and their evaluation *in vitro* and *in vivo*. *Note:* in this report, all polymers are drawn from their azide/norbornene (N) to alkyne (C) terminus; *L* and *D* labels are used to indicate the stereochemistry of each unit (wedge and dash bonds, respectively) akin to polypeptide nomenclature. *In vitro* evaluations of CUBPs revealed striking differences in toxicity and cell uptake across multiple cell lines for the 5AIEG-based CUBPs between the *L* and the *D* chiralities. Intriguingly, these differences were not observed in the case of 2AIEG-based CUBPs, implying rigidity in non-natural polymers may cause them to be less able to interact with biological systems. Furthermore, *in vivo* studies found pharmacokinetics

and biodistribution differences between *L* and *D* 5AIEG-based CUBPs, showing their potential translation into a delivery platform. Altogether, these results provide proof-of-principle that the stereochemistry and backbone rigidity of artificial polymers can be leveraged to tailor their interactions with biological systems.

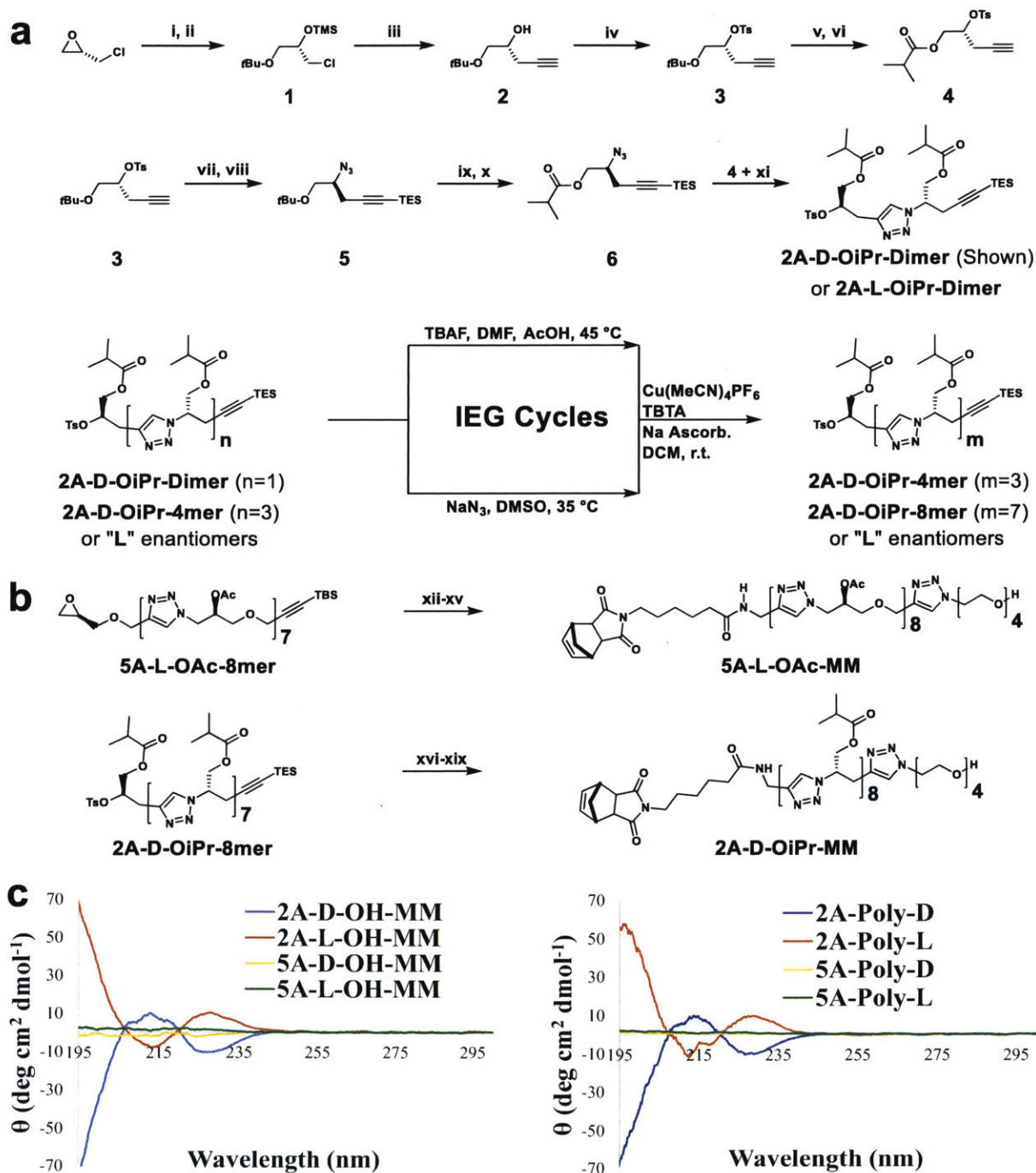


Figure 5.2. (a) Synthesis of 2AIEG oligomers up to the octamer. (i) *t*-BuOH, $\text{BF}_3 \cdot \text{OEt}_2$; (ii)

TMSCl, imidazole, DMF; (iii) lithium TMS acetylide, DMSO, THF, hexanes, r.t.; (iv) TsCl, 4-DMAP, TEA, DCM; (v) TFA, DCM; (vi) isobutyric anhydride, 4-DMAP, TEA, DCM; (vii) NaN₃, DMSO, 35 °C; (viii) NaHMDS, TESCl, THF; (ix) TFA, DCM; (x) isobutyric anhydride, 4-DMAP, TEA, DCM; (xi) Cu(MeCN)₄PF₆, TBTA, Na ascorbate, DCM. **(b)** Representative synthesis of chiral macromonomers **5A-L-OAc-MM** and **2A-D-OiPr-MM**. (xii) NaN₃, AcOH, DMF, 60 °C then Ac₂O, 4-DMAP; (xiii) **Nb-yne**, CuBr, PMDTA, Na ascorbate, DMF; (xiv) TBAF, THF; (xv) azido-tetraethyleneglycol, CuBr, PMDTA, Na ascorbate, DMF; (xvi) TBAF, AcOH, DMF; (xvii) azido-tetraethyleneglycol, Cu(MeCN)₄PF₆, TBTA, Na ascorbate, DCM; (xviii) NaN₃, DMSO; (xix) **Nb-yne**, CuBr, PMDTA, Na ascorbate, DMF. **(c)** (left) Overlapping CD spectra of the *L* and *D* enantiomers of the ester-deprotected macromonomers **5A-L-OH-MM**, **5A-D-OH-MM**, **2A-L-OH-MM**, and **2A-D-OH-MM**. (right) Overlapping CD spectra of the *L* and *D* enantiomers of the ester-deprotected CUBPs **5A-L**, **5A-D**, **2A-L**, **2A-D**.

5.2 Results and Discussions

Chiral Unimolecular-armed Bottlebrush Polymer (CUBP) Synthesis

The synthesis of our novel 2AIEG system is detailed in Figure 5.2a and 5.2b. First, the epoxide of enantiomerically pure epichlorohydrin (>99.5% ee) was opened by *t*-BuOH with the strong Lewis acid BF₃·OEt₂ and the resulting alcohol was temporarily protected with a trimethylsilyl (TMS) protecting group to yield **1** in high purity using only rotary evaporation and liquid-liquid extraction for purification. As previously reported, this methodology results in product with the same enantiopurity as the starting material. **1** is then treated with excess lithium (TMS)acetylide in the presence of DMSO to coordinate the lithium and make the acetylide more nucleophilic. Addition of MeOH upon completion of this reaction generates methoxide anions that deprotect all TMS protecting groups resulting in **2**. **2** undergoes standard tosylation conditions to generate **3**, which is the major building block for the alkyne and azide monomers. The alkyne monomer **4** is easily made through acid deprotection of **3** and subsequent protection of the alcohol with isobutyric anhydride. We chose to use an isobutyric ester instead of an acetyl group to both improve stability of the alcohol protecting group to potential hydrolysis and enhance solubility of the final products in organic solvents. To make the azide monomer, **3** is treated with a standard azidification procedure and the alkyne of the resulting azide is then protected with a triethylsilyl

(TES) protecting group to make **5**. It should be noted that the handedness of the stereocenter inverts quantitatively due to the S_N2 azidification reaction. **5** is reacted with the same acid deprotection and esterification conditions that were used to make **4** to generate the azide monomer **6**. **6** is coupled with **4** using standard CuAAC conditions to make enantiopure **2A-D-OiPr-Dimer** and **2A-L-OiPr-Dimer** at an almost 10 g scale.

We put these **2A-Dimers** through 2 IEG cycles. For each enantiomer, the TES-protected alkyne of one half of the materials was deprotected using 1.1 equivalents of TBAF and 2.2 equivalents of AcOH in DMF. Without AcOH, the hydroxide byproduct of standard TBAF deprotection leads to gradual hydrolysis of the ester side chains. Excessive AcOH will hydrogen bond to the fluoride anion and prevent silyl deprotection. The other half of each enantiomer is azidified with a standard sodium azide and DMSO procedure. The free alkyne and azidified halves were coupled using CuAAC conditions to make **2A-D-OiPr-4mer**, **2A-D-OiPr-8mer**, and their *L* enantiomer counterparts.

To create polymers of nanoparticle size, we combined our **5AIEG** and **2AIEG** systems with ring opening metathesis polymerization (ROMP), a highly efficient living polymerization approach. As shown in Figure 5.2C, we made MMs amenable to this polymerization by putting **5A-L-OAc-8mer**, **2A-D-OiPr-8mer**, and their enantiomers through a series of end group modifications. On one end, azidification and CuAAC was performed to couple on an alkyne functionalized norbornene. On the other end, the silyl-protected alkyne was deprotected and capped with a tetraethylene glycol unit. Modification of the alkyne is important to prevent the alkyne from interfering with the ROMP and to improve overall water solubility. In the future, the alkyne could be further functionalized with a cleavable therapeutic agent, imaging agent, or targeting ligand. It should be noted that it is not possible to ROMP MMs with either 5AIEG 16mers or 2AIEG 16mers as the higher concentration of triazoles adversely effect ROMP. Gel permeation chromatography (GPC, Figure S5.48) and matrix-assisted laser desorption ionization (MALDI, Figures S5.46 and S5.47) mass spectra data confirmed the MMs' unimolecular nature. Comparison of the CD spectra from the ester-deprotected **5A-L-OH-MM**, **5A-D-OH-MM**, **2A-L-OH-MM**, **2A-D-OH-MM**, **5A-L**, **5A-D**, **2A-L**, and **2A-D** (Figure 5.2D) demonstrate that the chiral centers of the 2AIEG system may interact far better to form ordered secondary structures than what is possible for the 5AIEG system.

Chiral Unimolecular-armed Bottlebrush Polymer (CUBP) Synthesis and Characterization

ROMPs of our novel chiral MMs were performed using bispyridyl-modified 3rd Grubbs initiator in dichloromethane (DCM), affording CUBPs. Separate polymerizations starting with **5A-L-OAc-MM**, **5A-D-OAc-MM**, **2A-L-OiPr-MM**, or **2A-D-OiPr-MM** (25:1 MM:**G3-Cat**) yielded the corresponding BPs **5A-Poly-L**, **5A-Poly-D**, **2A-Poly-L**, and **2A-Poly-D**. MM conversion was determined to be > 90% by GPC (Figure S5.48).

To deprotect these CUBPs, we first examined the deprotection of their corresponding MMs, including both the 5AIEG and 2AIEG-based systems. Following our previously reported procedure using methanol (MeOH) and excess potassium carbonate (K_2CO_3),³⁵ complete deprotection was observed, as evident by 1H NMR (Figures S5.19 to S5.26). The resulting deprotected MMs were subjected to dialysis and subsequent lyophilization, affording the final product.

We adapted this workflow to deprotect our CUBPs where the protected hydroxyl groups are in a sterically crowded environment. The deprotection of these CUBPs was done in two stages. First, the CUBPs were dissolved in a mixture of MeOH and DCM (1:1) with excess K_2CO_3 , and allowed to stir for 6 h at room temperature. Next, the solvent was removed and a mixture of acetone and water (1:1) were added. The reaction mixture was then allowed to stir for an additional 6 h at room temperature, affording the final CUBPs. As the CUBPs' solubility in organic solvents decreases as hydroxyl groups are gradually deprotected, adaptive changes in solvents are necessary to achieve complete deprotection. After reaction, the crude mixture was purified by dialysis and lyophilization.

1H NMR spectrum of deprotected BPs revealed a complete loss of resonances associated with the acetyl (for 5AIEG-based CUBPs) or isopropyl protons (for 2AIEG-based CUBPs) (Figures S5.28 to S5.35 and S5.36 to S5.43), confirming the successful removal of this protecting group to make the deprotected CUBPs **5A-L**, **5A-D**, **2A-L**, and **2A-D**. The resulting polymers were also soluble in water at high concentration (> 40 mg/mL), making them suitable candidates for subsequent biological studies. Furthermore, the 8 hydroxyl groups per arm provide immense potential for bottom-up therapeutic loading. This extremely high loading capability, combined with the ability to prepare a chiral delivery platform, could make our CUBPs a very powerful system and at the very least, a viable PEG replacement.

Dynamic light scattering (DLS) of CUBPs showed consistent hydrodynamic diameter (D_h) across these bottlebrushes, namely 3.2 ± 0.4 nm, 3.3 ± 0.7 nm, 2.8 ± 0.4 nm, and 2.5 ± 0.3 nm for **5A-L**, **5A-D**, **2A-L** and **2A-D** respectively. While, as hypothesized, rapid growth of MW via ROMP allowed our IEG-based chiral system to reach this biologically relevant size, further control can be achieved by utilizing brush-first ROMP, a well-established method in our group which cross-links brush polymers using drug-loaded or stimuli-responsive cross-linkers.⁴⁴⁻⁴⁷

To incorporate a near-infrared fluorescence (NIRF) imaging moiety for *in vitro* and *in vivo* studies, we prepared **Cy-M**, a Cyanine5.5-conjugated monomers. **Cy-M** was prepared via CuAAC of an alkyne-containing norbornene (Nb-yne) and Cyanine5.5-azide under identical ‘click’ conditions as mentioned above (Schemes S1 and S17). Fluorescent CUBPs were then prepared by adding **Cy-M** into the starting MM mixture and followed the procedures described above, forming the corresponding for **5A-L-Cy**, **5A-D-Cy**, **2A-L-Cy** and **2A-D-Cy**. These CUBPs are essentially identical as confirmed by GPC (Figure S5.48), making them ideal probes for examining how chirality affects biological entities with a built-in imaging moiety.

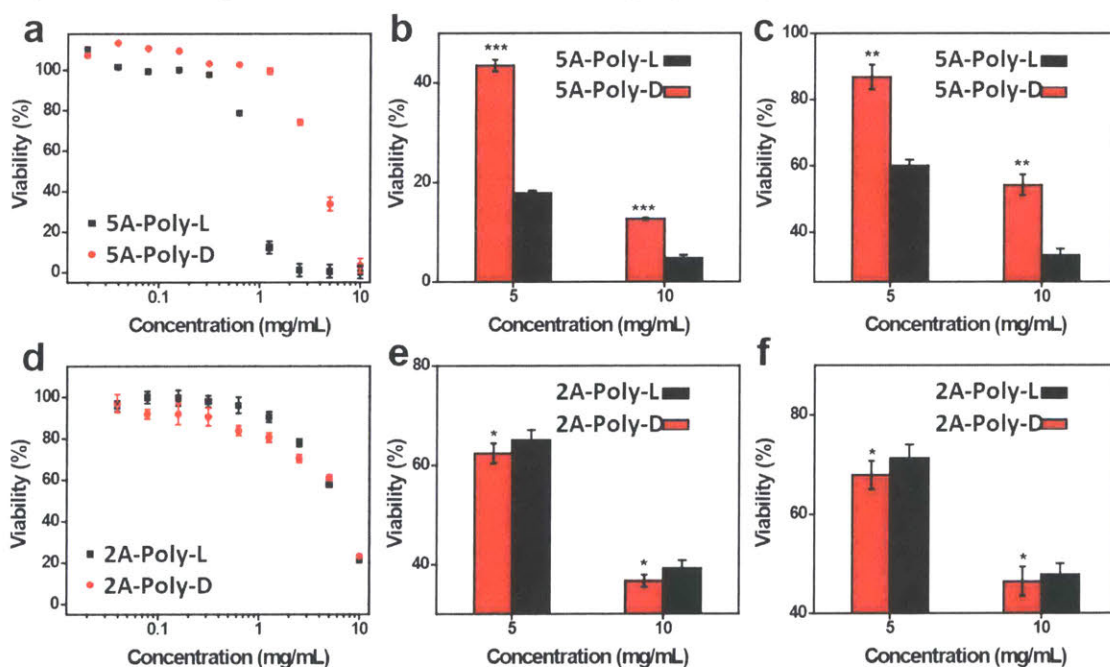


Figure 5.3. Cell toxicity of 5AIEG CUBPs in (a) HUVEC, (b) HeLa, (c) MCF cells, and 2AIEG CUBPs (d) HUVEC, (e) HeLa, (f) MCF cells. Viability was determined using CellTiter-Glo. Data are presented as mean \pm SEM ($n = 3$). Statistical comparison for viability curves (Figure 5.5a, 5.5d) were made using the Mann–Whitney U -test. Statistical comparisons for viability at set concentrations (10 or 5 mg polymer/mL, Figure 5.5b, 5.5c, 5.5e, 5.5f) were made using a two-tailed t test. *not significant, ** $p < 0.01$, *** $p < 0.0001$

***In vitro* Evaluation of CUBPs**

With these CUBPs in hand, we next evaluated their behaviors in an *in vitro* setting, beginning with cell toxicity testing (Figure 5.3). We first incubated these CUBPs in human umbilical vein endothelial cells (HUVEC), a well-established toxin-sensitive cell line. Interestingly, striking differences in viability between **5A-L** and **5A-D** were observed (Figure 5.3a), where the R enantiomer was significantly more toxic. The IC₅₀ observed for **5A-L** was 0.895 mg/mL, whereas the **5A-D** enantiomer exhibited an IC₅₀ of 3.994 mg/mL, a 4.5-fold difference. It is important to note that with the exception of the chiral hydroxyl groups, **5A-L** and **5A-D** were chemically identical, strongly suggesting the observed difference coming from their stereochemistry. In stark contrast, no differences in toxicity was observed between **2A-L** and **2A-D** when the same test was performed (Figure 5.3a), revealing the absence of the effect of the chiral hydroxyl groups upon their structural deviations from the 5AIEG. Statistical comparison between the viability curves for the *L* and *D* enantiomers were made using the Mann–Whitney *U*-test, revealing statistical differences for the 5AIEG CUBPs, but not the 2AIEG, consistent with our observations.

We then further examined this behavior in HeLa (cervical cancer) and MCF7 (breast cancer) cells (Figure 5.3). Consistent with our previous observations, differences in toxicity were observed for both cell lines in the case of 5AIEG, but not for 2AIEG-based CUBPs (Figure 5.3b-c and 5.3e-f). We incubated these cells with either 10 mg/mL or 5 mg/mL CUBPs. As these are aggressive adenocarcinoma, they appeared more viable even at 10 mg/mL CUBPs incubation. Therefore, the observed differences also diminished to certain extents. Nonetheless, statistically significant differences in viability was observed in both HeLa and MCF7 cell for 5AIEG-based CUBPs. For instance, with HeLa cells, at 10 mg/mL, $4.72 \pm 0.69\%$ viability was observed for **5A-L**, whereas $12.65 \pm 0.69\%$ viability was observed for **2A-L** ($p = 0.0004$). The same trend was also observed at 5.0 mg/mL incubation, with $17.82 \pm 0.48\%$ and $43.50 \pm 1.14\%$ viable cells for **5A-L** and **5A-D** respectively ($p < 0.0001$). In contrast, no statistically significant differences in viability was observed in the case of 2AIEG-based CUBPs, both for HeLa and MCF7 cells.

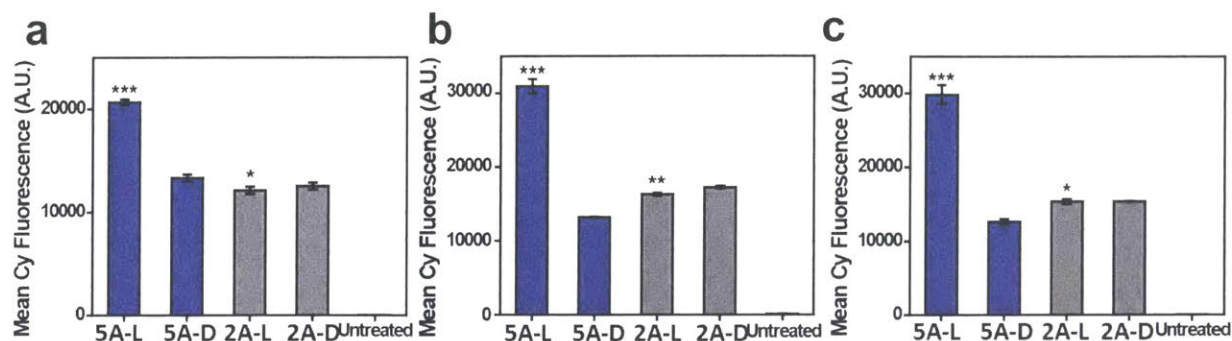


Figure 5.4. Quantification of CUBP cell uptake by flow cytometry in (a) HUVEC, (b) HeLa, and (c) MCF7 cells using Cyanine5.5 as detection dye. Data are presented as mean \pm SEM ($n = 4$). Statistical comparisons were made using a two-tailed t test. *not significant, ** $p < 0.01$, *** $p < 0.0001$

Importantly, in all cases, the observed toxicity across all CUBPs, including 5AIEG and 2AIEG-based, was very low. These CUBPs are well-tolerated by cells and possess comparably low toxicity to PEG-based species with similar bottlebrush architecture and molecular weight range.^{48,49} Hence, this positioned them as promising delivery platforms for therapeutic agents, especially given their structural tunability that could be directed at different translational applications. This approach can be conveniently realized through a block-copolymer synthesis where one block contains a therapeutic payload, in an analogous manner with their PEG-based counterpart, as commonly reported in the literature.⁵⁰⁻⁵²

Fascinated by these differences in toxicity, we then explored their potential causes, with the first candidate being cellular uptake. To be able to determine cell uptake by flow cytometry, Cy-loaded CUBPs were prepared as discussed above, resulting in **5A-L-Cy**, **5A-D-Cy**, **2A-L-Cy**, and **2A-D-Cy**. These polymers were incubated for 24 h with the same cell lines at 0.2 mg/mL, a concentration that exhibits no toxicity (Figure 5.3). We observed striking differences across all cell lines between **5A-L-Cy** and **5A-D-Cy**, but not between **2A-L-Cy**, and **2A-D-Cy** (Figure 5.4). **5A-L-Cy** were more effectively uptaken compared to **5A-D-Cy**; a difference of 1.5-, 2.3-, and 2.4-fold were observed for HUVEC, HeLa, and MCF7 respectively ($p < 0.0001$ for all cases). For 2AIEG-based CUBPs, no statistical differences were observed in HUVEC and MCF7 cells; while there was a statistically significant difference in the case of HeLa cells ($p < 0.0066$), only ~5% difference were observed. Altogether, this suggest a more efficient cellular uptake in the *L* enantiomer compared to its *D* counterpart, which can potentially contribute to its higher toxicity.

Again, chemical modifications deviation employed in the 2AIEG-based CUBPs diminished this chirality-induced biological difference.

This is, to our knowledge, the first example of precise rational chemical modifications directly translating to biological activity in polymeric platforms where the driving force is chirality. The 2AIEG platform differed from their 5AIEG counterpart in two aspects: a shorter distance between chiral centers (from 5 atoms to 2 atoms), and a hydroxyl group that is one methylene further away from the respective chiral centers (Figure 5.1). The first change increases both the density of the chiral hydroxyl groups and the rigidity of the polytriazole backbone. This change could potentially decrease the flexibility and subsequently the promiscuous binding of these CUBPs to certain receptors on cell surface or crucial protein corona components and hence, mask the effect of these chiral hydroxyl groups. The second change could also reduce the influence of the hydroxyl group as it is further away from the chiral center in the 2AIEG platform than its 5AIEG counterpart. As a combined result of these structure changes, chirality-induced differences both in *in vitro* toxicity and cellular uptake that were evident in the 5AIEG platform, were muted in the 2AIEG counterpart.

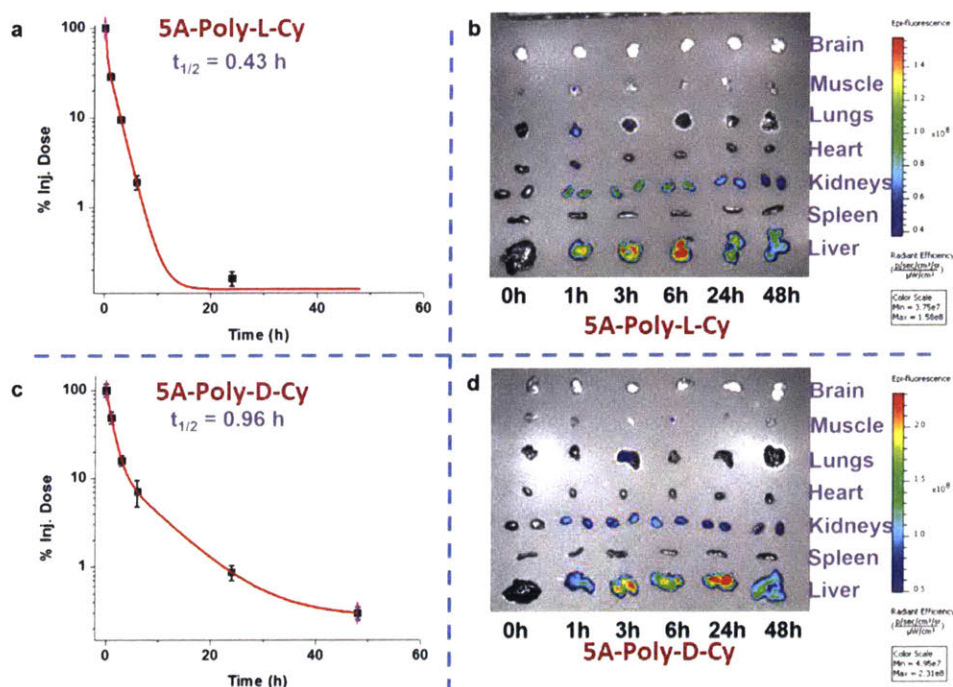


Figure 5.5. Pharmacokinetics (PK) and biodistribution (BD) in BALB/c mice ($n = 3$) of 5AIEG CUBPs. (a) PK and (b) BD of **5A-L-Cy**. (c) PK and (d) BD of **5A-D-Cy**. Cyanine5.5 ($\lambda_{ex}/\lambda_{em} = 640/700$ nm) was used for ex vivo NIRF analysis. Unit of radiant efficiency: $\frac{p/sec/cm^2/sr}{\mu W/cm^2}$

***In vivo* Pharmacokinetics (PK) and Biodistribution (BD) in BALB/c mice**

Inspired by the striking *in vitro* differences of 5AIEG CUBPs, we then set out to examine the effect of these enantiomeric CUBPs *in vivo*. In separate studies, **5A-L-Cy** and **5A-D-Cy** were delivered to BALB/c mice via tail-vein injections (2 mg CUBP in 200 μ L of 5% glucose). Blood samples were collected at different time points via cardiac puncture to constitute their pharmacokinetics PK; BD were also acquired from collected organ. Thanks to the conjugated Cy dye, ex vivo fluorescence imaging can be used to collect both of these data sets (Figure 5.5). Given their sub-5-nm size, rapid clearance from the bloodstream was expected and observed for both **5A-L-Cy** and **5A-D-Cy**, (Figure 5.5a and 5.5c). However, the circulation half-life ($t_{1/2}$) observed for these 2 CUBPs differed by a factor of 2.23: 0.43 h for **5A-L-Cy**, and 0.96 h for **5A-D-Cy**. Furthermore, clearances of these CUBPs were observed mainly at the liver and kidney sites, an expected behavior for NP species of this size range. Peak liver accumulation for **5A-L-Cy** was observed at 6 h post injections, whereas for **5A-D-Cy**, this was not observed until 24 h, consistent with **5A-D-Cy**'s longer circulation half-life. Furthermore, this is consistent with the higher cellular uptake observed *in vitro* for **5A-L-Cy**. Altogether, these observations clearly suggest differences in *in vivo* behavior between the two enantiomeric CUBPs **5A-L-Cy**, and **5A-D-Cy**. This is most likely due to different interactions between these chiral bottlebrushes with the in highly chiral *in vivo* environment, or the formation of distinct protein coronas that ultimately determined these CUBPs' *in vivo* fates.

5.3 Conclusion

We reported here the design, synthesis, characterization, *in vitro* and *in vivo* evaluation of enantiomeric CUBPs. Novel, ROMP-compatible stereocontrolled IEG-based MMs were prepared. We demonstrated the ability to rationally modify the IEG component of these MMs, including stereochemical sequence, length, and distance between sidechain groups. This resulted in 2 IEG-based MM systems with distinct features, namely 5AIEG and 2AIEG. CUBPs from these MMs were prepared and evaluated *in vitro* and *in vivo*. Striking differences were observed *in vitro* in term of toxicity and cellular uptake between the *L* and *D* enantiomers in the 5AIEG system across multiple cell lines, including HUVEC, HeLa, and MCF7; the *L* enantiomer was found to be more toxic and more efficiently uptaken into cells. Intriguingly, the aforementioned chemical alterations that led to the formation of the 2AIEG system were observed to have diminished this stereo-driven

differences. Furthermore, these observations readily translated to an *in vivo* context, where distinct PK and BD profiles were observed for the different enantiomers. Together, we demonstrated the ability to leverage stereochemistry to create synthetic polymer systems with tailorable interactions towards biological systems. This concept possesses immense potential both in drug delivery platform development, as well as mechanistic evaluation and probing of the biological milieu.

5.4 Supplementary Information

Materials / General Methods / Instrumentation

All reagents were purchased from commercial suppliers and used without further purification unless stated otherwise. 5-atom iterative exponential growth (5AIEG) octamer precursor **5A-L-OAc** and **5A-D-OAc** (Barnes, J. C.; Ehrlich, D. J.-C.; Gao, A. X.; Leibfarth, F. A.; Jiang, Y.; Zhou, E.; Jamison, T. F.; Johnson, J. A. Iterative Exponential Growth of Stereo- and Sequence-Controlled Polymers. *Nat. Chem.* 2015, 7, 810-815.) were prepared according to literature procedures using glycidal propargyl ether (**GPE**) monomers adapted from a more recent report. (Golder, M. R.; Jiang, Y.; Teichen, P. E.; Nguyen, H. V.-T.; Wang, W.; Milos, N.; Freedman, S. A.; Willard, A. P.; Johnson, J. A. Stereochemical Sequence Dictates Unimolecular Diblock Copolymer Assembly. *J. Am. Chem. Soc.* **2018**, 140, 1596-1599.) Norbornene precursor **c1**, (Patel, P. R.; Kiser, R. C.; Lu, Y. Y.; Fong, E.; Ho, W. C.; Tirrell, D. A.; Grubbs, R. H. Synthesis and Cell Adhesive Properties of Linear and Cyclic RGD Functionalized Polynorbornene Thin Films. *Biomacromolecules*, **2012**, 13, 2546-2553.) tetraethylene glycol precursor **c2**, (DeForest, C. A.; Tirrell, D. A. A Photoreversible Protein-Patterning Approach for Guiding Stem Cell Fate in Three-Dimensional Gels. *Nat. Mater.* **2015**, 14, 523-531.) and Grubbs 3rd generation bispyridyl catalyst **G3-Cat** (Love, J. A.; Morgan, J. P.; Trnka, T. M.; Grubbs, R. H. (2002) A Practical and Highly Active Ruthenium-Based Catalyst that Effects the Cross Metathesis of Acrylonitrile. *Angew. Chem. Int. Ed.* **2002**, 41, 4035-4037.) was prepared according to literature procedures with modifications specified in the following section.

Liquid chromatography mass spectrometry (LC/MS) was performed on an Agilent 1260 LC system equipped with a Zorbax SB-C18 rapid resolution HT column using a binary solvent system (MeCN and H₂O with 0.1% CH₃COOH). Recycling preparative HPLC was performed on a LaboACE system (Japan Analytical Industry) using a JAIGEL-2.5HR column. Size exclusion chromatography (SEC) analyses were performed on an Agilent 1260 Infinity setup with two Agilent PL1110-6500 columns in tandem and a 0.025 M LiBr DMF mobile phase run at 60 °C. The differential refractive index (dRI) of each compound was monitored using a Wyatt Optilab T-rEX detector. Column chromatography was carried out on silica gel 60F (EMD Millipore, 0.040–0.063 mm) or on aluminum oxide (Sigma-Aldrich, activated, neutral, Brockmann Activity I).

Nuclear magnetic resonance (NMR) spectra were recorded on Varian Inova-500 and Bruker AVANCE III-400 spectrometers, with working frequencies of 500 (^1H) and 125 (^{13}C) MHz, and 400 (^1H) and 100 (^{13}C) MHz, respectively. Chemical shifts are reported in ppm relative to the signals corresponding to the residual non-deuterated solvents: CDCl_3 : $\delta_{\text{H}} = 7.26$ ppm, MeOD: $\delta_{\text{H}} = 3.31$ ppm and $\delta_{\text{C}} = 77.16$ ppm; D_2O : $\delta_{\text{H}} = 4.79$. High-resolution mass spectra (HRMS) were measured on a Bruker Daltonics APEXIV 4.7 Tesla Fourier Transform Ion Cyclotron Resonance Mass Spectrometer (FT-ICR-MS) using an electrospray ionization (ESI) source. Matrix-assisted laser desorption/ionization-time of flight (MALDI-TOF) mass spectra were measured on a Bruker model MicroFlex instrument using α -cyano-4-hydroxycinnamic acid as the matrix. Chiral high-performance liquid chromatography (HPLC) was performed on an Agilent 1260 or an Agilent 1290 Infinity II system using a mixture of hexanes and isopropanol. Dynamic light scattering (DLS) measurements were performed using a Wyatt Technology Mobius DLS instrument. Bottlebrush polymer samples were prepared at 1 mg/mL in either nanopure water (MilliQ), PBS buffer, or 5% v/v glucose/nanopore water; disposable polystyrene cuvettes pre-cleaned with compressed air were used. Measurements were made in sets of 10 acquisitions, and the average hydrodynamic diameters were calculated using the DLS correlation function via a regularization fitting method (Dynamics 7.4.0.72 software package from Wyatt Technology).

Cell culture: MCF7 cells (ATCC) and HeLa cells (ATCC) were cultured in DMEM media (ATCC) supplemented with 10% fetal bovine serum (FBS, VWR) and 1% penicillin/streptomycin (Thermo Fisher Scientific). Human umbilical vein endothelial cells (HUVEC, Lonza) were cultured in EGM⁺ media (Lonza) supplemented with 1% penicillin/streptomycin. All cells were housed in 5% CO_2 humidified atmosphere at 37°C.

In vitro cell viability: HUVEC cells were plated at 10^4 cells/well (in 100 μL media) in 96-well collagen-coated plates and allowed for adhesion overnight, followed by the addition of one of the following bottlebrush polymers: **5A-L**, **5A-D**, **2A-L**, or **2A-D**. The plates were incubated for 48h, and cell viability was then determined using CellTiter-Glo assay (Promega).

In vitro cell uptake: Stock solutions of **5A-L-Cy**, **5A-D-Cy**, **2A-L-Cy**, or **2A-D-Cy** were prepared in PBS (2 mg/mL). Cells were plated in 24-well plates and allowed for adhesion overnight in 450 μL media; HeLa and HUVEC cells were plated at 2.5×10^4 cells/well, whereas MCF7 cells were plated at 5.0×10^4 cells/well. Polymer solutions were then added (50 μL), resulting in the final polymer concentration of 0.2 mg/mL. Cells were then incubated for pre-determined interval, and

then harvested for analysis. Cell uptake was characterized by flow cytometry using a FACS LSR II HTS instrument (BD Biosciences).

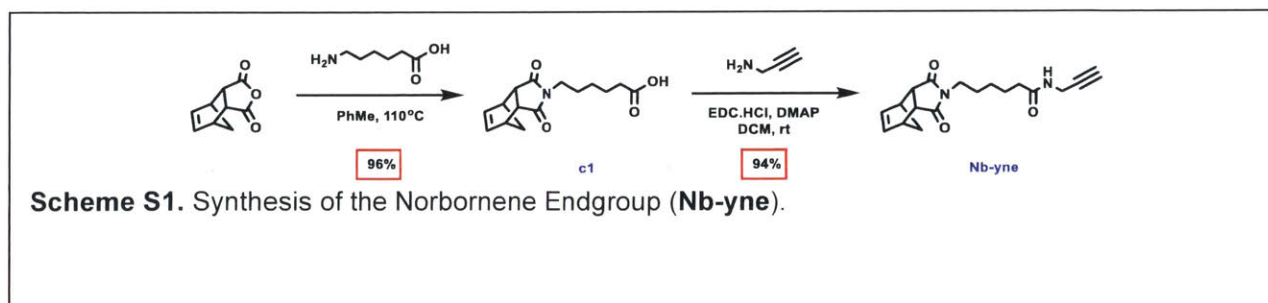
Animal usage: All experiments involving animals were reviewed and approved by the MIT Committee for Animal Care (CAC). BALB/c mice ($n=3$, female, 8-12 weeks old, Taconic) were used for pharmacokinetic and biodistribution studies after having receiving an alfalfa-free diet (TestDiet) for at least 2 weeks to minimize auto-fluorescence.

Pharmacokinetic and biodistribution studies: In separate pharmacokinetic studies, **5A-L-Cy**, **5A-D-Cy**, **2A-L-Cy**, or **2A-D-Cy** doses (2.0 mg/200 μ L) were injected into BALB/c mice (5 groups of $n=3$), and blood samples were taken at 1, 3, 6, 24, and 48h via cardiac puncture after euthanization in a CO₂ chamber, in addition to the control and 100% injected dose (ID). Samples were subjected to fluorescence imaging (IVIS, Cy5.5 $\lambda_{ex}/\lambda_{em} = 640/700$ nm, Xenogen). For biodistribution studies, organs from these BALB/c mice were harvested and subjected to fluorescence imaging (IVIS, Cy5.5 $\lambda_{ex}/\lambda_{em} = 640/700$ nm, Xenogen).

Imaging: ex vivo imaging was performed on an IVIS Spectrum-bioluminescent and fluorescent imaging system (Xenogen) at the Koch Institute for Integrative Cancer Research at MIT. Epi-fluorescence imaging was acquired through excitation of the Cy5.5 fluorophore ($\lambda_{ex}/\lambda_{em} = 640/700$ nm, exposure time 2-10s).

Synthetic Protocols

1) Norbornene Endgroup

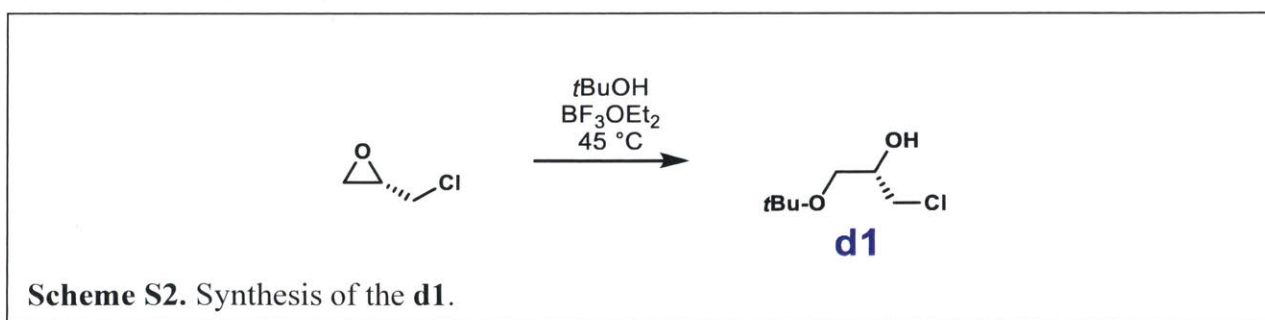


c1: a literature procedure (Patel, P. R.; Kiser, R. C.; Lu, Y. Y.; Fong, E.; Ho, W. C.; Tirrell, D. A.; Grubbs, R. H. Synthesis and Cell Adhesive Properties of Linear and Cyclic RGD Functionalized Polynorbornene Thin Films. *Biomacromolecules*, **2012**, *13*, 2546-2553.) was followed with slight modifications. Briefly, *cis*-5-norbornene-*exo*-2,3-dicarboxylic anhydride (500 mg, 3.0 mmol, 1.0

eq) and 6-aminohexanoic acid (480 mg, 3.7 mmol, 1.2 eq) were added to a round bottom flask (RBF) fitted with a condenser. Toluene (15 mL) was then added, and the solution was stirred overnight at 110°C. The mixture was then allowed to cool to room temperature, and concentrated under vacuum. DCM (150 mL) was then added, and the solution was washed with 1M HCl (3 × 150 mL) and brine (1 × 150 mL). The organic layer was collected, dried over Na₂SO₄, and concentrated under vacuum, affording the product as a white solid (830 mg, 96% yield). Characterization data agreed with the reported results.

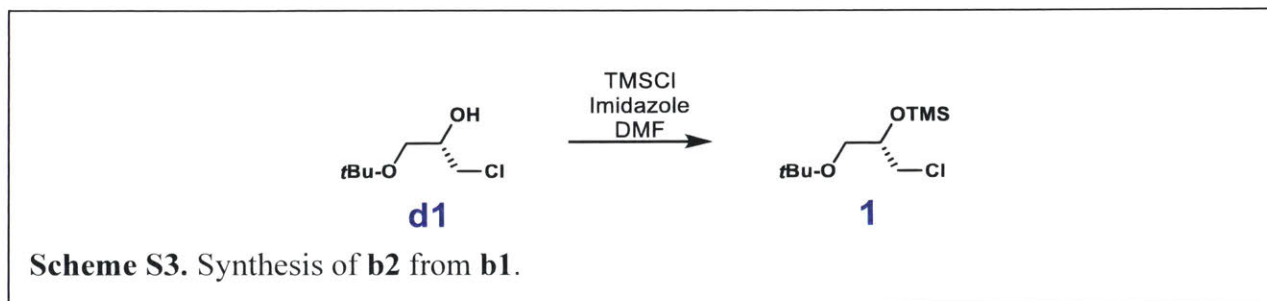
Nb-yne: into a RBF, **c1** (270 mg, 1.0 mmol, 1.5 eq), propargylamine (36 mg, 42 μL, 1.0 eq), *N*-(3-dimethylaminopropyl)-*N*'-ethylcarbodiimide hydrochloride (EDC.HCl) (180 mg, 1.0 mmol, 1.5 eq), and 4-dimethylaminopyridine (DMAP) (40. mg, 0.30 mmol, 0.5 eq), and DCM (35 mL) were added. The reaction mixture were stirred overnight and then concentrated under vacuum. Column chromatography (3% MeOH/DCM) of the crude mixture yielded product as a white solid (190 mg, 94% yield). HRMS-ESI: Calcd for C₁₈H₂₂N₂O₃: *m/z* = 315.1703 [*M* + H]⁺; Found: 315.1692 [*M*+H]⁺. ¹H NMR (400 MHz, CDCl₃, ppm) δ_H 6.28 (s, 2H), 5.70 (b, 1H), 4.04 (m, 2H), 3.45 (t, *J* = 7.2 Hz, 2H), 3.26 (s, 2H), 2.67 (s, 2H), 2.22 (t, *J* = 2.4 Hz, 1H), 2.18 (t, *J* = 7.6 Hz, 2H), 1.72 – 1.62 (m, 2H), 1.61 – 1.48 (m, 3H), 1.38 – 1.27 (m, 2H), 1.23 – 1.17 (d, 1H). ¹³C NMR (100 MHz, CDCl₃, ppm): δ_C 178.2, 172.3, 137.9, 79.8, 71.7, 47.9, 45.3, 42.9, 38.5, 36.2, 29.3, 27.5, 26.5, 25.0

2) 2-Atom IEG (2AIEG) Precursors

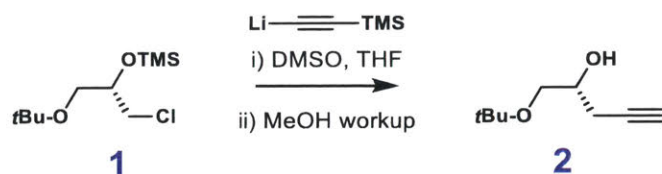


d1: (S)-Epichlorohydrin (100 g, 1.08 mol) was added dropwise to a solution of *t*-BuOH (300 g, 4.04 mol) and BF₃·OEt₂ (4.26 g, 30.0 mmol, 3.77 mL). The reaction solution was stirred at room temperature for 1 hour after which the reaction was heated to 45 °C and left to react overnight. 100 mL of water was then added to the solution and most of the *t*-BuOH was removed via reduced pressure. 400 mL of EtOAc was added to the reaction mixture and the solution was washed 2x

with 400 mL of water and 1x with 200 mL of brine. The organic layer was isolated, dried over Na₂SO₄, and concentrated under vacuum, affording the product as a clear liquid (140 g, 840 mmol, 78% yield). LRMS-ESI: Calcd for C₇H₁₅ClO₂: $m/z = 167.1 [M + H]^+$; Found: 167.1 $[M + H]^+$. ¹H NMR (500 MHz, CDCl₃, ppm) δ_H 3.91 (sext, $J = 5.5$ Hz, 1H), 3.64 (dd, $J = 5.5$ Hz, 4.5 Hz, 1H), 3.58 (dd, $J = 5.0$ Hz, 4.5 Hz, 1H), 3.46 (d, $J = 5.0$ Hz, 2H), 2.56 (d, $J = 5.0$ Hz, 1H), 1.20 (s, 9H). ¹³C NMR (125 MHz, CDCl₃, ppm): δ_C 73.5, 70.6, 62.3, 45.9, 27.4. The enantiomer of **d1** was also prepared in a similar fashion and has identical characterization to **d1**.

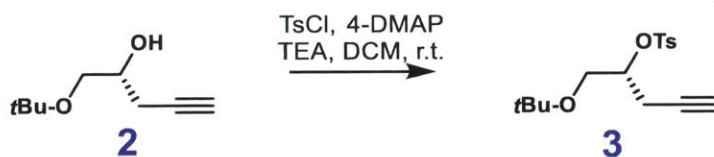


1: Imidazole (111 g, 1.63 mol) and DMF (400 mL) were added to **d1** (138 g, 831 mmol) and the solution was stirred until the imidazole was dissolved. TMSCl (177 g, 1.63 mol) was added gradually to the solution and the reaction was left to react overnight at room temperature. Upon completion, excess TMSCl and DMF were removed through reduced pressure. Throughout evaporation, the temperature was not allowed to exceed 60 °C to prevent degradation of the product. 300 mL of diethyl ether was then added to the mixture and stirred for half an hour. The organic solution was then extracted 3x with 200 mL H₂O, isolated, dried over Na₂SO₄, and concentrated under vacuum affording the product **1** as a clear liquid (170 g, 710 mmol, 85% yield). LRMS-ESI: Calcd for C₁₀H₂₃ClO₂Si: $m/z = 239.1 [M + H]^+$; Found: 239.1 $[M + H]^+$. ¹H NMR (500 MHz, CDCl₃, ppm) δ_H 3.91 (p, $J = 5.7$ Hz, 1H), 3.63 (dd, $J = 5.5$ Hz, 2.1 Hz, 1H), 3.49 (dd, $J = 12.6$ Hz, 1.8 Hz, 1H), 3.38 (dd, $J = 3.7$ Hz, 1.1 Hz, 1H), 3.33 (dd, $J = 3.2$ Hz, 0.9 Hz, 1H), 1.18 (s, 9H), 0.16 (s, 9H). ¹³C NMR (125 MHz, CDCl₃, ppm): δ_C 72.2, 63.7, 47.1, 27.5, 0.3. The enantiomer of **1** was also prepared in a similar fashion and has identical characterization to **1**.



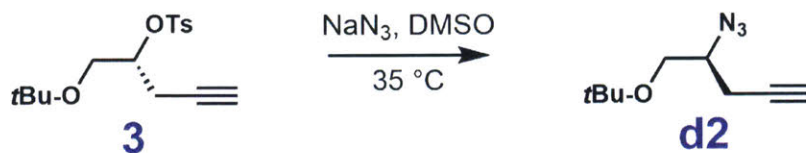
Scheme S4. Synthesis of **2** from **1**.

2: Trimethylsilylacetylene (113 g, 1.15 mol) was added to anhydrous THF (460 mL), and the solution was cooled to $-78\text{ }^{\circ}\text{C}$. A 2.5M solution of *n*-BuLi (460 mL) was added dropwise to the solution. The solution was allowed to warm to room temperature and kept inside a room temperature water bath. DMSO (300 mL) and then **1** (130 g, 546 mmol) were added to the reaction mixture and the reaction was left stirring for 4 hours. Completion of the reaction was checked through crude ^1H NMR. MeOH (30 mL) was then added very slowly dropwise to the solution to quench the reaction and remove all silyl protecting groups. Caution should be used as large quantities of gas will be released. 30 minutes after complete addition of MeOH, the majority of THF and other volatiles were removed under reduced pressure. 600 mL of diethyl ether was then added to the solution, which was then extracted 1x with 600 mL of H_2O and 2x with 300 mL of 5% LiCl solution. The organic layer was isolated, dried over Na_2SO_4 , and concentrated under vacuum, affording the product **2** as a slightly yellow liquid (54 g, 350 mmol, 63% yield) which was used without further purification. LRMS-ESI: Calcd for $\text{C}_9\text{H}_{16}\text{O}_2$: $m/z = 157.1$ [$M + \text{H}$] $^+$; Found: 157.0 [$M + \text{H}$] $^+$. ^1H NMR (500 MHz, CDCl_3 , ppm) δ_{H} 3.86 (sext, $J = 4.3$ Hz, 1H), 3.49 (dd, $J = 9.0$ Hz, 3.9 Hz, 1H), 3.36 (dd, $J = 9.0$ Hz, 6.5 Hz, 1H), 2.53 (d, $J = 4.9$ Hz, 1H), 2.45 (t, $J = 2.4$ Hz, 1H), 2.43 (t, $J = 2.7$ Hz, 1H), 2.02 (t, $J = 2.8$ Hz, 1H), 1.20 (s, 9H). ^{13}C NMR (125 MHz, CDCl_3 , ppm): δ_{C} 80.6, 73.3, 70.3, 69.1, 64.30, 27.5, 23.4. The enantiomer of **2** was also prepared in a similar fashion and has identical characterization to **2**.



Scheme S5. Synthesis of **3** from **2**.

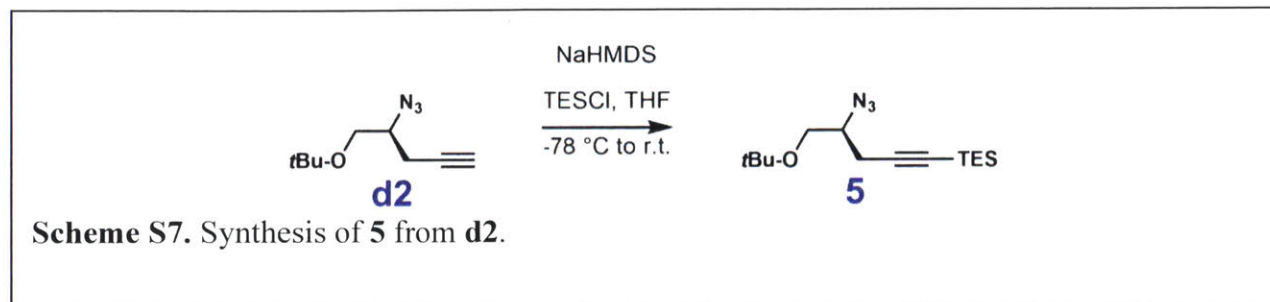
3: 4-DMAP (16.6 g, 136 mmol), triethylamine (51.5 g, 510 mmol), and DCM (600 mL) were added to **2** (53 g, 340 mmol). Tosyl chloride (71.3 g, 374 mmol) was then added portionwise into the solution and the reaction was left stirring overnight at room temperature. After completion of the reaction, DCM was removed under reduced pressure and 300 mL of EtOAc was added to the mixture. This organic solution was then extracted 1x with 300 mL of H₂O and 2x with 300 mL of pH=2 HCl solution. The organic layer was isolated, dried over Na₂SO₄, and concentrated under vacuum, affording the product **3** as a slightly yellow liquid (100 g, 320 mmol, 95% yield) which was used without further purification. LRMS-ESI: Calcd for C₁₆H₂₂O₄S: $m/z = 311.1 [M + H]^+$; Found: 311.1 $[M + H]^+$. ¹H NMR (500 MHz, CDCl₃, ppm) δ_H 7.81 (d, $J = 8.4$ Hz, 2H), 7.31 (d, $J = 8.2$ Hz, 2H), 4.54 (m, 1H), 3.50 (d, $J = 5.3$ Hz, 2H), 2.61 (dq, $J = 17.1$ Hz, 2.7 Hz, 1H), 2.56 (dq, $J = 16.5$ Hz, 3.1 Hz, 1H), 2.42 (s, 3H), 1.90 (t, $J = 2.7$ Hz, 1H), 1.08 (s, 9H). ¹³C NMR (125 MHz, CDCl₃, ppm): δ_C 144.8, 133.9, 129.7, 128.2, 79.1, 78.5, 73.6, 71.0, 61.7, 27.3, 21.8, 21.7. The enantiomer of **3** was also prepared in a similar fashion and has identical characterization to **3**.



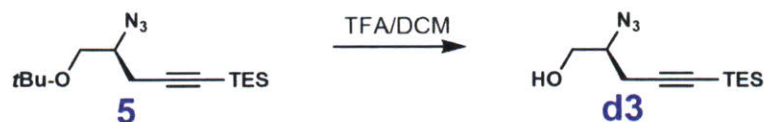
Scheme S6. Synthesis of **b5** from **b4**.

d2: NaN₃ (41.3 g, 636 mmol) and DMSO (500 mL) were added to **3** (66 g, 210 mmol) and the reaction was heated to 45 °C and left to react overnight. After completion of the reaction, 800 mL of EtOAc was added to the solution and this organic solution was extracted 1x with 800 mL of H₂O and 2x with 400 mL of 2% LiCl solution. The organic layer was isolated, dried over Na₂SO₄, and concentrated under vacuum. The crude product **d2** (31 g, 170 mmol, 81% yield) was used

without further purification. LRMS-ESI: Calcd for $C_9H_{15}N_3O$: $m/z = 182.1 [M + H]^+$; Found: 182.1 $[M + H]^+$. 1H NMR (500 MHz, $CDCl_3$, ppm) δ_H 3.60-3.47 (overlap, 3H), 2.03 (t, $J = 2.7$ Hz, 2H), 1.89 (t, $J = 2.8$ Hz, 1H), 1.19 (s, 9H). ^{13}C NMR (125 MHz, $CDCl_3$, ppm): 79.7, 78.9, 77.3, 73.4, 70.7, 63.3, 59.7. The enantiomer of **d2** was also prepared in a similar fashion and has identical characterization to **d2**.

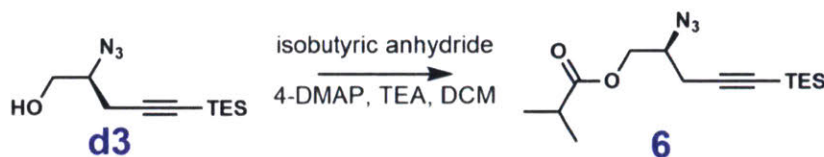


5: Anhydrous THF (550 mL) was added to **d2** (30 g, 160 mmol) and the solution was cooled to -78 °C. 1M solution of NaHMDS in THF (199 mmol, 199 mL) was added dropwise to the reaction solution. The reaction was left to stir for 30 minutes and then TESCl (37.4 g, 45.0 mL, 248 mmol) was added dropwise. The solution was allowed to warm to room temperature and left to react for 4 hours. Acetic acid (30 mL) was added to the solution to quench the reaction and THF was removed under reduced pressure. 100 mL of EtOAc was added to the solution and extracted 1x with 100 mL H_2O . The organic layer was isolated, dried over Na_2SO_4 , and concentrated under vacuum. The crude product was then purified with column chromatography (hexanes/EtOAc) to afford the final product **5** as a clear liquid (42 g, 140 mmol, 86% yield). LRMS-ESI: Calcd for $C_{15}H_{29}N_3OSi$: $m/z = 296.5 [M + H]^+$; Found: 296.5 $[M + H]^+$. 1H NMR (500 MHz, $CDCl_3$, ppm) δ_H 3.60-3.47 (overlap, 3H), 2.03 (t, $J = 2.7$ Hz, 2H), 1.89 (t, $J = 2.8$ Hz, 1H), 1.19 (s, 9H), 0.86 (q, 9H), 0.5 (t, 6H). ^{13}C NMR (125 MHz, $CDCl_3$, ppm): δ_C 103.3, 85.0, 73.7, 63.5, 60.3, 27.5, 22.8, 7.5, 4.5. The enantiomer of **5** was also prepared in a similar fashion and has identical characterization to **5**.



Scheme S8. Synthesis of **d3** from **5**.

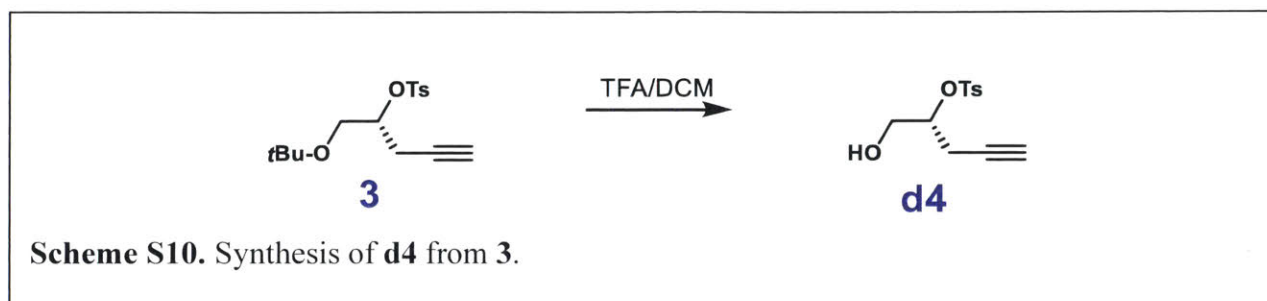
d3: A 1:1 solution of TFA and DCM (140 mL) were added to **5** (40 g, 130 mmol) and the solution was allowed to stir for 90 minutes. Progress of the reaction was tracked through TLC. Upon completion, TFA and DCM were removed through reduced pressure and the crude product was dissolved in 100 mL EtOAc and extracted 1x with 100 mL of H₂O and 1x with 100 mL of pH=1 HCl solution. The organic layer was isolated, dried over Na₂SO₄, and concentrated under vacuum. The crude product was then purified with column chromatography (hexanes/EtOAc) to afford the final product **d3** as a clear liquid (14 g, 58 mmol, 43% yield). LRMS-ESI: Calcd for C₁₁H₂₁N₃OSi: $m/z = 240.4 [M + H]^+$; Found: 240.4 $[M + H]^+$. ¹H NMR (500 MHz, CDCl₃, ppm) δ_H 3.60-3.47 (overlap, 3H), 2.03 (t, $J = 2.7$ Hz, 2H), 1.89 (t, $J = 2.8$ Hz, 1H), 0.86 (q, 9H), 0.5 (t, 6H). ¹³C NMR (125 MHz, CDCl₃, ppm): δ_C 102.5, 85.6, 85.6, 64.2, 62.3, 22.6, 7.5, 4.4. The enantiomer of **d3** was also prepared in a similar fashion and has identical characterization to **d3**.



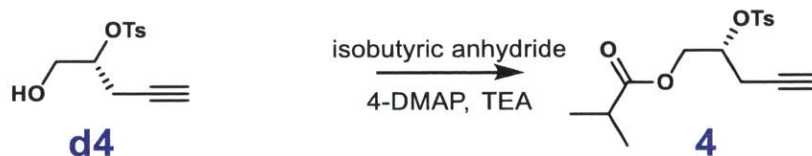
Scheme S9. Synthesis of **6** from **d3**.

6: 4-DMAP (1.3 g, 11 mmol), triethylamine (4.0 g, 5.5 mL, 40 mmol), and DCM (100 mL) were added to **d3** (6.3 g, 26 mmol). Isobutyric anhydride (7.19 g, 31.8 mmol) was then added dropwise into the solution and the reaction was left stirring for 2 hours. After completion of the reaction, DCM was removed under reduced pressure and 100 mL of EtOAc was added to the mixture. The organic solution was extracted 1x with 100 mL of H₂O and 2x with 100 mL of pH=1 HCl solution. The organic layer was isolated, dried over Na₂SO₄, and concentrated under vacuum. The crude product was purified by column chromatography (hexanes/EtOAc) to afford the final product **6** as

a clear liquid (5.6 g, 18 mmol, 69% yield). LRMS-ESI: Calcd for $C_{15}H_{27}N_3O_2Si$: $m/z = 310.5 [M + H]^+$; Found: 310.4 $[M + H]^+$. 1H NMR (500 MHz, $CDCl_3$, ppm) δ_H 4.28 (dd, $J = 10.7$ Hz, 3.3 Hz, 1H), 4.14 (dd, $J = 11.2$ Hz, 5.9 Hz, 1H), 3.75 (pent, $J = 5.4$ Hz, 1H), 2.60 (sept, $J = 5.8$ Hz, 1H), 2.53 (d, $J = 5.6$ Hz, 2H), 1.19 (d, $J = 5.9$ Hz, 6H), 0.97 (t, $J = 6.6$ Hz, 9H), 5.58 (q, $J = 6.5$ Hz, 6H). ^{13}C NMR (125 MHz, $CDCl_3$, ppm): δ_C 176.6, 101.8, 86.0, 65.2, 59.2, 34.0, 22.9, 19.0, 19.0, 7.5, 4.4. The enantiomer of **6** was also prepared in a similar fashion and has identical characterization to **6**.

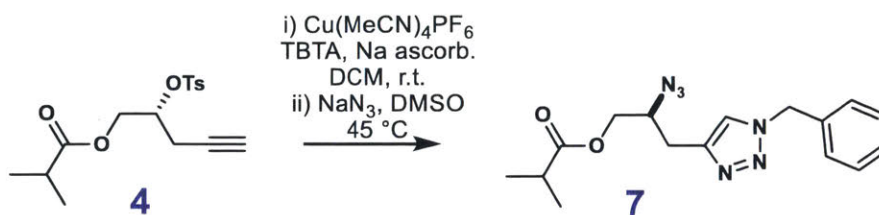


d4: A 1:1 solution of TFA and DCM (110 mL) were added to **3** (33 g, 110 mmol) and the solution was allowed to stir for 90 minutes. Progress of the reaction was tracked through TLC. Upon completion, TFA and DCM were removed through reduced pressure and the crude product was dissolved in 100 mL EtOAc and extracted 1x with 100 mL of H_2O and 1x with 100 mL of pH=1 HCl solution. The organic layer was isolated, dried over Na_2SO_4 , and concentrated under vacuum. The crude product was then purified with column chromatography (hexanes/EtOAc) to afford the final product **d4** as a clear liquid (19 g, 73 mmol, 67% yield). LRMS-ESI: Calcd for $C_{12}H_{14}O_4S$: $m/z = 255.3 [M + H]^+$; Found: 255.2 $[M + H]^+$. 1H NMR (500 MHz, $CDCl_3$, ppm) δ_H 7.83 (d, $J = 8.4$ Hz, 2H), 7.36 (d, $J = 8.3$ Hz, 2H), 4.64 (m, 1H), 3.91 (dd, $J = 12.6$ Hz, 3.3 Hz, 1H), 3.84 (dd, $J = 12.7$ Hz, 5.4 Hz, 1H), 2.59 (dq, $J = 5.7$ Hz, 2.9 Hz, 1H), 2.55 (dq, $J = 10.2$ Hz, 2.7 Hz, 1H), 2.46 (s, 3H), 1.97 (t, $J = 2.9$ Hz, 1H). ^{13}C NMR (125 MHz, $CDCl_3$, ppm): δ_C 145.1, 133.2, 129.8, 127.8, 80.2, 78.0, 71.4, 62.6, 21.5, 21.0. The enantiomer of **d4** was also prepared in a similar fashion and has identical characterization to **d4**.



Scheme S11. Synthesis of **4** from **d4**.

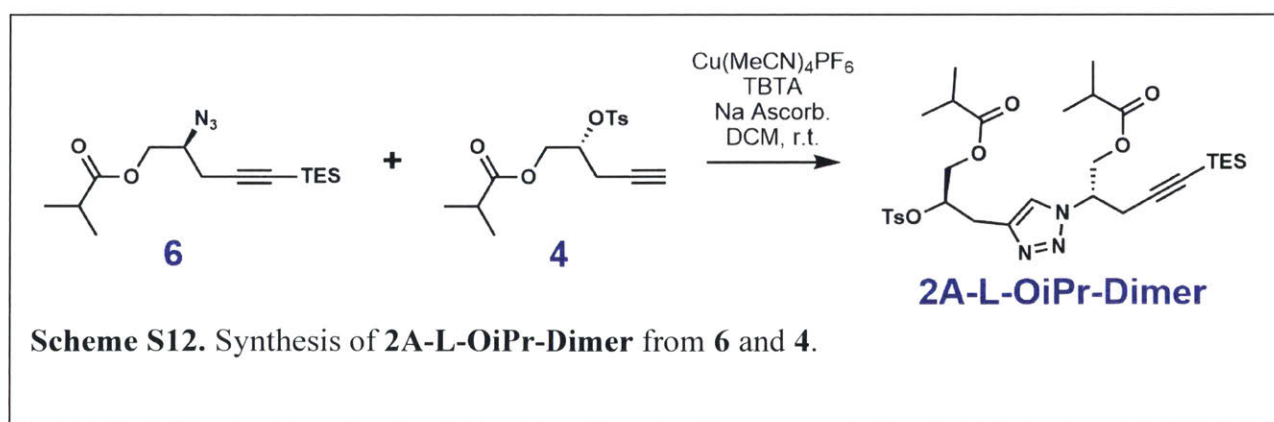
4: 4-DMAP (3.1 g, 25 mmol), triethylamine (7.6 g, 10 mL, 75 mmol), and DCM (100 mL) were added to **d4** (14.7 g, 56.5 mmol). Isobutyric anhydride (9.8 g, 62 mmol) was then added dropwise into the solution and the reaction was left stirring for 2 hours. After completion of the reaction, DCM was removed under reduced pressure and 100 mL of EtOAc was added to the mixture. The organic solution was extracted 1x with 100 mL of H₂O and 2x with 100 mL of pH=1 HCl solution. The organic layer was isolated, dried over Na₂SO₄, and concentrated under vacuum to afford the final product **4** as a clear liquid (16 g, 50 mmol, 89% yield). LRMS-ESI: Calcd for C₁₆H₂₀O₅S: *m/z* = 325.1 [*M* + H]⁺; Found: 325.1 [*M* + H]⁺. ¹H NMR (500 MHz, CDCl₃, ppm) δ_H 7.78 (d, *J* = 7.0 Hz, 2H), 7.32 (d, *J* = 6.8 Hz, 2H), 4.73 (m, 1H), 4.26 (dd, *J* = 10.2 Hz, 2.9 Hz, 1H), 4.16 (dd, *J* = 10.3 Hz, 5.3 Hz, 1H), 2.57 (dd, *J* = 5.3 Hz, 2.3 Hz, 2H), 2.42 (s, 3H), 2.40 (pent, *J* = 5.9 Hz, 1H), 1.98 (t, *J* = 2.3 Hz, 1H), 1.08 (d, *J* = 5.9 Hz, 3H), 1.07 (d, *J* = 5.8 Hz, 3H). ¹³C NMR (125 MHz, CDCl₃, ppm): δ_C 176.4, 145.1, 133.7, 129.9, 128.0, 127.9, 77.3, 76.8, 71.9, 63.5, 33.8, 21.9, 21.7, 18.9, 18.8. The enantiomer of **4** was also prepared in a similar fashion and has identical characterization to **4**.



Scheme S10. Synthesis of **7** from **3**.

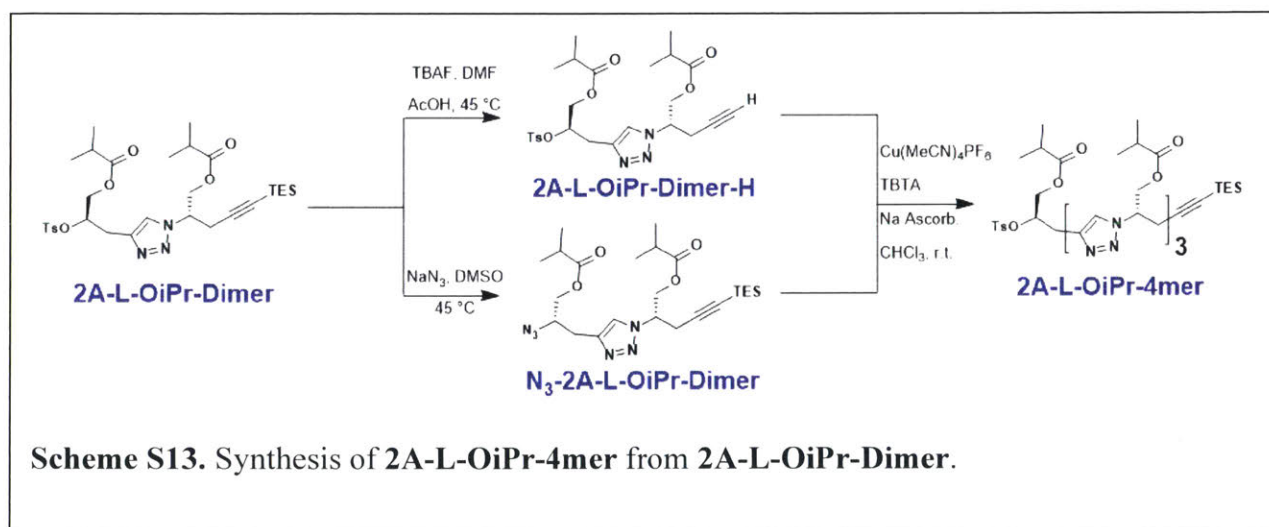
7: DCM (1.2 mL), benzyl azide () tris(benzyltriazolylmethyl)amine (TBTA) (6.4 mg, 0.012 mmol), Cu(MeCN)₄PF₆ (2.3 mg, 0.062 mmol), and sodium ascorbate (2.3 mg, 0.012 mmol) were added to **4** (20 mg, 0.062 mmol) in an oven-dried 20 mL scintillation vial. The reaction was left at room temperature and stirred overnight. Progress of the reaction was tracked through TLC. At

completion, EtOAc (10 mL) was added to the mixture which was extracted 3 times with 10 mL of water. The organic layer was isolated, dried over Na₂SO₄, and concentrated under reduced pressure. NaN₃ (8.1 mg, 0.12 mmol) and DMSO (240 μL) were added to the crude product and the mixture was heated to 45 °C and left to react overnight. EtOAc (10 mL) was added to the mixture which was extracted 3 times with 10 mL of 1% LiCl solution. The organic layer was isolated, dried over Na₂SO₄, and concentrated under reduced pressure. The crude product was loaded onto a silica column and purified with column chromatography (hexanes to DCM to 1% MeOH in DCM) to yield **7** (14 mg, 0.043 mmol, 69% yield). LRMS-ESI: Calcd for C₃₁H₄₇N₃O₇SSi: *m/z* = 329.4 [*M* + H]⁺; Found: 329.3 [*M* + H]⁺. ¹H NMR (500 MHz, CDCl₃, ppm) δ_H 7.37 (overlap, 3H), 7.34 (s, 1H), 7.26 (overlap with CDCl₃, 2H), 5.52 (s, 2H), 4.26 (dd, *J* = 9.5 Hz, 2.5 Hz, 1H), 4.11 (dd, *J* = 9.5 Hz, 5.5 Hz, 1H), 4.01 (m, 1H), 2.95 (dd, *J* = 12.5 Hz, 1.8 Hz, 1H), 2.87 (dd, *J* = 12.5 Hz, 7.0 Hz, 1H), 2.60 (sept, *J* = 5.0 Hz, 1H), 1.19 (d, *J* = 6.0 Hz, 6H). ¹³C NMR (100 MHz, CDCl₃, ppm): 176.7, 143.4, 134.7, 129.2, 129.2, 128.9, 128.1, 128.1, 122.2, 65.9, 60.3, 54.3, 34.0, 27.8, 19.0, 18.9. The enantiomer of **7** was also prepared in a similar fashion and has identical characterization to **7**. Both enantiomers were tested on a chiral HPLC to confirm enantiomeric purity.



2A-L-OiPr-Dimer: DCM (30 mL), tris(benzyltriazolylmethyl)amine (TBTA) (350 mg, 0.65 mmol), Cu(MeCN)₄PF₆ (160 mg, 0.43 mmol), and sodium ascorbate (160 mg, 0.81 mmol) were added to a mixture of **4** (5.5 g, 18 mmol) and **6** (6.2 g, 19 mmol) in an oven-dried 100 mL round bottom flask. The reaction was left at room temperature and stirred overnight. Progress of the reaction was tracked through TLC. At completion, the majority of DCM was removed under

reduced pressure and the crude product was loaded onto a silica column. Column chromatography (hexanes to DCM to 1% MeOH in DCM) was used to purify the desired product. **2A-L-OiPr-Dimer** was isolated as a slightly yellow viscous liquid (8.8 g, 14 mmol, 78% yield). LRMS-ESI: Calcd for C₃₁H₄₇N₃O₇SSi: $m/z = 634.9 [M + H]^+$; Found: 634.8 $[M + H]^+$. ¹H NMR (500 MHz, CDCl₃, ppm) δ_H 7.76 (d, $J = 8.3$ Hz, 2H), 7.58 (s, 1H), 7.33 (d, $J = 7.7$ Hz, 2H), 4.98 (m, 1H), 4.91 (m, 1H), 4.53 (overlap, 2H), 4.20 (dd, $J = 12.4$ Hz, 3.5 Hz, 1H), 4.02 (dd, $J = 12.4$ Hz, 6.5 Hz, 1H), 3.15 (m, 2H), 2.92 (m, 2H), 2.53 (sept, $J = 7.0$ Hz, 1H), 2.44 (s, 3H), 2.37 (sept, $J = 7.2$ Hz, 1H), 1.12-1.07 (overlap, 12H), 0.94 (t, $J = 7.9$ Hz, 9H), 0.55 (q, $J = 8.0$ Hz, 6H). ¹³C NMR (100 MHz, CDCl₃, ppm): 176.1, 176.1, 144.8, 141.0, 133.7, 129.7, 127.6, 122.0, 100.7, 86.4, 78.5, 63.8, 63.6, 58.6, 33.6, 33.5, 28.2, 23.3, 21.5, 18.7, 18.7, 18.6, 7.3, 4.1. **2A-D-OiPr-Dimer** was also prepared in a similar fashion and has identical characterization to **2A-L-OiPr-Dimer**.

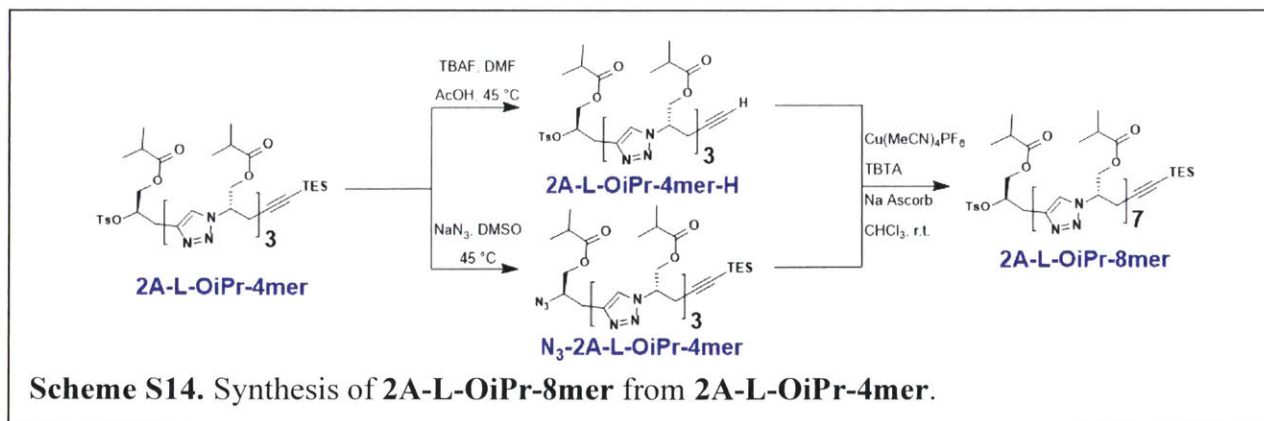


2A-L-OiPr-4mer: The **2A-L-OiPr-2mer-H** precursor to **2A-L-OiPr-4mer** was prepared by dissolving **2A-L-OiPr-2mer** (2.8 g, 4.4 mmol) in DMF (20 mL) in a 40 mL scintillation vial. AcOH (260 mg, 4.4 mmol) was added to this solution. A solution composed of a mixture of AcOH (260 mg, 4.4 mmol) and tetrabutylammonium fluoride (TBAF) (4.4 mL, 1M in THF, 4.4 mmol) was then added to reaction solution dropwise. Any additional excess AcOH will potentially slow down the reaction. The reaction was heated to 45 °C and left to react for 4 hours. The reaction was monitored by ¹H NMR to determine completion. After completion, 100 mL of EtOAc was added to the reaction mixture and extracted 3x with 100 mL 0.5% LiCl solution. The organic layer

was isolated, dried over Na₂SO₄ and concentrated under vacuum. The resulting yellow oil containing **2A-L-OiPr-2mer-H** and TES-F was used directly in the next step.

The **N₃-2A-L-OiPr-2mer** precursor to **2A-L-OiPr-4mer** was prepared by dissolving **2A-L-OiPr-2mer** (2.8 g, 4.4 mmol) in DMSO (26 mL), followed by the addition of NaN₃ (858 mg, 13.2 mmol). The reaction mixture was heated to 45 °C and allowed to stir for 12 h before 100 mL of EtOAc was added to the reaction mixture and the solution was extracted 3x with 100 mL 0.5% LiCl solution. The organic layer was dried over Na₂SO₄ and concentrated under vacuum. The resulting **N₃-2A-L-OiPr-2mer** was obtained as an off-white solid and was used in the next step without further purification.

Under an N₂ atmosphere, chloroform (50 mL), Cu(MeCN)₄PF₆ (120 mg, 0.33 mmol), TBTA (260 mg, 0.48 mmol), and sodium ascorbate (120 mg, 0.61 mmol) were added to **N₃-2A-L-OiPr-2mer** in a 100 mL round bottom flask. The mixture was stirred and sonicated until the Cu(MeCN)₄PF₆ and TBTA are dissolved. A solution of **2A-L-OiPr-2mer-H** in chloroform (10 mL) was then added slowly to the above solution. The reaction mixture was warmed to 35 °C and allowed to react overnight. The reaction was tracked by TLC. Upon completion, the solution was concentrated under reduced pressure until it becomes a viscous mixture, which was then loaded carefully onto a silica column. Column chromatography (100% DCM to 1.25% MeOH/DCM then 3.5% MeOH/DCM) yielded the product **2A-L-OiPr-4mer** (3.8 g, 3.7 mmol, 84% yield) as an off-white solid. ¹H NMR (500 MHz, CDCl₃, ppm) δ_H 7.76 (d, *J* = 8.1 Hz, 2H), 7.48 (s, 1H), 7.34 (d, *J* = 8.0 Hz, 2H), 7.26 (s, 1H), 7.19 (s, 1H), 5.07 (overlap, 2H), 4.98 (m, 1H), 4.91 (m, 1H), 4.55-4.39 (overlap, 4H), 4.15 (dd, *J* = 12.5 Hz, 3.5 Hz, 1H), 3.99 (dd, *J* = 12.4 Hz, 6.6 Hz, 1H), 3.40-3.33 (overlap, 4H), 3.13 (m, 2H), 2.90 (m, 2H), 2.55-2.44 (overlap, 6H), 2.36 (sept, *J* = 7.0 Hz, 1H), 1.12-1.05 (overlap, 24H), 0.93 (t, *J* = 7.9 Hz, 9H), 0.55 (q, *J* = 7.9 Hz, 6H). ¹³C NMR (125 MHz, CDCl₃, ppm): 176.4, 176.4, 176.3, 145.1, 141.9, 141.7, 141.4, 133.9, 130.0, 127.8, 122.8, 122.4, 121.7, 101.0, 86.5, 78.7, 64.8, 64.6, 63.9, 63.8, 60.1, 59.9, 58.8, 33.8, 33.80, 33.71, 28.4, 28.3, 28.1, 23.4, 21.7, 18.9, 18.9, 18.8, 7.5, 4.3. **2A-D-OiPr-4mer** was also prepared in a similar fashion and has identical characterization to **2A-L-OiPr-4mer**.



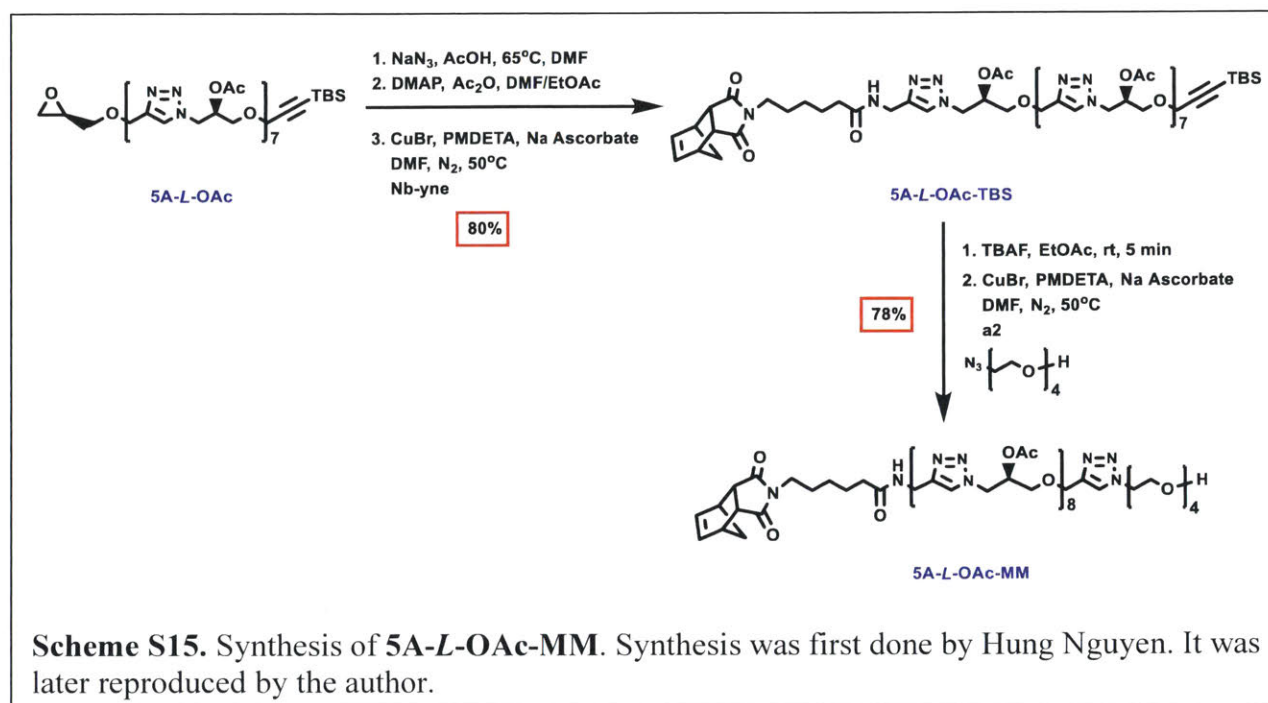
2A-L-OiPr-8mer: The **2A-L-OiPr-4mer-H** precursor to **2A-L-OiPr-8mer** was prepared by dissolving **2A-L-OiPr-4mer** (1.7 g, 1.7 mmol) in DMF (8.5 mL) in a 40 mL scintillation vial. AcOH (113 mg, 1.88 mmol) was added to this solution. A solution composed of a mixture of AcOH (113 mg, 1.88 mmol) and TBAF (1.88 mL, 1M in THF, 1.88 mmol) was then added to reaction solution dropwise. Any additional excess AcOH will potentially slow down the reaction. The reaction was heated to 45 °C and left to react for 4 hours. The reaction was monitored by ¹H NMR to determine completion. After completion, 100 mL of EtOAc was added to the reaction mixture and extracted 3x with 100 mL 0.5% LiCl solution. The organic layer was isolated, dried over Na₂SO₄ and concentrated under vacuum. The resulting yellow oil containing **2A-L-OiPr-4mer-H** and TES-F was used directly in the next step.

The **N₃-2A-L-OiPr-4mer** precursor to **2A-L-OiPr-8mer** was prepared by dissolving **2A-L-OiPr-4mer** (1.7 g, 1.7 mmol) in DMSO (17 mL), followed by the addition of NaN₃ (33 mg, 5.1 mmol). The reaction mixture was heated to 45 °C and allowed to stir for 12 h before 100 mL of EtOAc was added to the reaction mixture and the solution was extracted 3x with 100 mL 0.5% LiCl solution. The organic layer was dried over Na₂SO₄ and concentrated under vacuum. The resulting **N₃-2A-L-OiPr-4mer** was obtained as an off-white solid and was used in the next step without further purification.

Under an N₂ atmosphere, chloroform (10 mL), Cu(MeCN)₄PF₆ (20 mg, 0.054 mmol), TBTA (43 mg, 0.080 mmol), and sodium ascorbate (20 mg, 0.1 mmol) were added to **N₃-2A-L-OiPr-4mer** in a 40 mL scintillation vial. The mixture was stirred and sonicated until the Cu(MeCN)₄PF₆ and TBTA are dissolved. A solution of **2A-L-OiPr-4mer-H** in chloroform (10 mL) was then added slowly to the above solution. The reaction mixture was warmed to 35 °C and allowed to react overnight. The reaction was tracked by TLC. Upon completion, the solution was concentrated

under reduced pressure until it becomes a viscous mixture, which was then loaded carefully onto a silica column. Column chromatography (100% DCM to 1.25% MeOH/DCM then 3.5% MeOH/DCM) yielded the product **2A-L-OiPr-8mer** (1.9 g, 1.0 mmol, 56% yield) as an off-white solid. ^1H NMR (500 MHz, CDCl_3 , ppm) δ_{H} 7.83 (s, 1H), 7.82 (d, $J = 8.3$ Hz, 2H), 7.48 (s, 1H), 7.41 (s, 1H), 7.38 (d, $J = 8.0$ Hz, 2H), 7.26 (s, 1H), 7.24 (s, 1H), 7.09 (s, 1H), 7.08 (s, 1H), 5.33 – 4.99 (overlap, 10H), 4.92 (dd, $J = 11.8$ Hz, 8.9 Hz, 1H), 4.84 – 4.77 (overlap, 3Hw), 4.64 – 4.57 (overlap, 2H), 4.49 – 4.33 (overlap, 7H), 4.10 (m, 2H), 3.65 – 3.44 (overlap, 5H), 3.37 – 3.19 (overlap, 9H), 3.10 – 2.97 (overlap, 2H), 2.92 (dd, $J = 17.1$ Hz, 6.1 Hz, 1H), 2.62 – 2.41 (overlap, 10H), 2.29 (sept, $J = 7.0$ Hz, 1H), 1.17 – 0.91 (overlap, 57H), 0.55 (q, $J = 8.0$ Hz, 6H). ^{13}C NMR (125 MHz, CDCl_3 , ppm): 180.0, 177.3, 176.6, 176.5, 176.5, 176.4, 176.4, 176.3, 176.3, 176.3, 176.2, 176.2, 145.4, 143.1, 142.8, 142.6, 142.6, 142.5, 140.4, 133.6, 130.0, 129.9, 128.9, 127.7, 127.7, 126.0, 122.4, 121.4, 121.2, 121.1, 120.9, 120.7, 120.2, 101.5, 101.5, 85.7, 85.7, 78.7, 64.6, 64.5, 64.4, 64.4, 64.3, 64.2, 64.1, 64.1, 63.9, 63.8, 63.8, 63.7, 63.6, 61.5, 61.5, 61.4, 61.3, 61.2, 60.9, 59.2, 33.8, 33.7, 33.6, 33.6, 33.5, 29.3, 28.5, 28.4, 27.9, 27.7, 27.7, 27.5, 23.2, 21.6, 21.3, 19.0, 18.9, 18.9, 18.8, 18.7, 18.7, 18.7, 18.6, 18.6, 7.4, 4.2. **2A-D-OiPr-8mer** was also prepared in a similar fashion and has identical characterization to **2A-L-OiPr-8mer**.

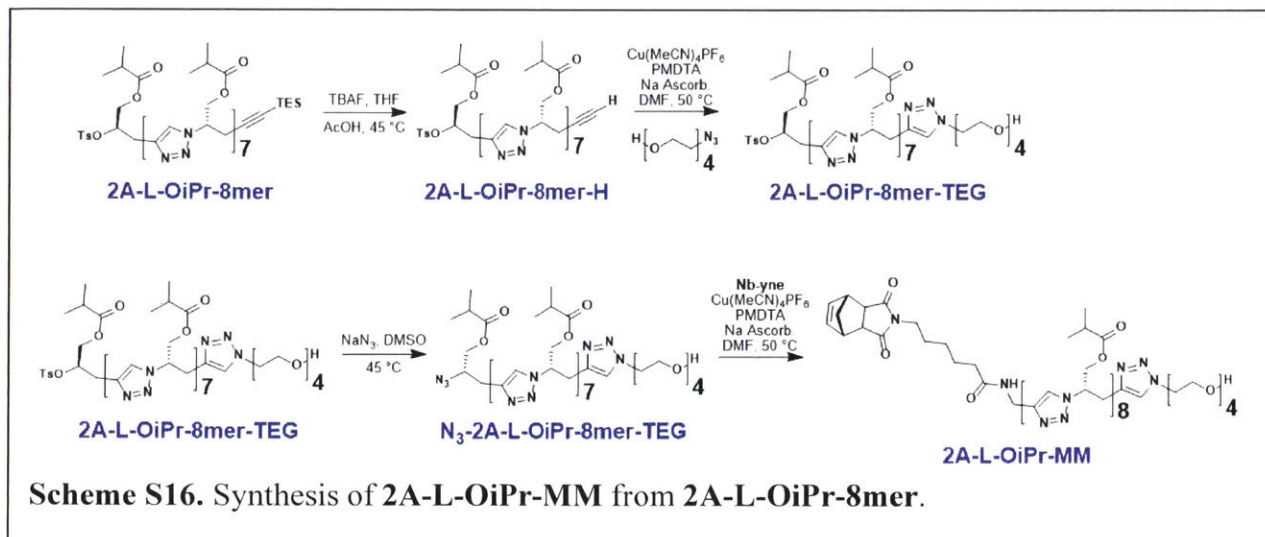
3) Macromonomer Synthesis



5A-L-OAc-TBS: In a RBF, **5A-L-OAc** (1.1 g, 0.70 mmol, 1 eq) was dissolved in DMF (7 mL), followed by the addition of acetic acid (63 mg, 60 μL , 1.1 mmol, 1.5 eq) and sodium azide (137 mg, 2.10 mmol, 3 eq). The reaction mixture was stirred at 65°C for 6 hours, and the DMF was then removed via rotary evaporator, leaving only ~0.5 mL of DMF. EtOAc (~5 mL) was then added, and the precipitated salt was filtered off. DMAP (43 mg, 0.40 mmol, 0.5 eq) and acetic anhydride (140 mg, 130 μL , 1.4 mmol, 2 eq) were added, and the mixture was stirred for 30 minutes. The mixture was then concentrated and pushed through a plug of silica gel using 6-7% MeOH/DCM. The resulting material was collected, concentrated under vacuum, and added to a RBF with DMF (4 mL), **Nb-yne** (340 mg, 1.1 mmol, 1.5 eq), copper (I) bromide (5 mg, 0.04 mmol, 0.05 eq), PMDETA (14 mg, 17 μL , 0.080 mmol, 0.1 eq), and sodium ascorbate (16 mg, 0.080 mmol, 0.1 eq). The reaction mixture was heated to 50°C and allowed to stir for 2 hours under nitrogen. The crude product was concentrated under vacuum and purified by column chromatography (0-10% MeOH/DCM), affording **5A-L-OAc-TBS** (1.3 g, 80% yield) as a white solid.

5A-L-OAc-MM: **5A-L-OAc-TBS** (1.2 g, 0.60 mmol, 1.0 eq) was dissolved in EtOAc (12 mL), followed by the slow addition of TBAF (1M in THF, 700 μL , 0.70 mmol, 1.1 eq). The reaction was stirred for 5 minutes, and MeOH (5 mL) was added, followed by 5-10 minutes of stirring. The

crude material was concentrated under vacuum and pushed through a silica gel plug using 2-3% MeOH/DCM. The resulting material was collected, concentrated under vacuum, and added to a RBF with DMF (5 mL), **c2** (“azido tetraethylene glycol”) (200 mg, 1.0 mmol, 1.5 eq), copper (I) bromide (4 mg, 0.03 mmol, 0.05 eq), PMDETA (11 mg, 10 μ L, 0.060 mmol, 0.1 eq), and sodium ascorbate (12 mg, 0.060 mmol, 0.1 eq). The reaction mixture was heated to 50°C and allowed to stir for 2 hours under nitrogen. The crude product was concentrated under vacuum and purified by column chromatography (2-14% MeOH/DCM), affording **5A-L-OAc-MM** (960 mg, 78% yield) as a white solid. MALDI: Calcd for C₉₀H₁₂₈N₂₉O₃₁: $m/z = 2110.93 [M+H]^+$; Found: 2111.572 $[M+H]^+$. ¹H NMR (500 MHz, CDCl₃, ppm) δ_H 7.83 (s, 1H), 7.67 (m, 7H), 7.58 (s, 1H), 6.42 (b, 1H), 6.27 (s, 2H), 5.31 – 5.25 (m, 8H), 4.70 – 4.54 (m, 32H), 4.51 – 4.41 (m, 3H), 3.87 (t, $J = 4.0$ Hz, 2H), 3.74 – 3.49 (m, 30H), 3.43 (t, $J = 6.0$ Hz, 2H), 3.25 (s, 2H), 2.67 (s, 2H), 2.18 (t, $J = 6.0$ Hz, 2H), 2.08 – 1.98 (br s, 24H), 1.67 – 1.60 (m, 2H), 1.57 – 1.47 (m, 3H), 1.33 – 1.26 (m, 2H), 1.21 – 1.17 (d, 1H). ¹³C NMR (100 MHz, CDCl₃, ppm): δ_C 178.2, 172.9, 170.0, 144.3, 137.9, 124.5, 124.1, 123.5, 72.6, 70.7, 70.6, 70.5, 70.3, 69.5, 68.2, 64.7, 61.7, 50.4, 50.1, 47.9, 45.3, 42.9, 38.5, 36.2, 35.0, 27.6, 26.6, 25.1, 21.0. This procedure was also implemented for the synthesis of the **5A-D-OAc-MM**, affording similar yield. MALDI: Calcd for C₉₀H₁₂₈N₂₉O₃₁: $m/z = 2110.93 [M+H]^+$; Found: 2111.449 $[M+H]^+$. ¹H NMR (400 MHz, CDCl₃, ppm) δ_H 7.83 (s, 1H), 7.67 (m, 7H), 7.58 (s, 1H), 6.42 (b, 1H), 6.27 (s, 2H), 5.32 – 5.28 (m, 8H), 4.70 – 4.54 (m, 32H), 4.51 – 4.42 (m, 3H), 3.87 (t, $J = 4.0$ Hz, 2H), 3.73 – 3.50 (m, 30H), 3.43 (t, $J = 6.0$ Hz, 2H), 3.25 (s, 2H), 2.66 (s, 2H), 2.18 (t, $J = 6.0$ Hz, 2H), 2.08 – 1.99 (br s, 24H), 1.67 – 1.60 (m, 2H), 1.57 – 1.47 (m, 3H), 1.34 – 1.26 (m, 2H), 1.21 – 1.17 (d, 1H). ¹³C NMR (100 MHz, CDCl₃, ppm): δ_C 178.2, 172.9, 170.0, 144.3, 137.9, 124.5, 124.1, 123.4, 72.6, 70.7, 70.6, 70.5, 70.3, 69.5, 68.2, 64.7, 61.7, 50.4, 50.1, 47.9, 45.3, 42.9, 38.5, 36.3, 35.0, 27.6, 26.6, 25.1, 21.0.

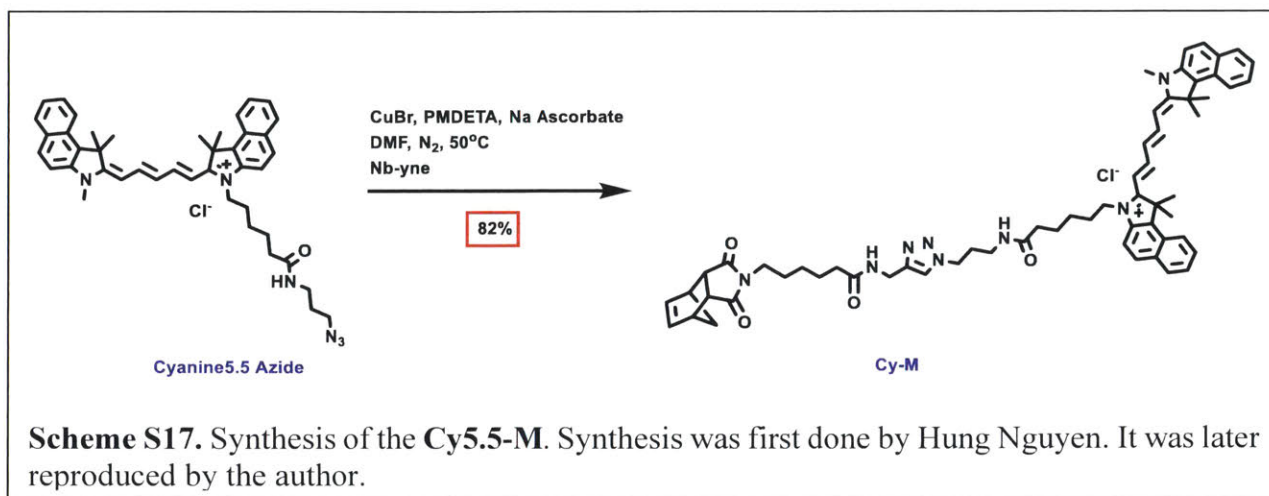


2A-L-OiPr-8mer-TEG: **2A-L-OiPr-8mer** (1.5 g, 0.84 mmol) was dissolved in DMF (8 mL), followed by the addition of AcOH (63 mg, 1.0 mmol). A solution of composed of a mixture of AcOH (63 mg, 1.0 mmol) and TBAF (1.04 mL, 1M in THF, 1.04 mmol) was then added to reaction solution dropwise. Any additional excess AcOH will potentially slow down the reaction. The reaction was heated to 45 °C and left to react for 4 hours. The reaction was monitored by ¹H NMR to determine completion. After completion, 100 mL of EtOAc was added to the reaction mixture and extracted 3x with 100 mL 0.5% LiCl solution. The organic layer was isolated, dried over Na₂SO₄ and concentrated under vacuum. The compound was then transferred to a 40 mL scintillation vial and DMF (10 mL), **c2** (466 mg, 2.22 mmol), Cu(MeCN)₄PF₆ (20 mg, 0.054 mmol), PMDETA (19 mg, 0.11 mmol), and sodium ascorbate (20 mg, 0.1 mmol) were also added to the vial. The reaction mixture was heated to 50 °C and allowed to stir for 2 hours under nitrogen. The reaction solution was run through a neutral alumina column with 5% MeOH/DCM to remove copper. The solvent was removed under reduced pressure and **2A-L-OiPr-8mer-TEG** was purified through preparatory GPC to yield **2A-L-OiPr-8mer-TEG** (1.0 g, 0.53 mmol, 64% yield) as a white solid.

2A-L-OiPr-8mer-TEG (1.0 g, 0.53 mmol) was dissolved in DMSO (15 mL) followed by the addition of NaN₃ (100 mg, 1.5 mmol). The reaction mixture was heated to 45 °C and allowed to stir for 12 h before 100 mL of EtOAc was added to the reaction mixture and the solution was extracted 3x with 100 mL 0.5% LiCl solution. The organic layer was dried over Na₂SO₄ and concentrated under vacuum which resulted in crude **N₃-2A-L-OiPr-8mer-TEG**. DMF (15 mL), **Nb-ynone** (630 mg, 2.0 mmol), Cu(MeCN)₄PF₆ (20 mg, 0.054 mmol), PMDETA (19 mg, 0.11

mmol), and sodium ascorbate (20 mg, 0.1 mmol) were also added to **N₃-2A-L-OiPr-8mer-TEG**. The reaction mixture was heated to 50 °C and allowed to stir for 2 hours under nitrogen. The reaction solution was run through a neutral alumina column with 5% MeOH/DCM to remove copper. The solvent was removed under reduced pressure and the crude product was purified through preparatory GPC to yield **2A-L-OiPr-MM** (820 mg, 0.39 mmol, 74% yield) as a white solid. MALDI-TOF-MS: Calcd for C₉₈H₁₄₄N₂₉O₂₃: $m/z = 2097.86 [M + H]^+$; Found: 2097.35 $[M + H]^+$. ¹H NMR (500 MHz, CDCl₃, ppm) δ 7.87 (s, 1H), 7.32 (s, 1H), 7.27 (s, 1H), 7.24 (s, 1H), 7.22 (s, 1H), 7.17 (s, 1H), 7.15 (s, 1H), 6.99 (t, $J = 5.7$ Hz), 6.87 (s, 1H), 6.29 (s, 2H), 5.49-5.34 (overlap, 5H), 5.28-5.04 (overlap, 10H), 4.98 (t, $J = 10.1$ Hz, 1H), 4.78-4.70 (overlap, 2H), 4.66-4.53 (overlap, 4H), 4.47-4.31 (overlap, 10H), 3.98-3.89 (overlap, 2H), 3.75-3.56 (overlap, 20H), 3.48-3.44 (overlap, 3H), 3.38 (dd, $J = 15.5$ Hz, 4.2 Hz), 3.31-3.16 (overlap, 11H), 2.85 (t, $J = 13.3$ Hz, 1H), 2.68 (s, 2H), 2.62 (sept, $J = 7.0$ Hz, 1H), 2.55 – 2.33 (overlap, 7H), 2.15 (pent, $J = 7.4$ Hz, 1H), (2.06, $J = 7.2$ Hz, 1H), 1.72-1.51 (overlap, 23H), 1.34-1.28 (overlap, 2H), 1.25-1.16 (overlap, 9H), 1.10-0.82 (overlap, 49H). ¹³C NMR (125 MHz, CDCl₃, ppm): 178.1, 177.1, 176.7, 176.7, 176.7, 176.7, 176.4, 176.3, 173.3, 146.5, 143.1, 143.0, 143.0, 142.8, 142.6, 142.5, 142.1, 137.9, 123.5, 121.1, 120.8, 120.7, 120.6, 120.4, 120.4, 119.8, 72.6, 70.6, 70.5, 70.5, 69.6, 65.0, 65.0, 64.8, 64.7, 64.5, 64.3, 64.1, 62.0, 61.8, 61.7, 61.6, 61.5, 61.4, 61.0, 60.8, 50.0, 47.9, 47.9, 45.2, 42.8, 38.4, 36.1, 35.3, 33.9, 33.8, 33.8, 33.7, 33.7, 33.7, 33.6, 29.0, 28.9, 28.0, 27.9, 27.9, 27.8, 27.8, 27.7, 27.5, 26.6, 25.2, 19.1, 19.0, 18.9, 18.9, 18.9, 18.9, 18.8, 18.8, 18.7, 18.7. **2A-L-OiPr-MM** was also prepared in a similar fashion and has identical characterization to **2A-L-OiPr-MM**.

4) Fluorescent Monomer Synthesis (Cy-M):



Cy5.5-M: **Nb-yne** (9 mg, 0.03 mmol, 1.5 eq) and Cyanine5.5 azide (Lumiprobe, 13 mg, 0.020 mmol, 1.0 eq) was dissolved in DMF (2 mL), followed by the addition of copper (I) bromide (1 mg, 0.001 mmol, 0.05 eq), PMDETA (1 mg, 1 μ L, 0.002 mmol, 0.1 eq), and sodium ascorbate (1 mg, 0.002 mmol, 0.1 eq). The reaction mixture was heated to 50°C and allowed to stir for 3 hours under nitrogen. The mixture was then allowed to cool to room temperature, and concentrated under vacuum. DCM (50 mL) was then added, and the solution was washed with brine (3 \times 50 mL). The organic layer was collected, dried over Na₂SO₄, and concentrated under vacuum. The crude mixture was then purified by column chromatography (0-15% MeOH/DCM), affording **Cy5.5-M** (31 mg, 82% yield) as a blue solid. HRMS-ESI: Calcd for C₆₁H₇₁N₈O₄Cl: m/z = 979.5593 [M + Cl]; Found: 979.5580 [M + Cl]. ¹H NMR (400 MHz, DMSO-*d*₆, ppm) δ _H 8.28 (d, J = 8.7 Hz, 2H), 7.78 (t, J = 11.2 Hz, 2H), 6.31 (s, 4H), 4.17 (s, 4H), 3.10 (s, 4H), 2.71 (s, 4H), 2.55 (br, 2H), 2.09 (d, J = 11.0 Hz, 2H), 1.53 (d, J = 9.5 Hz, 4H), 1.44 (br, 2H), 1.33 – 1.31 (d, J = 9.6 Hz, 2H), 1.22 – 1.09 (m, 2H). ¹³C NMR (100 MHz, CDCl₃, ppm): δ _C 178.1, 174.5, 173.8, 173.3, 152.3, 151.2, 144.3, 140.3, 139.4, 137.9, 134.1, 133.2, 132.2, 131.9, 131.0, 130.8, 130.4, 130.3, 128.3, 128.2, 128.0, 127.9, 126.2, 125.4, 125.1, 124.9, 122.1, 111.0, 110.4, 109.8, 104.5, 103.0, 51.3, 50.9, 48.0, 47.9, 45.3, 42.9, 38.7, 36.2, 36.1, 35.7, 29.8, 27.9, 27.7, 27.4, 26.8, 26.3, 25.4, 25.3.

5) Procedure for Bottlebrush Polymer Syntheses

Note: All ring-opening metathesis polymerization (ROMP) for bottlebrush polymer syntheses were performed in a glovebox under N₂ atmosphere; however, similar results are expected under

ambient conditions All ROMP reactions followed the same general procedure, which was modified from previously published literature. (Sowers, M. A.; McCombs, J. R.; Wang, Y.; Paletta, J. T.; Morton, S. W.; Dreaden, E. C.; Boska, M. D.; Ottaviani, M. F.; Hammond, P. T.; Rajca, A.; Johnson, J. A. Redox-Responsive Branched-Bottlebrush Polymers for *in vivo* MRI and Fluorescence Imaging. *Nat. Commun.* **2014**, *5*, 5460.)

b) 5A-Poly-L and 5A-Poly-L:

5A-Poly-L: To a vial containing a stir bar, **5A-L-OAc-MM** (34.0 mg, 16.0 μmol , 25 eq) was added. To another vial, a solution of Grubbs 3rd generation bispyridyl catalyst **G3-Cat** (0.02 M in DCM) was freshly prepared. DCM (289 μL) was then added to the **MM** vial, followed by the addition of **G3-Cat** solution (32 μL , 0.64 μmol , 1 eq) to give the desired **MM:G3-Cat** ratio of **25:1**, while achieving a total **MM** concentration of **0.05 M**, affording a yellow solution. The reaction mixture was allowed to stir for 12 hours at room temperature. To quench the polymerization, a drop of ethyl vinyl ether was then added, and an aliquot was taken out for GPC analysis. This procedure was also implemented for the synthesis of the **5A-Poly-D**.

c) 5A-Poly-L-Cy and 5A-Poly-D-Cy:

5A-Poly-L-Cy: Fresh solution of **Cy-M** in DCM was prepared (**Cy5.5-Stock**, 15.4 mg/mL). To a vial containing a stir bar, **5A-L-OAc-MM** (35.9 mg, 17.0 μmol , 25 eq) and **Cy-M** (44.9 μL from **Cy5.5-Stock**, 0.68 μmol , 1.0 eq) was added. To another vial, a solution of Grubbs 3rd generation bispyridyl catalyst **G3-Cat** (0.02 M in DCM) was freshly prepared. DCM (261 μL) was then added to the **MM** vial, followed by the addition of **G3-Cat** solution (34 μL , 0.68 μmol , 1 eq) to give the desired **MM:G3-Cat** ratio of **26:1**, while achieving a total **MM** concentration of **0.05 M**, affording a dark blue solution. The reaction mixture was allowed to stir for 12 hours at room temperature. To quench the polymerization, a drop of ethyl vinyl ether was then added, and an aliquot was taken out for GPC analysis. This procedure was also implemented for the synthesis of the **5A-Poly-D-Cy**.

d) 2A-Poly-L and 2A-Poly-D:

2A-Poly-L: To a vial containing a stir bar, **2A-L-OiPr-MM** (34 mg, 16 μmol , 25 eq) was added. To another vial, a solution of Grubbs 3rd generation bispyridyl catalyst **G3-Cat** (0.02 M in DCM) was freshly prepared. DCM (289 μL) was then added to the **MM** vial, followed by the addition of **G3-Cat** solution (32 μL , 0.64 μmol , 1.0 eq) to give the desired **MM:G3-Cat** ratio of **25:1**, while achieving a total **MM** concentration of **0.05 M**, affording a yellow solution. The reaction mixture was allowed to stir for 12 hours at room temperature. To quench the polymerization, a drop of ethyl vinyl ether was then added, and an aliquot was taken out for GPC analysis. This procedure was also implemented for the synthesis of the **2A-Poly-D**.

e) 2A-Poly-L-Cy and 2A-Poly-D-Cy:

2A-Poly-L-Cy: Fresh solution of **Cy-M** in DCM was prepared (**Cy5.5-Stock**, 15.4 mg/mL). To a vial containing a stir bar, **2A-L-OiPr-MM** (36 mg, 17 μmol , 25 eq) and **Cy-M** (44.9 μL from **Cy5.5-Stock**, 0.68 μmol , 1.0 eq) was added. To another vial, a solution of Grubbs 3rd generation bispyridyl catalyst **G3-Cat** (0.02 M in DCM) was freshly prepared. DCM (261 μL) was then added to the **MM** vial, followed by the addition of **G3-Cat** solution (34 μL , 0.68 μmol , 1.0 eq) to give the desired **MM:G3-Cat** ratio of **26:1**, while achieving a total **MM** concentration of **0.05 M**, affording a dark blue solution. The reaction mixture was allowed to stir for 12 hours at room temperature. To quench the polymerization, a drop of ethyl vinyl ether was then added, and an aliquot was taken out for GPC analysis. This procedure was also implemented for the synthesis of the **2A-Poly-D-Cy**.

f) Polyol Bottlebrush Polymer Formation via Deprotection:

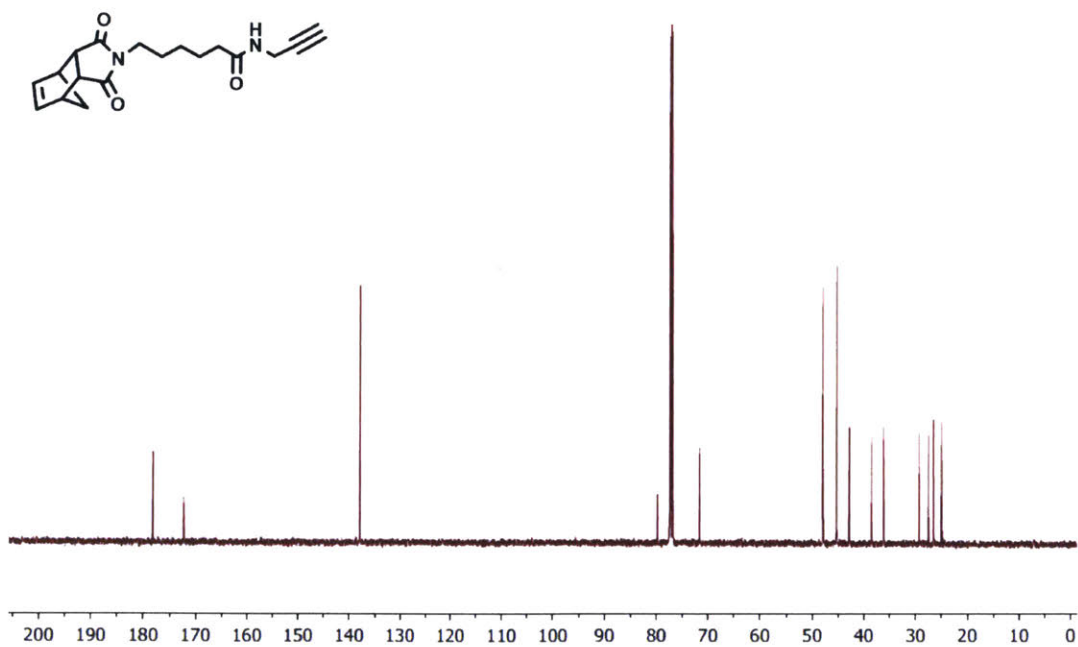
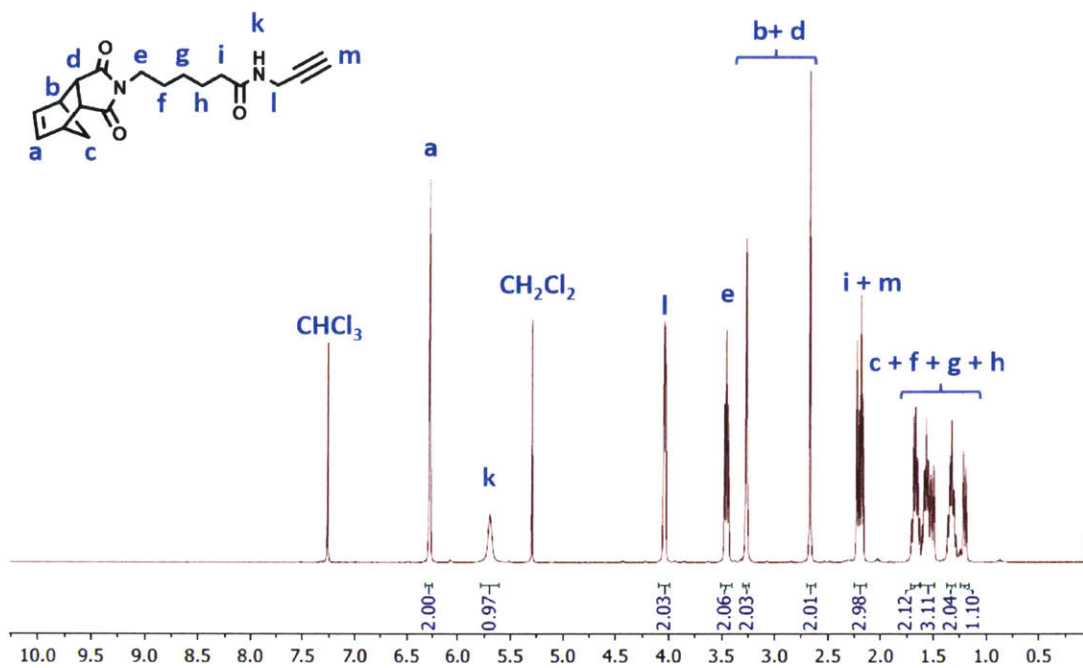
Upon quenching of the ROMP reaction mixture, the bottlebrush polymer was transferred into a 40 mL vial using 10 mL of a 1:1 mixture of DCM and MeOH. Excess potassium carbonate (~1 g) was then added, and the mixture was stirred for 5 hours. The solvent was removed via rotary evaporator, and 10 mL of a 1:1 mixture of acetone and water was added. Excess potassium carbonate (~1 g) was then added, and the mixture was stirred overnight. The bottlebrush polymer was then transferred into an 8kD MWCO dialysis tubing (Spectrum Laboratories), and the solution was dialyzed against water (3 \times 500 mL, solvent exchange every 6 hours). The collected solution was lyophilized, affording the product as an off-white solid for **5A-L**, **5A-D**, **2A-L**, **2A-D**, and a blue solid for **5A-L-Cy**, **5A-D-Cy**, **2A-L-Cy**, **2A-D-Cy**.

Table S5.1. Polymer Characterization

<i>Polymer</i>	<i>M_w (kDa)</i>	<i>D</i>	<i>CUBP</i>	<i>D_h</i>
5A-L-OAc-MM	2.111	1.201		
5A-D-OAc-MM	1.925	1.187		
5A-Poly-L	56.19	1.255	5A-L	3.2 ± 0.4
5A-Poly-D	60.66	1.268	5A-D	3.3 ± 0.7
2A-L-OiPr-MM	2.089	1.216		
2A-D-OiPr-MM	2.162	1.146		
2A-Poly-L	67.07	1.271	2A-L	2.8 ± 0.4
2A-Poly-D	59.78	1.212	2A-D	2.5 ± 0.3

Absolute molecular weights (M_w) were acquired using a light scattering detector with dn/dc values of 0.1210 for 5AIEG and 0.0775 for 2AIEG species.

Spectroscopic Characterization
Norbornene Endgroup (Nb-yne)



Macromonomers

5A-L-OAc-MM

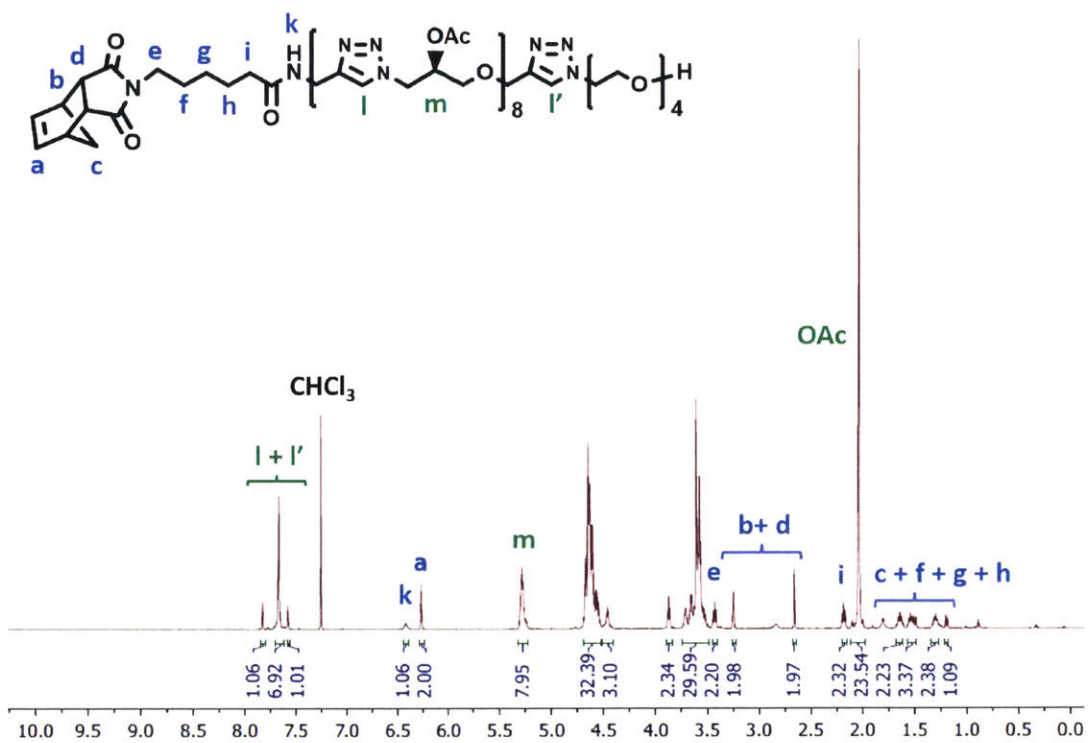


Figure S5.3. ¹H NMR of 5A-L-OAc-MM in CDCl₃.

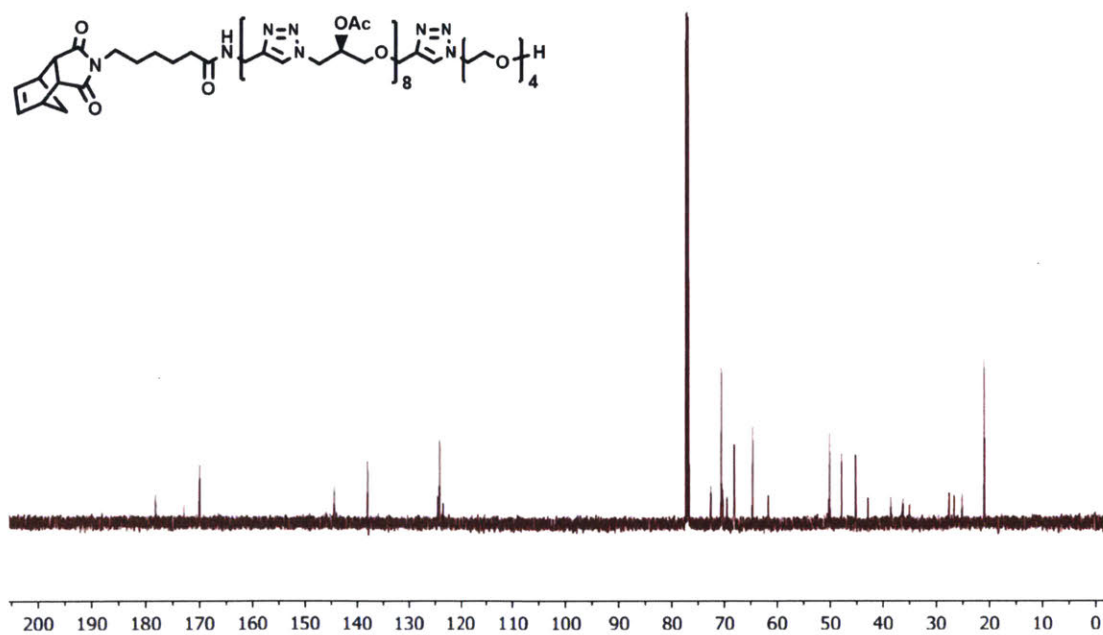


Figure S5.4. ¹³C NMR of 5A-L-OAc-MM in CDCl₃.

5A-D-OAc-MM

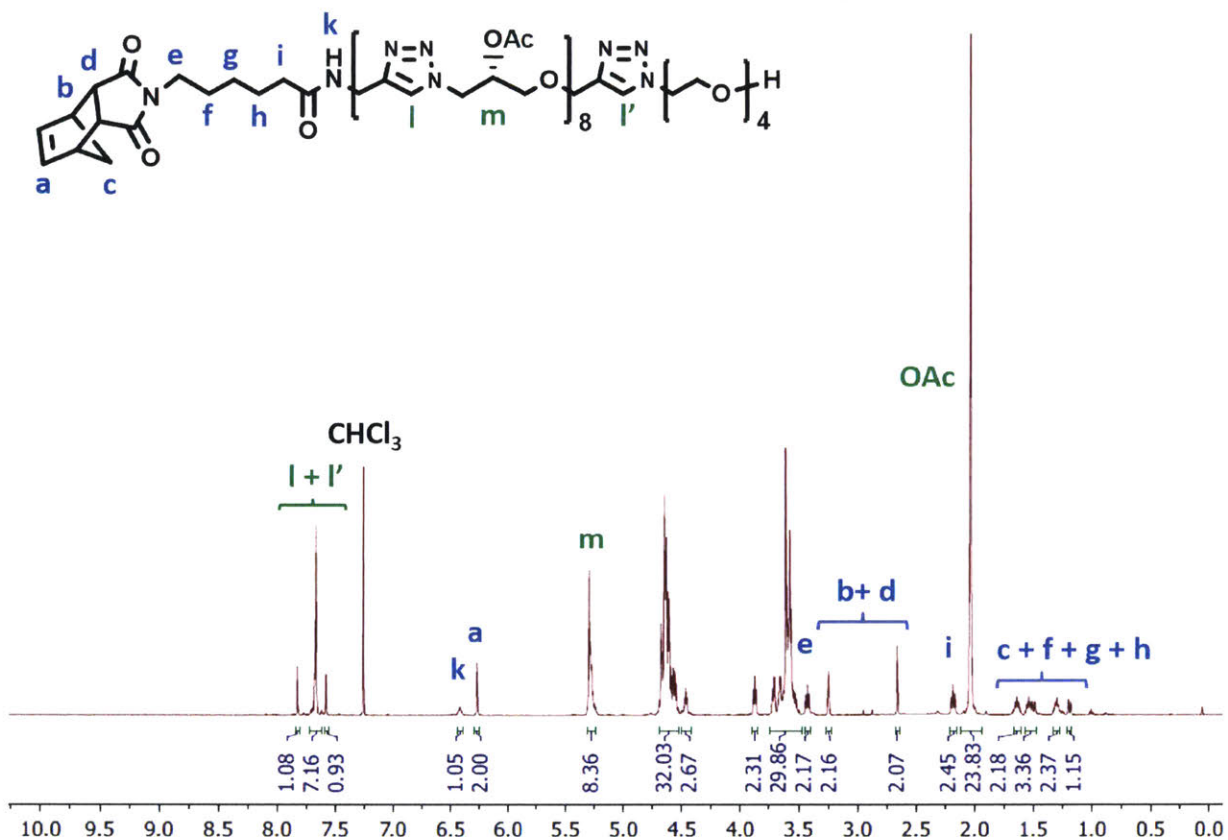


Figure S5.5. ¹H NMR of 5A-D-OAc-MM in CDCl₃.

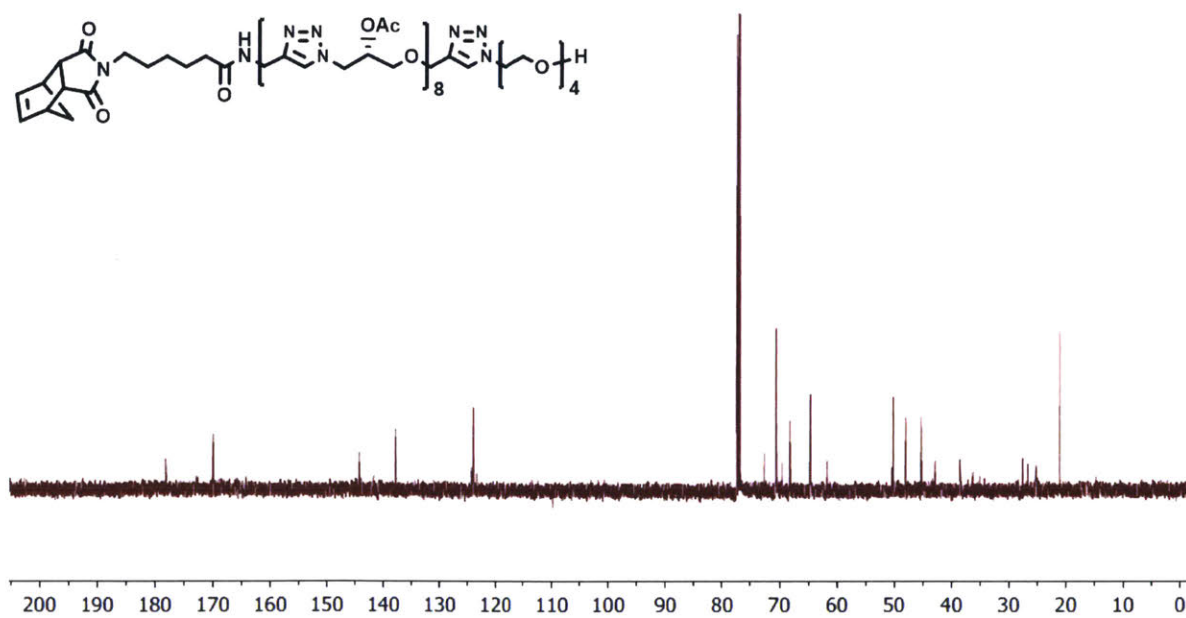


Figure S5.6. ¹³C NMR of 5A-D-OAc-MM in CDCl₃.

2AIEG

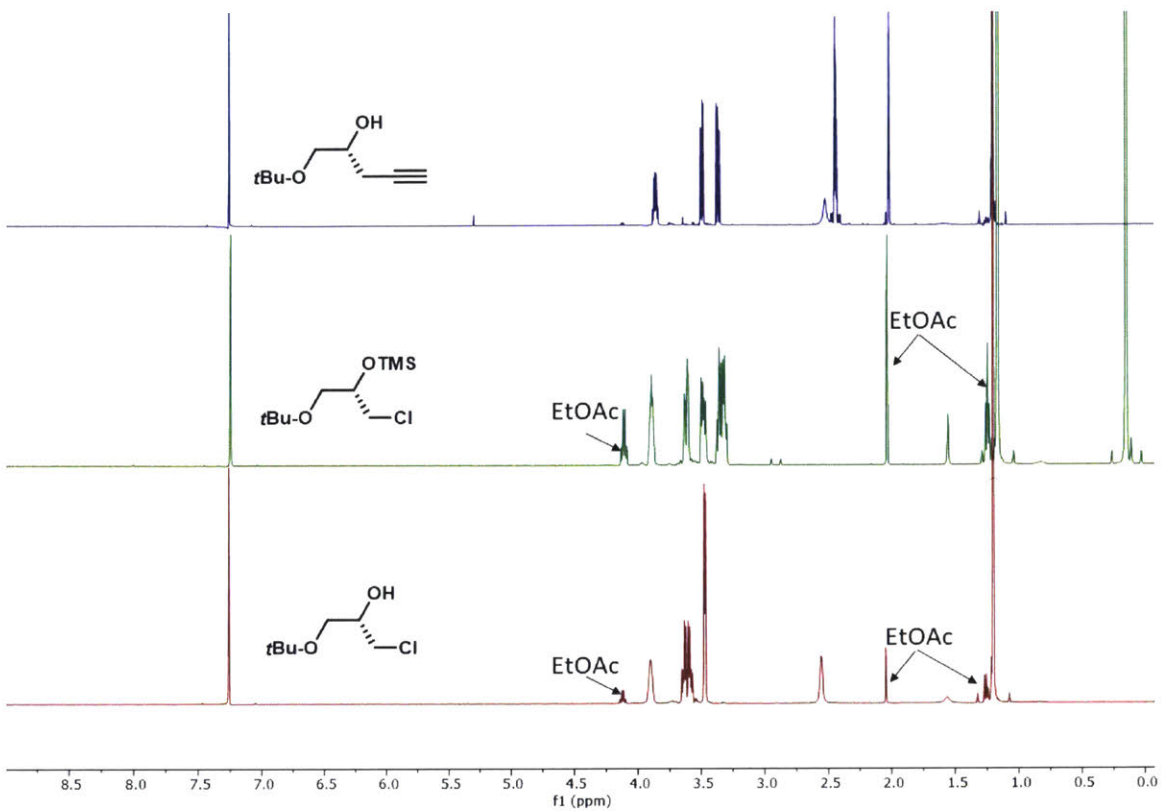


Figure S5.7. ^1H NMR of **d1**, **1**, and **2**. (500MHz, CDCl_3 , 298K). Enantiomer has identical spectra.

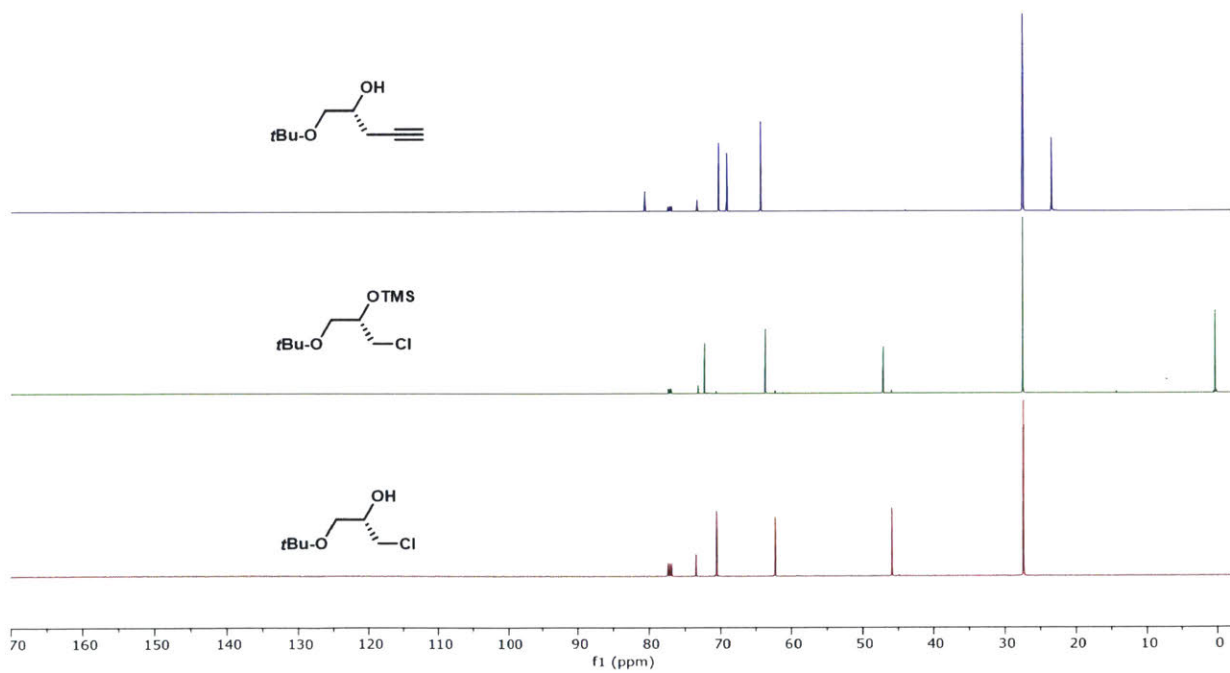


Figure S5.8. ^{13}C NMR of **d1**, **1**, and **2**. (125MHz, CDCl_3 , 298K). Enantiomer has identical spectra.

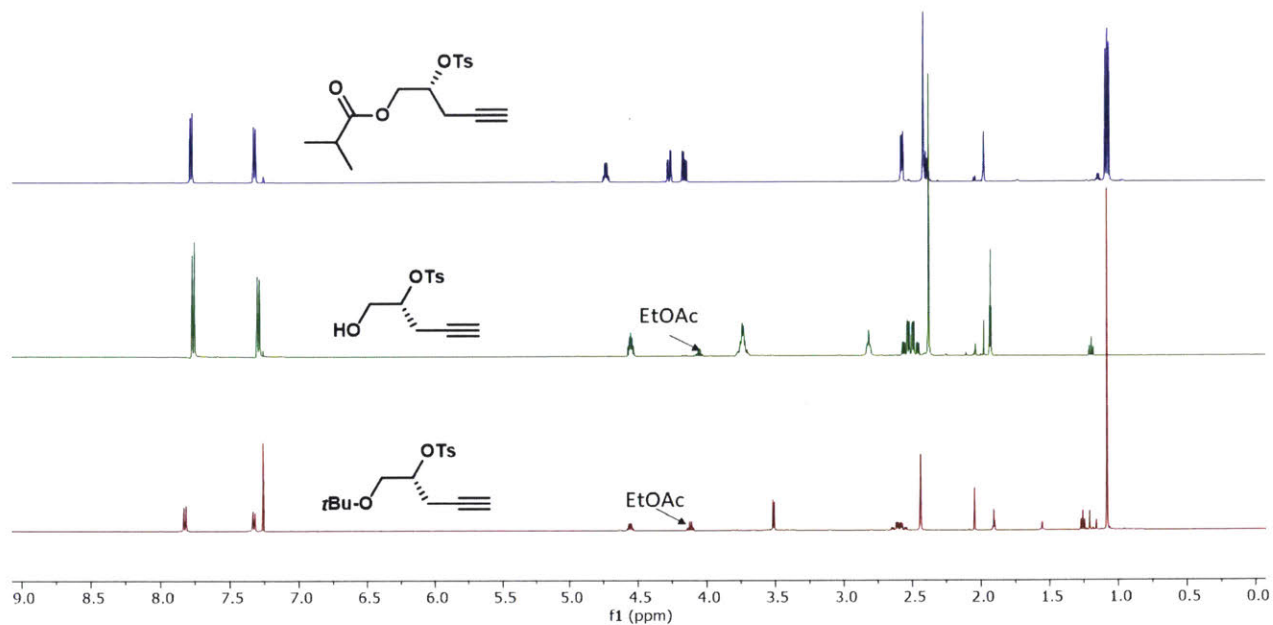


Figure S5.9. ^1H NMR of **3**, **d4**, and **4**. (500MHz, CDCl_3 , 298K). Enantiomer has identical spectra.

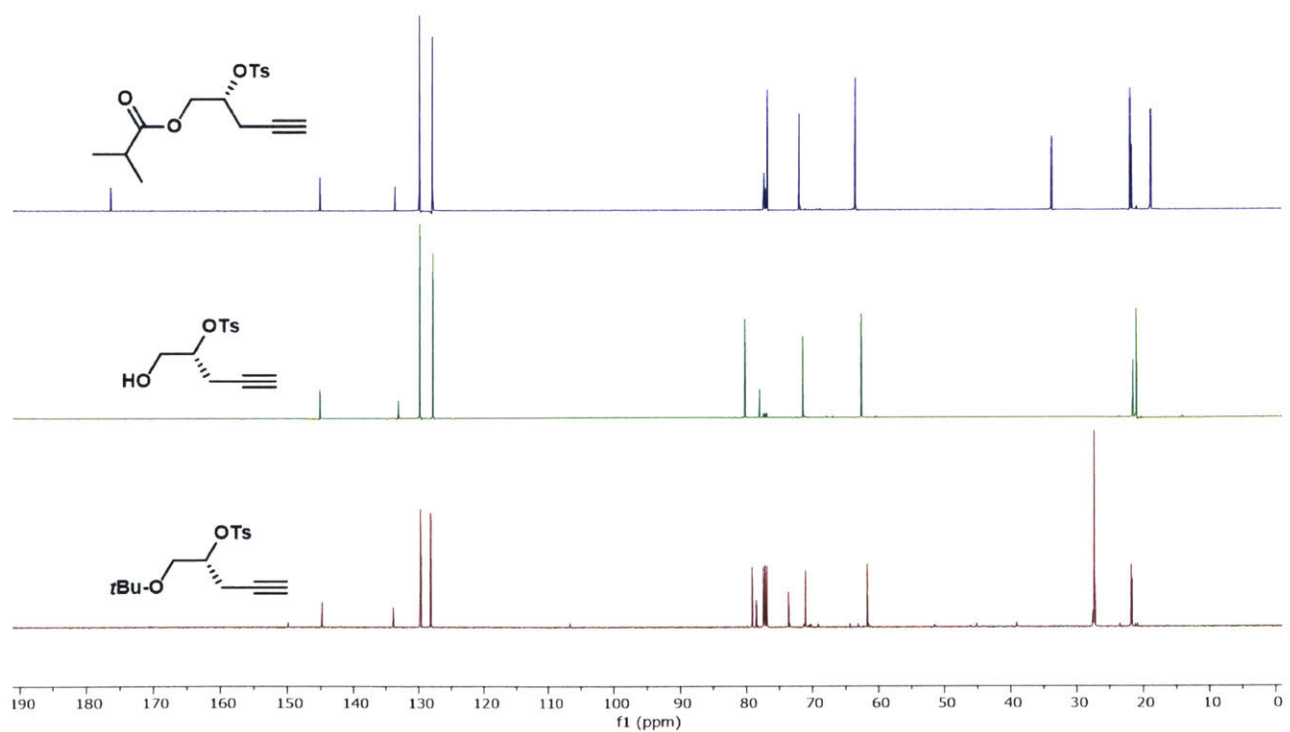


Figure S5.10. ^{13}C NMR of **3**, **d4**, and **4**. (125MHz, CDCl_3 , 298K). Enantiomer has identical spectra.

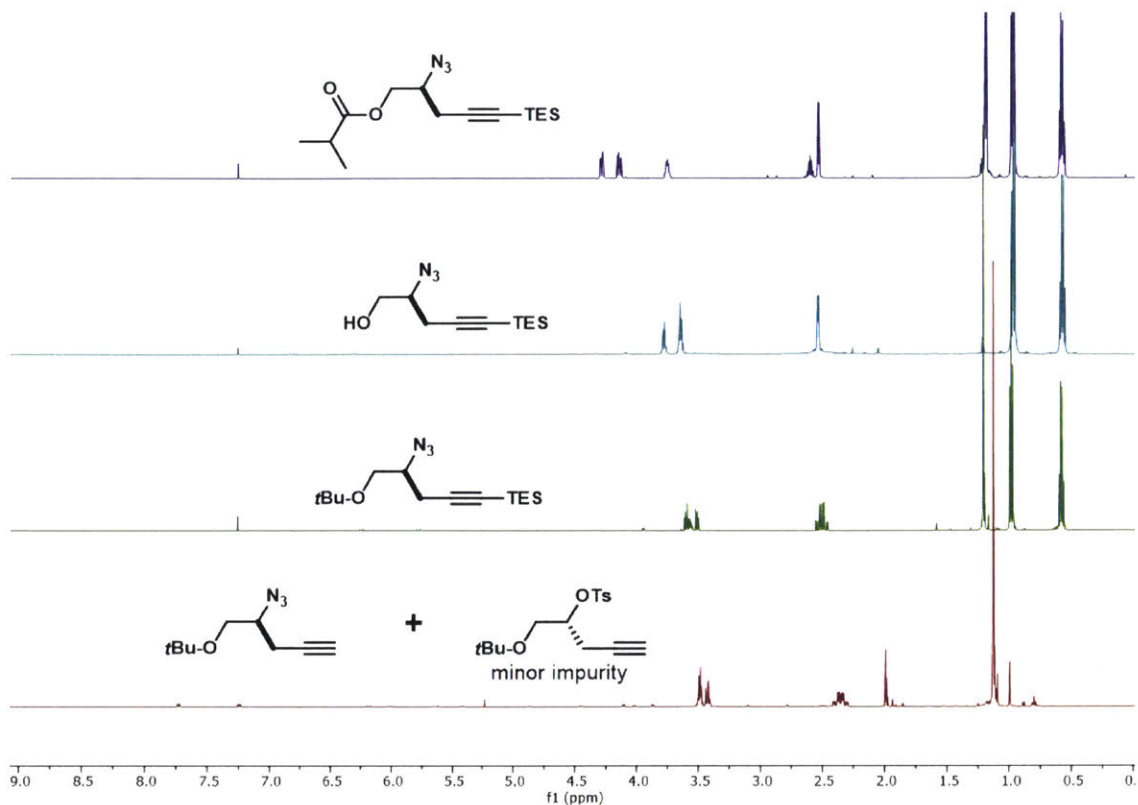


Figure S5.11. ^1H NMR of **d2**, **5**, **d4**, and **6**. (500MHz, CDCl_3 , 298K). Enantiomer has identical spectra.

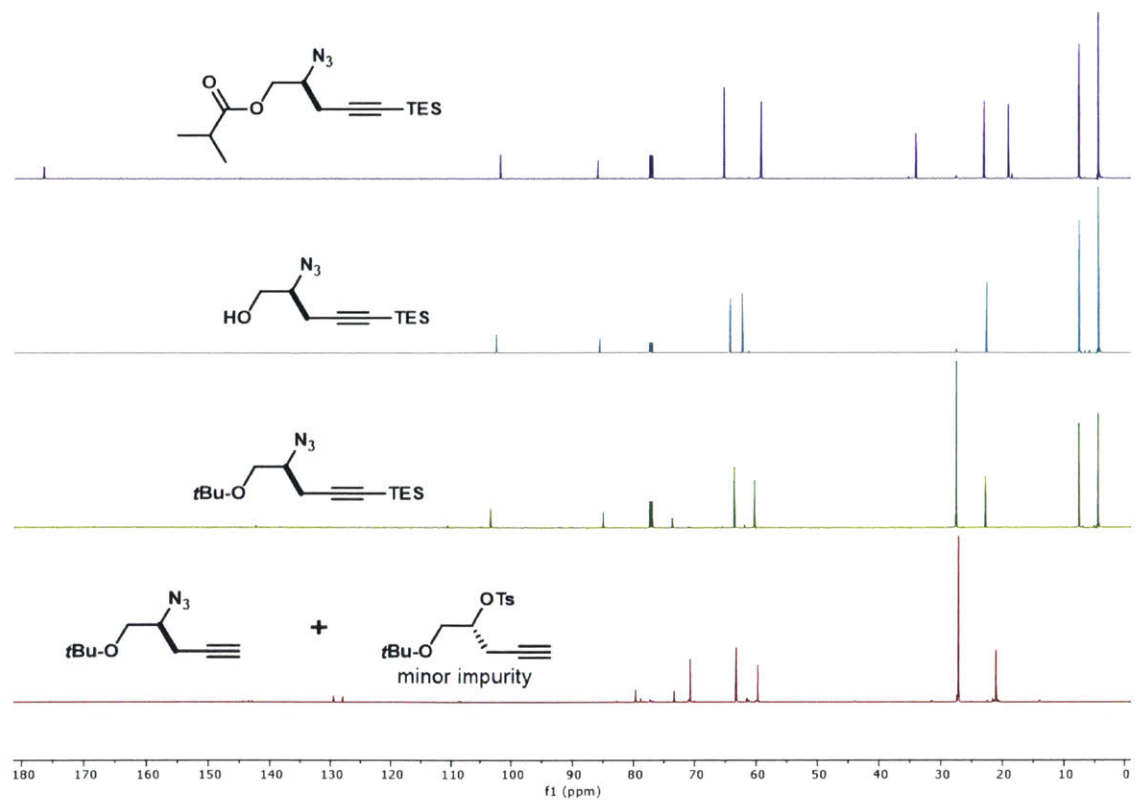


Figure S5.12. ^{13}C NMR of **d2**, **5**, **d4**, and **6**. (125MHz, CDCl_3 , 298K). Enantiomer has identical spectra.

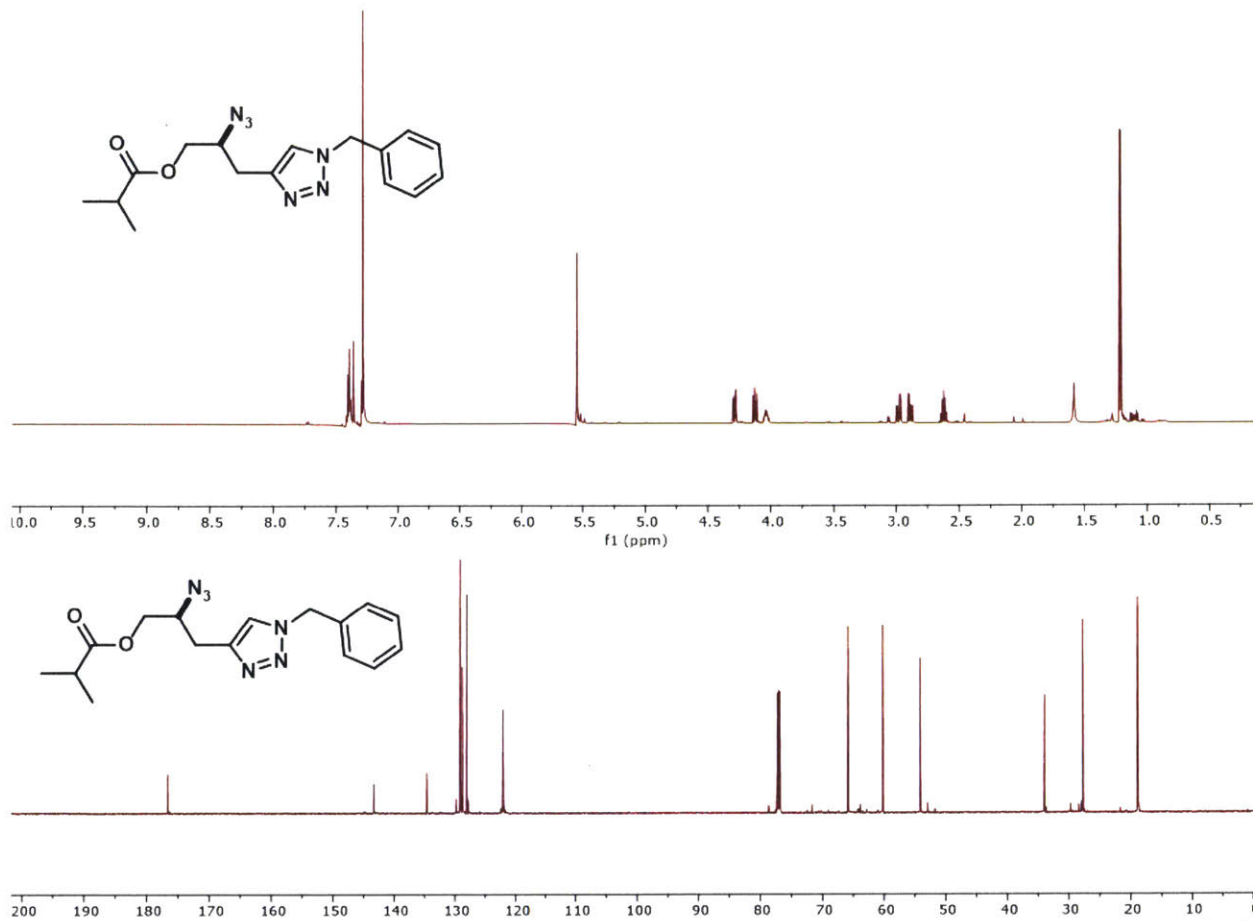


Figure S5.13. ^1H and ^{13}C NMR of 7. (500MHz and 125MHz, CDCl_3 , 298K). Enantiomer has identical spectra.

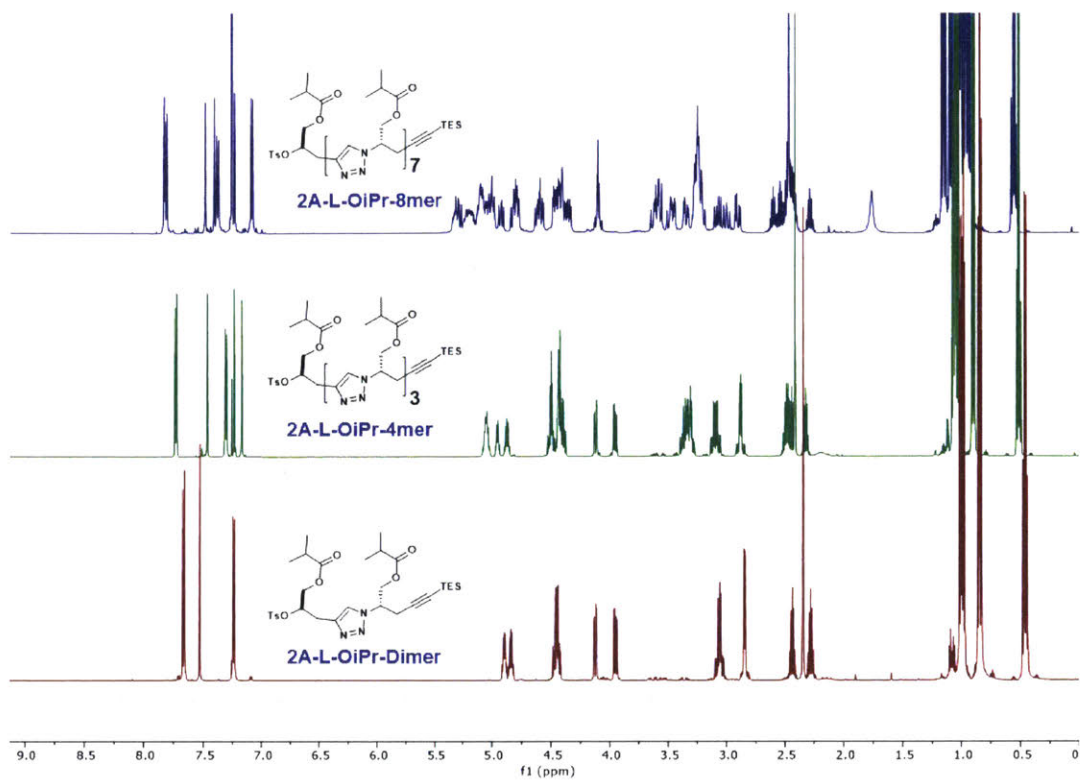


Figure S5.14. ^1H NMR of **2AIEG** oligomers (500MHz, CDCl_3 , 298K). Enantiomer has identical spectra.

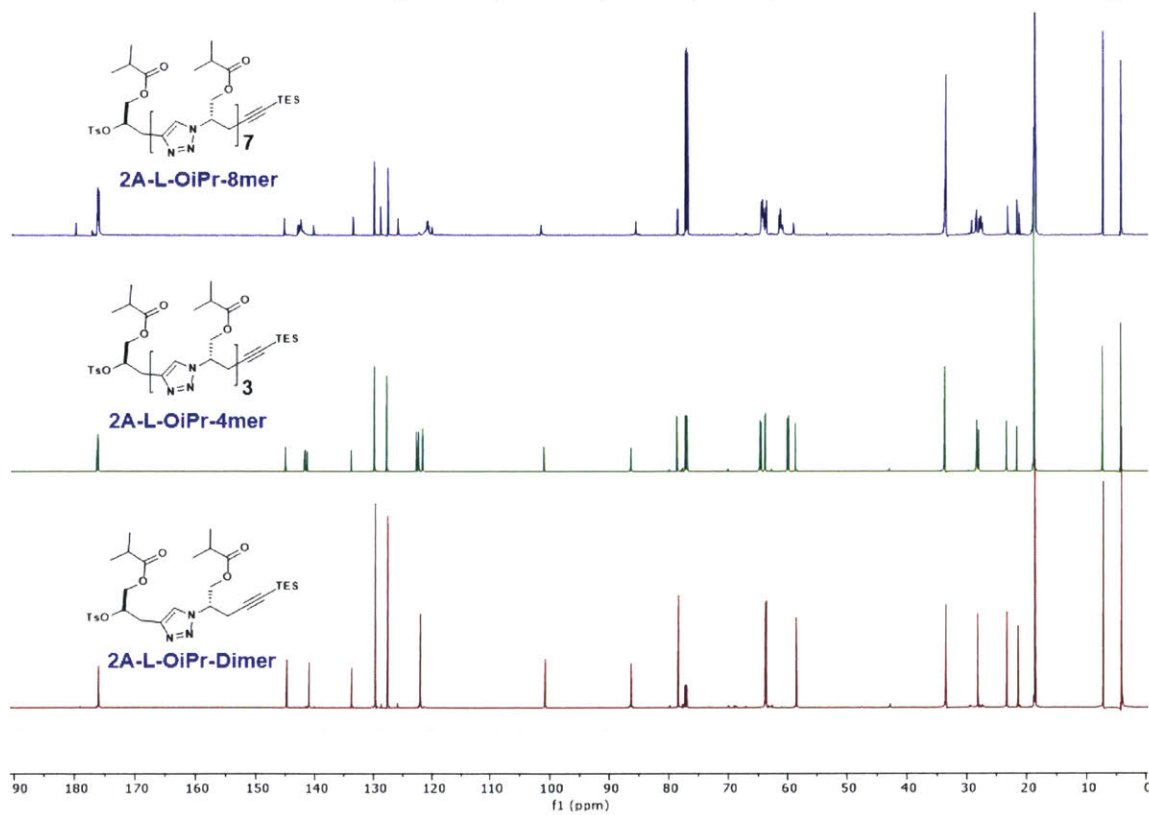


Figure S5.15. ^{13}C NMR of **2AIEG** oligomers (125MHz, CDCl_3 , 298K). Enantiomer has identical spectra.

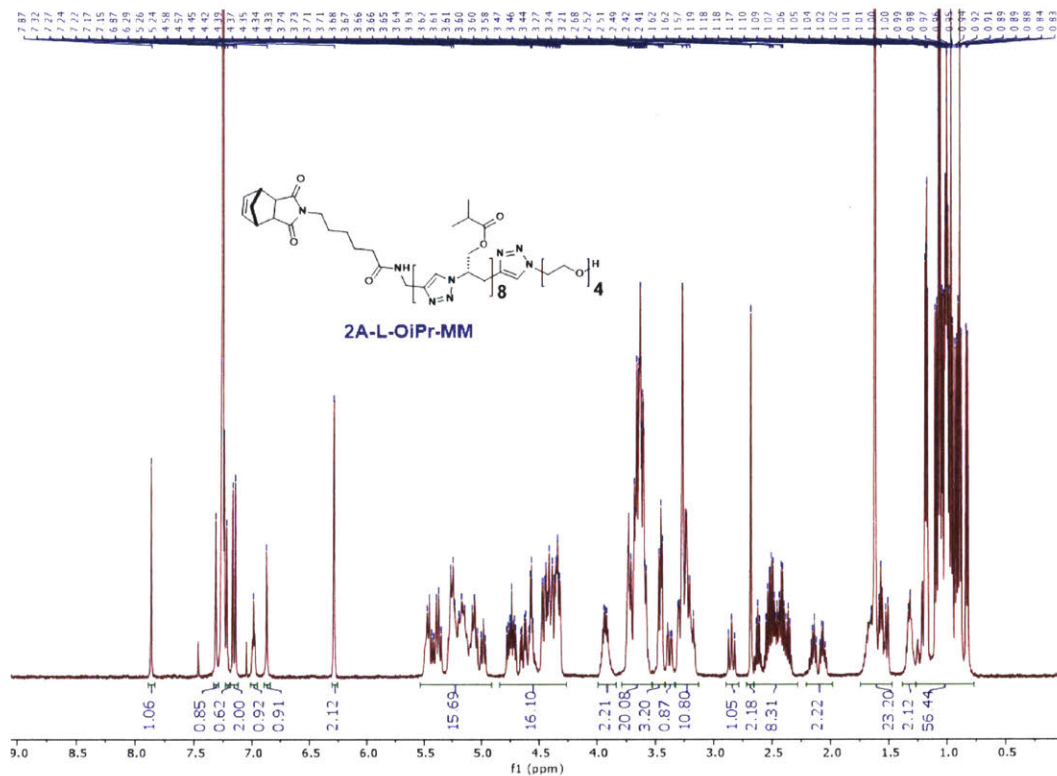


Figure S5.16. ^1H NMR of 2A-L-OiPr-MM (500MHz, CDCl_3 , 298K). Enantiomer has identical spectrum.

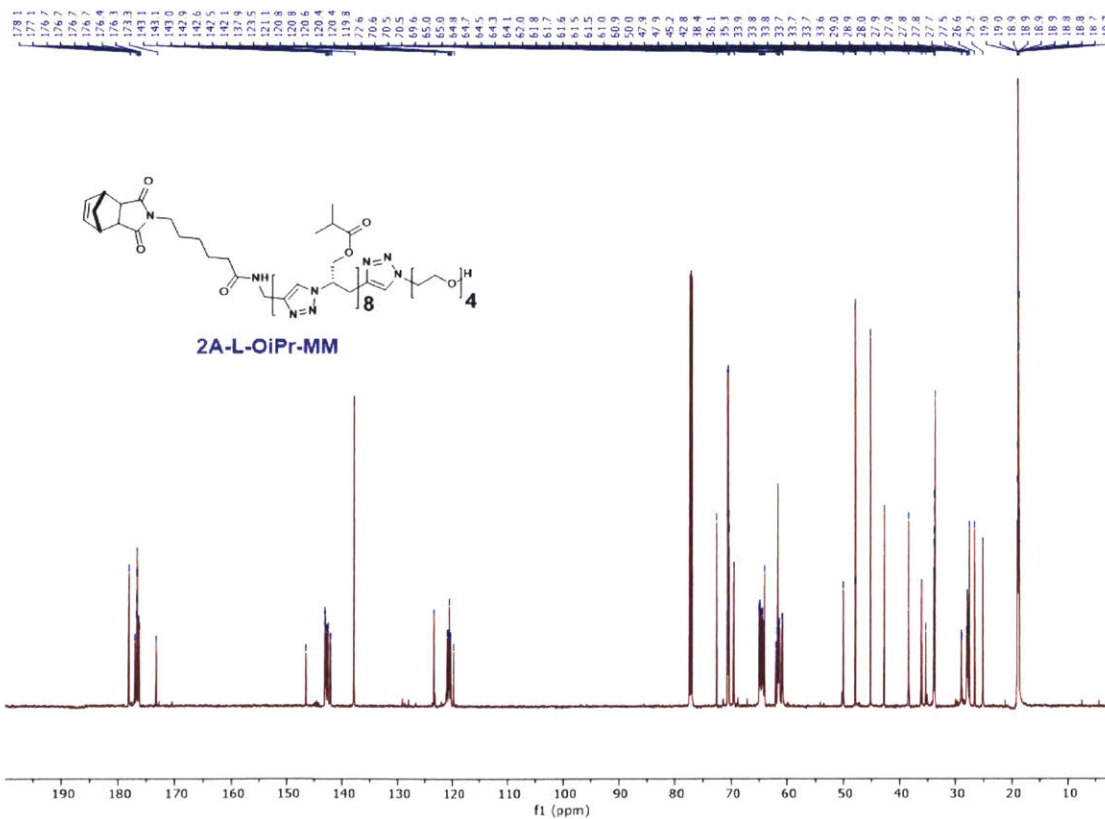


Figure S5.17. ^{13}C NMR of 2A-L-OiPr-MM (125MHz, CDCl_3 , 298K). Enantiomer has identical spectrum.

Deprotection of MMs

5A-L-OAc-MM

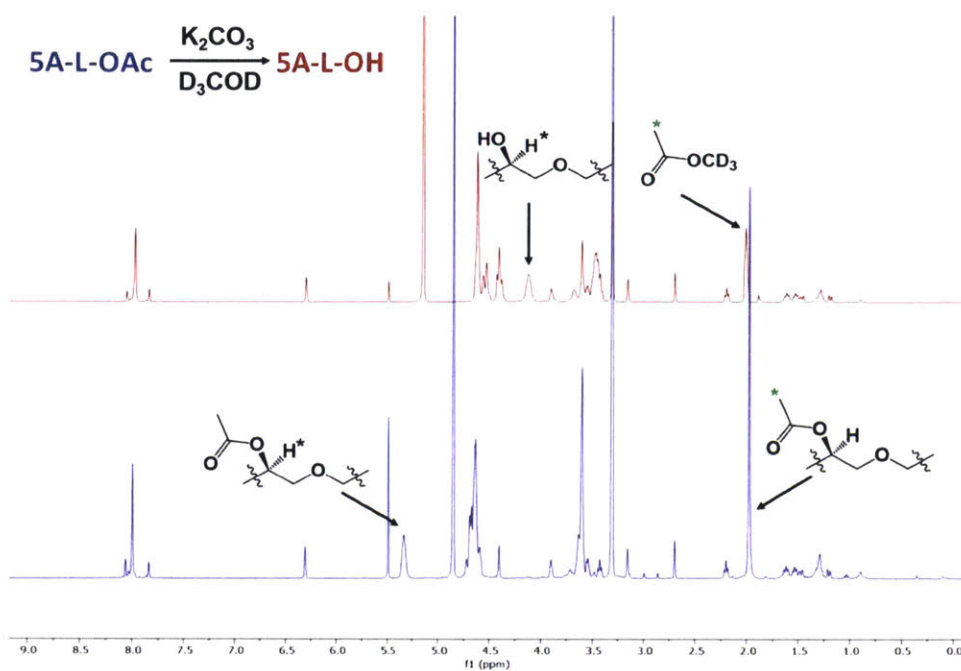


Figure S5.20. Stacked 1H NMR for the deprotection of **5A-L-OAc-MM** in $CDCl_3$.

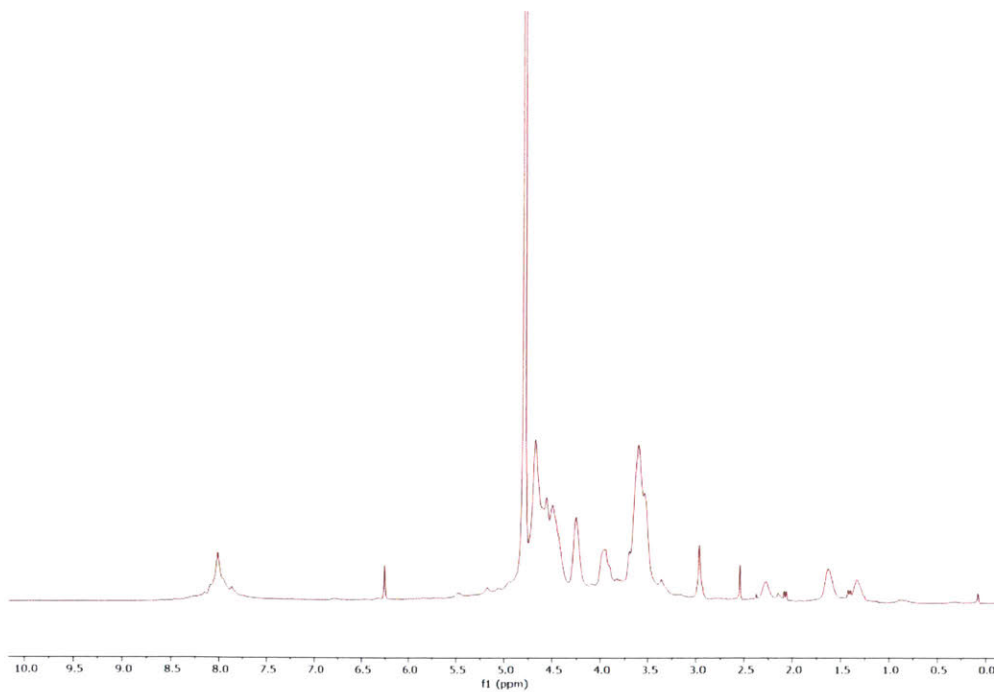


Figure S5.21. 1H NMR of the deprotected of **5A-L-OAc-MM** in D_2O .

5A-D-OAc-MM

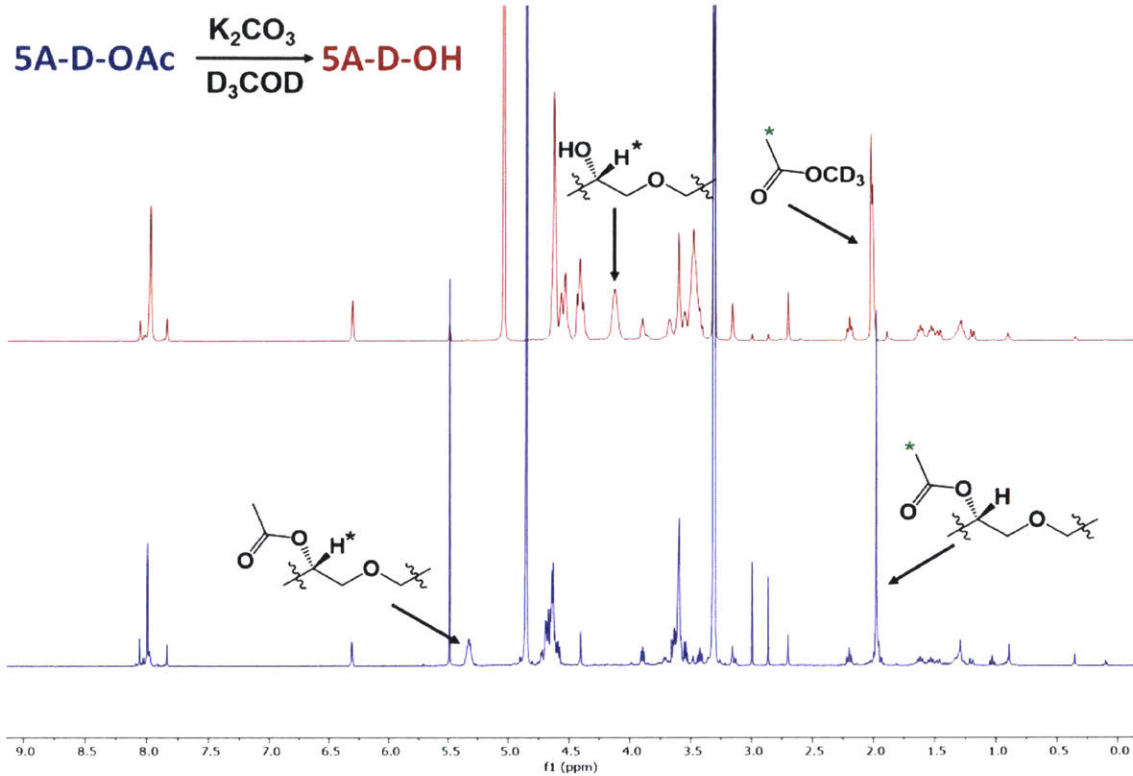


Figure S5.22. Stacked 1H NMR for the deprotection of 5A-D-OAc-MM in $CDCl_3$.

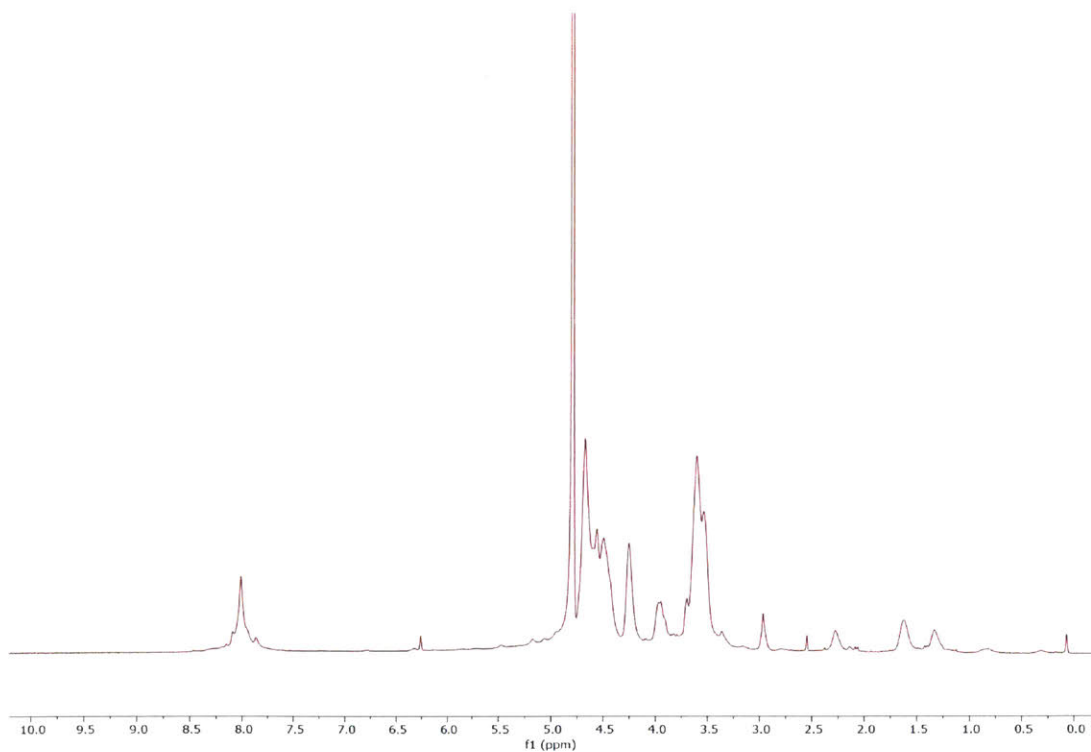


Figure S5.23. 1H NMR of the deprotected of 5A-D-OAc-MM in D_2O .

2A-L-OiPr-MM

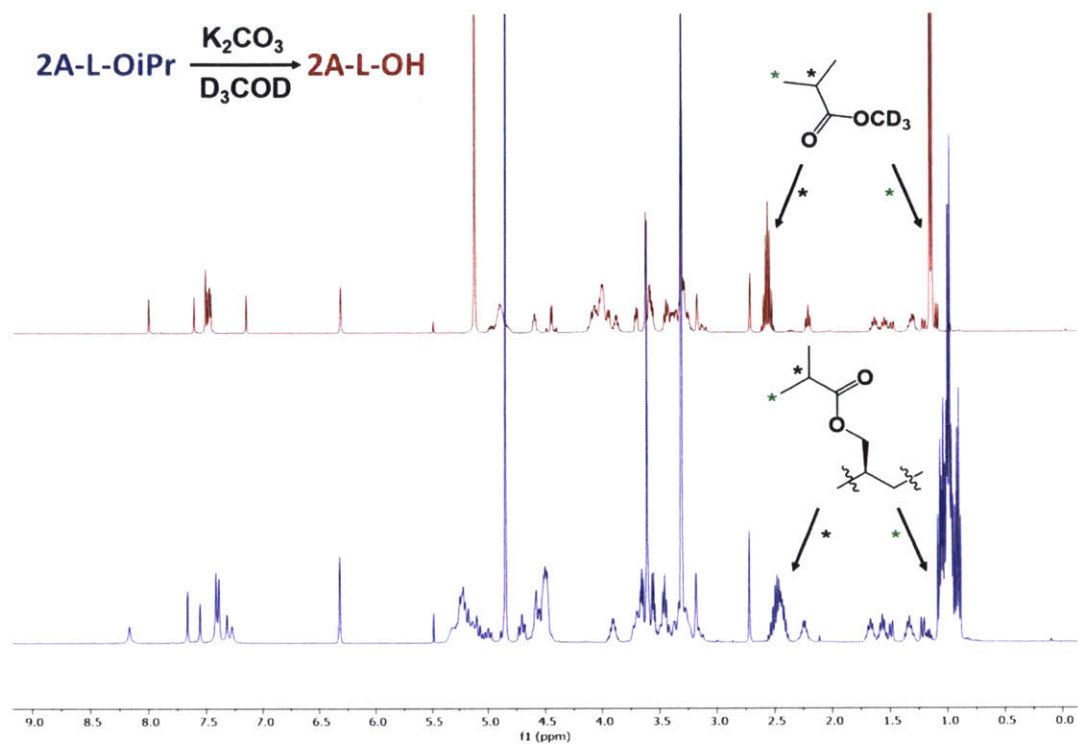


Figure S5.24. Stacked ¹H NMR for the deprotection of **2A-L-OiPr-MM** in CDCl₃.

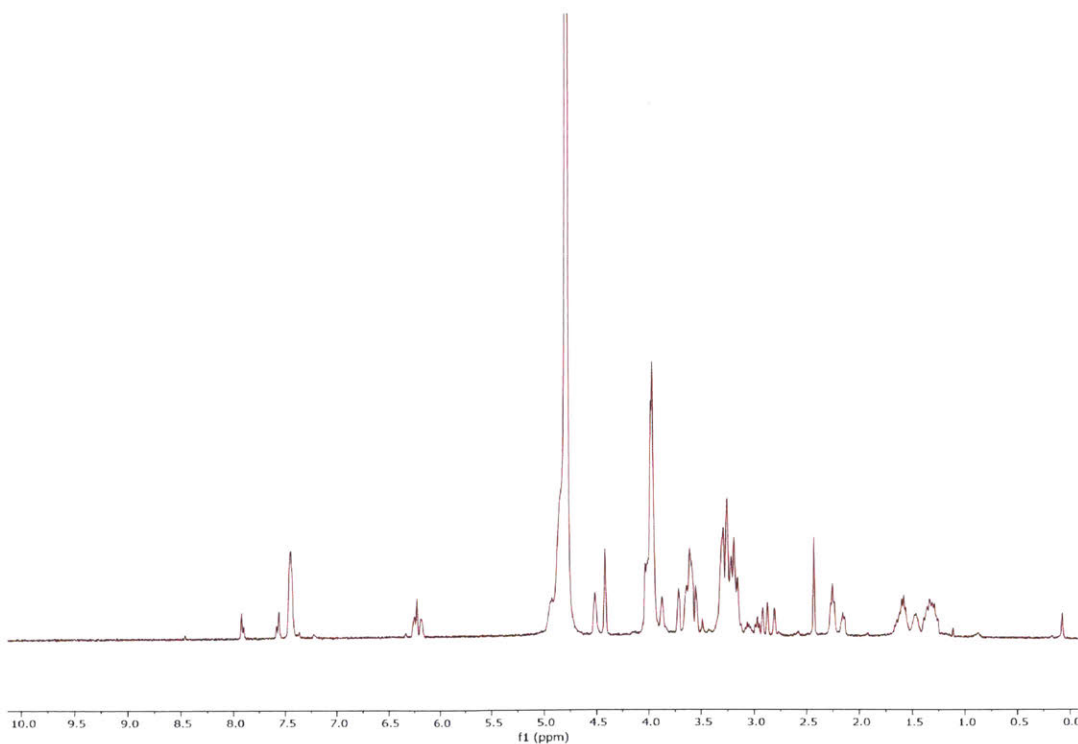


Figure S5.25. ¹H NMR of the deprotected of **2A-L-OiPr-MM** in D₂O.

2A-D-OiPr-MM

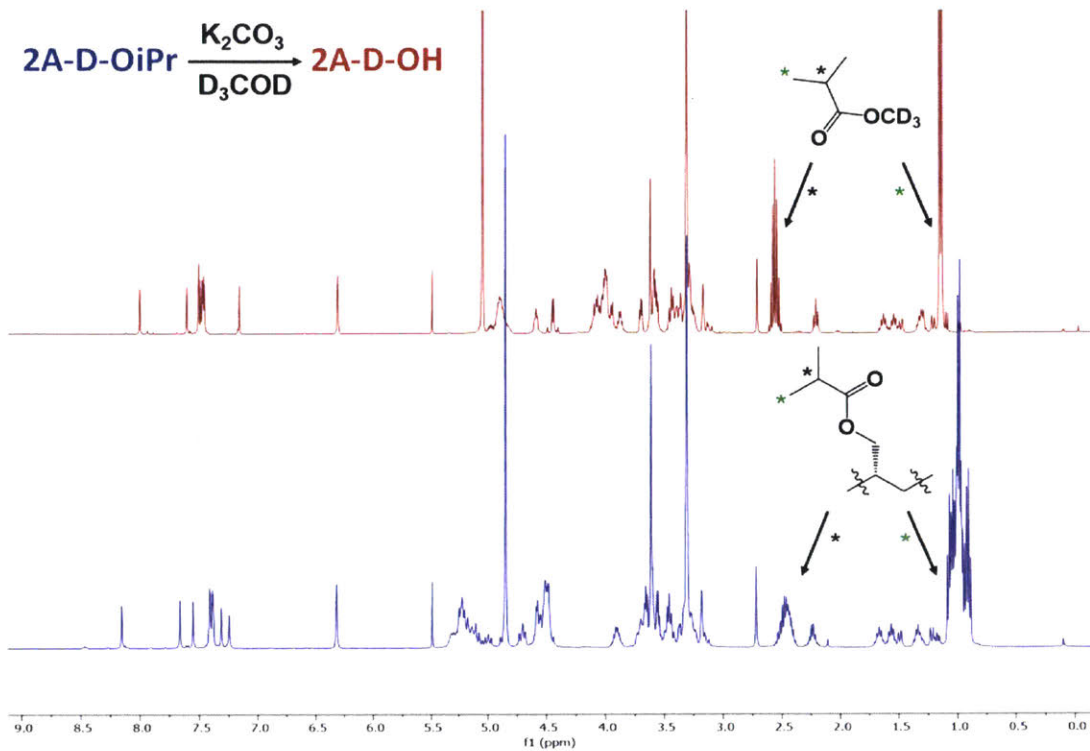


Figure S5.26. Stacked ¹H NMR for the deprotection of *2A-D-OiPr-MM* in CDCl₃.

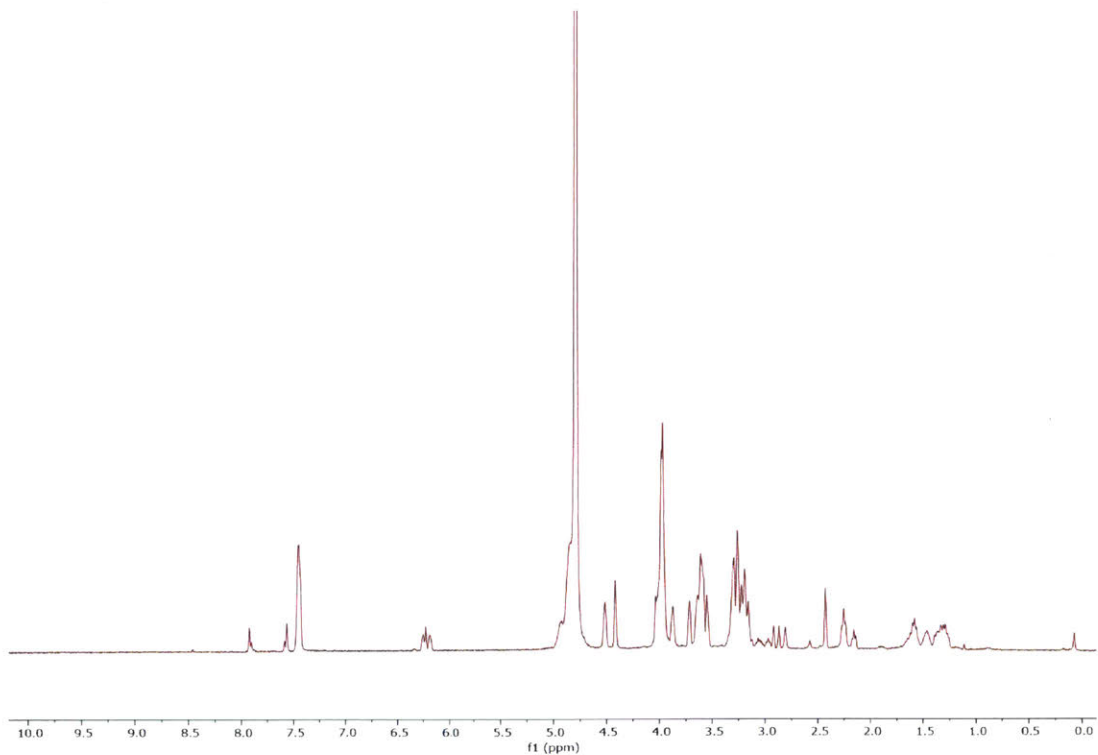


Figure S5.27. ¹H NMR of the deprotected of *2A-D-OiPr-MM* in D₂O.

Chiral Unimolecular-arm Bottlebrush Polymers (CUBP)

5A-Poly-L

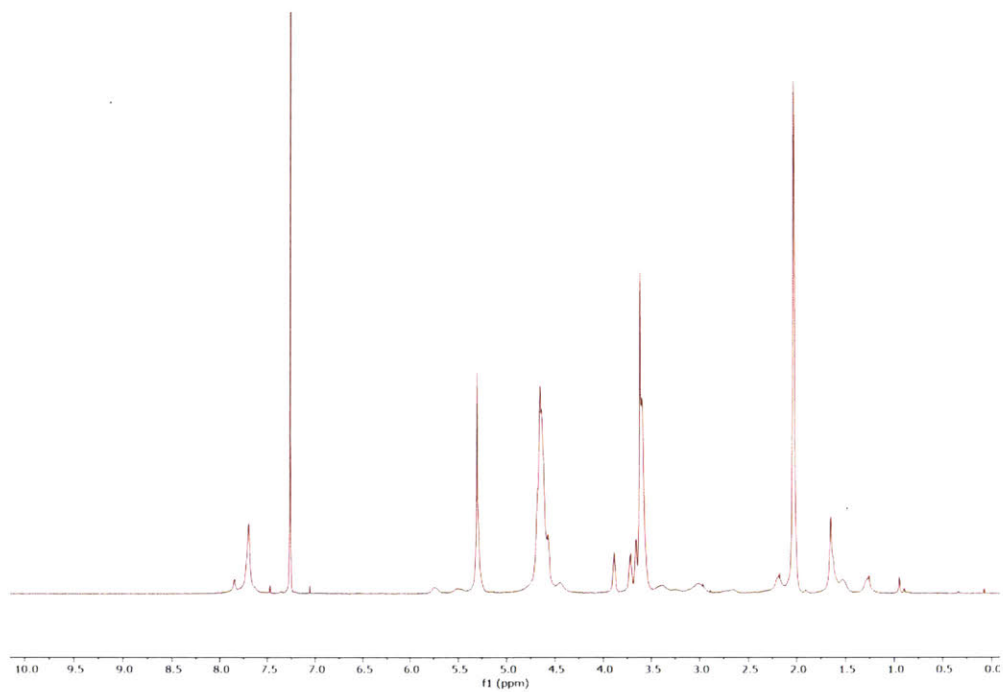


Figure S5.28. ^1H NMR of **5A-Poly-L** in CDCl_3 .

5A-Poly-D

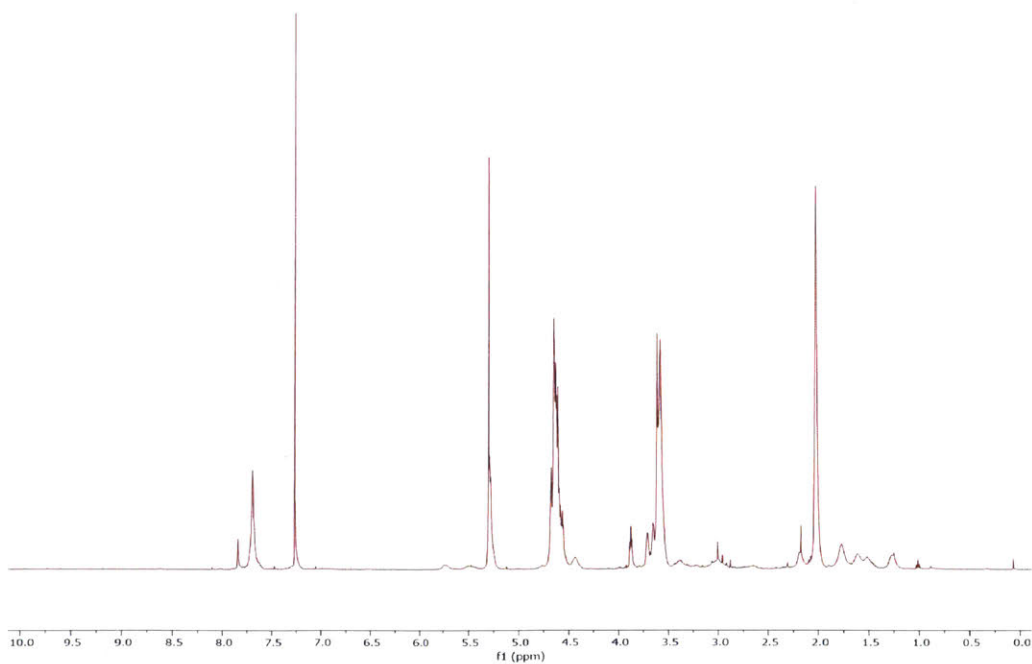


Figure S5.29. ^1H NMR of **5A-Poly-D** in CDCl_3 .

5A-Poly-L-Cy

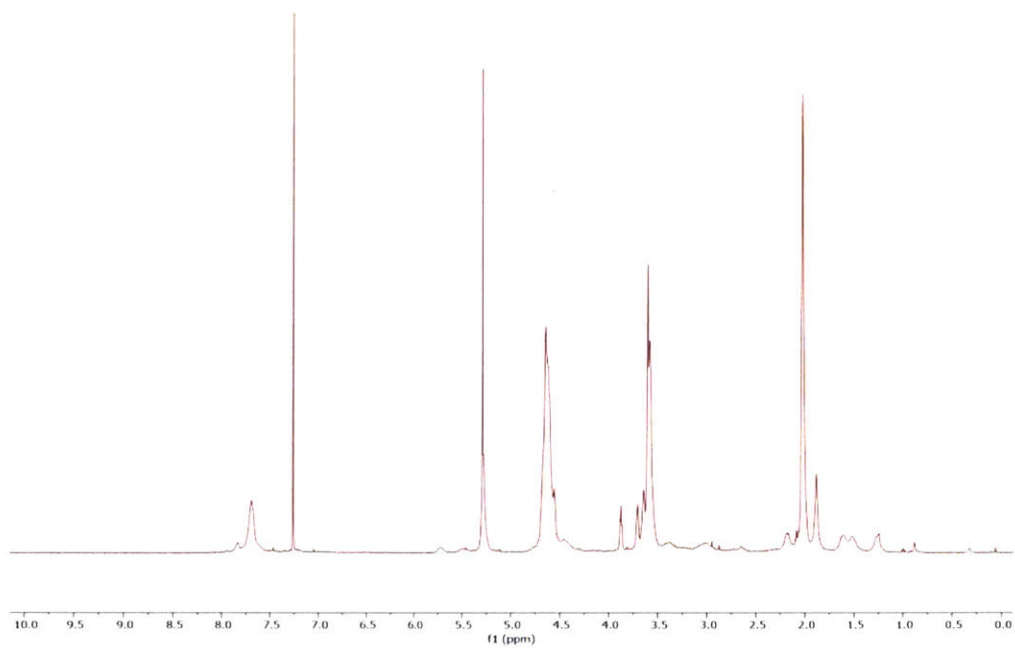


Figure S5.30. ^1H NMR of **5A-Poly-L-Cy** in CDCl_3 .

5A-Poly-D-Cy

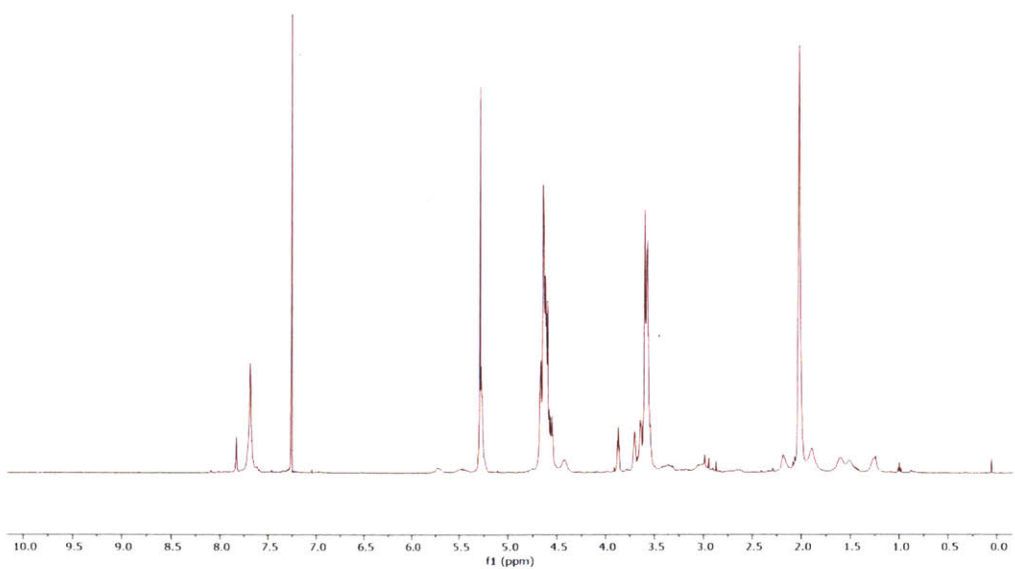


Figure S5.31. ^1H NMR of **5A-Poly-D-Cy** in CDCl_3 .

5A-L

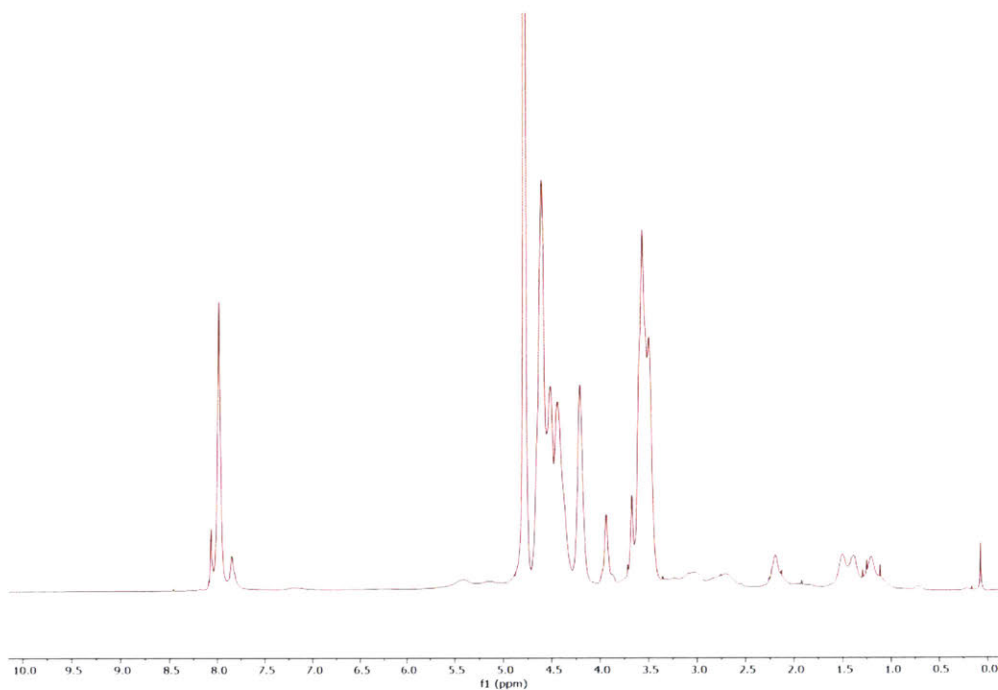


Figure S5.32. ^1H NMR of **5A-L** in D_2O .

5A-D

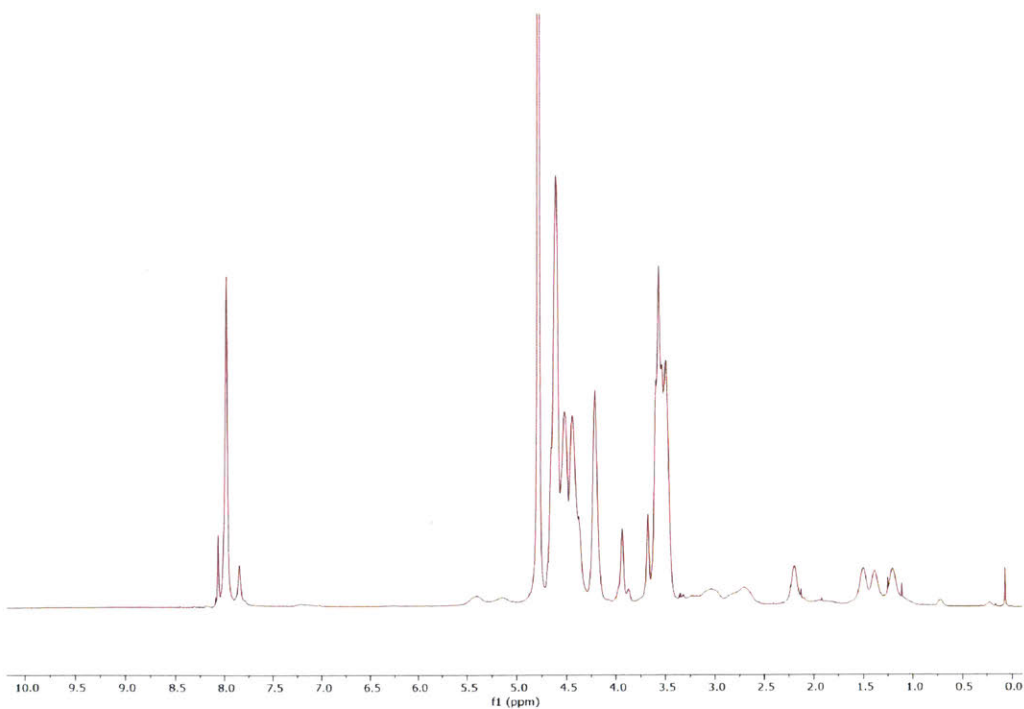


Figure S5.33. ^1H NMR of **5A-D** in D_2O .

5A-L-Cy

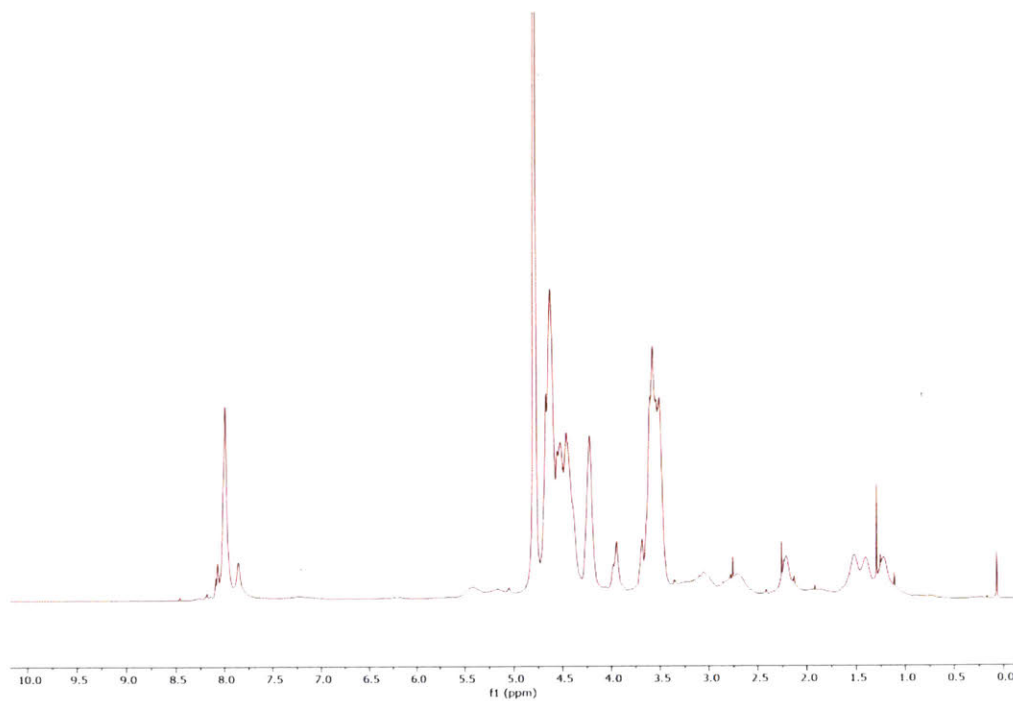


Figure S5.34. ^1H NMR of **5A-L-Cy** in D_2O .

5A-D-Cy

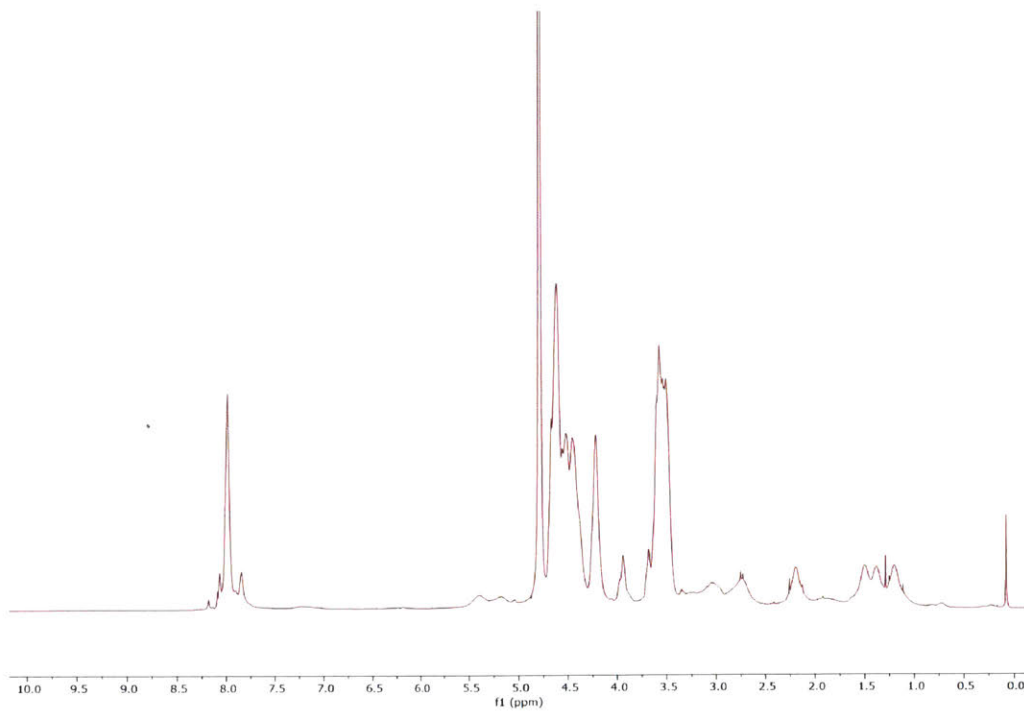


Figure S5.35. ^1H NMR of **5A-D-Cy** in D_2O .

2A-Poly-L

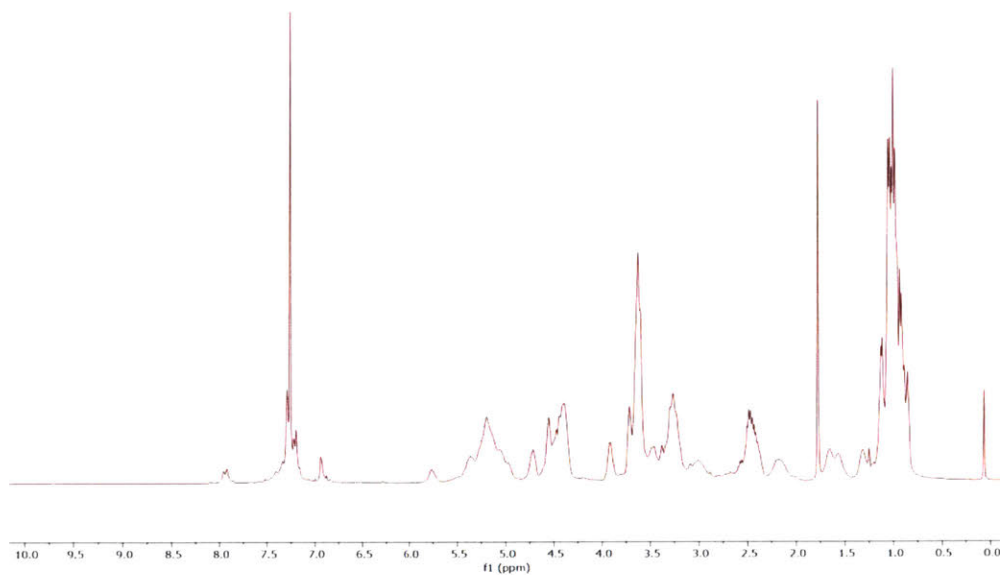


Figure S5.36. ^1H NMR of 2A-Poly-L in CDCl_3 .

2A-Poly-D

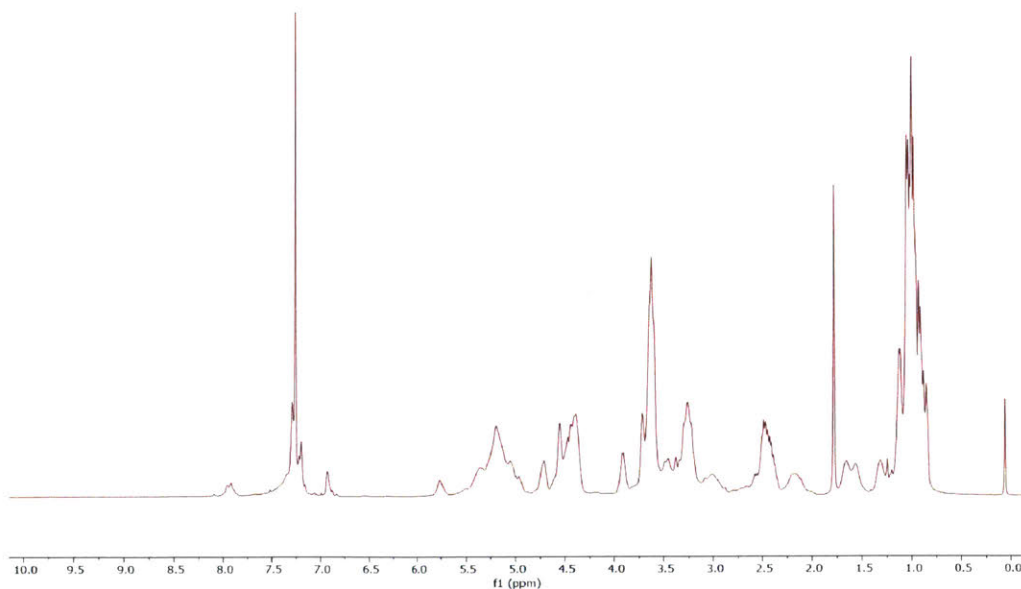


Figure S5.37. ^1H NMR of 2A-Poly-D in CDCl_3 .

2A-Poly-L-Cy

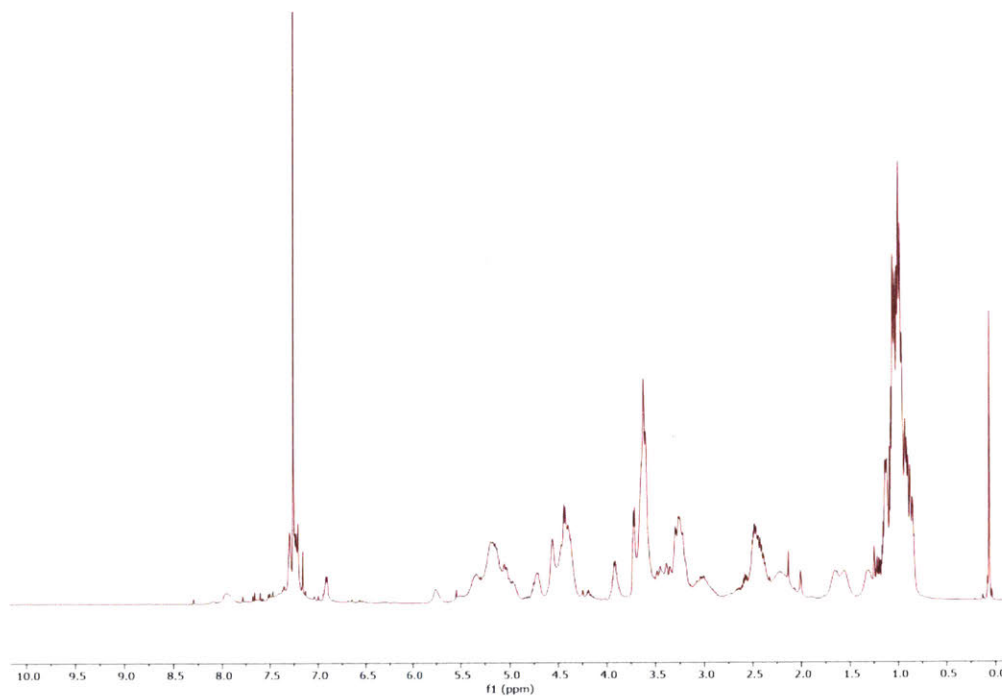


Figure S5.38. ^1H NMR of **2A-Poly-L-Cy** in CDCl_3 .

2A-Poly-D-Cy

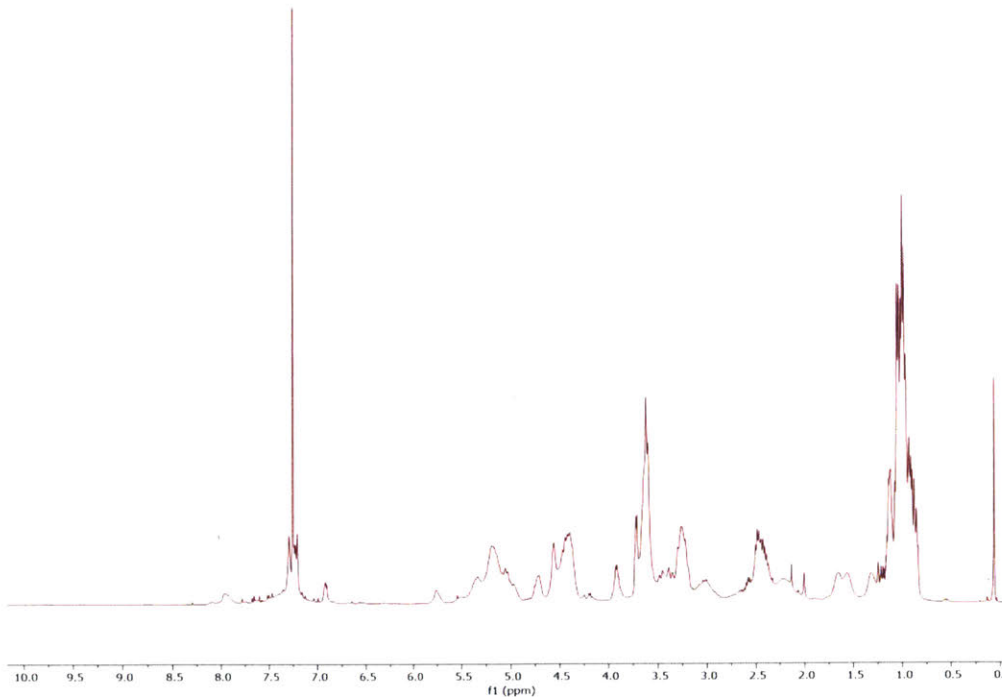


Figure S5.39. ^1H NMR of **2A-Poly-D-Cy** in CDCl_3 .

2A-L

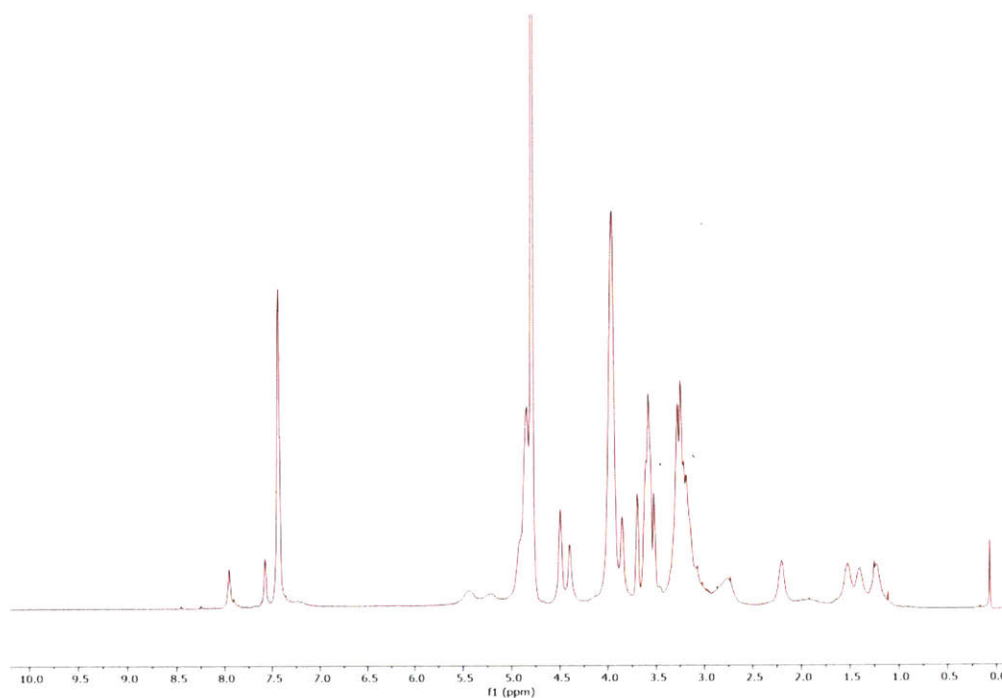


Figure S5.40. ^1H NMR of **2A-L** in D_2O .

2A-D

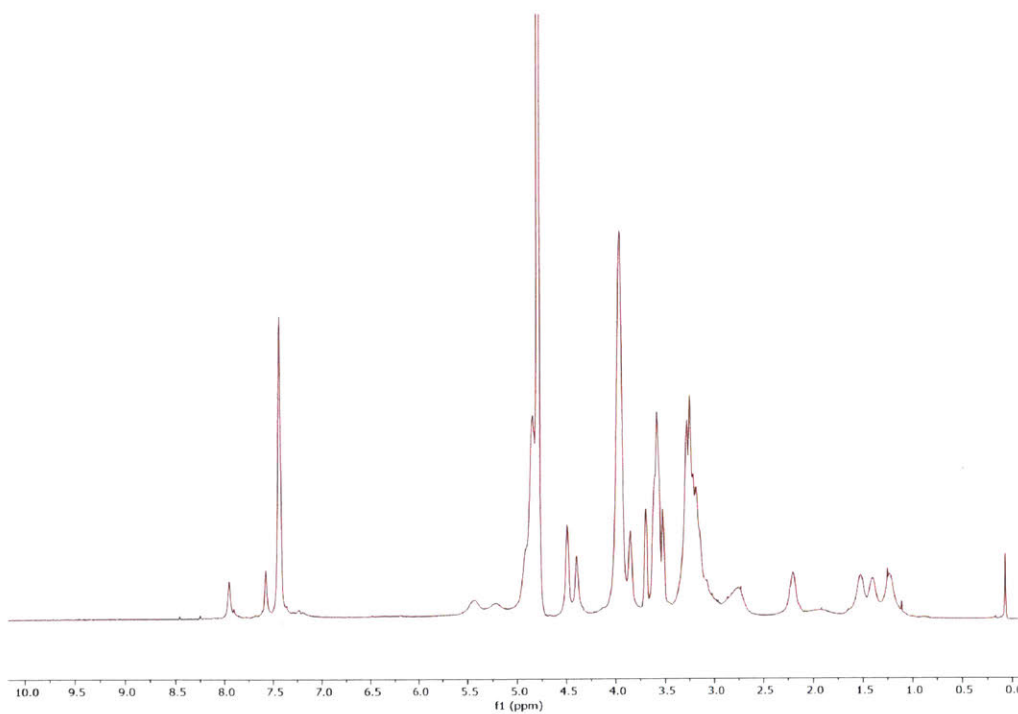


Figure S5.41. ^1H NMR of **2A-D** in D_2O .

2A-L-Cy

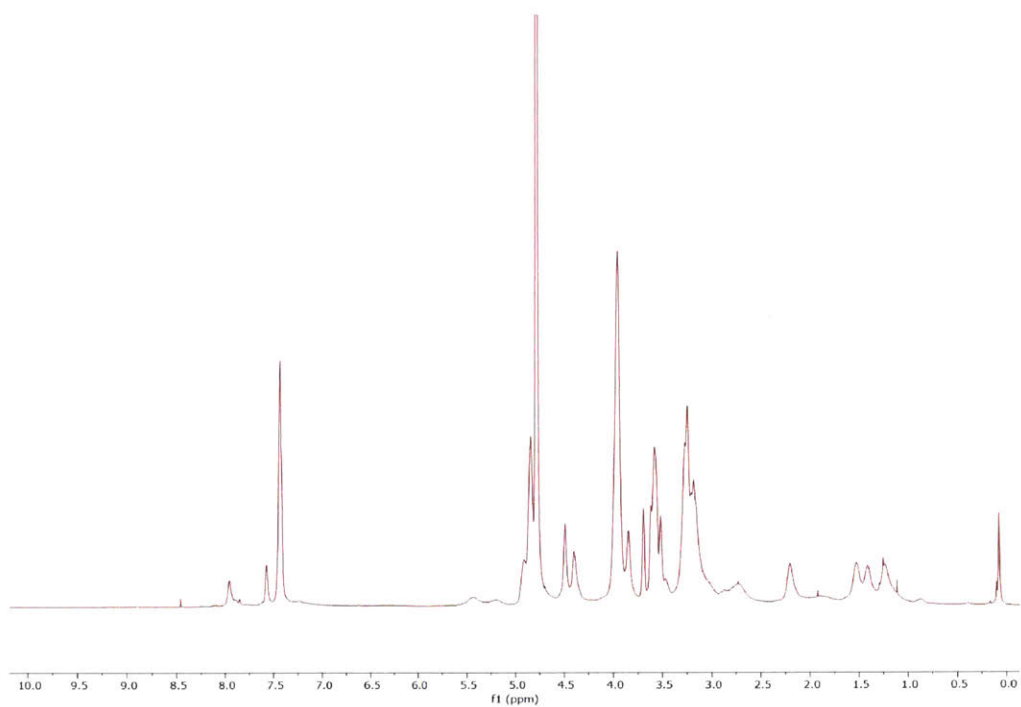


Figure S5.42. ^1H NMR of **2A-L-Cy** in D_2O .

2A-D-Cy

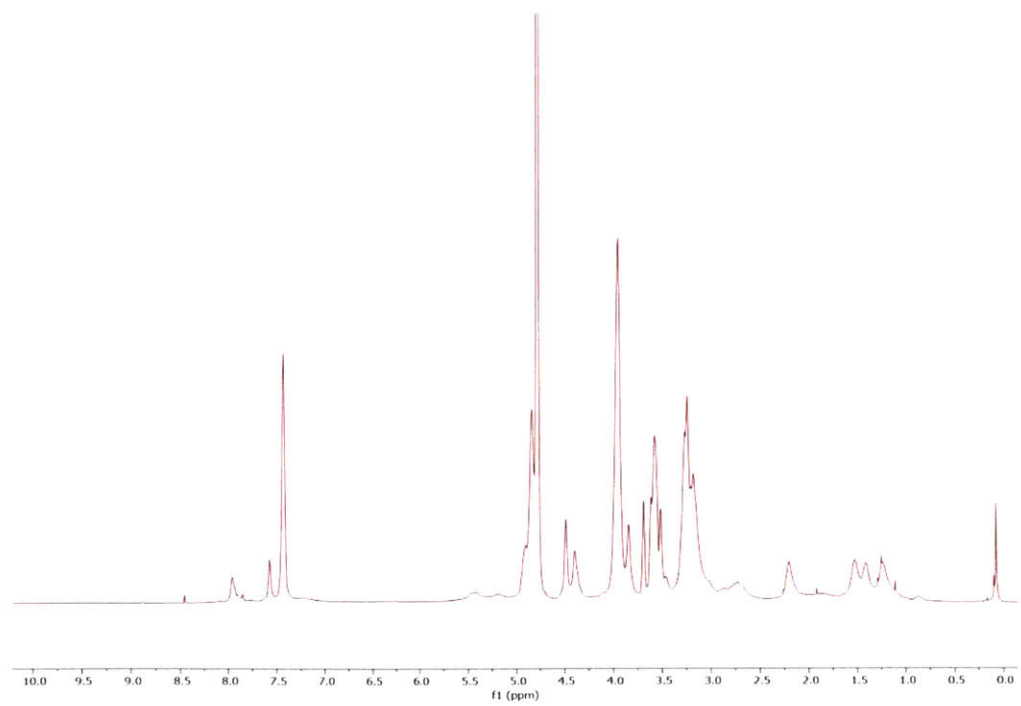


Figure S5.43. ^1H NMR of **2A-D-Cy** in D_2O .

Chiral HPLC

Column (wavelength): CHIRALCEL AD-H (230 nm)

Temperature: 23 °C

Mobile Phase: 10% isopropanol/hexanes, 1 mL/min

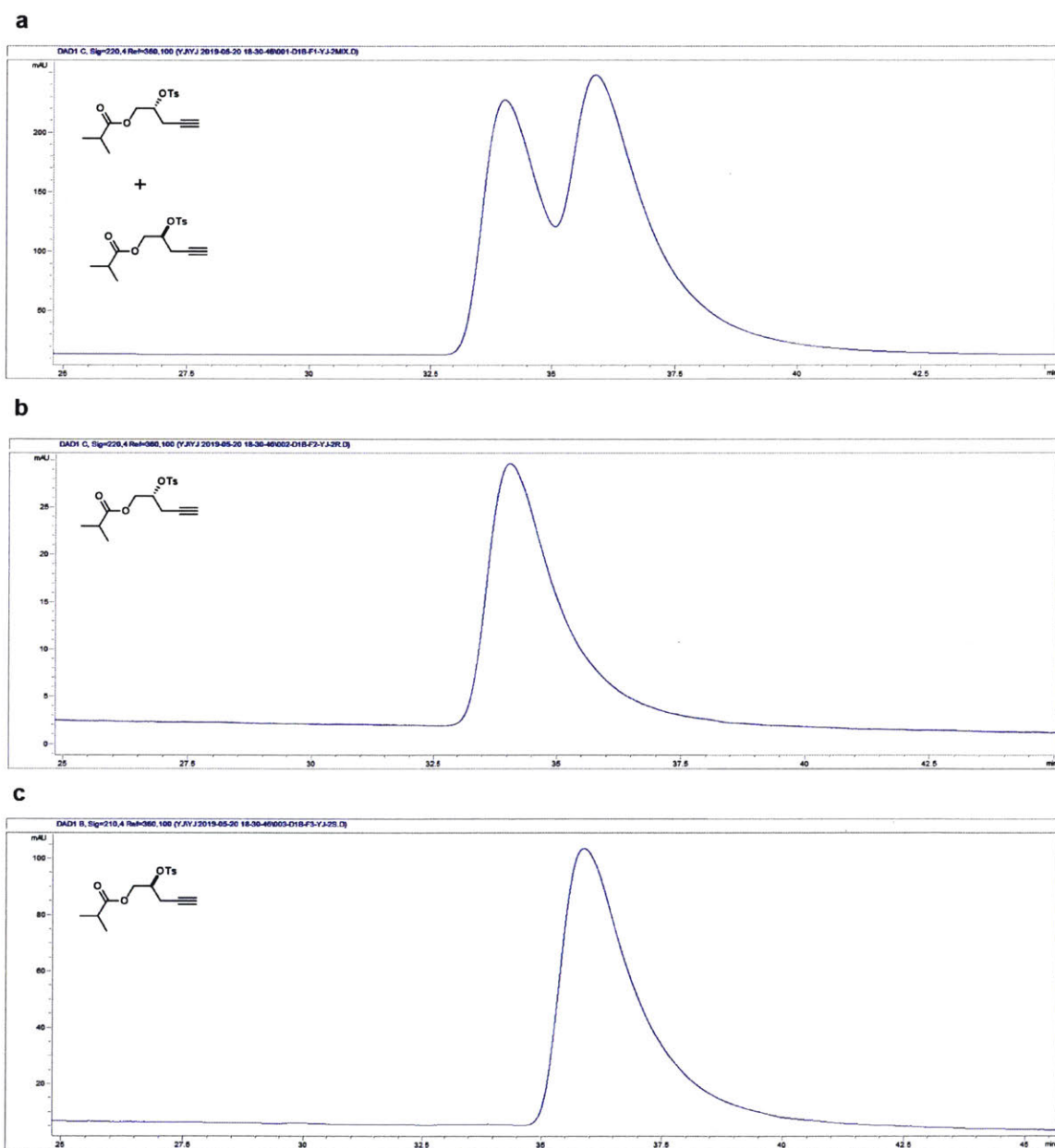
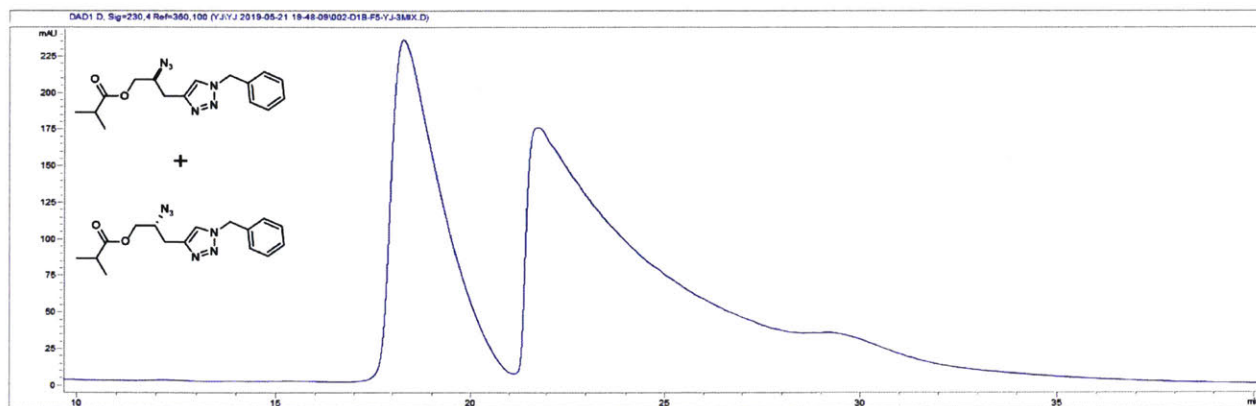
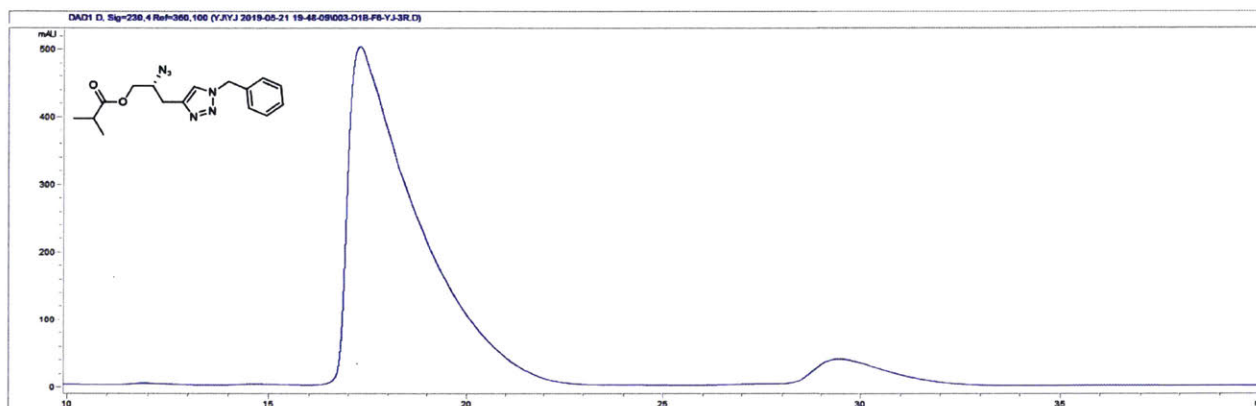


Figure S5.44. Chiral HPLC trace of (a) racemic mixture of **4** and its two individual enantiomers in parts (b) and (c).

a



b



c

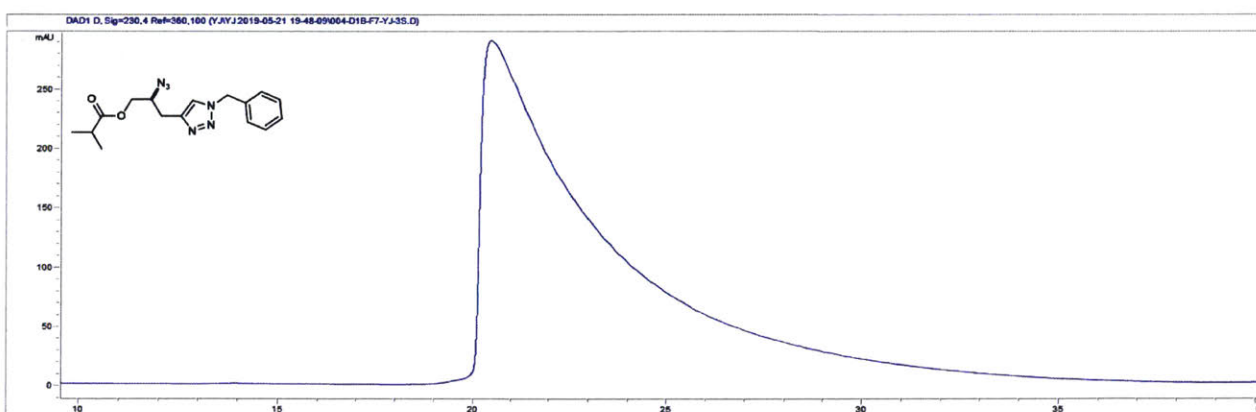


Figure S5.45. Chiral HPLC trace of **(a)** racemic mixture of **7** and its two individual enantiomers in parts **(b)** and **(c)**.

Spectrometric Characterization

Matrix-assisted laser Desorption/ionization Time-of-flight Mass Spectrometry (MALDI-TOF-MS)

5AIEG

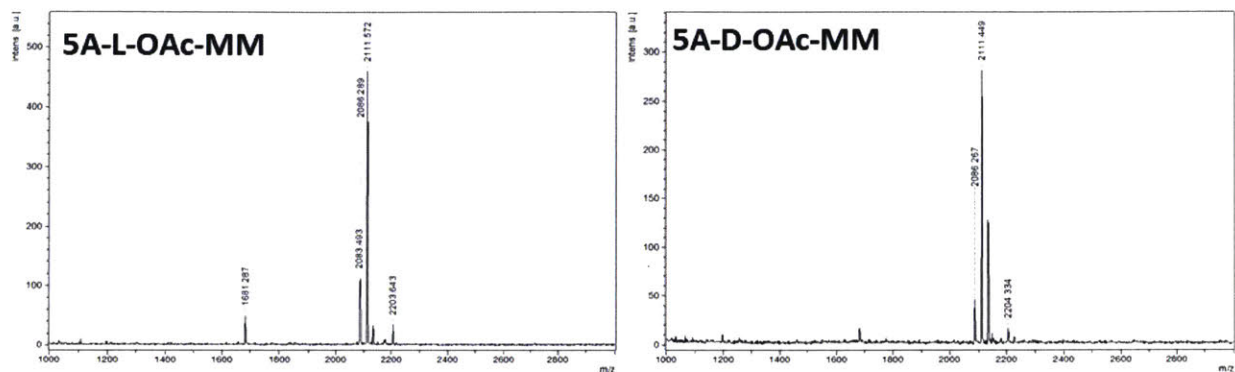


Figure S5.46. MALDI-TOF-MS of **5A-L-OAc-MM** and **5A-D-OAc-MM**. (Cald 2110.93 [M+H]⁺)

2AIEG

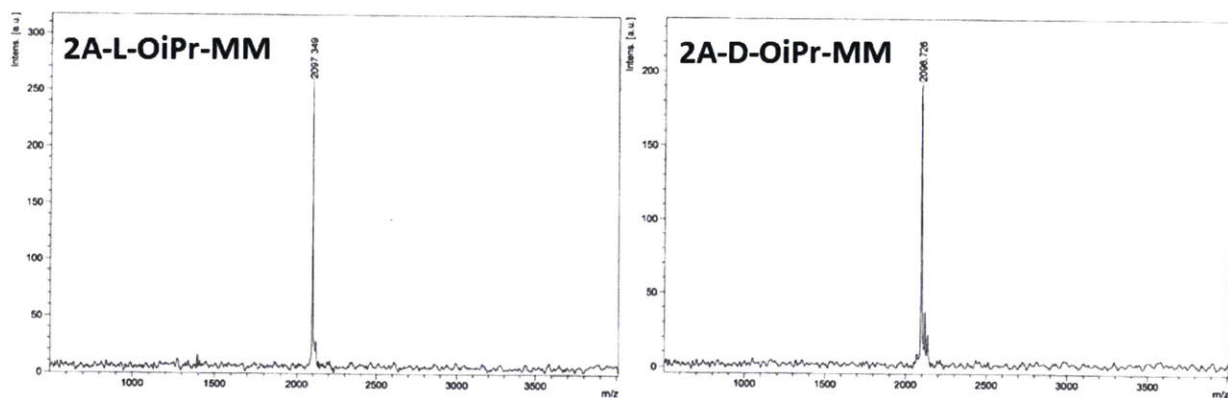


Figure S5.47. MALDI-TOF-MS of **2A-L-OiPr-MM** and **2A-D-OiPr-MM**. (Cald 2096.86 [M+H]⁺)

Size Exclusion Chromatography

Gel Permeation Chromatography (GPC) of Bottlebrush Polymers

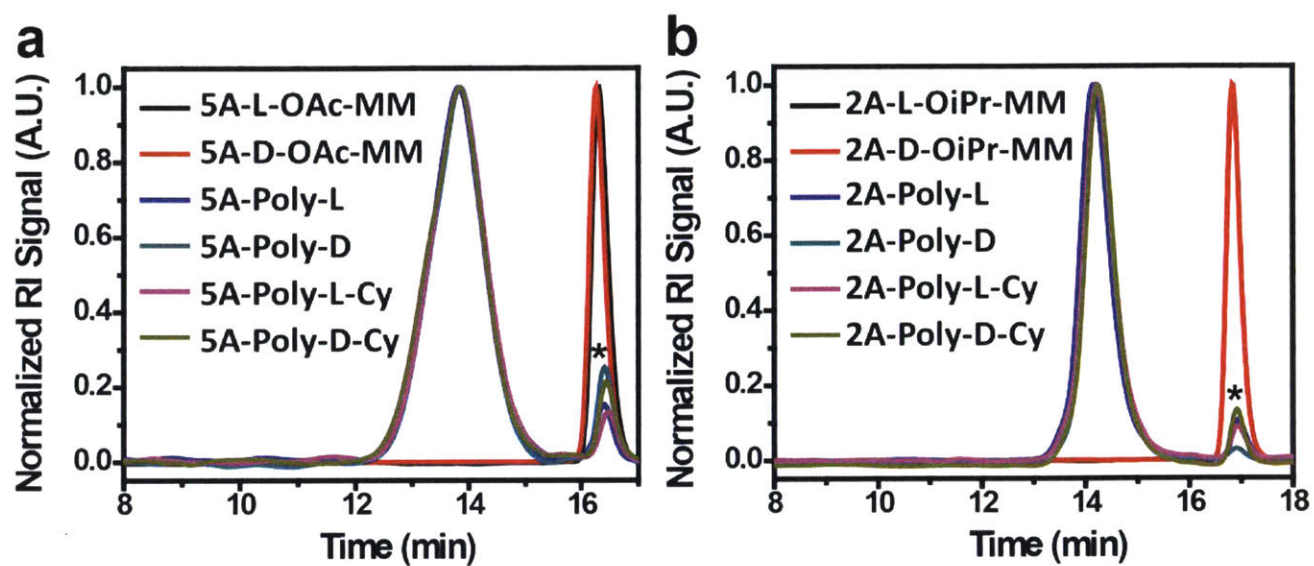


Figure S5.48. GPC traces of IEG MMs and the corresponding bottlebrush polymers for the (a) 5AIEG and (b) 2AIEG system. * denote residual MM in the crude reaction mixture prior to deprotection and dialysis. In all cases, a conversion of >90% was observed.

5.5 References

1. Lutz, J.-F.; Ouchi, M.; Liu, D. R.; Sawamoto, M. Sequence-Controlled Polymers. *Science*, **2013**, *341*, 1238149.
2. Bustamante, C.; Cheng, W.; Mejia, Y. X. Revisiting the Central Dogma One Molecule at a Time. *Cell*. **2011**, *144*, 480-497.
3. Schneider-Poetsch, T.; Yoshida, M. Along the Central Dogma—Controlling Gene Expression with Small Molecules. *Annu. Rev. Biochem.* **2018**, *87*, 391-420.
4. Lutz, J.-F. Sequence-Controlled Polymerizations: The Next Holy Grail in Polymer Science? *Polym. Chem.* **2010**, *1*, 55-62.
5. van Hest, J. C. M.; Tirrell, D. A. Protein-Based Materials, Toward a New Level of Structural Control. *Chem. Commun.* **2001**, *0*, 1897-1904.
6. Shi, J.; Votruba, A. R.; Farokhzad, O. C.; Langer, R. Nanotechnology in Drug Delivery and Tissue Engineering: From Discovery to Applications. *Nano Lett.* **2010**, *10*, 3223-3230.
7. Kakkar, A.; Traverso, G.; Farokhzad, O. C.; Weissleder, R.; Langer, R. Evolution of Macromolecular Complexity in Drug Delivery Systems. *Nat. Rev. Chem.* **2017**, *1*, 0063.
8. Elsabahy, M.; Heo, G. S.; Lim, S.-M.; Sun, G.; Wooley, K. L. Polymeric Nanostructures for Imaging and Therapy. *Chem. Rev.* **2015**, *115*, 10967.
9. Jokerst, J. V.; Lobovkina, T.; Zare, R. N.; Gambhir, S. S. Nanoparticle PEGylation for Imaging and Therapy. *Nanomedicine (Lond)*. **2011**, *6*, 715-728.
10. Otsukaa, H.; Nagasaki, Y.; Kataoka, K. PEGylated Nanoparticles for Biological and Pharmaceutical Applications. *Adv. Drug Deliv. Rev.* **2012**, *64*, 246-255.
11. Knop, K.; Hoogenboom, R.; Fischer, D.; Schubert, U. S. Poly(Ethylene Glycol) in Drug Delivery: Pros and Cons as Well as Potential Alternatives. *Angew. Chem. Int. Ed. Engl.* **2010**, *49*, 6288-6308.
12. Kolate, A.; Baradia, D.; Patil, S.; Vhora, I.; Kore, G.; Misra, A. PEG—A Versatile Conjugating Ligand for Drugs and Drug Delivery Systems. *J. Control Release* **2014**, *192*, 67-81.
13. Miura, Y.; Hoshino, Y.; Seto, H. Glycopolymers Nanobiotechnology. *Chem. Rev.* **2016**, *116*, 1673-1692.
14. Rabuka, D.; Forstner, M. B.; Groves, J. T.; Bertozzi, C. R. Noncovalent Cell Surface Engineering: Incorporation of Bioactive Synthetic Glycopolymers into Cellular Membranes. *J. Am. Chem. Soc.* **2008**, *130*, 5947-5953.
15. Godula, K.; Bertozzi, C. R. Synthesis of Glycopolymers for Microarray Applications via Ligation of Reducing Sugars to a Poly(Acryloyl Hydrazide) Scaffold. *J. Am. Chem. Soc.* **2010**, *132*, 9963-9965.
16. Gestwicki, J. E.; Cairo, C. W.; Strong, L. E.; Oetjen, K. A.; Kiessling, L. L. Influencing Receptor–Ligand Binding Mechanisms with Multivalent Ligand Architecture. *J. Am. Chem. Soc.* **2002**, *124*, 14922-14933.
17. Becer, C. R.; Gibson, M. I.; Geng, J.; Ilyas, R.; Wallis, R.; Mitchell, D. A.; Haddleton, D. M. High-Affinity Glycopolymer Binding to Human DC-SIGN and Disruption of DC-SIGN Interactions with HIV Envelope Glycoprotein. *J. Am. Chem. Soc.* **2010**, *132*, 15130-15132.
18. Yuan, L.; Zhang, F.; Qi, X.; Yang, Y.; Yan, C.; Jiang, J.; Deng, J. Chiral Polymer Modified Nanoparticles Selectively Induce Autophagy of Cancer Cells for Tumor Ablation. *J. Nanobiotechnol.* **2018**, *16*, 55.
19. Deng, J.; Yao, M.; Gao, C. Cytotoxicity of Gold Nanoparticles with Different Structures and Surface-Anchored Chiral Polymers. *Acta Biomater.* **2017**, *53*, 610-618.

20. Wang, X.; Gan, H.; Sun, T. Chiral Design for Polymeric Biointerface: The Influence of Surface Chirality on Protein Adsorption. *Adv. Func. Mater.* **2011**, *21*, 3276-3281.
21. Deng, J.; Wu, S.; Yao, M.; Gao, C. Surface-Anchored Poly(Acryloyl-*L(D)*-valine) with Enhanced Chirality-Selective Effect on Cellular Uptake of Gold Nanoparticles. *Sci. Rep.* **2016**, *6*, 31595.
22. Morris, M. C.; Deshayes, S.; Heitz, F.; Divita, G. Cell-Penetrating Peptides: From Molecular Mechanisms to Therapeutics. *Biol. Cell.* **2008**, *100*, 201-217.
23. Guidotti, G.; Brambilla, L.; Rossi, D. Cell-Penetrating Peptides: From Basic Research to Clinics. *Trends Pharmacol. Sci.* **2017**, *38*, 406-424.
24. Pooga, M.; Soomets, U.; Hallbrink, M.; Valkna, A.; Saar, K.; Rezaei, K.; Kahl, U.; Hao, J.-X.; Xu, X.-J.; Wiesenfeld-Hallin, Z.; Hokfelt, T.; Bartfai, T.; Langel, U. Cell Penetrating PNA Constructs Regulate Galanin Receptor Levels and Modify Pain Transmission *In Vivo*. *Nat. Biotechnol.* **1998**, *16*, 857-861.
25. Taylor, B. N.; Mehta, R. R.; Yamada, T.; Lekmine, F.; Christov, K.; Chakrabarty, A. M.; Green, A.; Bratescu, L.; Shilkaitis, A.; Beattie, C. W.; Das Gupta, T. K. Noncationic Peptides Obtained From Azurin Preferentially Enter Cancer Cells. *Cancer Res.* **2009**, *69*, 537-546.
26. Fowler, S. A.; Blackwell, H. E. Structure-Function Relationships in Peptoids: Recent Advances Toward Deciphering the Structural Requirements for Biological Function. *Org. Biomol. Chem.* **2009**, *7*, 1508-1524.
27. Yu, P.; Liu, B.; Kodadek, T. A High-Throughput Assay for Assessing the Cell Permeability of Combinatorial Libraries.. *Nat. Biotechnol.* **2005**, *23*, 746-751.
28. Kwon, Y. U.; Kodadek, T. Quantitative Evaluation of The Relative Cell Permeability of Peptoids and Peptides.. *J. Am. Chem. Soc.* **2007**, *129*, 1508-1509.
29. Tan, N. C.; Yu, P.; Kwon, Y. U.; Kodadek, T. High-Throughput Evaluation of Relative Cell Permeability Between Peptoids and Peptides. *Bioorg. Med. Chem.* **2008**, *16*, 5853-5861.
30. Wender, P. A.; Mitchell, D. J.; Pattabiraman, K.; Pelkey, E. T.; Steinman, L.; Rothbard, J. B. The Design, Synthesis, and Evaluation of Molecules that Enable or Enhance Cellular Uptake: Peptoid Molecular Transporters. *Proc. Natl. Acad. Sci. U. S. A.* **2000**, *97*, 13003-13008.
31. Wender, P. A.; Jessop, T. C.; Pattabiraman, K.; Pelkey, E. T.; VanDeusen, C. L. An Efficient, Scalable Synthesis of the Molecular Transport Octaarginine via a Segment Doubling Strategy. *Org. Lett.* **2001**, *3*, 3229-3232.
32. Wu, C. W.; Sanborn, T. J.; Zuckermann, R. N.; Barron, A. E. Peptoid Oligomers with α -Chiral, Aromatic Side Chains: Effects of Chain Length on Secondary Structure. *J. Am. Chem. Soc.* **2001**, *123*, 2958-2963.
33. Wu, C. W.; Sanborn, T. J.; Huang, K.; Zuckermann, R. N.; Barron, A. E. Peptoid Oligomers with α -Chiral, Aromatic Side Chains: Sequence Requirements for the Formation of Stable Peptoid Helices. *J. Am. Chem. Soc.* **2001**, *123*, 6778-6784.
34. Jumpei Morimoto, J.; Yasuhiro Fukuda, Y.; and Shinsuke Sando, S. Solid-Phase Synthesis of β -Peptoids with Chiral Backbone Substituents Using Reductive Amination. *Org. Lett.* **2017**, *19*, 5912-5915.
35. Lee, K. J.; Lee, S. W.; Yun, H.; Hyun, Y.-J.; Seo, C. D.; Lee, C. W.; Lim, H.-S. Oligomers of N-Substituted β^2 -Homoalanines: Peptoids with Backbone Chirality. *Org. Lett.* **2016**, *18*, 3678-3681.

36. Barnes, J. C.; Ehrlich, D. J.-C.; Gao, A. X.; Leibfarth, F. A.; Jiang, Y.; Zhou, E.; Jamison, T. F.; Johnson, J. A. Iterative Exponential Growth of Stereo- and Sequence-Controlled Polymers. *Nat. Chem.* **2015**, *7*, 810-815.
37. Golder, M. R.; Jiang, Y.; Teichen, P. E.; Nguyen, H. V.-T.; Wang, W.; Milos, N.; Freedman, S. A.; Willard, A. P.; Johnson, J. A. Stereochemical Sequence Dictates Unimolecular Diblock Copolymer Assembly. *J. Am. Chem. Soc.* **2018**, *140*, 1596-1599.
38. Jiang, Y.; Golder, M. R.; Nguyen, H. V.-T.; Wang, Y.; Zhong, M.; Barnes, J. C.; Ehrlich, D. J. C.; Johnson, J. A. Iterative Exponential Growth Synthesis and Assembly of Uniform Diblock Copolymers. *J. Am. Chem. Soc.* **2016**, *138*, 9369-9372.
39. Sheiko, S. S.; Sumerlin, B. S.; Matyjaszewski, K. Cylindrical Molecular Brushes: Synthesis, Characterization, and Properties. *Prog. Polym. Sci.* **2008**, *33*, 759-785.
40. Verduzco, R.; Li, X.; Pesek, S. L.; Stein, G. E. Structure, Function, Self-assembly, and Applications of Bottlebrush Copolymers. *Chem. Soc. Rev.* **2015**, *44*, 2405-2420.
41. Kawamoto, K.; Zhong, M.; Gadelrab, K. R.; Cheng, L.-C.; Ross, C. A.; Alexander-Katz, A.; Johnson, J. A. Graft-through Synthesis and Assembly of Janus Bottlebrush Polymers from A-branch-B Diblock Macromonomers. *J. Am. Chem. Soc.* **2016**, *138*, 11501-11504.
42. Bielawski, C. W.; Grubbs, R. H. Living Ring-Opening Metathesis Polymerization. *Prog. Polym. Sci.* **2007**, *32*, 1-29.
43. Johnson, J. A.; Lu, Y. Y.; Burts, A. O.; Xia, Y.; Durrell, A. C.; Tirrell, D. A.; Grubbs, R. H. Drug-loaded, Bivalent-bottle-brush Polymers by Graft-through ROMP. *Macromolecules.* **2010**, *43*, 10326-10335.
44. Liao, L.; Liu, J.; Dreaden, E. C.; Morton, S. W.; Shopsowitz, K. E.; Hammond, P. T.; Johnson, J. A. A Convergent Synthetic Platform for Single-nanoparticle Combination Cancer Therapy: Ratiometric Loading and Controlled Release of Cisplatin, Doxorubicin, and Camptothecin. *J. Am. Chem. Soc.* **2014**, *136*, 5896-5899.
45. Gao, A. X.; Liao, L.; Johnson, J. A. Synthesis of Acid-labile PEG and PEG-doxorubicin-conjugate Nanoparticles via Brush-first ROMP. *ACS Macro Lett.* **2014**, *3*, 854-857.
46. Nguyen, H. V.-T.; Chen, Q.; Paletta, J. T.; Harvey, P.; Jiang, Y.; Zhang, H.; Boska, M. D.; Ottaviani, M. F.; Jasanoff, A.; Rajca, A.; Johnson, J. A. Nitroxide-based Macromolecular Contrast Agents with Unprecedented Transverse Relaxivity and Stability for Magnetic Resonance Imaging of Tumors. *ACS Cent. Sci.* **2017**, *3*, 800.
47. Barnes, J. C.; Bruno, P. M.; Nguyen, H. V. T.; Liao, L.; Liu, J.; Hemann, M. T.; Johnson, J. A. Using an RNAi Signature Assay To Guide the Design of Three-drug-conjugated Nanoparticles with Validated Mechanisms, In Vivo Efficacy, and Low Toxicity. *J. Am. Chem. Soc.* **2016**, *138*, 12494-12501.
48. Sowers, M. A.; McCombs, J. R.; Wang, Y.; Paletta, J. T.; Morton, S. W.; Dreaden, E. C.; Boska, M. D.; Ottaviani, M. F.; Hammond, P. T.; Rajca, A.; Johnson, J. A. Redox-responsive Branched-bottlebrush Polymers for in vivo MRI and Fluorescence Imaging. *Nat. Commun.* **2014**, *5*, 5460.
49. Johnson, J. A.; Lu, Y.-Y.; Burts, A. O.; Lim, Y.-H.; Finn, M. G.; Koberstein, J. T.; Turro, N. J.; Tirrell, D. A.; Grubbs, R. H. Core-Clickable PEG-Branch-Azide Bivalent-Bottle-Brush Polymers by ROMP: Grafting-Through and Clicking-To. *J. Am. Chem. Soc.* **2011**, *133*, 559-566.
50. Li, Z.; Ma, J.; Cheng, C.; Zhang, K.; Wooley, K. L. Synthesis of Hetero-grafted Amphiphilic Diblock Molecular Brushes and Their Self-assembly in Aqueous Medium. *Macromolecules*, **2010**, *43*, 1182-1184.

51. Lu, X.; Jia, F.; Tan, X.; Wang, D.; Cao, X.; Zheng, J.; Zhang, K. Effective Antisense Gene Regulation via Noncationic, Polyethylene Glycol Brushes. *J. Am. Chem. Soc.* **2016**, *138*, 9097-9100.
52. Zou, J.; Yu, Y.; Li, Y.; Ji, W.; Chen, C.-K.; Law, W.-C.; Prasad, P. N.; Cheng, C. Well-Defined Diblock Brush Polymer–Drug Conjugates for Sustained Delivery of Paclitaxel. *Biomater. Sci.* **2015**, *3*, 1078-1084.